

LOCKHEED MARTIN ENERGY RESEARCH LIBRARIES



3 4456 051555D 5

CENTRAL RESEARCH LIBRARY
DOCUMENT COLLECTION

cy

ORNL-4370

UC-25 - Metals, Ceramics, and Materials

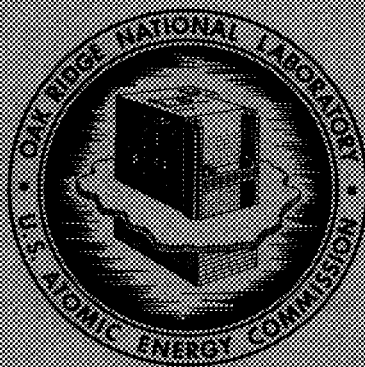
METALS AND CERAMICS DIVISION
ANNUAL PROGRESS REPORT
FOR PERIOD ENDING JUNE 30, 1960

OAK RIDGE NATIONAL LABORATORY
CENTRAL RESEARCH LIBRARY
DOCUMENT COLLECTION

LIBRARY LOAN COPY

DO NOT TRANSFER TO ANOTHER PERSON

If you wish someone else to see this
document, send in name with document
and the library will arrange a loan



OAK RIDGE NATIONAL LABORATORY
operated by
UNION CARBIDE CORPORATION
for the
U.S. ATOMIC ENERGY COMMISSION

Printed in the United States of America. Available from Clearinghouse for Federal
Scientific and Technical Information, National Bureau of Standards,
U.S. Department of Commerce, Springfield, Virginia 22151
Price: Printed Copy \$3.00; Microfiche \$0.65

LEGAL NOTICE

This report was prepared as an account of Government sponsored work. Neither the United States, nor the Commission, nor any person acting on behalf of the Commission:

- A. Makes any warranty or representation, expressed or implied, with respect to the accuracy, completeness, or usefulness of the information contained in this report, or that the use of any information, apparatus, method, or process disclosed in this report may not infringe privately owned rights; or
- B. Assumes any liabilities with respect to the use of, or for damages resulting from the use of any information, apparatus, method, or process disclosed in this report.

As used in the above, "person acting on behalf of the Commission" includes any employee or contractor of the Commission, or employee of such contractor, to the extent that such employee or contractor of the Commission, or employee of such contractor prepares, disseminates, or provides access to, any information pursuant to his employment or contract with the Commission, or his employment with such contractor.

Contract No. W-7405-eng-26

METALS AND CERAMICS DIVISION ANNUAL PROGRESS REPORT
for Period Ending June 30, 1968

J. H. Frye, Jr., Director
J. E. Cunningham, Assistant Director

Section Heads

G. M. Adamson, Jr.
B. S. Borie
W. O. Harms
C. J. McHargue
P. Patriarca

Compiled and Edited by Sigfred Peterson

OCTOBER 1968

OAK RIDGE NATIONAL LABORATORY
Oak Ridge, Tennessee
operated by
UNION CARBIDE CORPORATION
for the
U. S. ATOMIC ENERGY COMMISSION

LOCKHEED MARTIN ENERGY RESEARCH LIBRARIES



3 4456 0515550 5

Reports previously issued in this series are as follows:

ORNL-28	Period Ending March 1, 1948
ORNL-69	Period Ending May 31, 1948
ORNL-407	Period Ending July 31, 1949
ORNL-511	Period Ending October 31, 1949
ORNL-583	Period Ending January 31, 1950
ORNL-754	Period Ending April 30, 1950
ORNL-827	Period Ending July 31, 1950
ORNL-910	Period Ending October 31, 1950
ORNL-987	Period Ending January 31, 1951
ORNL-1033	Period Ending April 30, 1951
ORNL-1108	Period Ending July 31, 1951
ORNL-1161	Period Ending October 31, 1951
ORNL-1267	Period Ending January 31, 1952
ORNL-1302	Period Ending April 30, 1952
ORNL-1366	Period Ending July 31, 1952
ORNL-1437	Period Ending October 31, 1952
ORNL-1503	Period Ending January 31, 1953
ORNL-1551	Period Ending April 10, 1953
ORNL-1625	Period Ending October 10, 1953
ORNL-1727	Period Ending April 10, 1954
ORNL-1875	Period Ending October 10, 1954
ORNL-1911	Period Ending April 10, 1955
ORNL-1988	Period Ending October 10, 1955
ORNL-2080	Period Ending April 10, 1956
ORNL-2217	Period Ending October 10, 1956
ORNL-2422	Period Ending October 10, 1957
ORNL-2632	Period Ending October 10, 1958
ORNL-2839	Period Ending September 1, 1959
ORNL-2988	Period Ending July 1, 1960
ORNL-3160	Period Ending May 31, 1961
ORNL-3313	Period Ending May 31, 1962
ORNL-3470	Period Ending May 31, 1963
ORNL-3670	Period Ending June 30, 1964
ORNL-3870	Period Ending June 30, 1965
ORNL-3970	Period Ending June 30, 1966
ORNL-4170	Period Ending June 30, 1967

Contents

SUMMARY	xv
---------------	----

PART I. FUNDAMENTAL PROGRAMS

1. CRYSTAL PHYSICS	1
Internal Centrifugal Zone Growth	1
Molten-Salt Growth of Single Crystals	2
Self-Activated Thermoluminescence in Lanthanide- and Actinide-Doped Thorium Dioxide Crystals	2
Electron-Spin Resonance of $^{244}\text{Cm}^{3+}$ in ThO_2 and CeO_2	2
Flux Growth and Characterization of Hexagonal Germanium Dioxide Single Crystals	3
Hydrothermal Synthesis	3
Hydrothermal Synthesis, Optical Perfection, and Surface Topography of Quartz Grown in RbOH and Other Alkali Hydroxides	3
Infrared Spectra of Hydrothermally Grown Quartz	3
Further Studies in the System $\text{RbOH-SiO}_2\text{-Fe}_2\text{O}_3/\text{Fe-H}_2\text{O}$	3
Crystal Growth by the Verneuil Method	3
Diamagnetic Susceptibility of High-Purity Thorium Dioxide Crystals	4
Alternating-Current Mutual Inductance Bridge	4
2. DEFORMATION AND ANNEALING OF METALS	5
Development of Preferred Orientations in Cold-Rolled Niobium	5
Texture Inhomogeneities in Cold-Rolled Niobium	5
Texture Transition in Ordered Cu_3Au	6
The Recovery Characteristics of Niobium and Nb-40% V	8
3. DEFORMATION OF CRYSTALLINE SOLIDS	9
Substructure and Fracture in Pack-Rolled Foils of Copper and Iron	9
Plastic Deformation of Rhenium	9
Interaction of Slip Dislocations with Twins in Hexagonal-Close-Packed Metals	10
Dislocation Reactions in Hexagonal-Close-Packed Metals	10
Series Representation of Thermodynamic Functions of Binary Solutions	10
Representation of Textures as Axial and Biaxial Pole Figures	11

4. DIFFUSION IN SOLIDS	13
Use of Electrochemical Sectioning in the Study of Diffusion in Tungsten	13
Diffusion of ^{95}Nb and ^{188}W in Monocrystalline Tungsten	13
Short-Circuiting Effects on Tracer Diffusion in Tungsten	13
Cation Self-Diffusion in UN	14
Cation Self-Diffusion in UO_2 Single Crystals	14
Diffusion of Titanium in Modified Hastelloy N	14
5. ELECTRON MICROSCOPY	16
Bubble Growth Processes at Grain Boundaries in CVD Tungsten	16
Stress-Induced Growth of Gas Bubbles in Solids	16
Thermal Rejection and Growth of Gas Bubbles in Electrodeposited Nickel	17
Annealing Behavior of Voids in Irradiated Stainless Steel	17
Energy Stored in Silver Single Crystals	18
Phase Instability in Hastelloy N	18
Observation of Gas Bubbles in Solids	19
Electron Fractography for Studying Cavities	19
Electron Microscope-Microprobe Analysis of Precipitation	19
Preparation of Transmission Electron Microscopy Specimens from Tubing	19
6. ELECTRONIC PROPERTIES OF METALS AND ALLOYS	21
Mössbauer Measurements with ^{61}Ni in the Copper-Nickel System	21
Radiation Effects in Ordered Iron-Aluminum Alloys: Mössbauer Experiments Following Neutron Capture	22
Specific Heat of Uranium Mononitride from 1.3 to 4.6°K	23
Purification of Zirconium and Refractory Metals in an Ultrahigh-Vacuum Zone Refiner with Analysis of Partial Pressures	23
Preparation and Zone Purification of Hafnium Metal with Low Zirconium Content	23
Electrical Resistivity of Zirconium Alloys	23
Low-Temperature Specific Heats of Zirconium with 0 to 5% Additions of Nb, Mo, Re, Ru, Rh, and Pd	24
7. FUNDAMENTAL CERAMICS RESEARCH	26
Transport Properties of UN	26
Electrical Resistivity of $\text{U}(\text{C},\text{N})$	28
Ultrasonic Velocity Measurements in UN	28
8. PHYSICAL CERAMICS STUDIES	30
Deformation of Uranium Dioxide Single Crystals	30
Diffusion of Thorium in ThO_2	31
Some Fundamental Ideas from Topology and Their Application to Problems in Metallurgy	33
Compressive Creep of Uranium Mononitride	33

Compressive Creep of Uranium Dioxide	33
Activation Energy in Sintering	33
9. PHYSICAL PROPERTIES	35
Electronic Heat Transport Analysis	35
Thermal Conductivity and Electrical Resistivity of High-Purity Copper from 78 to 400°K	36
Physical Properties of Indium from 77 to 350°K	36
Physical Properties of Molybdenum from 77 to 1300°K	36
Physical Properties of Chromium	36
Thermal Conductivity of ThO ₂ and UO ₂ from 77 to 1300°K	37
Comments on "The Thermal Conductivity of UO ₂ at Very High Temperature Gradients"	37
Related Studies	37
Low-Temperature Axial Heat Flow Apparatus	37
Radial Heat Flow Apparatus	37
Electrical Heating Methods	38
Pulse Heating Calorimetry	38
10. SPECTROSCOPY OF IONIC MEDIA	39
Coordination of Transition Metal Ions in Melts	39
Nickel(II) in Molten LiBr-KBr and LiI-KI Mixtures	39
Liquidus Curve for the LiI-KI System and Liquid State Densities of LiI-KI and LiBr-KBr Melts	39
Nickel(II) in Molten ZnCl ₂ -CsCl Mixtures	40
Densities of Molten ZnCl ₂ and ZnCl ₂ -CsCl Mixtures	40
Nickel(II) in Molten CsAlCl ₄	40
Phase Studies and Electrical Conductivities of Systems Containing Aluminum Halides	40
Molybdenum(III) in Fluoride Melts	41
Nickel(II)-Nitrate Complexes in Molten Dimethyl Sulfone and Application to Identification of Nickel(II) Coordination in the Molten LiNO ₃ -NaNO ₃ -KNO ₃ Eutectic	41
Exchange Reactions Between Tetrahalo Complexes of Nickel(II) in Tetramethylene Sulfone	42
Densities of Solutions of LiI, LiBr, and LiClO ₄ in Tetramethylene Sulfone	42
Densities of Molten BiCl ₃ and BiCl ₃ -AlCl ₃ Mixtures	42
Phenomenological Analysis of the Effects of Temperature and Composition on the Absorption Spectra of Liquid Systems	42
Optical Spectra of Transition Metal Ions in Chloride Crystals	42
Nickel(II) at Approximately Octahedral Sites in Crystals	42
Nickel(II) at Approximately Tetrahedral Sites in Crystals	43
Crystal Structures of Cs ₃ MgCl ₅ ·Ni and Cs ₃ NiCl ₅ Down to 10°K	43
Cobalt(II) Centers at Approximately Octahedral Sites in Chloride Crystals	43
Redox Processes in Melts	43
Tellurium in the Electropositive Oxidation State One-Half	44
Spectroscopy of NO ₃ ⁻ in Melts	44
Ultraviolet Spectrum of the Nitrate Ion in Molten Mixtures of Alkali Metal Nitrates	44

Apparatus Development	44
Spectrophotometer Furnaces	44
Diamond-Windowed Cell for Molten Fluoride Spectroscopy	44
11. SUPERCONDUCTING MATERIALS	45
Superconducting Properties of a Tc-30 at. % V Alloy	45
Analytic Expression for Superconducting Critical Current Density	45
Rare Earth Structural Studies	45
12. SURFACE REACTIONS OF METALS	47
Oxidation of Nickel	47
X-ray Studies	47
Ellipsometer Studies	48
Refractory Metal Oxidation	49
Stress Development During Oxidation	49
Anodic-Film Sectioning of Tungsten	49
13. THEORETICAL RESEARCH	52
Constant Energy Surfaces for Aluminum by the Korringa-Kohn-Rostoker Method	52
Effect of $\langle 001 \rangle$ Uniaxial Tension on the Fermi Surface of Metallic Copper	52
Effect of Hydrostatic Pressure on the Fermi Surface of Metallic Gold	53
Calculation of the Band Structure of "Complex" Crystals	53
Calculation of the Wave Functions for the Electronic States in Metals	54
Valence States of Carbon in π -Electron Systems. I. Alternant-Hydrocarbon Ground States	54
Valence States of Carbon in π -Electron Systems. II. Excited States and Ions	54
<i>S</i> Limit in Helium. Movement of a System on an Energy Surface in Parameter Space	54
14. X-RAY DIFFRACTION	55
Routine Analyses	55
Crystal Structure of SrBe ₃ O ₄	56
Interpretation of Temperature Diffuse Scattering	56
Substructure and Perfection of UO ₂ Single Crystals	57
A High-Temperature Vacuum Sample Holder for the Kratky Camera	57
Automatic Balanced Filter Device for X-Ray Diffraction Experiments	57
Small-Angle X-Ray Scattering Investigation of Inhomogeneities in Aluminum-Zinc Alloys	57
Increased X-Ray Intensities by Use of Graphite as a Monochromator	58
Application of the Graphite Monochromator to Light Element X-Ray Spectroscopy	58
PART II. HIGH-TEMPERATURE MATERIALS PROGRAM	
15. PHYSICAL AND MECHANICAL METALLURGY OF HIGH-TEMPERATURE MATERIALS	59
Mechanical Properties of Refractory Alloys	59

Comparative Creep-Rupture Properties of Niobium Alloys	60
Effect of Fabrication Variables on Creep Rupture of Molybdenum Alloys	60
Time-Temperature Parameters for Creep Rupture of Refractory Alloys	61
Behavior of Refractory Alloys Under Dynamic Stresses	62
Physical Metallurgy of Refractory Alloys	62
Diffusivity, Solubility, and Permeability of Interstitials in Refractory Alloys	62
Development of Age-Hardening Refractory Alloys	62
Vaporization of Haynes Alloy No. 25 Under Stress	64
Brazing Alloy Development	64
Physical Properties of Molybdenum	66
Nondestructive Testing of Refractory Alloys	67
16. TUNGSTEN METALLURGY	68
Extrusion and Drawing of Tungsten and Tungsten Alloys	68
Extrusion Development	68
Hot-Plug Drawing Development	69
Chemical Vapor Deposition	70
Statistical Analysis of Tungsten Deposition	70
Effect of Deposition Conditions on the Orientation of CVD Tungsten and Molybdenum	71
Deposition of Tungsten-Rhenium Alloys	71
Effect of Gas Bubbles on Recrystallization and Grain Growth in CVD Tungsten	72
Creep-Rupture Properties of Wrought Tungsten Alloys	73
Tungsten Welding Development	73
17. ALKALI-METAL CORROSION OF HIGH-TEMPERATURE MATERIALS	76
Compatibility of Boiling Potassium with Refractory Alloys	76
Capsule Test Examinations	76
Forced-Circulation Loop Studies	77
Corrosion of Refractory Alloys by Lithium	78
Thermal-Convection Loop Tests	78
Forced-Circulation Loop Studies	78
Compatibility of NaK with Type 316 Stainless Steel and Nb-1% Zr Alloy in a Heat Rejection System	80
Interactions in Refractory-Metal-Alkali-Metal Systems Containing Oxygen	81
Effect of Oxygen in the Tantalum-Potassium System	81
Analysis of Corrosion Behavior in Terms of Solution Interaction Parameters	81
Partitioning of Oxygen Between Zirconium and Potassium and Between Zirconium and Sodium	83
Determination of Oxygen in Alkali Metals	84
18. NITRIDE FUELS DEVELOPMENT	85
Synthesis, Fabrication, and Characterization	85
Synthesis and Fabrication of UN and U(C,N)	85
Synthesis and Fabrication of (U,Pu)N	86
Characterization of Mixed Nitrides	86

Conversion of UO_2 to Carbonitride Fuels	86
Direct Conversion of Sol-Gel UO_{2+x} to $\text{U}(\text{C},\text{N})$	86
Kinetics of the UO_2 -C Reaction	87
Kinetics of the UC_2 - N_2 Reaction	88
Thermodynamic Studies	88
Thermodynamic Properties of UC-UN Solid Solutions	88
Vapor Pressure of Nitrogen over Nitrogen-Rich Uranium Nitride	89
A Consistent Set of Thermodynamic Values for Plutonium Mononitride	89
Compatibility of Cladding with Nitride Fuel	89
Thermodynamic Compatibility of Vanadium with Nitride Fuels	89
Compatibility of Nitride Fuels with Cladding Alloys	89
Active Carbon Produced by Reaction of Nitrogen with VC	90
Grain-Boundary Segregation of Oxygen in UN	90
Irradiation Performance of Nitride Fuels	90
Fuel-Cladding Thermal Conductance	90
Helium Bubble Migration in Uranium Mononitride in a Temperature Gradient	91
19. MATERIALS DEVELOPMENT FOR ISOTOPIC POWER SOURCES	92
Curium Program	92
Fabrication of Tungsten Capsules	92
Development of CVD Tungsten Cladding Techniques	92
Mechanical Properties of Capsule Materials	92
Vaporization of Refractory Alloys	94
Brazing Alloy Development	94
Physical Properties of T-111	94
Strontium Program	96
Compatibility	96
Welding	97
SNAP-21 Program	97
Electron-Beam Welding Development	97
Nondestructive Testing	99
SNAP-23 Welding Development	99
PART III. GENERAL FUELS AND MATERIALS RESEARCH	
20. FUEL ELEMENT FABRICATION DEVELOPMENT	101
Irradiation Testing of Miniature Fuel Plates	101
Preparation of UAl_x Particles	102
Determination of Powder Particle-Size Distribution of Research Reactor Fuels	103
Evaluation of a Device for the Determination of Powder Homogeneity After Blending	105
Void Volume in Aluminum Dispersion Fuel Plates	105
Influence of Alloying on the Swelling of UAl_x Dispersed in Aluminum	106
Nonuniform Deformation in Simulated Fuel Plates	107
Compressive Strengths of U_3O_8 - and UAl_3 -Aluminum Powder Metal Composites	108
Effect of Billet Feed Angle on the Curl of Rolled Plate	109
Flame-Produced Uranium Oxide Powders	109

Feasibility of Conversion of PuF_6 to PuO_2 by Chemical Vapor Deposition	110
Chemical Vapor Deposition of Silicon Carbide	110
Plate Surface Studies	111
Materials and Test Conditions	112
Results with 99.999% Aluminum	112
Results with 6061 Aluminum	114
21. IRRADIATION DAMAGE TO ALUMINUM	116
Effect of Neutron Irradiation on the Mechanical Properties of 1100 Aluminum	116
Density of Irradiated Aluminum	116
Effect of Neutron Irradiation on the Mechanical Properties of 6061 Aluminum	117
Effect of Cyclotron-Injected Helium on the Tensile Properties of Aluminum Alloys	117
Electron Microscopy of Irradiated X8001 Aluminum Alloy Hex Sheaths from HFIR	118
22. MECHANICAL PROPERTIES RESEARCH	120
Development of Titanium-Modified Type 304 Stainless Steel	120
Radiation Damage Resistance	120
Fabrication of Small-Diameter Stainless Steel Tubing	120
Development of Titanium-Modified Type 316 Stainless Steel	121
Effects of Titanium and Carbon Variations on Mechanical Properties and Radiation	
Damage of Incoloy 800	121
Effect of Titanium and Carbon on Mechanical Properties of Hastelloy N	122
Electron Microscopy of Irradiated EBR-II Fuel Cladding	122
Effect of Cyclotron-Injected Helium on the Creep-Rupture Properties of Stainless Steel	123
EBR-II Irradiation Experiments	124
23. NONDESTRUCTIVE TEST DEVELOPMENT	125
Electromagnetic Test Methods	125
Analytical Studies	125
Phase-Sensitive Eddy-Current Instrument	125
Temperature-Compensated Probes	129
Ultrasonic Test Methods	129
Fabrication of Reference Notches	129
Optical Visualization of Ultrasound	130
Frequency Analysis	130
Penetrating Radiation Methods	131
Holography	131
Quantitative Attenuation Measurement	132
24. SINTERED ALUMINUM PRODUCTS DEVELOPMENT	133
Primary Billet Process Development	133
Selection of a Process for the Consolidation of Ball-Milled Aluminum-Aluminum	
Oxide Flake	133
Effect of Impurities Introduced During Billet Fabrication on the Properties	
of Extruded Rod	133

Reproducibility of Product Fabricated from Billet Process B	134
Nondestructive Testing of Intermediate SAP Fabrication Products	136
Mechanical Property Studies	136
Anisotropy in Mechanical Properties of Extruded Commercial SAP Materials	136
Influence of Working in Various Directions on the Microstructure and High-Temperature Mechanical Properties of an Extruded SAP Alloy	136
Fracture Characteristics of SAP	137
Mechanical Properties of Commercial SAP	138
Development of New Dispersion-Strengthened Aluminum Alloys	140
25. SOL-GEL FAST REACTOR FUELS	142
Development of Fabrication Processes	142
Sphere-Pac Process Development	142
Pellet Development	143
Characterization of (U,Pu)O ₂ Fuels	143
Analytical Chemistry	143
Thermal Conductivity	143
Irradiation Testing	144
Uninstrumented Irradiation Tests	144
Instrumented Tests	145
Transient Irradiation Tests	149
Fast Flux Irradiation Tests	149
Applied Mathematics Development	149
26. JOINING RESEARCH ON NUCLEAR MATERIALS	151
Special Alloy Preparation	151
VARESTRAINT Testing	151
Hot-Ductility Testing	152
Electron-Beam Microprobe Analysis	153
27. ZIRCONIUM METALLURGY	156
Strain Behavior in Uniaxially Tested Zircaloy Tubing	156
Effect of Texture on the Torsional Yielding of Zircaloy Tubing	156
Textures in Deformed Zirconium Single Crystals	157
Examination of Orientation Factors for the Deformation Systems of Zirconium Under Biaxial Stress Conditions	157
Inhomogeneous Deformation in Zircaloy Tubing	157
Device for Studying Texture Variation Around Tubing	159
Texture Gradients in Thin-Walled Zircaloy Tubing	159
Tubing Fabrication	159
Hydride Orientation in Zircaloy Tubing	159
PART IV. REACTOR DEVELOPMENT SUPPORT	
28. ASSISTANCE IN RESEARCH REACTOR CORE PROCUREMENT	161
Fuel Assistance and Procurement	161

Fabrication of ATR Fuel Plates	162
Examination of Arc-Melting Techniques for the Preparation of UAl_x	162
Clumping of B_4C Powders in Dispersion Fuel Elements	163
Fuel Homogeneity	163
Welding Development	164
29. GAS-COOLED REACTOR PROGRAM	165
Bonding of Coated-Particle Fuels	165
Suppressing Infiltration of Pyrolytic Carbon into Porous Buffer Coatings During Application of Outer Coating Layers	167
Improved Computer Program for Predicting Coated-Particle Irradiation Behavior	168
Revised Comparison of Predicted and Observed Coated-Particle Irradiation Performance	169
High-Temperature Fast-Neutron Irradiation of Pyrolytic-Carbon-Coated ThO_2 Microspheres	170
Concrete for Prestressed Concrete Reactor Pressure Vessels	172
Properties of Nickel Alloy Weldments for Advanced HTGR Steam Generators	173
30. HEAVY SECTION STEEL TECHNOLOGY	175
31. HIGH FLUX ISOTOPE REACTOR MATERIALS DEVELOPMENT	179
HFIR Fuel Element Manufacture	179
Postirradiation Examination of HFIR Fuel Elements	182
Advanced Fuel Plate Fabrication	186
Characterization of Burned U_3O_8 Powders	189
Fuel-Plate-to-Side-Plate Welding Development	190
Coolant Channel Spacer Attachment	191
Alteration to the Fabrication Procedures for High Flux Isotope Reactor Control Plates	191
32. HIGH FLUX ISOTOPE REACTOR TARGET DEVELOPMENT	193
TRU Target Fabrication Operations	193
Analysis of HFIR Target Performance	194
TRU Inspection Results	195
Mechanical Properties	197
33. CLADDING MATERIALS FOR SNAP-8	198
34. MOLTEN-SALT REACTOR PROGRAM	200
MSRE Support	201
MSRE Materials Surveillance Program	201
Properties of Hastelloy N Surveillance Specimens	201
MSBR Development	202
Procurement and Evaluation of Special Grades of Graphite	202
Gas Impregnation of Graphite with Carbon	202
Surface Sealing Graphite with Molybdenum	203

Graphite Irradiation	204
Development of a Modified Hastelloy N with Improved Resistance to Irradiation	
Damage	205
Weldability of Hastelloy N	205
Residual Stress Measurements in Hastelloy N Welds	205
Oxidation of Hastelloy N	207
Corrosion	207
Graphite Brazing Development	208
Graphite-to-Hastelloy N Transition Joints	208
Radiation Stability of Brazing Alloys of Interest for Graphite	210
Nondestructive Testing of Graphite-to-Metal Joints	210
35. REACTOR EVALUATION	212
Computer Program Development	212
Fuel Fabrication Costs	212
Plant Optimization	213
Recycle Delay Code	213
Cost Analysis	213
Fuel Recycle Task Force	214
Desalination	214
HTGR Low Enrichment Study	214
HTGR Recycle Delay Analysis	215
Fuel Performance Analysis	215
Heavy-Water-Moderated Organic-Cooled Reactors	215
Heavy-Water-Moderated Light-Water-Cooled Reactor	216
Steam-Cooled Fast Breeder Reactors	216
Gas-Cooled Fast Reactors	217
Carbide-Fueled LMFBR	217
HTGR Evaluation	217
36. TERRESTRIAL LOW-POWER REACTOR	219
Materials Selection	219
Fuels Evaluation	219
37. THORIUM UTILIZATION	221
Thorium-Uranium Recycle Facility	221
TURF Building Construction and Procurement	221
Preparation of ^{233}U Fuel for the MSRE	224
Design of Fueled-Graphite Line	224
Fueled-Graphite Development	224
Particle Handling	224
Particle Coating	224
Particle Inspection	225
Bonding of Fuel Particles	227
Coating of High-Activity Particles	227
Irradiation of Thoria-Base Bulk Oxide Fuels	227

PART V. OTHER PROGRAM ACTIVITIES

38. METALLOGRAPHY	230
Alpha Metallography Facility	230
Electron Micrographic Examination of Radioactive Materials	230
Correlation of Composition and Heat Treatment with the Microstructures of Uranium Carbides	231
Electron Microprobe Analysis	233
Evaluation of the Bausch and Lomb Research II Metallograph	233
Quantitative Television Microscopy	233
39. ROVER ROCKET MATERIALS	235
Thermal Fatigue Properties of Nozzle Coolant Tubes	235
Effects of Space Environment on NERVA Materials	236
Outgassing of NERVA Fuel Elements	236
Adhesion of NERVA Materials	236
40. DISPERSION STRENGTHENING OF ALUMINUM-BASE ALLOYS	238
41. ARMY PULSED RADIATION FACILITY REACTOR ASSISTANCE	241
Evaluation of the APRFR Core	241
Core Alloy Development	242

PAPERS AND PUBLICATIONS

PAPERS AND ORAL PRESENTATIONS	243
PUBLICATIONS	251
ORGANIZATION CHART	261

Summary

PART I. FUNDAMENTAL PROGRAMS

1. Crystal Physics

Using our internal centrifugal zone growth technique, we continued studying the growth of crystals of UO_2 , UO_2 - ThO_2 solid solutions, and eutectic structures of the cermet UO_2 -W. Mechanical and temperature-sensing changes, made on the system to produce crystals of higher perfection, are being evaluated. Molten-salt solvent techniques continue to serve us well in the growth of ThO_2 , CeO_2 , GeO_2 , ZrSiO_4 , HfSiO_4 , and ThSiO_4 doped with transuranic and lanthanide ions for studies of thermoluminescence, optical absorption, and electron-spin resonance. Infrared spectra and optical perfection are being studied on hydrothermally grown quartz in various alkali hydroxide solvents. Single crystals of magnetic ferrites are being grown by the Verneuil method for the proposed electromagnetic neutron-beam chopper. Crystals approaching the desired physical size and perfection are being grown. The problem now is to optimize the neutron and magnetic properties within natural chemical constraints. The diamagnetic susceptibility of high-purity ThO_2 crystals was $-10.0 \times 10^{-8} \text{ cm}^3/\text{g}$.

2. Deformation and Annealing of Metals

In cold-rolled niobium we found important texture components that are not predictable from present theory. Certain fabricating conditions produced a sharp surface texture and a zone at intermediate depths that lacked some of the texture components typical of body-centered cubic metals. These texture inhomogeneities were analyzed in terms of the stress states existing at various fabrication stages. The texture developed in cold-rolled Cu_3Au depends upon the amount of order present at each stage of deformation. Thus both the copper-type and brass-type textures can be produced. The recovery kinetics of deformed niobium and niobium-vanadium alloys are being analyzed in terms of dislocation behavior.

3. Deformation of Crystalline Solids

We obtained textures and other structural information on metals deformed by rolling, including high deformations under unusual conditions. A general investigation of deformation in hexagonal-close-packed metals was begun. The experimental part is directed toward relating deformation substructures and work-hardening in rhenium. The primary theoretical consideration is given to dislocation-twin interactions in hexagonal metals in general.

A new series representation has been proposed for the thermodynamics of binary solutions.

4. Diffusion in Solids

Tracer lattice diffusion coefficients in monocrystalline tungsten were measured with high precision over a range of 1400 to 2400°C. Short-circuiting phenomena become dominant at the lower temperatures and are being investigated in detail. The alpha-energy degradation method is being used to investigate diffusion in UO_2 and in UN. We found that previous measurements on cation self-diffusion in UO_2 were characteristic of grain-boundary diffusion and not lattice diffusion, so published diffusion coefficients are at least two or three orders of magnitude in error. Data on titanium diffusion in modified Hastelloy N over the temperature range of 800 to 1250°C were obtained by serial sectioning by grinding. These data were used to predict corrosion behavior under Molten Salt Reactor operating conditions.

5. Electron Microscopy

Thermal and stress-assisted growth processes of grain-boundary gas bubbles in chemically vapor deposited tungsten are described and analyzed by existing models. Steps in the thermal rejection and precipitation of gas bubbles in electrodeposited nickel are outlined and explained in terms of gas-bubble nucleation and growth in a material supersaturated with vacancies. The annealing characteristics of voids in irradiated stainless steel are presented, and a model in which void shrinkage is

controlled by diffusion of vacancies from voids to dislocations is developed. The energy stored during deformation of silver single crystals is reported and related to work-hardening theories and dislocation structures. Complex precipitation reactions in Hastelloy N resulting from various thermomechanical treatments are described. Techniques for the observation of bubbles and cavities in solids are summarized. Electron microscope-microprobe techniques for studying precipitate particles in metals are described, and a procedure for the preparation of transmission electron microscopy specimens from tubing is outlined.

6. Electronic Properties of Metals and Alloys

In Mössbauer research, continued investigations of the Cu-Ni alloys with ^{61}Ni showed nearly linear isomer shifts of ^{61}Ni with atomic fraction nickel and indications of localization of electronic states, since after corrections for Doppler shifts the ^{61}Ni in the alloy has the same isomer shift as in pure nickel. Investigations of ordered Fe-Al alloys by neutron capture in ^{56}Fe at Karlsruhe revealed interesting information on displacements of iron nuclei during neutron irradiation.

The atomic heat of UN from 1.3 to 4.6°K obeyed $\gamma T + \beta(T/324)^3$, where γ was about 24 mj(gram-atom) $^{-1}$ deg $^{-2}$ varying with heat treatment; the magnitude of γ reflects 5f bands intersecting the Fermi surface. Zone purification of hafnium in ultrahigh vacuum successfully removed impurities other than zirconium. Low-temperature electrical resistivity of zirconium alloys dilute in Sc, Ti, or Hf and specific heats of alloys dilute in Nb, Mo, Re, Ru, Rh, or Pd were measured and associated with the electronic structures of the atoms involved.

7. Fundamental Ceramics Research

A multigroup effort has been started to study the properties and behavior of uranium mononitride (a potentially important fast-reactor fuel) to achieve a basic understanding of this refractory hard-metal type of ceramic compound. The program is in close liaison with the Nitride Fuel Development Program.

To date, preliminary band structure calculations have been made and a number of property measurements on UN are completed or are well under way, and these include: low-temperature specific heat (1.3 to 4.7°K), thermal conductivity (77 to 400°K), Seebeck coefficient (6 to 400°K), electrical resistivity (4.2 to 400°K), velocity of sound (300°K), self-diffusion of ^{233}U (1400 to 2100°K), and compressive creep (1400 to 1800°K).

8. Physical Ceramics Studies

Detailed electron microscope observations of dislocations in UO_2 single crystals show large numbers of dipoles and dipole loops after 1% strain and show dislocation tangles and dipole loops after 5% strain. Our study of diffusion of thorium in ThO_2 indicates that the diffusion coefficient is smaller near the surface and that grain boundary diffusion is dominant over a wide temperature range. The application of topology to problems in metallurgy is reviewed. Activation energies in sintering of ThO_2 are discussed. Compressive deformation studies of polycrystalline UN and UO_2 are under way.

9. Physical Properties

Theoretically based analyses of accurate physical property data available on a few metals and alloys allowed a separation of their electronic and lattice components of thermal conductivity. This provided several interesting theoretical consequences and guidelines for useful data extrapolation and for further research. Physical property studies on Cu, In, Mo, and Cr showed that available theory can only qualitatively explain thermal conductivity results. We found that the thermal resistivity of ThO_2 is controlled by Umklapp scattering, whereas that of UO_2 is largely controlled by spin-wave scattering of phonons. Contrary to the results of others, we found the thermal conductivity of UO_2 to be unaffected by large temperature gradients or compressive stresses. Several new apparatuses, which can extend our capacity to obtain accurate physical property measurements over a broad temperature range, were tested. These devices greatly enhance our measurement capacity for fundamental and applied research problems.

10. Spectroscopy of Ionic Media

Absorption spectra of molten salts are giving details about the oxidation states and structures of ionic entities in melts. Studies of chloride crystals doped with Ni(II) and Co(II) are testing the ability of ligand-field theory to describe the states of d^N configurations in distorted-cubic environments.

11. Superconducting Materials

The decomposition of single-phase Tc-30 at. % V alloys at 900°C yields a series of structures consisting of one superconducting phase dispersed in another. For these structures, we determined the critical temperatures, critical fields, and critical current densities and

can now plausibly relate the variation in these properties to the developing microstructures. An analytic expression for the variation of superconducting critical current density with applied field and temperature was developed; it is a quite satisfactory fit to most of our experimental data. The investigation of transformation kinetics and morphologies in rare earths was extended in two directions; selected rare earth alloys are being examined, and high-purity lanthanum crystals are being grown.

12. Surface Reactions of Metals

In a continuing attempt to understand the important influence of stress in the mechanism of oxidation of metals, we have extended our studies of the oxidation of niobium and tantalum to the range 700 to 900°C. By working at low oxygen pressures, we were able to isolate stress effects related to oxygen solution in the metal. Good agreement was obtained between surface stresses measured by our flexure technique and those computed on the basis of ideal bulk diffusion of oxygen in the specimens.

Further studies of the thin-film stage of the oxidation of nickel confirmed the existence of paths of easy diffusion in the NiO films and underscored their importance in the oxidation process. Ellipsometer studies of the NiO films led us to conclude that the refractive index of NiO changes with film thickness. There is some evidence that this change may be associated with a change in the concentration of Ni³⁺ ions in the films.

We also applied our anodic-film sectioning technique to a study of diffusion in tungsten. By using section thicknesses ranging down to 10 Å, we were able to measure diffusion coefficients as small as 5×10^{-13} cm²/sec. An Arrhenius plot is given for the diffusion of ⁹⁵Nb in tungsten over the range 1400 to 2400°C.

13. Theoretical Research

We have refined our techniques for band-theory calculations, successfully calculated properties of copper, aluminum, and gold, and extended the method to more complex solids. Calculations on the electronic states were also carried out for metal atoms, carbon in π -electron systems, and helium.

14. X-Ray Diffraction

The routine analyses performed during the reporting period are summarized. Crystal structures of La₂Be₂O₅ and SrBe₃O₄ were determined; we found only tetra-

hedral coordination of oxygen about beryllium in the former, but a mixture of trigonal and tetrahedral coordinations in the latter. An analytic separation of first- and second-order thermal diffuse scattering was derived. Experimental improvements in the measurement of small-angle x-ray scattering were made so that the sample temperature could be controlled between -170 and 450°C. Provision for automatic control of balanced filters was designed. Small-angle x-ray scattering measurements from aluminum-zinc alloys were begun; results indicate compositional inhomogeneities at all temperatures studied in the single-phase alpha field. Further experiments with highly oriented graphite continue to show the advantages of this material as an x-ray monochromator both in diffraction experiments and in fluorescence applications.

PART II. HIGH-TEMPERATURE MATERIALS PROGRAM

15. Physical and Mechanical Metallurgy of High-Temperature Materials

The creep-rupture properties of wrought C-129Y were found to be among the lowest for niobium-base alloys in the range 980 to 1200°C. Recrystallized and aged SU-16 alloy exhibited the highest strength we have observed for niobium-base alloys in this temperature range. Optimized heat treatment of the molybdenum alloy TZC did not give creep-rupture properties as good as those of niobium-modified TZM (Cb-TZM). In studies on time-temperature parameters for representation and extrapolation of creep-rupture data for refractory alloys, the Manson-Haferd parameter was superior to those of Dorn-Shepard and Larson-Miller. The elevated-temperature fatigue life of D-43 at the 1% plastic strain level was equal to or superior to that at room temperature, whereas in liquid nitrogen it was one-fifth of the room-temperature value.

The solubility and diffusivity of nitrogen in tungsten at 1800°K and 1 atm pressure were determined to be 28 ppm and 2.6×10^{-8} cm²/sec, respectively. Studies on strengthening of refractory alloys by controlled spinodal decompositions showed that Guinier-Preston zones in Nb-Hf and Ta-Hf alloys containing 40 to 65% Hf and quenched from 1730 to 1850°C grew rapidly on aging because of the existence of vacancy clusters. In 1000-hr creep tests on Haynes alloy No. 25 in high vacuum at 785°C, evaporation losses and amount of Laves-phase precipitate increased with stress. At a stress of 14,500 psi the rupture life in a vacuum of 1×10^{-8} torr was about one-half that of specimens tested in argon and one-tenth that of specimens tested in air.

The alloy Ti-21% V-25% Cr was outstanding for brazing Al_2O_3 and refractory metals as well as graphite to itself and to refractory metals. Brazing alloys of Ti-Zr-Ta and Ti-Zr-Nb were shown to be applicable for a variety of combinations of refractory materials, and the Ti-20% Zr-15% Ge alloy exhibited excellent wetting and flow characteristics on graphite for low-temperature brazing.

The electrical resistivity and thermoelectric power of high-purity molybdenum were measured from 100 to 1700°K, and the thermal conductivity was determined from 100 to 1250°K.

Improved techniques were developed for nondestructive evaluation of small tubing and rods of refractory alloys by fluorescent-penetrant, ultrasonic, and eddy-current techniques.

16. Tungsten Metallurgy

In the tungsten and tungsten alloy extrusion development program, 36 billets of tungsten and tungsten alloys were extruded as primary and duplex extrusions in the form of tube shells, round bars, and sheet bar. Extrusion temperatures ranged from 1650 to 1870°C and extrusion ratios varied from 3.6 to 9.6. Modification of the die design increased the life of the ZrO_2 -coated extrusion dies. In the hot-plug drawing program, the drawbench facilities were modified and temperature, lubricants, tooling, and other drawing conditions were investigated. A petroleum-base lubricant was far superior to glass for lubrication at temperatures greater than 1000°C. Unalloyed tungsten bar stock was successfully reduced 25% per pass at 1200°C and W-30% Re-30% Mo (at. %) was successfully reduced 30% in three passes at 1050°C without intermediate anneals.

Chemical vapor deposition (CVD) studies were performed on tungsten and tungsten-rhenium alloys. A statistically designed experiment produced a complete series of curves showing the effect of deposition parameters on the response variables for tungsten. An equation based on reaction-rate theory fitted the data better than a statistically derived third-order polynomial. The surface concentration of WF_6 was the controlling factor in deposit morphology. Orientation studies indicated that the {110} orientation desired for thermionic applications can be produced from WF_6 under certain conditions.

Gas bubbles less than 400 Å in diameter, fluorine impurity clusters, or both, were responsible for retarding recrystallization in rolled CVD tungsten containing 25 ppm F.

Creep-rupture studies for 1000 hr showed that at 1650°C the creep and rupture strengths of tungsten and its alloys decreased in the order, W-5% Re, W-25% Re, W, W-25% Re-30% Mo (at. %). At 2200°C the W-5% Re and W-25% Re alloys are equivalent and slightly stronger than tungsten.

Successful TIG welding of 1/16-in.-thick unalloyed tungsten sheet required preheating to at least 150°C. The ductile-to-brittle transition temperatures for welds in powder-metallurgy-derived tungsten were about 200°C higher than for unwelded material. No sigma phase was detected in W-26% Re weld metal deposited on unalloyed tungsten sheet.

17. Alkali-Metal Corrosion of High-Temperature Materials

The cumulative operating time of refractory-metal-boiling-potassium corrosion experiments has passed 100,000 hr, and the original objectives set for this program are essentially complete. Mass transfer has been seen only in unalloyed niobium, tungsten, and W-25% Re systems. In tungsten and W-25% Re the mass transfer effects were opposite to those expected from concentration-gradient considerations and are thought to be associated with gaseous impurities. Examination of an Nb-1% Zr loop containing a TZM nozzle-blade section revealed excellent compatibility of these materials in boiling potassium after forced-flow, engineering-scale testing at 1200°C for 3000 hr. A second forced-circulation loop constructed of the niobium alloy D-43 completed a scheduled 10,000-hr run at 1300°C with a load factor of 96%.

In tests of the niobium alloys D-43, Nb-1% Zr, and FS-85 in circulating lithium (1) zirconium and nitrogen were preferentially transported from hotter to cooler surfaces, (2) zirconium depletion was controlled by solid-state diffusion, (3) niobium mass transfer became significant at 1300°C, and (4) the corrosion rate was the same for any given temperature in the loop independent of location and direction of heat flux. The design, component procurement, and weld development were completed for the first in a series of forced-circulation lithium loop tests on tantalum and tungsten alloys at maximum temperatures of 1370 and 1540°C. A T-111 pump cell for the helical induction pump for these tests was successfully fabricated and tested to 815°C in potassium to verify its structural integrity and establish its performance characteristics.

Evaluation of a dissimilar-metal NaK radiator circuit with a type 316 stainless steel to Nb-1% Zr alloy surface area ratio of 5.5 showed a corrosion rate no

greater than 1×10^{-4} in./year and satisfactory mechanical properties after 6000 hr operation at 680°C .

In studies of the Ta-O-K system at 600, 800, and 1000°C we found a temperature-dependent threshold oxygen concentration in the tantalum at which potassium penetrates the tantalum; this threshold concentration is higher than that observed in similar studies of the Nb-O-Li and Ta-O-Li systems. The role of oxygen in the corrosion of refractory metals by alkali metals has been analyzed in terms of thermodynamic interaction parameters; oxygen activity coefficients derived from this approach offer a reasonable explanation for the distribution coefficient discrepancies previously reported in these systems.

A zirconium gettering technique was developed for oxygen determination in alkali metals in the concentration range 100 to 1000 ppm. The fast-neutron activation technique was proved effective for the determination of oxygen in potassium and lithium at concentrations as low as 20 ppm.

18. Nitride Fuels Development

We are developing nitride fuels for space-nuclear and liquid-metal fast breeder reactor (LMFBR) applications. For the latter, properly designed (U,Pu)N fuel pins can operate at significantly higher linear heat ratings and power densities than can mixed oxides. In addition, nitrides appear to have advantages over carbides in fabricability and compatibility with stainless steels and vanadium-base alloys, both candidate cladding materials for the LMFBR. The development program includes fabrication, characterization, thermodynamic studies, compatibility studies, and irradiation testing.

We developed processes for fabricating a wide variety of sizes and shapes to meet the needs of the fundamental and applied studies, maintaining impurity levels below 500 ppm O and 200 ppm C. We demonstrated processes for manufacture of single-phase $\text{UC}_x\text{N}_{1-x}$ for any value of x desired. We designed, built, and tested an apparatus for hot-pressing very high-density (U,Pu)N and developed capability for characterizing (U,Pu)N by differential thermal analysis, thermogravimetric analysis, metallography, x-ray diffraction, and hot-stage microscopy.

The kinetics of the conversion of UO_2 to UN was studied for sol-gel microspheres and powders, and the feasibility of producing high quality (U,Pu)(C,N) from aqueous reprocessing feed was demonstrated.

The limits of solubility of nitrogen and uranium in U(C,N) were determined, and we established that Vegard's law does not apply for UC-UN solid solutions.

Thermodynamic analysis indicates that UN in solid solution with UC is more stable than expected from ideal-solution behavior. The thermodynamic stability of PuN proved to be comparable to that of UN.

Vanadium and UN were found to be thermodynamically compatible. Compatibility problems with mixed nitrides and vanadium alloys should arise only when alloying additions of active components such as zirconium and titanium are involved or deleterious impurities are present.

19. Materials Development for Isotopic Power Sources

Support of isotopic power programs has included work on general technology programs, for ^{244}Cm and ^{90}Sr , and two application-oriented programs, SNAP-21 and SNAP-23.

In the Curium Program components for 3-in.-diam vented and 4-in.-diam nonvented capsules were extruded from arc-cast tungsten. These extrusions are the largest produced to date in tungsten. Chemical vapor deposition (CVD) of tungsten was evaluated as a possible cladding technique for curium fuels. On a 200-w electrically heated mockup nodule-free deposits were produced with only a 0.003-in. variation in thickness. A model was developed for predicting the creep behavior of a capsule fueled with an alpha-emitting isotope such as ^{244}Cm . Such a capsule would experience a constantly increasing stress and decreasing temperature. The behavior predicted by this model, based on creep data for constant load and constant temperature, was verified experimentally. Brazing alloys based on platinum and refractory metals are being developed for joining curium-fueled capsules to thermionic emitters. Several alloys with brazing temperatures in the range 1900 to 2300°C exhibit good wetting and flow characteristics. To aid in assessing the heat transfer characteristics of T-111 as a candidate cladding material, the electrical resistivity, specific heat, and total hemispherical emittance were determined in the range of 300 to 1700°K . Anomalously low values were determined for the electrical resistivity, and an instability in the total hemispherical emittance was also detected.

In the Strontium Program we assessed the compatibility of strontium fuels with alloys and determined the welding characteristics of these alloys. Nonradioactive compounds SrTiO_3 , Sr_2TiO_4 , and SrO were tested for compatibility with Hastelloy C, type 316 stainless steel, and Haynes alloy No. 25 for 1000 hr at 1100°C . The most inert compound was Sr_2TiO_4 . Type 304 stainless

steel was found to be a good stand-in for Hastelloy C in welding studies. Weld penetrations of up to 0.180 in. were obtained on both materials with the gas tungsten-arc process.

Welding and inspection procedures were developed for SNAP-21 fuel capsules. Electron-beam parameters were optimized for weld penetration and inspectability. Capsule components were ultrasonically inspected on a specially constructed scanning device, and in-cell inspection was successfully completed on two welded fuel-containing capsules. Electron-beam welding procedures are also being developed for sealing SNAP-23 fuel capsules. Initial studies resulted in acceptable welds on unpreheated capsules, but modifications will be required for fuel-containing capsules.

PART III. GENERAL FUELS AND MATERIALS RESEARCH

20. Fuel Element Fabrication Development

Emphasis on this program is now concentrated on improving fuel elements for research reactors. The potential improvements are being confirmed in loop irradiation tests. Samples containing highly loaded dispersions of both UAl_3 and U_3O_8 have been prepared and irradiated.

A major problem in preparation of UAl_3 powder fuels is minimizing the proportion of fines produced during comminution. A variety of comminuting techniques were tried with very little effect. The particle size distribution achieved during comminution was reproducible but depended on the procedure used for making the measurement.

The void volume in a dispersion-type fuel plate was shown to depend on both the type and concentration of the fuel; the highest void volume was achieved with a "burned" U_3O_8 .

Swelling of UAl_3 , which can cause dimensional problems during fabrication, is a two-stage process resulting from both release of gases and a diffusion-induced transformation. The latter may be retarded by the addition of small quantities of zirconium, silicon, or germanium to the alloy.

To assist vendors in understanding the processes for fabricating dispersion fuels, basic fabrication studies are being conducted. We demonstrated that dogboning occurs at both ends of a core, even if all reduction is from one direction, and is present whenever the core material is stronger than the cladding material. High-temperature compressive strength values of U_3O_8 and UAl_3 dispersion pellets were determined. As the volume fraction of the fuel is increased, the compressive

strength of the UAl_3 pellets continually increases, but that of oxide pellets reaches a maximum and then decreases. Especially at 5% plastic strain, large differences are found between the two.

Uranium oxide powder was prepared in a flame reactor from UF_6 , H_2 , and O_2 . The powder was characterized and is readily fabricable, after a treatment to remove excess fluorine. We demonstrated that PuO_2 powder could be made by chemical vapor deposition. Solid silicon carbide deposits with a wide range in stoichiometry, giving hardness ranging from 1331 to 3855 DPH (1-kg load), were also deposited. The most critical variables were deposition temperature and inlet-gas stream composition.

In an effort to decrease corrosion of aluminum, various anodizing techniques have been tested. With high-purity aluminum, the only one that resulted in a decrease was an oxalic acid bath. The film characteristics depended upon the bath temperature; lower temperatures appeared superior. The thickness of the corrosion film on a type 6061 aluminum specimen tripled when the specimen was held under strain.

21. Irradiation Damage to Aluminum

Irradiation damage to aluminum was until recently thought to be of little importance. The unexpected failure of some research reactor components due to neutron damage has stimulated research on the type and magnitude of aluminum irradiation damage at high neutron fluences.

We found that high neutron fluences near 10^{22} neutrons/cm² result in embrittlement of X8001, 1100, and 6061 alloys when deformed within a specific elevated temperature range, even though no significant change in ductility occurs at room temperature. Increases in strength are observed also. Starting with a neutron exposure of 5×10^{21} neutrons/cm², the density decreases linearly with increasing fluence. Irradiated in the Oak Ridge Research Reactor, 1100 aluminum decreased 1.5% in density at a fluence level of 1.5×10^{22} neutrons/cm². The irradiation produces about 10^{15} cavities/cm³, with diameters in the range of 100 to 600 Å. Cavities most likely give rise to swelling and can be removed by annealing at 260°C for 1 hr.

22. Mechanical Properties Research

The Mechanical Properties and LMFBR Cladding programs are closely related and have as their objectives the understanding of radiation damage to reactor materials and the development of modified alloys more resistant to radiation damage.

The development of types 304 and 304L stainless steel containing small amounts of titanium continues to appear promising. The radiation resistance after cyclotron and reactor irradiation of both the titanium-modified types 304 and 304L under high-temperature creep conditions is much superior to that of the standard compositions. The modified 304L stainless steel has been fabricated successfully into LMFBR-size tubing, and end cap welds in the alloy appear sound.

Type 316 stainless steel and Incoloy 800 both exhibit a maximum in postirradiation ductility as the titanium content is increased. In 50-lb vacuum-induction melts of the stainless steel the maximum in ductility occurs in the range of 0.1 to 0.3% Ti and at about 0.1% Ti in Incoloy 800.

The high-temperature creep-rupture properties of Hastelloy N are significantly influenced by the amounts of titanium and carbon in the alloy. Both the strength and ductility increase with titanium and carbon additions. This behavior is contrasted with the appearance of a maximum in the ductility as a function of titanium concentration observed in the other alloys studied.

The nuclear heating rate experiments in EBR-II were completed, and irradiation experiments have been designed, constructed, and installed in EBR-II. Type 304L stainless steel from a driver fuel pin in EBR-II was examined and found to contain voids that are attributable to displacement damage at 370 to 470°C. These voids begin to anneal (disappear) at 600°C and all are removed by annealing 1 hr at 900°C.

23. Nondestructive Test Development

We continued development of analytical techniques for the calculation of parameters for an induced electromagnetic field, with emphasis on closed-form solutions. Numerical values are being obtained on a time-sharing computer for many problems of interest to eddy-current testing. Improvements were made on the portable phase-sensitive eddy-current instruments. We are measuring the effective diameter of eddy-current fields and studying methods of decreasing the size. To minimize thermal drift materials with low-temperature coefficients are being investigated for fabrication of eddy-current coils.

Fabrication and measurement studies are continuing on notch reference standards for ultrasonic inspection. The schlieren system for viewing ultrasonic energy was modified to increase both the viewing area and the sensitivity; parabolic mirrors were substituted for collimating lenses and closed circuit television was used for display of images. An ultrasonic frequency analysis

system was developed to allow investigation of the significance of frequency in ultrasonic tests. Preliminary studies have already shown benefits for transducer analysis.

We are studying several parameters for the generation of holograms, using both single- and multiple-beam techniques. An electronic circuit was developed to allow real-time averaging of quantitative x-ray attenuation data during scanning of specimens.

24. Sintered Aluminum Products Development

Sintered aluminum products (SAP) are oxide-strengthened aluminum alloys produced by powder metallurgy. We have been engaged in a two-part program, to develop a billet fabrication process to produce SAP having uniform properties and to examine the causes and possible means of improving the low creep ductility of SAP without sacrificing strength.

A process for the fabrication of SAP has been selected from our development studies and evaluated on a small pilot plant scale. The properties within a particular billet made by this process are very uniform; the maximum range of strength observed is 2% of the mean. This SAP is approximately 20% stronger at 450°C than commercial SAP of equivalent oxide content. Several nondestructive test methods were developed to determine the flake thickness and oxide content of ball-milled flake. We scanned SAP billets using an x-ray attenuation method and established calibration curves. With this technique an 0.2% change in density or thickness of billet can be detected and used for process quality control. Secondary working studies showed that the structure and properties of SAP can be improved by hot working. The fracture of SAP from -200 to 450°C has been studied by electron microscopy. Three modes of fracture have been identified: separation, tearing, and shearing. All three show features characteristic of ductile failure even though the uniform elongations are often less than 1%.

25. Sol-Gel Fast Reactor Fuels

We continued the assessment of sol-gel-derived (U,Pu)O₂ fuel for fast reactors, particularly for the LMFBR's and the Fast Flux Test Facility. We installed equipment for fabrication and characterization of plutonium-bearing fuels, learned how to pack microspheres to specified densities, prepared the first sol-gel (U,Pu)O₂ pellets, developed analytical techniques for characterizing the fuel, and devised equipment for measuring thermal conductivity of packed powders.

Irradiation tests to 4 at. % burnup indicate that Sphere-Pac fuels will perform in the reactor comparably to pelletized fuels of similar smear density. Instrumented capsule irradiation tests were started to investigate the behavior of sol-gel-derived mixed oxide fuels as a function of fuel temperature. The first capsule was designed and operated satisfactorily. In addition, tests were designed for off-normal conditions such as power transients and for testing in the EBR-II. Calculation methods required for irradiation testing and for the analysis of the results were developed.

26. Joining Research on Nuclear Materials

We have studied the effects of Al, Ti, P, and S, individually and collectively, on the weldability of Incoloy 800. Both the VARESTRAINT Test and the Duffer's Gleeble were employed.

Aluminum and titanium additions to the ternary (Fe-Ni-Cr) Incoloy 800 composition increased the alloy's susceptibility, as measured by the VARESTRAINT Test, to weld-metal hot cracking; however, the degree of cracking was considerably less than that exhibited by commercial Incoloy 800 plate. Similar results with these two elements were also obtained with the Gleeble heat-affected zone tests. The presence of aluminum and titanium decreased the Zero Ductility Temperature (ZDT) from approximately 2450°F for the ternary to about 2400°F. Phosphorus and sulfur did not decrease the ZDT below the 2400°F level. This apparent innocuous effect of phosphorus and sulfur may be due to their association with titanium and/or aluminum.

27. Zirconium Metallurgy

We made continued progress in relating the anisotropy of uniaxial and biaxial plastic properties of zirconium alloys to crystallographic texture. We also related the orientation of the hydride in Zircaloy tubing to texture. Deformation studies on single crystals showed how the development of texture is controlled by the fabrication stress state and the availability of slip and twinning modes. Inhomogeneous deformation was observed in zirconium alloy tubing and its origin was identified as variations in texture around the tubing. Also, we found variations in texture through the tubing wall. All of these texture variations are strongly influenced by processing history. An experimental tubing fabrication study is in progress to relate, in detail, fabrication variables to texture and thereby to permit texture control in commercially fabricated material.

PART IV. REACTOR DEVELOPMENT SUPPORT

28. Assistance in Research Reactor Core Procurement

During the year technical assistance was furnished to the AEC in preparing specifications for fuel elements, in making technical audits of fuel manufacturers, and in discussions of the fabrication of dispersion fuel elements. Assistance in procurement and inspection was provided in the purchase of fuel cores for AF-NETR and PM-4.

A limited number of short-range development problems were pursued to assist the fuel element manufacturers. We found that even with ORNL fabricating procedures, much more dogboning was encountered with UAl_3 than with U_3O_8 , and the amount is a function of the fuel concentration. We demonstrated that arc melting of UAl_3 need not result in the presence of free uranium, but considerable variation in structure and composition might be expected. Segregation of B_4C burnable poison results when finer than desired particles are exposed to moisture, which causes clumping; it may be avoided by vacuum drying. Electron-beam welding has been shown to have potential as a positive technique for attaching the fuel plates in research reactors.

In an attempt to compare relative sensitivities for measuring fuel homogeneity by x-ray attenuation and by scanning radiographs, difficulty has been encountered in obtaining standard curves with the accuracy previously obtained for the x-ray attenuation machine. Some, but not all, of the increase in spread was traced to machining errors. When standards are established for variation in fuel content, the size aperture must be considered. The minimum visually detectable fuel increase in a high quality radiograph of a dispersion plate is 7% for a spot diameter of 0.125 in. or 8% for an 0.078-in.² area.

29. Gas-Cooled Reactor Program

All-ceramic nuclear fuels consisting of (Th,U)O₂ and (Th,U)C₂ fuel particles coated with composite coatings of pyrolytic carbon and SiC offer considerable advantages as fission-product-retaining fuel for high-temperature gas-cooled reactors. Much of our support for the Program consisted of developing fabrication techniques for bonding coated particles into rods for loading into graphite fuel elements and testing coated particles and coating materials. During the development of bonding methods we modified the coating design to avoid cracking of coatings. In other coating studies we developed a technique to avoid infiltration of dense

carbon into buffer coatings during application of outer coating layers on coated particles. A revised version of STRETCH, our computer program for predicting irradiation behavior of coated particles, was published and used to improve our correlation of results from two experiments in the ETR. Results from DFR irradiations showed that failure of carbon coatings can be induced by fast-neutron effects alone and that densification or swelling of coatings occurs as they approach an equilibrium density between 1.8 and 1.9 g/cm³. An important new activity concerns the study of concretes proposed for prestressed concrete reactor pressure vessels. We are characterizing the individual constituents and cast concrete shapes of three concrete mixes being used in mechanical properties studies at other laboratories.

30. Heavy Section Steel Technology

The Oak Ridge National Laboratory has been given the responsibility of directing the AEC-sponsored portion of the Heavy Section Steel Technology Program. This phase of the program is an engineering effort to develop the technology of fracture mechanics to the point where it is capable of defining the safe behavior of a nuclear pressure vessel. We are represented as consultants on the Program Office's Technical Staff. In addition, we satisfy the needs of those experimental programs that require the experience and facilities available in our Division. Specific topics in this report cover the depth of heat-affected zone due to flame cutting of thick steel sections and the interpretation of the microstructures prevalent at the various depth locations in the quenched, tempered, and stress-relieved ASTM A533 Grade B steel plate.

31. High Flux Isotope Reactor Materials Development

The second HFIR fuel element production contract was completed on schedule and a third started. A total of 60 fuel assemblies have been shipped to ORNL; all are capable of being used at full design power, but only one outer and 18 inner elements met all portions of the specifications. The causes of the fuel-element waivers and fuel plate rejects are tabulated. The reject rates for the various periods for the fuel plates during this year were 20.1, 9.99, and 4.84% with a total reject rate for 42,000 plates of only 10.7%.

After a cooling period of one year, a used HFIR fuel element was destructively examined in the ORNL hot cells. Other than a slight expansion at the center line, no dimensional changes were found. In a metallographic examination, no evidence of potential failure within the

plates or of excessive swelling was found. The fuel element appeared to be in excellent shape. The blistering temperatures found in postirradiation heat treatments were considerably higher than had been previously reported.

Full-size HFIR plates containing high loadings of both U₃O₈ and UAl₃ were fabricated. In the HFIR plates with unfueled filler sections, dogboning of UAl₃ cores was not as severe as in comparable flat-cored plates. However, the insert did extrude beyond the core both longitudinally and laterally. Such an extrusion was not found with the high loaded oxide plates. The so-called burned U₃O₈, which has possibilities as a cheaper fuel, was characterized. It falls far short of the present HFIR specifications, but the seriousness of the deviations has not been determined.

We demonstrated that good quality electron-beam welds could be made within the small bore of the HFIR inner side plates. Using a low-inertia, electronically controlled spot welding machine with samples, spacers were attached to dummy aluminum fuel plates with a uniform penetration of about 0.003 in.

32. High Flux Isotope Reactor Target Development

The goal of the Transuranium Project is to produce gram quantities of the heavier transuranium elements for research. Plutonium, americium, and curium from the Savannah River were fabricated at ORNL into target elements that are being irradiated in the High Flux Isotope Reactor at approximately 3×10^{15} neutrons cm⁻² sec⁻¹. The target elements are removed periodically and reprocessed to separate the product actinides and recover the target actinides, which are fabricated into recycle targets and returned to HFIR.

Our tasks have included the design, fabrication, and validation of suitable targets, the development of equipment and techniques for fabricating them, and monitoring their performance in HFIR. Our investigation of the premature failure of target elements exposed in the HFIR indicated that the cladding had embrittled from fast neutron irradiation to such an extent that it was unable to accommodate by straining the buildup of fission gas pressure. During the year, the remote TRU target fabrication line was operated to fabricate recycle targets containing ²⁴⁴Cm, ²⁵²Cf, ²⁴⁸Cm, and ²⁵³Es. Although minor difficulties have been experienced with the remote equipment for fabrication of these targets, satisfactory targets have been made and necessary target schedules have been met. In addition to this work, we irradiated aluminum

materials in target elements in our search for a better cladding alloy and in our search for an explanation for the embrittlement of aluminum cladding by fast neutron irradiation. The irradiation of target elements containing lower loadings of isotopes and greater pellet porosity continued during the year.

33. Cladding Materials for SNAP-8

We measured the postirradiation mechanical properties of several candidate SNAP-8 cladding materials. These materials included standard Hastelloy N; several modified Hastelloy N's containing various amounts of titanium, zirconium, and niobium; Hastelloy X; type 304 and titanium-modified type 304L stainless steel; and several heats of Incoloy 800 with various titanium levels. Several of these materials exhibited higher fracture strains and strengths than the standard Hastelloy N that was actually chosen. This decision was based on the other desirable properties of Hastelloy N and our mechanical property measurements showing that the properties were adequate.

34. Molten-Salt Reactor Program

Surveillance specimens in the MSRE showed excellent compatibility of graphite and Hastelloy N with the appropriate reactor environments. The same decrease in strength and ductility of Hastelloy N was observed in these environments as had been noted for comparable neutron doses in helium. Progress is reported on physical characterization of commercial graphites for MSBR use, sealing the graphite surface with molybdenum or pyrolytic carbon (carbon is better), and irradiation of graphite in the HFIR. Commercial melts of titanium-modified Hastelloy N showed excellent mechanical properties after irradiation at 650°C, but thermally induced changes in precipitation during irradiation at 760°C reduced the properties of some heats to near those of the standard alloy.

High-restraint welds were made satisfactorily in 1/2-in.-thick plates of 100-lb heats of titanium-modified Hastelloy N, but similar welds in a 5000-lb melt cracked profusely, probably because of some deleterious impurity in the large melt. In a highly restrained weld thermal stresses above the yield stress can exist and cause small cracks to form during service and lead to failure. We developed a technique for measuring the residual stresses in welds. Postweld annealing at 870°C reduced the thermal stresses in a 1/2-in. plate from 55,000 to 5000 psi.

Vacuum melting decreased the oxidation resistance of standard Hastelloy N appreciably by removing silicon

and other impurities. The oxidation rate of the titanium-modified alloy seems adequate for continuous service up to 760°C.

All of our fluoride salt-Hastelloy N thermal convection loops continue to show corrosion rates of only a few ten-thousandths of an inch per year. The new coolant salt NaBF₄-8% NaF is somewhat more aggressive than the other fluoride salts, but the corrosion rate after 4000 hr of operation is about 5×10^{-4} in./year. Where comparable, titanium-modified Hastelloy N exhibited a lower corrosion rate than the standard alloy. We are running a loop containing a fused salt to determine whether the cheaper type 304L stainless steel could be used in cooler parts of the system. This loop has operated without incident for 44,000 hr at a peak temperature of 675°C, and removable specimens indicate a corrosion rate of about 2×10^{-3} in./year.

We are testing two techniques for joining Hastelloy N to graphite; direct brazing and use of a transition joint with thin slices of several nickel-tungsten alloys. Joints were made by both techniques, and we developed a pulse-echo ultrasonic technique that can detect whether the joints are bonded.

35. Reactor Evaluation

We continued to assist the AEC in analyzing the potential of various reactor systems by evaluating fuel fabrication costs and fuel element performance. Our emphasis this year was on updating *Civilian Nuclear Power, A Report to the President - 1962* and evaluating reactors for desalination. We updated our code for estimating fuel fabrication costs for pin-type fuel elements and developed computer codes for optimizing plant expansions and determining when recycle of fuel should be undertaken in a growing nuclear power economy. In addition, we started the development of a model and computer code for performance of pin-type fuel elements.

36. Terrestrial Low-Power Reactor

Existing knowledge indicates that titanium is the preferred structural metal for a pressurized water reactor with maximum simplicity and requiring minimum maintenance. Uranium dioxide pellets in a metal tube should satisfactorily meet requirements of a 50-Mwyr core life at a peak linear heat rating of 5.9 kw/ft.

37. Thorium Utilization

To use thorium as a source of energy by converting it to fissionable ²³³U, it is necessary to develop economi-

cal fuels, to characterize the physical and chemical nature of such fuels, and to demonstrate the technical and economic feasibility of recycling such fuels. Our responsibilities are the characterization of fuel, the testing of fuel under irradiation, and the development of processes for refabrication of fuel elements that are prototypic of designs useful for power reactors. The principal current objective is to demonstrate the refabrication of high-temperature gas-cooled reactor fuel elements in the Thorium-Uranium Recycle Facility (TURF), an \$8 million research and development facility whose construction was just completed.

We are developing remotely operative processes and equipment to refabricate fueled-graphite elements in the TURF. We concentrated on the critical areas required for refabrication of HTGR fuel elements, doing very little design of pilot-scale equipment. We essentially completed the development of a pneumatic system to transfer pyrolytic-carbon-coated particles between steps in the process with negligible abrasion. The 5-in. engineering-scale particle coating furnace system achieved routine operation, and we built a prototype remotely operated coating system based on our experience. We coated several batches of special particles containing high-activity isotopes such as ^{233}U and ^{239}Pu .

The TURF was received from the contractor, placed into operation, and used to prepare ^{233}U -bearing fuel for the Molten Salt Reactor Experiment.

PART V. OTHER PROGRAM ACTIVITIES

38. Metallography

A completely contained alpha metallography glove box line was fabricated, equipped, and leak checked. It consists of eight boxes in line for specimen preparation and microscopic examination. Two isolated boxes are for hardness testing, mensuration, and photomacrography. We added electron microscopy to our responsibilities in the High Radiation Level Examination Laboratory. Replicating techniques were developed to allow us to examine highly radioactive ($>30,000$ r/hr) specimens routinely. A catalog of photomicrographs of arc-cast and heat-treated uranium carbides was reported; chemical analyses and x-ray data were provided. A newly developed commercial metallograph was evaluated; some operating and performance problems were corrected by working with the manufacturer. We continued the evaluation of an image analyzing computer for quantitative metallography and compared

results with those of other methods. We continued to improve techniques and capabilities of x-ray microprobe analyses, using computer programming and achieving element detection of amounts as low as 40 ppm.

39. Rover Rocket Materials

Multiple-tube bundles of Hastelloy X and type 347 stainless steel, which simulated rocket nozzle configurations, were tested in thermal fatigue, and the results were correlated with the test parameters and the low-cycle fatigue properties of the alloys. Thermal cycles typical of nozzle service conditions produced intergranular failures in 23 to 87 cycles in both materials. Studies on the effects of gaseous contamination on the adhesion of rocket engine materials have been expanded. Adhesion is harder to produce with engineering materials than with pure metals under only static normal-force loading. Surface shearing produces adhesion in some of the engineering materials. Oxygen inhibited adhesion more than hydrogen for the materials that exhibit significant adhesion in ultrahigh vacuum. Preliminary studies indicate that outgassing of the reactor fuel elements will determine the gaseous environment for the engine components. Since this outgassing cannot be estimated from existing data, we have begun to determine the quantity, species, and rate of outgassing under simulated space conditions.

40. Dispersion Strengthening of Aluminum-Base Alloys

The technical feasibility of a method of dispersion hardening aluminum by the fine particle embedment principle was demonstrated. One such alloy was significantly stronger at 450°C than a conventional SAP with 11% Al_2O_3 , yet it contained only 4% oxide. Another alloy showed improved low-strain-rate fracture ductility with good strength at 450°C when compared to SAP.

41. Army Pulsed Radiation Facility Reactor Assistance

Assistance was provided during fabrication and coating of U-10% Mo core components for the Army Pulsed Radiation Facility Reactor, and the core was subjected to metallurgical evaluation after having been tested to damage in the ORNL Critical Experiments Facility. Thermal and inertial stresses induced during energy pulsing caused damage in the form of cracking and buckling of fuel rings, bending of regulating rods,

and permanent set to core-alloy bolts. The U-10% Mo gamma phase was retained during the test, and aluminum plating adhered better than nickel plating. No significant change in mechanical properties of the core

alloy was observed. Preliminary studies in an alloy development program indicate that a 70% increase in neutron yield with no sacrifice in pulse width is possible with U-10% Nb as compared to U-10% Mo.

Part I. Fundamental Programs

1. Crystal Physics

G. W. Clark

The growth of single crystals of high-melting-point materials is our central theme. Such crystals are often required to characterize physical properties uniquely. Some technical devices require very specific single crystals for their operations. Frequently, it is difficult to obtain suitable crystals; hence, we are conducting a continuing program to provide crystals needed in research, to devise and improve methods of crystal growth, and to develop increased understanding of crystal growth processes and kinetics. We are growing crystals by several methods; by internal centrifugal zone growth, from molten-salt solvents, from supercritical aqueous systems, and by the general Verneuil method. Some of these crystals have been used by other groups in investigations of electron-spin resonance, optical and magnetic properties, deformation, fission-gas release, neutron damage by x-ray analysis, and a possible neutron-beam chopper. Also, we are investigating selected physical properties, both those related to the crystal-growth process and those important for characterizing new compounds.

INTERNAL CENTRIFUGAL ZONE GROWTH

D. E. Hendrix¹ G. W. Clark
A. T. Chapman²

We are continuing the study of growth of crystals of UO_2 , $\text{UO}_2\text{-ThO}_2$ solid solutions, and eutectic structures of the cermet $\text{UO}_2\text{-W}$ by our internal centrifugal zone

growth (ICZG) technique.³ A preheated ceramic or cermet rod moves slowly through a radio-frequency induction coil, causing progressive melting (2800 to 3300°C) and recrystallization inside a solid shell. Thermal gradients favorable to the formation of a single crystal or eutectic matrix along the rod axis are promoted by rotation of the rod under specific conditions. Crystals or eutectic matrices approximately 1 cm in diameter and 4 cm long can be grown within 2° of specific orientations by seeding the melt.

By changing to a lower impedance induction coil design we have reduced the problem of arcing and attendant sudden temperature decreases⁴ which in turn has doubled the probability of obtaining crack-free samples. We made mechanical and temperature sensing changes, which we believed will produce crystals of higher perfection.

The perfection of UO_2 crystals grown by our method, arc-melted specimens, and vapor-grown crystals have been appraised. This work is summarized in Chapter 14 of this report.

¹On loan to Metallurgy Department, Laboratory Division, Oak Ridge Gaseous Diffusion Plant.

²Consultant from Georgia Institute of Technology, Atlanta, Georgia.

³A. T. Chapman and G. W. Clark, *Metals and Ceramics Div. Ann. Progr. Rept. June 30, 1965*, ORNL-3870, pp. 3-4.

⁴D. E. Hendrix, A. T. Chapman, and G. W. Clark, *Metals and Ceramics Div. Ann. Progr. Rept. June 30, 1967*, ORNL-4170, pp. 3-4.

MOLTEN-SALT GROWTH OF SINGLE CRYSTALS

C. B. Finch G. W. Clark

The molten-salt solvent (flux) technique is the primary and often sole method of producing single crystals of refractory materials that (1) melt incongruently, (2) have high-temperature solid phase transformations, (3) decompose or sublime at or before melting, or (4) are glass formers. Such materials include numerous silicates, germanates, and pure oxides (such as CeO_2 and GeO_2). It typically enables crystal growth at temperatures considerably below the high melting points of many refractory oxides. However, it has the disadvantages relative to crystal growth from a pure melt of a slower rate of crystal growth for high crystal perfection and at best a trace of solvent contamination in the resulting crystals.

We continued to improve the existing methods^{5,6} for refractory-oxide crystal growth at 1000 to 1300°C from such solvents as $\text{Li}_2\text{O}\cdot 2\text{WO}_3\text{-B}_2\text{O}_3$ and $\text{Li}_2\text{O}\cdot 2\text{MoO}_3$. We grew additional 3-mm ThO_2 and CeO_2 single crystals doped with less than 500 ppm $^{244}\text{Cm}^{3+}$, $^{231}\text{Pa}^{5+}$, Gd^{3+} , Tm^{3+} , Eu^{3+} , or Ca^{2+} for electron spin resonance and thermoluminescence studies. We also grew pure and Gd^{3+} -doped crystals of tetragonal (zircon structure) ZrSiO_4 , HfSiO_4 , and ThSiO_4 to 4 mm from $\text{Li}_2\text{O}\cdot 2\text{WO}_3$ and $\text{Li}_2\text{O}\cdot 2\text{MoO}_3$ at 1150 to 1200°C by existing methods.^{7,8} The electron spin resonance spectrum of Gd^{3+} is being studied in these silicates. In a special glove box at the Transuranium Research Laboratory we grew 3-mm crystals of CaWO_4 doped with $^{243}\text{Am}^{3+}$ from $\text{Na}_2\text{O}\cdot 2\text{WO}_3$ solvent by cooling from 1250 to 850°C at 2°/hr. The resulting crystals are being used for optical absorption and emission studies. The crystals have a green fluorescence with ultraviolet excitation at 77°K and offer potential as a laser material.

Self-Activated Thermoluminescence in Lanthanide- and Actinide-Doped Thorium Dioxide Crystals⁹

C. B. Finch L. J. Nugent¹⁰
G. K. Werner¹¹ M. M. Abraham¹²

Thermoluminescence in the range 125 to 180°C was found for ThO_2 crystals doped with Eu^{3+} , Gd^{3+} , Dy^{3+} , Er^{3+} , Tm^{3+} , Yb^{3+} , and $^{244}\text{Cm}^{3+}$. In each case the thermoluminescence emission spectrum is characteristic of the rare-earth tripositive ion and identical to the spectrum obtained by ultraviolet excitation. In the lanthanide cases the energy released in thermo-

luminescence arises from the 4-Mev (1.39×10^{10} -year half-life) alpha-particle emission from naturally occurring ^{232}Th . In the $^{244}\text{Cm}^{3+}$ case, the thermoluminescence energy arises primarily from the more intense 6-Mev (17.6-year half-life) alpha-particle emission from ^{244}Cm . The alpha energy is primarily absorbed in the crystal (at room temperature) where it creates storage sites capable of releasing energy to excite the rare-earth ion at the elevated temperatures. The storage sites can also be created by 2537-A radiation, and they are slowly removed by visible light. Paramagnetic resonance measurements on the Tm^{3+} -doped crystals confirm that neither Tm^{2+} nor Tm^{4+} ions are present in the activated samples, indicating that the dipositive or tetrapositive ions are in general not involved in the energy transfer or storage process. Some possibilities for an energy transfer mechanism are discussed, and this new phenomenon should occur for most of the tripositive rare-earth ions in ThO_2 .

Electron-Spin Resonance of $^{244}\text{Cm}^{3+}$ in ThO_2 and CeO_2 (Ref. 13)

M. M. Abraham¹² G. W. Clark
C. B. Finch

The ESR spectra of $^{244}\text{Cm}^{3+}$ -doped ThO_2 and CeO_2 single crystals were measured at approximately 10 GHz and liquid helium temperatures. Sites of cubic symmetry were observed in both hosts with the crystal field splitting larger than the microwave quanta used. The ground states are Γ_6 doublets, indicating that the fourth-order parameter of the cubic crystal field Hamiltonian is negative. The g-value was 4.484 ± 0.002 for ThO_2 and 4.475 ± 0.002 for CeO_2 .

⁵C. B. Finch and G. W. Clark, *J. Appl. Phys.* 36(7), 2143-45 (1965).

⁶C. B. Finch and G. W. Clark, *J. Appl. Phys.* 37(10), 3910 (1966).

⁷C. B. Finch and G. W. Clark, *Am. Mineralogist* 49, 782-85 (1964).

⁸A. A. Ballman and R. A. Laudise, *J. Am. Ceram. Soc.* 48(3), 130-33 (1965).

⁹Abstract of paper to be presented at the 7th Rare-Earth Research Conference, San Diego, California, October, 1968.

¹⁰Chemistry Division.

¹¹Physics Division.

¹²Solid State Division.

¹³Abstracted from *Phys. Rev.* 168, 933 (1968).

Flux Growth and Characterization of Hexagonal Germanium Dioxide Single Crystals^{1,4}

C. B. Finch G. W. Clark

Single crystals of hexagonal GeO_2 up to $2 \times 2 \times 3$ mm were grown from $\text{Li}_2\text{O} \cdot 2\text{MoO}_3$ and $\text{Li}_2\text{O} \cdot 2\text{WO}_3$ fluxes by slow-cooling from 1100 to 950°C no faster than $1^\circ\text{C}/\text{hr}$. Optically clear crystals contain 50 ppm Mo (or W) and 30 ppm Li as impurities.

HYDROTHERMAL SYNTHESIS

Hydrothermal Synthesis, Optical Perfection, and Surface Topography of Quartz Grown in RbOH and Other Alkali Hydroxides^{1,5}

Otto C. Kopp^{1,6} G. W. Clark

Quartz has been grown hydrothermally in iron-lined vessels from 0.5 *N* RbOH, CsOH, and KOH in the ranges 340 to 460°C and 800 to $1800 \text{ kg}/\text{cm}^2$. Although other phases (mica, zeolite) also nucleate, crystals of good quality have been grown at rates up to 0.6 mm/day along the *c*-axis.

Infrared Spectra of Hydrothermally Grown Quartz

O. C. Kopp^{1,6} G. W. Clark
P. A. Staats^{1,1}

Infrared spectroscopic investigation of quartz crystals grown hydrothermally in various solvents (NaOH, KOH, RbOH, and CsOH) reveals that their absorption spectra are very similar. Analysis of samples grown in each of these solvents, as well as the natural quartz used as nutrient, suggests that all of the crystals contain some Na^+ (0.98-Å radius), whereas the larger alkali ions ($\text{K}^+ = 1.33 \text{ Å}$, $\text{Rb}^+ = 1.49 \text{ Å}$, $\text{Cs}^+ = 1.65 \text{ Å}$) are preferentially excluded. The source of the Na^+ ions appears to be both the nutrient and trace impurities in the solvents. Kats^{1,7} previously noted that he was not able to electrodiffuse ions larger than K^+ into the quartz lattice. We shall try to grow purer quartz crystals (i.e., lacking

the alkalis and traces of iron and aluminum found in most quartz) through careful selection of starting materials. Such quartz may possess a more perfect crystal lattice and consequently behave as a more perfect oscillator, have less absorption in the infrared due to defects, and maintain its strength to higher temperatures.^{1,8}

Further Studies in the System RbOH-SiO₂-Fe₂O₃/Fe-H₂O

O. C. Kopp^{1,6} L. A. Harris^{1,9}

In addition to the normal black mica, a green mica produced at temperatures below 350°C and a possible pyroxene phase have been previously reported.^{2,0} X-ray powder diffraction data and optical study confirm that two distinct mica phases exist in this system. Their stability appears related to the oxygen fugacity^{2,1} in the system at operating conditions. Electron microprobe analysis indicates that the pyroxene phase is rubidium free but contains sodium. Analysis of the 0.5 *N* RbOH solvent used reveals the presence of $60 \mu\text{g}/\text{ml}$ of sodium in the solvent, sufficient to form traces of the sodium iron pyroxene acmite ($\text{NaFeSi}_2\text{O}_6$).

CRYSTAL GROWTH BY THE VERNEUIL METHOD

G. W. Clark H. A. Mook^{1,2}

The heart of an electromagnetic neutron-beam chopper is a single crystal of certain magnetic ferrites. After a concerted, unsuccessful effort to obtain the desired crystals commercially, we embarked on a cooperative program. We are growing crystals in the ferrite system approaching the desired perfection and physical size. At the present time we are searching for an appropriate mixed compound with optimum neutron and magnetic properties while conforming to nature's constraints on site occupation and our ability to control growth conditions. For evaluation, we have grown the following ferrites: lithium-manganese, lithium-manganese-nickel, lithium-manganese-titanium, lithium-titanium, and magnesium-manganese-zinc.

^{1,8}D. T. Griggs and J. D. Blacic, *Science* 147, 292 (1965).

^{1,9}X-ray Diffraction Group.

^{2,0}O. C. Kopp, G. W. Clark, and L. A. Harris, *Metals and Ceramics Div. Ann. Progr. Rept. June 30, 1967*, ORNL-4170, p. 6.

^{2,1}H. P. Eugster and D. R. Wones, *J. Petrol.* 3, 82-125 (1962).

^{1,4}Abstracted from paper accepted for publication in *The American Mineralogist*.

^{1,5}Abstracted from paper accepted for publication in the *Journal of Crystal Growth*.

^{1,6}Consultant from the University of Tennessee.

^{1,7}A. Kats, *Philips Res. Rept.* 17, 133-95 (1962).

DIAMAGNETIC SUSCEPTIBILITY OF HIGH-PURITY THORIUM DIOXIDE CRYSTALS

H. M. Smith G. W. Clark

The diamagnetic susceptibility of high-purity ThO₂ crystals was measured, with our Faraday apparatus, at 298 and 79°K. The gram susceptibility was determined as $-10.0 \pm 0.1 \times 10^{-8}$ cm³/g, and the molar susceptibility as $-26.3 \pm 0.3 \times 10^{-6}$ cm³/mole. As expected, the susceptibility is temperature-independent over the range studied. These susceptibility measurements are the most precise yet reported for ThO₂ and are being compared with theoretically calculated values. The results to date indicate that the experimentally determined diamagnetic susceptibility is approximately one-half the theoretical value. The difference between the experimental and theoretical results may be due to

“high-frequency” or temperature-independent paramagnetism of the Th⁴⁺ ion. A similar study is in progress on high-purity CeO₂ crystals.

ALTERNATING-CURRENT MUTUAL INDUCTANCE BRIDGE

H. M. Smith G. W. Clark

An ac mutual inductance apparatus for the precise measurement of the principal magnetic susceptibilities is nearing completion. The bridge is a Cryotronics model ML-17B, operating at 17 Hz. It will be capable of measuring the principal magnetic susceptibilities of 2 to 4-mm single crystals over the entire range of 2 to 300°K. Plans for the use of this apparatus include the measurement of the principal susceptibilities of UN, UO₂, several lithium lanthanide molybdates, and several lanthanide germanomolybdates.

2. Deformation and Annealing of Metals

Carl J. McHargue

We are studying the deformation behavior of polycrystalline metals by comparing the preferred orientation developed under a variety of conditions with that predicted from single-crystal behavior. An analysis of the results can give an important insight into the mechanical and plastic properties of complex engineering materials. Studies on the properties of individual crystal defects and their interaction provide the information needed to make such an analysis.

DEVELOPMENT OF PREFERRED ORIENTATIONS IN COLD-ROLLED NIOBIUM¹

R. A. Vandermeer J. C. Ogle

The preferred crystallographic orientations (texture) developed in randomly oriented polycrystalline niobium during rolling were studied by x-ray diffraction. The evolution of texture at both the surface and center regions of the rolled strip was carefully examined as a function of increasing reduction in thickness throughout the range 43 to 99.5%. Certain aspects of the center texture development in niobium are in agreement with the predictions of a theory by Dillamore and Roberts,² but others cannot be explained by the theory in its present form. Above 87% reduction by rolling, a distinct texture unlike the center texture appeared in the surface layers. The present results are compared with previous results obtained from other body-centered cubic metals and alloys.

TEXTURE INHOMOGENEITIES IN COLD-ROLLED NIOBIUM³

R. A. Vandermeer J. C. Ogle

Two types of depth-dependent texture inhomogeneities were observed in niobium specimens cold

rolled various amounts up to 99.5% reduction in thickness. We feel that nonuniform plastic deformation during rolling was responsible for both these inhomogeneities.

The first type of texture inhomogeneity is characterized by a zone at intermediate depths that lacks certain strong orientations that are present in the surface and central layers of the rolled stock. The texture in the surface and center zones consisted of (1) B orientations, a range of orientations extending from $\{111\}\langle 112 \rangle$ to $\{112\}\langle 110 \rangle$, (2) $\{001\}\langle 110 \rangle$ orientations, and to a lesser extent (3) A' orientations ranging from $\{111\}\langle 110 \rangle$ to $\{112\}\langle 110 \rangle$. The texture in the intermediate zone was primarily $\{001\}\langle 110 \rangle$, lacking the B and A' orientations. This type of inhomogeneity was observed only in thick specimens rolled to 70% or less reduction in thickness or only when for each rolling pass the ratio of the geometrical zone of deformation to the average thickness of that zone was less than about 1.0. According to the work of Tarnovskii, Pozdeyev, and Lyashkov,⁴ rolling under these conditions is similar to the compression of thick plates with rigid ends. The inhomogeneity apparently arises because of an important interaction at the boundary between the plastically deforming material in the zone of deformation and the adjacent nondeforming material; this interaction restricts the manner in which deformation proceeds and evidently causes the stress states acting to deform the workpiece to vary from one depth to another.

The second type of texture inhomogeneity involved the formation of a unique texture in the surface layers of rolled strip. We believe that this surface texture was probably a result of a shear deformation in the surface layers for the following reasons:

1. High friction forces between work piece and rolls are necessary to produce and maintain this texture. Thus lack of lubrication and high reductions per pass favor the formation of the surface texture.

¹ Abstract of *Trans. Met. Soc. AIME*, 242, 1317-26 (1968).

² I. L. Dillamore and W. T. Roberts, *Acta Met.* 12, 281 (1964).

³ Summary of paper to be submitted for publication.

⁴ I. Ya. Tarnovskii, A. A. Pozdeyev, and V. B. Lyashkov, *Deformation of Metals During Rolling*, First English ed. translated from Russian, Pergamon, New York, 1965.

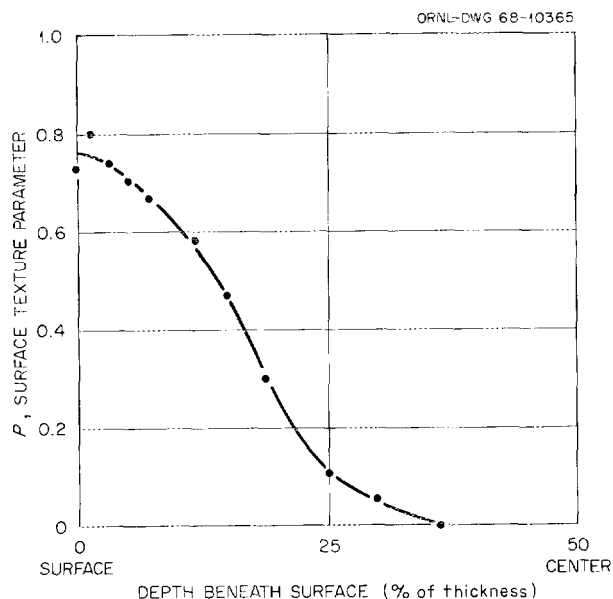


Fig. 2.1. Variation of Surface Texture Parameter, P , with Depth Beneath the Surface. P is defined such that it approaches 1 for a very strong surface texture and approaches 0 when no surface texture is present.

- The depth dependence of the amount of surface texture, shown in Fig. 2.1, is in qualitative agreement with a theory⁵ of the mechanism of metallic friction.
- Other factors being constant, a critical value of reduction per pass⁶ is necessary to generate a substantial amount of surface texture (see Fig. 2.2). This is consistent with the view that a shear mode of deformation occurs only when the shear stresses in the surface layers exceed a certain maximum shear stress characteristic of the material.
- A parallel situation exists for face-centered cubic metals, for which the unique surface texture has been definitely shown to be a shear texture.

The inhomogeneity arises then because, although the surface layers deform by a shear mode, the interior of the strip deforms by the more customary squeezing or compressional mode of deformation.

⁵E. G. Thomsen, C. T. Yang, and S. Kobayashi, *Mechanics of Plastic Deformation in Metal Processing*, Macmillan, New York, 1965.

⁶A theoretical treatment of the rolling process can show that the higher the reduction per pass the greater are the frictional forces (i.e., shear stresses) at work on the specimen surface.

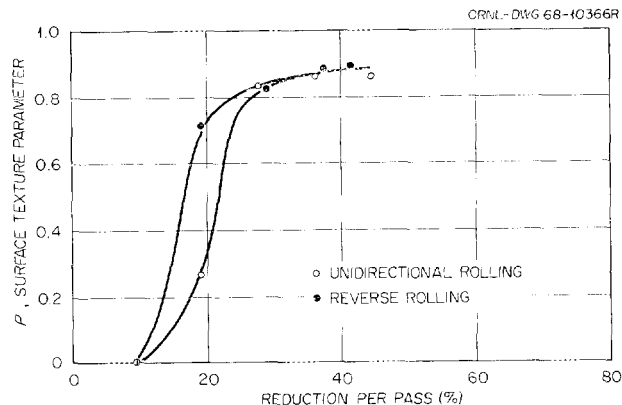


Fig. 2.2. Variation of the Surface Texture Parameter, P , with Reduction Per Pass for Niobium Stock Rolled to 81 to 90% Reduction in Thickness at Approximately Constant Reductions Per Pass.

TEXTURE TRANSITION IN ORDERED Cu_3Au (Ref. 7)

E. A. Starke, Jr.⁸ J. C. Ogle
C. J. Sparks, Jr.⁹

X-ray diffraction techniques were used to determine the texture of ordered and disordered Cu_3Au after various amounts of rolling. The ordered samples had an initial long-range-order parameter of $S \approx 1$. The grain size of both the ordered and disordered samples was the same, and the initial textures of both were also identical and approximately random.

No differences in the deformation textures of the ordered and disordered materials were detected up to 30% reduction, and the pole figures resembled those of pure copper. However, with reductions larger than 30% and less than 50%, a marked deviation from the copper texture developed in the ordered material. This deviation is analogous to that produced in α brass after reduction greater than 70 to 80%. Figures 2.3 and 2.4 show the (111) pole figures for the disordered and ordered samples after 42% reduction. After reduction of 55% and greater the texture of the ordered alloy returned to that of pure copper and disordered Cu_3Au . This is attributed to the destruction of long-range order with increasing deformation. Figure 2.5 shows that 40%

⁷The results of this study have been accepted for presentation at the 1968 Denver Conference on Application of X-Ray Analysis and will be published in *Advances in X-Ray Analysis*, vol. 12.

⁸Consultant from the Georgia Institute of Technology, Atlanta.

⁹X-Ray Diffraction Group.

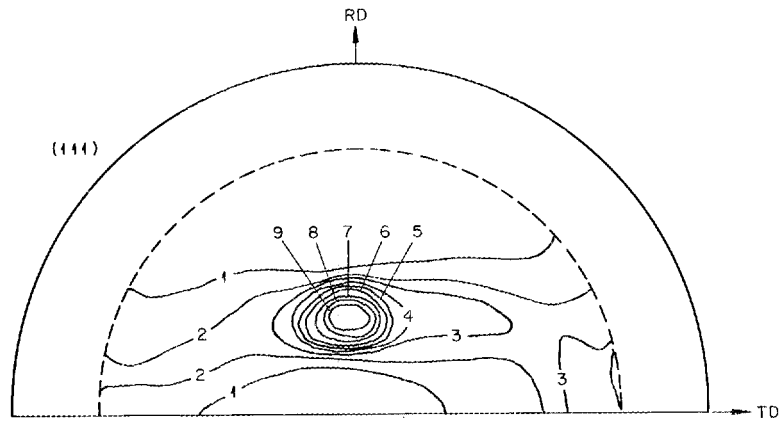


Fig. 2.3. Pole Figure for Disordered Cu_3Au Rolled 42% at 25°C .

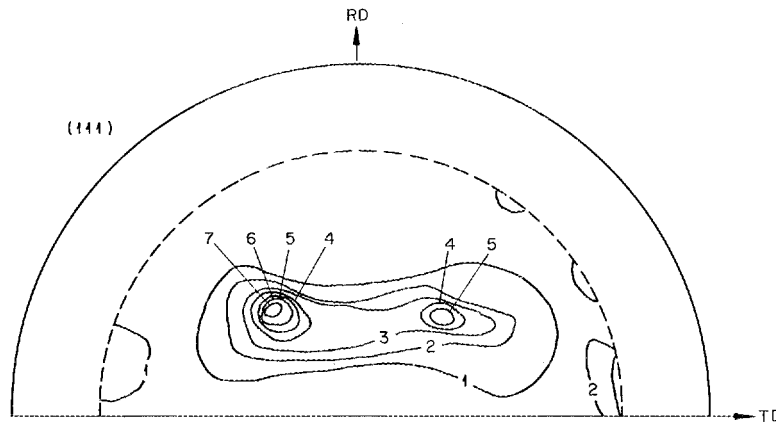


Fig. 2.4. Pole Figure for Ordered Cu_3Au Rolled 42% at 25°C .

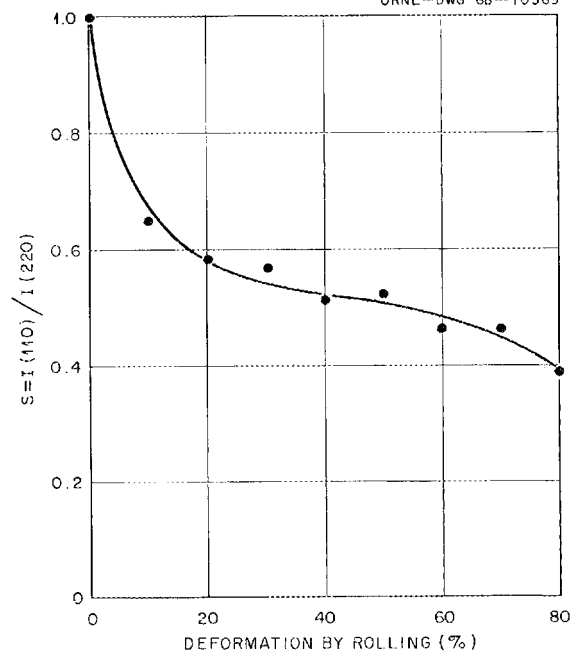


Fig. 2.5. Variation of Long-Range-Order Parameter in Cu_3Au with the Deformation by Rolling.

reduction by rolling has reduced the long-range-order parameter in Cu_3Au by approximately 50%.

We are examining the differences in these textures in light of the general theories of deformation twinning, cross slip, stacking fault energies, and dislocation interaction.

THE RECOVERY CHARACTERISTICS OF NIOBIUM AND Nb-40% V

P. Guthrie¹⁰

The x-ray diffraction profiles of niobium cold rolled at room temperature and at liquid-nitrogen temperature indicate definite differences in the microstrain distributions and effective particle sizes. For 10% cold rolling at room temperature the particle size obtained for the [200] direction is 1230 Å, whereas a similar deformation at 77°K (at which niobium is observed to twin) exhibits a [200] particle size of 1020 Å. After a recovery anneal at 700°C for 63 hr, at which time the recovery rate has essentially diminished to zero, these particle sizes increased to 2060 and 1270 Å respectively. A summary of the root-mean-squared strains corresponding to these particle sizes is given by Fig. 2.6. Deformation at 77°K produces greater strains over larger distances than does similar deformation at room temperature. After recovery at 700°C is complete, both strain distributions are essentially equivalent. However, the specimen deformed at 77°K has undergone a greater decrease in RMS strain while undergoing a much smaller increase in particle size.

¹⁰ORAU Fellow.

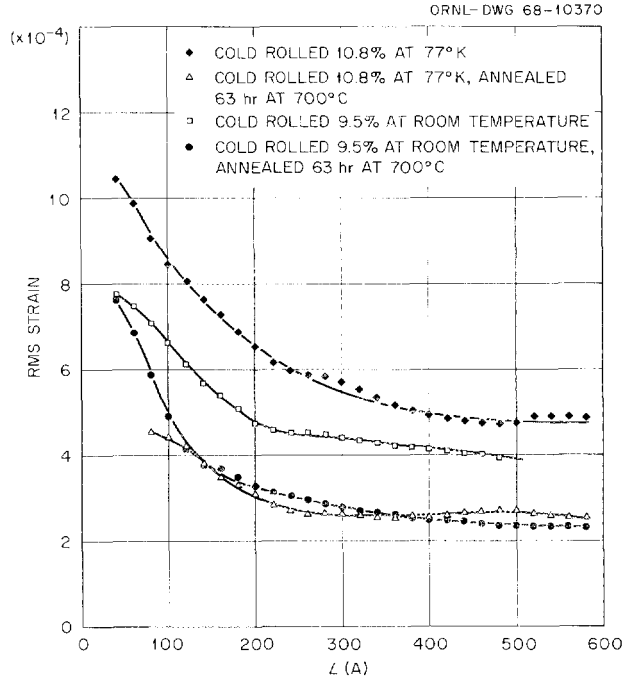


Fig. 2.6. Strain Distributions in $\langle 200 \rangle$ for Cold-Rolled and Recovery-Annealed Niobium. L is a parameter related to the number of planes over which the strain is averaged.

Future plans are to correlate this type of profile analysis with dislocation substructures as observed by transmission electron microscopy and with flow stress analysis as determined by tensile testing. In addition, we plan to extend these analyses to Nb-40% V, which produces two distinctly different dislocation arrays under mild deformation, one above the twinning transition temperature of 140°C and the other below this temperature.

3. Deformation of Crystalline Solids

R. O. Williams

Our interests cover most of the field of deformation of metals and alloys — how this depends upon prior structures and what kind of structures result from deformation. The following abstracts are typical of the current work. The interest in thermodynamics also falls within this field since the nonrandomness of the atoms is important in the deformation of alloys and is in turn presumably related to the thermodynamics.

SUBSTRUCTURE AND FRACTURE IN PACK-ROLLED FOILS OF COPPER AND IRON¹

R. W. Carpenter J. C. Ogle²

The work reported last year³ concerning the rolling and recrystallization substructure in very thin foils of copper and iron has been extended to consideration of the fracture mechanism characteristic of pack-rolled foils. Pack-rolled foils in general begin to develop pinholes at a thickness of 2 to 5 μ , instead of the shear cracks usually associated with fracture during rolling of ductile metals. No cause for this different fracture behavior was apparent in substructure observations made by electron microscopy or in the deformation textures of pack-rolled copper or iron. The stress distribution in foils during pack rolling was considered in some detail. As a result of the difference in flow stress between the austenitic stainless steel pack and the iron or copper foil, a large hydrostatic stress was induced in the foil during pack rolling. The magnitude of this hydrostatic stress depended on the difference in flow stress of the pack and foil and the difference in thickness of the jacket and foil; under the conditions of the work reported here the hydrostatic pressure was estimated to be 2.00×10^5 and 1.88×10^5 psi for copper and iron respectively. It is well known that if a normally ductile metal is plastically deformed under a

large hydrostatic pressure, in addition to the deviatoric stresses necessary to cause plastic flow, the growth of shear cracks will be suppressed or prevented and the total elongation to fracture greatly increased.⁴ Ductile fracture can be divided into two steps: (1) the nucleation of cracks and (2) the growth and coalescence of cracks during subsequent plastic strain to form the final fracture surface. The crack nuclei formed in step (1) have been shown to be associated with nonmetallic inclusions in the deforming metal.⁵ Optical metallographic analysis was not possible on the thin foils used here; however, such investigation did establish the presence of inclusions in 130- μ -thick starting material. We conclude that the pinholes observed in copper and iron represent shear crack nuclei that did not enlarge upon further reduction because of the large hydrostatic stress present during pack rolling.

PLASTIC DEFORMATION OF RHENIUM

R. W. Carpenter

The deformation behavior of the metal rhenium is of interest in general because it is of the hexagonal-close-packed type and in particular because its deformation-hardening rate is reported to be very high.⁶ Cylindrical single crystals of rhenium (0.125 in. diam \times 4 in. long) with [2110] parallel to the cylindrical axis have been grown by the electron-beam floating-zone technique. Some of these crystals were used to develop a method of preparation of rhenium specimens for transmission electron microscopy⁷ based on the high-voltage jet method developed by DuBose and Stiegler.⁸ Others were used in preliminary deformation experiments in compression along the $[2\bar{1}\bar{1}0]$ zone axis. We observed

¹Submitted to *Transactions of the Metallurgical Society of AIME* for publication.

²Structure of Metals Group.

³R. W. Carpenter and J. C. Ogle, *Metals and Ceramics Div. Ann. Progr. Rept. June 30, 1967*, ORNL-4170, pp. 13–14.

⁴P. W. Bridgman, *Studies in Large Plastic Flow and Fracture*, McGraw-Hill, New York, 1952.

⁵K. E. Puttick, *Phil. Mag.* 4, 964 (1959).

⁶A. T. Churchman, *Trans. Met. Soc. AIME* 218, 262 (1960).

⁷R. W. Carpenter and H. Paris, accepted by *Journal of Applied Physics* for publication.

⁸C. K. H. DuBose and J. O. Stiegler, *Rev. Sci. Instr.* 38, 694–95 (1967).

profuse formation of twins during such deformation at stresses above about 6800 psi; the stress drops accompanying twinning were in general not larger than about 850 psi. Transmission electron microscopic examination of some of these twins indicated that thickening is difficult, with most twins having thicknesses less than 4 μ . We have not observed stacking faults in deformed rhenium. This work will be continued.

INTERACTION OF SLIP DISLOCATIONS WITH TWINS IN HEXAGONAL-CLOSE-PACKED METALS⁹

M. H. Yoo

Possible interaction between the perfect dislocations of six slip systems along with a *c* dislocation and the $\{10\bar{1}2\}\langle 10\bar{1}1\rangle$, $\{10\bar{1}1\}\langle 10\bar{1}2\rangle$, $\{11\bar{2}2\}\langle 11\bar{2}3\rangle$, and $\{11\bar{2}1\}\langle 1\bar{1}26\rangle$ twins in hexagonal-close-packed metals have been analyzed from both the crystallographic and the energetic points of view. We identified 24 distinct types of possible interactions with the aid of transformation matrices. Those that are more probable to occur on the basis of crystallographic constraints were selected for further analysis of their energetic feasibilities.

An approximate solution to the long-range elastic interaction between a straight dislocation and a coherent twin interface was obtained by use of the anisotropic energy factors. No long-range interaction exists for a dislocation if its Burgers vector is parallel to the interface (e.g., a basal screw dislocation and the $\{10\bar{1}2\}$ twin). For the basal mixed dislocations of cadmium and zinc, the interaction with the $\{10\bar{1}2\}$ twin is strongly attractive, which indicates that incorporation of basal dislocations into the $\{10\bar{1}2\}$ twin is energetically feasible, and twin growth will take place as a result. On the other hand, the interaction between basal mixed dislocations and the $\{10\bar{1}2\}$ and $\{11\bar{2}1\}$ twins is always repulsive for Mg, Re, Zr, Ti, or Be. This indicates that a local stress concentration will develop due to a dislocation pileup at the interface, which may become a source for the nucleation of conjugate twins or twins of other type and even for the formation of a crack, depending on the cleavage strength of the metal.

DISLOCATION REACTIONS IN HEXAGONAL-CLOSE-PACKED METALS¹⁰

M. H. Yoo

A number of dislocation reactions involving straight perfect dislocations in hexagonal metals (Cd, Zn, Mg, Co, Zr, Ti, and Be) were studied with a particular

interest in those associated with $\langle c + a \rangle$ dislocations. According to an energy criterion that takes into account the effect of elastic anisotropy, the interaction between a prismatic dislocation and a sessile major dislocation,

$$\frac{1}{3} [11\bar{2}0]_{(1\bar{1}00)} + [0001] \rightarrow \frac{1}{3} [11\bar{2}3]_s, \quad (1)$$

where the subscript *s* denotes screw orientation, is found to produce an attractive junction, which under applied stress may become a source for $\langle c + a \rangle$ dislocations. This implies that $\langle c + a \rangle$ dislocations will be generated when and where prismatic slip is active in the presence of *c* dislocations. We found that $\langle c + a \rangle$ dislocations in the hexagonal metals are unstable with respect to $\langle c + a \rangle$ dislocation reactions as pure edge in $\{11\bar{2}2\}$ glide planes and rather stable in pure screw orientation. We also found that under suitable stress states twin interfaces can be the sources of $\langle c + a \rangle$ dislocations when the reactions

$$2 \cdot \frac{1}{3} [2\bar{1}\bar{1}0]_m + 2b_t \rightarrow \frac{1}{3} [\bar{1}\bar{1}23]_t, \quad (2)$$

$$\frac{1}{3} [\bar{2}110]_m + \frac{1}{3} [\bar{1}\bar{1}20]_m + 2b_t \rightarrow \frac{1}{3} [\bar{2}11\bar{3}]_t, \quad (3)$$

and

$$[0001]_m + b_t \rightarrow \frac{1}{3} [\bar{1}\bar{1}23]_t, \quad (4)$$

occur, respectively, at the $(1\bar{1}02)$, $(11\bar{2}2)$, and $(11\bar{2}1)$ twin interfaces, where the *m* and *t* subscripts denote the matrix and the twin, and nb_t refers to the Burgers vector of the corresponding zonal twin dislocation.

SERIES REPRESENTATION OF THERMODYNAMIC FUNCTIONS OF BINARY SOLUTIONS

R. O. Williams

A new series was constructed expressly for representing the compositional dependence of thermodynamic functions for binary solutions. The first three

⁹ Abstract of paper presented at the symposium on "Plastic Deformation in H.C.P. Metals," the 97th Annual Meeting of AIME, New York, Feb. 27-29, 1968.

¹⁰ Abstract of paper to be presented at the 1968 Fall Meeting of the Metallurgical Society of AIME, Detroit, Oct. 14-17, 1968.

members are

$$Z_1 = 4x - 4x^2, \quad (1)$$

$$Z_2 = 4x - 10x^2 + 10x^4 - 4x^5, \quad (2)$$

$$Z_3 = 4x - 18x^2 + 70x^4 - 84x^5 + 28x^6, \quad (3)$$

where x is the fraction of component 2. The integral functions would be expressed as

$$T = AZ_1 + BZ_2 + CZ_3, \quad (4)$$

relative to the pure components, where T represents the heat of mixing, the excess free energy, or the excess entropy, and the constants A , B , and C are to be evaluated to provide the best representation of the data. The series is defined such that the third derivative is zero at $x = 0$ and 1 , so that the excess stability ($d^2 G^E/dx^2$) is a constant at these compositions. This condition appears to be satisfied by real solutions according to the work of Darken.¹¹ The members are also approximately orthogonal. The first term is used to describe regular solutions and was originally due to Margules.¹² The higher terms that Margules included do not satisfy Darken's condition.

From the definition of partial molar quantities, it follows that the above series can be converted into a second representing the partial molar quantities and using the same coefficients. Specifically for component 2

$$\bar{Z}_1^2 = 4 - 8x + 4x^2, \quad (5)$$

$$\bar{Z}_2^2 = 4 - 20x + 10x^2 + 40x^3 - 50x^4 + 16x^5, \quad (6)$$

and

$$\begin{aligned} \bar{Z}_3^2 = 4 - 36x + 18x^2 + 280x^3 - 630x^4 \\ + 504x^5 - 140x^6, \quad (7) \end{aligned}$$

such that

$$\bar{T}^2 = A\bar{Z}_1^2 + B\bar{Z}_2^2 + C\bar{Z}_3^2. \quad (8)$$

In Fig. 3.1 we have graphed both the integral and partial molar terms.

There are a number of advantages of the present series. To evaluate the coefficients most simply the experimental data must be a linear function of these coefficients. This condition has been met by only part

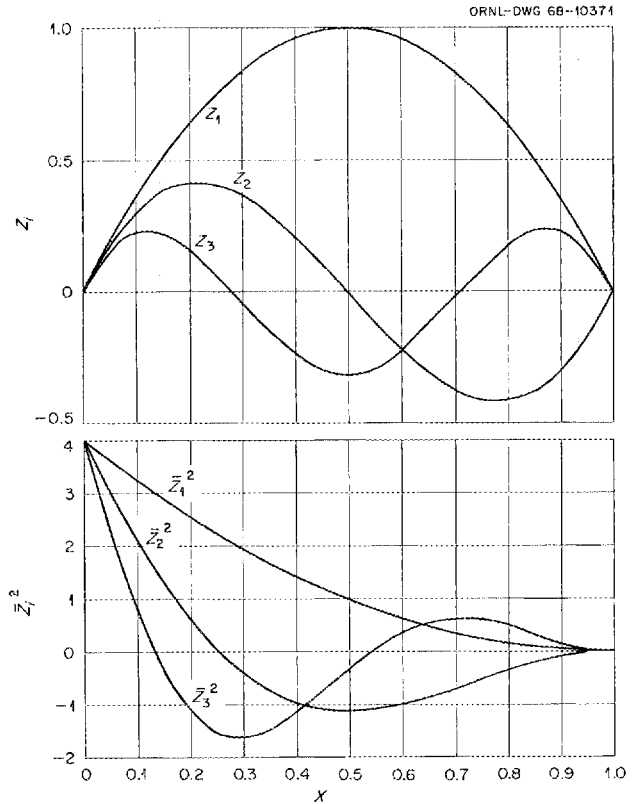


Fig. 3.1. The Partial and Molar Forms of the First Three Members of the Series for Representing Thermodynamic Functions of Solutions.

of the prior proposals. Also, it is desirable that the coefficients be as independent as possible so that they will describe the systems as graphically as possible and will exhibit only small changes depending on the data and the number of terms used. The present series is markedly superior in these respects. As already pointed out, this series must satisfy Darken's excess stability condition, whereas most others do not.

There are many advantages of having analytical expressions for the thermodynamic functions. The above expressions illustrate an example; if either partial or integral data are fitted by a set of constants then one immediately has the complete representation without recourse to any integration. This result is not new but it does not appear to be widely appreciated.

REPRESENTATION OF TEXTURES AS AXIAL AND BIAxIAL POLE FIGURES

R. O. Williams

The mathematical treatment by means of which experimental data for fiber textures may be converted

¹¹L. S. Darken, *Trans. Met. Soc. AIME* 239, 80 (1967).

¹²M. Margules, *Sitzber. Akad. Wiss. Wien* 104, 1243 (1895).

into axial pole figures has shown that prior methods were not optimum, but it did not entirely succeed in showing the best forms of the solutions.¹³ This problem was further examined in some detail, and various solutions were compared. One particularly interesting development was that the linear method in fact turns out to be based upon a very general series, which may well prove superior to the spherical harmonics. We anticipate that a report covering this work and including all necessary programs and data can be prepared shortly.

The rolling textures for copper, brass, and aluminum have been represented as biaxial pole figures,¹⁴ and the required mathematical treatment figures have been reported.¹⁵

¹³R. O. Williams, *J. Appl. Phys.* 38, 4029–33 (1967).

¹⁴R. O. Williams, *Trans. Met. Soc. AIME* 242, 105 (1968).

¹⁵R. O. Williams, "Analytical Methods for Representing Complex Textures by Biaxial Pole Figures" to be published in *Journal of Applied Physics*, August 1968.

4. Diffusion in Solids

T. S. Lundy

During this reporting period we concentrated our research efforts on three main topics – tracer diffusion in tungsten, uranium diffusion in both UO_2 and UN, and titanium diffusion in modified Hastelloy N. The first program is being conducted jointly with R. E. Pawel of the Surface Reaction of Metals Group and part of the work is reported in Chap. 12. The last program was a joint effort with C. E. Sessions of the Mechanical Properties Group and was in support of the Molten Salt Reactor Program.

USE OF ELECTROCHEMICAL SECTIONING IN THE STUDY OF DIFFUSION IN TUNGSTEN¹

R. E. Pawel² T. S. Lundy

A microsectioning technique based on metal anodization and subsequent removal of the anodic oxide film was developed and used to determine the concentration profiles of ^{95}Nb in tungsten single crystals after diffusion at 1800°C . The anodization characteristics of tungsten pertinent to quantitative serial sectioning were studied, and several techniques for increasing the efficiency of isotope removal during chemical dissolution of the anodic film were tried. The resulting data were highly self-consistent and demonstrate the value of the method in investigating diffusion behavior in tungsten, particularly at low temperatures.

DIFFUSION OF ^{95}Nb AND ^{188}W IN MONOCRYSTALLINE TUNGSTEN

R. E. Pawel² T. S. Lundy

Experiments to determine lattice diffusion coefficients for ^{95}Nb in monocrystalline tungsten have been completed and are reported in Chap. 12. We are currently measuring lattice diffusion coefficients for ^{188}W in tungsten.³ Initial measurements from 1800 to

¹Abstracted from *J. Electrochem. Soc.* **115**, 233–37 (1968).

²Reactions at Metal Surfaces Group; see Chap. 12.

³The radioisotope was supplied through the courtesy of J. J. Pinajian, Isotopes Division.

2400°C show that the diffusion coefficient at any given temperature is about one-third that for ^{95}Nb . The activation energies for these two diffusing species appear to be about equivalent. Our measured values for ^{188}W agree reasonably well with previous work by Andelin, Knight, and Kahn⁴ (2660 to 3230°C) but lie significantly below values by Danneberg⁵ (2000 to 2700°C) and are one to two orders of magnitude below values by Neumann and Hirschwald⁶ (1740 to 2100°C). Apparently, at the lower temperatures investigated in the last two papers^{5,6} short-circuiting mechanisms were the dominate transport processes rather than lattice diffusion.

SHORT-CIRCUITING EFFECTS ON TRACER DIFFUSION IN TUNGSTEN

T. S. Lundy R. E. Pawel²

The influence of short-circuiting paths on measured diffusion coefficients can be quite large. Here we consider detailed penetration data for the diffusion of ^{95}Nb into one polycrystalline sample of tungsten. The sample was diffusion annealed for 8 hr at 1399°C and then sectioned by the extremely precise technique previously described. The overall penetration plot is shown in Fig. 4.1. Although one cannot resolve all the details in this one figure, one can see that the slope (and therefore the apparent diffusion coefficient) varies over about six orders of magnitude. The true lattice diffusion coefficient obtained from the initial portion of this plot as well as from data for monocrystalline tungsten is about 3×10^{-18} cm^2/sec . Depending upon the techniques used for sectioning and analyzing such data it is easy to imagine that one could have measured diffusion coefficients (and thought they were due to lattice diffusion)

⁴R. L. Andelin, J. D. Knight, and M. Kahn, *Trans. Met. Soc. AIME* **233**, 19–24 (1965).

⁵W. Danneberg, *Metallwiss. Tech.* **15**, 11–15 (October 1961).

⁶G. M. Neumann and W. Hirschwald, *Z. Naturforsch.* **21a**, 812–15 (1966).

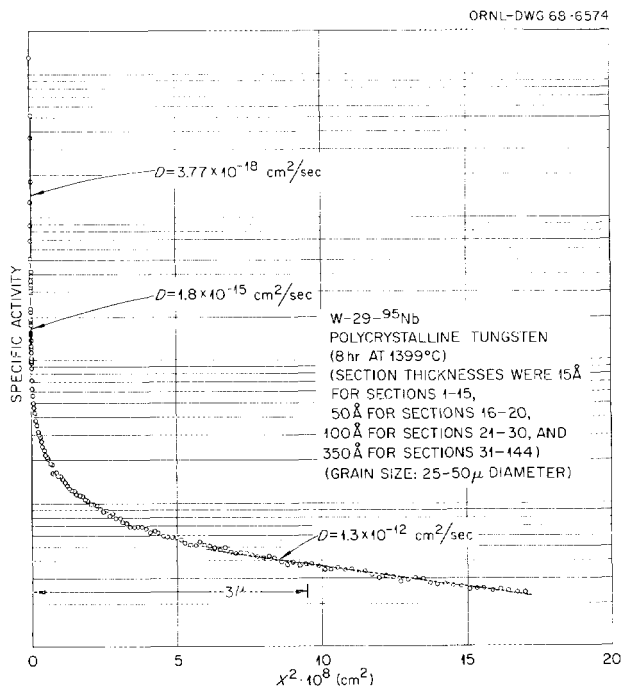


Fig. 4.1. Penetration Profile for Diffusion of ^{95}Nb in Polycrystalline Tungsten.

that were many orders of magnitude too large. As Harrison⁷ pointed out, when the grain size for polycrystalline material is small relative to the penetration distances involved, then plots of penetration data will appear to be Gaussian (logarithm of activity linear in distance squared) for the semiinfinite diffusion couple having a plane surface source of tracer even if all the atomic transport is along grain boundaries. We believe that data of the type presented here for diffusion in polycrystalline tungsten may be instrumental in explaining previous anomalous results on diffusion in such body-centered cubic systems as β -zirconium⁸ and β -titanium,⁹ where Arrhenius plots are markedly non-linear.

CATION SELF-DIFFUSION IN UN

D. K. Reimann¹⁰

The diffusion of ^{233}U in large-grained polycrystalline UN_{1+x} was measured for two compositions, one close to the phase boundary between UN and UN + U(l) and

⁷L. G. Harrison, *Trans. Faraday Soc.* 57, 1191-99 (1961).

⁸J. I. Federer and T. S. Lundy, *Trans. Met. Soc. AIME* 227, 592-97 (1963).

⁹J. F. Murdock, T. S. Lundy, and E. E. Stansbury, *Acta Met.* 12, 1033-39 (1964).

¹⁰Temporary noncitizen employee from Germany.

one about halfway between this phase boundary and the boundary between UN and U_2N_3 . The following results were obtained in the respective temperature ranges:

1. Close to UN + U(l):

$$D = 3.24 \times 10^{-7} \exp(-60,000/RT)$$

$$\text{for } 1100 < T < 1600^\circ\text{C}.$$

2. Intermediate pressure range:

$$D = 7.54 \times 10^{-2} \exp(-105,000/RT)$$

$$\text{for } 1420 < T < 1820^\circ\text{C}.$$

Experiments close to the phase boundary between UN and U_2N_3 will be run, and the temperature ranges will be extended.

Similar experiments will be run with small-grained sintered UN to obtain information on grain-boundary diffusion of uranium in UN.

CATION SELF-DIFFUSION IN UO_2 SINGLE CRYSTALS

D. K. Reimann¹⁰

From diffusion experiments on UO_2 single crystals in the temperature range from 985 to 1400°C, diffusion coefficients were estimated to be two or three orders of magnitude smaller than those reported by several investigators¹¹⁻¹³ for polycrystalline material. On large-grained polycrystalline UO_2 , appreciable grain-boundary diffusion was detected autoradiographically.

Experiments at high temperatures (1800 to 2100°C) are presently being done to establish true lattice diffusion coefficients for uranium in UO_2 .

DIFFUSION OF TITANIUM IN MODIFIED HASTELLOY N (Refs. 14-15)

C. E. Sessions¹⁶ T. S. Lundy

The nickel-base alloy Hastelloy N was developed as a containment material for the Molten-Salt Reactor Ex-

¹¹A. B. Auskern and J. Belle, *J. Nucl. Mater.* 3(3), 311-19 (1961).

¹²R. Lindner and F. Schmitz, *Z. Naturforsch.* 16a, 1373-78 (1961).

¹³S. Yajima, H. Furuya, and H. Hirai, *J. Nucl. Mater.* 20, 162-70 (1966).

¹⁴Work supported by the Molten Salt Reactor Program.

¹⁵Abstract of paper submitted to *Journal of Nuclear Materials*.

¹⁶Mechanical Properties Group.

periment. The alloy is composed basically of nickel and molybdenum, elements that are essentially noble to the fluoride fuel mixture used in this reactor. However, continuing studies of the alloy have indicated that the addition of 0.5 to 1.0% titanium greatly reduces the susceptibility of the alloy to helium-bubble damage occurring from neutron irradiation. Corrosion studies have shown a tendency for selective removal of the less noble constituents such as chromium, titanium, and iron. This removal rate may be controlled by solid state diffusion in the alloy.

With this problem in mind we determined the diffusion coefficients for ^{44}Ti in titanium-modified Hastelloy N from 800 to 1250°C. Standard serial sectioning involving specimen grinding and gamma spectroscopy were used. The data could be fitted by the

Arrhenius expression:

$$D = (15.3 \pm 2.2) \exp \left(-\frac{72,000 \pm 3300}{RT} \right) \text{ cm}^2/\text{sec}.$$

We have used these data to predict the atomic mobility at reactor service temperature (700°C) and to predict the rate of titanium mass transfer. In a typical molten-salt breeder reactor the maximum rate of loss by diffusion of titanium from the alloy at 700°C would result in an increase of no more than 5 to 10 ppm titanium in the salt in two years of operation. Titanium diffusion at and below 700°C is limited principally to "short circuit" paths such as grain boundaries and results in negligible depletion of titanium even from thin cross sections.

5. Electron Microscopy

J. O. Stiegler

The mechanical and physical properties of metals are altered, usually for the worse, by the presence of internal cavities that develop under service conditions. For example, voids formed by fast-neutron irradiation strengthen metals, reduce their ductility, and cause gross swelling; part per million quantities of insoluble gases precipitate as bubbles, which severely restrict high-temperature ductility; and deformation processes open cavities on grain boundaries, which then grow into cracks and cause premature failure. We are using the electron microscope to detect, characterize, and follow the development of cavities formed by these processes. We are working closely with the LMFBF and aluminum programs in studying voids generated by fast-neutron irradiation and are supplementing these programs with studies of voids introduced into metals by quenching. In conjunction with the tungsten metallurgy program we have examined gas bubbles in chemically vapor deposited tungsten^{1,2} and creep cavities³ and cracks in powder-metallurgy material. We are extending the range of test conditions and grades of material to better define the nature of creep deformation. We are conducting companion studies on various grades of nickel containing gaseous and solid impurity elements to clarify their role in the creep process. We are also studying precipitation phenomena and irradiation damage and their influence on elevated-temperature deformation in the complex alloy Hastelloy N used in the Molten Salt Reactor Experiment. Subjects that are based primarily on microstructural observations are

reported in this chapter; other work is included in Part II, Chapter 16; Part III, Chapters 21 and 22; and Part IV, Chapter 34.

BUBBLE GROWTH PROCESSES AT GRAIN BOUNDARIES IN CVD TUNGSTEN⁴

A. Wolfenden K. Farrell

Recent measurements of gas bubbles on the grain boundaries in chemically vapor deposited (CVD) tungsten after various annealing treatments² are analyzed in terms of three models of bubble growth in solids. These models are (1) bubble migration and coalescence, (2) bubble dissolution and reprecipitation, and (3) the so-called *in situ* touch-and-merge process. The bubbles had average diameters in the range 0.08 to 5.6 μ . For such bubbles, growth by bodily migration and coalescence at the times and temperatures used is shown to be highly improbable whether the migration occurs by surface diffusion, volume diffusion, or vapor transport.

The general pattern of the experimentally observed bubble growth can be most closely described by the model of bubble dissolution and reprecipitation. This growth is characterized by an activation energy of approximately 92 kcal/gram-atom, which is close to that for self-diffusion of tungsten in the grain boundaries. At high annealing temperatures bubble growth is enhanced by the so-called *in situ* touch-and-merge process, in which the bubbles grow until they touch without migrating.

STRESS-INDUCED GROWTH OF GAS BUBBLES IN SOLIDS⁵

J. O. Stiegler K. Farrell H. E. McCoy

By an electron fractographic technique, we studied the stress-induced growth of grain-boundary gas bubbles in creep specimens of CVD tungsten. When the specimen was stressed to 4000 psi at 1650°C in a vacuum

¹K. Farrell, B.T.M. Loh, and J. O. Stiegler, "Morphologies of Bubbles and Voids in Tungsten," *ASM (Am. Soc. Metals) Trans. Quart.* 60, 485-93 (1967).

²K. Farrell, J. T. Houston, and A. C. Schaffhauser, "The Growth of Grain-Boundary Gas Bubbles in Chemically Vapor Deposited Tungsten," pp. 363-90 in *Proceedings of the Conference on Chemical Vapor Deposition of Refractory Metals, Alloys, and Compounds, Gatlinburg, Tennessee, September 12-14, 1967*, ed. by A. C. Schaffhauser, American Nuclear Society, Hinsdale, Ill., 1967.

³J. O. Stiegler, K. Farrell, B.T.M. Loh, and H. E. McCoy, "Nature of Creep Cavities in Tungsten," *ASM (Am. Soc. Metals) Trans. Quart.* 60, 494-503 (1967).

⁴Summary of a paper presented at the 97th Annual AIME Meeting, New York, February 1968 (to be published).

⁵Abstract of *J. Nucl. Mater.* 25, 340-43 (1968).

the bubbles expanded only slightly. When the stress was increased to 6000 psi, unlimited bubble growth occurred, linking the bubbles to form cracks. The results are consistent with a model in which breakaway growth of bubbles occurs above a critical stress that depends on the size of the bubble. A surface energy of 2100 ergs/cm^2 at 1650°C for the environment of the bubbles was deduced from the observations.

THERMAL REJECTION AND GROWTH OF GAS BUBBLES IN ELECTRODEPOSITED NICKEL⁶

K. Farrell J. T. Houston

Gas bubbles and voids generated in nuclear reactor components by neutron irradiation may contribute to hardening, dimensional instability, and loss in high-temperature ductility. Similar effects ought to arise in unirradiated materials if they contain sufficient holes or gas bubbles of suitable sizes. A study of such unirradiated materials might therefore provide information pertinent to the irradiation problem. Hence we have been examining gas bubble formation in electrodeposited nickel. Electrodeposited nickel should provide a system of entrapped lattice vacancies and gas atoms whose combination during suitable annealing ought to ensure extensive bubble nucleation. Nickel is also similar in other properties to the stainless steels and nickel-base alloys used in nuclear reactors.

The annealing behavior of a 9-mm-diam electrolytic nickel rod was studied. Hardness measurements showed that it softened rapidly even at low annealing temperatures. This was followed by a slower softening process with an activation energy of $70 \pm 5 \text{ kcal/mole}$. During slow softening gas bubbles about 60 Å in diameter were observed by transmission electron microscopy after anneals at 500°C . Chemical analyses revealed that most of the hydrogen evolved from the specimens before or during the formation of the tiny bubbles. With increasing annealing treatment the gas bubbles coarsened and large grain-boundary bubbles developed. These large bubbles caused significant swelling, the activation energy for which was measured from density changes as $46 \pm 4 \text{ kcal/mole}$. Swelling and softening ceased at about 6% swelling, and grain growth occurred simultaneously.

Support for the view that electrodeposits are supersaturated with lattice vacancies is drawn from published evidence, and the above results are discussed in terms of

gas bubble nucleation and growth in a material supersaturated with vacancies.

We conclude that the slow softening process is determined by bubble coarsening within the grains, which in turn is controlled by bulk self-diffusion in the nickel. Swelling results largely from the grain-boundary bubbles, but because the gas supply to these bubbles depends on dissolution of bubbles within the grains the activation energy for the swelling process is a compromise between that for bulk self-diffusion and that for self-diffusion in the grain boundaries.

ANNEALING BEHAVIOR OF VOIDS IN IRRADIATED STAINLESS STEEL

B.T.M. Loh E. E. Bloom J. O. Stiegler

By transmission electron microscopy, we followed the annealing of voids in sections of a fuel pin irradiated in EBR-II. Both isothermal and isochronal annealing treatments were given to materials containing various initial void distributions. In all cases, small voids were eliminated more rapidly than large ones, resulting in a decrease in void density and a shift of the distribution of remaining voids to larger sizes. The temperature at which all voids were eliminated by a 1-hr anneal depended on the initial density and size distribution.

The changes in density and size distributions of voids were calculated as functions of annealing time and temperature for a model in which void shrinkage is controlled by diffusion of vacancies from voids to dislocations. The dissolution rate of a void is calculated by assuming a steady-state diffusion of vacancies from a spherical void to the surrounding matrix with the boundary conditions that the vacancy concentration at the void surface is $C_0 \exp(2\gamma\Omega/rkT)$ and is some average value, \bar{C} , at the midpoint between voids, where r is the radius of the void, C_0 is the equilibrium concentration of vacancies in the matrix at temperature T , and γ and Ω are the surface tension and the atomic volume of the matrix, respectively. Dislocations are the sole sinks for the excess vacancies and can be eliminated by absorbing vacancies. The drain rate of vacancies into the dislocations is estimated by solving the diffusion equation (assuming steady state) for cylindrical symmetry with the boundary conditions $C = C_0$ at the core radius of the dislocation, and $C = \bar{C}$ at the midpoint between dislocations. The stress-induced drift due to vacancy-dislocation interaction is neglected. Initially, \bar{C} is assigned a value corresponding to the concentration at the surface of a void of the most probable size, and rapidly it reaches some value that regulates the whole kinetic process to a quasi-steady state such that the

⁶Summary of a paper presented at the 97th Annual AIME Meeting, New York, February 1968.

total number of vacancies leaving the voids is approximately the number absorbed by the dislocations. The value of \bar{C} fluctuates slightly and decreases with annealing time.

Calculations performed for this model have shown the following points.

1. If the measured activation energy for self-diffusion of 67.1 kcal/mole for Fe in Fe-11.3% Ni-17.5% Cr-1.3% Mo alloy is used, this model predicts a faster rate of void dissolution than is observed. A value of the activation energy about 70 kcal/mole provides a better fit.

2. If the rate of elimination of dislocations is assumed to be proportional to the number of vacancies absorbed by dislocations (the case for climb of interstitial dislocation loops), the dissolution rate of voids is too high for the observed initial dislocation density (approx $10^{11}/\text{cm}^2$). Also the experimental data indicate a much faster rate of annihilation of dislocations during the earlier stages of annealing. Thus, in addition to climb, direct annihilation of dislocation loops by migration and glide can play an important role in reducing the dislocation density in the earlier stages. An exponentially decreasing function is then adopted to describe the decrease in dislocation density and enables the model to fit the observed data reasonably. The justification for such a function remains to be explored.

3. With the modifications given above, the predicted void densities for long-time annealing are low compared with the experimental results. Adjustment of the parameters to slow down the dissolution rate of voids decreases the agreement for the short-time annealing results. For long annealing time gases may diffuse to the voids and slow the rate of shrinkage. We are now incorporating this effect into the model.

4. Since voids with surface concentration higher than \bar{C} shrink, and since the surface concentration is an exponential function of $1/r$, small voids dissolve rapidly while the large ones may even grow. The net result of this is a shift of the distribution of remaining voids to larger sizes, which agrees well with the observed results.

ENERGY STORED IN SILVER SINGLE CRYSTALS⁷

A. Wolfenden

As part of a series of experiments⁸⁻¹³ on the determination of the stored energy of cold work, a single-step calorimeter was used to measure the energy relations involved in the room-temperature tensile deformation of single crystals of silver. The data are discussed in terms of theories of work hardening. The values of the stored energy were linearly related to the square

of the shear stress, the constants of proportionality being orientation dependent. An explanation of these effects was sought in terms of the dislocation structure after deformation.

PHASE INSTABILITY IN HASTELLOY N (Ref. 14)

R. E. Gehlbach H. E. McCoy

Hastelloy N, although basically a solid-solution alloy, does exhibit changes in mechanical properties and microstructure as a result of various thermomechanical treatments. Since this alloy is intended for use at temperatures up to 850°C and is presently used in the MSRE, it is important that we understand the nature of the precipitation processes and the effect on mechanical behavior.

Identification and characterization of the precipitate involved several complementary techniques. These include optical metallography, transmission electron microscopy, extraction replication, x-ray diffraction, and electron probe microanalysis. In addition, chemical analysis using a microprobe attachment for the electron microscope and electron diffraction were employed for identifying individual particles, agglomerates, and grain-boundary films on extraction replicas without interference from the matrix. We have used these techniques to resolve differences in precipitates that show the same diffraction pattern and relate the microstructure to mechanical properties.

The microstructure is characterized by stringers of a massive primary precipitate of the $\text{Ni}_3\text{Mo}_3\text{C}$ type. Exposure to the range 500 to 1000°C results in the precipitation of particles of the $\text{Ni}_2\text{Mo}_4\text{C}$ type in the grain boundaries. In air-melted heats, which contain approximately 0.6% Si, the carbide-type precipitates are

⁷ Abstract of a paper submitted for publication.

⁸ A. Wolfenden, Ph.D. Thesis, University of Liverpool, 1965.

⁹ A. Wolfenden and A. S. Appleton, *Rev. Sci. Instr.* **38**, 826-30 (1967).

¹⁰ A. Wolfenden, *Acta Met.* **15**, 971-78 (1967).

¹¹ A. Wolfenden and A. S. Appleton, *Acta Met.* **16**, 915-25 (1968).

¹² A. Wolfenden, "The Ratio of Stored to Expended Energy During the Deformation of Copper and Aluminum Single Crystals at 78°K," accepted for publication in *Acta Metallurgica*.

¹³ A. Wolfenden, "Autographically Recording Sensitive Gas Flowmeter," accepted for publication in *Review of Scientific Instruments*.

¹⁴ Abstract of paper to be presented at the International Symposium on Structural Stability in Superalloys, Pittsburgh, Pa., Sept. 4-6, 1968.

enriched in silicon and are not dissolved at high annealing temperatures but melt and transform to a noncarbide phase. In vacuum-melted heats with low silicon contents, the carbides do go into solid solution.

We find that the only precipitates that form in air-melted alloys at temperatures as high as 1180°C are complex pseudocarbides of the $\text{Ni}_3(\text{Mo,Cr})_3(\text{C,Si})$ and $\text{Ni}_2(\text{Mo,Cr})_4(\text{C,Si})$ types. The quantity of the precipitates and their behavior are highly silicon dependent; this impurity stabilizes the particles, preventing their being taken into solid solution at high annealing temperatures and causing them to melt and transform to the high-temperature phase. We have found that this latter phase is probably the δ -NiMo intermetallic and is probably responsible for the increased embrittlement at high annealing temperatures.

OBSERVATION OF GAS BUBBLES IN SOLIDS¹⁵

J. O. Stiegler K. Farrell

The techniques available for detecting and measuring gas bubbles in solids are briefly described and their application and limitations are reviewed. These techniques include transmission and replication electron microscopy, conventional optical microscopy, field ion microscopy, x-ray absorption microscopy, small-angle x-ray scattering, residual electrical resistivity, and precision density measurements. Most of the information that we now have on the sites, sizes, and shapes of gas bubbles in solids has been obtained by the first three of these techniques. Some of these results are illustrated for irradiation-induced bubbles in type 304 stainless steel and for bubbles in chemically vapor-deposited tungsten.

ELECTRON FRACTOGRAPHY FOR STUDYING CAVITIES¹⁶

K. Farrell J. O. Stiegler

The advantages and limitations of a direct carbon replication technique for the study of fracture surfaces in brittle materials containing cavities are outlined. Some recent observations obtained this way on creep cavities in high-grade commercial tungsten are described and discussed in terms of published observations made by other methods. Finally, caution is urged in the use of a shadowgraphic electron microscopy technique that has been used to examine holes in solids.

¹⁵Summary of a paper presented at the 97th Annual AIME Meeting, New York, February 1968 (to be published).

¹⁶Summary of paper accepted for publication in *Metalurgia*.

ELECTRON MICROSCOPE-MICROPROBE ANALYSIS OF PRECIPITATION¹⁷

R. E. Gehlbach

Understanding the role of microstructure in mechanical and physical properties of alloy systems necessitates the identification of precipitated phases occurring in these materials. We found that an electron probe microanalyzer accessory to the electron microscope, used in conjunction with standard electron microscope specimens, provides the means for obtaining a quick and reliable analysis of individual precipitate particles. The uniqueness of this tool is apparent when extraction replicas are used, permitting without matrix interference chemical analysis along with usual electron microscopy and diffraction of individual particles (1) in the same spatial distribution as the bulk material, (2) of the thin dendritic morphology often present in grain boundaries, (3) of a size or distribution too fine to be resolved by conventional microprobe techniques, and (4) in quantities not detectable by x-ray diffraction analysis of extraction residues.

In applying this tool to our research problems, we have made observations that would not have been possible without the use of this type of microanalyzer. For example, the fine carbide precipitating in grain boundaries of Hastelloy N on aging is the η_2 type instead of the η_1 type that is present in the matrix, although the lattice parameters of both these M_6C -type carbides are indistinguishable. Of more significance, silicon appears to play a major role in the formation of precipitate particles commonly identified as carbides. We identified precipitates containing elements having a deleterious effect on properties, such as sulfides. We were also successful in determining and identifying oxidation and corrosion products.

PREPARATION OF TRANSMISSION ELECTRON MICROSCOPY SPECIMENS FROM TUBING¹⁷

C.K.H. DuBose C. Jones

The application of transmission electron microscopy to engineering materials requires techniques for preparing specimens from intricate structures. Suitable flat tabs can be cut or ground from massive pieces and thinned by standard techniques, but small-diameter,

¹⁷Abstract of a paper presented at the 22nd AEC Metallography Group Meeting at San Diego, Calif. on June 19-21, 1968 (to be published in the Proceedings).

thin-walled tubing presents special problems that can not be handled in this way. We describe modifications to the ORNL jet polishing technique that enable good specimens to be prepared from tubing rapidly and reliably using a minimum of material.

The tube is first sectioned into small pieces that can be accommodated in the electron microscope by the following procedure, which was devised to prevent deformation of the tube during cutting. A rod is inserted in a short length of the tubing to give a snug fit, and a slitting saw is used to make longitudinal cuts spaced about $\frac{1}{8}$ in. apart on the circumference of the tubing. A band about $\frac{1}{4}$ in. long at one end of the tube is left unslitted to keep the tubing attached to the rod. The tubing-rod composite is then sliced into $\frac{1}{8}$ -in. lengths to produce curved tubing sections roughly $\frac{1}{8}$ in. square. A fixture that allows accurate location of the slits can be used for remote operation.

Jet polishing is then used to prethin or dimple these pieces. The inner contour can be retained in the dimple

by proper selection of the current density. The outer contour can not be maintained as accurately, but flat-bottomed dimples can be produced. Final thinning until a hole forms in the dimpled region is done in a polishing cell equipped with a light source and a photocell detector.¹⁸

Special features of a glove-box facility for thinning alpha-contaminated materials are described along with modifications to the specimen holder to allow it to accept curved pieces.

The use of this technique is illustrated with examples of the microstructures of a fuel pin irradiated in EBR-II and a target hex-sheath irradiated in HFIR, both to fast-neutron fluences in excess of 10^{22} neutrons/cm².

¹⁸C.K.H. DuBose and J. O. Stiegler, *Semiautomatic Preparation of Specimens for Transmission Electron Microscopy*, ORNL-4066 (February 1967).

6. Electronic Properties of Metals and Alloys

J. O. Betterton, Jr.

Our main objectives were the study of transition metal alloys and of radiation defects in Fe-Al alloys and the purification of the metals zirconium and hafnium for galvanomagnetic studies. Low-temperature specific heat experiments with the ceramic material UN, with the magnetic material holmium, and with the superconducting materials cubic Zr-Nb and Zr-N are starting. The program on low-temperature specific heats of zirconium with small alloying additions is now ending. Mössbauer research continues with studies of ^{61}Ni in Cu-Ni alloys and of ^{58}Fe in ordered Fe-Al alloys.

MÖSSBAUER MEASUREMENTS WITH ^{61}Ni IN THE COPPER-NICKEL SYSTEM

John C. Love¹ Gordon Czjzek Felix E. Obenshain²

Several advances in technique for measuring the Mössbauer resonance of the 67.4-keV gamma transition of ^{61}Ni were made, and the studies of the resonance in nickel alloys are in progress. The results for the copper-nickel alloys are discussed here.

The major technical difficulty has been the preparation of a suitable nonmagnetic source. The nature of the problem and our solution has been discussed.³ Briefly, we found that Ni-14 at. % V highly enriched in ^{64}Ni is nonmagnetic at 4.2°K and may be used directly following bombardment with 22-MeV protons. The reaction $^{64}\text{Ni}(p,\alpha)^{61}\text{Co}(\beta)^{61}\text{Ni}$ populates the first excited state of ^{61}Ni with 100% efficiency. Since the beta decay half-life is only 99 min, the data-collection time is severely limited. The gamma counting equipment has been improved so that data may be collected at about 10^5 counts/sec in the 67.4-keV line with a negligible decrease in resolution in the gamma spectrum. For these experiments we used a multiscaler Mössbauer spectrometer that accepts these high counting rates and

can measure energy shifts of the nickel resonance line to a precision of ± 0.001 mm/sec (and to an order of magnitude better than that for the ^{57}Fe resonance, which is used for calibration).

The linear dependence on concentration exhibited by several magnetic properties of the copper-nickel system has often been cited as evidence favoring a simple rigid-band model. These elements are neighbors in the periodic table and form substitutional solid solutions throughout the concentration range with no change in crystal structure and only a small change in lattice parameter for all concentrations of the system from that of pure nickel (3.517 Å) to the value for pure copper (3.608 Å). The saturation magnetic moment per atom and the Curie temperature decrease linearly with copper concentration over most of the pertinent range of composition and extrapolate to zero at 53 and 57 at. % Cu, respectively. The spectroscopic g factor for nickel in the alloys was independent of composition and equal to that of pure nickel. Thus, the average number of uncompensated spins per atom of the alloy is a linear function of composition.⁴

A well-known interpretation of these properties is the rigid-band model. This model suggests that the outer electronic states of the copper and nickel atoms in the alloy share common d bands and common $s-p$ conduction bands, which overlap in energy. For pure nickel, the $3d$ subband (all $3d$ states with the same spin) has approximately 0.6 hole per atom. The rigid-band model further suggests that the $4s-p$ electrons are donated by the copper and progressively fill the holes in the partially empty $3d$ subband as the copper concentration is increased. This provides a very simple explanation for the disappearance of ferromagnetism in the alloys at about 60% Cu. Since the isomer shift of the Mössbauer absorption line is proportional to the total electronic charge density $\rho(0)$ within the nuclear

¹Oak Ridge Graduate Fellow from Ohio State University under appointment with Oak Ridge Associated Universities.

²Physics Division.

³F. E. Obenshain, J. C. Love, and G. Czjzek, *Phys. Div. Ann. Progr. Rept. Dec. 30, 1967*, ORNL-4230, pp. 35-39.

⁴J. Crangle, "The Intrinsic Magnetic Properties of Transition Elements and Their Alloys," pp. 51-68 in *Electronic Structure and Alloy Chemistry of the Transition Elements*, ed. by P. Beck, Interscience Publishers, London, 1963.

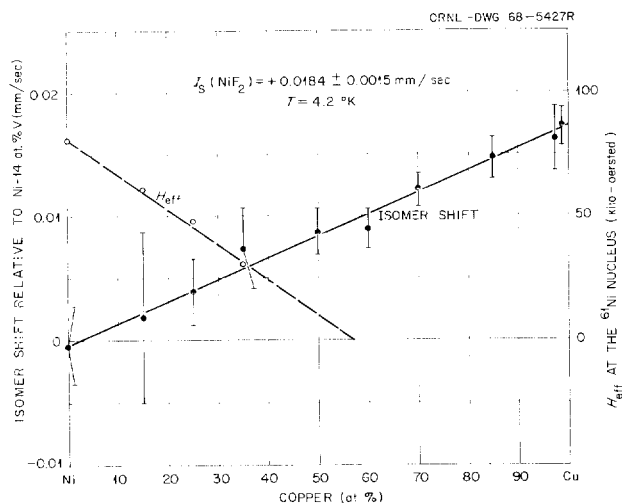


Fig. 6.1. The Energy Shift and Magnetic Hyperfine Field at the ^{61}Ni Nucleus in the Copper-Nickel Series of Alloys.

volume, one may expect to test this model by observing the isomer shift as a function of concentration. One expects to see a nonlinear dependence of the isomer shift on concentration, possibly a break in the slope near 60% Cu, if there is in fact a transfer of s to d character of the conduction electrons.

Our measurements of the energy shift and the magnetic splitting (as represented by an effective magnetic field H_{eff} at the nucleus) for the ^{61}Ni resonance are displayed as a function of alloy concentration in Fig. 6.1. To eliminate temperature shifts, source and absorber were immersed in a common liquid helium bath. Both the observed shift and H_{eff} can be well represented by linear functions of composition.

The entire range of shifts is only about 1/40 of the minimum observable line width $2\Gamma_0 = 0.77$ mm/sec, and it may be explained by the change in the zero-point energy of the nickel as a function of alloy concentration. The Debye model yields an approximate expression for the velocity shift due to a difference in zero-point energy, which leads to a change of 78°K in the Debye temperature for the observed shifts if one assumes no change in $\rho(0)$. A more detailed comparison with phonon spectra for copper and nickel also indicates that the change in $\rho(0)$ is very small. These results indicate that the rigid-band model does not provide an adequate description of the electronic structure of these alloys⁵ or that $\rho(0)$ is not related in such a simple way to the band structure and other effects must be considered.

The effective magnetic field at ^{61}Ni decreases linearly from $H_{eff} = 80$ kilo-oersteds for nickel and extrapolates to zero for 57 at. % Cu in Ni. These measurements

and others that we have made for the iron-nickel and cobalt-nickel systems show that H_{eff} for ^{61}Ni generally follows a Slater-Pauling dependence for alloys of nickel with $3d$ transition metals.

RADIATION EFFECTS IN ORDERED IRON-ALUMINUM ALLOYS: MÖSSBAUER EXPERIMENTS FOLLOWING NEUTRON CAPTURE⁶

W. G. Berger⁷ G. Czjzek

We have taken Mössbauer spectra with ^{57}Fe in ordered iron-aluminum alloys with the 14.4-keV level populated by thermal-neutron capture in ^{56}Fe . The capture process is followed by emission of high-energy γ rays, which impart recoil energies between about 100 and 545 eV to the ^{57}Fe nuclei. These energies are well above the displacement threshold; therefore the Mössbauer γ rays are originating from nuclei that have certainly been displaced from their lattice positions.

Comparison of the Mössbauer spectra obtained in this way with spectra taken with the same materials used as resonance-absorbers gave the following results. In alloys with 35 to 52 at. % Al (FeAl order, paramagnetic), the center of the (n,γ) -Mössbauer line is shifted towards lower energy by an amount that depends on the aluminum concentration. In a specimen with 26 at. % Al (Fe_3Al order, ferromagnetic), the (n,γ) -spectrum is qualitatively different from the absorption spectrum. At most a small fraction of the displaced nuclei can be in positions equivalent to normal iron lattice sites in Fe_3Al . Analysis of the data leads us to the conclusion that the final positions of the recoiled nuclei are either interstitial positions or lattice positions in close association with several point defects.

Experiments at temperatures between 80 and about 750°K are in progress to give information about the stability and the type of defects involved.

⁵ Recently, N. D. Lang and H. Ehrenreich, *Phys. Rev.* **168**, 605 (1968), have considered the dependence on pressure of the Curie temperature of nickel and the copper-nickel alloys. The rigid-band model yielded poor results for the copper-nickel alloys, but they obtained good agreement with experiment for a "minimum polarity" model according to which the number of d holes per Ni atom stays constant at all concentrations. Our results would support this conclusion.

⁶ Research performed by W. G. Berger and G. Czjzek while Czjzek was on a one-year research assignment at Kernforschungszentrum Karlsruhe, Institut für Angewandte Kernphysik, Karlsruhe, Germany.

⁷ Kernforschungszentrum Karlsruhe, Institut für Angewandte Kernphysik.

SPECIFIC HEAT OF URANIUM MONONITRIDE FROM 1.3 TO 4.6°K (Ref. 8)

J. O. Scarbrough H. L. Davis⁹
W. Fulkerson¹⁰ J. O. Betterton, Jr.

The atomic heat of uranium mononitride was measured from 1.3 to 4.6°K and found to be of the form $\gamma T + \beta(T/\theta_D)^3$, where γ was 24.79 ± 0.05 mj gram-atom⁻¹ deg⁻², the Debye temperature θ_D was $324 \pm 7^\circ\text{K}$, and $\beta = 12\pi^4 R/5$ ($R =$ gas constant). The large value of γ (35 times the value for copper) apparently results from the Fermi surface intersecting narrow $5f$ electronic bands. The above values refer to a UN sample heat treated in nitrogen for 6.5 hr at 2250°C. The same sample before this heat treatment had a measured $\gamma = 24.07 \pm 0.08$ mj gram-atom⁻¹ deg⁻² and $\theta_D = 322 \pm 13^\circ\text{K}$. The shift in γ may be due to a small change in stoichiometry caused by the heat treatment.

Although the Debye temperature obtained from the present work, 324°K, disagrees with previous specific heat estimates of 276 to 289°K, it does agree fairly well with the value 347 to 362°K obtained from room-temperature velocity-of-sound measurements.

No changes were observed in the specific heat upon application of magnetic fields up to 35 kilogauss, suggesting the absence of any appreciable magnetic contribution to the total specific heat for temperatures below 4.7°K.

PURIFICATION OF ZIRCONIUM AND REFRACTORY METALS IN AN ULTRAHIGH-VACUUM ZONE REFINER WITH ANALYSIS OF PARTIAL PRESSURES¹¹

D. S. Easton J. O. Betterton

An electron-beam zone refiner has been developed to produce high-purity zirconium and other metals for use in high-field galvanomagnetic studies. A quadrupole gas analyzer monitored the environment during zoning. We measured resistance ratios ($R_{300^\circ\text{K}}/R_{4.5^\circ\text{K}}$) and applied other analytical methods to provide indications of purity levels. A successful zone refining of zirconium from oxygen was accomplished by use of large numbers of zone passes. The low partial pressures in the system made these lengthy operations possible without contamination from the environment. Resistivity ratios of up to 1300 in zirconium were achieved.

⁸ Abstract of paper submitted to *Physical Review*.

⁹ Theory Group.

¹⁰ Fundamental Ceramics Studies Group.

¹¹ Abstract of paper for presentation at the Electrochemical Society Meeting, Boston, May 5, 1968.

PREPARATION AND ZONE PURIFICATION OF HAFNIUM METAL WITH LOW ZIRCONIUM CONTENT¹²

D. S. Easton J. O. Betterton

Iodide hafnium¹³ was zone refined in a 5×10^{-11} -torr vacuum, increasing the resistance ratio from 31 to 300. Partial pressure analysis with a mass spectrometer showed extensive outgassing of H₂, CO, CO₂, CH₄, and C₂ and C₃ hydrocarbons. The final resistance ratio was dominated by the 0.15 at. % Zr impurity, which did not zone-separate or evaporate. This means that remaining impurities, mainly oxygen and carbon, were about 0.004 at. % in the purest part of the zone-refined bar. This purification was supported by the decrease in hardness (150 to 90 DPH) and by the very low pressures observed over the liquid metal in the final stages of zone refining. Further improvements in the resistance ratio of hafnium will depend on lowering the zirconium content of the initial material.

ELECTRICAL RESISTIVITY OF ZIRCONIUM ALLOYS

J. O. Betterton D. S. Easton

Resistivities of zirconium alloys in the temperature range 4 to 300°K vary in the following manner. With solutes to the left of zirconium and in the same column of the periodic table, the compositional dependence is near $Ax(1-x)$ where $x =$ atomic fraction solute. There is near agreement with Matthiessen's rule that the temperature dependence of the alloy resistivity is independent of composition. Solutes of this type, of which Sc, Ti, and Hf were tested, produce relatively small increases in resistivity, as shown in Fig. 6.2. The second class of solutes, with positions to the right of zirconium in the periodic table and with greater numbers of valency electrons, behave differently. Here the alloying resistivity rises to a high maximum on the zirconium-rich side of the system. Also the resistivity increases for 1 at. % solute are much larger, Matthiessen's rule is not obeyed, and the actual resistivity of many of these alloys decreases with increase in temperature. In alloys such as Zr-5 at. % Ru and Zr-15 at. % In, the effect is so strong that these alloys are

¹² Abstract of paper to be presented at the Symposium on Preparation and Purification of Ultrapure Metals, Electrochemical Society, Montreal, Canada, Oct. 6 to 11, 1968.

¹³ Purity given by the following contents (at. %): 99.7 Hf, 0.15 Zr, 0.04 C, 0.04 H, 0.01 each of Fe, Si, Al, and O; and 0.2 sum of remaining impurities.

Table 6.1. Effect of Temperature on Resistivity of Zirconium Alloys

Temperature (°K)	Resistivity ($\mu\text{ohm-cm}$)						
	Pure Zirconium	Alloys with Same or Fewer Electrons Per Atom ^a			Alloys with More Electrons Per Atom ^a		
		Zr-10 Hf	Zr-10 Ti	Zr-10 Sc	Zr-15 In	Zr-15 Nb	Zr-5 Ru
300	42.3	46.4	58.5	62.5	169	106	115
4.2	0.1	4.1	12.2	22.1	175	105	111

^aCompositions in atomic percent.

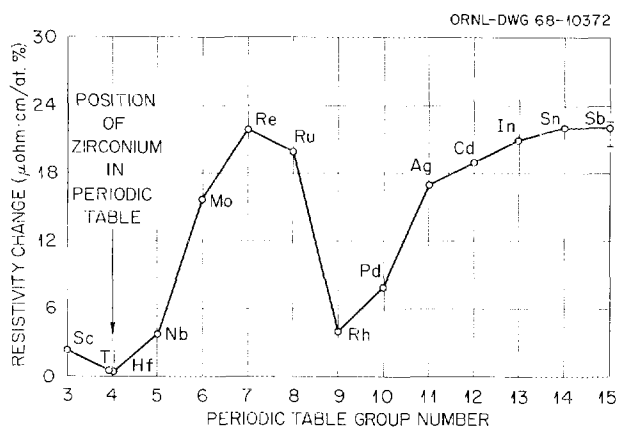


Fig. 6.2. Change in Resistivity Per Atomic Percent Solute Plotted Against Group Number of Solute for Dilute Zirconium Alloys at 4.2°K.

temperature-independent resistors. These temperature effects are illustrated in Table 6.1.

Although a complete interpretation of the above effects is not available, the resistivity results suggest that virtual d -band states are involved in a manner similar to that proposed by Friedel¹⁴ to explain similar resistivity changes in copper and aluminum alloys. For the solutes with more electrons, the effects shown in Fig. 6.2 appear to indicate that a single virtual state forms at various energies near the Fermi surface for various solutes. The other excess electrons are apparently bound to the solute at considerably lower energies. For the solutes with the same number or fewer electrons per atom than zirconium, the virtual bound states are absent, and only the smaller effects from atomic potential differences and interband transitions are observed in these alloys.

¹⁴J. Friedel, *Can. J. Phys.* 34, 1190 (1956).

LOW-TEMPERATURE SPECIFIC HEATS OF ZIRCONIUM WITH 0 TO 5% ADDITIONS OF Nb, Mo, Re, Ru, Rh, AND Pd

J. O. Betterton J. O. Scarbrough

In the approximation that the conduction electrons are independent, the electronic specific heat coefficient γ is equal to $\frac{2}{3} \pi^2 k^2 N(E_f)$ where $N(E_f)$ is the density of electronic states at the Fermi surface. As discussed by Krebs¹⁵ and Clogston,¹⁶ a similar formula relates the linear specific heat coefficient to the density of electronic states of an electron gas where there is an electron-phonon interaction. The electron-phonon interaction in zirconium has been estimated by the isotope effect in the superconductivity,¹⁷ and the phonon enhancement may be appreciable in pure zirconium.¹⁸ However, we assume that the phonon enhancement factor does not change for alloying 0 to 5 at. % of the various solutes below. This assumption is partly justified by the experimental observation that the interaction V in the BCS superconductivity formula, $T/\theta_D = \exp[-1/N(E_f)V]$, is approximately constant throughout these alloys. Knowing that the difference in the attractive electron-phonon interactions and the repulsive screened Coulomb and exchange interactions remains the same, the assumption that both interactions are nearly constant with alloying seems more plausible than to assume equal and opposite changes in the interactions.

¹⁵K. Krebs, *Phys. Letters* 6, 31 (1963).

¹⁶A. M. Clogston, V. Jaccarino, and Y. Yafet, *Phys. Rev.* 134, A650 (1964); A. M. Clogston, *Phys. Rev.* 136, A8 (1964).

¹⁷E. Bucher, J. Muller, J. L. Olsen, and C. Palmy, *Phys. Letters* 15, 303 (1965).

¹⁸J. O. Betterton, Jr., and J. O. Scarbrough, *Phys. Rev.* 168, 715-25 (1968).

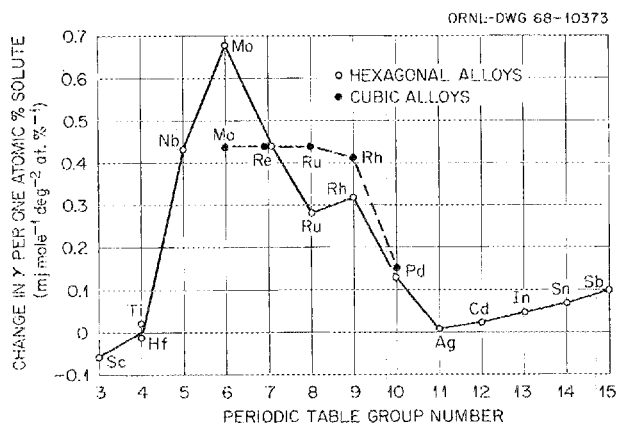


Fig. 6.3. Change of Electronic Specific Heat Coefficient Per Atomic Percent Solute in Zirconium-Rich Alloys Plotted Against Group Number of Solute.

The changes in γ per atomic percent addition of various solute elements to zirconium are very dependent upon the position of the solute elements in the periodic table, as is shown by Fig. 6.3. The solid curve represents the change of the electronic specific heat coefficient in hexagonal alloys. The body-centered cubic phase¹⁹ is retained in the alloys of zirconium with more than 1 to 2% Mo, Re, Ru, or Rh. For the

cubic alloys, the changes in γ per atomic percent solute are given by the dashed curve in Fig. 6.3. Earlier measurements of the effects of other elements^{18,20} in hexagonal zirconium are included in Fig. 6.3 to illustrate zirconium alloying more fully. Like in the resistivity increments in Fig. 6.2, a large increase in γ occurs with solutes from groups 5 to 9, in agreement with the apparent formation of virtual-bound states in these alloys. The main difference between the two curves is in the large extra alloying resistivity with the B-subgroup solutes of groups 11 through 15, which have a filled 4d-shell on the ion and which have no correspondingly large increase in γ during the same alloying. Alloys with solutes to the left and in the same column as zirconium in the periodic table and with B-subgroup elements have relatively small γ effects, related to the band structure of the solvent and reflecting changes in the average number of electrons per atom.

¹⁹A small amount of omega phase, with complex hexagonal structure, forms in these retained cubic alloys, and we are neglecting this in the present discussion.

²⁰G. D. Kneip, Jr., J. O. Betterton, Jr., and J. O. Scarbrough, *Phys. Rev.* 131, 2425-32 (1963).

7. Fundamental Ceramics Research

W. Fulkerson

The Fundamental Ceramics Research Program has been established to encourage a more coordinated effort of basic ceramics research in the Metals and Ceramics Division. Uranium mononitride, a potentially important fast reactor fuel, has been selected as a basis material for achieving this coordination. By concentrating on one material the efforts of various groups specializing in particular types of research, we can get a good overall understanding of this important nuclear fuel and, at the same time, provide a basis for mutual interest between the groups to stimulate more exchange of information and ideas. For example, there is a close liaison between this program and the Nitride Fuel Development Program (Part III, Chapter 18 of this report). Most of the specimens used in this work have been supplied through the courtesy of the Ceramics Technology Group, and there has been a cross fertilization of ideas for pertinent basic and applied research between the two programs.

Uranium mononitride is interesting not only because it is an important nuclear fuel but also because it is a member of an increasingly important class of materials, the refractory hard metals, which also include other isomorphous nuclear fuels such as UC, US, and UP as well as HfC and ZrC, the materials with the highest known melting points. These compounds are brittle and hard at ordinary temperatures, but they exhibit electrical conductivity characteristic of a metal. More fundamental information about this class of materials is needed before the full technological potential of the class can be realized. The philosophy of this program is that if an understanding of one member of the group is achieved, then obtaining an understanding of the whole class will become much easier. Indeed it is difficult to see how the class can be understood generally unless at least one member is thoroughly investigated.

In addition to the work reported below on transport properties and on the velocity of sound, a significant amount of the UN research that has been started as a result of this program is reported in other chapters of this report. Preliminary first-principals band theory calculations, which are reported in Chapter 13, indicate

that narrow $5f$ bands are near or at the Fermi energy. This is qualitatively corroborated by a very high density of states deduced from low-temperature specific heat measurements (Chapter 6). The self-diffusion of ^{233}U in UN as a function of nitrogen pressure and temperature is reported in Chapter 4. This information should be valuable in interpreting the mechanical behavior of UN, such as the compressive creep, the measurement of which has been initiated (Chapter 8) as a prelude to studying the rate and mechanism of dislocation motion. In-reactor measurements of fission gas release and of the effect of irradiation on the thermal diffusivity are in progress in the Reactor Chemistry Division.¹

The success of this research depends, of course, on the availability of high-quality, well-characterized specimens of suitable size and configuration. For this reason the Ceramics Technology Group is improving the quality of pressed and sintered materials and the Crystal Physics Group is preparing to grow controlled single crystals by an arc-melting technique.

TRANSPORT PROPERTIES OF UN

J. P. Moore² W. Fulkerson
D. L. McElroy²

The thermal conductivity (80 to 400°K), electrical resistivity (4.2 to 400°K), and absolute Seebeck coefficient (6 to 400°K) were measured on a pressed and sintered 98.6%-dense UN rod. The measurements between 77 and 400°K were made with the ORNL absolute longitudinal heat flow apparatus³ with probable errors of 1.2, 0.4, and 1.1% for the three properties, respectively. These data together with literature values for the thermal conductivity and electrical resistivity at higher temperatures were used to try to separate the electrical and lattice portions of the thermal conductivity. The results, although somewhat ambiguous,

¹R. M. Carroll and J. G. Morgan, Reactor Chemistry Division.

²Physical Properties Group.

³J. P. Moore, D. L. McElroy, and R. S. Graves, *Can. J. Phys.* 45, 3849-65 (1967).

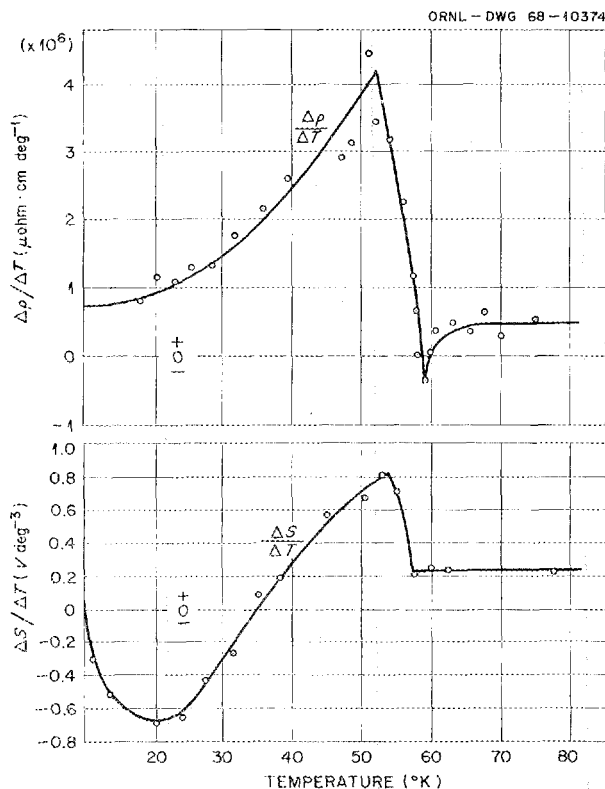


Fig. 7.1. The Temperature Coefficients of Electrical Resistivity and Absolute Seebeck Coefficient in the Vicinity of the Antiferromagnetic-to-Paramagnetic Transformation.

indicate that the lattice conductivity peaks in the range 200 to 500°K and that the high-temperature limit of the Lorenz function is greater than the Sommerfeld value of $2.443 \times 10^{-8} \text{ (v/deg)}^2$, perhaps by as much as 30%. Further measurements at higher temperatures will be necessary to verify the higher Lorenz function. The peaking in the lattice thermal conductivity is undoubtedly due to the scattering of phonons by spin disorder in analogy to the situation in UO_2 , which also undergoes an antiferromagnetic-to-paramagnetic transformation at low temperatures.⁴

The electrical resistivity and the absolute Seebeck coefficient exhibit a sharp change in slope in the vicinity of the Néel point, as is shown in Fig. 7.1. The resistivity ρ below the Néel point may be fitted by the expression

$$\rho = 7.5 + 6.15 \times 10^{-3} T^{2.38} \text{ } \mu\text{ohm}\cdot\text{cm}, \quad (1)$$

where the temperature-dependent term is thought to be

⁴O. Béthoux, P. Thomas, and L. Weil, *Compt. Rend.* 253, 2043 (1961).

predominantly magnetic in origin. The Seebeck coefficient goes through a minimum at 33°K and then rises again to a local maximum at 10°K. This low-temperature peak is probably due to magnon drag.

Even above the Néel point the electrical resistivity continues to rise rapidly but at a decreasing rate until at high temperatures the ρ vs T function becomes nearly linear. If this linear behavior is interpreted as being due to the usual electron-phonon scattering in a metal, then the magnetic contribution can be separated out. If we further assume that the magnetic resistivity is roughly proportional to the magnetic entropy⁵ (because the magnetic resistivity is due to spin disorder scattering and the entropy is a measure of this disorder), we can deduce that the magnetic specific heat $C_{p \text{ mag}}$ is

$$C_{p \text{ mag}} \propto T \frac{d\rho_{\text{mag}}}{dT}. \quad (2)$$

The proportionality constant is determined by assuming that $C_{p \text{ mag}}$ is equal to the difference between the extrapolation of the low-temperature specific heat of Scarbrough *et al.* (Chapter 6 of this report) and the normalized average data at 14.1°K of Westrum and Barber⁶ and of Counsell *et al.*⁷ The temperature dependence of $C_{p \text{ mag}}$ thus obtained is shown in Fig. 7.2. The large high-temperature tail is particularly important since the magnetic entropy obtained from this phenomenological analysis was $0.63 \text{ cal deg}^{-1} \text{ mole}^{-1}$ with about two-thirds of the total occurring above the Néel temperature. This is to be compared with a value of only 0.15 deduced by Counsell *et al.*⁷ by assuming that the $C_{p \text{ mag}}$ was zero above the Néel point. The large tail on $C_{p \text{ mag}}$ is not unreasonable judging from the results^{8,9} on other magnetic compounds such as UO_2 and CrBr_3 . The subtraction of $C_{p \text{ mag}}$ from the total specific heat values yields a smooth curve for the remainder even through the Néel point region.

⁵W. Fulkerson, J. P. Moore, and D. L. McElroy, *J. Appl. Phys.* 37, 2639-53 (1966). Note that the proportionality, Eq. (2), must fail in detail at or near the Néel point since for a 2 or 3° range $d\rho_{\text{mag}}/dT$ is negative, as shown in Fig. 7.1.

⁶E. F. Westrum, Jr., and C. M. Barber, *J. Chem. Phys.* 45, 635 (1966).

⁷J. F. Counsell, R. M. Dell, and J. F. Martin, *Trans. Faraday Soc.* 62, 1 (1966).

⁸D. W. Osborne and E. F. Westrum, Jr., *J. Chem. Phys.* 21, 1884 (1953).

⁹L. D. Jennings and W. N. Hansen, *Phys. Rev.* 139, A1694 (1965).

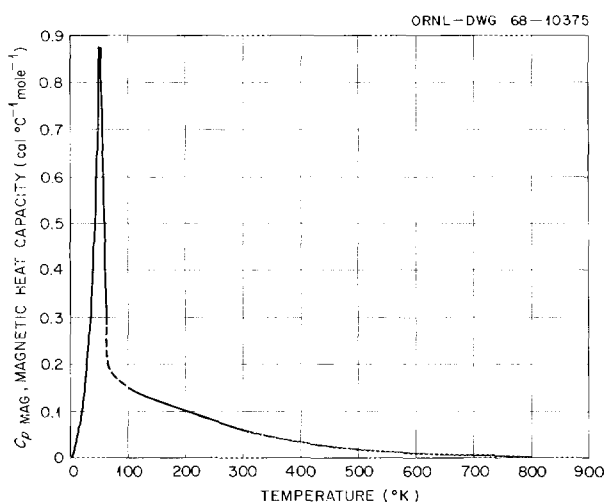


Fig. 7.2. The Magnetic Specific Heat of UN as Deduced from the Magnetic Electrical Resistivity.

ELECTRICAL RESISTIVITY OF U(C,N)

C. V. Dodd¹⁰ J. M. Leitnaker¹¹
 R. A. Potter¹¹ J. P. Moore²
 W. Fulkerson

Recently, Ohmichi and Kikuchi¹² found that the electrical resistivity of U(C,N) solid-solution alloys of compositions ranging all the way from pure UN to pure UC was considerably lower than would be obtained if a Vegard-type law existed for resistivity. Of course, the normal behavior for an alloy is that the resistivity will be higher than a linear combination of the pure component resistivities, so the behavior of U(C,N) is anomalous. We verified the phenomenon at room temperature for nearly equimolar alloys and estimate the resistivity of theoretically dense UN_{0.55}C_{0.45} to be about 30% below the linear combination result. Furthermore, neutron diffraction showed no long-range ordering of the nitrogen or carbon atoms.¹³

A possible explanation for this anomaly is that the large magnetic resistivity component of UN is somehow reduced more by the addition of UC (UC is weakly paramagnetic at all temperatures) than the total resistivity is increased by random impurity scattering. A similar anomaly has been observed near the Néel point

due to alloying chromium with certain elements.¹⁴ Interestingly, the thermal conductivity does not show the same anomaly, and this apparently indicates (assuming that the Lorenz function is not reduced by alloying) that the lattice portion of the thermal conductivity (more than 50% of the total at room temperature for UN) is not increased above a linear combination of the pure component values.

ULTRASONIC VELOCITY MEASUREMENTS IN UN

H. L. Whaley¹⁰ R. A. Potter¹¹
 W. Fulkerson

Longitudinal and shear ultrasonic velocity measurements at 5 MHz have been made at room temperature on four pressed-and-sintered UN specimens ranging in density from 92.8 to 98.5% of theoretical. The uncertainty of the measurements, which were by a pulse-echo technique, was estimated to be about 1%. The velocity results are given in Table 7.1 and divide themselves into two groups, with the two lower density specimens giving velocities lower than those for the higher density specimens but identical to each other. These results do not lead to an unambiguous conclusion about the effect of porosity on velocity and they indicate that some specimen difference besides density is important.

Table 7.2 shows the elastic constants calculated on the basis of the two sets of measured velocities and the theoretical density of UN, 14.32 g/cm³. Also given in Table 7.2 are various estimates of the Debye temperature, θ_D , θ_M , and θ_V . The values θ_D and θ_M were calculated from elastic constants by the formula by James¹⁵ and correspond to specific heat and x-ray measurements, respectively. The value of θ_V was

¹⁴A. L. Trego and A. R. Mackintosh, *Phys. Rev.* 166, 495 (1968).

¹⁵R. W. James, *Theoretical Principles of the Diffraction of X-rays*, G. Bell and Sons, Ltd., London, 1948.

Table 7.1. Ultrasonic Velocities for UN Specimens of Different Density

Density (% of theoretical)	Ultrasonic Velocity (cm/sec)	
	Longitudinal	Shear
	× 10 ⁵	× 10 ⁵
92.8, 95.0	4.52	2.57
97.0, 98.5	4.75	2.64

¹⁰Nondestructive Testing Group.

¹¹Ceramics Technology Group.

¹²T. Kikuchi, Japan Atomic Energy Research Institute, Tokai Establishment, private communication, Oct. 19, 1967.

¹³W. C. Koehler, Solid State Physics Division, private communication, Feb. 28, 1968.

Table 7.2. Elastic Constants and Debye Temperatures Calculated for Theoretically Dense UN from Ultrasonic Velocity Data

	Poisson's Ratio, σ	Elastic Moduli (dynes/cm ²)			Debye Temperature (°K)		
		Young's	Shear	Bulk	θ_D	θ_M	θ_V
Set I ^a	0.26	2.39×10^{12}	0.95×10^{12}	1.66×10^{12}	347	357	349
Set II ^b	0.27	2.59×10^{12}	1.00×10^{12}	1.88×10^{12}	362	372	359

^aCalculated from velocities measured for the 92.8 and 95.0%-dense samples.

^bCalculated from velocities measured for the 97.0 and 98.5%-dense samples.

calculated directly from the velocities of sound.¹⁶ These values of the Debye temperature 347 to 372°K should be compared with the values of $324 \pm 7^\circ\text{K}$ obtained by Scarbrough *et al.* (see Chapter 6 of this report) from low-temperature specific heat measurements. Although the measurements were taken at different temperatures, the usual thermal expansion correction to the Debye temperature would only be about 1%, and the agreement between the results is reasonable. Furthermore, since 5 MHz is about one-millionth the Debye frequency, the velocity measure-

ments should correspond to the long-wavelength harmonic portion of the frequency spectrum, just as low-temperature lattice specific heat should be indicative of this harmonic region. The agreement between the two results is not as close as that obtained for the similar compound UC, for which values of 330 and 320 were obtained from elastic constants and specific heat measurements, respectively.¹⁷ Further velocity measurements on UN, especially at temperatures below the Néel point, seem warranted.

¹⁶O. L. Anderson, "Determination and Some Uses of Isotropic Elastic Constants of Polycrystalline Aggregates Using Single Crystal Data," p. 43 in *Physical Acoustics*, Vol. III, Part B, W. P. Mason, ed., Academic Press, New York, 1965.

¹⁷L. G. Graham and R. Chang, "The Elastic Properties of Uranium Carbide Between 4.2 and 300°K," pp. 409-422 in *Intern. Symp. Compounds of Interest in Nucl. Reactor Technol.*, Boulder, Colo., 1964, *Nucl. Met.*, Vol. 10, American Institute of Mining, Metallurgical, and Petroleum Engineers, New York, 1964.

8. Physical Ceramics Studies

C. S. Morgan

These studies are aimed at improving the basic understanding and practical technology of solid state processes in ceramics through investigation of the mechanisms of deformation and sintering. To better interpret deformation and sintering studies in ThO_2 , we investigated diffusion of thorium in ThO_2 . The diffusion studies cast doubt that volume diffusion transport of material plays a significant role except in very long-term processes. Topological studies of sintering are intended to implement the means of describing sintering masses and to clarify the application of topological concepts in metallurgy.

DEFORMATION OF URANIUM DIOXIDE SINGLE CRYSTALS¹

C. S. Yust C. J. McHargue

Single crystals of uranium dioxide, grown in this division by the Internal Centrifugal Zonal Growth technique,² were deformed in compression to nominal strains of 1 and 5%. The crystals were oriented to promote slip on only one slip system of the family $\{100\}\langle 110\rangle$. The strain rate and temperature ranges studied were 10^{-3} to 10^{-1} /min and 750 to 1400°C. The dislocation density of the as-grown crystals was $2 \times 10^6/\text{cm}^2$. Sections of the deformed specimens cut both parallel and perpendicular to the slip planes were examined by transmission electron microscopy. The dislocation substructures at a strain of 1% consisted of numerous dipoles and dipole loops, the edge components of the dipoles lying along $\langle 110\rangle$ directions. A typical dislocation configuration at 1% strain is shown in Fig. 8.1. At 5% strain extensive dislocation tangles were present as well as the dipole configurations, as shown in Fig. 8.2. In the dislocation arrangements we noted particular features that can be related to several of the theories of dipole formation,

but no definitive statement as to the mechanism of formation of the dipoles in UO_2 can be made. However, these results present the first detailed electron microscope observations of dislocations in deformed uranium dioxide.

The critical resolved shear stress on the $\{100\}\langle 110\rangle$ slip system was measured as a function of temperature, as was the variation in the appearance of the load-deflection curve with temperature level. Of particular interest is the markedly serrated load-deflection behavior observed at 1150°C and the minimum in the shear stress curve at 950°C. Both of these effects can be rationalized in terms of impurity effects on the charge of the dislocations.

The dislocation density as a function of strain was determined from the electron micrographs by counting the intersections of the dislocation images with a series

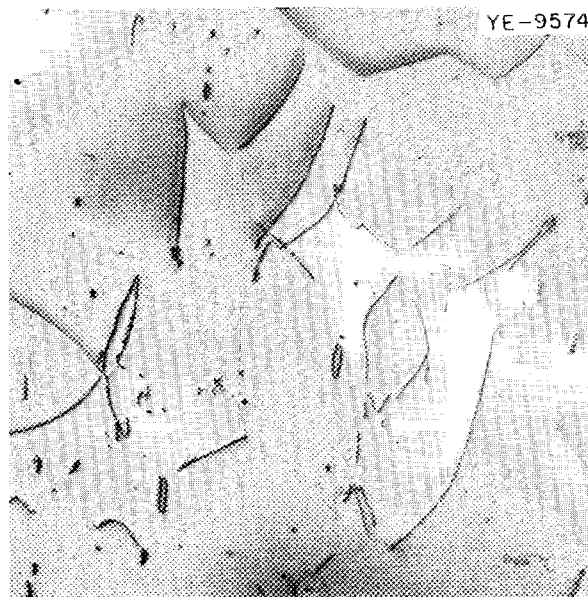


Fig. 8.1. A Typical Dislocation Configuration on a Slip Plane in Deformed Single-Crystal UO_2 at 1% Strain. The deformation strain rate and temperature were, respectively, 1.4×10^{-3} /min and 1150°C. 10,000X.

¹ Abstracted from paper to be submitted for publication.

² A. T. Chapman and G. W. Clark, "Growth of UO_2 Single Crystals Using the Floating-Zone Technique," *J. Am. Ceram. Soc.* 48, 494-95 (1965).

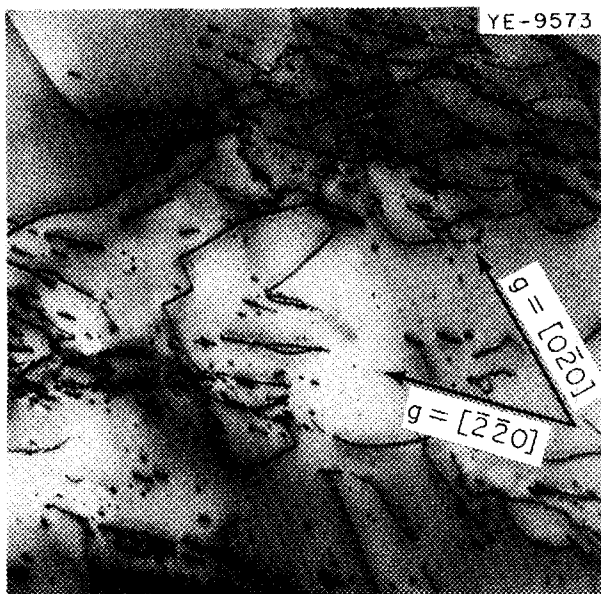


Fig. 8.2. The Dislocation Configuration on a Slip Plane in Deformed Single-Crystal UO_2 at 5% Strain. The deformation strain rate and temperature were, respectively, $5.6 \times 10^{-3}/\text{min}$ and 1150°C . 10,000X.

of concentric circles. An estimate of the thickness of the observed foil is required to determine the density of dislocations, and the results of several techniques indicated that the UO_2 foils were approximately 2500 Å thick. The dislocation densities of the deformed specimens at 1 and 5% strain, respectively, were $6 \times 10^8/\text{cm}^2$ and $1.2 \times 10^9/\text{cm}^2$. The calculated dislocation densities were used in conjunction with the measured strain rate, the known Burgers vector, and the orientation of the specimen to calculate the average dislocation velocity as a function of the average shear stress and temperature. These data, plotted as average velocity against the reciprocal of the shear stress, show that the shear stress required to produce a given dislocation velocity is a minimum at 950°C , in agreement with the observed minimum in the critical resolved shear stress curve.

DIFFUSION OF THORIUM IN ThO_2

L. E. Poteat³ C. S. Morgan

We have studied extensively sintering and deformation in ThO_2 specimens. To interpret these results, we studied diffusion of ^{230}Th in ThO_2 . Diffusion coeffi-

icients were determined on single crystals, sintered powder specimens, and specimens prepared from ThO_2 sol, giving a range of grain sizes from extremely large to a few microns.

An organic chelate of ^{230}Th was placed on the specimen surface, dried, and annealed. Diffusion anneals were conducted in air below 1800°C and in argon at higher temperatures. Penetration of the isotope was determined by sectioning, the alpha particle energy spectra degradation, or both.

The diffusion coefficients were determined from the penetration data by the solution for Fick's law for an infinitely thin film on a semi-infinite solid. The diffusion coefficients thus obtained represent a measure of the rate of movement of the isotope through the specimen. However, their meaning in terms of transport mechanisms is not certain, because a differentiation between grain-boundary, dislocation-pipe, and volume diffusion has not been made.

Diffusion coefficients for single crystals are shown in Fig. 8.3, results for sintered specimens in Fig. 8.4, and a comparison of crystals and polycrystal specimens in

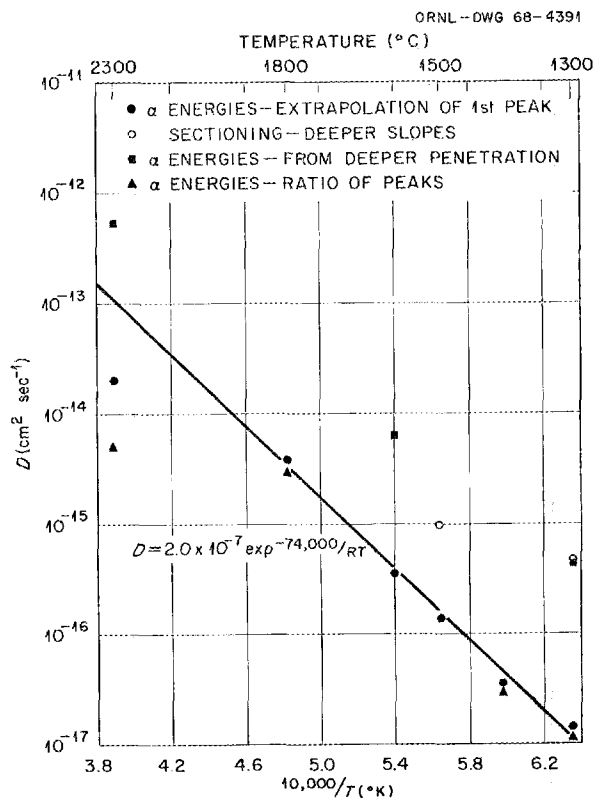


Fig. 8.3. Diffusion Coefficients of Thorium in ThO_2 Single-Crystal Specimen.

³Consultant from Clemson University, Clemson, S.C.

Fig. 8.5. Two distinctive features stand out. First, the diffusion is increased by decreasing grain size. Grain-size measurements on specimens annealed at 1300°C indicate that the diffusion coefficient is roughly proportional to the grain boundary (or subgrain boundary) content. Second, the results indicate an increase in the diffusion coefficient as the measurement zone moves

deeper into the specimen. This is further illustrated in Table 8.1.

A short investigation is being made of the effect of lattice imperfections on diffusion in thorium. A crystal with dislocations added by pressing in 800-grit SiC powder during an anneal at 1400°C showed more degradation of the alpha spectra, indicating more diffusion, than an untreated crystal annealed with it. Specimens containing small amounts of CaO, added by coprecipitation, had sharply higher rates of isotope penetration.

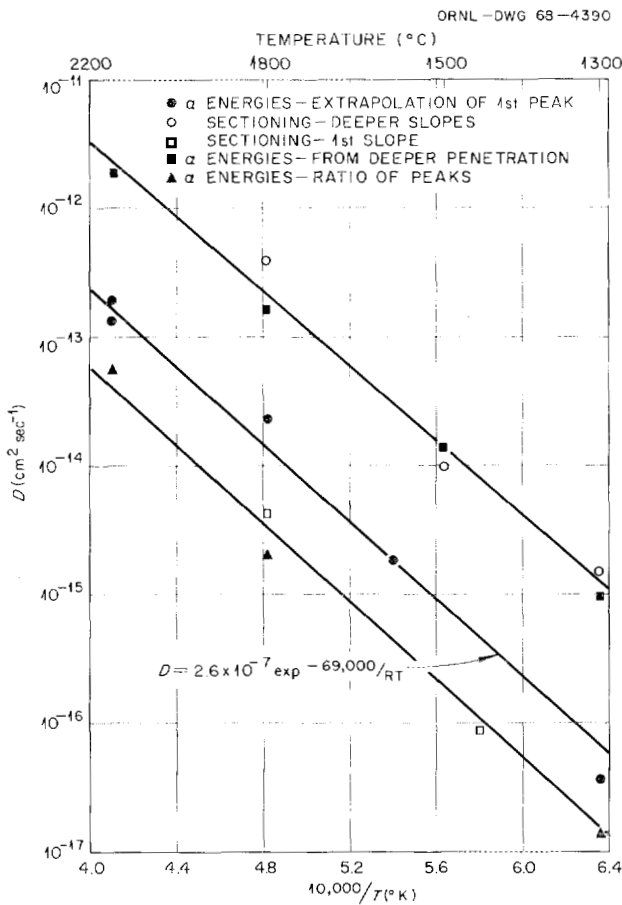


Fig. 8.4. Diffusion Coefficients of Thorium in ThO₂ Sintered Powder Specimen.

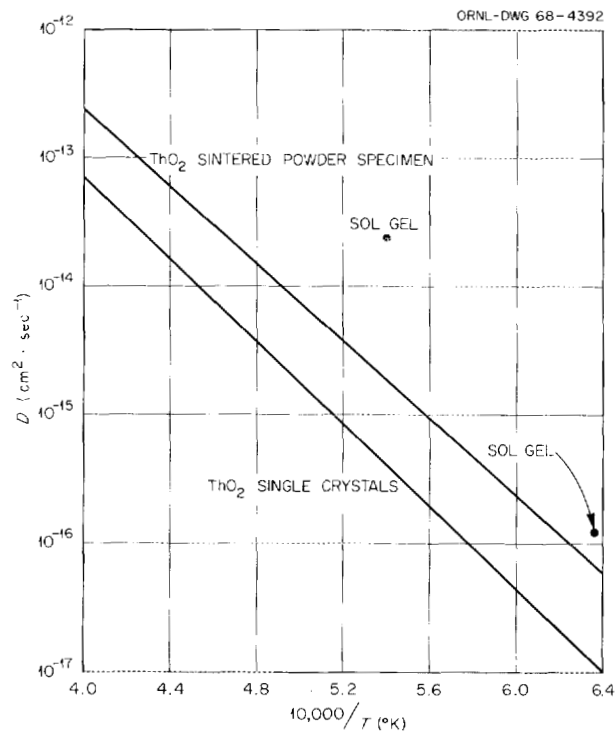


Fig. 8.5. Comparison of Diffusion Coefficients of Thorium in Mono- and Polycrystalline Thorium.

Table 8.1. Effect of Depth on Diffusion Coefficients Measured for Thorium in ThO₂

Method of Determining the Diffusion Coefficient	Approximate Depth (μ)	Diffusion Coefficient (cm ² /sec)		
		Sintered Powder, 1300°C	Single Crystal, 2300°C	Sol Gel, 1000°C
Ratio of α energy peaks	0.26	1.3 × 10 ⁻¹⁷	5.2 × 10 ⁻¹⁵	1.7 × 10 ⁻¹⁷
Extrapolation of first peak	0.2-0.6	3.7 × 10 ⁻¹⁷	1.4 × 10 ⁻¹⁴	2.6 × 10 ⁻¹⁷
Use of lower α energies	0.4-1.2	9.7 × 10 ⁻¹⁶	5.5 × 10 ⁻¹³	9.8 × 10 ⁻¹⁶
Sectioning	0.5-10	1.5 × 10 ⁻¹⁵		

In summary, over a wide temperature range a substantial part of the thorium transport in thoria appears to be in grain or subgrain boundaries. The reduced diffusion rate near the surface may be due to the influence of surface forces on atom movement in these defects.

SOME FUNDAMENTAL IDEAS FROM TOPOLOGY AND THEIR APPLICATION TO PROBLEMS IN METALLURGY⁴

Lida K. Barrett⁵ C. S. Yust

Some fundamental concepts and theorems from topology that relate to properties of surfaces and solids of the standard physical types have been reviewed. The Euler-Poincare characteristic of surfaces and solids has been used as a unifying theme, both for the presentation of the relevant topology and as the means of interrelating the cases in which a topological approach has been made to metallurgical problems. The determination of the Euler-Poincare characteristic from maps on surfaces has been discussed, and the evaluation of this quantity by means of the Betti numbers has also been demonstrated. The application of the Euler-Poincare characteristic to solids has been considered, as has the relationship of this characteristic to connectivity of surfaces and solids. We show that topological properties permit the grouping of all real three dimensional surfaces into a few classes and make clear the basic structural relationships common to the members of each class.

The topological concepts are used as a basis for the presentation of the work of several authors in which topology has been applied to the analysis of the interfaces in solid systems. The identification of concepts in mathematical terms has permitted the application of mathematical facts to validate or correct results that were originally presented empirically.

COMPRESSIVE CREEP OF URANIUM MONONITRIDE

L. L. Hall C. S. Yust

We are measuring the compressive creep characteristics of polycrystalline uranium mononitride. The specimens are prepared from UN powder by pressing and sintering in nitrogen; they have a fired density 95%

⁴Abstracted from a paper submitted for publication.

⁵Consultant from the University of Tennessee.

of theoretical and a grain size of approximately 10 μ . The experiments will cover from 1100 to 1600°C and stresses of from 3000 to 6000 psi. The test atmosphere is Ar-4% H₂. A sufficient partial pressure of nitrogen exists in this mixture as an impurity to maintain the UN phase over the temperature range of these tests; the hydrogen minimizes the possibility of oxidation. This range of experimental conditions overlaps and extends the data of Vandervoort, Barmore, and Cline⁶ on compressive creep of UN. The data collected to date are in agreement with those of Vandervoort *et al.* over part but not all the range of conditions. The slope of the plot of logarithm of strain rate at constant stress against reciprocal temperature is somewhat lower than that of the earlier data, suggesting a lower activation energy. Additional measurements are required to completely establish the creep properties of the UN specimens.

COMPRESSIVE CREEP OF URANIUM DIOXIDE

L. L. Hall C. S. Morgan

We are studying the compressive deformation of polycrystalline UO₂ specimens made by sol-gel. Specimen preparation involved evaporation of UO₂ sol, grinding, forming, isostatic pressing, and sintering. The specimens were sintered in hydrogen at 1750°C after a slow rate of temperature increase with a two-day hold at 800°C to 92% of theoretical density. Extensive deformation occurred over the 700 to 1500°C range. The specimens usually exhibited classical metallic yield behavior. The yield stress was above 20,000 psi at 1300°C. A preliminary value of the activation energy of the deformation process, which is thought to be a complex mixture of plastic flow and grain boundary sliding, is 40 kcal/mole at a stress of 23,300 psi and temperature around 1250°C. Further studies will include deformation of (U,Pu)O₂.

ACTIVATION ENERGY IN SINTERING

C. S. Morgan

Study of the mechanisms of material transport in sintering of powder compacts involves a number of problems that are not yet satisfactorily resolved. Our observation of nonisothermal densification kinetics

⁶R. R. Vandervoort, W. L. Barmore, and C. F. Cline, *Compressive Creep of Polycrystalline Uranium Mononitride in Nitrogen*, UCRL-70709 (preprint), (Oct. 9, 1967).

indicates that dislocation motion is frequently important.^{7,8} The sintering process has been observed

⁷C. S. Morgan and C. S. Yust, *J. Nucl. Mater.* 10, 182-90 (1963).

⁸C. S. Morgan, C. J. McHargue, and C. S. Yust, *Proc. Brit. Ceram. Soc.* 3, 177-84 (1965).

further by determining the activation energies by comparing the densification rates before and after small temperature changes. Values obtained were often higher when the temperature was raised than when it was lowered. These results are being extended and analyzed in terms of a material transport model involving dislocation motion.

9. Physical Properties

D. L. McElroy

We now know that two necessary steps are involved in obtaining a useful understanding of heat transport in solids over a broad temperature range. First, one must have accurate physical property data on well-characterized solids, and to obtain these we have developed several independent, overlapping, and accurate methods of measurement. Second, these data must be critically examined to test the adequacy of the theories. This two-step study is yielding the desired understanding needed to make reliable property predictions beyond the range of existing data on materials of considerable scientific and engineering importance.

Consequently, our research is applicable to other fundamental and applied areas and is coordinated with certain programs. Other sections of this report describe our studies on UN (Part I, Chapter 7), Mo (Part II, Chapter 15), T-111 (Part II, Chapter 19), (U,Pu)O₂ (Part III, Chapter 25), concrete (Part IV, Chapter 29), and thermal contact resistance (Part II, Chapter 18). Some of our work involves heat transport in electrical insulators, such as our recently completed study on silicon.¹ We have recently made an extensive review² of accurate temperature measurements, since these are required for our work. Developments in this field may allow improvements in our measurements.

ELECTRONIC HEAT TRANSPORT ANALYSIS³

R. K. Williams W. Fulkerson
J. P. Moore D. L. McElroy

Two independent methods for separating the electronic and lattice portions of the thermal conductivity

¹W. Fulkerson, J. P. Moore, R. K. Williams, R. S. Graves, and D. L. McElroy, *Phys. Rev.* 167(3), 765–82 (1968).

²D. L. McElroy and W. Fulkerson, "Temperature Measurement and Control," pp. 105–267 in *Techniques in Metals Research, Vol. I, Techniques of Materials Preparation and Handling, Part I*, R. F. Bunshah, ed., Interscience Publishers, New York, 1968.

³This section is largely summarized from a paper prepared by W. Fulkerson and R. K. Williams to be submitted to the *Canadian Journal of Physics*.

Table 9.1. Comparison of Thermal Conductivity Component Separation Results at 300°K

Element	L/L_0^a		$100 (\lambda_L/\lambda)^b$	
	Alloying Method	Curve Fitting Method	Alloying Method	Curve Fitting Method
W	1.20	1.10	8	14
Mo	<i>c</i>	1.09	<i>c</i>	2
Cr		1.15		28
Fe	0.87	0.74	18	31
Cu		0.94		<i>d</i>
Al		0.88		<i>d</i>
In		0.99		<i>d</i>

$$^aL_0 = (\pi/3)(k/e)^2 = 2.443 \times 10^{-8} \text{ v}^2/\text{°K}^2.$$

^b λ_L is the lattice component of the total thermal conductivity λ .

^cAlloying method yields very uncertain results at 300°K.

^dNegligible.

λ of metals and alloys were developed. An alloying method analyzes the composition dependence of the two λ components at a given temperature, whereas the curve fitting method is based on temperature dependences assumed for the two λ components of a single composition. Table 9.1 summarizes the results obtained by applying this analysis to several elements. Data for tungsten and iron and some of their dilute alloys were used to compare the two methods, and the results of this comparison were very encouraging. Only the curve fitting method could be applied to accurate data available for Cu, Al, In, Cr, and Pt. For the relatively simple metals Cu, Al, and In in the limiting value L_∞ of the high-temperature Lorenz function $L(T)$ was slightly less than the Sommerfeld limit L_0 . For Cr, Mo, and W the limiting high-temperature Lorenz number was significantly greater than L_0 . For platinum the high-temperature Lorenz function was not constant, although it was larger than L_0 . The lattice portion of the thermal conductivity was significant for W, Fe, Cr, and Pt, amounting to as much as 58% and 25% of the total for Fe and W, respectively, at 100°K. The lattice thermal conductivity of Mo seems anomalously small compared with that of W and Cr.

These findings have interesting theoretical consequences and are also useful for extrapolation. The analyses are being used to guide further research but cannot be extended to other elements until needed accurate physical property data are available. Our ultrahigh-vacuum furnace for electrical resistivity ρ and thermoelectric power S measurements to 2500°K has provided some of the needed data for tantalum (see Part II, Chapter 19). In addition, a modification to our absolute longitudinal apparatus now allows eight steady-state λ , ρ , and S data points per day, providing supporting data for the component separation study on other elements.

THERMAL CONDUCTIVITY AND ELECTRICAL RESISTIVITY OF HIGH-PURITY COPPER FROM 78 TO 400°K (Ref. 4)

J. P. Moore D. L. McElroy
R. S. Graves

A guarded axial heat flow technique for accurately measuring thermal conductivity, electrical resistivity, and Seebeck coefficient from 78 to 400°K on small rod samples is described in detail. Results on a 99.999%-pure polycrystalline copper specimen ($\rho_{273.16^\circ\text{K}}/\rho_{4.2^\circ\text{K}} = 900$) are compared with the results of previous investigators.

The behavior of the electrical resistivity and the thermal conductivity is discussed in terms of existing theoretical equations. Although copper is a relatively simple monovalent metal, little agreement between the experimental thermal conductivity results and theory was found. The behavior of the experimental electrical resistivity from 100 to 1200°K was explained in terms of an approximation to the Bloch-Grüneisen equation.

PHYSICAL PROPERTIES OF INDIUM FROM 77 TO 350°K (Ref. 5)

M. Barisoni R. K. Williams
D. L. McElroy

The electrical resistivity, thermal conductivity, and Seebeck coefficient of three high-purity indium specimens were studied between 77 and 350°K in a guarded longitudinal heat flow apparatus. Two of the three specimens were single crystals of known orientation. Data obtained from these samples were used to extract

⁴ Abstracted from *Can. J. Phys.* 45, 3849–65 (1967).

⁵ Abstract of paper to be in the Proceedings of the Seventh Conference on Thermal Conductivity, National Bureau of Standards, Gaithersburg, Md., Nov. 13–16, 1967.

values for the transport properties along the two principal crystallographic axes. The third sample was coarse grained. Electrical resistivity data are in reasonable agreement with the temperature variations reported for high-purity indium resistance thermometers. Application of the results of this study to the behavior of resistance thermometers is discussed. The thermal conductivity data for all samples are consistently lower than values obtained in another investigation, and the differences do not correlate with the differences in the electrical resistivity measurements.

PHYSICAL PROPERTIES OF MOLYBDENUM FROM 77 TO 1300°K (Ref. 6)

R. K. Williams J. P. Moore
R. S. Graves T. E. Banks
D. L. McElroy

Electrical resistivity, absolute Seebeck coefficient, and thermal conductivity data were obtained from 77 to 1300°K on an arc-cast, hot-rolled sample from Climax Molybdenum Company. Other samples studied included a zone-refined high-purity molybdenum, an arc-cast sample obtained from GE-NMPO, and Mo–0.5% Ti. The results differ significantly from previous measurements reported for molybdenum, and analysis of the results leads to an interesting behavior for the electronic and lattice components (see Part II, Chapter 15).

PHYSICAL PROPERTIES OF CHROMIUM

J. P. Moore R. K. Williams
D. L. McElroy

The electrical resistivity, thermal conductivity, and absolute Seebeck coefficient of two high-purity chromium specimens were measured⁷ from 77 to 400°K. No anomaly was observed in any of these properties near 122°K, where a local minimum occurs in the elastic constants. At the Néel temperature the Seebeck coefficient and the electrical resistivity dropped sharply and the thermal conductivity had a broad shallow minimum. In addition, the electrical resistivity between 310 and 317°K was also sensitive to temperature gradients. Within experimental accuracy limits,

⁶ Abstract of paper accepted for presentation at the Eighth Conference on Thermal Conductivity, Purdue University, West Lafayette, Ind., Oct. 7–10, 1968.

⁷ Paper to be published in the Proceedings of the Seventh Conference on Thermal Conductivity, National Bureau of Standards, Gaithersburg, Md., Nov. 13–16, 1967.

these properties do not show hysteresis near the Néel temperature on thermal cycling from 77 to 400°K.

The above work on chromium was extended⁸ by measurements of electrical resistivity ρ and absolute Seebeck coefficient S on a high-purity chromium specimen from 400 to 1200°K. Values of ρ , S , and λ determined from 77 to 400°K on a chromium sample previously measured at the Naval Ordnance Laboratory agreed within 5% with our previous data on chromium. These new results yield a Lorenz function for the NOL chromium that agrees within $\pm 0.5\%$ with our previous findings on chromium.

THERMAL CONDUCTIVITY OF ThO₂ AND UO₂ FROM 77 TO 1300°K (Ref. 9)

J. P. Moore R. S. Graves
D. L. McElroy

The thermal conductivity λ of 93%-dense ThO₂ and 98%-dense UO₂ was measured from 77 to 1300°K. An absolute longitudinal heat flow apparatus yielded results with a probable accuracy of $\pm 1.2\%$ from 77 to 400°K. A radial heat flow apparatus yielded results with a probable accuracy of $\pm 1.5\%$ from 300 to 1300°K. The results from the two methods agreed to better than 1% in the range of overlap. The λ data were compared with results of previous studies on ThO₂ and UO₂ to obtain a temperature-dependent density correction. The thermal resistance $1/\lambda$ was analyzed in terms of phonon scattering processes including Umklapp scattering, spin-wave scattering, and impurity scattering.

COMMENTS ON "THE THERMAL CONDUCTIVITY OF UO₂ AT VERY HIGH TEMPERATURE GRADIENTS"¹⁰

W. Fulkerson D. L. McElroy
J. P. Moore

Patrassi claims that below 900°C large temperature gradients on UO₂ in a radial heat flow system yield thermal conductivity λ values lower than small gradients because of thermal stresses. Our radial heat flow

results, which need repeating, show some superficial evidence of this at very small temperature differences. However, new data were obtained from our longitudinal comparative heat flow apparatus on a UO₂ single crystal with various temperature gradients and compressive stress levels to simulate the Patrassi test. These results revealed no effect of temperature gradient or stress level on λ of UO₂.

RELATED STUDIES

A major part of our physical properties studies involves the development of accurate measuring equipment. Several pertinent activities are described below.

Low-Temperature Axial Heat Flow Apparatus

R. W. Williams D. L. McElroy

A low-temperature axial heat flow apparatus patterned after our 77 to 400°K apparatus was designed to measure thermal conductivity, electrical resistivity, and Seebeck coefficient in the range 20 to 80°K. This apparatus will be used to study the effects of magnetic transitions, such as occur in UN near 50°K and UO₂ near 30°K. Initial tests will attempt to measure thermal arrests associated with the condensation of gases in metals, such as hydrogen in irradiated aluminum or fluorine in CVD tungsten.

We are attempting a first-principle, independent-particle approximation calculation to determine the sign of one of the terms contributing to the Seebeck coefficient of copper.

Radial Heat Flow Apparatus

P. H. Spindler D. L. McElroy
J. P. Moore R. S. Graves

We constructed a dual-purpose radial heat flow system to extend thermal conductivity measurements on powders to 4 atm and 1400°K (see Part III, Chapter 25). In addition to freeing our other radial apparatus for needed work, this second radial system will allow tests on a 1-in.-diam solid specimen rather than the 3-in.-diam specimen currently required. It will also allow us to test small commercially available platinum resistance thermometers for temperature transducers that may increase our ability to detect temperature differences by 150 fold over present thermocouples.

⁸Paper to be presented at the Eighth Conference on Thermal Conductivity, Purdue University, West Lafayette, Ind., Oct. 7-10, 1968 and published in the proceedings.

⁹Abstract of paper submitted to the *Journal of the American Ceramic Society*.

¹⁰Summary of comments on a paper by E. Patrassi, *J. Nucl. Mater.* 22, 311-19 (1967); published in *J. Nucl. Mater.* 26, 223-26 (1968).

Electrical Heating Methods

K-H. Bode R. K. Williams

Several new equations that relate thermophysical properties to measurable quantities were derived from the one-dimensional heat conduction equation for a current-carrying wire. When used with a single experimental arrangement, these new relations indicate experimental measurements to yield thermal conductivity values in different ways. In addition, this experimental arrangement allows thermal conductivity determinations using solutions developed by others, thus affording a meaningful comparison of different evaluation methods.¹¹

Our vacuum radial heat flow apparatus was converted to allow needed intercomparison of various electrical heating methods for measuring the thermal conductivity of electrical conductors.

¹¹Abstract of paper by K-H. Bode to be presented at the Eighth Conference on Thermal Conductivity, Purdue University, West Lafayette, Indiana, Oct. 7-10, 1968 and published in the proceedings.

Pulse Heating Calorimetry

T. G. Kollie M. Barisoni
D. L. McElroy

The energetics of ferromagnetic materials are being studied by determining specific heat, electrical resistivity, and thermoelectric power of iron, nickel, and alloys near Ni_3Fe , which have order-disorder transitions.

A new pulse-heating calorimeter that incorporates a specimen furnace to reduce heat losses was used to measure the specific heat of iron to 1800°K . Specimen heat losses limited the attainable accuracy of the first pulse-heating calorimeter.¹² Both calorimeters are mated to a recording system that obtains data accurate to 1 part in 10^4 at the rate of 2000 readings/sec. A new data acquisition system is being obtained that will equal this capacity and provide on-line computation of specific heat. The specific heat of alloy T-111 was measured from 400 to 1200°K (see Part II, Chapter 19).

¹²T. G. Kollie, *Rev. Sci. Instr.* 38(10), 1452-63 (1967).

10. Spectroscopy of Ionic Media

G. P. Smith

Our prime objective is information on the structure and behavior of ionic entities in molten salts, especially those entities formed by transition and posttransition metal ions. The method of study is optical absorption spectroscopy. An important second line of research is the spectroscopy of transition metal ions in halide crystals. At present this research is probing the utility and limitations of ligand-field theory as a description of the states of dN configurations in distorted-cubic environments. The results also provide basic data on spectroscopic parameters needed for the molten salt investigations. A third area of research is a study in sulfone¹ media of some transition metal complexes that also occur in molten salts. By using sulfones as solvents one can measure some basic ionic properties that cannot be determined by direct measurements on molten salts. Measurements of nonspectroscopic properties, such as crystal structure and density, support the spectroscopic research directly.

During the year we began research on some molten salt reactor problems, particularly the behavior of transition metal fission products in molten fluoride systems. Another cooperative program was begun with G. Mamantov at the University of Tennessee, who is measuring the electrochemical behavior of nonclassical bismuth ions in molten salt media. We reported discovery of these ions last year and are helping Mamantov get his program under way.

COORDINATION OF TRANSITION METAL IONS IN MELTS

In molten salt solutions transition metal ions form light-absorbing centers consisting of the central ion, its coordination shell of anions, and an outer shell predominantly of solvent cations. Most of the following reports describe a continuing study of nickel(II) centers, which are particularly useful for establishing basic principles, but we have begun studies of molybde-

num(III) centers in support of the molten salt reactor program.

Supporting research described here concerns complexation in sulfone media, phase relations in salt systems, and densities and electrical conductivities of molten salts.

The final report concerns a general phenomenological analysis of the effect of temperature and solvent composition on absorption. Although this analysis was undertaken to clarify the interpretation of molten salt spectra, it has broad applications to liquid-state spectroscopy in general.

Nickel(II) in Molten LiBr-KBr and LiI-KI Mixtures²

C. R. Boston C. H. Liu³
G. P. Smith

The previous study⁴ of the equilibrium between T- and O-type nickel(II) centers in LiCl-KCl melts has been extended to the corresponding bromide and iodide systems. The principal finding is that the T-O equilibrium is shifted increasingly in favor of T centers as the halide becomes heavier. An analysis of possible controlling factors leads us to believe that the increasing size of the anion ($\text{Cl}^- < \text{Br}^- < \text{I}^-$) is at least a major consideration.

Liquidus Curve for the LiI-KI System and Liquid State Densities of LiI-KI and LiBr-KBr Melts⁵

L. R. Lieto⁶ C. H. Liu³

The liquidus curve of the lithium iodide-potassium iodide system was measured by a visual-thermal

² Accepted for publication in *Inorganic Chemistry*.

³ Consultant from Arizona State University.

⁴ J. Brynestad, C. R. Boston, and G. P. Smith, *J. Chem. Phys.* 47, 3179-89 (1967).

⁵ Accepted for publication in *Journal of Chemical and Engineering Data*.

⁶ AEC Predoctoral Fellow from Arizona State University.

¹ Sulfones are organic materials of the type R_2SO_2 .

method. The densities of the eutectics in this and the lithium bromide-potassium bromide systems were determined by the buoyancy method as functions of temperature.

Nickel(II) in Molten ZnCl_2 -CsCl Mixtures⁷

G. P. Smith W. E. Smith⁸

J. Brynstad

We are continuing to study the behavior of nickel(II) centers in molten ZnCl_2 -CsCl mixtures. At least three kinds of T centers and an O center occur in this system. One of the T centers, T_1 , is the familiar NiCl_4^{2-} anion surrounded by Cs^+ ions. The others are T_2 , found at low temperatures in melts containing 50 to 70 mole % ZnCl_2 , and T_3 , found in melts containing over about 90 mole % ZnCl_2 . Each type has a distinctive spectrum. At 350 to 400°C and 50 mole % ZnCl_2 , Ni^{2+} is present largely as T_2 centers. Increasing the ZnCl_2 content converts T_2 centers to O centers until at roughly 70 mole % ZnCl_2 mostly O centers are present. These change little between about 70 and 90 mole % ZnCl_2 , but at about 90 mole % ZnCl_2 , T_3 centers appear. In going from 90 to 100 mole % ZnCl_2 the T_3 /O ratio rapidly increases, but we do not yet understand some features of the spectra for melts containing 98 to 100 mole % ZnCl_2 . Future research will include a study of all compositions at high temperatures and a more detailed examination of 98 to 100 mole % ZnCl_2 melts at all temperatures.

Densities of Molten ZnCl_2 and ZnCl_2 -CsCl Mixtures⁹

W. E. Smith⁸ G. P. Smith

Liquid state densities of ZnCl_2 and ZnCl_2 -CsCl mixtures containing from 1.0 to 75.0 mole % CsCl were measured as functions of temperature. The excess molar volume was positive and large near 60.0 mole % CsCl and negative and small near pure ZnCl_2 .

Nickel(II) in Molten CsAlCl_4

J. Brynstad G. P. Smith

A qualitative theoretical analysis indicates that liquid media consisting of an alkali metal tetrachloroaluminate plus small amounts of the alkali-metal chloride or AlCl_3

should provide an exceptionally favorable situation for studying the acid-base properties of the chloro complexes of Ni^{2+} . A knowledge of these acid-base properties is of key importance in understanding the coordination behavior of Ni^{2+} in molten chloride salts and in understanding the nature of chemical bonding in nickel complexes in general.

Research on this topic is still in its early stages, but it is already clear that the theoretical expectations will be fulfilled. As the pCl of CsAlCl_4 is altered by additions of small amounts of CsCl or AlCl_3 a succession of chloronickel complexes is formed. Each has a sharp, well defined spectrum indicating an orderly molecular ion. There are reasons for believing that the very elusive complexes NiCl_3^- and NiCl^+ are among the observed species.

Phase Studies and Electrical Conductivities of Systems Containing Aluminum Halides¹⁰

C. R. Boston

Preliminary research shows that nickel(II) centers in chloride melts containing significant amounts of AlCl_3 have very interesting coordination behavior. (See preceding report.) To obtain some basic properties of such melts in support of planned spectroscopic research, we are studying phase equilibria and electrical conductivities of the CsCl-AlCl_3 , KCl-AlCl_3 , and NaBr-AlBr_3 systems at temperatures up to 1000°C and pressures up to 175 atm.

Most alkali halide-aluminum halide mixtures exhibit a two-liquid region on the AlX_3 -rich side, usually between 80 and 100 mole % AlX_3 . Seldom has the consolute temperature been reported for this two-liquid region. Our applications require these consolute temperatures, and attempts to measure them gave interesting results. For CsCl-AlCl_3 and KCl-AlCl_3 at compositions near the midpoint of the two-liquid region the boundary between the two liquid phases did not disappear with increasing temperature as expected for normal consolute behavior. Instead, the boundary between the upper (AlCl_3 -rich) liquid phase and the vapor phase disappeared with critical opalescence and other behavior characteristic of critical phenomena. The temperature at which this occurred was $349 \pm 1^\circ\text{C}$ for both systems and was unaffected by successive volume reductions. The critical point of pure AlCl_3 was

⁷Parts of this report appeared in W. E. Smith, J. Brynstad, and G. P. Smith, *J. Am. Chem. Soc.* 89, 5983-84 (1967).

⁸Visitor from England, now at University College, London.

⁹Published in *J. Chem. Eng. Data* 13, 123-24 (1968).

¹⁰Research performed at Atomics International, Canoga Park, Calif. We are grateful to S. J. Yosim and L. F. Grantham of Atomics International for their hospitality and technical aid.

determined with the same material and technique as was used for the mixtures and gave a value of $350 \pm 2^\circ\text{C}$. Since this value is essentially the same as the "critical" temperature of the mixtures it would appear that the upper liquid phases in the mixtures do not exhibit consolute behavior. Of the alkali halide-aluminum halide mixtures reported in the literature, only NaBr-AlBr₃ shows a consolute temperature. We found a value of $255 \pm 2^\circ\text{C}$, compared with the literature¹¹ value of 232°C .

The conductivity of pure AlCl₃ was measured from the melting point (192°C) through the critical point (350°C) and up to 600°C . Specific conductances were about 10^{-7} /ohm-cm, about one-tenth the literature values,^{12,13} probably due to the high purity of our AlCl₃. A maximum in the specific conductance vs temperature curve occurs near 300°C .

Conductivities were measured for KCl-AlCl₃ mixtures from 15 to 100 mole % AlCl₃ except the two-liquid region (80 to 99 mole % AlCl₃). The temperature effect on conductivity was determined at each composition from the liquidus to 1000°C except for AlCl₃-rich melts, where a maximum temperature of 600°C was reached. When equivalent conductance (based on MX vs AlX₃) was plotted against composition, a well defined minimum occurred at 33 mole % AlCl₃ and an even sharper maximum at 50 mole % AlCl₃. (A similar plot using specific conductance instead of equivalent conductance had the same shape with the minimum shifted to 40 mole % AlCl₃.) Similar measurements are under way on NaBr-AlBr₃ mixtures, and the results so far are quite similar to those just described for KCl-AlCl₃, with minimum and maximum in the equivalent conductance plot at 33 and 50 mole % AlBr₃, respectively. The minimum is actually slightly more pronounced for the bromide system. This would seem to rule out the formation of anions of the type AlX_n³⁻ⁿ with $n > 4$ as an explanation for this minimum since a high coordination number for aluminum, unlikely for chloride, would be even less likely for the larger bromide.

Maxima in the conductivity vs temperature curves were observed for compositions corresponding to the compounds KAlCl₄ and NaAlBr₄ at approximately 1000 and 880°C , respectively. Grantham and Yosim¹⁴

¹¹J. Kendall, E. D. Crittenden, and H. K. Miller, *J. Am. Chem. Soc.* 45, 963 (1923).

¹²K. N. Semenenko and T. N. Naumova, *Zh. Neorgan. Khim.* 9, 1316-22 (1964).

¹³W. Biltz and A. Voigt, *Z. Anorg. Allgem. Chem.* 126, 39-53 (1923).

¹⁴L. F. Grantham and S. J. Yosim, *J. Chem. Phys.* 38, 1671 (1963); 45, 1192 (1966).

have shown that this temperature t_{max} of maximum conductivity is linearly dependent on the heat of vaporization. Using their formula and the observed t_{max} one finds approximate values for the heat of vaporization of 12 kcal/mole for KAlCl₄ and 11 kcal/mole for NaAlBr₄.

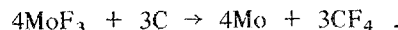
Molybdenum(III) in Fluoride Melts

L. M. Toth¹⁵ J. P. Young¹⁶

As an initial phase of a program in support of the Molten Salt Reactor Project, we are studying the spectra of molybdenum(III) centers in fluoride melts. Molybdenum is an important neutron poison produced by fission.

Molybdenum trifluoride¹⁷ at concentrations up to 1 wt % in molten LiF-34 mole % BeF₂ was studied in windowless containers¹⁸ made of graphite, copper, and platinum. The spectra agree with that theoretically predicted for octahedral MoF₆³⁻. We are attempting to verify these theoretical predictions by spectroscopic and x-ray diffraction measurements¹⁹ on K₃MoF₆.

Solutions of MoF₃ in the molten LiF-BeF₂ solvent are reasonably stable in copper and platinum containers at 450 to 700°C but react with graphite in such a way that the Mo(III) concentration (measured spectroscopically) decreases by first-order kinetics with the deposition of metallic molybdenum. This suggests the reaction



Nickel(II)-Nitrate Complexes in Molten Dimethyl Sulfone and Application to Identification of Nickel(II) Coordination in the Molten LiNO₃-NaNO₃-KNO₃ Eutectic²⁰

C. H. Liu³ J. Hasson²¹
G. P. Smith

Nickel(II) was shown potentiometrically to form successive 1:2 and 1:3 complexes in dimethyl sulfone at

¹⁵On loan from the Reactor Chemistry Division.

¹⁶Analytical Chemistry Division.

¹⁷Supplied by C. F. Weaver, Reactor Chemistry Division.

¹⁸J. P. Young, *Anal. Chem.* 36, 390 (1964).

¹⁹The diffraction measurements are being made by G. D. Brunton, Reactor Chemistry Division.

²⁰Accepted for publication in *Inorganic Chemistry*. Parts of this research were carried out at the Brookhaven National Laboratory.

²¹Brookhaven National Laboratory.

125°C, and the values of the formation constants were determined. These potentiometric results were confirmed by spectrophotometric measurements, and the ligand-field spectra of the nickel(II) species involved were determined. The spectrum of nickel(II) in the molten $\text{LiNO}_3\text{-NaNO}_3\text{-KNO}_3$ eutectic at 125°C was measured and found to correspond closely to that of the 1:3 complex. We concluded that the $\text{Ni}(\text{NO}_3)_3^-$ complex is the principal species in the nitrate melt and that its nitrate ions are bidentate with the coordinated oxygens arranged in a distorted octahedral array. Present evidence rules against the occurrence of $\text{Ni}(\text{NO}_3)_4^{2-}$ in significant amounts in the melt although it occurs in certain crystalline compounds.

Exchange Reactions Between Tetrahalo Complexes of Nickel(II) in Tetramethylene Sulfone

L. R. Lieto⁶

We are measuring equilibrium constants for exchange reactions between tetrahedral tetrahalonickelate(II) complexes in tetramethylene sulfone as functions of temperature. The primary effort to date has been on purification of tetramethylene sulfone to a sufficient degree to prevent oxidation of iodide ions and on the development of computer programs for the analysis of the spectrophotometric data.

Densities of Solutions of LiI, LiBr, and LiClO_4 in Tetramethylene Sulfone

L. R. Lieto⁶

Liquid-state densities of the system 1 *M* LiClO_4 and 1 *M* (LiI + LiBr) in tetramethylene sulfone were determined from room temperature to approximately 145°C by the buoyancy method. Density was measured at approximately 30°C intervals. The concentration of either halide constituent varied from 0.0 *M* to 1.0 *M* by 0.25 *M* units.

Densities of Molten BiCl_3 and $\text{BiCl}_3\text{-AlCl}_3$ Mixtures²²

C. R. Boston

The "float" method was used to measure the liquid-state densities of BiCl_3 and $\text{BiCl}_3\text{-AlCl}_3$ mixtures containing 20.0, 35.0, and 60.0 mole % AlCl_3 , as functions of temperature. Substantial negative excess molar volumes were found.

Phenomenological Analysis of the Effects of Temperature and Composition on the Absorption Spectra of Liquid Systems²³

J. Brynestad G. P. Smith

We critically analyzed the theory of isosbestic points and showed that the rules previously proposed for interpreting these points in terms of the number of absorbing species or the number of independent reaction parameters are unreliable. We went on to develop the theory of linearly related spectra and demonstrated that it is much more useful to show that linear relations hold than it is to show that isosbestic points are present.

OPTICAL SPECTRA OF TRANSITION METAL IONS IN CHLORIDE CRYSTALS

We are measuring at low temperatures high-resolution spectra of chloride crystals that contain Ni(II) or Co(II) ions to study the splitting of cubic degeneracies by environments with small distortions from cubic symmetry. We are attempting to rationalize the results in terms of ligand-field theory. Since these spectra are of the same type that we study in molten salts, the crystal measurements support the molten salt research in basic ways.

Nickel(II) at Approximately Octahedral Sites in Crystals

G. E. Shankle²⁴

When alkali chloride crystals are doped with divalent 3d transition metal ions, the nearest-neighbor chlorides about the transition metal ions are distorted from an octahedral configuration, at least partly because alkali metal ion vacancies must be present for charge compensation. Optical spectra of Ni^{2+} ions at liquid-nitrogen and liquid-helium temperatures in single crystals of LiCl containing approximately 0.5 to 1.0 mole % NiCl_2 suggest that this distortion may be considerable. Normally degenerate electronic states of Ni^{2+} appear to be split by the noncubic environment. The magnitude of this splitting is directly related to the amount and type of distortion about the Ni^{2+} ions. We are calculating the extent of distortion by ligand-field theory containing adjustable parameters representing noncubic environments. These parameters are adjusted

²²Published in *J. Chem. Eng. Data* **13**, 117-18 (1968).

²³Published in *J. Phys. Chem.* **72**, 296-300 (1968).

²⁴AEC Predoctoral Fellow from the University of Tennessee.

until the observed spectra are reproduced as closely as possible.

Splittings of the ground state of Ni^{2+} are being studied by magnetic-resonance techniques in cooperation with M. M. Abraham of the Solid State Physics Division. These data will provide an independent and complementary check of the optical results.

In addition to electronic-state splitting, the LiCl:Ni system shows well-defined vibrational progressions of several electronic bands. These progressions are due to the annihilation or creation of phonons during electronic excitation. These phonons may be modes of the host lattice or localized modes of the NiCl_6^{4-} complex.

To help identify the source of the progression, the system $\text{CdCl}_2:\text{NiCl}_2$ is being studied. CdCl_2 has a very different crystal structure from LiCl , hence different host normal modes, but the local structure about Ni^{2+} is similar (but not identical). Thus, both the optical spectra and progressions of $\text{CdCl}_2:\text{Ni}$ and LiCl:Ni may show similarities and differences that would help explain both results.

Nickel(II) at Approximately Tetrahedral Sites in Crystals

T. W. Couch²⁵

We are studying in detail the well-resolved spectra of Cs_3NiCl_5 and $\text{Cs}_3\text{MgCl}_5:\text{Ni}$ at low temperatures and less thoroughly $\text{Cs}_2\text{MgCl}_4:\text{Ni}$, $\text{Cs}_2\text{ZnCl}_4:\text{Ni}$, and $\text{Cs}_3\text{ZnCl}_5:\text{Ni}$. In all these systems nickel is surrounded by a distorted tetrahedron of chlorides. Analysis of the results in terms of ligand field theory takes the distortion into account. H. L. Davis of the Theoretical Group guided the development of a computer program to generate the matrix elements for a d^8 ion in arbitrary symmetry via the tensor operator approach.

Polarized optical spectra were obtained for oriented crystals of Ni^{2+} -doped Cs_3MgCl_5 at 5, 80, and 300°K. The crystals are uniaxial positive, and the coordination symmetry about Mg^{2+} , for which Ni^{2+} substitutes, is a distorted tetrahedron of nearest-neighbor chlorides with D_{2d} symmetry. At low temperatures the electronic bands show an extensive polarized fine structure consisting of subbands that arise from interactions between vibrational modes of the crystal and the electronic states of Ni^{2+} . In a particularly notable instance we measured 67 sharp, polarized subbands that arise from transitions to two electronic states whose (0,0) lines are very close together. We are endeavoring to locate the electronic origins of all the electronic bands and account for their energies in terms of a six-parameter ligand-field model appropriate for D_{2d} symmetry. The six parameters being used are a single spin-orbit

coupling constant (ξ), two electron repulsion integrals (B and C), and three crystal-field potential parameters (A_2^0 , A_4^0 , and A_4^4). We then sort out the vibrational fine structure in terms of progressions on fundamental frequencies.

The analysis for Cs_3NiCl_5 at 5°K is nearly complete and yields the values $B = 766 \text{ cm}^{-1}$, $C = 3259 \text{ cm}^{-1}$, $\xi = 522 \text{ cm}^{-1}$, $A_2^0 = -3489 \text{ cm}^{-1}$, $A_4^0 = 8347 \text{ cm}^{-1}$, and $A_4^4 = 6566 \text{ cm}^{-1}$.

Crystal Structures of $\text{Cs}_3\text{MgCl}_5:\text{Ni}$ and Cs_3NiCl_5 Down to 10°K

T. W. Couch²⁵ H. L. Yakel²⁶
C. J. Sparks²⁶

By x-ray diffraction measurements we showed that $\text{Cs}_3\text{MgCl}_5:\text{Ni}$ and Cs_3NiCl_5 have the space group $I4/mcm$ (isostructural with Cs_3CoCl_5) from room temperature down to 10°K and determined the lattice parameters. These data are essential for interpretation of the optical spectra described above.

Cobalt(II) Centers at Approximately Octahedral Sites in Chloride Crystals

F. C. Gilmore²⁴

Fairly detailed studies were made of the spectra of Co(II) in pseudooctahedral sites in chloride crystals. The actual site symmetries are almost O_h for $\text{KMgCl}_3:\text{Co}$ and D_{3d} for RbCoCl_3 , CsCoCl_3 , $\text{CsMgCl}_3:\text{Co}$, $\text{MgCl}_2:\text{Co}$, and $\text{CdCl}_2:\text{Co}$. In $\text{LiCl}:\text{Co}$ we believe the site symmetry of cobalt is C_{2v} . The spectra of these systems were measured at room temperature, 77°K, and approximately 4°K. At the lower temperatures several bands showed vibrational fine structure. The results are being analyzed in terms of ligand field theory.

Despite the known distortions and some polarization effects, the approximation of O_h symmetry leads to a satisfactory rationalization of the results. Within this approximation the ligand-field parameter Dq is roughly correlated with the distances between Co^{2+} and its nearest-neighbor chlorides, and values of the electron repulsion integral B and the spin-orbit coupling constant are reduced about 20% from their free-ion values.

REDOX PROCESSES IN MELTS

Our previous research on redox processes in melts concerned the oxidation states of bismuth in chloride

²⁵Graduate student from the University of Tennessee.

²⁶X-Ray Diffraction Group.

and bromide systems. This posttransition element was found to have a wide variety of nonclassical ions unknown in other media. Research elsewhere showed that the neighboring element lead forms the nonclassical ion Pb_2^{2+} in molten chloride salts, and we recently determined its absorption spectrum. To find out whether or not these ions are confined to the sixth period, we studied the metalloid tellurium with results that are reported below.

We also began studying redox processes for titanium in chloride melts, but the results are not ready for presentation because we encountered new oxidation states and have not yet untangled the chemistry involved. This research is being done by J. Brynestad, S. von Winbush,²⁷ and H. L. Yakel.²⁶

TELLURIUM IN THE ELECTROPOSITIVE OXIDATION STATE ONE-HALF²⁸

N. J. Bjerrum²⁹ G. P. Smith

The novel entity Te_{2n}^{n+} has been prepared in molten salt solutions and as a compound with the stoichiometry Te_2AlCl_4 . The solutions were made up by elemental tellurium reacting with dilute solutions of tellurium tetrachloride in the molten $AlCl_3$ - $NaCl$ eutectic. There are clear indications of other novel entities in solution with formal oxidation states between zero and one-half. We are determining the value of n for Te_{2n}^{n+} .

SPECTROSCOPY OF NO_3^- IN MELTS

We are phasing out a study of the Stark effect shift on the lowest energy transition of NO_3^- produced by the electric fields of surrounding ions in molten salt media. Experimental measurements on this program were completed several years ago, but the analysis of the data has been involved. Work on weakly interacting ions was completed this year and is reported here. Profile analyses of the data for strongly interacting ions were also computed, but correlation of the data is still in progress.

ULTRAVIOLET SPECTRUM OF THE NITRATE ION IN MOLTEN MIXTURES OF ALKALI METAL NITRATES³⁰

C. R. Boston D. W. James³¹
G. P. Smith

The effects of composition and temperature on the first ultraviolet band of NO_3^- in molten mixtures of alkali metal nitrates were determined. The energy of the

band maximum E_{max} is a linear function of mole fraction for $NaNO_3$ - $RbNO_3$ and KNO_3 - $RbNO_3$ mixtures and shows small positive deviations from linearity for $LiNO_3$ - $NaNO_3$, $LiNO_3$ - KNO_3 , and $LiNO_3$ - $CsNO_3$. The f number shows moderate deviations from linearity for all these systems. With increasing temperature E_{max} decreases and f increases. These results are in line with an earlier theoretical analysis and with studies of mixtures containing multicharged cations.

APPARATUS DEVELOPMENT

Spectrophotometer Furnaces³²

C. R. Boston G. P. Smith

We developed two types of resistance-heated furnaces for molten salt spectrophotometry that have low thermal gradients in the cell space. One furnace fits the standard sample compartment of a Cary model 14 spectrophotometer and operates up to 400°C. The other is used with the Cary model 14H high-temperature spectrophotometer at temperatures up to 1000°C.

Diamond-Windowed Cell for Molten Fluoride Spectroscopy

L. M. Toth¹⁵

Although windowless cells have been extremely useful for molten fluoride spectroscopy, a windowed cell is needed to improve the accuracy of absorptivity values and permit better control of vaporization and the covering gas phase. The problem is that no window material is completely immune to attack by all fluoride melts of interest. After making an extensive survey³³ of available information and testing several alternative approaches, we decided that diamond windows in a graphite cell would offer many advantages for studying systems not reduced by carbon.³⁴ We are developing such a cell in which diamond plates $5 \times 5 \times 1$ mm will be used as windows.

²⁷Consultant from Fisk University.

²⁸Accepted for publication in *Journal of the American Chemical Society*.

²⁹Visitor from the Technical University of Denmark.

³⁰Published in *J. Phys. Chem.* 72, 293-95 (1968).

³¹University of Queensland, Australia.

³²Submitted for publication.

³³L. M. Toth, *Containers for Molten Fluoride Spectroscopy*, ORNL-TM-2047 (Nov. 8, 1967).

³⁴Successful use of diamond windows for fluoride containment in metal cells is reported by G. G. Cocks, J. B. Schroeder, and C. M. Schwartz, "The Spectroscopy of Fused Salts," *Progress Relating to ANP Application, February-April 1957*, BMI-1185, p. 13.

11. Superconducting Materials

G. R. Love

We are studying the effects of metallurgical variables on the properties of superconducting materials. Of concern are the effects on current-carrying capacity in a magnetic field of such things as morphology, compositions, and spacings of two-phase structures; mechanical strain; preferred orientation; aging and transformation reactions; and fabrication and heat-treatment procedures. For the studies to be meaningful, we must have a considerable knowledge of the physical metallurgy and phase diagrams of the systems of interest. Few systems have been studied, and they have not been studied in sufficient detail. Consequently, much of the effort is devoted to establishing a background of information on the transformation kinetics and products, morphologies, phase diagrams, precipitation and aging reactions, and rates of formation of intermetallic compounds. The alloy systems of primary interest are those based on niobium and technetium.

SUPERCONDUCTING PROPERTIES OF A Tc-30 at. % V ALLOY

C. C. Koch G. R. Love

The alloy Tc-30 at. % V has been examined as a function of aging time at 900°C to correlate superconducting property changes with physical property variations. The alloy, as quenched from above 1200°C, is apparently single phase with the CsCl structure and is strongly supersaturated in technetium. Holding at 900°C allows the alloy to approach equilibrium by rejecting the technetium-rich hexagonal phase as a plate-like precipitate. Both the CsCl-type phase and the hexagonal phase are superconductors, and we are able to determine separately many properties of each phase within the aggregate as a function of precipitation time. The observed changes in upper critical field and critical temperature suggest that the daughter phases approach their equilibrium compositions relatively slowly at 900°C. The maximum in critical current density, on the other hand, occurs at quite short aging times — indeed before the maximum physical hardness for this heat treating temperature. We tentatively identified the

defect morphology responsible for the high current densities in this alloy to be the array of hexagonal-phase particles on sub-boundaries in the matrix (see the following section).

ANALYTIC EXPRESSION FOR SUPERCONDUCTING CRITICAL CURRENT DENSITY

G. R. Love

We have taken the model description for flux-flow in a superconductor given by Anderson and Kim¹ with a slightly more careful definition of some of the terms. Judicious choice of boundary conditions and elementary application of rate theory to this model then allow us to write generalized expressions for critical current density as a function of temperature and applied field. Two adjustable (semiempirical) parameters are available to the model description. From one of these we deduce the distance between flux-pinning sites in a superconductor; from the other, the total strength of the pinning interactions. The fit of the model expression to experimental results is adequate to excellent, and the apparent separation between pinning sites deduced from it is plausibly related to the observed microstructures of type II superconductors such as Nb-Zr, Nb-Ti, and the Tc-V described above.

RARE EARTH STRUCTURAL STUDIES

C. C. Koch C. J. McHargue

An investigation of the influence of deformation on the face-centered cubic to double hexagonal close packed phase transformation in cerium² has been completed.³ Work is continuing on the phase transformations between close-packed structures in intrarear-earth alloy systems. Of special interest is the mode

¹P. W. Anderson and Y. B. Kim, *Rev. Mod. Phys.* **43**, 39-43 (1964).

²C. C. Koch and C. J. McHargue, *Metals and Ceramics Div. Ann. Progr. Rept. June 30, 1967*, p. 50.

³C. C. Koch and C. J. McHargue, to be published in *Acta Metallurgica*.

of transformation from hexagonal close packed to the rhombohedral samarium-type structure. This transformation is diffusionless and may be induced by plastic deformation. The kinetics and morphology are being studied by electrical resistance measurements and optical and electron microscopy.

Pure lanthanum metal is being zone-refined in our new electron-beam melting apparatus. We hope to

achieve pure single crystals as starting material for a study of the superconducting properties of the various phases of lanthanum related to its metallurgical structure. At present, we have increased the grain size from about 50μ to about 1.5 mm (in a 3-mm ingot) and have decreased the fraction of second phase (presumably oxide) to less than 1% by volume.

12. Surface Reactions of Metals

J. V. Cathcart

Our assignment is to study the fundamentals of the oxidation of metals and alloys and related phenomena. Much of our work is concerned with the role of stress in oxidation mechanisms. We have shown that stresses arise during oxidation in both surface oxide layers and the substrate metal in many systems. These stress effects may involve the gross distortion, rupture, or both of the oxide film and the metal, in some instances leading to the mechanical failure of the specimen. They may also be more subtly manifested in terms of the development of paths of easy diffusion in the oxide films. In both cases, these stress effects can be responsible for orders of magnitude changes in the oxidation rate. An investigation of these phenomena is clearly essential to a complete understanding of the oxidation process.

Activities of this group during the past year involved studies of both types of stress effects. Our studies of stress effects in tantalum and niobium were concentrated in the range 700 to 900°C and at sufficiently low oxygen pressures that the major reaction was solution of oxygen in the metals. These experiments were designed to characterize further the very large stresses attendant upon oxygen solution in the surface layers of a metal. Similar experiments in which the oxygen pressure was raised to the point that a significant thickness of oxide formed provided an opportunity to observe additional flexure effects associated with the presence of films.

Our x-ray studies of the thin-film stage of oxidation of nickel were extended and showed conclusively that the development of paths of easy diffusion in NiO films is as crucial a part of the oxidation mechanism for nickel as it is for copper. Ellipsometer measurements on growing NiO films provided information regarding the changes of the optical properties of these films with thickness.

We also extended our diffusion measurements to tungsten, using the very sensitive anodic-film sectioning technique we developed for tantalum and niobium. In addition, a search for a protective coating for aluminum

alloys in a HFIR-type reactor environment was carried out in this group. The results are reported in Part III, Chapter 20 of this report.

OXIDATION OF NICKEL

J. V. Cathcart G. F. Petersen

X-Ray Studies

Our study of the thin-film stage of oxidation of nickel at 500°C and 1 atm O₂ pressure was extended to include the (311). The (311) is the most slowly oxidizing of all major planes of nickel. As in the case of the (311) of copper, the oxide film was well oriented and exhibited but a single epitaxial relationship with the substrate. The films were composed of an array of mosaic blocks a few hundred angstroms in diameter, but the mosaic spread (see Fig. 12.1) was quite small, making the subboundaries rather inefficient as paths of easy diffusion. This fact, we believe, accounts for the slow rate of oxidation of the (311).

The average *d*-spacing and the mosaic spread of the (311) films were determined by the x-ray technique previously described.¹ The *d*-spacing measures the average strain in the film and was determined in a direction normal to the film surface. The mosaic spread was expressed as the width at half-maximum intensity of rocking curves for the films.

These data along with the results for the other three major planes of nickel as well as comparative results from our previous work on copper are summarized in Figs. 12.1 and 12.2. As may be seen, the oxide films on copper and nickel differed considerably in the way their mosaic spread and average *d*-spacing varied with film thickness. Note that the average strain in the NiO films was virtually zero, although an analysis of the line shapes of the diffraction peaks for these films indicated the presence of a substantial strain gradient. The cause

¹B. S. Borie, C. J. Sparks, Jr., and J. V. Cathcart, *Acta Met.* 10, 691-97 (1962).

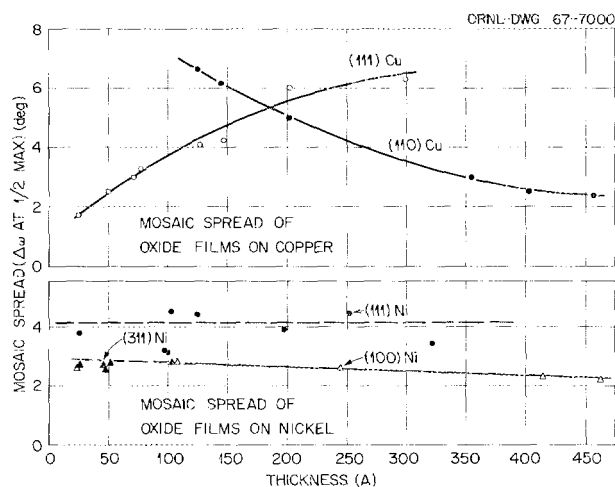


Fig. 12.1. Mosaic Spread as a Function of Film Thickness for Oxide Formed in Several Crystal Planes of Copper and Nickel.

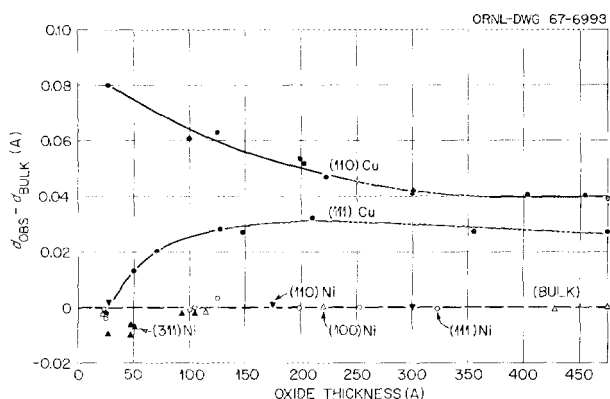


Fig. 12.2. Average d -Spacing for Oxide Films Formed on Several Crystal Planes of Copper and Nickel.

and significance of these differences is still not completely understood, but, as previously reported,² the basic conclusions drawn from our x-ray studies of the thin-film stage of oxidation are:

1. The films all contain many paths of easy diffusion.
2. The extent and efficiency of these short-circuit diffusion paths vary with crystal plane of the substrate.
3. The observed rates of oxidation of different crystal planes correlate directly with the above variation in the efficiency of paths of easy diffusion in the oxide.

²J. V. Cathcart and G. F. Petersen, *Metals and Ceramics Div. Ann. Progr. Rept. June 30, 1967*, ORNL-A170, pp. 51–52.

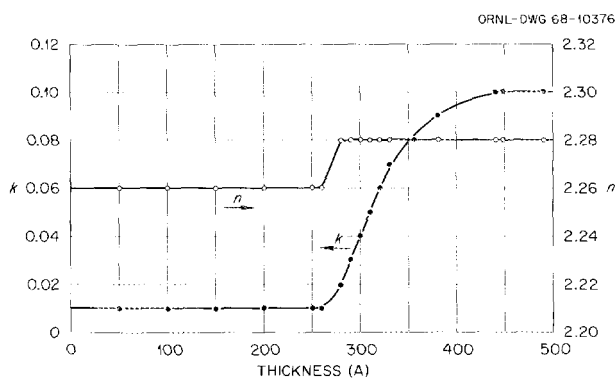


Fig. 12.3. Variation of the Real and Imaginary Parts of the Refractive Index at 5461 Å of NiO Films Growing on the (100) of Nickel at 500°C.

These conclusions relative to the importance of short-circuit diffusion in the oxidation process are identical to those drawn from our previous work with copper. Thus the oxidation behavior of nickel appears to be entirely consistent with the main feature of the oxidation model we proposed for copper.

Ellipsometer Studies

During our nickel oxidation work we used an ellipsometer to investigate the optical properties of the NiO films. An ellipsometer measures the relative phase change and amplitude reduction suffered by a beam of polarized light on reflection from the surface of a film-covered specimen. From these quantities one may calculate a film thickness provided the refractive index of the film is known. However, reliable values for the refractive index are generally unavailable for thin films, and it is usually necessary, as in our case, to resort to a computerized curve-fitting procedure to obtain both thickness values and the refractive index.

We discovered that the refractive index n_2 was a function of film thickness in growing NiO films. Furthermore, despite the fact that NiO has a cubic crystal structure at 500°C, the measurement temperature, n_2 varied with the crystallographic orientation of the substrate. Figure 12.3 shows the variation of the real and imaginary parts of the refractive index of the oxide as a function of the thickness of an oxide film growing on the (100) of nickel. Here we express the refractive index as $n_2 = n - ik$, where n is the real part and the imaginary part k is related to the absorption

³R. Newman and R. M. Chrenko, *Phys. Rev.* **114**, 1507–11 (1959).

coefficient. The measurements were made at a wavelength of 5461 Å.

The absorption spectrum of NiO in the visible region consists of a line spectrum associated with the Ni^{2+} ions superimposed on a continuous background that increases with increasing energy. The magnitude of the background increases as the NiO departs from stoichiometric composition.³ The mechanism of this effect is not known, but it is presumed to be related to the concentration of trivalent nickel ions in the oxide.

The wavelength at which our ellipsometer measurements were made lies between two peaks of the line spectrum of NiO; therefore, our results may reflect changes in the background absorption and, hence, the Ni^{3+} concentration, as the NiO films increase in thickness. From the point of view of the oxidation mechanism of nickel, these results are of special interest in that they offer the possibility of measuring the concentration of Ni^{3+} in the growing oxide film. Since the diffusing species in NiO is believed to be cation vacancies, whose concentration ought in turn to be related to that of Ni^{3+} , we may be in a position to describe the changes in vacancy concentration in NiO films during the thin-film stage of oxidation. Such information would be most valuable in testing the validity of current oxidation theories such as that of Fromhold.⁴ Of course, we have measured k at only one wavelength, and a firm interpretation of our results awaits a more complete determination of the absorption spectrum of the films.

REFRACTORY METAL OXIDATION

R. E. Pawel J. V. Cathcart

Stress Development During Oxidation

We continued our measurements of the strain arising in tantalum and niobium specimens during gaseous oxidation. Recent experiments conducted from 700 to 900°C, in which the flexure of thin specimens oxidizing on one side was measured, helped to establish further some of the important characteristics of stress generation due to the dissolution of a reactant into the surface layers of a solid. In these experiments, the oxygen pressures were low enough to prevent excessive oxide formation, and the oxygen-diffusion rates were

sufficiently high that diffusion distances were generally of the same order as the specimen thickness. The correlation between the flexure behavior and that computed on the basis of ideal bulk diffusion of oxygen was very satisfactory. For example, Fig. 12.4 illustrates typical maximum bending stress values during oxidation and subsequent vacuum annealing, in this case for a niobium specimen held at 800°C. During the oxidation period, the bending stresses increased rapidly and would have resulted in plastic deformation of the specimen if oxidation had not been stopped. Calculation of surface stresses from the bending stress values suggested that the surface concentration of oxygen increased with oxidation time over a wide range of pressure. During annealing of the oxidized specimen, the maximum bending stress decreased at a decreasing rate in accord with that calculated on the basis of a redistribution of the dissolved oxygen. The calculated stress values are shown as rectangles in Fig. 12.4 and agree well with the experimental data. The triangular points indicate the bending stress values (normalized to 16 min) that would be expected for a constant oxygen concentration at the surface of the specimen during both the oxidation and annealing period. Obviously, this latter model is not accurate for the conditions of this experiment.

Similar experiments at higher initial oxygen pressures (or for longer oxidation times) exhibited the additional effect of stresses in the growing oxide films. We are modifying our experimental procedures to obtain a more quantitative description of the stress in these films and to test any possible correlations between changes in the state of this stress and the oxidation kinetics.

Anodic-Film Sectioning of Tungsten

An experimental technique for sectioning, which utilizes the high degree of uniformity exhibited by anodic films, was developed for tungsten⁵ and is being applied to the investigation of tracer diffusion in this metal. Basically, by allowing the specimen to be sectioned into uniform layers from about 10 to 400 Å in thickness, the method permits the determination of extremely steep concentration gradients and thus is a particularly useful tool for studying diffusion at low temperatures and for observing the interplay of volume and short-circuit diffusion mechanisms.

Utilizing this technique, we have now examined the diffusion characteristics of ^{95}Nb in tungsten over a

⁴A. T. Fromhold, Jr., *J. Phys. Chem. Solids* 24, 1309-23 (1963).

⁵R. E. Pawel and T. S. Lundy, *J. Electrochem. Soc.* 115, 233-37 (1968).

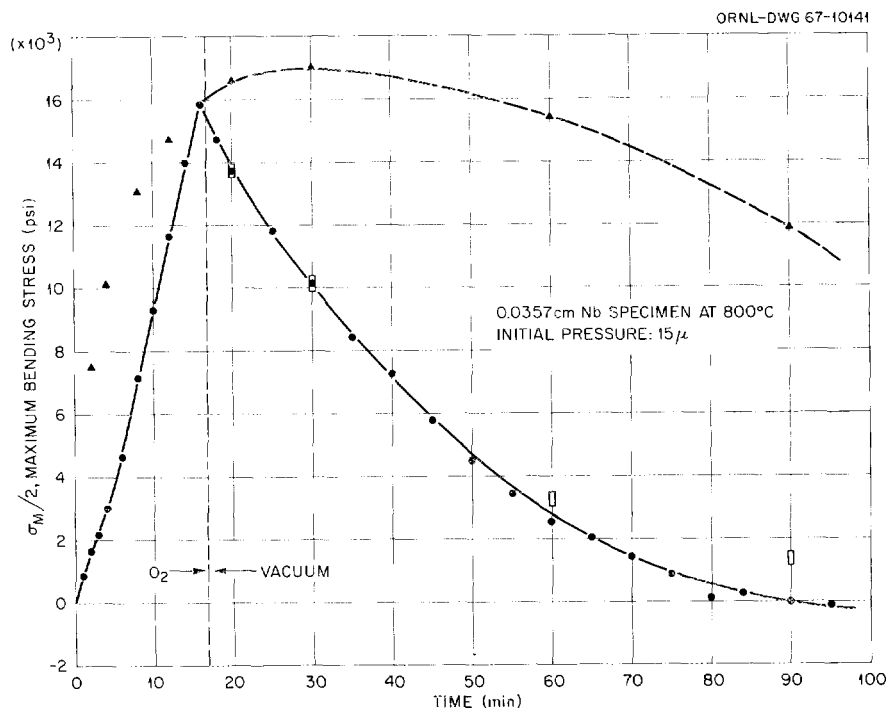


Fig. 12.4. Flexure Behavior During Oxidation-Annealing Experiment at 800°C for Niobium Specimen. Oxygen pressure for first 16 min was approximately 0.015 torr. • Maximum bending stress, experimental data; □ bending stress computed on the basis of oxygen redistribution via volume diffusion during vacuum anneal; ▲ bending stress computed on the basis of a constant oxygen concentration at the surface.

wide temperature range. The standard tracer methods were applied, subject to the restrictions associated with the very small diffusion distances involved after diffusion at the lower temperatures. A serious experimental difficulty was encountered in that portions of the ^{95}Nb tended to remain on the surface of the specimen during chemical dissolution of the anodic layer. This problem was resolved by use of ultrasonic vibration during dissolution. Although the thickness calibration for the amount of tungsten removed per section is not yet as precise as desired for section thicknesses less than about 25 Å, we have nevertheless sectioned several specimens to nominal thicknesses as small as 15 and 10 Å with no anomalies apparent in the resulting penetration profiles.

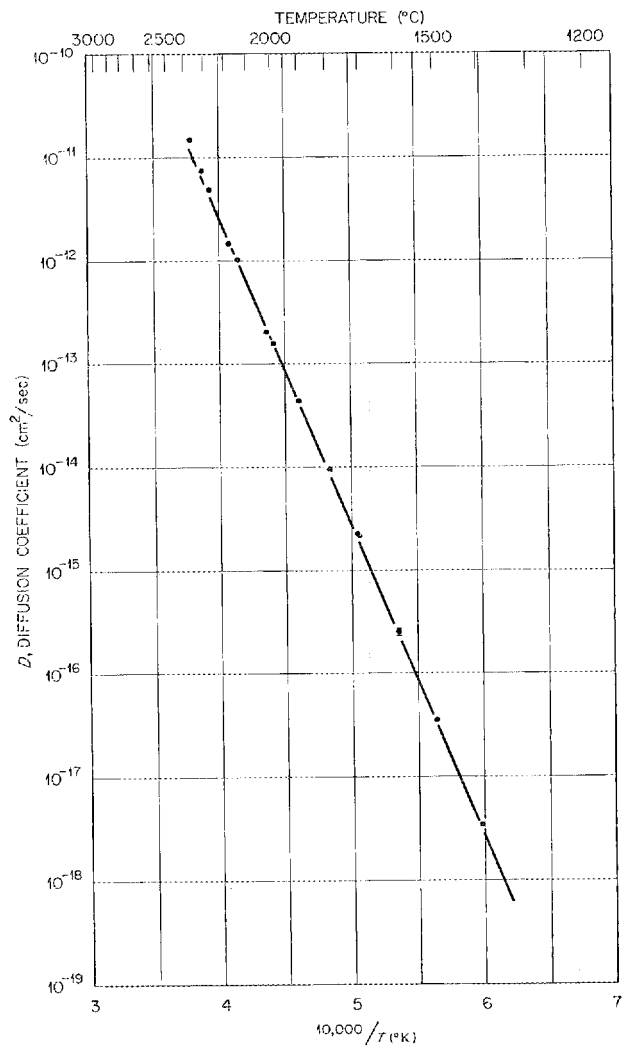
The values of the lattice diffusion coefficients for niobium in tungsten from 1400 to 2400°C obtained in this investigation are presented in Arrhenius form in Fig. 12.5. The data may be described by the equation:

$$D = 2.8 \exp(-137,000/RT) \text{ cm}^2/\text{sec},$$

with maximum deviations (based on 90% confidence) of about 1 and 5% for Q and D_0 , respectively. Our procedures are thus producing highly self-consistent values for bulk diffusion parameters. Furthermore, since errors associated with the use of the more conventional sectioning techniques become very large when dealing with diffusion coefficients smaller than about $10^{-13} \text{ cm}^2/\text{sec}$, the range of temperature now open to critical investigation is markedly increased.

The present emphasis of the experimental work is on the determination of the diffusion parameters for several metals in tungsten, including those for self-diffusion. Characteristics of short-circuit diffusion are also being studied. This work is being done in association with the Diffusion in Solids Group, and other work using this method is reported in Chapter 4 of this report.

Fig. 12.5. Temperature Dependence of the Lattice Diffusion Constant of ^{95}Nb in Tungsten.



13. Theoretical Research

Bernard Borie

We are investigating a number of phenomena in solids and also in atoms and molecules. Much of our effort has gone into band-theory calculations by the Korringa-Kohn-Rostoker method using techniques that we have developed. Work that we have done in addition to that described below includes fundamental investigations on electronic states and theoretical help to other groups and individuals in the Division.

CONSTANT ENERGY SURFACES FOR ALUMINUM BY THE KORRINGA-KOHN-ROSTOKER METHOD

J. S. Faulkner

Previous first-principles band theory calculations have all been interpreted as demonstrating that the third zone electron surface is multiply connected in a manner that is similar to the free-electron result. The discussions of these calculations have emphasized that the inability to calculate the Fermi energy to better than a few hundredths of a rydberg casts some doubt on this feature of the Fermi surface. Using an extension of previously developed programs we calculated the constant energy surfaces for aluminum by searching in 561 directions in 1/48 of the Brillouin zone (25,478 directions in the full zone). With a modest expenditure of computer time we found the Fermi energy for several different potentials to better than 0.001 rydberg. This is sufficient accuracy to remove the ambiguity discussed above. We find that it is possible to construct potentials that lead to a third zone electron surface that is not multiply connected, although the parts on a given square face are connected to each other, a result that is in agreement with the most recent experimental indications. Even some of the potentials used in previous calculations give this result. Other features of the density of states function and the Fermi surface for aluminum were investigated.

EFFECT OF $\langle 001 \rangle$ UNIAXIAL TENSION ON THE FERMI SURFACE OF METALLIC COPPER

H. L. Davis

Calculations were performed relating to the change of copper's electronic band structure upon application of uniaxial tension along the $\langle 001 \rangle$ direction. We used modifications of our constant-energy-search techniques¹ based on the Korringa-Kohn-Rostoker method for band theory calculations. With these techniques the Fermi energies for potentials corresponding to strained and unstrained cases were obtained to four-figure accuracy by direct numerical solution of the one-electron eigenvalue problem. The potentials were obtained by a standard method² of superposition of free atom charge densities and use of the Slater exchange approximation. As is illustrated by the results of Table 13.1, these procedures lead to calculated changes of the Fermi surface with uniaxial tension that compare favorably with the only available direct experimental information³ on how copper's Fermi surface deforms with the considered stress. Our calculations are also consistent with the qualitative interpretation, which MacFarlane and Rayne⁴ gave their ultrasonic attenuation data, that the deformation properties of copper's Fermi surface are strongly anisotropic.

These calculations, when coupled with our previous hydrostatic pressure calculations,⁵ demonstrate for the first time that the relatively simple potential prescription² appears to be very promising in its ability to

¹J. S. Faulkner, H. L. Davis, and H. W. Joy, *Phys. Rev.* **161**, 656-64 (1967).

²L. F. Mattheiss, *Phys. Rev.* **133**, A1399 (1964).

³D. Shoenberg and B. R. Watts, *Phil. Mag.* **15**, 1275 (1967).

⁴R. E. MacFarlane and J. A. Rayne, *Phys. Rev.* **162**, 532 (1967).

⁵H. L. Davis, J. S. Faulkner, and H. W. Joy, *Phys. Rev.* **167**, 601-607 (1968).

Table 13.1. Effect of Tension
Along the (001) Direction
on Cross-Sectional Areas
of the Fermi Surface of Copper

Area	$d(\ln A)/d(\ln A_0)^a$	
	Experimental ^b	Calculated
[001] belly	2.4 ± 0.5	3.2
[001] rosette	-2.1 ± 0.8	-2.2
[100] belly	not measured	-0.5
[100] rosette	not measured	2.8
[101] dog's bone	not measured	-7.4
[110] dog's bone	not measured	18.3
[111] belly	not measured	-1.0
[111] neck	not measured	2.7

^a A is the cross-sectional area and A_0 is the diametral area of a free-electron sphere whose volume remains exactly half that of the Brillouin zone.

^bShoenberg and Watts, *Phil. Mag.* 15, 1275 (1967).

quantitatively describe changes of metallic band structure potentials with changes in lattice spacing and lattice symmetry. Such a demonstration has a bearing on attempts to calculate electron-phonon interactions in metals and also implies that modern band theory techniques will enable improvements to be made on historical calculations⁶ of elastic constants for metals.

EFFECT OF HYDROSTATIC PRESSURE ON THE FERMI SURFACE OF METALLIC GOLD

H. L. Davis

In an attempt to further extend our work on the effect of lattice deformations on electronic band structures, preliminary calculations were performed relating to the change of the Fermi surface of metallic gold with hydrostatic pressure. Using our constant-energy-search techniques,¹ based on the Korringa-Kohn-Rostoker method of band theory, we calculated detailed Fermi surfaces corresponding to lattice spacings a and $0.99a$, where a is the normal lattice constant of gold. In obtaining these Fermi surfaces, separate potentials, based on the Mattheiss prescription,² were calculated for each lattice spacing using free atom wave functions.⁷ As is illustrated by Table 13.2, these

⁶K. Fuchs, *Proc. Roy. Soc. (London), Ser. A* 153, 622 (1936).

⁷The necessary atomic gold wave functions were calculated by T. C. Tucker of the Mathematics Division. His method is given by C. W. Nestor *et al.*, *Relativistic and Non-Relativistic SCF Wave Functions*, ORNL-4027 (December 1966).

Table 13.2. Hydrostatic Pressure
Variation of Two Cross-Sectional
Areas of the Fermi Surface of Gold

Area	$\Delta A/A\Delta P$ (cm ² /kg)	
	Experimental ^a	Calculated
[111] neck	1.97×10^{-6}	2.34×10^{-6}
[111] belly	2.84×10^{-7}	3.25×10^{-7}

^aFrom I. M. Templeton, *Proc. Roy. Soc. (London) Ser. A* 232, 413 (1966).

procedures lead to changes in gold's Fermi surface with pressure that compare favorably with the only available direct experimental information.⁸

CALCULATION OF THE BAND STRUCTURE OF "COMPLEX" CRYSTALS

H. L. Davis

A rather extensive computer code was developed for calculating the electronic band structure for crystals having two atoms per unit cell. This code is based on extensions of the Korringa-Kohn-Rostoker method of band theory given by Segall⁹ and by Treusch and Sandrock.¹⁰ Since no group theory is used as a basis of the code, the same code works equally well for all crystal symmetries having two atoms per unit cell. This code has been successfully debugged by performing test calculations and comparing with published results¹¹⁻¹³ on TiO, Be, and KCl. In all cases, our test calculations agreed with published results to within about 0.002 rydberg.

We started to apply this code to the calculation of the electronic band structure of uranium nitride. These "first attempt" calculations show the Fermi energy of this metallic compound intersects a narrow f -band, which is consistent with low-temperature specific heat data in Chapter 6 of this report. Furthermore, the calculations would indicate that the strong binding (high-temperature strength) of this compound is due to a covalent s - p band a few electron volts below the Fermi energy. We hope that as good single crystal specimens

⁸I. M. Templeton, *Proc. Roy. Soc. (London) Ser. A* 292, 413 (1966).

⁹B. Segall, *Phys. Rev.* 105, 108 (1957).

¹⁰J. Treusch and R. Sandrock, *Phys. Status Solidi* 16, 487-97 (1966).

¹¹V. Ern and A. C. Switendick, *Phys. Rev.* 137, A1927-36 (1965).

¹²J. H. Terrell, *Phys. Rev.* 149, 526-34 (1966).

¹³P. D. DeCicco, *Phys. Rev.* 153, 931-38 (1967).

of this compound become available, further experimental data can be folded into the present calculation to enable the band structure of UN to be determined more accurately.

CALCULATION OF THE WAVE FUNCTIONS FOR THE ELECTRONIC STATES IN METALS

H. L. Davis

To theoretically study and attempt to calculate many of the interesting physical properties of real metals requires a knowledge of the details of the wave functions for the band structure electrons. Extensive modifications have been made on our existing¹ one atom per unit cell band structure computer code, which enable normalized wave functions for any of the band electrons to be obtained. To check the results, the wave functions were numerically determined by the two separate methods analytically derived by Ham and Segall.¹⁴ Since detailed agreement was obtained between calculations based on the two methods and because of other involved reasons, we believe our resulting wave function codes are successfully debugged.

Our first attempt to apply these codes has been toward a theoretical study of the Knight shift of metallic copper. For this study it is necessary to calculate $\langle |\psi(0)|^2 \rangle$, which represents the electronic probability density at a nucleus averaged over the Fermi surface. Using our best previously calculated¹ Fermi surface of copper, based on the Chodorow potential and the new wave function codes, we calculated $1.38 \times 10^{25}/\text{cm}^3$ for the above quantity. This is to be compared with recent^{15,16} attempts to extract an experimental estimate of this quantity from Knight shift data, which fall in the range 1.1×10^{25} to $1.5 \times 10^{25}/\text{cm}^3$.

VALENCE STATES OF CARBON IN π -ELECTRON SYSTEMS. I. ALTERNANT-HYDROCARBON GROUND STATES¹⁷

Harris J. Silverstone¹⁸ Hubert W. Joy

When the molecular wave function is described in part by molecular-orbital theory, new terms (Coulomb self-repulsion integrals) enter the valence-state energy over and above the classic valence-bond valence state of Van Vleck. Atomic orbitals for π -electron theory are obtained by minimizing the energy of carbon in a

valence state appropriate for alternant-hydrocarbon ground states. The $2p\pi$ orbital so obtained with a nonintegral- n "double" basis, with a simple valence-bond σ wave function and a simple molecular-orbital σ wave function, gives a one-center Coulomb repulsion integral $\langle 2p\pi 2p\pi | 1/r_{12} | 2p\pi 2p\pi \rangle = 12.38$ ev, compared with the semiempirical value of about 11 ev.

VALENCE STATES OF CARBON IN π -ELECTRON SYSTEMS. II. EXCITED STATES AND IONS¹⁹

Hubert W. Joy Harris J. Silverstone¹⁸

Changes in atomic orbitals (AO) brought about by changes in molecular wave functions are studied by minimizing the energy of carbon in atomic valence states appropriate for ions and excited states of alternant hydrocarbons. We found that positive-ion and triplet-state $2p\pi$ AO's are more contracted than in alternant hydrocarbon ground states. Negative-ion and excited-singlet $2p\pi$ AO's are more expanded than those for the ground states. These AO changes may be negligible for large molecules but are increasingly important for molecules smaller than naphthalene.

S LIMIT IN HELIUM. MOVEMENT OF A SYSTEM ON AN ENERGY SURFACE IN PARAMETER SPACE²⁰

George S. Handler²¹ Hubert W. Joy

As part of a variational examination of angular correlation in electronic systems, a careful examination of the movement of a system on an energy surface in parameter space has been made. The results indicate that the surface is highly convoluted and that minimization techniques must take explicit account of this. An eight-term result close to the S limit in helium is given.

¹⁴F. S. Ham and B. Segall, *Phys. Rev.* **124**, 1786 (1961).

¹⁵A. Narath, *Phys. Rev.* **163**, 232 (1967).

¹⁶L. H. Bennett, R. W. Mebs, and R. E. Watson, *Bull. Am. Phys. Soc.* **13**, 690 (1968).

¹⁷Abstracted from *J. Chem. Phys.* **47**(4), 1384-92 (Aug. 15, 1967).

¹⁸Department of Chemistry, The Johns Hopkins University, Baltimore, Maryland.

¹⁹Abstracted from *Mol. Phys.* **13**(2), 149-56 (1967).

²⁰Abstracted from *J. Chem. Phys.* **47**(12), 5074-77 (1967).

²¹Department of Chemistry, University of Georgia, Athens.

14. X-Ray Diffraction

H. L. Yakel

Our purposes reflect both the extent to which other groups rely on x-ray diffraction as an adjunctive analytic tool in the solution of their problems and basic research programs in which x-ray diffraction methods are of principal importance. Boundaries between these aspects often overlap, and experience has shown that work of fundamental interest may evolve from initially routine experiments.

Our laboratory continues to serve both purposes. We perform routine measurements, such as those described below, at an increasingly efficient rate thanks to the use of improved experimental procedures and computer techniques. In areas of fundamental research, we pursue theoretical and experimental studies of high- and low-angle x-ray scattering from imperfect crystalline solids and investigate crystal structures of uncommon interest.

ROUTINE ANALYSES

O. B. Cavin¹ L. A. Harris
J. E. Epperson R. M. Steele
H. L. Yakel

Some pertinent results of diffraction analyses of the more than 1400 samples submitted to our laboratory during the reporting period may be found in appropriate sections of this report. Although it is not possible to describe each problem in detail, we present here a brief classification of the kinds of experiments performed, some results of inherent interest, and a general overview of the reaction of automation and computer technology on our routine procedures.

We have performed desired analyses requiring the use of powder and single-crystal diffractometry and film techniques. Phase analysis, lattice-parameter estimation, crystal orientation and perfection studies, preferred orientation measurements, crystal-structure analysis, strain and particle-size analysis, and the investigation of phase transformations at elevated temperatures are representative of these tasks. We have also assisted the Ceramics Group in the optical microscopy of cement aggregates.

An M₆C-type precipitate was identified² in Hastelloy N, but it is clear that in this alloy silicon rather than only carbon must play a major role in the precipitate's formation. We attempted to deduce the probable atom positions from knowledge of the elemental composition and the relative powder diffraction line intensities.

Phases present in beryllium-rich beryllium-boron alloys³ were studied by powder and single-crystal diffraction methods. Decomposition of hafnium-tantalum and hafnium-niobium alloys⁴ was examined by the Debye-Scherrer method with the use of flat, highly oriented graphite monochromators⁵ to achieve higher line-to-background intensity ratios at minimal increases in exposure time. Lattice parameters of solid solution alloys in lanthanide-lanthanide and Fe-Ni-Cu systems were measured.⁶ Results are collected in Table 14.1.

We demonstrated⁷ that the crystal structures of Cs₃MgCl₅ and Cs₃NiCl₅ are isotypic with the reported⁸ structure of Cs₃CoCl₅. Values of the lattice parameters of Cs₃NiCl₅ were obtained at liquid nitrogen and liquid helium temperatures; this experiment also confirmed the absence of a phase transition in the compound in the temperature range studied. Single-crystal x-ray diffraction data⁹ from a novel phase TiAl₂Cl₈ were collected with an automated diffractometer.¹⁰ Unit-cell

¹Now in Materials Compatibility Group.

²Work performed in cooperation with R. E. Gehlbach, Electron Microscopy Group; related microstructural studies are reported in Chap. 5.

³Work performed in cooperation with R. L. Hamner and T. G. Godfrey, Ceramics Group.

⁴Work performed in cooperation with C. T. Liu, Physical Metallurgy Group, and discussed in Part II, Chap. 15.

⁵C. J. Sparks, *Metals and Ceramics Div. Ann. Progr. Rept. June 30, 1966*, ORNL-3970, pp. 57-58.

⁶Work performed in cooperation with members of the Crystal Physics Group.

⁷Work performed in cooperation with T. W. Couch, Spectroscopy of Ionic Media Group.

⁸H. M. Powell and A. F. Wells, *J. Chem. Soc.* 1935, 359.

⁹Work performed in cooperation with J. Brynstad, Spectroscopy of Ionic Media Group.

¹⁰Work performed on an instrument made available by J. H. Burns, Transuranium Research Laboratory, Chemistry Division.

Table 14.1. Crystallographic Data for New Alloys and Compounds

Composition (at. %)	Crystal System	Lattice Parameter (Å)		Remarks
		a_0	c_0	
(Cr,Ni,Mo) ₆ (C,Si)	Cubic	11.028 ± 0.004		Hastelloy N ppt. Space group Fd3m
42.5Fe-42.5Ni-15Cu	Cubic	3.582 ± 0.001		fcc ^a
35Fe-35Ni-30Cu	Cubic	3.586 ± 0.001		fcc
27.5Fe-27.5Ni-45Cu	Cubic	3.590 ± 0.001		fcc
10Gd-90Y	Hexagonal	3.6479 ± 0.0003	5.7381 ± 0.0009	hcp ^b
60Gd-40Y	Hexagonal	3.6425 ± 0.0002	5.760 ± 0.002	hcp
80Gd-20Y	Hexagonal	3.6386 ± 0.0004	5.771 ± 0.002	hcp
69Gd-31Sc	Hexagonal	3.5585 ± 0.0004	5.6379 ± 0.0008	hcp
80Gd-20Sc	Hexagonal	3.5894 ± 0.0003	5.6938 ± 0.0006	hcp
SmF ₂	Cubic	5.740 ± 0.001		CaF ₂ type
YbF ₂	Cubic	5.594 ± 0.001		CaF ₂ type
Cs ₃ MgCl ₅	Tetragonal	9.23 ± 0.02	14.88 ± 0.02	Cs ₃ CoCl ₅ type
Cs ₃ NiCl ₅	Tetragonal	9.228 ± 0.009	14.53 ± 0.02	Cs ₃ CoCl ₅ type
TiAl ₂ Cl ₈	Monoclinic ^c	13.000 ± 0.003	11.772 ± 0.003	

^aFace-centered cubic Al structure type.

^bHexagonal close-packed A3 structure type.

^c $b_0 = 7.711 \pm 0.002$, $\beta = 92^\circ 37' \pm 1'$.

dimensions for these compounds are included in Table 14.1.

With a monotonic increase in the number of routine x-ray diffraction analyses requested each year, the continued ability of the group to efficiently perform its work rests on the incorporation of automation and computer methods in both the experiments themselves and the analysis of their results. We attempted to move in this direction during the past year through use of such experimental devices as patch-board-programmed or tape-controlled single-axis diffractometer drives and through development of local and remote-access computer programs for evaluation of results.

CRYSTAL STRUCTURE OF SrBe₃O₄ (Ref. 11)

L. A. Harris H. L. Yakel

The compound SrBe₃O₄ forms hexagonal crystals, space group P62c, with unit cell dimensions $a_0 = 4.5961 \pm 0.0002$ Å and $c_0 = 8.9300 \pm 0.0004$ Å. We determined its crystal structure using three-dimensional Patterson and difference-Fourier methods and refined it by iterative least-squares procedures.

¹¹Abstract of paper to be submitted for publication to *Acta Crystallographica*.

The structure consists of pseudo-close-packed layers of oxygen and strontium atoms with beryllium atoms in tetrahedral and trigonal interstices. Each strontium atom has six oxygen-atom neighbors arranged about it in a trigonal prism with three additional oxygen-atom neighbors offset from the prism face centers. The mixture of tetrahedral and trigonal beryllium-oxygen atom coordinations is similar to the mixture reported¹² in Ca₁₂Be₁₇O₂₉ and may reflect the instability of the compound.

INTERPRETATION OF TEMPERATURE DIFFUSE SCATTERING¹³

Bernard Borie

An alternative formulation of temperature diffuse scattering theory is described. The result is in terms of the mean atomic displacements rather than the usual normal mode representation. The theory leads to a direct relation between first- and second-order diffuse intensity, which, by iteration, allows for a correction for the second-order contribution without approximation. This theory should be useful for highly anharmonic thermal motion.

¹²L. A. Harris and H. L. Yakel, *Acta Cryst.* 20, 295-301 (1966).

¹³Abstract of paper submitted to *Acta Crystallographica*.

SUBSTRUCTURE AND PERFECTION OF UO₂ SINGLE CRYSTALS¹⁴

A. T. Chapman¹⁵ D. E. Hendrix^{16,17}
C. S. Yust¹⁸ O. B. Cavin¹
G. W. Clark¹⁶

The quality of single crystals of uranium dioxide grown by three different techniques – vapor growth, arc-fusion, and internal centrifugal zone growth (ICZG) developed at ORNL – was compared by etch-pit patterns, transmission electron microscopy, and x-ray topography. Good correlation of results obtained by these experimental techniques was shown; however, substructure differences in crystals obtained by each of the methods exist.

A HIGH-TEMPERATURE VACUUM SAMPLE HOLDER FOR THE KRATKY CAMERA¹⁹

R. W. Gould²⁰ R. W. Hendricks

A furnace was designed for small-angle x-ray scattering studies of samples in vacuum at temperatures from ambient up to 450°C. Provision was made for heating and cooling the specimen at rates as great as 200°C/min between any two temperatures within the operating range. The sample holder could also be used for studies at temperatures down to -170°C.

AUTOMATIC BALANCED FILTER DEVICE FOR X-RAY DIFFRACTION EXPERIMENTS²¹

J. S. Arrington, Jr.²² R. W. Hendricks
W. J. Mason²²

An automatic balanced filter box that may be used on most standard x-ray diffraction tubes was constructed. It is designed to be used in conjunction with a wide variety of automated x-ray diffraction experiments to

¹⁴ Abstract of paper for Fall Meeting of the Nuclear Division of the American Ceramic Society, Urbana, Illinois, Sept. 19–22, 1967.

¹⁵ Consultant from the Georgia Institute of Technology, Atlanta.

¹⁶ Crystal Physics Group.

¹⁷ Now in Metallurgy Department, Oak Ridge Gaseous Diffusion Plant.

¹⁸ Physical Ceramic Studies Group.

¹⁹ Abstracted from *J. Sci. Instr.* Ser. 2 1, 681 (June 1968).

²⁰ Summer participant from the University of Florida, Gainesville, 1967.

²¹ Abstract of paper to be published in the *Journal of Applied Crystallography*.

²² Engineering Division, Y-12 Plant.

change Ross filters and insert attenuators into the incident x-ray beam on receipt of appropriate commands from the control system. The positions of the filters and attenuators may be displayed at all times by feedback signals generated by a combination of light sources and photocells.

SMALL-ANGLE X-RAY SCATTERING INVESTIGATION OF INHOMOGENEITIES IN ALUMINUM-ZINC ALLOYS²³

R. W. Hendricks R. W. Carpenter²⁴

A high-temperature small-angle x-ray scattering (SAXS) investigation was conducted over a range of temperatures in the single-phase region of aluminum-zinc alloys containing 30.7, 40.7, and 50.9 at. % Zn.

The increasing SAXS at decreasing angles is evidence of clustering within the solid solution. The average sizes of the clusters present in this temperature region have been obtained from the slope of the Guinier plot and are listed in Table 14.2. It should be emphasized that these clusters are not a second phase but are composition fluctuations within a single phase field.

These clusters are nearly half the size of those reported by other workers for aluminum-zinc alloys at lower temperatures in the two-phase field, corresponding to G-P zones in the early stages of precipitation. The present results indicate that it is not possible to obtain a "random" solid solution in the aluminum-zinc alloy system, even by superheating to within approximately 50°C of the solidus, and that the clusters present in the single-phase region probably have a strong influence on nucleation of second phases at lower temperatures.

We are analyzing the scattering curves in detail to recover the radial distribution functions for these alloys and to estimate the temperature of the coherent miscibility gap.

²³ Abstract of paper presented at the Annual Meeting of AIME, New York, February 25–29, 1968.

²⁴ Deformation of Crystalline Solids Group.

Table 14.2. Size of Clusters
in Aluminum-Zinc Alloys

Composition (at. % Zn)	Mean Cluster Radius (Å)			
	352°C	362°C	380°C	410°C
30.7	9.1	7.3		6.5
40.7	10.5	7.6	7.2	6.8
50.9	7.1			7.1

Part II. High-Temperature Materials Program

15. Physical and Mechanical Metallurgy of High-Temperature Materials

W. O. Harms

The purpose of this program is to provide a broad, base-technology evaluation of high-temperature alloys for use in high-performance nuclear reactors and isotopic heat sources for advanced space, terrestrial, and civilian power applications. Principal emphasis is placed on tantalum-, niobium-, molybdenum-, and vanadium-base alloys for systems that use alkali metals as thermodynamic working fluids and heat-transfer media. Some work on superalloys is included because of the more immediate need for these materials in thermoelectric power devices. Tungsten and tungsten-base alloys are investigated in the Tungsten Metallurgy Program and covered in Chapter 16 of this document.

This work is needed because lack of materials information continues to limit several advanced reactor

and isotopic power projects to development of components rather than prototype power systems. This situation can, in large measure, be rectified by systematic development and characterization of high-temperature alloys that are adequately creep resistant, fabricable, weldable, and structurally stable under the designated service conditions.

In the text that follows, frequent reference is made to commercial refractory alloys by their trade designations. The nominal compositions of these alloys are listed in Table 15.1.

MECHANICAL PROPERTIES OF REFRACTORY ALLOYS

J. R. Weir, Jr.

Our objective is to establish the comparative mechanical properties of promising refractory alloys from 1000 to 1650°C. Primary consideration is given to collecting 1000-hr creep-rupture data on materials in typical metallurgical conditions produced by alloy vendors. The program includes studies on the response of these alloys to other heat treatments to establish optimum strength, ductility, and stability. Also, creep data are being analyzed in terms of time-temperature parameters, to assist in program planning as well as to establish limits on the extent to which data may be extrapolated. Another activity includes fatigue studies on refractory metals to assist in the stress analysis of specific structures.

Table 15.1. Nominal Compositions of Refractory Alloys

Designation	Base	Alloying Elements (wt %)
B-66	Niobium	5 Mo, 5 V, 1 Zr
C-129Y	Niobium	10 Hf, 10 W, 0.1 Y
Cb-752	Niobium	10 W, 2.5 Zr
Cb-753	Niobium	5 V, 1.25 Zr
D-43	Niobium	10 W, 1 Zr, 0.1 C
FS-85	Niobium	27 Ta, 10 W, 1 Zr
SU-16	Niobium	11 W, 3 Mo, 2 Hf, 0.08 C
TZM	Molybdenum	0.5 Ti, 0.08 Zr, 0.02 C
Cb-TZM	Molybdenum	0.5 Ti, 0.08 Zr, 0.02 C, 1.5 Nb
TZC	Molybdenum	1.2 Ti, 0.25 Zr, 0.15 C
T-111	Tantalum	8 W, 2 Hf
T-222	Tantalum	9.6 W, 2.4 Hf, 0.01 C

Comparative Creep-Rupture Properties of Niobium Alloys

R. L. Stephenson

Recent work on niobium-base alloys has concentrated on C-129Y and SU-16. The 1000-hr creep-rupture strengths of these materials are compared with other alloys¹ in Fig. 15.1. Alloy C-129Y has exceptional fabricability, thermal stability, and ductility at cryogenic temperatures,² as indicated in the figure, these favor-

¹J. R. Weir *et al.*, *Metals and Ceramics Div. Ann. Progr. Rept.* June 30, 1967, ORNL-4170, pp. 65-69.

²Wah Chang Corporation, *Columbium and Tantalum Alloy Technical Information*, Vol. II, August 1966.

ORNL-DWG 67-6756R

C-129Y: COLD WORKED
 SU-16a: 1 hr AT 1200°C
 SU-16b: 1 hr AT 1600°C, 3 hr AT 1200°C
 FS-85a: 1 hr AT 1370°C
 FS-85b: 1 hr AT 1595°C
 D-43: STRESS RELIEVED 10 min AT 1205°C
 D-43M: ½ hr AT 1650°C, 25% COLD WORK, AND 1 hr AT 1425°C
 Cb-752a: 1 hr AT 1315°C
 Cb-752b: 1 hr AT 1595°C
 B-66: COLD WORKED 50%
 Cb-753: 1 hr AT 1205°C
 Nb-1% Zr: COLD WORKED

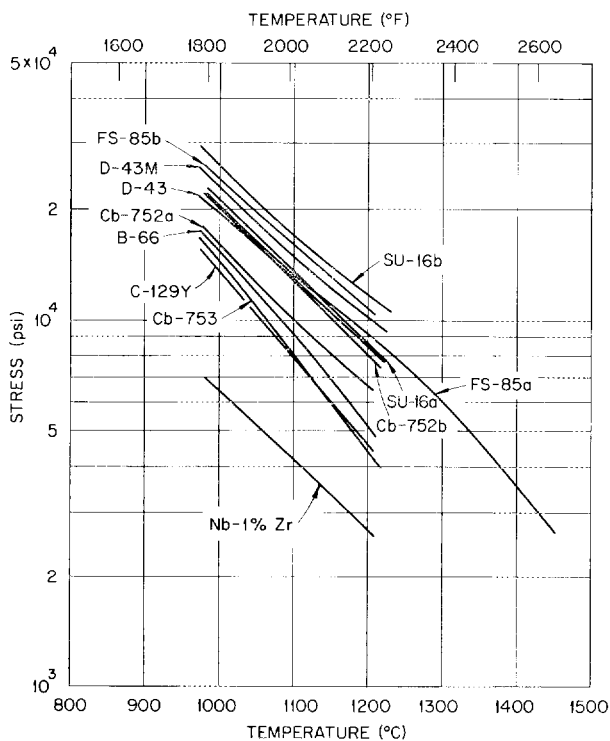


Fig. 15.1. Stress to Produce Rupture in 1000 hr as a Function of Temperature for Selected Niobium-Base Alloys.

able properties are achieved only by sacrificing high-temperature strength. The alloy is comparable in properties to Cb-753, one of the weakest of the second-generation niobium alloys. However, we tested C-129Y in the wrought condition, and some improvement in strength could result from optimization of heat treatment.

Alloy SU-16 was tested in two thermal conditions: (1) stress relieved at 1200°C, designated SU-16a, and (2) recrystallized at 1600°C and aged 3 hr at 1200°C, designated SU-16b. In the stress-relieved condition, the strength of this alloy is comparable to that of D-43 and FS-85 in similar metallurgical states. The recrystallization and aging treatment produces the highest strength we have observed in any niobium alloy.

Effect of Fabrication Variables on Creep Rupture of Molybdenum Alloys

R. L. Stephenson

Our work on molybdenum alloys has included the creep-rupture testing of TZC in two metallurgical

ORNL-DWG 67-6755R

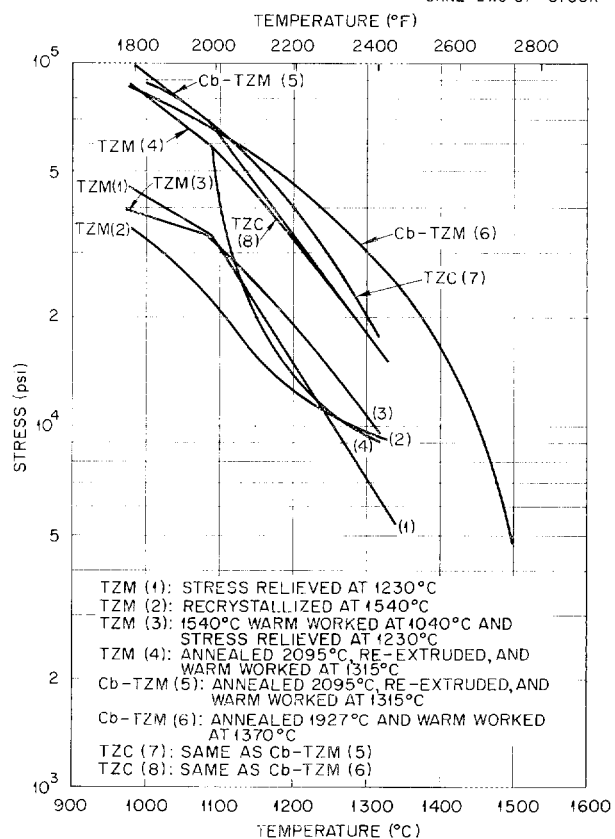


Fig. 15.2. Stress to Produce Rupture in 1000 hr as a Function of Temperature for Selected Molybdenum-Base Alloys.

conditions, and the results are shown in Fig. 15.2 along with previous data¹ for other molybdenum alloys. The histories are as follows: TZC(7) was solution treated at 2095°C, reextruded, and warm worked at 1315°C; TZC(8) was solution treated at 1925°C, warm worked at 1370°C, and stress relieved at 1205°C. The TZC(7) alloy exhibited somewhat better strength than TZC(8) at 1200°C but offers no distinct advantage over Cb-TZM. The high strength of Cb-TZM(6) at 1300°C encouraged us to perform additional tests at 1500°C. Although this investigation is incomplete, the trend of data indicates a significant drop in strength between 1300 and 1500°C.

Time-Temperature Parameters for Creep Rupture of Refractory Alloys

R. W. Swindeman R. L. Stephenson

Since creep is a thermally activated process, it is attractive to make use of the accelerated rate of high temperature to predict creep strength at lower temperatures and for longer times. Many time-temperature parameters have been developed for this purpose, and we are investigating the fit of our creep data on refractory metals to several of these.

Of particular interest are the Larson-Miller,³ Dorn,⁴ and Manson-Haferd⁵ parameters, since these are commonly used for engineering applications. A least-squares technique, suggested by Manson and Mendelson,⁶ is being used to calculate the parametric constants. The fit of the three parameters to creep-rupture data varies with the alloys and their heat treatments. In general, the three parameters yield about the same fit for an individual alloy. The niobium alloy FS-85 is one of the exceptions. The parametric master curves and predicted isothermal curves for 1% creep of this alloy are shown in Figs. 15.3 and 15.4. The fit of the Manson-Haferd parameter appears to be superior to those of the Dorn-Shepard and Larson-Miller parameters; it also predicts more conservative stresses upon extrapolation to low temperatures.

³F. R. Larson and J. Miller, "A Time-Temperature Relationship for Rupture and Creep Stress," *Trans. ASME (Am. Soc. Mech. Engrs.)* 74(5), 765-771 (July 1952).

⁴L. Orr, O. D. Sherby, and J. E. Dorn, "Correlations of Rupture Data for Metals at Elevated Temperatures," *Trans. Am. Soc. Metals* 46, 113-28 (1954).

⁵S. S. Manson and A. M. Haferd, *A Linear Time-Temperature Relation for Extrapolation of Creep and Stress-Rupture Data*, NACA-TN-2890 (1953).

⁶S. S. Manson and A. Mendelson, *Optimization of Parametric Constants for Creep-Rupture Data by Means of Least Squares*, N-62-70249 (March 1959).

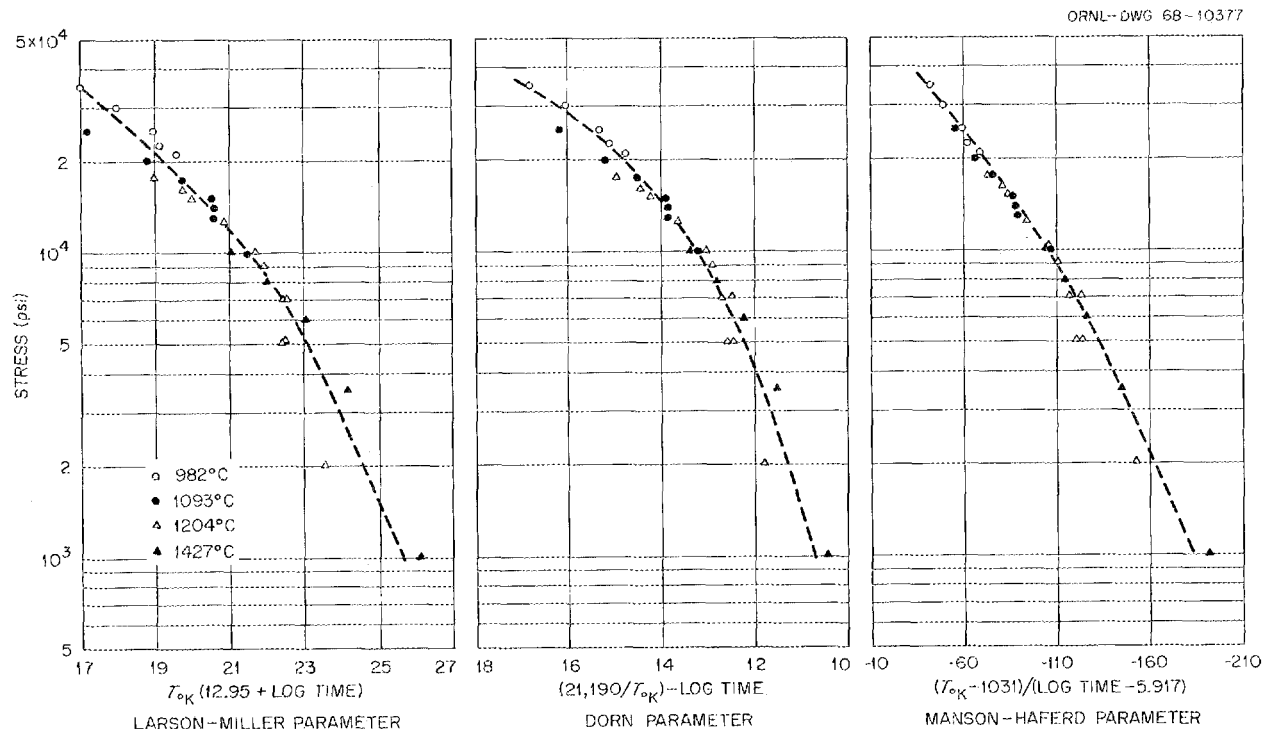


Fig. 15.3. Fit of Three Time-Temperature Parameters to 1% Creep Data for FS-85.

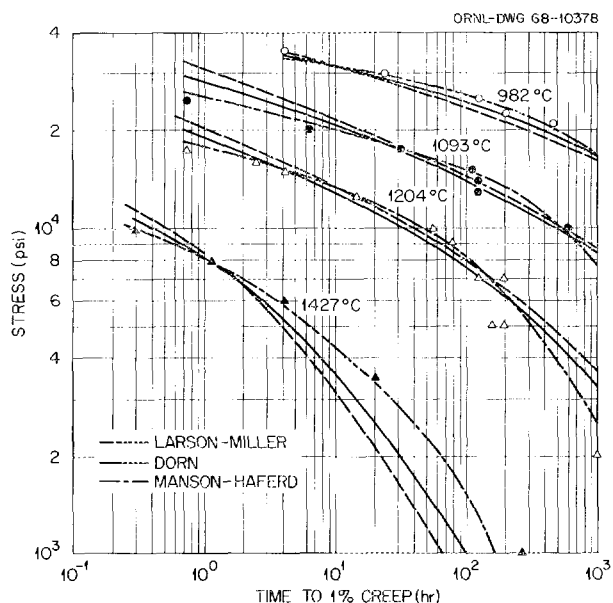


Fig. 15.4. Comparison of Isothermal 1% Creep Data for FS-85 to Curves Predicted by Three Time-Temperature Parameters.

Behavior of Refractory Alloys Under Dynamic Stresses

R. W. Swindeman

The low-cycle fatigue life of D-43 at the 1% plastic strain level was established over the temperature range from liquid nitrogen to 1205°C. At elevated temperatures the life is equal to or superior to that at room temperature, but in liquid nitrogen the life is one-fifth the room-temperature value and cleavage failure occurs with very little crack growth. Data for plastic strain range vs life are shown for three temperatures in Fig. 15.5.

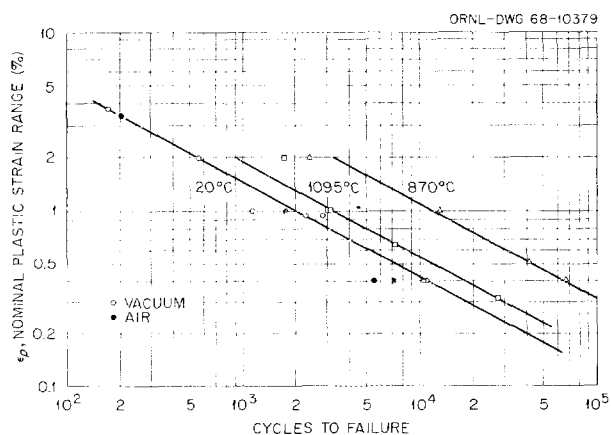


Fig. 15.5. Plastic Strain Fatigue of D-43 at Three Temperatures.

PHYSICAL METALLURGY OF REFRACTORY ALLOYS

H. Inouye

Diffusivity, Solubility, and Permeability of Interstitials in Refractory Alloys

R. L. Wagner

The diffusivity and solubility of nitrogen in tungsten are being determined as part of a broader program aimed at assessing the ability of candidate refractory-alloy fuel cladding to contain and not react deleteriously with the decomposition products, such as oxygen, carbon, and nitrogen, of ceramic fuels.

The degassing rate of the small amount of nitrogen in a suitably engassed 0.040-in.-diam tungsten wire was measured in an ultrahigh vacuum system with the aid of a mass spectrometer and calibrated conductances. The values of the diffusivity and solubility at 1800°K obtained in this study are compared with the literature values in Table 15.2. The disagreement between the various sets of data is due in part to the difficulty in measuring the small quantities of nitrogen in tungsten.

Table 15.2. Diffusivity and Solubility of Nitrogen in Tungsten at 1800°K

Investigator	Diffusivity (cm ² /sec)	Solubility at 760 torr of N ₂ (ppm)
Frauenfelder ^a	1.7×10^{-7}	3.0
Norton ^b	2.2×10^{-7}	0.17
ORNL	2.6×10^{-8}	28

^aR. Frauenfelder, *Permeation, Diffusion, and Solution of Nitrogen in Tungsten and Molybdenum Final Report*, WERL-2823-28 (June 1967).

^bF. J. Norton and A. L. Marshall, *Trans. AIME* 156, 135 (1944) and S. Dushman, *Scientific Foundations of Vacuum Technique*, Wiley, New York, 1962, p. 562.

Development of Age-Hardening Refractory Alloys

C. T. Liu

We are investigating the feasibility of improving the high-temperature strength of refractory alloys through the controlled precipitation of stable second phases, such as intermetallic compounds, products of spinodal decomposition, and products of ordering reactions.

Listed in Table 15.3 are some characteristic temperatures and properties of two niobium-base and two tantalum-base systems in which transformation by

Table 15.3. Characteristic Temperatures and Properties of Four Binary Refractory Alloy Systems in which Spinodal Decompositions are Possible

Alloy System	Solidus Temperature at Symmetrical Composition (°C)	Critical Temperature (°C)		Temperature Depression Due to Coherent Strain, $T_c - T_s$ (°C)	Eutectoid Temperature (°C)	Lattice Misfit (%)
		Chemical Spinodal ^a T_c	Coherent Spinodal ^b T_s			
Ta-Hf	2160	1660	1110	550	1020	5.9
Nb-Hf	2050	1800	1380	420	830	5.7
Ta-Zr	2040	1780	750	1030	800	8.5
Nb-Zr	1860	970	230	740	610	8.2

^aChemical spinodal: locus of points where second derivative of the free energy with respect to composition is zero.

^bCoherent spinodal: locus of points defining a region within the miscibility gap where coherent precipitation occurs.

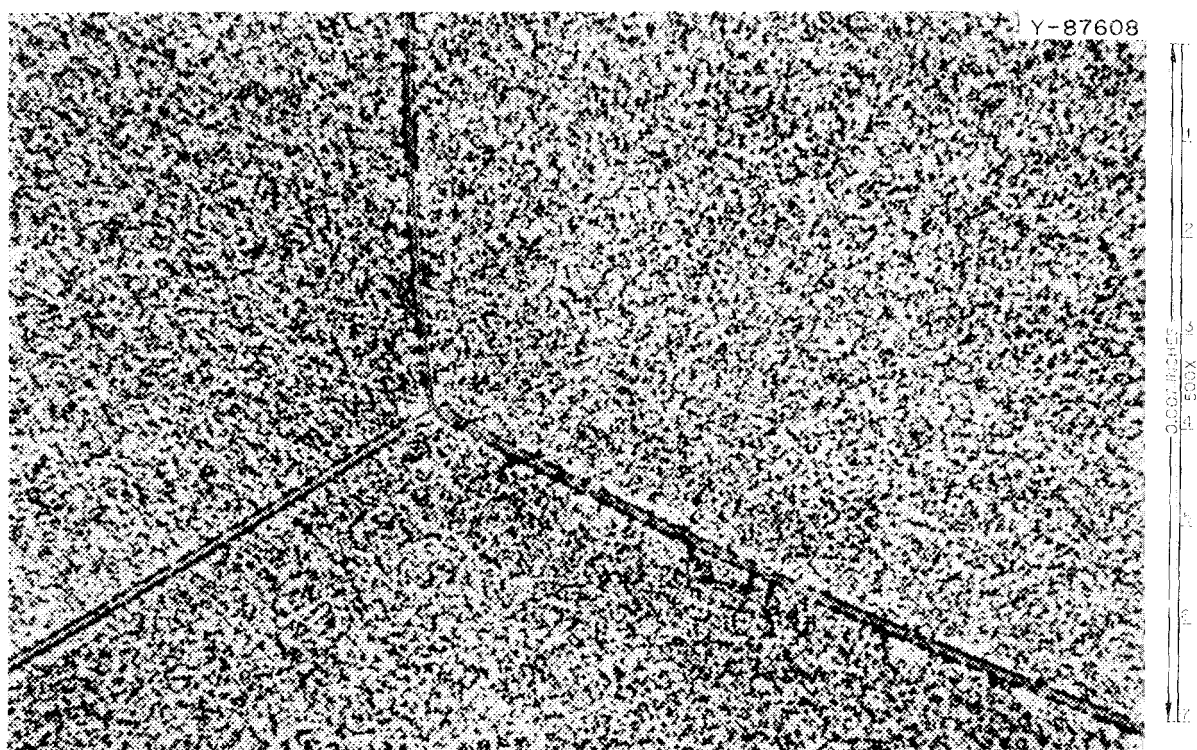


Fig. 15.6. Microstructure of Nb-40% Hf Aged 6 hr at 1000°C, Showing Typical Morphology of Precipitate in a Specimen Aged to Promote Spinodal Decomposition. Etchant: 1 part HF, 10 parts HNO₃, 5 parts H₂O.

spinodal decompositions is possible. When properly controlled, these transformations can lead to the precipitation of fine dispersions of daughter phases uniformly distributed throughout the grains.

Debye-Scherrer x-ray diffraction patterns of Nb-Hf and Ta-Hf alloys containing 40 to 65% Hf and quenched from 1730 to 1850°C show the presence of Guinier-Preston (G-P) zones, as evidenced by the small-angle scattering and strong diffuse streaks associ-

ated with the main Bragg reflections. The rapid growth of the G-P zones on aging seems to be governed by the existence of vacancy clusters. The morphology typical of the precipitate in an aged specimen is shown in Fig. 15.6.

Hardness data for a Nb-53% Hf alloy as a function of aging temperature is shown in Fig. 15.7. The highest rate of coarsening, corresponding to the valley of the hardness plot, occurs at 1050°C. The high hardness

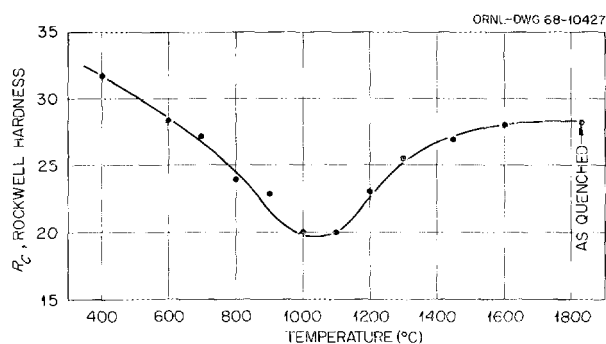


Fig. 15.7. Effect of Aging Temperature on the Room-Temperature Hardness of Nb-53% Hf Alloy for 3-hr Aging Treatments.

value for the quenched specimen indicates a high decomposition rate for the spinodal reaction, in agreement with the detection of G-P zones by x-ray diffraction in the quenched specimens.

Vaporization of Haynes Alloy No. 25 Under Stress

D. T. Bourgette

Haynes alloy No. 25 was creep tested under 1 to 2×10^{-8} torr at 785°C and stress levels of 2100 to 15,000 psi to correlate evaporation losses and microstructure with stress and the observed creep behavior. In 1000-hr tests, evaporation losses and the amount of Laves-phase precipitate increased with stress.

Evaporation had a significant effect on the creep properties. For example, a 0.012-in.-thick specimen tested at 1×10^{-8} torr and 14,500 psi ruptured in 246 hr at 785°C , but a control specimen tested in argon at 1 atm ruptured in 540 hr. These results may be compared with a rupture life of 2500 hr at 815°C and 15,000 psi in air.⁷ The times to 1% plastic strain for the vacuum-tested samples were 1/8 to 1/15 of those for comparably stressed air tests.

Section thickness is an important test parameter with respect to creep in vacuum because of the evaporation mode exhibited by complex alloys containing high-vapor-pressure elements.⁸ Initial results showed that a 0.012-in.-thick specimen ruptured in 246 hr, whereas a 0.030-in. specimen failed in 741 hr when tested at 785°C and approximately 15,000 psi. Since the evaporation losses per unit area were nearly the same, the

⁷R. Widmer *et al.*, *Mechanisms Associated with Long Time Creep Phenomena*, AFML-TR-65-181 (June 1965).

⁸D. T. Bourgette, *Vaporization Phenomena of Haynes Alloy No. 25 to 1150°C*, ORNL-TM-1786 (May 1967).

change in composition of the thinner specimen was more severe.

BRAZING ALLOY DEVELOPMENT

N. C. Cole D. A. Canonico
G. M. Slaughter

A number of brazing alloys have been developed that satisfy the requirements previously discussed;⁹ that is, that they melt and flow in a temperature range of 1300 to 1900°C and wet and braze refractory metals, graphite, and aluminum oxide. Ideally, the filler metals should be capable of joining these materials to each other as well as to themselves, and a number have been developed that do, indeed, satisfy this general requirement.

Systems within which the most acceptable alloys have been developed are given in Table 15.4; a brazing temperature range is shown for those systems in which more than one composition satisfied the requirements. As reported last year,⁹ the Ti-21% V-25% Cr alloy is outstanding in its ability to join Al_2O_3 and refractory metals. We have now found this alloy to be equally applicable for joining graphite to itself and to refractory metals. Microstructures of graphite-to-tantalum, Al_2O_3 -to- Al_2O_3 , and graphite-to-graphite brazes made with this composition are shown in Fig. 15.8.

Compositions exhibiting almost as much promise were also developed within the Ti-Zr-Ta system. For example, the 47.5% Ti-47.5% Zr-5% Ta alloy satisfactorily brazed refractory metals, Al_2O_3 , and graphite at approximately 1650°C . This system is rather unique in that it appears to possess solid solubility over its

⁹N. C. Cole and D. A. Canonico, *Metals and Ceramics Div. Ann. Progr. Rept. June 30, 1967*, ORNL-4170, pp. 73-74.

Table 15.4. Systems Containing Acceptable Brazing Alloy Compositions

Brazing Alloy System	Brazing Temperature (°C)	Materials Brazed		
		Refractory Metals	Graphite	Al_2O_3
Ti-V-Cr	1550-1650	x	x	x
Ti-Zr-Ta	1650-2100	x	x	x
Ti-Zr-Ge	1300-1600	x	x	
Ti-Zr-Nb	1600-1700	x	x	
Ti-Zr-Cr	1250-1450	x		
Ti-Zr-B	1400-1600	x		
Ti-V-Nb	1650	x		
Ti-V-Mo	1650	x		

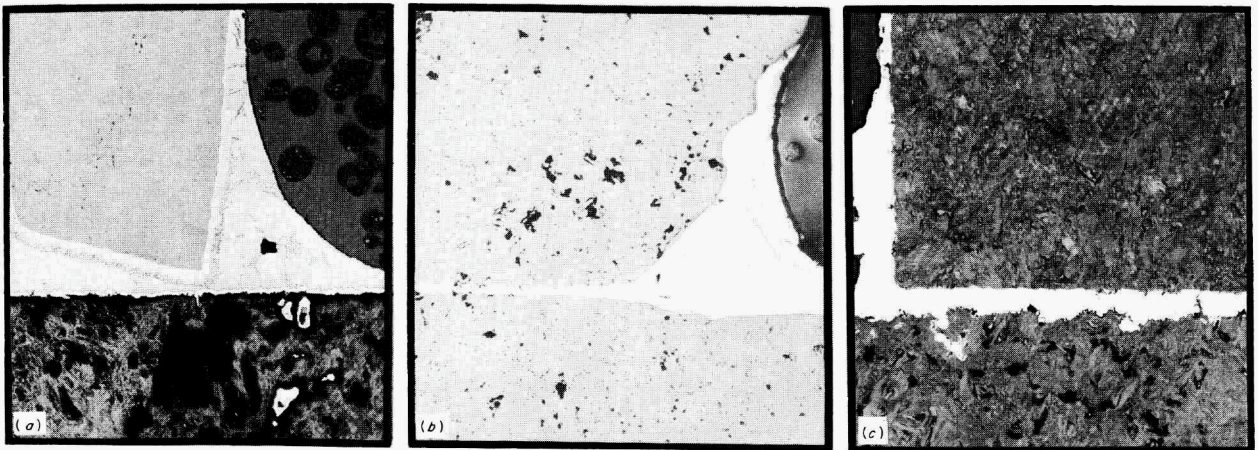


Fig. 15.8. T-Joints Brazed with Ti-21% V-25% Cr. (a) Tantalum to graphite. (b) Al₂O₃ to Al₂O₃. (c) Graphite to graphite. 100X. Reduced 36.5%.

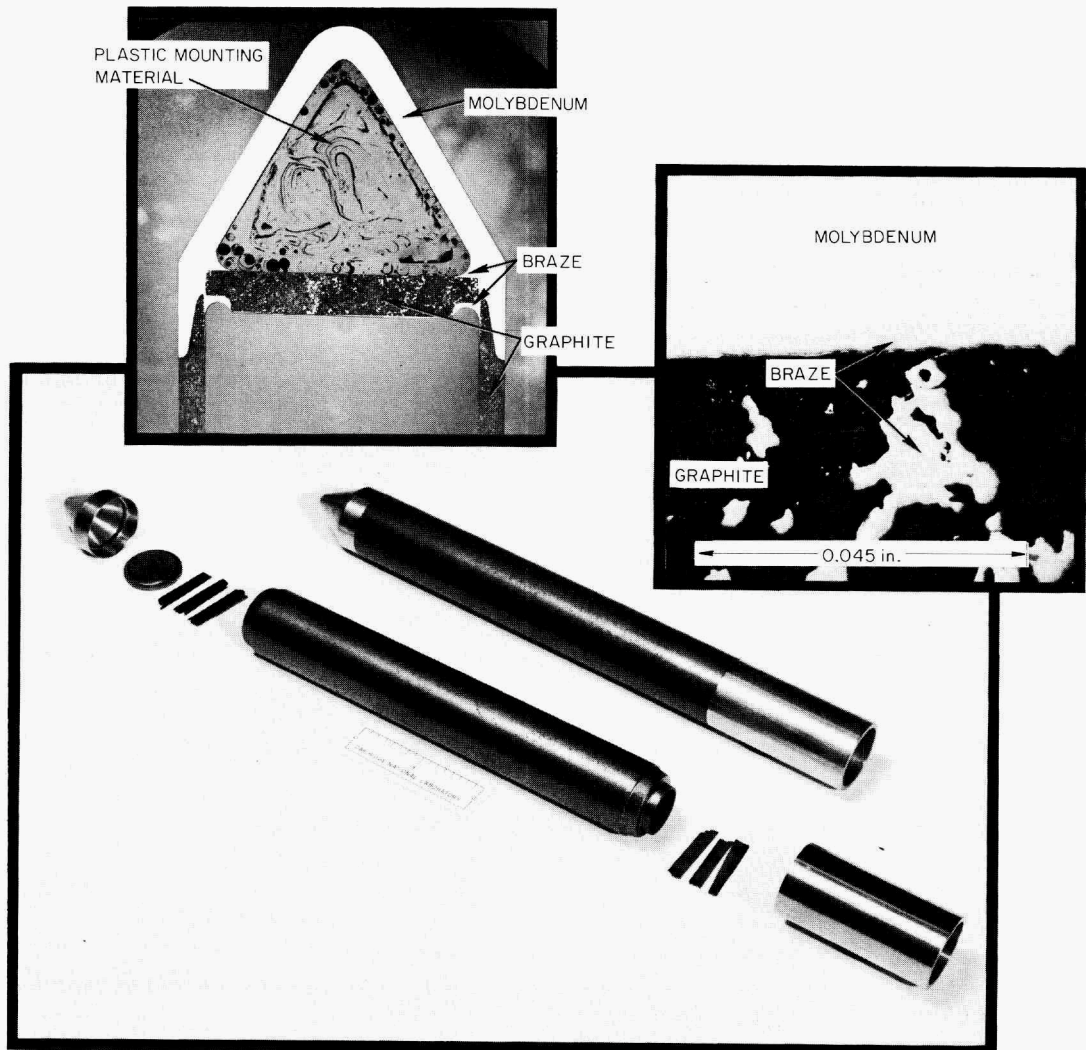


Fig. 15.9. Components for Cesium Diffusion Experiment Involving Graphite-to-Molybdenum Joints Brazed with 47.5% Ti-47.5% Zr-5% Nb Experimental Alloy.

entire composition range and, moreover, exhibits a relatively narrow liquidus-solidus separation. This latter feature is important in minimizing liquation of low-wetting constituents during heatup. The behavior of the Ti-Zr-Nb system is similar. Both systems should be applicable for developing a number of alloys for use over a wide temperature range.

The 47.5% Ti-47.5% Zr-5% Nb alloy has been successfully used to fabricate a component required for a cesium diffusion experiment. This alloy was used to make two graphite-to-graphite brazes and a molybdenum-to-graphite braze simultaneously at 1600°C. Figure 15.9 shows the individual components, the brazes that were made, and the excellent wettability and flowability of the alloy on both molybdenum and graphite.

In addition, several alloys useful at lower temperatures (1250 to 1300°C) were developed for joining refractory metals and graphite. Of particular note is Ti-20% Zr-15% Ge, which has shown an outstanding ability to wet and flow on graphite. Metallographic evaluation showed that not only does the filler metal flow into the capillary of joints but it also flows along and covers the flat surfaces of graphite sheets.

PHYSICAL PROPERTIES OF MOLYBDENUM

R. K. Williams J. P. Moore
D. L. McElroy

We measured the electrical resistivity and thermoelectric power of 99.97%-pure molybdenum (CMX-WB-LB-1 grade) from 100 to 1700°K and the thermal conductivity from 100 to 1250°K. The material had been arc-cast, hot rolled, and given a recrystallization anneal. The electrical resistivity ratio ($\rho_{273^\circ\text{K}}/\rho_{4.2^\circ\text{K}}$) of the material was found to be 142, indicating that impurity effects should have been negligible over most of the temperature range investigated. Smoothed values for the physical properties are shown in Table 15.5, and thermal conductivity data from another recent study¹⁰ are included for comparison. Our data for thermal conductivity λ and resistivity ρ can be correlated from 100 to 1250°K to

¹⁰A. D. Feith, *Measurements of the Thermal Conductivity and Electrical Resistivity of Molybdenum*, GE-TM-65-10-1 (1965).

Table 15.5. Physical Properties of Recrystallized Molybdenum Corrected for Thermal Expansion

Temperature (°K)	Thermal Conductivity (w cm ⁻¹ °K ⁻¹)		Electrical Resistivity (μohm-cm)	Absolute Seebeck Coefficient (μV/°K)
	This Study	Feith ^a		
100	1.752		0.930	+0.20
200	1.477		3.235	+2.93
300	1.401		5.561	+5.80
400	1.337		7.960	8.07
500	1.277		10.451	10.48
600	1.231		13.021	12.85
700	1.195		15.649	14.79
800	1.167		18.333	16.03
900	1.143		21.051	16.87
1000	1.123		23.815	17.35
1100	1.106		26.613	17.56
1200	1.094	0.863	29.432	17.47
1300	1.08 ^b	0.849	32.301	17.15
1400	1.07 ^b	0.835	35.209	16.64
1500	1.05 ^b	0.821	38.183	15.91
1600	1.04 ^b	0.807	41.201	14.78
1700	1.03 ^b	0.794	44.305	13.16

^aA. D. Feith, *Measurements of the Thermal Conductivity and Electrical Resistivity of Molybdenum*, GE-TM-65-10-1 (1965).

^bExtrapolated from $\lambda = 2.67 \times 10^{-8} T/\rho + 7/T$.

±0.5% by the equation

$$\lambda = 2.67 \times 10^{-8} \left[1 - \exp \left(-\frac{T}{90} + 0.214 \right) \right] \frac{T}{\rho} + \frac{7}{T},$$

where T is the absolute temperature. The constants obtained from this fit indicate that the Lorenz number of molybdenum exceeds the Sommerfeld value ($2.443 \times 10^{-8} \text{ v}^2/\text{K}^2$) at high temperatures and is similar to the Lorenz number we found for tungsten. This result is not in agreement with that of Feith,¹⁰ whose thermal conductivity values for molybdenum are 27 to 29% less than ours in the range of overlap. This illustrates the need for accurate measurements of thermal conductivity for the determination of the behavior of the Lorenz value at high temperatures. The $7/T$ term represents the lattice contribution, which is smaller than we found for tungsten.

NONDESTRUCTIVE TESTING OF REFRACTORY ALLOYS

R. W. McClung K. V. Cook

The specific techniques employed for nondestructive evaluation of refractory alloys are selected according to the materials and their configurations. Fluorescent

penetrants were used to evaluate the outer surfaces of the alloys, and very few significant discontinuities were detected by this procedure. At least one ultrasonic technique was used for the detection of internal flaws, and in some instances radiography and eddy currents were also applied. Many of the parts evaluated were small (1/4 to 1 in. OD × 1 to 6 in. long), and neither eddy currents nor ultrasonic techniques could be readily applied because of inadequate three-dimensional scanning mechanisms. Eddy-current and ultrasonic scanners were assembled from portions of 6-in. metal lathes and a small jeweler's lathe. Both mechanisms are now operable and adequate for developmental work.

Significantly, some of the cylindrical specimens of refractory alloys evaluated contained discontinuities oriented both parallel and perpendicular to the cylinder axis. Because it is necessary to inspect for transverse flaws if the material must be of high quality, we modified our tubing tank scanner facility to allow the inspection of small-diameter tubing (1/8 to 1 in. OD) for transverse oriented flaws. This redesigned facility allows a much quicker, simple mechanical adjustment for various tubing sizes for both longitudinal and transverse inspections.

A large portion of our work was devoted to the preparation of appropriate reference standards by electric discharge machining and subsequent evaluation of materials under study. Additional work of this type is discussed in Part III, Chapter 23 of this report.

16. Tungsten Metallurgy

W. O. Harms

Tungsten is of interest for advanced reactor systems employing ultrahigh-temperature liquid-metal-cooled circuits, thermionic conversion, and the Brayton Cycle. This interest stems from the fact that tungsten has a number of attractive properties including high melting point, good high-temperature strength, high thermal and electrical conductivities, high thermionic emission, and compatibility with many fuel materials and coolants. The goal of this program is to develop economical methods for producing high-quality tungsten and tungsten alloy tubing having good high-temperature creep resistance, microstructural stability, low-temperature ductility, and weldability. The program encompasses two areas of tubing fabrication — one by modification of conventional techniques based on extrusion, tube reducing, and warm drawing, and the other by direct chemical vapor deposition (CVD) through the hydrogen reduction of heavy-metal halides — and a complete physical-metallurgical evaluation of both. The materials being investigated include unalloyed tungsten, tungsten-rhenium alloys, other solid-solution-strengthened alloys, and dispersion- and precipitation-hardened alloys. All materials are consolidated by arc-casting, powder-metallurgy, or CVD techniques. More basic studies designed to elucidate the mechanisms controlling the metallurgical and mechanical behavior of tungsten and the role of selected alloying elements are included.

Percentage compositions given in this chapter are atomic percentages, as is customary for the tungsten alloys covered.

EXTRUSION AND DRAWING OF TUNGSTEN AND TUNGSTEN ALLOYS

W. R. Martin

The metalworking program on tungsten has as its objective the development of new or improved techniques for the fabrication of tungsten products with improved properties and quality. The fabrication of

tubing by floating-mandrel extrusion¹ and hot-plug drawing is emphasized.

Extrusion Development

R. E. McDonald C. W. Dean

Continuing our investigation of tungsten and tungsten alloy extrusions,¹ we extruded 36 billets in the past year as primary and duplex extrusions in the form of tube shells, round bar, and sheet bar. Extrusion temperatures ranged between 1650 and 1870°C and extrusion ratios varied from 3.6 for primary extrusions to 9.6 for duplex tube-shell extrusions. Primary extrusion temperatures were dropped from 2200 to 1870°C in an effort to improve the surface condition of the extruded products. Modification of the die design increased the life of the ZrO₂-coated dies.

Billets of arc-cast unalloyed tungsten, W-25% Re, W-26% Re, W-5% Re, and W-30% Re-30% Mo were extruded as round bars and then swaged to small-diameter rod for mechanical property specimens. Arc-cast unalloyed tungsten and W-25% Re sheet bar was rolled to 0.060-in.-thick sheet for mechanical property specimens.

Two 4-in.-diam arc-cast tungsten billets were extruded at 1750°C to produce nominal 2-in.-OD × 1/4-in.-wall tube shells for vented 1-kw curium isotope test capsules. Two 6-in.-diam arc-cast tungsten billets were extruded at 1850°C to produce nominal 3-in.-diam × 1/4-in.-wall pipe for unvented 1-kw curium isotope capsules. The 6-in. billets required extrusion tooling and pressures that exceeded the capability of our press and were extruded at the Fansteel Metals Center, Baltimore, under our supervision.

We analyzed the extrusion of tungsten and tungsten alloys in terms of extrusion conditions and properties of the extruded product. Large reductions can be made

¹R. E. McDonald and G. A. Reimann, *Floating-Mandrel Extrusion of Tungsten and Tungsten-Alloy Tubing*, ORNL-4210 (February 1968).

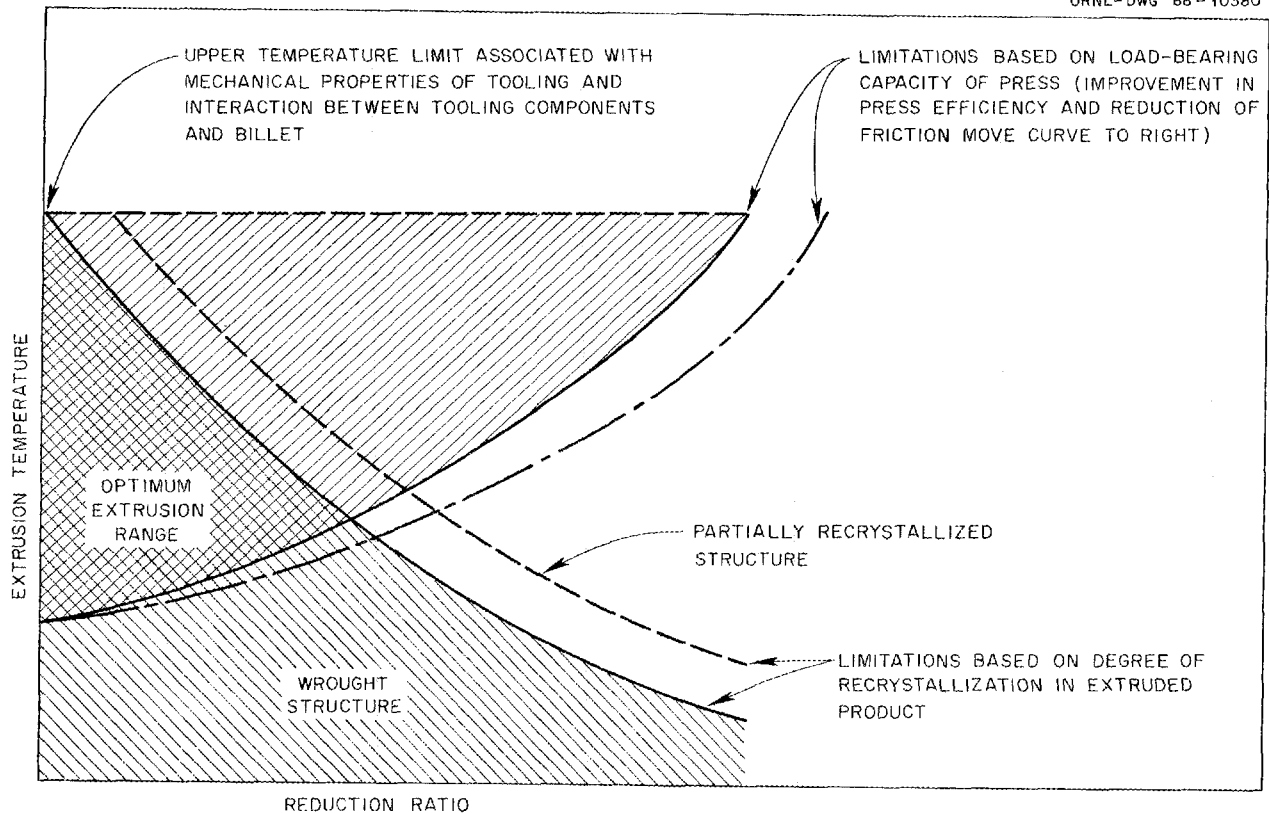


Fig. 16.1. Schematic Representation for Selection of Extrusion Conditions in Terms of Properties of Final Product and Capability of the Extrusion Press.

at temperatures that are restricted only by the chemical reactions between tooling and billet. Since the properties of the extruded product vary significantly with metallurgical structure, a second limitation needs to be imposed concerning the properties of the extruded part. To optimize the properties of tungsten for use at temperatures below the recrystallization temperature, a wrought structure is preferred over a recrystallized structure. Thus for a given reduction, an upper limit to the extrusion temperature is needed to prevent recrystallization. Absolute extrusion conditions for optimizing the properties of a tungsten extrusion vary with alloy composition and procedural details, such as transfer time from the billet furnace and extrusion speed. In general, the optimum extrusion range will be as shown in the double-crosshatched region in Fig. 16.1. Restriction of the extrusion conditions to this range should assist subsequent operations, such as the machining of components from extrusion billets and the cold- or warm-drawing of tubes and rods.

Hot-Plug Drawing Development

G. A. Reimann

Development of plug drawing techniques for reducing primary and duplex-extruded tungsten alloy tubes has continued. The drawbench modifications deemed necessary for this investigation were completed and include (1) a heated die head to maintain dies at 450°C , (2) a furnace to heat tube shells to 1000°C or higher, (3) a long-stroke mandrel advance and retraction system, and (4) a variable-volume pump to control drawing speed. The modified drawbench is shown in Fig. 16.2, and a close-up of the heated die head with the zirconia-insert die is shown in Fig. 16.3.

While feasibility of hot drawing had been demonstrated previously² at 700°C , the limitations of the process had not been established. In the past year,

²G. A. Reimann, *Metals and Ceramics Div. Ann. Progr. Rept. June 30, 1967*, ORNL-4170, p. 81.

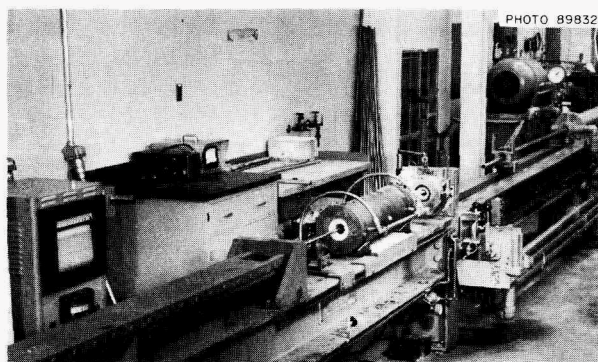


Fig. 16.2. Hydraulic Drawbench, Modified for Elevated-Temperature Plug Drawing of Refractory Metals.

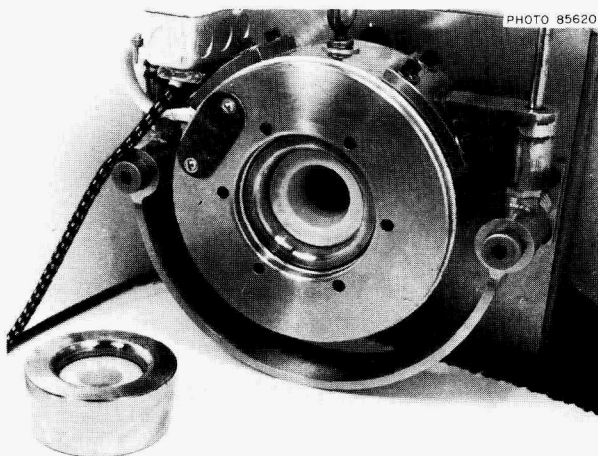


Fig. 16.3. Close-Up of Heated Die Head and Zirconia-Insert Die.

temperature, lubricants, tooling, and other drawing conditions were investigated.

The gas-fired muffle furnaces operated very effectively in the range 1000 to 1300°C but were not satisfactory at lower temperatures, principally because of nonuniform heating by the gas ports. A resistance furnace probably will be required for the lower temperatures.

A number of glass compounds and Fiske 604, a petroleum-base hot-die lubricant, were investigated as

lubricants at elevated temperatures. Glass lubricants were not effective because the oxide film formed on the tungsten tubes prevented satisfactory adherence of the glass coating; in addition, for thin-walled tubing insufficient heat was retained between the cooler die and plug to maintain glass fluidity, so the die, tube, and plug became cemented together by the solidifying glass. For drawing temperatures above 1000°C, the petroleum-base lubricant gave the best results.

The steel-cased vitrified zirconia dies (Fig. 16.3) have performed very well and appear to be well suited for this application. Numerous drawing plugs with zirconia shells have failed, and additional development work is needed in this area.

Unalloyed tungsten bar stock was successfully reduced 25% per pass at 1200°C and W-30% Re-30% Mo tubing was successfully reduced 30% in three passes at 1050°C. No intermediate anneals were required in either case.

CHEMICAL VAPOR DEPOSITION

W. R. Martin

By chemical vapor deposition (CVD), we are producing tungsten and tungsten alloys in shapes and with properties not obtainable by conventional metalworking processes. Our effort has been concentrated in three areas: (1) optimizing the deposition process with respect to deposition parameters and developing a theoretical approach to predict the variations, (2) examining the effect of deposition conditions on the orientation of tungsten and molybdenum, and (3) continuing our study on the conditions controlling the uniformity of composition and properties in deposits of tungsten-rhenium alloys.

Statistical Analysis of Tungsten Deposition

W. C. Robinson, Jr.

The purpose of this study was to (1) optimize the tungsten deposition process in a chosen system with respect to total deposition, deposition efficiency, and thickness uniformity; (2) develop a method for accurate specification of engineering response variables from first principles; and (3) identify the principal variables that control the formation of nodular growths. We developed an experimental design that allowed the response variables to be represented by a third-degree

polynomial in the independent experimental variables.³ It required 81 experiments. The results showed that the CVD process is sufficiently reproducible to be fitted by a mathematical model. A complete series of curves showing the effect of deposition parameters on the response variables was generated for our experimental range and enabled optimization of the deposition parameters in this range.

An equation based on gas-phase diffusion and reaction kinetics theory was derived and was found to fit the data better than the statistically derived third-degree polynomial.⁴ This equation involves three constants, all of which represent combinations of physical parameters of the reacting components. If the values of these basic parameters were measured independently, one could calculate the deposition characteristics of a system directly from our equation.

Nodular growths occurred in 25 of the 81 deposits. Correlation of the experimental parameters at the point of origin of nodules in these deposits did not identify a unique parameter responsible for nodule formation. We then calculated the surface concentration of the gas phase at all points where nodule deposition began. In 24 of the 25 runs, nodules developed when the mole fraction of WF_6 at the surface dropped below 0.009. Since temperature, pressure, and hydrogen and hydrogen fluoride concentrations were widely scattered for all runs, both with and without nodules, it became apparent that WF_6 surface concentration was the controlling factor in deposit morphology. With this information we have been able to predict and explain many of the previously unexplained phenomena encountered in CVD systems.

Effect of Deposition Conditions on the Orientation of CVD Tungsten and Molybdenum⁵

J. I. Federer W. C. Robinson
R. M. Steele

Tungsten deposited from WF_6 typically has a columnar grain structure with {100} planes oriented parallel to the substrate. Our purpose was to determine qualitatively from x-ray diffractometer intensities whether {110}-oriented tungsten and molybdenum, the most favorable orientation for thermionic application, can be deposited from WF_6 and MoF_6 .

The principal orientation in tungsten deposited at a hydrogen-to- WF_6 ratio of 10 in the range 600 to 1200°C was {100} parallel to the substrate. However, in the range 800 to 1000°C grains with {110} and {310}

planes parallel to the substrate appeared with the maximum proportion of {110}-oriented grains equivalent to that in randomly oriented tungsten powder. Attempts to reproduce this orientation in slightly larger samples at hydrogen-to- WF_6 ratios of 1.5, 3.0, 10.0, and 20.0 at 800 and 1000°C were unsuccessful. Thin tungsten layers deposited on {110}-oriented molybdenum substrates approached random orientation. Annealing at 1800 and 1900°C did not improve the {110} component of the orientation.

The principal orientation in molybdenum deposited at 800 and 1000°C was {100} parallel to the substrate, which changed to a very strong {211} orientation on annealing at 1800°C. At a deposition temperature of 1200°C the {100} orientation was very weak, and substantial intensities were observed for {110}, {211}, {111}, and {321} planes. Annealing at 1800°C produced very strong {100} and {211} orientations.

Thus, the goal of depositing {110}-oriented tungsten and molybdenum from WF_6 and MoF_6 was not realized. However, tungsten deposits approaching a random orientation have resulted from certain deposition conditions and substrates, suggesting that the {110} orientation can be produced under certain conditions.

Deposition of Tungsten-Rhenium Alloys

J. I. Federer

Tungsten-rhenium alloy tubing and sheet for metallurgical and mechanical property evaluation are being deposited by the hydrogen reduction of WF_6 and ReF_6 . Basic requirements for the deposits are uniformity of composition and a coherent grain structure.

The technique of delivering the WF_6 - ReF_6 mixture directly by means of an injector into the hot zone of a

³W. C. Robinson, F. H. Patterson, J. D. Fleming, and C. W. Gorton, "Chemical Vapor Deposition Statistical Parametric Study," pp. 109-25 in *Proceedings of the Conference on Chemical Vapor Deposition of Refractory Metals, Alloys, and Compounds, September 12-14, 1967*, ed. by A. C. Schaffhauser, American Nuclear Society, Hinsdale, Illinois, 1967.

⁴F. H. Patterson, W. C. Robinson, and T. L. Hebble, *The Statistical Design and Analysis of Vapor Deposition Experiments*, ORNL-TM-2066 (December 1967).

⁵This section is summarized largely from J. I. Federer, W. C. Robinson, and R. M. Steele, "Effect of Deposition Conditions on the Orientation of Chemical Vapor-Deposited Tungsten and Molybdenum," pp. 287-95 in *1967 IEEE Conference Record of the Thermionic Conversion Specialist Conference, October 30-November 1, 1967, Palo Alto, California*, Institute of Electrical and Electronic Engineers, New York, 1968.

heated mandrel⁶ was discontinued. Although uniformity of composition in both the axial and thickness direction was obtained, the deposits had a noncoherent or nodular grain structure when the thickness exceeded about 0.02 in. Nodules formed in deposits containing nominally 1, 5, 7, and 25% Re prepared with hydrogen-to-($WF_6 + ReF_6$) ratios ranging from 10 to 30 and temperatures from 650 to 950°C.

Alloys were successfully deposited on resistance-heated mandrels contained within a relatively large cold-wall chamber. Rod, tubular, and sheet-type substrates were used in this apparatus. Deposits containing nominally 5 and 25% Re were prepared at a hydrogen-to-($WF_6 + ReF_6$) ratio of 15, pressures of 5 to 10 torr, and temperatures from 600 to 950°C. The results of typical experiments are summarized below.

1. Nominal 5% Re alloys were generally uniform in composition along the deposit, and the composition was not particularly sensitive to temperature. Nominal 25% Re alloys were more uniform in composition when deposited at 750°C than at 600 or 950°C. In deposits that were uniform in composition the WF_6 -to- ReF_6 ratio apparently remained constant along the deposition surface.

2. The surfaces of all nominal 5% Re alloys made were smooth; thicknesses ranged up to 0.075 in. Surfaces of nominal 25% Re alloys were smooth for thicknesses of about 0.025 in. or less and rough for greater thicknesses.

3. The thickness of the deposits gradually decreased from the gas-inlet end of the apparatus toward the outlet end as WF_6 and ReF_6 became depleted. Reversing the direction of gas flow at regular intervals improved thickness uniformity.

By use of the external coating method 5/8 to 1-1/2-in.-wide X 18-in.-long sheets of nominal 5 and 25% Re alloys were deposited. These were uniform in both composition and thickness within about $\pm 5\%$ of the average values for thicknesses up to about 0.025 in. As the thickness increased, heat loss to the water-cooled electrodes resulted in rhenium-rich deposits on the cooler ends of the substrates and maximum thickness at the center.

EFFECT OF GAS BUBBLES ON RECRYSTALLIZATION AND GRAIN GROWTH IN CVD TUNGSTEN⁷

A. C. Schaffhauser K. Farrell

We are studying the properties of wrought CVD tungsten since the CVD process offers advantages, particularly in the production of thin-wall tubing, in supplying feed material for secondary working operations. We determined the deformation characteristics, recrystallization temperature, and ductile-to-brittle transition temperature (DBTT) of CVD tungsten sheet containing 25 ppm F rolled at temperatures between 400 and 1000°C to reductions of 40 to 95%. Previously we showed that fluorine impurities and the associated gas-bubble formation and growth that occurs on annealing have a large effect on the properties of undeformed CVD tungsten.⁸ The present studies showed that the

⁶J. I. Federer and W. R. Martin, *Metals and Ceramics Div. Ann. Progr. Rept. June 30, 1967*, ORNL-4170, pp. 84-85.

⁷Abstracted from a paper presented at the 97th AIME Annual Meeting, New York, February 25-29, 1968.

⁸A. C. Schaffhauser and R. L. Heestand, *Metals and Ceramics Div. Ann. Progr. Rept. June 30, 1967*, ORNL-4170, pp. 88-89.

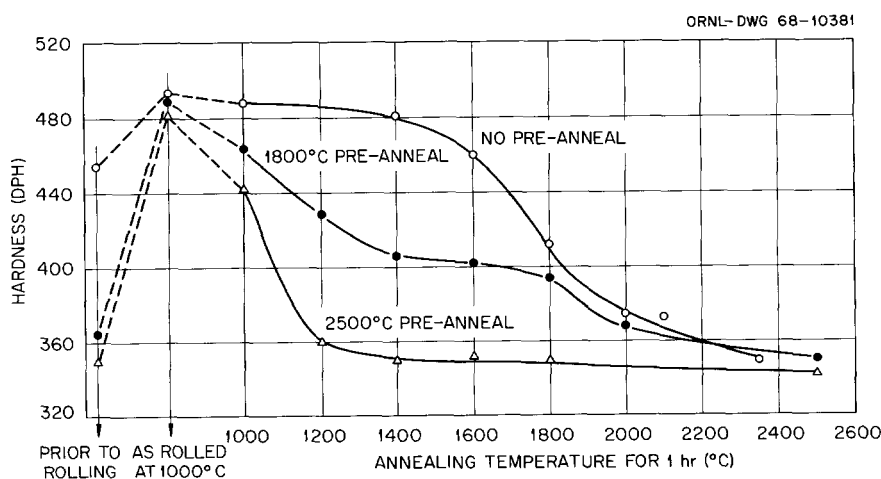


Fig. 16.4. Effect of Annealing Temperature on the Hardness of As-Deposited and Preannealed CVD Tungsten Sheet Rolled 80% at 1000°C.

properties of wrought CVD tungsten are also affected by gas bubbles.

The columnar grain structure of CVD tungsten was completely destroyed and a fine cellular substructure developed for reductions of 80% by rolling above 500°C. These samples did not recrystallize in 1 hr below 1800°C and recrystallized completely only after annealing above 2100°C, which is significantly higher than the 1100 to 1400°C recrystallization temperatures for conventionally produced tungsten. A fine distribution of gas bubbles smaller than 400 Å in diameter was observed in the substructure of samples annealed between 1400 and 1800°C. Additional samples, pre-annealed at 1800 and 2500°C to precipitate larger bubbles before rolling, recrystallized at much lower temperatures, as seen from the hardness data presented in Fig. 16.4. These data show that the gas bubbles smaller than 400 Å in diameter, unprecipitated fluorine impurity clusters, or both are responsible for retarding recrystallization in this material.

At annealing temperatures above 1800°C, gas bubbles cover a large fraction of the grain-boundary area and inhibit grain growth after recrystallization. The retarded recrystallization and limited grain growth in the rolled CVD tungsten results in a lower DBTT than that of high-purity, conventionally produced tungsten sheet annealed above 1400°C.

CREEP-RUPTURE PROPERTIES OF WROUGHT TUNGSTEN ALLOYS

R. L. Stephenson

Our objective is to evaluate the creep-rupture properties of tungsten alloys from 1650 to 2200°C for times extending to 1000 hr. The test specimens are machined from products derived from powder, arc-melting, and CVD consolidation processes. Wrought arc-cast tungsten, W-5% Re, W-26% Re, and W-25% Re-30% Mo in the form of 1/4-in.-diam rod have been emphasized.

The stress-rupture data generated at 1650 and 2200°C are shown in Fig. 16.5 along with data for W-25% Re, produced by the same process⁹ but in sheet form and annealed at 1760°C. The trend of the data at 1650°C indicates W-5% Re to be the strongest alloy, followed by W-25% Re, tungsten, and W-25% Re-30% Mo. The strength advantage of the binary alloys is reduced

⁹R. R. Lowery and G. Asai, *An Evaluation of W-25 Re Produced by Both Arc-Melting and Powder Metallurgy*, USBM-RC-1274 (Feb. 19, 1968).

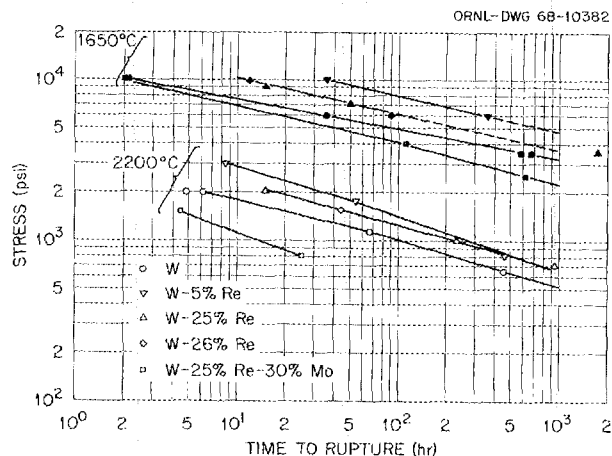


Fig. 16.5. Stress-Rupture Data for Tungsten and Tungsten Alloys.

at the lower stresses and longer rupture lives. At 2200°C the W-5% Re and W-25% Re alloys are equivalent and slightly stronger than tungsten at 1000 hr. The W-25% Re and W-26% Re alloys are equivalent at both temperatures, in spite of the fact that they represent different product forms and heat treatments.

Creep rates were observed to follow the same trend in relative strengths as the rupture data.

TUNGSTEN WELDING DEVELOPMENT

N. C. Cole G. M. Slaughter

We are studying the effects of welding on the properties of tungsten and tungsten-rhenium alloys produced by powder metallurgy, arc casting, and chemical vapor deposition (CVD).

We have found that a minimum workpiece preheat of 150°C is necessary to consistently produce welds free from cracking in 1/16-in.-thick tungsten sheet. Higher preheats did not appear to be beneficial; however, configurations involving more severe stress concentrations or more massive parts may require higher temperatures.

The large grain size of welds and the recrystallized heat-affected zone in tungsten and its alloys are largely responsible for the increase in ductile-to-brittle transition temperature (DBTT) observed after welding. The DBTT values for welds in typical powder metallurgy unalloyed tungsten and GE-15, a proprietary powder

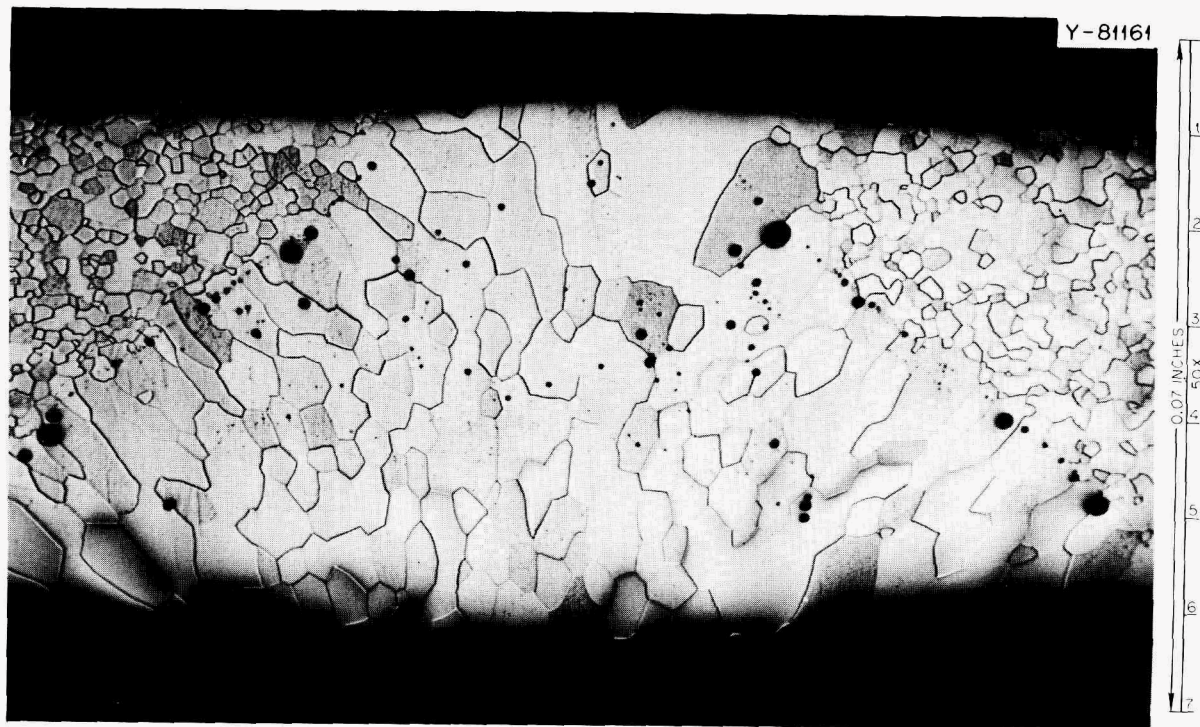


Fig. 16.6. Tungsten-Arc Weld in a Typical Wrought Powder-Metallurgy Tungsten Product. Gross porosity is evident, particularly along the fusion line. Etchant: $\text{H}_2\text{O}_2\text{-NH}_4\text{OH}$.

metallurgy product,¹⁰ were 325 and 385°C, respectively, compared to a DBTT of 150°C for both types of material in the unwelded condition.

The quality of a weldment depends to a great extent upon the method used in consolidating the base metals. Welds in arc-cast and electron-beam-melted base metals are essentially free from porosity; however, welds in powder-metallurgy tungsten are characterized by gross porosity, particularly along the fusion line (Fig. 16.6). The amount of this porosity is considerably reduced in welds in the GE-15 alloy.

The unusual as-deposited microstructure of CVD tungsten causes an unusual weld heat-affected zone. The base metal is composed primarily of large columnar grains with a fine-grained substrate surface. During welding, the fine grains in the heat-affected zone grow, but the large columnar grains do not. Consequently, if the fine-grained substrate surface is removed before welding, the weldment does not contain a metallo-

graphically detectable heat-affected zone. In worked CVD material (such as extruded and drawn tubing) the weld heat-affected zone exhibits the normal recrystallized grain structure.

The amount of residual fluorine in CVD tungsten has a great effect on its weldability. A fluorine content greater than 20 ppm is sufficient to cause cracking in the heat-affected zone. This cracking, as seen in Fig. 16.7, is caused¹¹ by rapid bubble formation and growth in the grain boundaries as the temperature exceeds 2500°C. At the high temperatures involved in welding, the bubbles are able to consume much of the grain boundary area; this effect, combined with the stress produced during cooling, causes the grain boundaries to pull apart, forming a crack.

¹¹K. Farrell, J. T. Houston, and A. C. Schaffhauser, "The Growth of Grain Boundary Gas Bubbles in Chemically Vapor Deposited Tungsten," pp. 363-90 in *Proceedings of the Conference on Chemical Vapor Deposition of Refractory Metals, Alloys, and Compounds, Gatlinburg, Tennessee, September 12-14, 1967*, ed. by A. C. Schaffhauser, American Nuclear Society, Hinsdale, Illinois, 1967.

¹⁰Powder metallurgy tungsten produced by General Electric Co., Cleveland.

Previously, the tungsten-arc welding of a simulated tungsten loop with W-26% Re filler wire was described.¹² Further studies showed that sigma phase was present in certain areas of the weld metal. Although popular belief is that the use of W-26% Re filler metal avoids sigma formation during fabrication and use, microsegregation during solidification may produce localized areas having a high propensity toward its formation.

We have not successfully reproduced this condition in subsequent bead-on-plate studies. Weld metal of W-26% Re deposited on unalloyed tungsten sheet has not revealed any sigma phase. Hardness traverses do show that as-deposited weld metal is harder than the unalloyed tungsten base metal, but upon aging at 900, 1200, 1600, and 2000°C for up to 1000 hr, the hardness decreases as the aging time and temperature increase. In fact, after aging for 1000 hr at 1200°C, the hardness of the weld metal reaches that of the base metal.

¹²N. C. Cole and G. M. Slaughter, *Metals and Ceramics Div. Ann. Progr. Rept. June 30, 1967*, ORNL-4170 pp. 90-92.

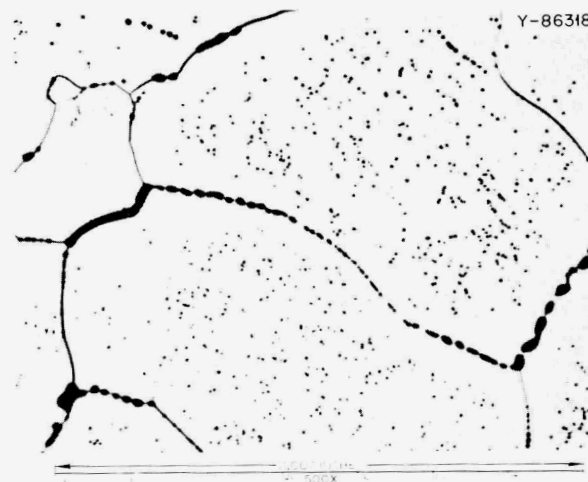
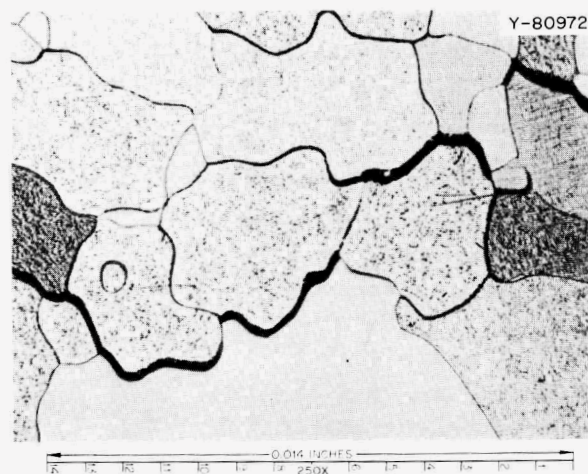
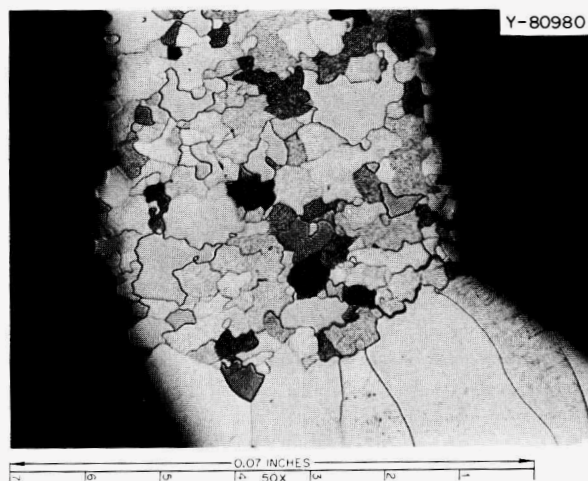


Fig. 16.7. Cracking and Bubble Formation in Chemical Vapor Deposited Tungsten at Three Magnifications. Etchant: $H_2O_2-NH_4OH$.

17. Alkali-Metal Corrosion of High-Temperature Materials

J. H. DeVan A. P. Litman
W. O. Harms

Auxiliary electrical or ion-propulsion requirements for space vehicles necessitate power plants of high efficiency that will operate at high temperatures. Nuclear power systems have been proposed for these applications in which alkali metals are used to transfer heat, drive a turbogenerator, and lubricate rotating components.¹ Accordingly, we are studying the corrosion properties of candidate alkali metals, primarily lithium and potassium, under conditions of interest for space applications. Because of the relatively high temperatures ($>1000^{\circ}\text{C}$), the studies are largely concerned with refractory-metal container materials.

COMPATIBILITY OF BOILING POTASSIUM WITH REFRACTORY ALLOYS

J. R. DiStefano D. H. Jansen
B. Fleischer

A program to investigate the compatibility of refractory metals with boiling alkali metals has been in progress using refluxing capsules, natural-circulation loops, and forced-circulation loops.² Tests are being conducted at 1100 to 1400°C with durations ranging from 100 to 5000 hr. Materials under investigation include alloys based on Nb, Ta, Mo, and W.

The investigation of corrosion under boiling conditions has involved refluxing capsules and both natural and forced-circulation loops. Most tests incorporate insert specimens to provide quantitative data on the rate of dissolutive attack. Engineering-scale forced-circulation loops also provide data on the corrosion-erosion resistance of potential nozzle and turbine-blade materials.

¹W. O. Harms and A. P. Litman, "Compatibility of Materials for Advanced Space Nuclear Power Systems," paper 67-WA/AV-1 presented at the meeting of the American Society of Mechanical Engineers, Pittsburg, Pa., November 1967, and accepted for publication in *Nuclear Applications*.

²J. R. DiStefano, D. H. Jansen, and B. Fleischer, *Metals and Ceramics Div. Ann. Progr. Rept. June 30, 1967*, ORNL-4170, pp. 93-94.

Table 17.1 summarizes the conditions and results of tests conducted during the past year. These tests have effectively completed the original objectives set for our potassium program and have brought the cumulative operating time for refractory-metal-boiling-potassium systems to over 100,000 hr. Potassium studies for the coming year will be limited to the completion of tests on tungsten- and molybdenum-base alloys.

Capsule Test Examinations

Capsule tests now in progress or recently completed are summarized in Table 17.1. Experiments with unalloyed niobium have shown an interesting contrast to our earlier capsule studies with niobium alloys. As discussed previously,^{2,3} the alloys of niobium, which as a class contain a minimum of 1% Zr, were resistant to attack in boiling potassium at temperatures up to 1300°C for times as long as 5000 hr. Unalloyed niobium, on the other hand, exhibited heavy attack in refluxing potassium initially containing less than 10 ppm O and was virtually destroyed in potassium to which 300 ppm O was added. As seen in Table 17.1, a similar oxygen addition had very little effect on Nb-1% Zr under comparable test conditions.

Unalloyed tungsten, like niobium, showed extensive attack in a 5000-hr refluxing capsule test at 1300°C. The test used tungsten with two different fabrication histories - insert specimens had been made by the chemical vapor deposition (CVD) process and the capsule by extrusion of powder-metallurgically produced material. Corrosion effects in this capsule were identified more with mass transfer occurring between the CVD and extruded material than with any concentration gradient that may have existed between condenser and boiler regions. Likewise, in an arc-cast

³J. H. DeVan, A. P. Litman, J. R. DiStefano, and C. E. Sessions, "Lithium and potassium corrosion studies with refractory metals," pp. 675-95 in *Alkali Metal Coolants* (Proceedings of a Symposium, Vienna, 28 November-2 December, 1966) International Atomic Energy Agency, Vienna, 1967.

Table 17.1. Summary of Boiling-Potassium-Refractory-Alloy Compatibility Tests

Material ^a		Temperature (°C)		Test Duration (hr)	Condensing Rate (g min ⁻¹ cm ⁻²)	Weight Change (mg/cm ²)	Results
Insert	Container	Boiler	Condenser				
Refluxing Capsules							
W ^b	W	1315	1240	5000	0.33	-93 to +188	Mass transfer between CVD inserts and powder metallurgically produced capsule
Nb ^c	Nb		1200	5000	0.32	<i>d</i>	Very heavy attack
Nb	Nb		1210	5000	0.40	<i>d</i>	Heavy attack
Nb-1% Zr ^c	Nb-1% Zr	1230	1210	5000	0.38	-3 to +1	No evidences of attack
<i>e</i>	W-25% Re		1180	5000	0.30		Examination in progress
<i>e</i>	W-25% Re	1250	1210	5000	0.33		Mass transfer deposit near top of vapor zone
Nb-1% Zr	Nb-1% Zr	1215	1200	950	0.28		Test in progress
Nb ^b	Nb		1200	1200	0.30		Test in progress
Natural-Circulation Loop							
TZM	TZM	1240	1160	<i>f</i>	0.29		Test in progress
Forced-Circulation Loops							
TZM	Nb-1% Zr	1200	450	3000	165 g/min		Nozzle-blade specimens showed negligible attack; mass transfer of loop components limited to zirconium migration from boiler to vapor and condenser regions
D-43	D-43	1300	840	10,000	280 g/min		Examination in progress

^aCompositions of alloys identified here and in the text of this chapter by commercial names are listed in Table 15.1.

^bChemically vapor deposited material.

^cPotassium contained approximately 300 ppm O before test.

^dInsert specimens bonded to capsule.

^eNo insert specimens available.

^fLoop has completed 4000 hr of a scheduled 5000-hr test.

W-25% Re capsule (Table 17.1) we observed a heavy mass transfer deposit in the condenser region of the capsule, a mass transport effect opposite to that expected from concentration gradient considerations. We suspect that impurities, possibly halogens, may have given rise to gas transport effects that dominated the usual concentration gradient effects in these capsules.

Forced-Circulation Loop Studies

Metallurgical analysis of the Nb-1% Zr alloy loop FCL-6 containing a TZM nozzle-blade test section was completed (Table 17.1) and a summary report is being written. The examinations revealed excellent compatibility of potassium with Nb-1% Zr and TZM alloys under engineering conditions. Mass transfer and erosion were minimal. The only visual evidence of mass transfer deposits was noted in the nozzle and blade test section and in the boiler nucleation rings. The deposits in

the test section were mostly ZrO₂ and chromium, the chromium apparently coming from the stainless steel pump cell, which operated with inlet and outlet temperatures of 400 and 540°C, respectively. Zirconium migrated from the upper region of the boiler to all other parts of the system. Except for the zirconium-rich deposits in the test section, zirconium migration could be detected only by direct electron-beam microprobe analysis of the piping surfaces.

A pumped loop (FCL-8) of similar design, fabricated of D-43 alloy and containing D-43 nozzle-blade specimens, completed 10,000 hr of operation at design conditions (Table 17.1). The loop, operated by Reactor Division personnel, was shut down in June 1968 after having been on line 96% of the time since startup in March 1967. The down time was mostly associated with electrical and instrument problems external to the vacuum chamber. Examination of this loop is in progress.

CORROSION OF REFRACTORY ALLOYS BY LITHIUM

C. E. Sessions J. H. DeVan
B. Fleischer

Interest in lithium stems from the attractive properties of this metal as a heat-transfer fluid in high-performance nuclear reactor systems. Refractory alloys based on Nb, Ta, W, and Mo have demonstrated low solubilities in lithium, and, by virtue of their superior high-temperature strength, appear ideally suited as container materials. Accordingly, we are investigating the detailed corrosion behavior of refractory metals in lithium from the standpoint of mass transfer resistance and the effects of oxygen on grain-boundary penetration.

Thermal-Convection Loop Tests

The thermal-convection loop affords a convenient means for studying mass transfer properties of liquid metals moving through a temperature gradient. Our current program makes use of the thermal-convection approach for the following purposes: (1) to compare the corrosion resistance of niobium, tantalum, and tungsten alloys in flowing nonisothermal lithium and (2) to measure in the niobium and tantalum systems the magnitude and the time dependence of corrosion reactions, which are controlled by solid-state diffusion processes.

In tests of the niobium-base alloys D-43, Nb-1% Zr, and FS-85 in circulating lithium, we have observed the following mass transfer effects:⁴

1. The alloy constituents zirconium and nitrogen are preferentially transferred from hotter to cooler surfaces in loop tests operated at maximum temperatures of 1200 and 1300°C.
2. Zirconium concentration gradients measured below the surfaces of hot-leg specimens indicate that zirconium depletion is controlled by a solid-state diffusion process. The gradients are of the same form as those computed under the assumption that zirconium surface concentrations remain fixed throughout the test.
3. Mass transfer of niobium is insignificant at 1200°C but accounts for a large fraction of insert weight

⁴C. E. Sessions and J. H. DeVan, "Thermal Convection Loop Tests of Refractory Alloys in Lithium," pp. 326-31 in 1967 IEEE Conference Record of the Thermionic Conversion Specialist Conference, October 30-November 1, 1967, Palo Alto, California, Institute of Electrical and Electronic Engineers, New York.

changes in loops operated at 1300°C. The higher rate of niobium transfer at 1300°C is also manifested by the appearance of niobium deposits at the heater entrance.

4. Mass-transfer profiles in these systems indicate that components of the refractory alloy enter and leave the lithium at commensurate rates. The solute concentrations in the lithium change very little from point to point around the loops, so that the corrosion rate is the same for any given temperature independent of location and direction of heat flux.

The corrosion properties of these niobium-base alloys are now being compared with those of tantalum alloys containing tungsten and hafnium. The first such test, that of the alloy T-222, is being examined after operating 3000 hr at 1350°C. Future tests have also been programmed to evaluate tungsten-base alloys.

Forced-Circulation Loop Studies

The mechanical, piping, electrical, and instrument design of the advanced forced-circulation liquid lithium loop (FCLLL-1) was completed. For economic reasons we adopted a test-bed-loop approach so that we can study the compatibility of several refractory alloys in lithium at 20 ft/sec. A simplified schematic of the basic loop system is shown in Fig. 17.1 and a general

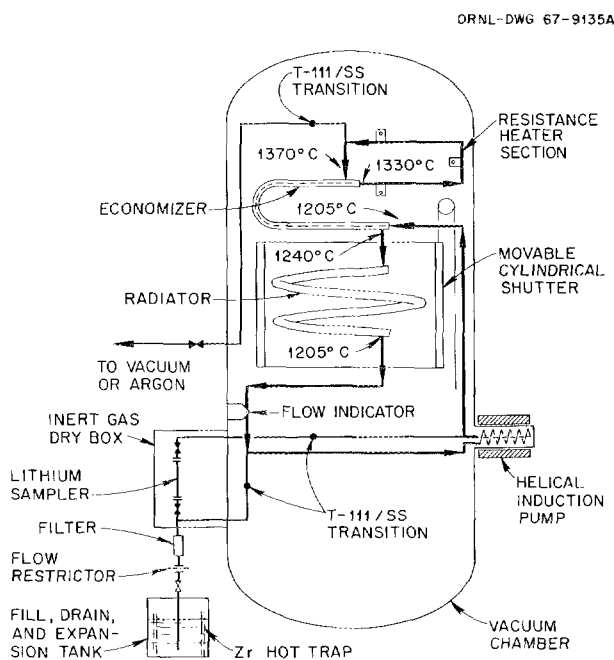


Fig. 17.1. Schematic Representation of Forced-Flow Liquid Lithium Loop.

description of the forced-circulation lithium loop program is presented in Table 17.2. Future loops, FCLLL-2 and -3, will be operated in the same test stand with the heater and economizer sections of FCLLL-1 replaced. Approximately 100 specimens have been fabricated for insertion in the loops to study changes in weight, composition, and mechanical properties. All supporting equipment for FCLLL-1 has been procured and fabricated.

Techniques were developed for making butt and nozzle-type welds, Nb-1% Zr to T-111 welds, and field welds. As-welded field-type joints have been exposed to lithium in capsule tests and show no evidence of

Table 17.2. Test Conditions and Materials for Forced-Circulation Lithium Loops with Maximum Velocity of 20 ft/sec

Loop	Maximum Temperature ^a (°C)	Materials ^b	
		Hot Leg	Specimens
FCLLL-1	1370	T-111	T-111
FCLLL-2	1370	T-111	Tungsten alloys
FCLLL-3	1540	Tungsten alloy	Tungsten alloys

^aMinimum: 1205°C.

^bCold leg: T-111.

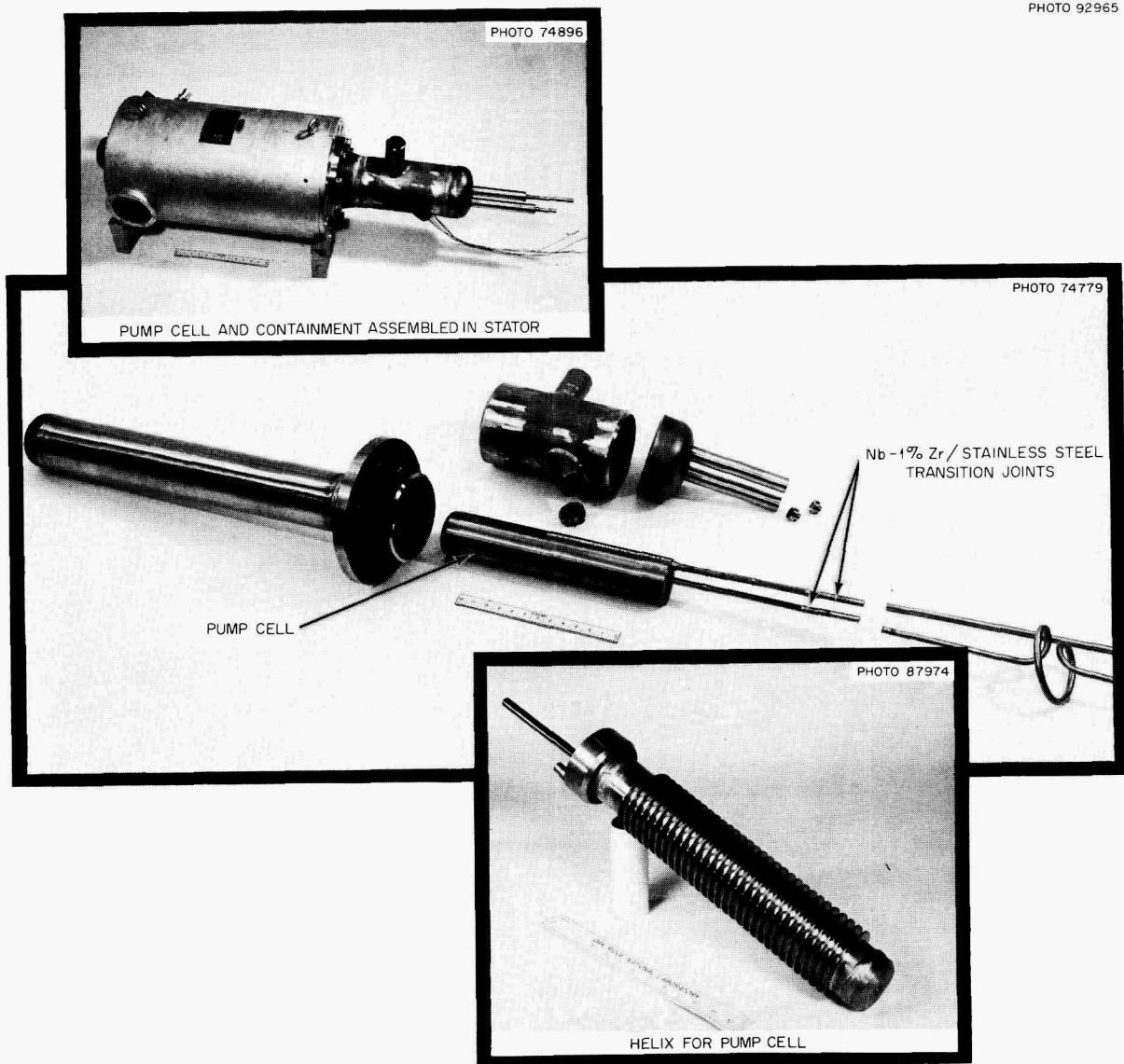


Fig. 17.2. T-111 Helical Induction Pump and Associated Stainless Steel Containment.

corrosion damage. High-purity zirconium foil has been procured for hot-trap purification of lithium.

A T-111 pump cell for the helical induction pump was successfully fabricated and tested to 815°C in potassium to verify its structural integrity and establish its performance characteristics. A photograph of this pump cell is included in Fig. 17.2. Measured performance closely matched predicted behavior. Extrapolation to 1205°C, the operating temperature in lithium, indicated a satisfactory flow rate of 5.8 gpm at 450 v and 41 psi developed head. All T-111 material for FCLLL-1 has been procured and about 95% of the parts have been fabricated in preparation for welding of assemblies.

COMPATIBILITY OF NaK WITH TYPE 316 STAINLESS STEEL AND Nb-1% Zr ALLOY IN A HEAT REJECTION SYSTEM⁵

A. P. Litman W. J. Leonard

Evaluation of a SNAP-50-type dissimilar-metal radiator circuit with a stainless steel-to-refractory alloy surface area ratio of 5.5 was completed. The test system consisted of a parallel-tube, air-cooled radiator fabri-

⁵Summary of papers presented at the USAEC Corrosion Symposium, Columbus, Ohio, May 6-8, 1968, and at the American Nuclear Society, Toronto, Ontario, Canada, June 10-13, 1968.

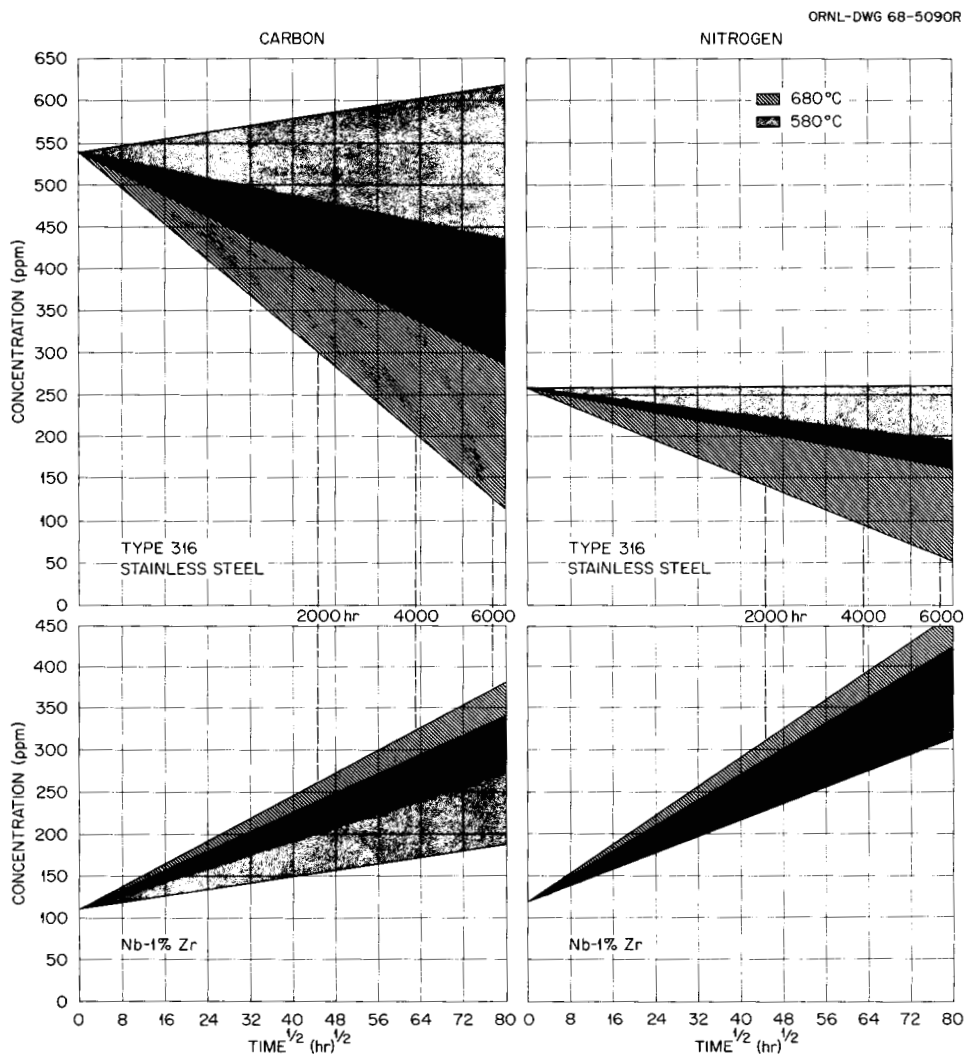


Fig. 17.3. Effect of Time and Temperature on Carbon and Nitrogen Migration in Nb-1% Zr and Type 316 Stainless Steel Simultaneously Exposed to Polythermal Eutectic NaK.

cated from type 316 stainless steel and a heated section made from Nb-1% Zr. The loop, containing numerous replaceable and permanent refractory alloy and stainless steel specimens, circulated eutectic NaK (78% K) at 8.4 ft/sec (Reynolds number of 100,000 in the hot section) for 6000 hr with a heater outlet temperature of 680°C and a temperature difference of approximately 100°C.

Weight changes on the specimens were minimal (maximum approximately $0.1 \text{ mg cm}^{-2} \text{ month}^{-1}$), and dimensional changes were too small to be measured. The major corrosion effect was solid-state diffusion-controlled mass transfer of carbon and nitrogen from the stainless steel to form thin layers, approximately 0.0001 in. thick, of Nb²N and NbC on the refractory alloy. The bulk movement of these interstitial elements as functions of time and temperature is shown in Fig. 17.3. Changes in the mechanical properties of the alloys are shown in Table 17.3 and indicate that adequate ductility and strength at room and elevated temperatures remained after test.

The experiment led to a better definition of acceptable residence times and temperature conditions for Nb-1% Zr alloy and type 316 stainless steel exposed together in NaK. A low system corrosion rate, no greater than 0.0001 in./year, plus satisfactory post-test mechanical properties, indicate high reliability for the dissimilar-metal heat rejection complex operating at 680°C - a reliability that can reasonably be extrapolated to 10,000 hr service life.

Table 17.3. Mechanical Properties of Type 316 Stainless Steel and Nb-1% Zr Alloy After Exposure in Bimetallic NaK System

Exposure Temperature (°C)	Test Temperature (°C)	Tensile Elongation (%)	Ultimate Tensile Strength (psi)
Type 316 Stainless Steel			
			×10 ³
None	25	64	86
565	25	51	87
680	25	29	95
None	680	51	49
565	680	38	51
680	680	30	53
Nb-1% Zr Alloy			
None	25	22	56
605	25	44	40
680	25	43	40
None	680	10	43
605	680	22	29
680	680	30	29

INTERACTIONS IN REFRACTORY-METAL-ALKALI-METAL SYSTEMS CONTAINING OXYGEN

R. L. Klueh

Effect of Oxygen in the Tantalum-Potassium System

We are continuing⁶ to study the Ta-O-K system at 600, 800, and 1000°C. The effect of oxygen on the compatibility between tantalum and potassium depends upon whether the oxygen is in the potassium or the tantalum. An increase in the oxygen concentration of the potassium leads to an increase in the solubility of tantalum in potassium. We believe that this effect can be explained phenomenologically in terms of the effect of oxygen on the activity coefficient of tantalum in potassium, as discussed in the next section.

At each of the test temperatures there was a threshold oxygen concentration in the tantalum at which potassium penetrated the tantalum. This threshold oxygen concentration increased with temperature (between 100 and 600 ppm below 800°C and between 600 and 1000 ppm at 1000°C) and was unaffected by the oxygen concentration of the potassium. Examples of penetration at 600°C of tantalum containing 600 and 1300 ppm O are shown in Figs. 17.4 and 17.5, respectively. The amount of attack (and depth of penetration) increased with the initial oxygen concentration of the tantalum. Note that both transcrystalline and grain-boundary attack are present in Fig. 17.5. When the specimen shown in Fig. 17.4 was etched, only grain-boundary attack was detected.

Qualitatively, the results are similar to those obtained by DiStefano⁷ for the Nb-O-Li and Ta-O-Li systems. The chief difference is that a lower threshold oxygen concentration is required for penetration by lithium than by potassium.

Analysis of Corrosion Behavior in Terms of Solution Interaction Parameters⁸

Studies of the compatibility between refractory metals (principally niobium and tantalum) and the alkali metals sodium and potassium have shown that the

⁶R. L. Klueh, *Metals and Ceramics Div. Ann. Progr. Rept. June 30, 1967*, ORNL-4170, p. 96.

⁷J. R. DiStefano, *Corrosion of Refractory Metals by Lithium*, ORNL-3551 (April 1966).

⁸Papers summarizing this work were presented at the NACE Annual Conference in Cleveland, Ohio, March 18, 1968, and at the USAEC Corrosion Symposium in Columbus, Ohio, May 6, 1968.

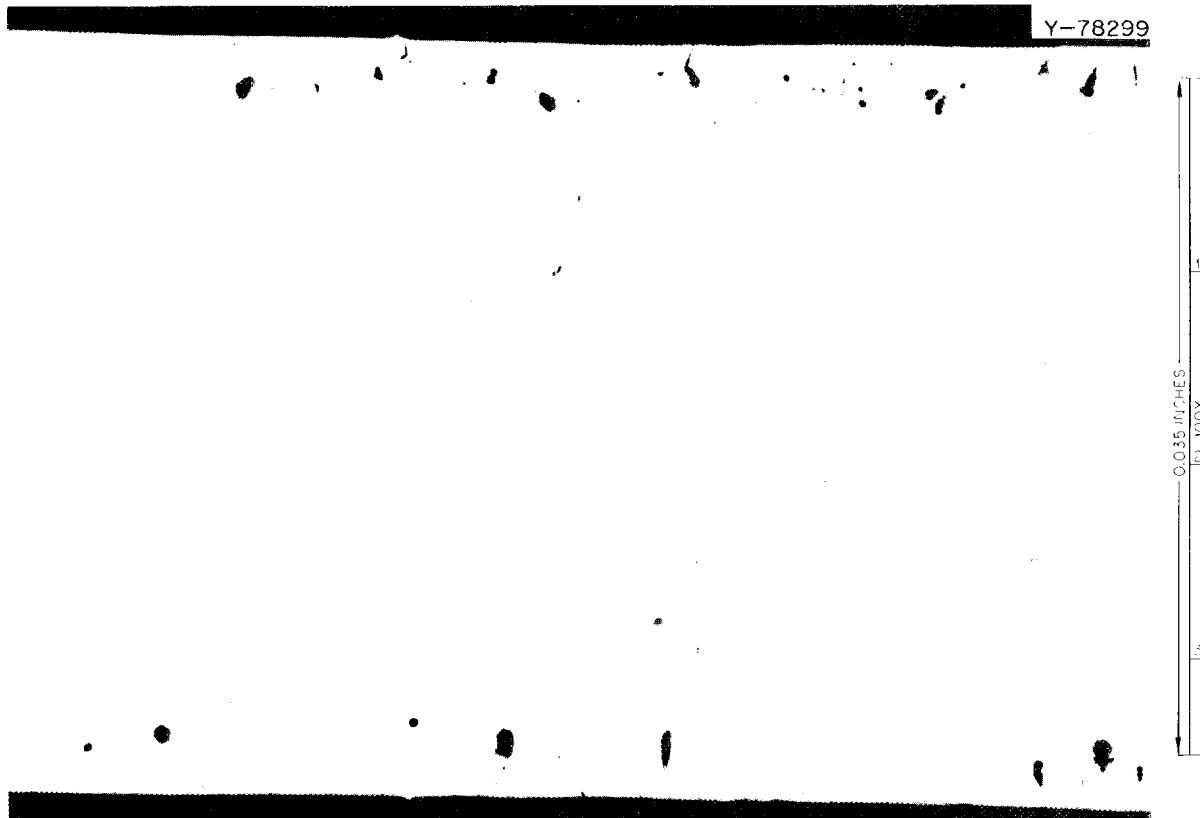


Fig. 17.4. Tantalum that Initially Contained 600 ppm O After Exposure to Potassium for 500 hr at 600°C. Unetched.

dissolution of the refractory metal in the alkali metal depends upon the concentration of oxygen in the alkali metal. Also, the experimentally determined oxygen equilibrium distribution coefficient at a given temperature (the ratio of the oxygen concentration in the refractory metal to that in the alkali metal at equilibrium) is generally much smaller than the theoretically calculated value. These observations have generally been explained by postulating the formation of a double oxide containing atoms of the refractory metal, alkali metal, and oxygen.⁹

As an alternative to the double oxide hypothesis, we propose that at equilibrium a liquid ternary solution exists in equilibrium with the solid and that oxygen affects the solubility of the refractory metal by decreasing the activity coefficient of the refractory metal in the liquid. Under this assumption, the system can be characterized in terms of the interaction

parameters developed by Wagner¹⁰ for the interaction between the refractory metal and the oxygen in the potassium. This interaction parameter for the Nb-O-K system is defined as

$$\epsilon_{\text{Nb}}^{(\text{O})} = \left(\frac{\partial \ln \gamma_{\text{Nb}}}{\partial N_{\text{O}}} \right),$$

where γ_{Nb} is the activity coefficient of the niobium and N_{O} is the atom fraction of the oxygen in the potassium. Once $\epsilon_{\text{Nb}}^{(\text{O})}$ is determined experimentally, solubility data for oxygen in pure potassium can be used to empirically represent the activity coefficient of oxygen in the ternary solution as a function of the niobium concentration of the solution.

The phase rule has been used to check the hypothesis for the Nb-O-K, Nb-O-Na, and Ta-O-Na systems. In all cases the solubility of the refractory metal increases with the oxygen concentration of the alkali metal.

⁹C. Tyzack, "The Behavior of Materials in Liquid Sodium," p. 251 in *Advances in Materials (Inter-Disciplinary Symposium)*, The Institution of Chemical Engineers, London, 1964.

¹⁰C. Wagner, *Thermodynamics of Alloys*, Addison-Wesley, Cambridge, Mass., 1952.



Fig. 17.5. Tantalum that Initially Contained 1300 ppm O After Exposure to Potassium for 500 hr at 600°C. Etched in a solution of H₂O, HNO₃, and NH₄HF.

Furthermore, these tests show that the concentration of oxygen in solid solution finally achieved in the refractory metal increases regularly with the initial oxygen level of the alkali metal. Both observations suggest that there are two condensed phases present at equilibrium rather than the three phases required by the double oxide hypothesis. Also the activity coefficients derived by the interaction parameter approach offer a reasonable explanation for the distribution coefficient discrepancy discussed above.

PARTITIONING OF OXYGEN BETWEEN ZIRCONIUM AND POTASSIUM AND BETWEEN ZIRCONIUM AND SODIUM^{1 1}

R. L. Klueh

We have completed our investigation of the use of zirconium gettering of oxygen in alkali metals as an analytical technique for oxygen determination.^{1 2} This investigation required an analysis of the oxygen parti-

tioning occurring between zirconium and liquid potassium and sodium. In both systems the partition coefficient (the ratio of the oxygen content in zirconium to that in the alkali metal) was relatively large ($>10^4$). Accordingly, under the conditions employed for these studies, essentially all of the oxygen initially in the liquid metal was gettered by the zirconium.

Therefore, one is able to determine the oxygen in potassium or sodium to very low concentrations simply by exposing the liquid metal to zirconium and directly measuring the amount of oxygen gettered. To test the technique we conducted recovery experiments at 800°C in which known oxygen additions were made to potassium and sodium, which were then exposed to zirconium tabs in molybdenum containers. Recoveries of 90% or greater were obtained for oxygen concentrations (in potassium or sodium) in the range of 100 to 1000 ppm.

^{1 1} Abstracted from topical report in preparation.

^{1 2} A. P. Litman and J. W. Prados, *Electrochem. Technol.* 3, 228-33 (1965).

DETERMINATION OF OXYGEN IN ALKALI METALS

J. H. DeVan J. E. Strain¹³

The fast-neutron activation facility described previously^{14,15} has been used routinely during the past year for the determination of oxygen in alkali and refractory metals. A unique feature of this facility is that the alkali metal is protected by an inert atmosphere rather than by the usual encapsulation procedure, so the oxygen background associated with the specimen holder is greatly reduced. Thus we have successfully determined oxygen in both lithium and potassium at levels of less than 20 ppm. Sodium has not yet

been analyzed for oxygen because of the high-energy beta radiation associated with ^{20}F , a product of fast-neutron reaction with sodium. However, we are presently evaluating different beta discrimination techniques that we believe will make this analysis feasible.

This system is also being used to measure the oxygen levels in our refractory metal corrosion specimens before and after exposure. This technique makes possible the nondestructive analysis of our whole test specimen ($1 \times 1/2 \times 0.040$ in.). The specimen is transported to and from the neutron generator in a polyethylene holder and under an argon atmosphere. Because the analysis is nondestructive, the same specimen can be analyzed before and after testing. Oxygen has been determined in the range of 27 to 2700 ppm in specimens of V, Nb, Ta, and Nb-Zr alloys, and the results show reasonable agreement with vacuum fusion analyses on the same specimens. A series of refractory-metal oxygen standards is being prepared by oxidizing tantalum and niobium test coupons to known oxygen levels and performing repetitive analyses.

¹³Analytical Chemistry Division.

¹⁴A. P. Litman and J. E. Strain, *Metals and Ceramics Div. Ann. Progr. Rept. June 30, 1966*, ORNL-3970, pp. 82-83.

¹⁵J. E. Strain and J. H. DeVan, *Metals and Ceramics Div. Ann. Progr. Rept. June 30, 1967*, ORNL-4170, p. 96.

18. Nitride Fuels Development

J. L. Scott W. O. Harms

Uranium mononitride is attractive for space reactors because of its high density, high thermal conductivity, and excellent high-temperature stability. These features permit its operation at higher heat ratings and specific power than the more standard UO_2 . The excellent properties of UN suggest that mixed (U,Pu)N will be attractive as fuel for liquid-metal-cooled fast breeder reactor (LMFBR) systems. To be sure, the fast-neutron capture cross section of nitrogen is somewhat higher than that of oxygen or carbon. This disadvantage, however, is offset by the higher specific power possible with the nitride fuels, which, in turn, enables shorter doubling times despite reduced breeding gains.

Our program involves fuel fabrication, determination of physical and thermodynamic properties, compatibility studies, and irradiation studies. Part of the program is directed toward development of carbonitride fuels. A carbonitride might offer significant advantages over either pure carbide or nitride because of (1) a lower-cost fuel cycle involving aqueous processing; (2) a greater plasticity above 600°C , which minimizes the effects of fuel swelling at a given temperature; and (3) better control of stoichiometry and fission-product reactivity at high burnups.

Uranium nitride is an interesting material from a fundamental viewpoint, and is being investigated under the Fundamental Ceramics Research Program described in Part I, Chapter 7.

SYNTHESIS, FABRICATION, AND CHARACTERIZATION

Synthesis and Fabrication of UN and U(C,N)

R. A. Potter

We are continuing to extend our capability for the preparation of pressed-and-sintered specimens of UN and selected U(C,N) compositions. The UN synthesis scheme and equipment¹ remain essentially unchanged.

¹R. A. Potter, *Metals and Ceramics Div. Ann. Progr. Rept. June 30, 1967, ORNL-4170, pp. 97-98.*

In addition to preparing engineering test pieces, we are now fabricating specimens of various sizes and geometries for the fundamental studies described in Part I, Chapter 7.

Several representative specimens are shown in Fig. 18.1. For the large samples, we adopted a different method of pressing. We preformed the specimens in steel dies, transferred them to rubber bags, evacuated and sealed these, and isostatically pressed the specimens at about 30 tsi. Sintered pieces can be ground to close tolerances by conventional ceramics machining processes.

We prepared specimens of $\text{UC}_x\text{N}_{1-x}$ in which x ranged from 0.0 to 1.0 by reaction of UN powder with spectrographic grade carbon. The equilibrium pressure for a given temperature and composition set the conditions for synthesis as well as sintering. The reacted powders were cooled under a constantly decreasing nitrogen pressure to prevent either precipitation of graphite or formation of U_2N_3 . Sintered specimens of the resultant U(C,N) powder were then prepared in a manner similar to that used for UN.

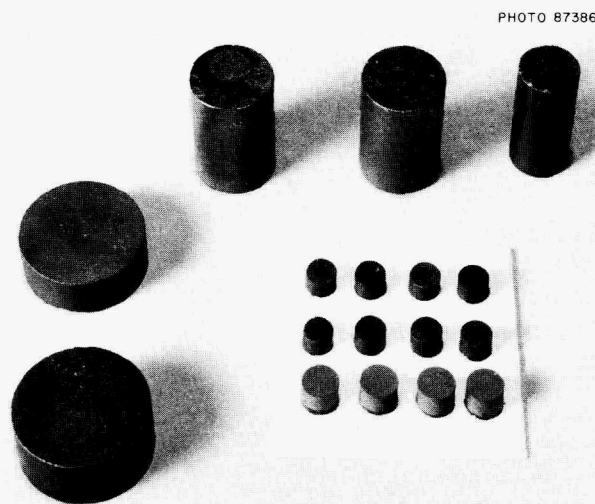


Fig. 18.1. UN Specimens Sintered at 2250°C in 1 atm N_2 to a Density Greater than 95% of Theoretical.

Synthesis and Fabrication of (U,Pu)N

E. S. Bomar J. D. Sease
J. D. L. Harrison² Ji Young Chang

A facility was prepared for the synthesis, fabrication, and characterization of high-quality (U,Pu)N. Process capability includes conversion of mixed oxide to mixed nitride, synthesis of nitrides from metallic uranium and plutonium alloys, and pellet manufacture by cold pressing and sintering and by hot pressing.

Glove boxes provide primary containment of the experimental materials. Services are provided in a modular, overhead arrangement and allow the operation of boxes with either air or inert atmosphere, as required by the chemical compounds to be examined. Ten glove boxes have been equipped with instruments to control the argon supply from a bulk source connected to the overhead services and have been checked thoroughly for leaktightness.

Synthesis and sintering equipment includes two Pt-50% Rh-wound, controlled-atmosphere, water-cooled tube furnaces capable of temperatures to 1700°C. These are to be used primarily for preparation of mixed nitrides. The design allows their use for investigating the sintering characteristics of a variety of fuels. Environments available are argon, controlled argon-hydrogen mixtures, nitrogen, and vacuum (10^{-5} torr). A tungsten resistance furnace capable of operating at 3000°C under a vacuum of 1×10^{-5} torr or at 2400°C in nitrogen was designed and is being built.

A hot-pressing unit was designed, built, and installed in a glove box for use in fabrication of high-density nitrides. The press is inductively heated, has a graphite die and controlled atmosphere, and can operate above 2000°C. A total force of 10 tons can be applied by a hydraulically driven ram capable of sustained operation at preset force levels. A transducer allows us to infer from the physical position of the ram the extent of pressing. An electronic readout plots the change of pellet length as a function of time and records the temperature.

We also have the capability of cold-pressing and sintering nitride fuels. Powder conditioning equipment now available in glove boxes includes both a centrifugal-force grinder and a conventional ball mill.

Characterization of Mixed Nitrides

E. S. Bomar J. M. Leitnaker Ji Young Chang

Equipment was installed in glove boxes for characterizing plutonium fuel materials by a variety of techniques: differential thermal analysis to 1200°C, thermogravimetric analysis to 1200°C, hot-stage microscopy to

1350°C, and x-ray diffraction by both the Debye-Scherrer and diffractometer methods.

CONVERSION OF UO_2 TO CARBONITRIDE FUELS

Because low fuel-cycle cost is an important criterion for an LMFBR fuel, we are investigating the synthesis, fabrication, and performance of carbonide fuels. Carbonitrides are easier to prepare and, therefore, less expensive than pure nitrides. They are prepared by reaction of oxide fuel powders with an excess of carbon in a nitrogen environment. We are attempting to discover the basic mechanisms of this conversion so that we can optimize the efficiency of the conversion on a practical scale. Methods for producing both U(C,N) and (U,Pu)(C,N) from sol-gel feed, a natural product of aqueous processing, are emphasized in this development program.

Direct Conversion of Sol-Gel UO_{2+x} to U(C,N)

J. M. Leitnaker R. L. Beatty
K. J. Notz³ K. E. Spear

A method was developed but not optimized for the production of U(C,N) by direct conversion of sol-gel UO_{2+x} . Three steps are involved. (1) Undried gel with carbon added is dropped directly into a furnace at 1500°C, where it is converted in about 15 min to a sesquinitride phase containing some oxygen and carbon. (2) Most of the sesquinitride phase is converted to a mononitride phase at 1600°C by sequential 15-min exposures to nitrogen and argon. (3) Complete conversion to carbonitride and sintering is effected by exposure to a sintering cycle such as that described by Potter and Fréchet⁴.

The products obtained by this procedure contain less than 1000 ppm O and varying amounts of carbon, depending on the starting materials used, and the density has been only about 70% of theoretical. The process has not been optimized with respect to carbon particle size, temperature, and nitrogen flow rate. The success of the process clearly depends upon the high reaction rates associated with the rapid heating of the gel in step 1. Rapid heating prevents those processes, such as sintering of the UO_2 or the formation of a continuous carbide layer on the surface of the oxide particles (see next section), that would otherwise severely reduce the rate at which gaseous reaction products are evolved. The results also suggest that a

²On assignment from AERE, Harwell, England.

³Chemical Technology Division.

⁴R. A. Potter and V. D. Fréchet, *Metals and Ceramics Div. Ann. Progr. Rept. June 30, 1967*, ORNL-4170, pp. 98-99.

U-O-N phase is an intermediate product in the overall reaction.

Kinetics of the UO_2 -C Reaction

T. B. Lindemer

In connection with our carbonitride studies we investigated the kinetics and mechanisms of the reaction of high-density UO_2 sol-gel microspheres with spectrographic grade graphite powder. The experiments were performed from 1400 to 1750°C in flowing argon at 400 torr.

The rate of heating from 1000°C to the reaction temperature had a profound effect on the kinetics of the reaction. For heating rates greater than 30°C/min the reaction rates were up to 5 times those for heating rates of 20°C/min and less.

The mechanisms responsible for this effect were revealed by metallographic examination of partially converted microspheres. At the lower heating rates, a continuous layer of " UC_2 " formed on the surface of the microspheres, as shown in Fig. 18.2; the rate-controlling mechanism was grain-boundary or volume diffusion of oxygen through this layer, as determined

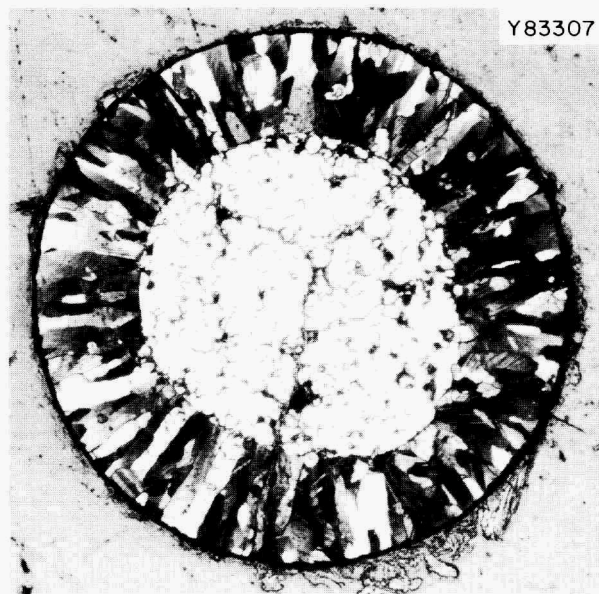


Fig. 18.2. Sol-Gel UO_2 Microsphere Showing Continuous " UC_2 " Layer After Partial Reaction with Carbon for 90 min at 1700°C After Heating from 1000°C at a Rate Less than 20°C/min. 200X. Etched with H_2O - HNO_3 -acetic acid.

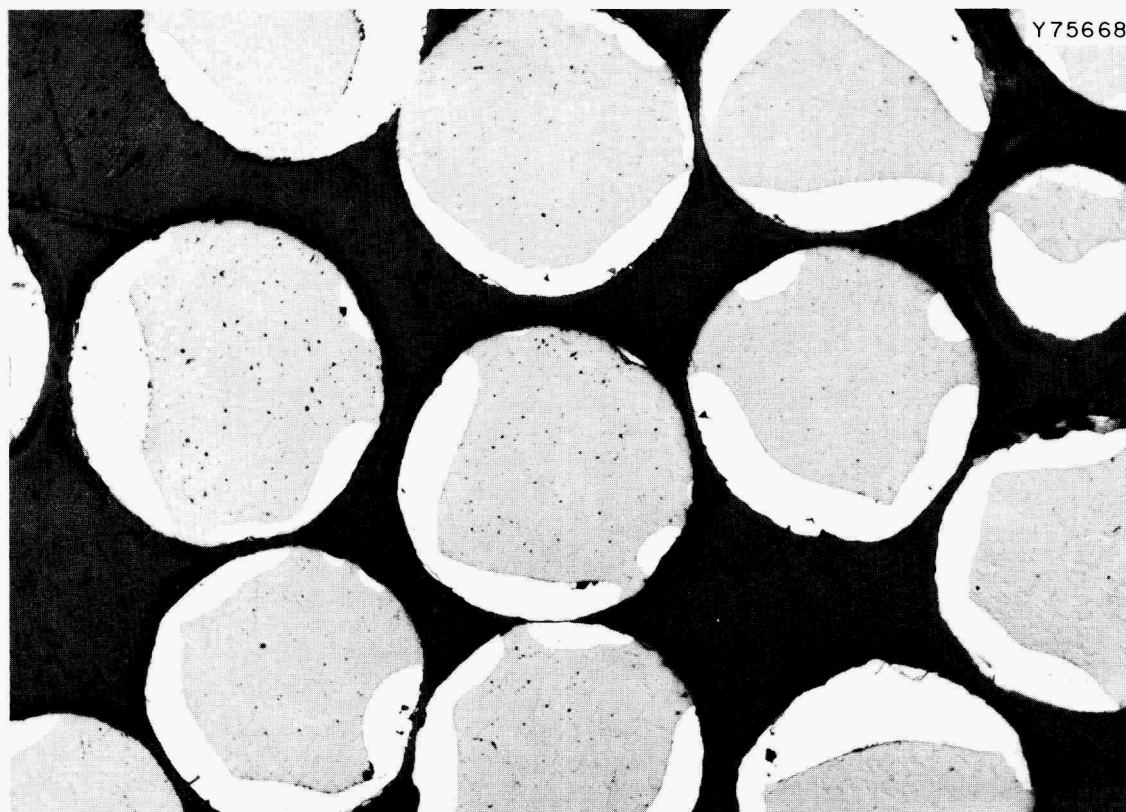


Fig. 18.3. Sol-Gel UO_2 Microspheres Showing Discontinuous Carbide Layers After Reaction with Carbon for 60 min at 1600°C After Heating at a Rate Greater than 30°C/min. 100X. As polished.

by a fit of the experimental data with a model for diffusion control.^{5,6} The activation energy for this process was determined to be 93 ± 10 kcal/mole. At the higher heating rates both "UC₂" and UC formed, but as discontinuous layers, as shown in Fig. 18.3. In this case, oxygen apparently leaves the reaction interface and proceeds readily through the UO₂ to the surface of the microsphere.

Kinetics of the UC₂-N₂ Reaction

T. B. Lindemer

We have investigated the kinetics of the UC₂-N₂ reaction from 1400 to 1900°C because of its relevance to the preparation of carbonitrides. A typical microstructure of a partially reacted microsphere after exposure to nitrogen for 24 hr at 1600°C is shown in Fig. 18.4. The core of this particle consists of "UC₂" that originally contained less than 1 vol % free carbon, and the two-phase region surrounding the core contains U(C,N) of varying composition and a precipitate of reaction-product free carbon. The outer layer is also free carbon produced by the reaction. Comparison of reaction rates, as determined from quantitative metallography, with previously constructed theoretical models⁵⁻⁸

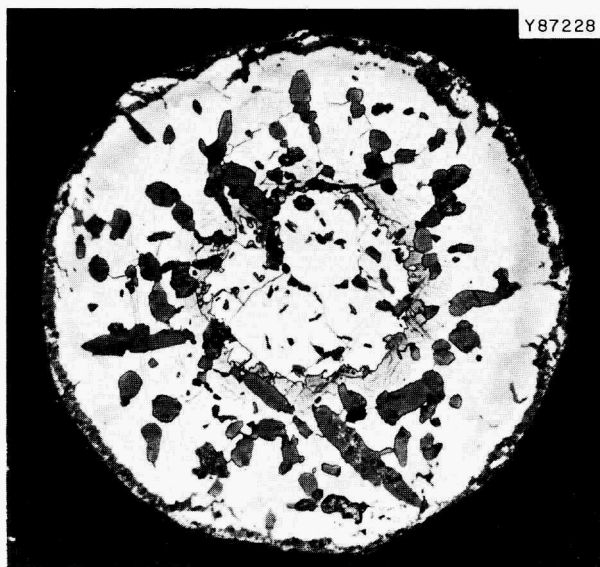


Fig. 18.4. Microstructure of Partially Reacted "UC₂" Microsphere After Exposure to Nitrogen for 24 hr at 1600°C. The core is "UC₂," the region surrounding the core is U(C,N) of variable composition and free carbon (dark-gray phase) produced by the reaction, and the surface layer is also free carbon. 200X. Etched with H₂O-HNO₃-acetic acid. Reduced 22%.

leads us to believe that a mechanism at the "UC₂"-[U(C,N) + C] interface is rate-controlling.

THERMODYNAMIC STUDIES

The thermodynamic properties of nitride fuels are studied on a continuing basis to help define problems that might arise in advanced concepts of space and civilian power-breeder reactor systems. Thermodynamic analyses of questions concerning stability at high temperatures and compatibility with candidate cladding alloys, including the effects of fission products, not only provide guidance for the experimental program but also help interpret experimental results.

Thermodynamic Properties of UC-UN Solid Solutions

J. M. Leitnaker R. A. Potter
K. E. Spear W. R. Laing⁹

X-ray diffraction studies¹⁰ showed that UC-UN solid solutions deviate significantly from Vegard's law and that the width of the single-phase region representing this continuous series of solid solutions in the ternary phase diagram is narrow. The composition of solid solutions in this system as a function of the lattice parameter a_0 (in angstroms) is given by

$$\frac{\text{moles N}}{\text{moles (N + C)}} = 1.00 - 13.2488r + 42.5072r^2 + (2.13035 \times 10^2)r^3 - (1.37677 \times 10^4)r^4,$$

where $r = (a_0 - 4.8892)$. These results coupled with measurements of lattice parameters as a function of nitrogen pressure¹¹ let us conclude that UC-UN solid solutions show negative deviations from ideal (Raoult's law) behavior.

⁵R. E. Carter, *J. Chem. Phys.* 34, 2010-15 (1961).

⁶R. E. Carter, *J. Chem. Phys.* 35, 1137-38 (1961).

⁷W. M. McKewan, *Trans. Met. Soc. AIME* 212, 791-93 (1958).

⁸S. Yagi and D. Kuni, *Fifth Symposium on Combustion*, pp. 231-44, Reinhold Publishing Corp., New York, 1955.

⁹Analytical Chemistry Division.

¹⁰J. M. Leitnaker, R. A. Potter, K. E. Spear, and W. R. Laing, "The Lattice Parameter of U(C,N) as a Function of Composition," submitted for publication to the *Journal of the American Ceramic Society*.

¹¹J. M. Leitnaker, "The Ideality of the UC-UN Solid Solution," pp. 317-30 in *Thermodynamics of Nuclear Materials, 1967*, International Atomic Energy Agency, Vienna, 1968.

Vapor Pressure of Nitrogen over Nitrogen-Rich Uranium Nitride

K. E. Spear H. Inouye

The vapor pressures of nitrogen over uranium nitride with nitrogen-to-uranium ratio greater than 1.0 were measured between 900 and 1500°C by a technique described elsewhere.¹² Fifteen series of measurements representing 87 different nitrogen concentrations in uranium showed that the nitrogen pressure continuously decreased for constant temperatures as the nitrogen-to-uranium ratio was decreased from about 1.2 to 1.09. We saw no evidence of the two-phase region UN + U₂N₃ reported by Müller and Ragass¹³ for a nitrogen-to-uranium range of 1.01 to 1.57 at 1200°C and nitrogen pressure of about 100 torr. Our results show that the nitrogen pressure at 1200°C decreases continuously from 38 torr at a nitrogen-to-uranium ratio of about 1.2 to 2.3×10^{-7} torr at a nitrogen-to-uranium ratio of 1.09.

At a nitrogen-to-uranium ratio of about 1.64, the equilibrium nitrogen pressure over the sample at 900°C was 6.25 torr, compared to the value of about 500 torr reported by Bugl and Bauer.¹⁴ Furthermore, our results at 900°C indicate that a two-phase field extends from a nitrogen-to-uranium ratio of about 1.3 to 1.6 compared to a reported range of 1.00 to 1.54 for UN-U₂N₃. The cause of this significant disagreement among the various investigators is not known.

A Consistent Set of Thermodynamic Values for Plutonium Mononitride¹⁵

K. E. Spear J. M. Leitnaker

Literature values for the heat of formation $\Delta H_{f,298}^{\circ}$ of PuN range from -70 to -76 kcal/mole. If estimated entropy and high-temperature heat capacity data are used to derive a reasonable set of high-temperature thermal functions for PuN, then $\Delta H_{f,298}^{\circ}$ values obtained from equilibrium data by both second- and third-law methods agree. The equilibrium data are from

¹²H. Inouye and J. M. Leitnaker, *J. Am. Ceram. Soc.* 51, 6-9 (1968).

¹³O. F. Muller and H. Ragass, "Disorder in Cubic Uranium Sesquinitride," pp. 257-64 in *Thermodynamics of Nuclear Materials, 1967*, International Atomic Energy Agency, Vienna, 1968.

¹⁴J. Bugl and A. A. Bauer, *J. Am. Ceram. Soc.* 47, 425-29 (1964).

¹⁵Abstracted from paper accepted for publication in the *Journal of the American Ceramic Society*.

measurements from 700 to about 3040°K. A calorimetric value of -70.2 kcal/mole reported for $\Delta H_{f,298}^{\circ}$ for PuN appears to disagree with the derived equilibrium value of -76.0 kcal/mole, but this difference might be explained by a composition uncertainty.

COMPATIBILITY OF CLADDING WITH NITRIDE FUEL

The compatibility of nitride fuels with candidate cladding alloys must be thoroughly investigated and understood if these fuel materials are to be considered seriously for use in LMFBR systems. The problem is complicated because of the several multicomponent cladding alloys under consideration and the important effects of burnup on the composition, constitution, and nitrogen activity of the fuel. Our approach is to investigate systematically the thermodynamics and kinetics of those interactions involving components of the fuel and the cladding, as well as certain fission and transmutation products, that are pertinent to the compatibility problem. A selected number of compatibility-couple experiments are included in this program.

Thermodynamic Compatibility of Vanadium with Nitride Fuels

K. E. Spear J. M. Leitnaker

The free energies for reactions of vanadium metal with UN, PuN, or mixed nitride to form the hexagonal V₂N phase plus condensed U, Pu, or U-20 at. % Pu were calculated from available thermodynamic data. The free energies of reaction, which are believed to be accurate to at least 1500°C, are all positive.

Experiments designed to test the above calculations involving uranium nitride and to fix other equilibrium tie-lines in the ternary U-V-N phase diagram have begun. Preliminary results indicate that vanadium metal will not reduce UN to uranium metal at 1400 to 1600°C and no intermetallic compounds are formed.

Compatibility of Nitride Fuels with Cladding Alloys

J. D. L. Harrison¹⁶

The object of this work is to observe the out-of-reactor interaction between nitrides of nominal compositions UN, UN_{0.95}C_{0.05}, UN_{0.95}O_{0.05}, and

¹⁶On assignment from AERE, Harwell, England.

UN_{0.90}C_{0.05}O_{0.05} with stainless steel types 316L, 304L, and ORNL-modified 304 containing 0.2% Ti and with V-5% Ti-15% Cr. Sandwiches of each alloy and each nitride composition were heated in initially evacuated and welded stainless steel capsules to 800°C for 1000 hr and are being examined metallographically and by electron microprobe analysis.

To limit the possibility of unwanted interactions through the gas phase, each capsule contained nitride of only one composition and steel of one composition in contact with the nitride. To limit interaction between the sandwiches and the capsule bodies, each of which was made of type 316 and 321 stainless steels, each sandwich is surrounded by a 0.005-in. wrap of the sandwich metal.

Contact between the layers of the sandwiches is maintained by an axial compressive load on each capsule sufficient to deform a bellows closure and thus transfer the load to the contents of the capsules. Several capsules are stacked inside a loosely fitting Inconel tube. This tube encloses the capsules in an atmosphere of pure flowing argon and acts as the tension member that applies the compressive load to the stack of capsules through an internal spring and push rods.

Active Carbon Produced by Reaction of Nitrogen with VC

K. E. Spear J. M. Leitnaker

The reaction of VC with nitrogen between 1600 and 1200°C at 600 torr was found to produce, in addition to V(C,N), carbon in a form more active than graphite. This behavior is similar to that observed previously in reactions of UC with nitrogen.¹¹ In contrast, V(C,N) produced from VN and graphite did not produce "active" carbon when treated with nitrogen to reverse the reaction.

Grain-Boundary Segregation of Oxygen in UN

J. D. L. Harrison¹⁶

Westbrook,¹⁷ measuring grain-boundary microhardness, demonstrated that grain-boundary segregation of impurities occurs in several metal-oxide systems at impurity concentrations well below the solubility limits. Such segregation can influence greatly those properties of a polycrystalline material that depend on grain-boundary structure and diffusion rates.

¹⁷J. H. Westbrook, "Impurity Effects at Grain Boundaries in Ceramics," p. 263 in *Science of Ceramics*, vol. III, British Ceramic Society, 1967.

Measurements of the grain-boundary microhardness of arc-melted low-oxygen UN and of sintered UN contaminated with oxygen have not shown any significant differences from the bulk microhardness. Any differences may have been obscured by the effects of absorbed surface water vapor. Subsequent experiments have revealed both for UN and UN_{0.8}C_{0.2} that the microhardness increases when the surface is cleaned by cathodic etching and protected from subsequent gaseous contamination by toluene. Definitive work on grain-boundary microhardness in this system can probably not be done until better techniques for cleaning and preserving the surfaces have been devised.

IRRADIATION PERFORMANCE OF NITRIDE FUELS

While our program on irradiation behavior of nitride fuels for civilian power-breeder concepts has not progressed to the stage of actual irradiation testing, we have performed out-of-reactor experiments and analyses to provide guidance in planning our test program. Methods for improving the thermal conductance between fuel and cladding have been investigated because with lower temperatures less fuel swelling occurs and burnup limits can be extended. Experiments involving helium injection in UN followed by annealing in a temperature gradient have been performed to provide insight into the mechanism of swelling and fission-gas bubble behavior.

Fuel-Cladding Thermal Conductance

R. K. Williams T. E. Banks D. L. McElroy

Our objective is to improve the permissible power generation rating of fuel elements by decreasing the thermal contact resistance associated with the fuel-cladding interface. Emphasis is placed on nitride and carbide fuels, which have relatively high thermal conductivities. The conditions and results of the tests are summarized in Table 18.1.

All data that have been collected fit the relationship $R_c = A\sigma^n$, where R_c is the thermal contact resistance, σ is the compressive stress, and A and n are material constants. The results show that the contact resistance for interfaces between stainless steel and UN is not very sensitive to the hardness of the stainless steel and that the value of this resistance can be significantly reduced by using a material that is soft, has a high thermal conductivity, or both.

Table 18.1. Conditions and Results of Thermal Contact Resistance Measurements in Vacuum at 50°C

Contacting Materials ^a	Hardness ^b (DPH)	RMS Surface Roughness (μ in.)	Thermal Conductivity at 50°C ($w\text{ cm}^{-1}\text{ }^{\circ}\text{C}^{-1}$)	Contact Resistance R_c at Compressive Stress of 1000 psi ($^{\circ}\text{C cm}^2\text{ w}^{-1}$)	Materials Constants ^c	
					A	n
Copper	50	14–15	4.0	0.17	550	-1.17
T-1 tool steel	835	3–4	0.16			
Type 302 stainless steel ^d	340	3–4	0.1	1.16	1156	-1.00
T-1 tool steel	835	3–4	0.16			
Type 302 stainless steel ^e	415	5	0.1	2.24	569	-0.80
UN	525	6–8	0.14			
Type 302 stainless steel ^d	340	3–4	0.1	2.40	990	-0.87
UN	525	6–8	0.14			
Type 302 stainless steel ^f	166	5	0.1	1.88	437	-0.79
UN	525	6–8	0.14			

^aFirst material listed in given couple was a thin foil and the second was a bulk specimen.

^b50-g load for foils, 1-kg load for bulk specimens.

^cFrom relationship $R_c = A\sigma^n$, where σ is the compressive stress in psi.

^dMill designation: Half Hard.

^eMill designation: Full Hard.

^fMill designation: Annealed.

Helium Bubble Migration in Uranium Mononitride in a Temperature Gradient¹⁸

S. C. Weaver J. E. Spruiell¹⁹

We studied helium bubble migration in uranium mononitride from 985 to 1585°C with gradients from 75 to 880°C/cm. Uranium nitride specimens were inoculated with 250-keV helium ions from a Cockroft-Walton accelerator and examined by electron microscopy by use of replicas of longitudinal sections (parallel to the temperature gradient), thin-film transmission samples, and replicas of fractured surfaces.

The bubbles migrated up the temperature gradient at velocities ranging from 300 Å/sec at 985°C to greater than 11,000 Å/sec at 1585°C. The bubbles appeared to move by a surface diffusion mechanism. From measurements of the migration distances, an approximate surface diffusion coefficient for UN was calculated to be

$$D_s = 1.92 \times 10^3 \exp(-42,200/RT) \text{ cm}^2/\text{sec}.$$

Although the bubbles migrated great distances, they were not observed to coalesce during the heat treatments. We think this was because of stress fields in the UN matrix surrounding the bubbles that caused the bubbles to repel each other. These stress fields were presumably caused by high non-equilibrium internal pressures in the gas bubbles.

¹⁸ Abstracted from ORNL-TM-2016 (December 1967).

¹⁹ Consultant from the University of Tennessee.

19. Materials Development for Isotopic Power Sources

R. G. Donnelly

Support of isotopic power programs includes work on general technology programs for ^{244}Cm and ^{90}Sr , and two application-oriented programs, SNAP-21 and SNAP-23. In addition, materials consulting was provided on the Isotope Kilowatt Program design evaluation study.

On the Curium Program we are selecting, developing, and testing encapsulating materials for ^{244}Cm -fueled heat sources for use in space. The immediate concern is for thermionic generator applications in the range of 1600 to 2000°C. This temperature range limits the choice of container materials to the refractory metals.

The purpose of the Strontium Program is to select optimum encapsulating materials and to develop capsule sealing techniques for ^{90}Sr -fueled isotopic heat sources designed to power thermoelectric generators. These generators require fuel capsule operation at temperatures to about 1000°C for extended periods of time. Iron-, nickel-, and cobalt-base alloys are the primary candidate encapsulation materials.

The SNAP-21 generators are designed for undersea applications and the SNAP-23 generators are for terrestrial applications. Qualified and reproducible welding and inspection procedures are necessary to better assure the integrity of the fuel containers for both normal and possible accident conditions.

CURIUM PROGRAM

Fabrication of Tungsten Capsules

R. E. McDonald

Two concepts are being investigated in the capsule testing portion of the Curium Program. These are vented and nonvented capsules fueled with 1 kw (thermal) of a ^{244}Cm fuel. With the technology developed over the past few years for the extrusion of tungsten,¹ two unalloyed arc-cast tungsten billets were

extruded in the Materials Processing Laboratory to produce pipe for the 3-in.-diam vented capsules. Two larger billets were extruded at the Fansteel Metals Center under our supervision to produce pipe for 4-in.-diam unvented capsules. Details of these extrusions are presented in Chapter 16 of this report. These four extrusions represent the largest arc-cast tungsten pipe extruded to date. Capsule bodies were machined from the extruded pipe, and end caps are being forged.

Development of CVD Tungsten Cladding Techniques

W. C. Robinson, Jr.

The chemical vapor deposition (CVD) technique was evaluated for the buildup of a heavy-wall tungsten vessel on a thin-wall tungsten container for curium fuel because this technique has the advantage of providing a capsule with no welds. This work required the development of a method for simulating the fueled thin-wall capsule and a modification of the usual deposition parameters to allow for the unusually high thermal gradients expected in the assembly during deposition.

Tungsten crucibles 1/2 in. in diameter \times 2 in. long with an 0.030-in. wall thickness were used to simulate a 200-w (thermal) curium-fueled container on which a deposit was to be made. The steep temperature gradient obtained with a 200-w internal heater in the bottom third of the capsule was balanced with an induction heater to produce a uniform temperature over the entire length of the sleeve. Parameters were ultimately determined for the production of a nodule-free deposit with a maximum variation of 0.003 in. from the mean deposition thickness.

Mechanical Properties of Capsule Materials

R. W. Swindeman R. L. Stephenson

A significant fraction of the helium produced by the alpha decay of ^{244}Cm will probably be released by the fuel at thermionic temperatures. To assure integrity of a

¹R. E. McDonald and G. A. Reimann, *Floating-Mandrel Extrusion of Tungsten and Tungsten Alloy Tubing*, ORNL-4210 (February 1968).

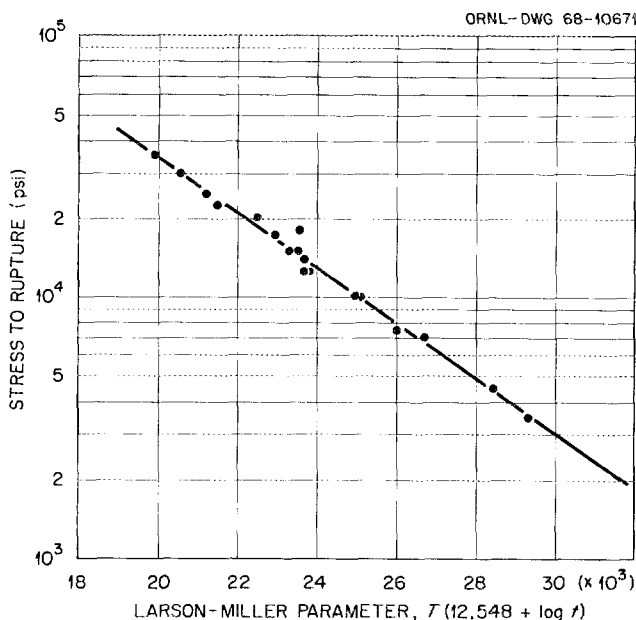


Fig. 19.1. Larson-Miller Parameter for T-111 Generated from Constant-Load Isothermal Creep Data. T is the temperature in $^{\circ}\text{K}$, and t is the time in hours.

capsule containing this isotope, the designer must either include a vent to exhaust the helium or provide sufficient void space to maintain stresses in the capsule wall at a tolerable level. In the nonvented concept one can take advantage of the predictable pressure-temperature history and optimize the design in terms of the power, weight, and life requirements.^{2,3}

The objective of the mechanical testing program is to obtain creep and rupture data for candidate capsule materials such as tungsten and tantalum alloys. Collecting data suitable for design purposes is emphasized. In addition, some tests are performed to assess the validity of the assumptions used in the design model.

With the decay of the curium fuel an unvented capsule will experience an increasing pressure but decreasing temperature, the latter affording an improvement in the creep resistance of the capsule material. Advantage may be taken of this behavior if a suitable model is available to predict creep under varying stress and temperature from constant-load, isothermal creep data. Three basic assumptions are required. (1) The fraction of damage incurred at any stress and tempera-

²J. P. Nichols and D. R. Winkler, *A Program for Calculating Optimum Dimensions of Alpha Radioisotope Capsules Exposed to Varying Stress and Temperature*, ORNL-TM-1735 (April 1967).

³R. L. Stephenson, *An Approximate Method for Determining Allowable Stress Rates for Capsules Containing Helium-Producing Isotopes*, ORNL-TM-1436 Rev. (November 1965).

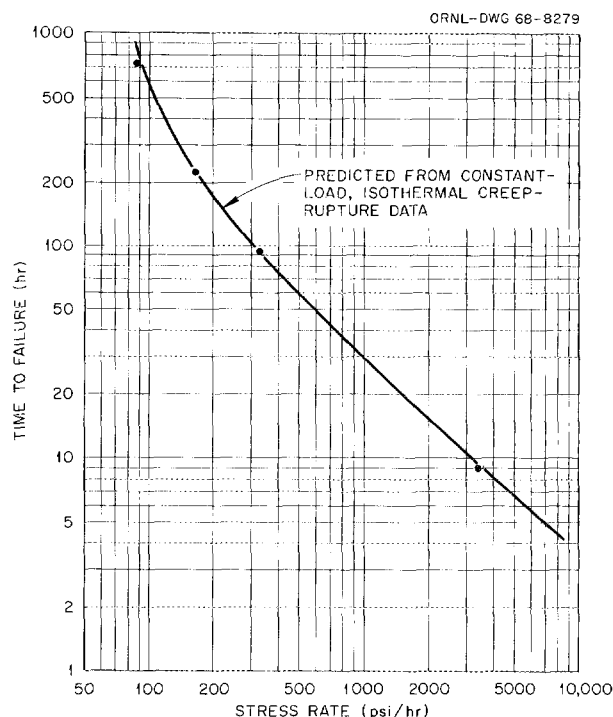


Fig. 19.2. Rupture Life of T-111 as a Function of Stress Rate for Constant Stress Increase Rate and Exponential Decrease of Temperature from 1315°C .

ture is given by the ratio of time spent under those conditions to the time to failure under those conditions; when the sum of all the damage fractions is unity, failure occurs. (2) The time to failure at any stress and temperature may be interpolated from a parametric curve, based on experimental data, that relates time, temperature, and stress. (3) The parametric curve may be extrapolated to times, temperatures, or stresses outside the range of actual experimental data.

Because the equipment required to test the validity of these assumptions for tungsten and Ta-10% W is not yet available, we tested the tantalum alloy T-111 at lower temperatures. Figure 19.1 shows a time-temperature-stress correlation for rupture of T-111 based on the Larson-Miller parameter and constant-load isothermal data. Using this correlation we calculated the rupture life of T-111 under conditions of varying stress and temperature. Four tests were then performed in which the stress rate was maintained at a constant value during each test, while the temperature was decreased from 1315°C at an exponential rate corresponding to that for an alpha-emitting isotope with a half-life of 1 year. Experimental and calculated behavior for a number of stress rates are compared in Fig. 19.2. The agreement is very good.

Vaporization of Refractory Alloys

R. L. Wagner

The vaporization of TZM at pressures less than 10^{-7} torr and at $1650 \pm 35^\circ\text{C}$ was found to occur by the selective loss of the more volatile components. For example, after 67 hr the concentrations of titanium and zirconium in the deposit formed in a cooler portion of the system were seven times those in the original alloy. Extending the exposure time progressively decreased the concentration of these components in the deposit as a result of their depletion from the alloy. Since the vaporized components are important with respect to creep resistance of this alloy, these results indicate that the maximum permissible service temperature for TZM in vacuum is below 1650°C .

Brazing Alloy Development

N. C. Cole D. A. Canonico

The efficiency of an isotopically powered thermionic generator depends on good heat transfer from the heat source to the thermionic emitter. Optimum heat transfer would be obtained with a continuous metallurgical bond, and brazing appears to be an attractive joining method for this application.

Current technology indicates that the prime candidate material for both the capsule and emitter will be tungsten. Hence, the first requirements for braze filler metals are that they wet and flow on tungsten. In addition, brazing temperatures are limited on the high side to the melting point of pure Cm_2O_3 (2200 to 2300°C) and on the low side (approx 1900°C) by the requirement for some strength at operating temperatures of 1650 to 1850°C . Stability in vacuum at these temperatures is also required.

Table 19.1. Brazing Temperatures of Experimental Alloys for Brazing Tungsten

Alloy	Composition (wt %)	Brazing Temperature ($^\circ\text{C}$)
New Alloys		
100	Pt-30W	2300
110	Pt-50Rh	2050
Alloys Previously Developed		
4D	Ta-25Ti-25Zr	2100
TVN	V-30Ta-30Nb	2000
TVT ^a	V-35Ti-30Ta	1750

^aBrazing temperature outside the desired range.

We developed four new highly promising alloys and reevaluated a number of other alloys that were previously developed for refractory alloy brazing under the High-Temperature Materials Program. The compositions and brazing temperatures of some of these alloys are presented in Table 19.1. Several of the previously developed alloys appear to satisfy the wetting, flow, and temperature requirements; however, the high vapor pressure of some of the alloying elements, such as titanium and zirconium, may compromise the usefulness of these alloys. Accordingly, we undertook the development of new brazing alloys that do not include elements with high vapor pressures.

The first four alloys listed in Table 19.1 were used to make simulated capsule-to-emitter brazes. Visually, all of the brazes exhibited good filleting and flow characteristics. These specimens have undergone nondestructive tests including radiographic, penetrant, and ultrasonic inspections. All were considered acceptable based on the first two tests. However, two (4D and 110) exhibited nonbond indications during ultrasonic testing. These indications in all instances were localized and represented no more than 10% of the total cross-sectional area of the specimen.

Physical Properties of T-111

D. L. McElroy M. Barisoni
T. G. Kollie

The temperature dependences of certain physical properties are needed to 2200°K at pressures less than

Table 19.2. Smoothed Values of Electrical Resistivity and Specific Heat of T-111 from 300 to 1600°K

Temperature ($^\circ\text{K}$)	Electrical Resistivity ($\mu\text{ohm-cm}$)	Specific Heat ($\text{cal g}^{-1} \text{ }^\circ\text{C}^{-1}$)
300	17.65	
400	21.75	0.0341
500	25.86	0.0347
600	29.84	0.0354
700	33.80	0.0360
800	37.55	0.0366
900	41.35	0.0372
1000	45.00	0.0377
1100	48.60	0.0381
1200	52.20	0.0384
1300	55.75	
1400	59.25	
1500	62.75	
1600	66.20	

10^{-6} torr to properly assess the heat transfer characteristics of the candidate curium-fuel containment materials. The properties of interest are thermal conductivity, electrical resistivity, total hemispherical emittance, and specific heat. The development of methods to measure the thermal conductivity of these materials to these high temperatures is described in Part I, Chapter 9 of this report.

We completed a series of measurements of the electrical resistivity, emittance, and specific heat of T-111. Smoothed values of the resistivity and specific heat as functions of temperature between 300 and 1600°K are given in Table 19.2. The values of the resistivity are greater than those determined for unalloyed tantalum, but the increase with temperature is smaller than expected for a 10% alloy (T-111 contains 8% W and 2% Hf). Furthermore, these values are nominally 1.7 $\mu\text{ohm-cm}$ lower than we previously obtained on another T-111 sample.⁴ The causes for these effects are receiving further study. The specific heat of T-111 exhibits greater temperature dependence

than reported for unalloyed tantalum, suggesting that the addition of 8% W increases the electronic density of states. This effect may, in turn, be related to the electrical resistivity anomaly cited above.

The total hemispherical emittance of T-111 is shown in Fig. 19.3 as a function of temperature for various surface and thermal treatments. This property is unstable in the range of 800 to 1150°K, an effect that is similar to that observed for pure tantalum.⁵ The emittance E_t of sample C during cooling from 1700°K in a vacuum of 5×10^{-7} torr can be represented by

$$E_t = 0.013 + 1.31 \times 10^{-4} T, \quad 1200 \text{ to } 1700^\circ\text{K}. \quad (1)$$

⁴J. P. Moore, R. S. Graves, and T. G. Kollie, *Metals and Ceramics Div. Ann. Progr. Rept. June 30, 1967*, ORNL-4170, pp. 77-78.

⁵G. L. Abbott, *Total Normal and Total Hemispherical Emittance of Polished Metals - Part III*, WADD-TR-61-94 (1963).

ORNL-DWG 58-7473

- T-111, POLISHED, SAMPLE A
- T-111, 11- μ in., ANNEALED
- ◇ T-111, SAMPLE C ON REHEATING
- ▲ Ta, ON HEATING (REF 1)
- T-111, 11- μ in., SAMPLE B
- ◆ T-111, SAMPLE C ON COOLING FROM 1700°K
- ▲ Ta, ON COOLING FROM 1700°K (REF 1)

⁴G. L. ABBOTT, *TOTAL NORMAL AND TOTAL HEMISPHERICAL EMITTANCE OF POLISHED METALS - PART III*, WADD-TR-61-94, U.S. NAVAL RADIOLOGICAL DEFENSE LABORATORY (1963).

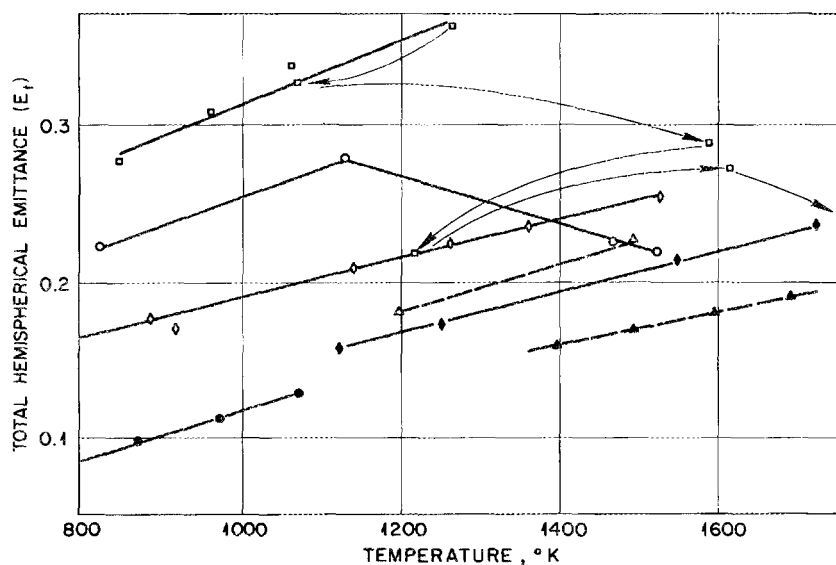


Fig. 19.3. The Temperature Dependence of the Total Hemispherical Emittance of T-111 and Tantalum for Various Thermal Treatments and Surface Finishes.

On further cooling to below 1200°K, the emittance increases to values represented by

$$E_t = 0.058 + 1.31 \times 10^{-4} T, \quad 700 \text{ to } 1200^\circ\text{K}. \quad (2)$$

If the sample is not heated above 1600°K, the latter equation can be used to determine E_t in the range 700 to 1500°C.

STRONTIUM PROGRAM

Compatibility

J. R. DiStefano

Isotopic fuels such as SrTiO_3 , Sr_2TiO_4 , and SrO are currently being developed for use in thermoelectric

power conversion systems. To provide a reliable container for these heat sources, we are examining the compatibility of nickel, iron, and cobalt alloys — Hastelloy C, type 316 stainless steel, and Haynes alloy No. 25, respectively — with these compounds at temperatures to 1100°C. Nonradioactive strontium compounds have been used in the initial phase of this program to simplify handling and evaluation.

The test system is shown schematically in Fig. 19.4. The results of tests for 1000 hr at 1100°C indicate that Sr_2TiO_4 is the most inert strontium compound. No significant weight, chemical, or microstructural changes were noted in either the alloys or fuel specimens in tests involving Sr_2TiO_4 . Weight losses and subsurface voids were found in the alloys exposed to SrTiO_3 . A surface

ORNL-DWG 68-10672

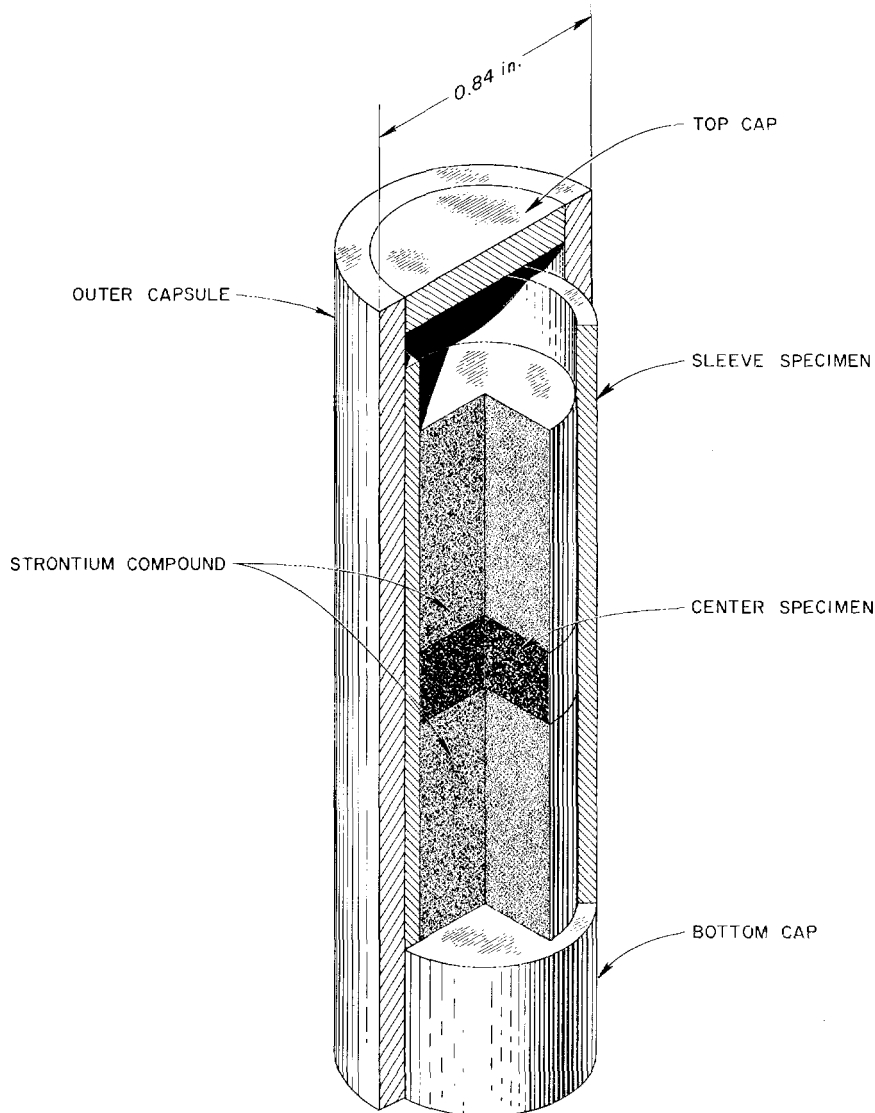


Fig. 19.4. Schematic Drawing of Compatibility Test Capsule.

reaction zone containing large amounts of Cr, Mn, Ti, and O was present in the SrTiO₃. Each alloy specimen exposed to SrO exhibited a weight gain, an increase in oxygen concentration, and a reaction zone 0.003 to 0.004 in. deep.

Room-temperature tensile tests of the sleeve specimens indicated that the interactions did not significantly alter the yield strength, ultimate tensile strength, or ductility of the alloys. Although a considerable weakening of the alloys occurred compared with before-test data on as-received material, the same effects were noted in control specimens that were heat treated in argon for 1000 hr at 1100°C. This effect, therefore, was attributed to grain growth and other microstructural changes not related to interactions with the strontium compounds. Longer time tests are under way, and those involving ⁹⁰Sr have been scheduled.

Welding

D. A. Canonico

Improvements in weld penetration capability are of interest for strontium-fueled heat sources. Although adequate penetration has been achieved by the electron-beam welding technique,⁶ there is incentive to improve weld penetration with the simpler gas tungsten-arc (GTA) welding equipment.

During the past year we investigated various parameters and joint designs for increasing weld penetration capability by the GTA process. Test welds were made on flat-plate specimens with a simple butt-joint configuration. No weld filler metal was added. First we used type 304 stainless steel. Although not a candidate capsule material, this material was selected because of its low relative cost and ready availability. Hastelloy C was also used when it became available. The butt-joint was used and a wide range of welding parameters, including preheat, were investigated. In addition, we studied the method of chilling the specimen during welding. These studies included gripping the specimen very close to the weld as well as about 1 in. away. The effect of variations in joint design and of titanium additions was studied briefly.

The results of these experiments are summarized in Table 19.3 for welds made with the optimum welding parameters. Penetrations of approximately 0.150 in. were achieved when the specimen was properly chilled. Preheating the weld to 300°C to simulate the effect of a

⁶R. G. Donnelly, *Metals and Ceramics Div. Ann. Progr. Rept. June 30, 1967*, ORNL-4170, pp. 230-31.

Table 19.3. Effect of Preheat and Joint Design on GTA Weld Penetration for Type 304 Stainless Steel and Hastelloy C

Joint Design	Preheat (°C)	Weld Penetration ^a (in.)
Type 304 Stainless Steel		
Butt	None	0.132 ^b
	300	0.180
Hastelloy C		
Butt	None	0.156
	300	0.180
Open	None	0.155
	300	0.172
Titanium insert	None	0.163
	300	0.172

^aWelding conditions: 300 amp, 10 v, 12 in./min travel speed, 1/8-in.-diam W-2% ThO₂ electrode, helium torch gas, chill grip level with top of joint.

^bChill grip approximately 1 in. below top of joint.

strontium fuel increased the depth of penetration to approximately 0.180 in., which is about 75% of the end cap thickness used. Table 19.3 shows that the two alternate joint designs (open and titanium insert) offer no advantage over the simple butt design.

SNAP-21 PROGRAM

Electron-Beam Welding Development

R. W. Gunkel

The SNAP-21 heat source capsule is a thick-walled Hastelloy C tube, 3.200 in. in diameter × 3.310 in. long, with 0.200-in.-thick walls and end caps. Gas tungsten-arc welding was first investigated for welding the caps in this capsule, but it failed to consistently produce joints having the required 0.100 in. penetration of defect-free weld metal without melting the edge of the capsule.⁶ This edge must be retained as a reference for ultrasonic inspection of the weld area. Electron-beam welding was subsequently investigated, and it produced high-quality joints having the desired combination of penetration and inspectability.

The weld geometry shown in Fig. 19.5(a) met the penetration and inspectability requirements on all nonpreheated capsules and on most capsules preheated to 300°C (the expected temperature of an isotopically fueled capsule of this design). However, edge melting was encountered in some of the preheated capsules, and methods were investigated to ensure a narrower weld.

The addition of a beam-corrector coil to the electron gun created a narrower and deeper weld of the type shown in Fig. 19.5(b). With such a narrow weld, however, a small amount of misalignment or out-of-roundness could lead to incomplete fusion. With ap-

propriate changes in beam focus together with the beam-corrector coil, we could produce joints of the type shown in Fig. 19.5(c). With this weld the joint is completely fused and the capsule edge can be reliably prevented from melting.

PHOTO 93027

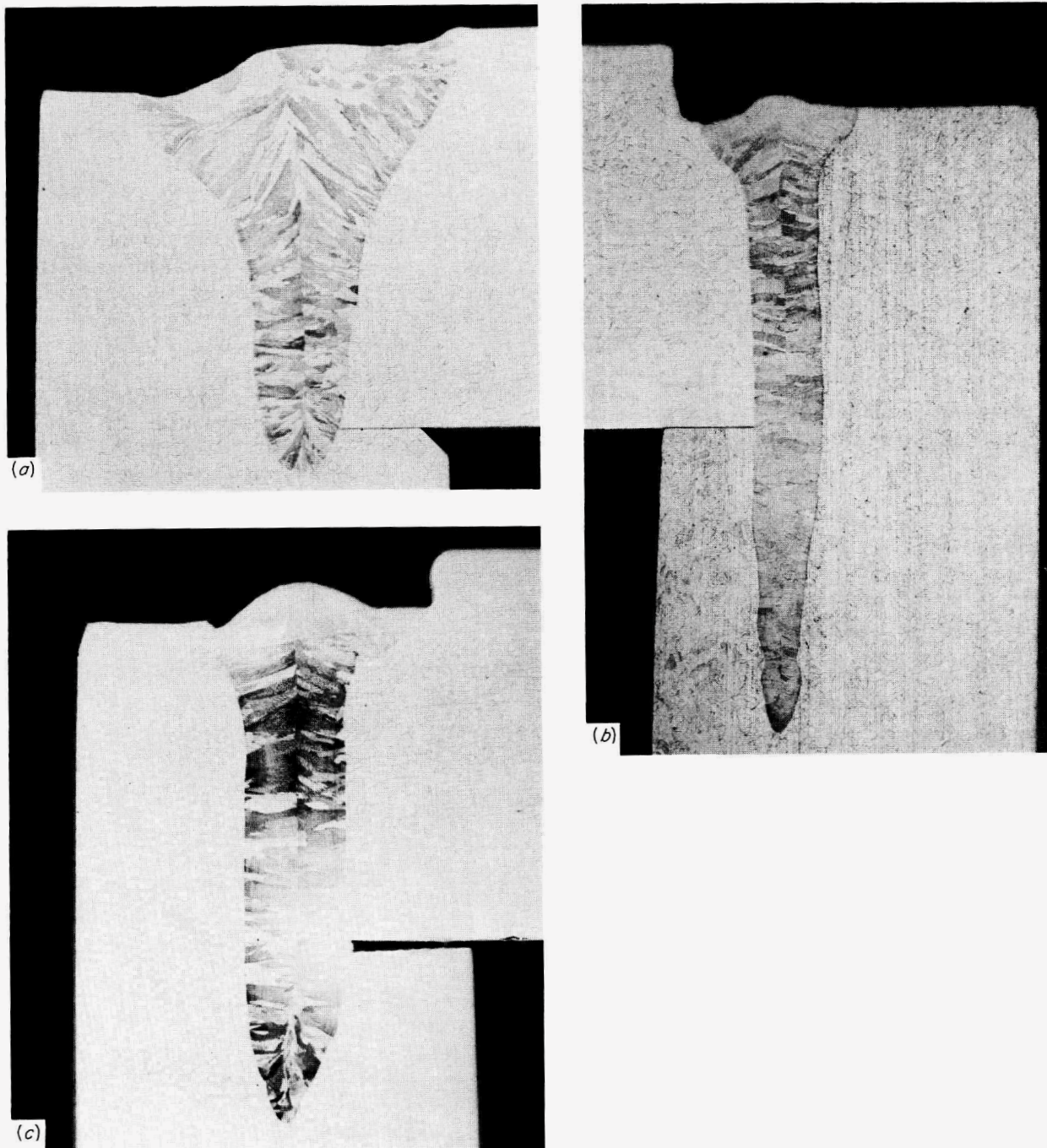


Fig. 19.5. Cross Sections of SNAP-21 Electron-Beam Welds. (a) Initial weld geometry in which corner melting was occasionally encountered. (b) Narrow weld, alignment critical. (c) Optimum joint geometry. Etched. 16X. Reduced 19%.

Nondestructive Testing

K. V. Cook

We have adapted nondestructive testing techniques for two separate tasks. The first is testing the capsule material and the initial bottom closure weld before fueling. The second is remote inspection of the closure weld of fueled capsules.

We designed and fabricated a mechanical scanning system for capsule parts. This system duplicates the scan required for the hot-cell ultrasonic inspection of the closure welds. With this and the electronic portion of the SNAP-21 scanner we evaluated bottom closure weldments of unfueled capsules in our laboratory by the same technique to be used on fueled capsule closure welds in the hot cell. Fluorescent penetrants were also used for inspection of the bottom welds.

We drafted preliminary acceptance criteria for the ultrasonic inspection of closure welds based on the interpretation of an *x-y* recording of the cylindrical joint area as projected on a plane surface. A sample recording of our ultrasonic reference standard made to simulate a SNAP-21 capsule is shown in Fig. 19.6. Each diagonal pen trace represents one circumferential path around the capsule, and the spacing between traces represents an 0.006-in. increment along the capsule axis. The traces are skewed so that the vertical deflection of the pen caused by discontinuity indications can be detected. Holes with diameters from 0.015 to 0.070 in. were machined on a circumference about 1/8 in. from the top of the mockup capsule and

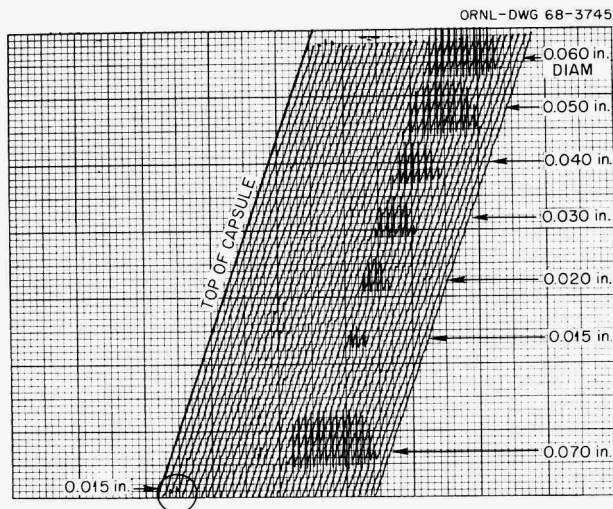


Fig. 19.6. Recording of Ultrasonic Response from SNAP-21 Capsule Calibration Standard with Various Hole Sizes.

at such a radial depth as to simulate flaws at the weld joint. An 0.015-in.-diam electro-discharge machined (EDM) hole served as the primary reference. This standard is used to calibrate and to recheck calibration of our ultrasonic instrumentation during inspection of all SNAP-21 capsule closure weldments.

Two fueled capsules were evaluated ultrasonically by remote techniques in a hot cell. Four closure welds (two bottom and two top) were inspected and found to be acceptable according to the criteria adopted.

SNAP-23 WELDING DEVELOPMENT

R. W. Gunkel

The SNAP-23 heat source capsule is a thick-walled Hastelloy C tube, 5 in. in diameter \times 7.860 in. long, with 0.400-in.-thick walls and 0.600-in.-thick end caps. The original specification required a minimum weld penetration of 0.110 in. with an edge-weld design that included an 0.062-in.-diam machined groove 0.120 in. below the surface at the base of the weld. The purpose of this groove is to prevent propagation of cracks from the root of the weld and to promote plastic deformation in a region other than that including the weld metal if the capsule is subjected to high hydrostatic pressure during operation.

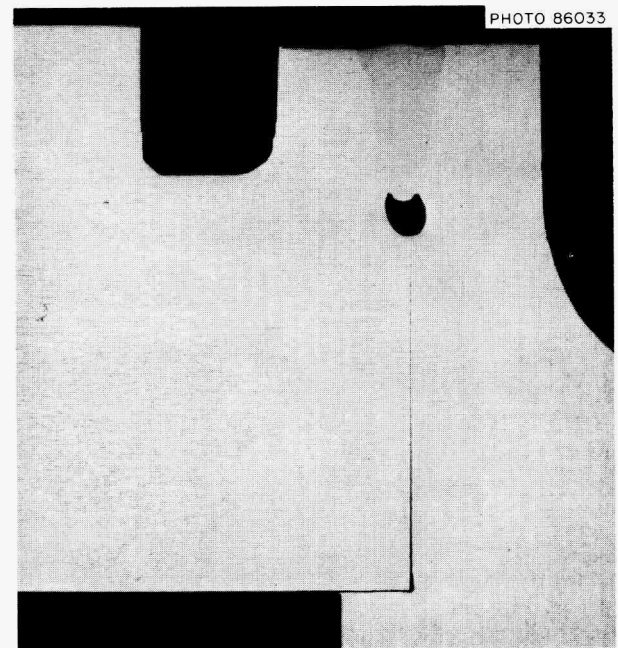


Fig. 19.7. Cross Section of a SNAP-23 Joint Electron-Beam Welded Without Preheat. Etched, 7X. Reduced 29%.

Techniques were developed for making satisfactory welds when the base metal was not preheated (Fig. 19.7). However, several attempts to produce similar welds in specimens preheated to 300 to 400°C (the temperature range for a fueled capsule) were unsuccessful. With preheat, the groove was filled with weld

metal and the effect of the groove was therefore nullified. In an attempt to solve this problem we are conducting experiments on joints in which the groove is larger and is located at a lower position with respect to the root of the weld.

Part III. General Fuels and Materials Research

20. Fuel Element Fabrication Development

G. M. Adamson, Jr.

Program emphasis was shifted this year and redirected toward better research reactor performance by improving present types of fuel elements rather than by developing new fuel systems. This upgrading can be accomplished by increased fuel loadings permitting longer core lives, by improved fabrication processes, and by higher fuel plate recovery rates. Current efforts are on aluminum-base dispersion-type fuel plates containing powdered U_3O_8 or UAl_x as the fuel. The work on this program is closely integrated with other work on research reactor fuel elements reported in Part IV, Chapters 28 and 30.

IRRADIATION TESTING OF MINIATURE FUEL PLATES

M. M. Martin W. R. Martin

Miniature fuel plates have been prepared to study the fabricability of aluminum-base dispersion fuels and for an irradiation experiment in the G-12 loop at the ETR. The motivations for our irradiation program are (1) to increase the loading of HFIR by 25%, (2) to investigate the utilization of a cheaper grade of U_3O_8 in HFIR, and (3) to evaluate the performance of UAl_x compounds as alternate fuels. The loop, which permits testing of 24 plates in 6 tier positions, is being shared with Idaho Nuclear Corporation. In ORNL experiments, several levels of fuel concentration are being examined; the lower limit is that now being used in HFIR, while the upper represents a 25% increase. The fuel dispersions, which are clad with aluminum alloy

6061, include two grades of U_3O_8 and two grades of uranium-aluminum intermetallics dispersed in a matrix of 101 aluminum. The dispersoid and matrix materials are characterized in Table 20.1. Irrespective of the type and quantity of fuel, identical pressing and rolling conditions were used to fabricate the plates.¹

In general, the plates fabricated for irradiation testing met all specifications. The only problem encountered was excessive core thickness (dogboning) near both ends of the fueled region of the plates. Table 20.2 defines the degree of localized core thickening for various test compositions. Maximum core thickening of 52 to 66% above the average thickness appears to be the rule for the UAl_x -bearing plates of highest loading. The UAl_x -aluminum composites of lower loading and also dispersions of both types of U_3O_8 in aluminum exhibited increases of only 21 to 26%. We deemed these deviations acceptable for the irradiations of miniature fuel plates.

Irradiation of ORNL plates in cycle 93A began on December 8, 1967, and after 567 Mwd exposure ($<3 \times 10^{20}$ fissions/cm³ of core), a fission release in the loop shut the reactor down. The contamination came from an Idaho Nuclear sample located in tier 4. Our plates in tiers 1 and 3 were bowed whereas our plates in tier 5 were not. Hot-cell examination of the bent plates at ORNL and also thermal test of dimensional stability on

¹M. M. Martin, W. J. Werner, and C. F. Leitten, Jr., *Fabrication of Aluminum-Base Irradiation Test Plates*, ORNL-TM-1377 (February 1966).

Table 20.1. Characterization of Fuel Dispersoids and Matrix Aluminum

Type of Material	Uranium Concentration (wt %)	Method of Preparation	Powder			
			Density (g/cm ³)	Size Range ^a of Principal Particles (μ)	Fines <44 μ (wt %)	Surface Area (m ² /g)
Atomized Al (Alcoa 101)		Atomization of molten aluminum	2.696	<44	90	0.22
Burned U ₃ O ₈	84.51	Burning uranium metal chips	7.60	105-44	3	0.35
High-fired U ₃ O ₈	84.66	"Dead-burned" U ₃ O ₈ (Y-12 process) ^b	8.22	88-44	3	0.04
Arc-cast UAl _x	75.20	Arc-casting uranium and aluminum metals	7.10	88-44	10	0.11
Solid-state reaction UAl ₃	73.70	Reaction of uranium hydride with aluminum at 1000°C	6.70	105-44	10	0.09

^aUranium-bearing materials were crushed, separated into mesh fractions, and then recombined and blended to achieve the desired particle size distribution.

^bFuel for the High Flux Isotope Reactor.

Table 20.2. Observations of Core Thickening in Miniature Fuel Plates Clad with Aluminum

Reference Plate	Fuel Dispersoid			Average Core Thickness ^a (in.)	Maximum Thickening ^b (%)
	Type	Core Concentration (wt %)	Loading of ²³⁵ U (g)		
0-56-955	High-fired U ₃ O ₈	50.2	2.75	0.0198	21
0-3-892	Burned U ₃ O ₈	44.8	2.21	0.0196	22
0-56-876	Burned U ₃ O ₈	51.0	2.75	0.0212	23
0-24-958	Arc-cast UAl _x	48.6	2.20	0.0206	26
0-57-879	Arc-cast UAl _x	58.5	2.76	0.0207	55
0-57-962	Arc-cast UAl _x	58.9	2.75	0.0197	52
0-57-966	Arc-cast UAl _x	58.8	2.75	0.0199	66
0-57-972	Solid-state reaction UAl ₃	57.4	2.75	0.0199	56

^aThe desired fuel core thickness is 0.020 in. ± 15%.

^bValues based on average.

unirradiated samples failed to reveal the cause of distortion.

Ten additional plates similar to those that bowed and those from the previous test that were still satisfactory are now being irradiated in the G-12 loop during ETR cycle 96. These plates were inserted in cycles 93E and 94A, in which they received greater than 5000 Mwd exposure. The total irradiation exposure in cycle 96 is nearly complete and the experiment is operating satisfactorily. The plates will be scheduled for return to ORNL for postirradiation evaluation upon completion of cycle 96.

PREPARATION OF UAl_x PARTICLES

M. M. Martin W. R. Martin

Uranium-aluminum intermetallic fuel (UAl_x) is used for several research reactors and is under consideration for a high-loading long-life core for HFIR. In the preparation of intermetallics for experimental fuel dispersions, the principal problem has been the reduction of the arc-cast button to the desired particle size of -140 +325 mesh with a minimum of -325-mesh fines.

We investigated comminution of both hyperstoichiometric and hypostoichiometric UAl_3 compositions, which contained, respectively, 69 and 75 wt % U. A characteristic of the two materials was that they burn or emit sparks when scratched or hammered in air. Preliminary studies using crushing devices such as a diamond mortar and pestle and a rotating disk pulverizer yielded at least 40% fines. In an attempt to decrease the yield of fines, we crushed the hypostoichiometric UAl_3 with a hammer mill rotating at 3250 rpm. Various combinations of (1) hole diameters from 0.250 to 0.020 in. for the internal mill screens and (2) size of particles fed to the mill were tried. Regardless of these crushing conditions, the mill produced mostly particles that were retained on a 140-mesh sieve; of the material that passed through the 140-mesh sieve, the ratio of $-140 +325$ mesh fraction to fines was essentially 1.

While somewhat contradictory to the above results, the hypostoichiometric UAl_3 was brittle and shattered profusely when struck a sharp blow, while the hyperstoichiometric material resisted initial breakup to -4 mesh particles. The malleable nature of this material caused severe deterioration of the screens in the hammer mill. In contrast, we milled 7 kg of hypostoichiometric UAl_3 to -4 mesh with only slight evidence of screen wear.

To produce a sufficient quantity of UAl_x particles of the desired size for fabrication studies, we crushed the -4 -mesh material obtained above in a 2.5-liter stainless steel rod mill. The advantage of this device in comparison to jaw, hammer, or ball mills is that the large particles supposedly hold the rods apart. Crushing of the smaller particles is therefore delayed until the larger sizes have been reduced. After being crushed in the rod mill, the powders were sieved twice on a Ro-Tap shaker for a total of 30 min. The fines ($<44 \mu$) from both -140 -mesh hypostoichiometric and -100 -mesh hyperstoichiometric UAl_3 compounds again accounted for about half the distribution. A heat treatment for 2 hr at $1000^\circ C$ in an atmosphere of argon caused little if any decrease in fines production during rod milling.

From the above results we conclude that the yield of fines from arc-cast UAl_x was not affected by the crushing methods investigated to date. To minimize production of fines, all particles of the desired size should be removed from the crushing device as soon as possible after the desired size has been achieved.

DETERMINATION OF POWDER PARTICLE-SIZE DISTRIBUTION OF RESEARCH REACTOR FUELS

M. M. Martin W. R. Martin

In aluminum-base dispersion fuel plates, the particle size of the uranium-bearing phase may affect irradiation performance, measurement of uranium homogeneity, and fabricability of the plates. The characterization of the starting fuel powder is important to any detailed research program on powder metallurgy fuel plates.

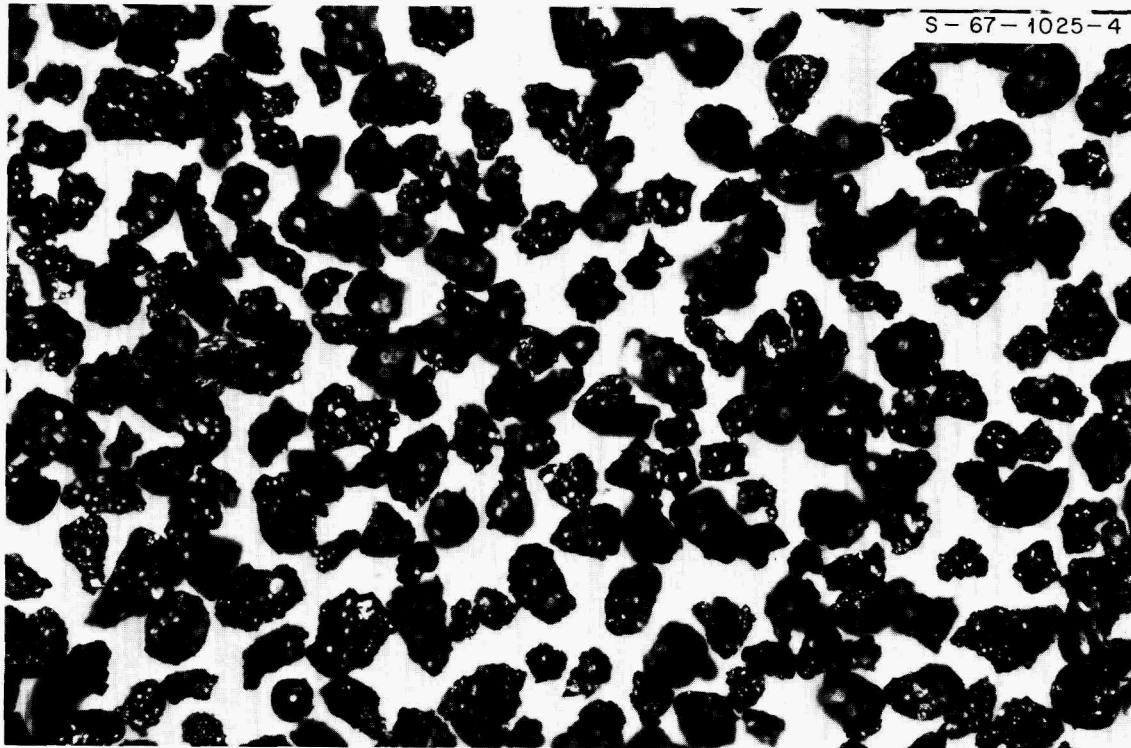
We have experienced considerable difficulty in characterizing the particle-size distribution of research reactor fuels with the accuracy desired for developmental work. For example, we desired three U_3O_8 blends from HFIR grade oxide in which the distributions are (1) 100% 88 to 74μ ; (2) evenly divided between 88 to 74μ , 74 to 63μ , 63 to 53μ , and 53 to 44μ ; (3) 100% less than 44μ . To prepare the experimental blends, we separated the as-supplied U_3O_8 particles into known mesh fractions and then recombined in the desired proportion. The powders were sieved twice with a Ro-Tap shaker to effect the separation. The weighed proportions were then blended obliquely for 2 hr inside a glass bottle that contained approximately 75% mixing void volume. To determine the actual distribution, we performed particle-size analyses on the three prepared blends and on the as-supplied U_3O_8 . The results, which are given in Table 20.3, indicate gross departure of the actual from the desired distribution.

Table 20.3 illustrates the problem of interpreting particle-size distributions encountered in the characterization of experimental U_3O_8 blends. The values are reproducible within approximately ± 3 wt %, which is adequate for production operations. Surface area measurements indicated little, if any, differences in particle size for the three blends and as-supplied material. As shown in the table, the distribution depends significantly upon the method of analysis. The Coulter Counter and photographic techniques, which are considered to be the most accurate methods, measure, respectively, the volume and major cross-sectional area of each particle. The distribution from the Ro-Tap sieve shaker using U.S. standard sieves represents essentially the minor area of the particles. When comparing the results in Table 20.3 for methods A, B, and C, one should therefore expect the distribution to shift successively to indicate more material at the larger sizes.

Table 20.3. Particle-Size Distributions of U_3O_8 Blends

Powder Blend Designation	Method of Analysis ^a	Wt % of Particles with Indicated Sizes Less Than						Surface Area (m ² /g)
		44 μ	53 μ	63 μ	74 μ	88 μ	105 μ	
As-supplied	A	9	33	51	78	100	100	0.054
	B	2	14	36	72	96	100	
	C	1	3	12	33	61	92	
	D	1	13	40	70	98	100	
Blend 1	A	0	0	0	12	100	100	0.053
	B	0	0	0	37	87	100	
	C	0	0	0	4	32	87	
Blend 2	A	2	33	60	78	100	100	0.057
	B	1	6	34	73	93	100	
	C	1	2	11	37	66	94	
Blend 3	A	100	100	100	100	100	100	0.060
	B	19	71	94	100	100	100	
	C	5	28	68	94	100	100	

^aA: Ro-Tap testing sieve shaker, 100 g sample, 15 min duration. B: Coulter Counter, sample dispersed in 1 wt % aqueous NaCl solution. C: Photomicrograph and Zeiss particle counter, 95X magnification. D: Cenco-Meizer sieve shaker, 100-g sample, 30 min at setting 5.

Fig. 20.1. Photomicrograph of High-Fired U_3O_8 . As polished. 100X.

The distribution of the as-supplied U_3O_8 as determined by a Cenco-Meizer shaker and U.S. standard sieves should represent the major cross-section area of the particles. Although these devices use screens, they impart only a circular motion to the particles, so the possibility of standing a long narrow particle on end is not great. The photomicrographic and Cenco techniques should therefore give comparable results. Surprisingly, the Coulter Counter, which measures particle volume, and the Cenco results show good agreement. To explain this discrepancy, we observed that particle-size determinations using shaking devices depend greatly upon the duration of agitation. For example, 5 hr of screening on the Cenco is equivalent to 45 min on the Ro-Tap.

The four methods for determining particle-size distribution should give identical results only on idealized spherical particles. Figure 20.1 illustrates the particle shape of the as-supplied U_3O_8 that was used to prepare the blends. Although the larger particles approximate spheres, the smaller ones are more irregular. We conclude that the four examined methods will produce reproducible results when properly controlled and should be comparable if the particles are spherical. However, for irregularly shaped particles, particle-size distribution depends on the method of analysis. Consistency of particle shape for a given particle preparation process will, therefore, be very important to show similar particle-size distributions from batch to batch.

EVALUATION OF A DEVICE FOR THE DETERMINATION OF POWDER HOMOGENEITY AFTER BLENDING

A. K. Chakraborty B. E. Foster
S. D. Snyder

The application of x-ray attenuation for the determination of green density, segregation, and homogeneity of the powder blends is being examined. The purpose is to find a direct method, other than statistical, to evaluate blending homogeneity of mixtures of aluminum and UAl_3 or U_3O_8 powders and to subsequently relate the data to the distribution of fuel in the compact and fuel plate stages of fabrication.

We designed and fabricated a mechanical device, shown in Fig. 20.2, which allows us to sample the blend without significantly disturbing the powders. The blender consists of a powder blending cavity with aluminum-beryllium sampling trays. The aluminum tray frames are inserted into the blending capsule before the powders are loaded. After blending, two thin polished

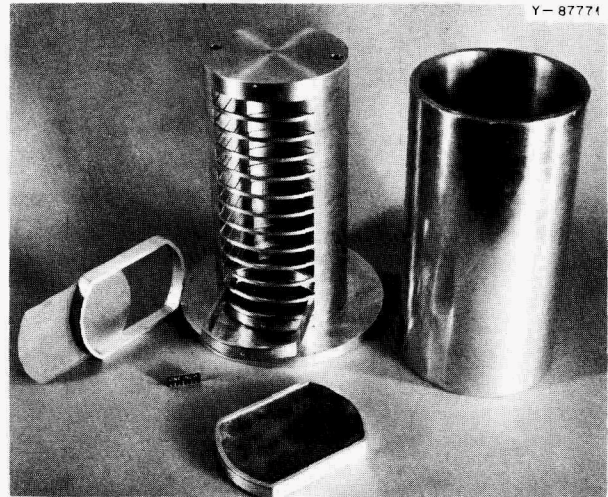


Fig. 20.2. Individual Components of the "Top Hat" Blending Device.

beryllium plates are pushed into grooves in the top and bottom of each of the aluminum frames to enclose the powders and allow the extraction of the powders from any level of the blending capsule.

We are now completing the demonstration of the technique on aluminum-iron binary powders. Sampling techniques using only aluminum powders have been completed and indicate that density variations within $\pm 2\%$ can be determined. With the device, we expect that nonuniform mixing of two powders can be studied as a function of powder characterizations and blending conditions.

VOID VOLUME IN ALUMINUM DISPERSION FUEL PLATES

M. M. Martin W. R. Martin

The control of swelling in fuel dispersions by introduction of fabrication voids has been used by several investigators to explain variations in irradiation performance.^{2,3} If this concept is real, we must understand the fabrication factors that control the final void volume in plate-type fuel elements to obtain consistent and improved irradiation performance. We have therefore established the effect of fuel compound concentration on the void volume present in fuel plates for several different fuels.

²M. J. Graber *et al.*, "Superior Irradiation Performance of Stainless-Steel Cermet Fuel Plates Through Use of Low-Density UO_2 ," *Trans. Am. Nucl. Soc.* 10(2), 482-83 (November 1967).

³J. R. Weir, *A Failure Analysis for the Low-Temperature Performance of Dispersion Fuel Elements*, ORNL-2902 (May 27, 1960).

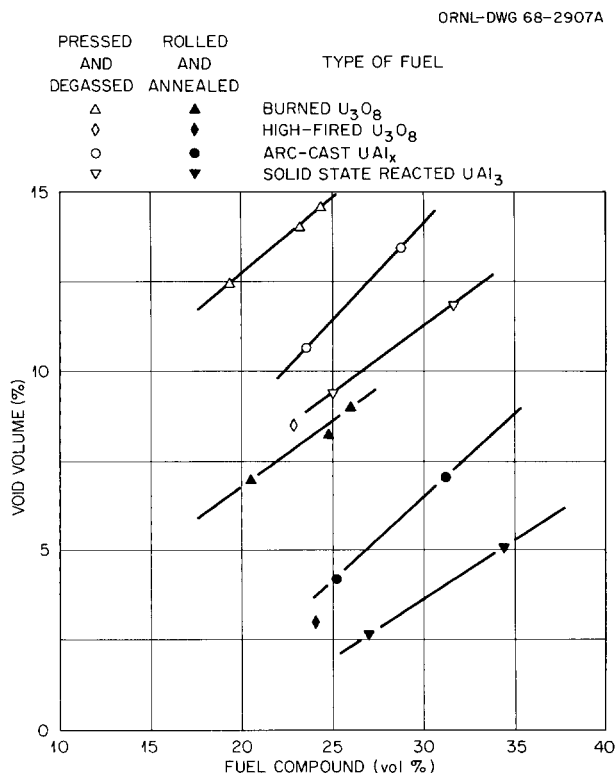


Fig. 20.3. Effect of Fuel Compound Concentration on Void Volume.

Full-size and miniature dispersion fuel plates have been fabricated with various uranium loadings from two grades of U_3O_8 and two grades of uranium-aluminum intermetallic. Characteristics of the dispersoid and matrix materials were given in Table 20.1. Irrespective of the type and quantity of fuel, identical pressing and rolling conditions were used to fabricate the plates.^{4,5}

The void volume data for the miniatures are given in Fig. 20.3. From these data, one concludes that void volume is a function of type and amount of fuel. Most importantly, the plates that contain arc-cast intermetallic exhibit slightly more voids than those with high-fired U_3O_8 and stoichiometric UAl_3 prepared by the hydride method. However, the void volume obtained for plates containing the burned U_3O_8 is much

⁴M. M. Martin, W. J. Werner, and C. F. Leitten, Jr., *Fabrication of Aluminum-Base Irradiation Test Plates*, ORNL-TM-1377 (February 1966).

⁵M. M. Martin, J. H. Erwin, and C. F. Leitten, Jr., "Fabrication Development of the Involute-Shaped High Flux Isotope Reactor Fuel Plates," pp. 268-89 in *Research Reactor Fuel Element Conference, September 17-19, 1962, Gatlinburg, Tennessee, TID-7642, Book I* (1963).

greater than for any other fuel examined. The significant increase in voids for this fuel results from extensive fragmentation of the fuel particles during fabrication. From the void volume irradiation damage concept, we conclude that the irradiation performance of burned U_3O_8 -aluminum dispersions should be better than that of dispersions of high-fired U_3O_8 , arc-cast UAl_x , and solid-state-reaction UAl_3 in aluminum.

The void volume measured for full-size plates was about 2% more than that noted for the miniature plates. The reason for the increase is not known. However, this points out that irradiation performance predicted from miniature plates may be conservative for full-size plates.

INFLUENCE OF ALLOYING ON THE SWELLING OF UAl_x DISPERSED IN ALUMINUM

A. K. Chakraborty W. R. Martin

Compacts of UAl_x dispersed in aluminum swell and distort when heated. The swelling is often sufficient to cause dimensional problems during assembly and hot rolling. The use of additives such as Ge, Si, Sn, or Zr in various concentrations is being studied as a method for minimizing such swelling. Hot-stage metallography, electrical resistance, and dilatometer measurements are being used to study the swelling problem.

A specially constructed dilatometer permitted the simultaneous measurement of the change in length of the pellets and the pressure of gas released at specified times and temperatures. A highly structured sensitive

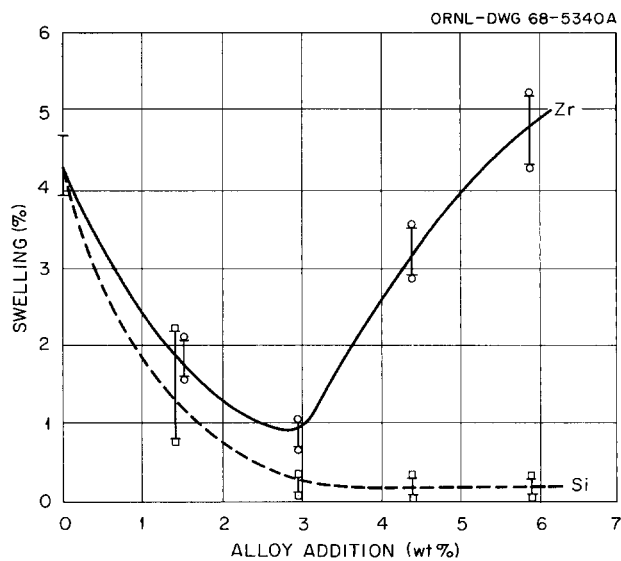


Fig. 20.4. Swelling Behavior of 40 wt % $U(Al,Si)_3$ and $U(Al,Zr)_3$ Fuel Compacts at 600°C. The compacts were heat treated for 0.5 to 8 hr at 10^{-3} torr.

electrical resistivity measurement was used to show that the swelling was actually a two-step phenomenon. Initially, it is caused by the expansion of the entrapped gases, causing grain boundary and powder surface separation. This is then followed by a diffusion-induced transformation that occurs in a preferred direction. Measurement of the kinetics of swelling at different temperatures showed the rate to be very temperature sensitive. However, the amount of gas released varied only slightly with temperature. We therefore concluded that at the higher temperatures swelling was greater because of loss of strength of the aluminum matrix, which enables more surface separation, and because of a higher transformation rate.

Added elements such as germanium, silicon, and zirconium reduced the swelling by reducing the rate of transformation to UAl_4 . Swelling behavior of 40 wt % $U(Al, Si)_3$ and $U(Al, Zr)_3$ fuel compacts at 600°C as a function of amount of additive is shown in Fig. 20.4. The most effective additions in reducing swelling were 3% Zr, Si, or Ge.

NONUNIFORM DEFORMATION IN SIMULATED FUEL PLATES

J. H. Erwin W. R. Martin

Differences in the compressive mechanical properties of core, cover plate, and frame materials at the rolling temperature may be the primary cause of nonuniform deformation of a composite fuel plate. The shape of the core after nonuniform deformation is often similar to that of a "dogbone," as shown in Fig. 20.5, and hence is known by that name. In our initial studies we used wrought materials with different elevated-temperature mechanical properties to study the development of "dogbone" or inhomogeneous reduction in simulated fuel plates. At 500°C the

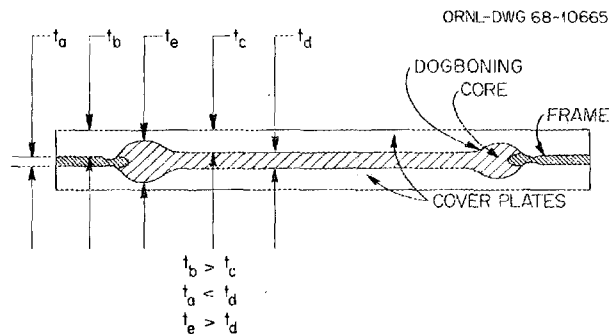


Fig. 20.5. Schematic of Composite Fuel Plate Showing Nonuniform Deformation of Core, Cover Plate, and Frame.

compressive yield strength of type 1100 aluminum is slightly lower than that of X8001, but type 6061 aluminum is stronger. Rolling billets were constructed from X8001 aluminum frames and cover plates 4 in. wide \times 9-1/2 in. long. Each frame contained two 1-3/4-in.-wide \times 1-in.-long tandem cavities separated 2-1/2 in. The frames, 1/4 in. thick, were assembled with 1/8-, 1/4-, and 1/2-in.-thick cover plates to make 1/2-, 3/4-, and 1-1/4-in.-thick billets. A type 1100 and a type 6061 aluminum alloy simulated core 0.002 in. smaller than the cavities in all dimensions were placed in each frame. The billets were heated to 500°C and rolled in multiples of 20% reduction per mill pass with a 12- \times 14-in. mill. Unlike normal fabrication practice but to accentuate differences, all reductions were made in the same billet feeding direction. After each reduction, the billets were opened and thickness contour measurements describing the frame and core reduction were obtained.

An examination of the rolled frame and core to compare the relative thicknesses reveals that the reduction of the components is approximately symmetrical at the ends of the cores; the frame is thicker

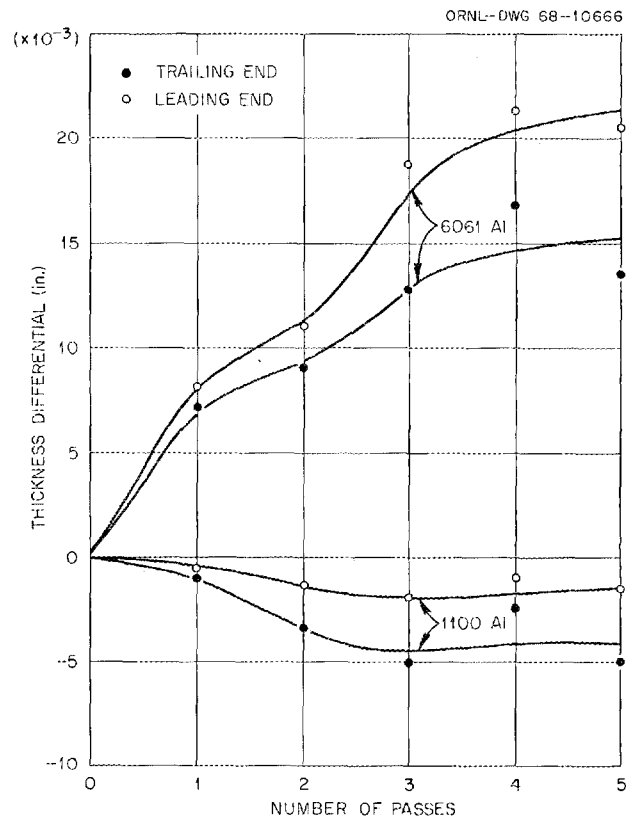


Fig. 20.6. Deformation of Simulated Fuel Plate Billets Rolled at 20% Reduction per Pass at 500°C.

adjacent to the type 1100 aluminum core and thinner adjacent to the type 6061 aluminum core. The non-uniformities in the reduction of the core in these billets through five 20% mill passes are shown in Fig. 20.6.

The thickness differentials were altered significantly when we varied the thickness of the cover plates. With six 20% mill passes, the average dogbone in the type 6061 aluminum cores was 110, 118, and 135% of the average core thickness, respectively, in billets assembled with 1/8-, 1/4-, and 1/2-in.-thick cover plates.

We conclude that the strength of the core relative to other fuel plate materials is indeed important. Dog-boning is observed when the core material is stronger than the frame and cover plates. Cover plate thickness is important also.

COMPRESSIVE STRENGTHS OF U_3O_8 - AND UAl_3 -ALUMINUM POWDER METAL COMPOSITES

J. H. Erwin W. R. Martin

With the problems of dogboning encountered with hot rolling of dispersion fuel plates, as discussed above, differences in compressive strength between the various billet components must exist at the rolling temperature, 500°C. To evaluate the magnitude of the strength differences existing between the fuel mixtures at fuel plate rolling temperatures, we investigated the compressive strength of U_3O_8 and UAl_3 dispersions in 101 aluminum over the range of 0 to 40 vol % from 25 to 550°C.

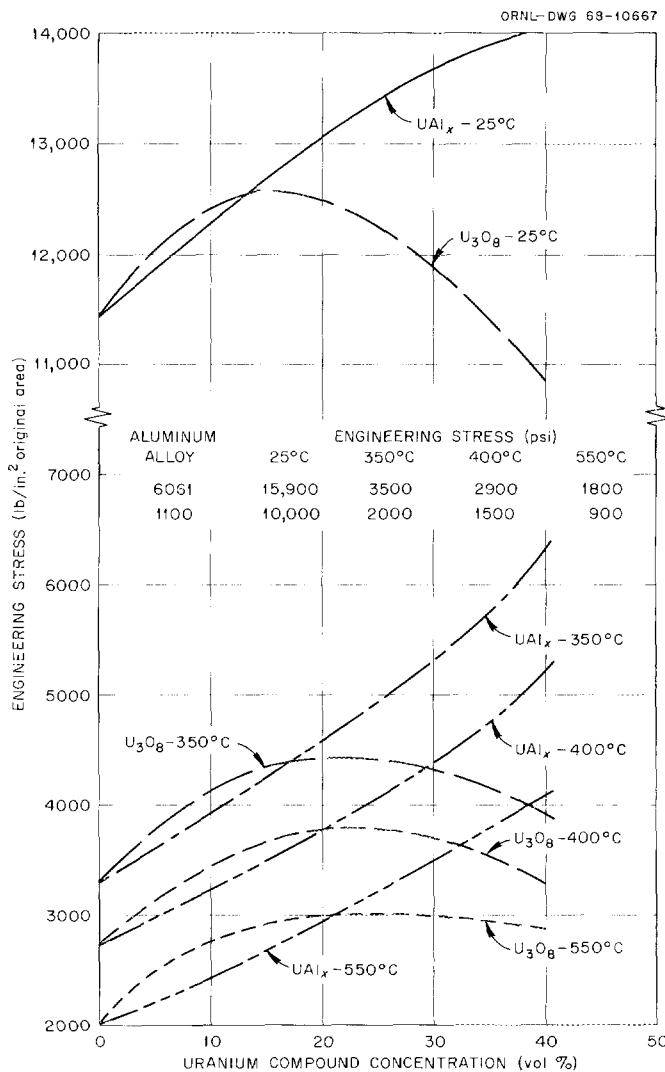


Fig. 20.7. Effect of Fuel Concentration and Temperature on the Compressive Strength of Fuel Dispersions in 101 Aluminum. Corresponding similarly determined values for cladding alloys are listed for comparison.

The fuel-aluminum powder mixture was processed by normal powder metallurgy procedures to produce 0.5-in.-diam \times 0.5-in.-long compacts pressed at 22.5 tsi. The compacts were degassed 2 hr at 500°C and less than 5×10^{-2} torr. Each compression test required three compacts of the same fuel composition stacked to produce a smooth test cylinder 0.5 in. in diameter \times 1.5 in. long. Each test was continued to approximately 5% deformation on an Instron universal testing machine operated at a crosshead speed of 0.002 in./min.

The compressive strength corresponding to 5% plastic strain in the U_3O_8 and UAl_x fuel-aluminum powder mixtures at 0 to 40 vol % are compared in Fig. 20.7 at 25, 350, 400, and 550°C. For the lower volume percentages of fuel, the properties of the compacts are similar. However, above a certain volume percentage, which increases with temperature, the curves cross and the UAl_3 compacts show much higher compressive stresses. The U_3O_8 compacts decrease in strength at the higher fuel concentrations.

EFFECT OF BILLET FEED ANGLE ON THE CURL OF ROLLED PLATE

J. H. Erwin W. R. Martin

"Curl" describes the deviation from flatness of a plate issuing from a rolling mill. It results from nonuniform plastic deformation of the entering billet and is produced during the initial reduction passes. Although the external manifestation of curl is easily corrected and hence unimportant, a serious part of the phenomenon is changes in the shape and location of the fuel core end. Its study is thus an important adjunct to both fuel-plate development studies and commercial fabrication. The mechanism of uneven metal flow depends upon frictional forces both within and without the rolling billet and may be ascribed to a number of interrelated factors. Since the predominant external factor is roll friction, we began an investigation relating curl to unbalanced friction on the billet surface.

If the billet is fed at an elevated angle, the roll friction may be increased on the top roll to shift deformation and make the issuing plate curl downward. Figure 20.8 shows the relationship found between billet feed angle and plate curl from five sample plates rolled at each of seven billet feed angles. The simulated billets were $1/4 \times 4 \times 9\text{-}1/2$ -in. X8001 aluminum. These were rolled at 500°C on a 12- \times 14-in. mill at 20% reduction. The deflection was measured at 1-in. intervals along the rolled plate length to determine the curl produced. From these data it is obvious that if curl is to be

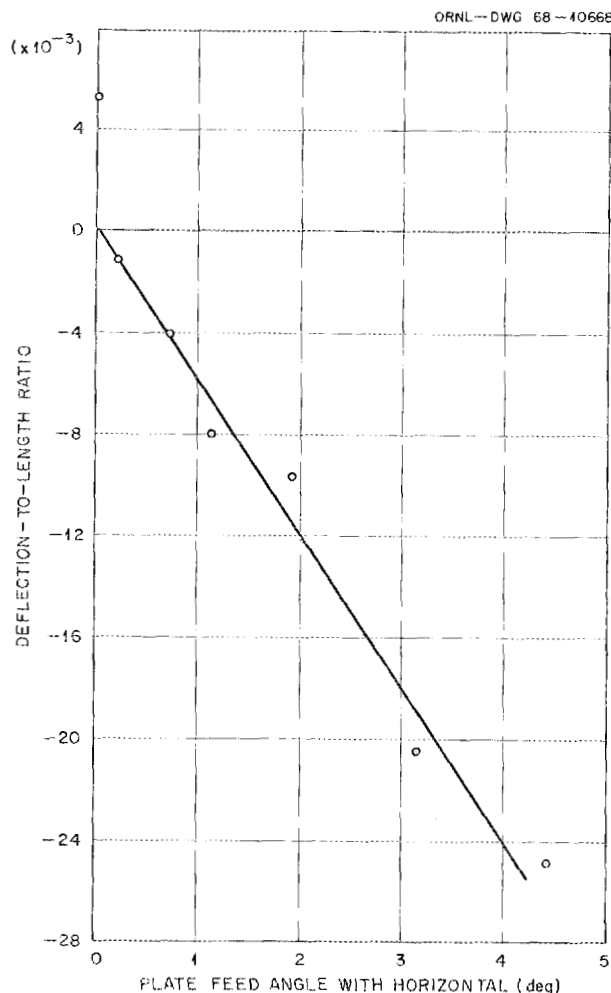


Fig. 20.8. Effect of Feed Angle on Curl Produced in Rolled Plate; $1/4$ -in.-thick X8001 Aluminum Was Reduced 20% at 500°C with a 12 \times 14-in. Mill.

avoided in commercial fabrication operations, close control of the feed angle to the mill is required.

FLAME-PRODUCED URANIUM OXIDE POWDERS⁶

J. I. Federer W. C. Robinson, Jr.
W. R. Martin

Uranium oxide powder was prepared in a flame reactor by reaction of UF_6 , H_2 , and O_2 . The powder product was characterized according to phases and impurities, particle size distribution, and sinterability.

⁶J. I. Federer, W. C. Robinson, Jr., and F. H. Patterson, *Conversion of UF_6 to UO_2 in a Flame Reactor*, report in preparation.

Studies are continuing to optimize the product with respect to purity and particle size.

Uranium oxide has been prepared from gas mixtures in which the O_2 -to- UF_6 ratio varied from 1 to 34. Initially, the reaction occurred in a H_2 - F_2 flame. Later the UF_6 - H_2 - O_2 reaction was found to be self-sustaining after ignition. The principal product in each experiment was UO_2 . Other compounds identified in some powder batches by either x-ray or chemical analysis include UO_3 , U_3O_8 , UO_2F_2 , $U(OH)_4$, and UF_4 . The fluorine content of as-prepared powder usually ranged between 4 and 10 wt % but was reduced to 30 ppm or less by heat treating the powder in dry hydrogen at $1000^\circ C$. After this defluorination treatment, x-ray analysis indicated only UO_2 present.

A sieve analysis of as-prepared powder indicated that the particle size ranged from greater than 250μ to less than 44μ . However, electron microscopy showed that the powder was highly agglomerated and that the true particle size of a typical batch ranged from 0.012 to 0.038μ . The surface area for this powder was about $15 m^2/g$. Defluorination at $1000^\circ C$ caused the particles to grow to several microns.

Defluorinated powder was isostatically pressed into pellets at 10,000, 30,000, and 50,000 psi and sintered at 1200, 1400, 1600, and $1800^\circ C$. A density of 97% of theoretical was obtained in pellets pressed at 50,000 psi and sintered as low as $1400^\circ C$. Subsequent studies showed that severe cracking occurred in pellets pressed from as-prepared powder and sintered in dry hydrogen at $1400^\circ C$. Some cracking also occurred in such pellets sintered in wet hydrogen. However, no cracking occurred in pellets pressed from defluorinated powder and sintered in either dry or wet hydrogen.

Powder mixtures of UO_2 and tungsten were also prepared in the flame reactor from the reactants mentioned previously and WF_6 . The purpose of these experiments was to determine the feasibility of preparing duplex powder. The initial product of the reaction was a powder mixture of UO_2 and $W_{20}O_{58}$. After defluorination at $1000^\circ C$ in hydrogen, the powder consisted of UO_2 and tungsten. Powder mixtures containing approximately 18, 34, and 52 wt % W were pressed into pellets and sintered at $1750^\circ C$. During sintering the tungsten agglomerated in pellets containing about 18 wt % W and became the continuous phase in pellets of higher tungsten content. Thermal conductivity (λ) measurements⁷ accurate to $\pm 5\%$ were made from 25 to $75^\circ C$. Pellets with 52 wt % W had a λ value of $0.14 w cm^{-1} ^\circ C^{-1}$ and those with 33 wt % W had a value of 0.10 at $50^\circ C$. These values are consistent with a continuous tungsten phase. Pellets containing 18 wt % W had a λ value less than that of

theoretically dense UO_2 ($0.08 w cm^{-1} ^\circ C^{-1}$), apparently due to porosity and cracks.

FEASIBILITY OF CONVERSION OF PuF_6 TO PuO_2 BY CHEMICAL VAPOR DEPOSITION

W. C. Robinson, Jr. W. R. Martin

We undertook to establish the feasibility of converting PuF_6 to PuO_2 in a one-step process by chemical vapor deposition. The process is analogous to the UF_6 conversion process and involves the reaction of PuF_6 vapor, hydrogen, and steam. A remote apparatus with facilities for fluorination of PuF_4 to PuF_6 and subsequent conversion of PuF_6 to PuO_2 was designed and constructed, and the feasibility experiments were completed. X-ray analyses of the powder product confirmed the presence of PuO_2 only.

CHEMICAL VAPOR DEPOSITION OF SILICON CARBIDE

J. E. Spruiell⁸

We determined the effect of deposition parameters on the characteristics of silicon carbide produced by chemical vapor deposition from silicon tetrachloride-methane-hydrogen mixtures. The deposits were characterized by determining (1) deposit density and soundness, (2) phases present, (3) surface appearance, (4) hardness, and (5) deposition rate.

Decreasing the pressure in the deposition chamber reduced the deposition rate, but pressure did not have a major effect on other deposit characteristics within the range investigated (<1 to 180 torr). The variables found to have the greatest effects on other deposit characteristics were deposition temperature and inlet gas stream composition. X-ray diffraction analysis showed that deposits formed below approximately $1250^\circ C$ contained free silicon as a second phase. At about $1250^\circ C$ and above, deposits containing only silicon carbide were formed for certain ranges of silicon-carbon and hydrogen-silicon mole ratios in the inlet gas stream. Above approximately $1350^\circ C$ and for low silicon-carbon ratios in the inlet gas stream, the deposits contained free graphite. The bulk of the silicon carbide in the deposits was the cubic beta phase; however, a small amount of one or more of the hexagonal alpha phases was also present.

The surface morphology of the deposits varied markedly, as shown in Fig. 20.9, and the smoother

⁷Work performed by the Physical Properties Group.

⁸Consultant from the University of Tennessee.

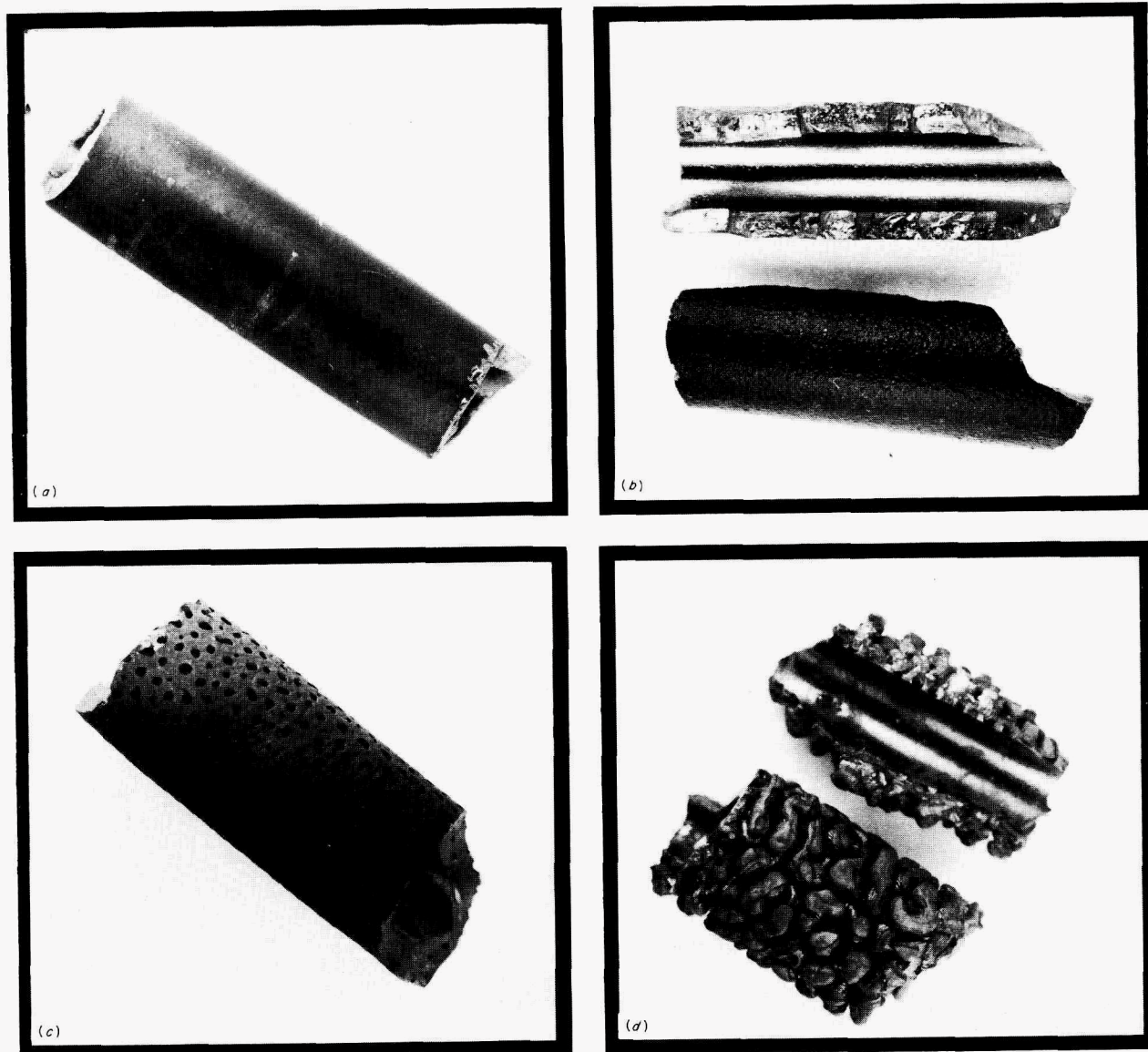


Fig. 20.9. Surface Morphologies of Silicon Carbide Deposited at (a) 1175°C, (b) 1400°C, (c) 1350°C, and (d) 1400°C.

deposits were associated with low deposition temperatures, fine-grained "laminar" microstructures, and often the presence of free silicon. Although deposition temperature was most important, surface morphology also depended on the inlet gas stream composition.

The deposition rate was a function of temperature and inlet gas stream composition as well as pressure. Typically, the deposition rate at 100 torr increased from about 0.005 to 0.010 in./hr at 1300°C to about 0.030 to 0.040 in./hr at 1500°C.

The hardnesses of the deposits were all very high even when they contained as much as 65 vol % Si; the range

was 1331 to 3855 DPH (1-kg load). The higher hardnesses were associated with higher proportions of silicon carbide in the deposits.

PLATE SURFACE STUDIES

J. V. Cathcart

The very high heat flux that exists across the surface of fuel elements in reactors such as HFIR enhances the corrosion rate of the 6061 aluminum alloy cladding. The thickness of the layer of corrosion product may reach 0.002 in. during the life of the fuel element. This

rate of corrosion does not threaten the structural integrity of the fuel elements, but the corrosion layer does pose a serious barrier to heat flow and thereby limits the fuel loading that may be used.

The purpose of our research is to develop a coating for aluminum and its alloys that will significantly reduce the extent of this corrosion in high-temperature water. We have chosen to use anodic oxide films as the coating. Aluminum forms a variety of anodic films, depending on the anodizing conditions. The films may be porous or dense, and changes in both their mechanical properties and corrosion resistance may be produced. Our aim is to find the right combination of variables so as to optimize the protectiveness and thermal conductivity of the films.

Materials and Test Conditions

Our corrosion tests fall into two categories: (1) screening tests conducted in static water at 200°C, and (2) flowing loop tests in which a large heat flux occurs across the specimen-to-water interface. The latter tests are being conducted in cooperation with John Griess of the Reactor Division.

Most of the screening tests have been performed on 99.999% Al specimens. Pure aluminum is much more subject to corrosion in water at 200°C than is type 6061 aluminum, and for a starting point we have assumed that anodic treatments that are beneficial for pure aluminum would also be beneficial to type 6061. All test specimens were in the form of electropolished coupons 0.5 × 0.75 × 0.025 in. Tests were run in distilled water at 200°C and 225 psi in a stainless steel autoclave. After test, the weight change of the specimens was measured, and the specimen surface and a cross section through the oxide were examined by optical and electron microscopy.

Results with 99.999% Aluminum

Corrosion of Pure Unanodized Aluminum. — Pure aluminum has very poor corrosion resistance in water at 200°C. For example, one of our typical test specimens was converted completely into oxide in a test lasting only 24 hr. In addition to the formation of a surface oxide layer, pronounced grain-boundary attack also occurred. The latter phenomenon was accompanied by a large stress buildup, which severely deformed the specimen and doubtlessly accelerated the corrosion process. Others, notably Draley and Ruther,⁹ have suggested that this grain-boundary attack is the consequence of the solution of atomic hydrogen in the metal followed by the precipitation of hydrogen gas in

the grain boundaries. The corrosion product is boehmite.

Effect of Anodization and the Composition of the Anodizing Bath. — We found that anodization may provide considerable corrosion protection for pure aluminum, but the degree of protection is very much a function of the composition of the anodizing bath. Aluminum specimens were anodized in baths containing 1 wt % H₂SO₄, H₃PO₄, oxalic acid, boric acid, Na₃PO₄, and Na₂CO₃. Only in the case of the oxalic acid bath was a significant decrease in corrosion rate observed. The degree of protection was a function of film thickness (see Fig. 20.10). Note that for a film 0.00012 in. thick, breakdown did not begin until after 450 hr at 200°C.

Structure of the Oxalic Acid Films. — A typical porous anodic film on aluminum consists of a close-packed array of roughly hexagonal cells of oxide 1000 to 3000 Å in diameter.¹⁰ Running down the center of each cell is a micropore a few hundred angstroms in diameter. The pores terminate at a "barrier layer" of dense oxide, which separates them from the substrate metal. The thickness of the barrier layer depends on the anodizing voltage and appears to range from 5 to 10 Å/v. For 65 v in a 1 wt % oxalic acid bath at 26°C, we formed films with a cell size of approximately 1500 Å and an estimated barrier layer thickness of 300 Å. The pore size was not determined.

Corrosion of Anodic Films on Aluminum. — Films formed in oxalic acid were not completely inert to

⁹J. E. Draley and W. E. Ruther, *Corrosion* 12, 480t–90t (1956).

¹⁰G. C. Wood, J. P. O'Sullivan, and B. Vaszko, *J. Electrochem. Soc.* 115, 618–20 (1968).

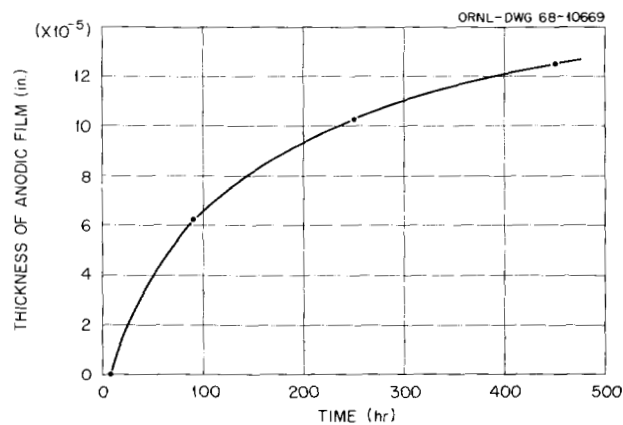


Fig. 20.10. Time Required for the Beginning of Breakdown of Anodic Coating as a Function of Anodic Film Thickness.



Fig. 20.11. Indirect Replica of the Surface of a 99.999% Aluminum Specimen Anodized for 20 min at 65 v in a 1 wt % Oxalic Acid Solution at 26°C. Specimen was exposed to water at 200°C for 336 hr. 36,000X.

water at 200°C. The film converted to boehmite at the water-to-oxide interface. Figure 20.11 shows the surface of a specimen anodized for 20 min at 65 v at a bath temperature of 26°C and then exposed to water at 200°C for 336 hr. The surface was originally smooth and featureless; after attack, however, well-formed crystallites of boehmite are plainly visible.

Figure 20.12 shows the same film in cross section. The pore structure of the film is apparent. The dark band at the top of the micrograph is thought to be the layer of corrosion product. The dark rectangles in the aluminum are etch pits formed when the specimen was etched before replication. The role of the pore structure and the barrier layer in the corrosion process are still uncertain, but the results obtained when the tempera-

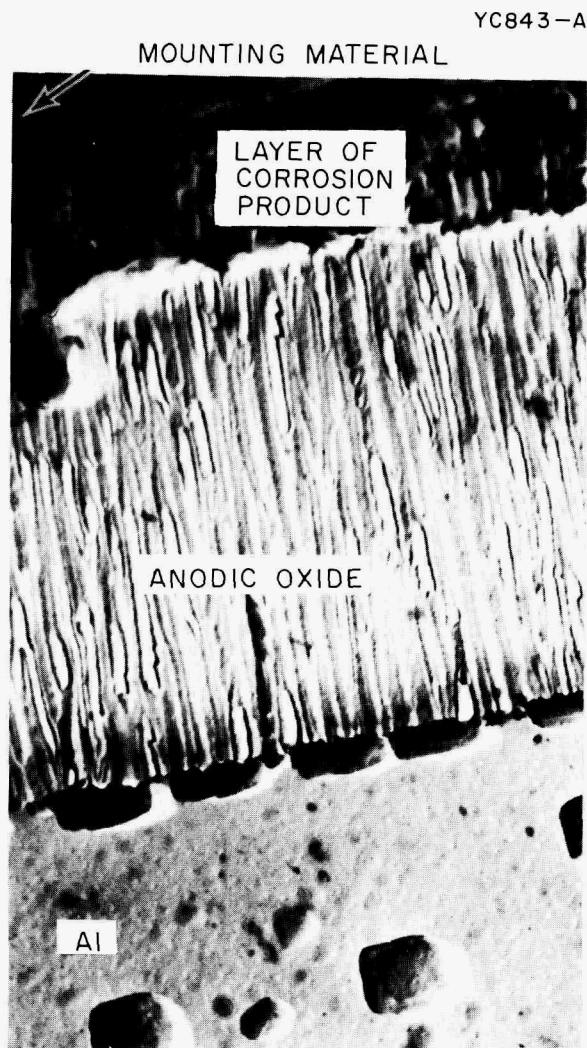


Fig. 20.12. Cross Section of Specimen Shown in Fig. 20.11. Specimen was etched lightly in dilute HF before replication. 10,000X.

ture of the anodizing bath was changed (see below) suggest that they are important.

The eventual breakdown of the films occurred at localized spots on the specimen. Once the aluminum substrate was exposed, the rate of corrosion was accelerated greatly. Large stresses developed, visibly deformed the specimen, and contributed to the further breakdown of the anodic film in adjacent areas.

Effect of Additions to the Anodic Films. — The porous nature of the anodic films formed in oxalic acid makes them ideal for absorbing various materials from solution. In an effort to enhance the corrosion resistance of the films, CrO_4^{2-} , PO_4^{3-} , and Ni^{2+} ions were absorbed in the pores of the films by refluxing anodized

specimens in appropriate solutions containing these ions. The nickel was added as nickel formate, and the specimens were annealed in either air or hydrogen before being subjected to corrosion. Thus the nickel was present either as NiO or metal during corrosion. In no case, however, was a significant improvement in the corrosion properties of the films observed.

Temperature of the Anodizing Bath. — The anodizing characteristics of aluminum are sensitive to the temperature of the anodizing bath. We investigated three temperatures: 3, 16, and 26°C. The current variation that occurs during anodization at these three temperatures is summarized in Fig. 20.13. The initial current surge that occurred when voltage was first applied to the cell was followed by a sharp drop and a slower recovery to a steady state. This behavior is probably related to the initial formation of a relatively thick barrier layer and its subsequent thinning as the pore structure develops. Note that the limiting current density decreased with decreasing temperature, indicating the formation of a thicker barrier layer, an alteration of the pore structure of the film, or both.

These changes in the character of the anodic films have an important and beneficial effect on the corrosion properties of the films. For example, a film formed at 16°C had a lifetime in water at 200°C at least four times that of a comparable film formed at 26°C. An autoclave test of a film formed at 3°C is in progress.

Conclusions from Screening Tests with Pure Aluminum. — Anodic films as thin as 0.0001 in. can provide very substantial corrosion protection for aluminum in water at 200°C for several hundred hours. The com-

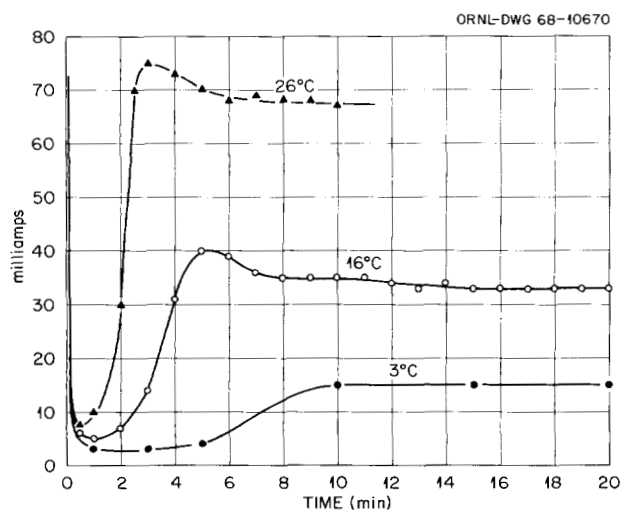


Fig. 20.13. Cell Current Variation During Anodizing at Different Temperatures. 1 wt % oxalic acid bath at 65 v.

position of the anodizing bath is crucial to the formation of protective anodic films. Of the various baths investigated, only the oxalic acid bath was effective. Bath temperature also is an important parameter; lowering it substantially improved the corrosion resistance of the films.

Results with 6061 Aluminum

Screening Tests. — The corrosion film on 6061 aluminum reached a thickness of only a few tens of microinches in periods up to 200 hr in static water at 200°C; however, Griess's¹¹ flowing loop tests indicated that a roughly hundredfold increase in the corrosion rate of the alloy occurs when the heat flux across the specimen surface reaches approximately 1×10^6 Btu $\text{hr}^{-1} \text{ft}^{-2}$. The films formed under these conditions are compact layers of boehmite that show no signs of cracking or porosity. These results suggested that the enhanced corrosion rate might be caused by a strain gradient related to the thermal gradient across the film.

To test this hypothesis, we mounted an unanodized 6061 aluminum specimen in a quartz jig in such a way that the specimen was under strain during corrosion. The oxide film thickness after 192 hr at 200°C was about 0.00012 in., approximately triple that on a control specimen.

Figure 20.14 is an electron micrograph of the surface of this specimen and shows well developed crystallites of boehmite covering the specimen. In cross section (Fig. 20.15), the film is clearly polycrystalline and compact.

Flowing Loop Tests. — We feel that the screening tests just described give an indication of the causes of the corrosion enhancement associated with the presence of a large heat flux; however, a definitive check of the effect of an anodic film on the corrosion of type 6061 aluminum clearly requires the more stringent test conditions provided by the flowing loop apparatus. The specimen in the loop test is an integral part of the loop and takes the form of a rectangular slot 0.078 \times 0.5 \times 6 in. The walls of this narrow slot serve as the test specimen and must be anodized before the unit is incorporated into the loop.

The results of the first loop test were rather inconclusive. The failure of an electrical connection forced the premature shutdown of the test, and, more importantly, temperature measurements along the surface of

¹¹J. C. Griess, H. C. Savage, and J. L. English, *Effect of Heat Flux on the Corrosion of Aluminum by Water. Part IV. Tests Relative to the Advanced Test Reactor and Correlation with Previous Results*, ORNL-3541 (February 1964).



Fig. 20.14. Indirect Replica of the Surface of an Unanodized 6061 Aluminum Specimen Corroded Under Strain for 192 hr in Water at 200°C. 13,000X. Reduced 37.5%.

the test section were sufficiently similar to those from previous tests with unanodized specimens as to suggest that the anodic film was much thinner than predicted.

Before beginning the second loop test, we revised our anodizing procedures. The cathode was a thin stainless steel strip stretched down the center axis of the test specimen. The anodizing solution was pumped through the specimen during anodization, thus sweeping out gas bubbles that formed. Furthermore, the specimen was



Fig. 20.15. Cross Section of Specimen Shown in Fig. 20.14. The micrograph shows the water oxide interface and a portion of the boehmite layer. Specimen was etched lightly in dilute HF before replication. 36,000X. Reduced 37.7%.

held at 16°C during anodization to take advantage of the enhanced corrosion resistance exhibited by anodic films formed at low temperatures. While we could not examine the interior of the test specimen itself after anodization, mockups of the loop specimens were anodized and cross-sectioned, and their interior surfaces were completely and evenly coated with an anodic film. This second loop test is now in progress.

21. Irradiation Damage to Aluminum

W. R. Martin

Aluminum has been extensively and successfully used in research reactors for years. The effect of irradiation on aluminum has been largely an increase in strength with neutron exposure, and the magnitude of any adverse irradiation effect has been small. However, some new research reactors, such as HFIR, operate at higher fuel element temperatures and higher neutron fluxes. At fluxes of approximately 10^{15} neutrons cm^{-2} sec^{-1} aluminum is exposed to fluences greater than 10^{22} neutrons/ cm^2 in times that are relatively short. Since the failure of HFIR target elements,¹ an elevated-temperature embrittlement problem with aluminum irradiated to doses of approximately 10^{22} neutrons/ cm^2 has been confirmed.²

Our program has been to determine the type and magnitudes of property changes during irradiation and seek the causes of those property changes for several aluminum alloys of interest in current research reactors. This work is related to the structural materials irradiation damage program reported in Chapter 22 of this report. Damage to HFIR targets is discussed further in Part IV, Chapter 32.

EFFECT OF NEUTRON IRRADIATION ON THE MECHANICAL PROPERTIES OF 1100 ALUMINUM

R. T. King J. R. Weir, Jr.

The effects of neutron irradiation on the tensile properties of 1100 aluminum from the N_f tray of the Oak Ridge Research Reactor have been determined.³

¹A. L. Lotts, E. J. Manthos, J. E. Van Cleve, E. L. Long, Jr., R. T. King, and J. R. Weir, Jr., *Metals and Ceramics Div. Ann. Progr. Rept. June 30, 1967*, ORNL-4170 pp. 187-91.

²J. E. Cunningham, *Severe Radiation Damage to Aluminum Alloys*, ORNL-TM-2138 (March 1968).

³S. S. Hurt, III, "Experience with Neutron Damage to Beryllium and Aluminum Lattice Components at the ORR," *Trans. Am. Nucl. Soc.* **10** (Supplement), 11-12 (July 1967).

Plate specimens irradiated to fluences ranging from 0.19×10^{22} to 1.3×10^{22} neutrons/ cm^2 (>1 Mev) at 60°C were tested in air at a strain rate of 0.266/min at temperatures from 20 to 370°C .

Irradiation to about 1.2×10^{22} neutrons/ cm^2 increased the yield strength and ultimate strength by factors of approximately 4 and 2, respectively, over the entire range of tensile-test temperatures. The ductility showed a pronounced minimum between 200 and 260°C ; in this range the irradiated alloy strained less than 6% to failure.

Specimens irradiated in the ORR to fluences ranging from 0.19×10^{22} to 1.3×10^{22} neutrons/ cm^2 were tensile tested at 30 and 200°C . At 30°C the yield and ultimate tensile strengths increased rapidly with increasing fluence, but the ductility did not change. However, although the yield and ultimate strengths at 200°C increased with increasing fluence, the ductility decreased rapidly from 50% at 0.19×10^{22} neutrons/ cm^2 to 5.9% at 1.3×10^{22} neutrons/ cm^2 .

As observed² for the X8001 alloy, annealing for 1 hr at 537°C before testing at a temperature of low postirradiation ductility (200°C) recovered both the ductility and strength of the 1100 aluminum.

DENSITY OF IRRADIATED ALUMINUM

E. L. Long, Jr.

Immersion densities were measured on 1100-aluminum specimens that had been sectioned from an ORR N_f tray.³ The aluminum was irradiated at about 60°C and received a maximum fluence of 1.5×10^{22} neutrons/ cm^2 (>1 Mev). As shown in Fig. 21.1, the density decreased linearly with increasing fast neutron fluence. A 1.5% decrease in density was measured at a fluence level of 1.5×10^{22} neutrons/ cm^2 . As would be expected, the measured decrease in density of the aluminum could be correlated with the flux profile along the length of the N_f tray.

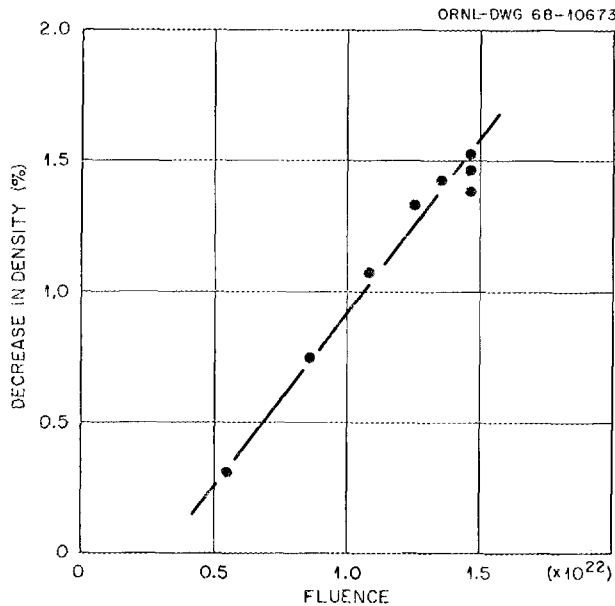


Fig. 21.1. Effect of Total Fast-Neutron Fluence (>1 Mev) on the Immersion Density of 1100 Aluminum from the N_f Tray of the ORR.

EFFECT OF NEUTRON IRRADIATION ON THE MECHANICAL PROPERTIES OF 6061 ALUMINUM

R. T. King J. R. Weir, Jr.

To determine whether the neutron irradiation damage in X8001 aluminum^{1,2} also occurs in other aluminum-base alloys, we tensile tested 6061-T6 aluminum from the hydraulic tube of the High Flux Isotope Reactor (HFIR). Ring tensile specimens were cut from regions exposed to fluences of either 6.16×10^{21} or 2.3×10^{21} neutrons/cm² (>0.82 Mev) at approximately 60°C. The tensile tests were performed in air at a crosshead speed of 0.002 in./min at temperatures ranging from 20 to 370°C.

Neutron irradiation caused a two- to threefold increase in ultimate strength over the range of test temperatures, and the strength increased with increasing fluence. A marked ductility minimum was observed between 150 and 315°C. The ductility after exposure to 6.16×10^{21} neutrons/cm² (>0.82 Mev) was lower than that after 2.3×10^{21} neutrons/cm² (>0.82 Mev). Annealing at 537°C for 1 hr before testing at 200°C recovered both the strength and ductility of 6061 aluminum. Thus, both the strength and ductility behavior of the 6061 alloy are qualitatively similar to the behavior of the X8001 alloy.

EFFECT OF CYCLOTRON-INJECTED HELIUM ON THE TENSILE PROPERTIES OF ALUMINUM ALLOYS

R. T. King J. R. Weir, Jr.

Several possible mechanisms for the embrittlement of irradiated aluminum have been proposed as either separately responsible for the neutron damage or interacting synergistically to produce the observed behavior. These are:

1. The production of helium by the $Al(n,\alpha)$ reaction with fast neutrons. This is similar to the cause of high-temperature embrittlement in iron- and nickel-base alloys used in fast reactors. As much as 6×10^{-6} atom fraction of helium is produced during the irradiation of aluminum to 1×10^{22} fast neutrons/cm² in the High Flux Isotope Reactor.
2. The production of hydrogen by the $Al(n,p)$ reaction with fast neutrons. As much as 10^{-4} atom fraction of hydrogen is generated during the irradiation of aluminum to 1×10^{22} fast neutrons/cm² in the HFIR. Substantially larger amounts of hydrogen may be recoiled into the HFIR cladding from the aqueous environment. Another possible source of hydrogen is that released during the oxidation of aluminum by water.
3. The production of silicon by the $^{27}Al(n,\gamma)$ reaction with a thermal neutron followed by a beta decay to ^{28}Si . Approximately 1% Si is produced by exposure of aluminum to approximately 2×10^{22} neutrons/cm² (thermal).
4. Displacement damage can cause strengthening and loss of ductility in metals, but embrittlement of aluminum is observed at temperatures for which displacement damage can be removed by annealing.

We determined the effect of cyclotron-injected helium on the X8001-0 6061-0, and 1100-0 alloys and SAP containing 7.5 wt % Al_2O_3 . Approximately 5×10^{-6} atom fraction of uniformly dispersed helium was injected into these alloys at temperature below 100°C. These specimens and suitable control specimens were then tensile tested in air at 0.266/min strain rate between 20 and 425°C.

The yield strengths, ultimate strengths, and uniform elongations of the alloys were not changed by the cyclotron-injected helium. However, the total elongation to failure of the X8001 and 1100 alloys decreased by as much as 50% at test temperatures above approximately one-half their absolute melting points ($0.5T_m$).

The 6061-0 and SAP alloys did not exhibit any marked decrease in ductility above $0.5T_m$.

The loss in high-temperature ductility is not clearly related to intergranular fracture processes as is the case in iron- and nickel-base alloys. No metallographic or transmission electron microscopy evidence was found to support an intergranular fracture mechanism above $0.5T_m$, where helium affects the intergranular fracture process of other face-centered-cubic metals.

ELECTRON MICROSCOPY OF IRRADIATED X8001 ALUMINUM ALLOY HEX SHEATHS FROM HFIR

J. O. Stiegler K. Farrell
C. K. H. DuBose

Transmission electron microscopy has been used to characterize the microstructure of X8001 aluminum alloy hex sheaths irradiated in the Savannah River Reactor (SRL) and in the High Flux Isotope Reactor (HFIR). Specimens have been examined in the unirradiated and as-irradiated states as well as after various annealing and deformation treatments. The irradiation occurred at 55°C in HFIR and probably at a slightly lower temperature at SRL. The material irradiated only in HFIR received a thermal fluence of 2.7×10^{22} neutrons/cm², whereas that exposed in both reactors received 6.4×10^{22} . The fast fluence (>0.8 Mev) was 1.0×10^{22} neutrons/cm² for both.

The hex sheaths were 30% cold worked before insertion in the reactors, and their microstructures consisted of a fairly coarse distribution of cigar-shaped precipitate particles, usually longer than about 0.5μ , in a well-defined matrix of subgrains of average size about 1μ . In the as-irradiated condition the precipitate and the subgrain boundaries were retained but the matrix was sprinkled with white spots ranging from 100 to 600 Å in diameter, which we determined to be voids and not gas-filled bubbles. Regions within about 1000 Å of subgrain boundaries and precipitate particles were free

of voids. Preliminary counts of the voids in the specimen irradiated in HFIR alone gave $0.9 \times 10^{15}/\text{cm}^3$. The void density in a specimen exposed in the SRL and then in HFIR was $1.9 \times 10^{15}/\text{cm}^3$. The voids in the specimen irradiated in HFIR only were larger, as is illustrated in Fig. 21.2. The large thermal neutron fluence received in the Savannah River Reactor presumably affected growth and perhaps also nucleation of voids during the subsequent HFIR irradiation. Silicon atoms produced by the reaction of ^{27}Al with thermal neutrons may be responsible for the difference.

A 1-hr anneal at 120°C of the material irradiated in HFIR did not alter the void distribution appreciably nor did it change the subgrain size. However, it did result in the appearance of small dark spots between the voids, which we believe are solid precipitate particles involving the silicon transmutation product. Such a precipitate was not present in unirradiated material given the same heat treatment.

The voids were completely eliminated by a 1-hr anneal at 260°C , and the irradiation-induced precipitate coarsened. The size of the subgrains appeared unchanged. However, in unirradiated material recrystallization commenced during a 1-hr anneal at 200°C and was complete in 1 hr at 250°C with a tenfold increase in the grain size. Thus, recrystallization was retarded in the irradiated material, even in the absence of voids.

The voids were also eliminated by cold work. Specimens were reduced about 65% in thickness by pressing at room temperature or 120°C . During the deformation the radiation-induced precipitate interacted extensively with dislocations. The loads required to press irradiated specimens were more than twice those required to press unirradiated specimens.

These metallographic observations illustrate the complex nature of high-fluence radiation damage in aluminum alloys. They show that one must consider not only displacement damage and the hydrogen, helium, and silicon produced by nuclear reactions but also the influence of the initial microstructure and its response to their presence.

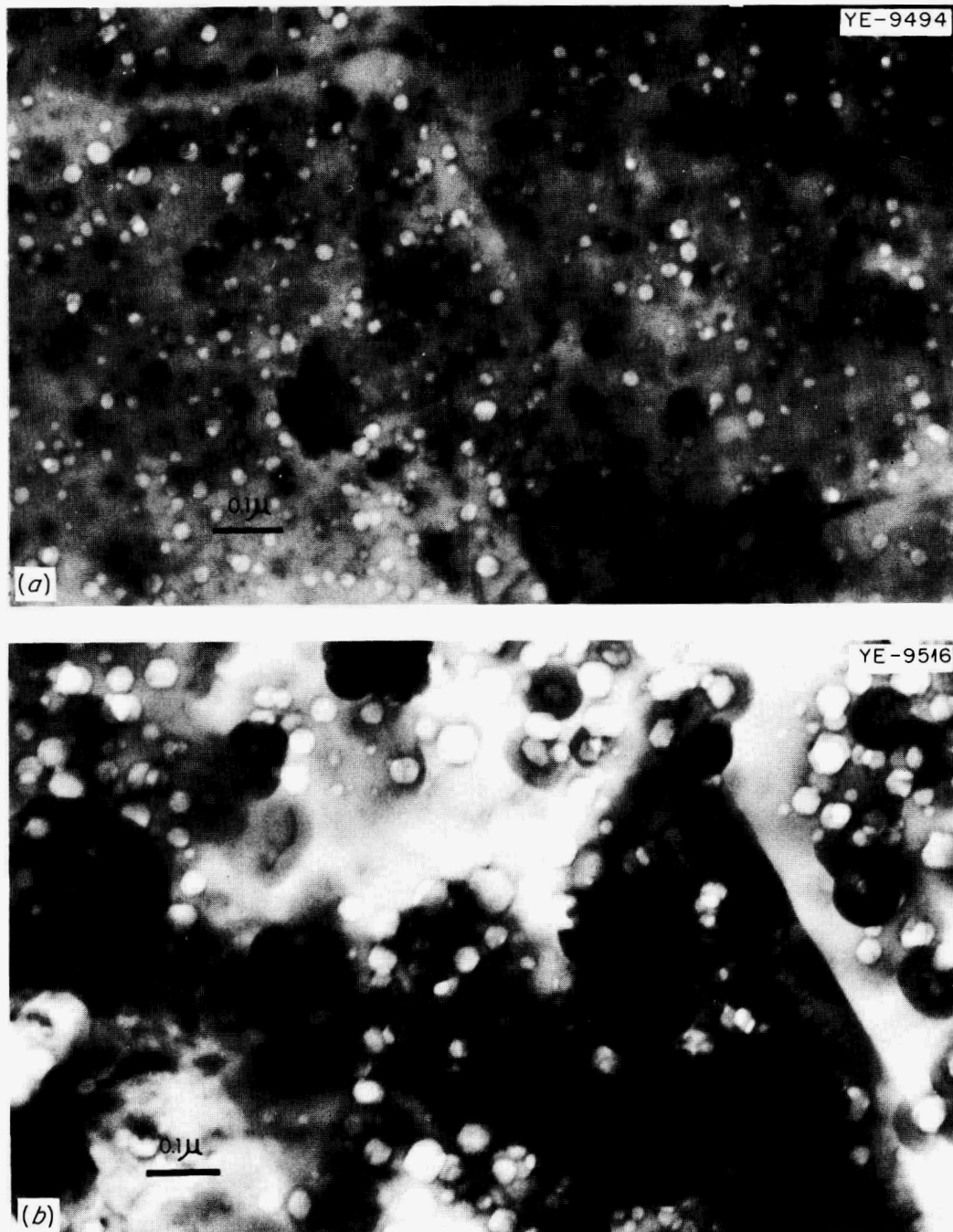


Fig. 21.2. Transmission Electron Micrographs of Sections Taken from HFIR Target Hex Sheaths. 100,000X. (a) Irradiated at SRL and HFIR. (b) Irradiated in HFIR. A subgrain boundary with an associated zone free of voids is visible on the right side of the micrograph.

22. Mechanical Properties Research¹

J. R. Weir, Jr.

These programs are closely related and have as their objectives the understanding of radiation damage to important reactor materials and the development of modified alloys more resistant to radiation damage. Emphasis has been placed on types 316 and 304 stainless steels and the titanium-modified versions of both. Incoloy 800, Hastelloy N, and certain vanadium alloys are also in various stages of investigation. Insufficient work has been done on the vanadium alloys to warrant reporting here.

Additional work on Hastelloy N is reported in Part IV, Chapters 33 and 34, of this report.

DEVELOPMENT OF TITANIUM-MODIFIED TYPE 304 STAINLESS STEEL

Radiation Damage Resistance

E. E. Bloom

The basis for selecting a titanium addition to the austenitic stainless steels to reduce the irradiation-induced loss of elevated-temperature ductility has been discussed previously.^{2,3} Tensile and creep-rupture properties of types 304 and 304L stainless steels containing titanium in concentrations up to 0.5% have been investigated. Within this range an alloy containing 0.15 to 0.25% Ti has optimum postirradiation ductility. The effects of annealing temperature, thermal aging, and irradiation on the mechanical properties of 50- and 1500-lb heats having titanium contents within this range have been extensively investigated. In the an-

nealed condition the creep-rupture properties of the titanium-modified alloy are superior to those of standard type 304 and 304L stainless steels having an equal grain size and carbon content. Upon thermal aging at 600 or 700°C the strength of the titanium-modified alloy decreases and becomes approximately equal to that of the standard alloy.⁴ The postirradiation ductility and strength properties are sensitive functions of preirradiation annealing temperature. When the alloy is annealed 1 hr at 925°C before irradiation the postirradiation ductility is optimum, is essentially independent of tensile test temperature between 700 and 900°C, and increases as the strain rate is reduced in creep-rupture tests at 700°C. In contrast, the postirradiation ductility of standard types 304 and 304L stainless steels annealed and irradiated under the same conditions decreases with increasing test temperature or decreasing strain rate.

These effects appear to result primarily from the effect of titanium on the intergranular fracture process, making crack initiation and propagation more difficult and thus reducing the susceptibility to elevated-temperature irradiation embrittlement.

Fabrication of Small-Diameter Stainless Steel Tubing

G. A. Reimann

We have been producing tubing from the titanium-modified low-carbon grade of type 304 stainless steel. Ingots were forged, machined into billets, and extruded into tube shells. Three separate approaches were investigated for reducing as-extruded tube shells to the final size. Plug drawing and mandrel swaging produced unsatisfactory tubing, but mandrel drawing produced the final size without difficulty, and satisfactory tubing was produced in 28 to 32 passes of about 15% reduction each. The mandrel drawing approach involved four swaging passes after extrusion to reduce the cross

¹Including LMFBR Cladding and Structural Materials Development.

²W. R. Martin and J. R. Weir, "Solutions to the Problems of High-Temperature Irradiation Embrittlement," pp. 440-57 in *Effects of Radiation on Structural Metals Spec. Tech. Publ. 426*, American Society for Testing and Materials, Philadelphia, December 1967.

³E. E. Bloom and J. R. Weir, "Development of Austenitic Stainless Steels with Improved Resistance to Elevated-Temperature Irradiation Embrittlement," Paper presented at ASTM Annual Meeting, July 25, 1968; to be published in the proceedings.

⁴E. E. Bloom, *Effect of Titanium Additions on the Stress-Rupture Properties of Type 304 Stainless Steel*, ORNL-TM 1807 (June 1967).

section to within the capacity of the drawbench. Tube-reducing will replace the swaging step in the future.

The microstructure of the finished tubing is shown in Fig. 22.1, where the titanium nitride precipitate can be observed. The precipitate particles were larger in the

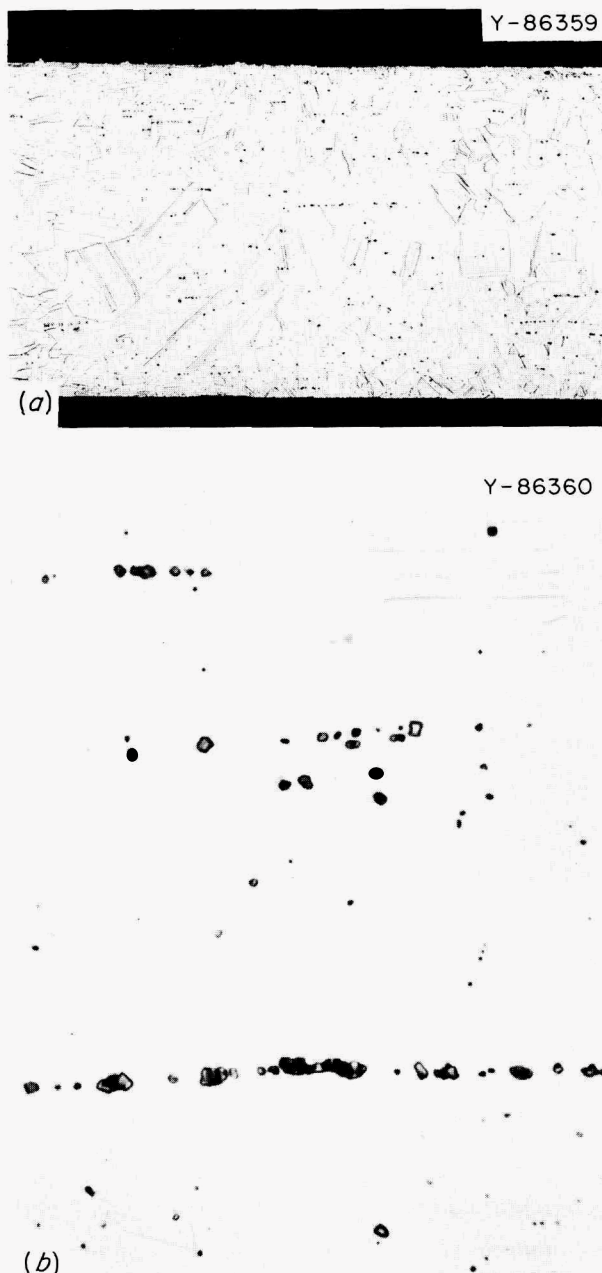


Fig. 22.1. Microstructure of Longitudinal Section of Finished 0.250-in.-OD X 0.016-in.-Wall Tube. Except for crushed nitride crystals, no second phase is evident. (a) 100X. (b) 1000X.

as-cast structure but have been fractured into smaller pieces and strung out in the direction of working.

DEVELOPMENT OF TITANIUM-MODIFIED TYPE 316 STAINLESS STEEL

E. E. Bloom

Type 316 stainless steel is an austenitic alloy that has potential as a cladding material for liquid-metal-cooled fast breeder reactors. As in other austenitic alloys, neutron irradiation causes a severe loss of the elevated-temperature ductility. In an attempt to improve the mechanical properties in both the unirradiated and irradiated conditions, we have altered the composition by the addition of titanium in concentrations up to 0.6%. In the annealed condition and at a test temperature of 650°C, titanium concentrations from 0.1 to 0.3% significantly improved the ultimate tensile strength and time to rupture in creep-rupture tests at 35,000 psi. As a result of thermal aging (2000 hr at 650°C) before test, the strength properties of the 0.1 to 0.3% Ti alloys are reduced to values similar to those of standard type 316 stainless steel. Postirradiation tensile and creep-rupture ductilities of 0.1 to 0.3% Ti alloys are lower than for the unirradiated condition but significantly higher than those of type 316 stainless steel irradiated and tested under the same conditions. Creep-rupture fractures at 650°C are intergranular in unirradiated type 316 stainless steel and transgranular in the titanium-modified alloys.

EFFECTS OF TITANIUM AND CARBON VARIATIONS ON MECHANICAL PROPERTIES AND RADIATION DAMAGE OF INCOLOY 800

D. G. Harman

Several 100-lb heats of vacuum-melted Incoloy 800 were tested at elevated temperatures. The nominal commercial composition was used except that both the carbon and titanium concentrations were intentionally varied. High carbon (approx 0.12%) alloys with titanium levels from below 0.02 to 0.38% and low carbon (approx 0.03%) alloys with 0.10 to 0.31% Ti were studied. All alloys contained 0.22% Al.

The specific alloy composition had a significant effect on the mechanical properties of both unirradiated and irradiated material. Especially prominent was the effect of titanium on the postirradiation creep ductility, which increased significantly up to 0.1% Ti but then decreased sharply with further titanium additions.

Creep elongations measured at 700 and 760°C after high-temperature irradiation were three times higher for the 0.1% Ti alloys than for the other titanium alloys. No direct effect of carbon content on ductility was found.

Metallurgical structure and testing conditions were important considerations. Postirradiation ductility increased with decreasing grain size and strain rate. Low strain rate (i.e., low stress) creep elongations as high as 100% were observed at 700°C for fine grained 0.1% Ti alloys irradiated to 3×10^{20} neutrons/cm² (thermal) at 700°C.

EFFECT OF TITANIUM AND CARBON ON MECHANICAL PROPERTIES OF HASTELLOY N

C. E. Sessions

Thermal neutron irradiation damage in Hastelloy N results from transmutation of boron to helium, which interacts with grain boundaries under stress to cause premature creep-rupture failure with low fracture strains. Small additions of active getters such as zirconium, hafnium, and titanium have been shown⁵ to significantly reduce the magnitude of the high-temperature damage, and we are studying the effects of these alloying additions on the properties of the alloy. We are defining the titanium-carbon interactions so that we can better understand the role of titanium in reducing the boron-helium damage.

We find that the creep strength at 650°C is increased significantly with both carbon and titanium additions. The creep elongation is approximately constant for carbon contents up to 0.05% but increases significantly at higher concentrations. This verifies the beneficial influence of gross grain boundary precipitation on creep ductility. For increasing titanium contents from 0 to 1.0%, the creep elongation at 40,000 psi and 650°C increased continuously from 12 to 27%. The creep

fractures at 650°C are intergranular in Hastelloy N, and the fracture characteristics do not change significantly with either titanium or carbon additions. This observation is contrary to the observed effects of titanium on the fracture mode of type 304 stainless steel.⁴

We thus see primarily a strengthening of the alloy with titanium and carbon additions and are evaluating the optimum titanium-to-carbon ratio for thermal stability and also for improved resistance to irradiation damage. We have not defined the mechanisms of ductility enhancement in these alloys but feel that generally a gettering of deleterious impurities is the most likely role of titanium.

ELECTRON MICROSCOPY OF IRRADIATED EBR-II FUEL CLADDING⁶

J. O. Stiegler E. E. Bloom J. R. Weir, Jr.

Specimens of type 304L stainless steel irradiated at temperatures between 370 and 472°C to fast neutron fluences of 0.8 to 1.4×10^{22} neutrons/cm² have been examined by transmission electron microscopy. The specimens were sections cut from the cladding of a spent driver fuel element that had been irradiated in the EBR-II and supplied by Argonne National Laboratory.

Two structural features, voids and dislocation loops, were present in all specimens. Table 22.1 lists the approximate irradiation temperature, fast neutron fluence, and void density for each of five conditions; void density values are based on a count of the number of

⁵H. E. McCoy and J. R. Weir, "Development of a Titanium-Modified Hastelloy with Improved Resistance to Radiation Damage," paper presented at 71st Annual Meeting of ASTM, Irradiation Damage Conference, June 24-27, 1968, San Francisco.

⁶Abstract of paper presented at the Fourteenth Annual Meeting of the American Nuclear Society, Toronto, Canada, June 9-13, 1968.

Table 22.1. Irradiation Conditions and Void Density Measurements in Type 304L Stainless Steel

Specimen	Irradiation Temperature (°C)	Fast Neutron Fluence (neutrons/cm ²)	Void Concentration (cm ⁻³)	Cladding Density Decrease (%)
		$\times 10^{22}$	$\times 10^{15}$	
1	370	0.8	1.4	0.07
2	398	1.2	1.3	0.15
3	438	1.4	1.3	0.17
4	465	1.3	0.9	0.16
5	472	0.9	0.4	0.08

voids per unit area on photomicrographs and an assumed foil thickness of 1000 Å. A comparison of the results for specimens 1 with 5 and 2 with 4 indicates that for a fixed fluence, the void density decreases with increasing irradiation temperature. On the basis of void size distribution and concentration, we calculated the density decreases given in Table 22.1.

The distribution of voids was remarkably homogeneous. Variations observed between different micrographs from the same specimen probably reflect differences in foil thickness. It is significant, however, that no voids were detected in the grain boundaries. In fact, the void density within about 0.1μ of the boundary was reduced, probably due to the annihilation of voids at the boundary or the influence of the boundary on the void formation process.

A very complex dislocation substructure was present in each of the five sections. At the lower irradiation temperatures the structure was so complicated that individual loops could not be observed. At 472°C , however, well-defined loops were resolved. These loops lie on $\{111\}$ and appear faulted, suggesting that they are Frank sessile loops formed by the precipitation of interstitial atoms. The loops ranged in diameter from 200 to 900 Å and were present to a density of about $2 \times 10^{15}/\text{cm}^3$.

Changes in microstructure as a result of postirradiation annealing were examined for specimen 3. After 1 hr at 600°C the dislocation loops disappeared and were replaced by a dislocation network. At progressively higher annealing temperatures the dislocation density decreased, and after 1 hr at 900°C the dislocation density was comparable to that of an unirradiated

annealed specimen. Concurrent with changes in loop and dislocation structure, we observed that the void density began to decrease. Measurements of void size distribution after annealing indicated that the smaller voids annealed more rapidly. All voids were removed in 1 hr at 900°C .

EFFECT OF CYCLOTRON-INJECTED HELIUM ON THE CREEP-RUPTURE PROPERTIES OF STAINLESS STEEL

R. T. King J. R. Weir, Jr.

The loss in high-temperature ductility of stainless steel after neutron irradiation is due to transmutation-produced helium. This damage was simulated in two LMFBR candidate cladding materials, type 304 stainless steel and 0.2% Ti-type 304L stainless steel, by cyclotron-injecting a uniform concentration of 2×10^{-5} atom fraction of helium into sheet specimens of both materials after annealing for 1 hr at 925 or 1038°C . These specimens and suitable control specimens were creep-rupture tested in argon at 600 and 700°C , over 30,000 to 55,000 psi and 14,000 to 20,000 psi stress ranges, respectively.

The ductility of the type 304 stainless steel is severely reduced by 20 ppm of helium at both 600 and 700°C . However, the titanium-modified type 304L stainless steel, which shows improved resistance to neutron irradiation damage, is not as severely affected by 20 ppm of cyclotron-injected helium as the type 304 stainless steel (See Fig. 22.2). Martin and Weir² have discussed the effects of small additions of titanium on stainless steel.

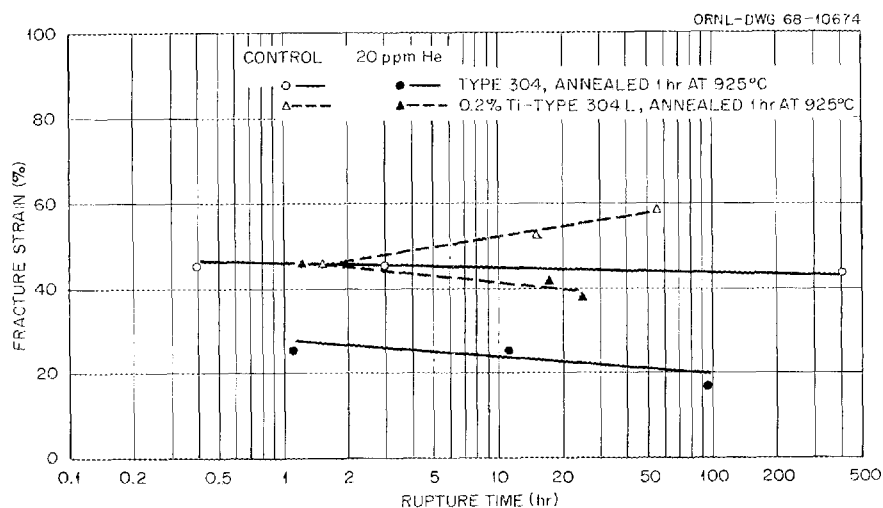


Fig. 22.2. Effect of Helium Injection on Fracture Strain vs Rupture Time Curves for Type 304 and 0.2% Ti-Type 304L Stainless Steels at 600°C .

EBR-II IRRADIATION EXPERIMENTSE. E. Bloom J. R. Weir, Jr. A. F. Zulliger⁷

To allow the design of subsequent materials irradiation experiments, we determined the axial distribution of the nuclear heating rate for rows 2 and 7 of the EBR-II. Susceptors were placed in the central tube of a seven-tube subassembly. A gas gap was provided between the susceptor surface and the inner wall of the tube to act as a heat transfer barrier. Susceptors were designed on the basis of published heating rates to operate at temperatures between 500 and 800°C. Melt wires having melting points both above and below the design temperature were placed in each susceptor. In each susceptor the melt wires had a range of melting points such that the susceptor temperature that would result from a variation of $\pm 50\%$ from the calculated

heating rates could be measured. Postirradiation examination of the susceptors placed the operating temperature between the melting points of two wires. Nuclear heating rates were then calculated. In the row 2 experiment the melt wires having the lower melting points showed no signs of melting, whereas in the row 7 experiment melt wires at several locations had melted. These results indicated that in row 2 at the reactor midplane, the nuclear heating rate was less than 4.0 w/g (in stainless steel at a reactor power of 45 Mw), compared to a calculated value of approximately 7.2 w/g. In row 7 at the reactor midplane the measured value was 0.8 w/g, compared to a calculated value of approximately 2 w/g.

The information provided by this experiment has been used in the design of two subassemblies, which are being irradiated in row 2 and 7 positions. The materials included in the subassemblies are types 304, 304L, titanium-modified 304 and 304L, and 316L stainless steels, Incoloy 800, V-20% Ti and nickel 270.

⁷General Engineering Division.

23. Nondestructive Test Development

R. W. McClung

This program is designed to develop new and improved methods of examining reactor materials and components. To achieve this we study the pertinent physical phenomena, develop instrumentation and other equipment, devise application techniques, and design and fabricate reference standards. Among the subjects being actively pursued are electromagnetics (with major emphasis on eddy currents), ultrasonics, holography, and penetrating radiation.

ELECTROMAGNETIC TEST METHODS

C. V. Dodd J. W. Luquire¹
W. E. Deeds¹ W. G. Spoeri

Analytical Studies

We continued research and development on both analytical and empirical bases. We derived a number of integral equations that represent solutions to various problems related to electromagnetic phenomena.²⁻⁴ The cases solved that are of particular interest to eddy-current testing are shown in Fig. 23.1 and the effects for which the solutions are applicable are listed as follows: cases 1, 5, and 6, coil impedance and defect sensitivity; cases 2 and 3, phase and amplitude of voltage and defect sensitivity; case 4, coil impedance.

We have written computer programs that allow calculation of these effects in minutes on a time-sharing computer. Consequently, these programs are highly beneficial in the design of actual eddy-current tests. The

two curves in Fig. 23.2 show how coil impedance in a given test situation varies with cladding thickness for one conductor clad on two base materials having different conductivities. Figure 23.3 shows the variation in phase shift with an incremental variation in metal thickness for four different thickness ranges as a function of both coil and metal parameters. These curves allow us to choose the optimum parameters to obtain maximum sensitivity over a particular thickness range.

We determined that the signal due to a defect can be expressed as the product of a defect sensitivity factor, a defect shape-and-orientation factor, and the defect volume. The defect sensitivity factor is a mutual- or self-inductance function and depends only on the coil system, the frequency, the specimen conductivity, and the location of the defect. Figure 23.4 is a typical plot of the defect sensitivity factor as a function of location. The defect shape-and-orientation factor calculated for a spheroidal flaw as a function of orientation and ratio of axes is shown in Fig. 23.5.

We made a series of experimental measurements of coil impedance for the case of a coil above a single conducting plane for comparison with calculated values. The results are shown in Fig. 23.6. The agreement between calculated and measured values is excellent in the areas of accurate measured values. (At the lower frequencies the measured values are relatively inaccurate.) The disagreement between measured and calculated points is within the limit of experimental error in all cases.

Phase-Sensitive Eddy-Current Instrument

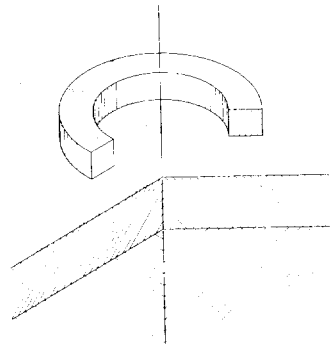
Portable Instrument. — Work has continued on the portable phase-sensitive eddy-current instrument. We constructed printed circuit boards to simplify maintenance and prepared templates so that the circuit boards can be constructed more economically. The instrument and circuit board layout were photographed so prints could be distributed externally through the ORNL

¹Consultant from the University of Tennessee.

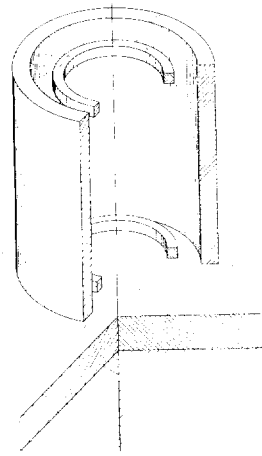
²C. V. Dodd, *Solutions to Electromagnetic Induction Problems*, ORNL-TM-1842 (June 1967). Ph.D. Thesis, the University of Tennessee.

³C. V. Dodd and W. E. Deeds, "Electromagnetic Forces in Conductors," *J. Appl. Phys.* 38(13), 5045-51 (December 1967).

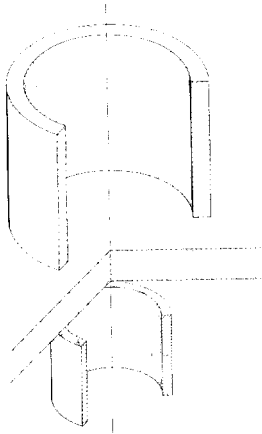
⁴C. V. Dodd and W. E. Deeds, "Analytical Solutions to Eddy-Current Probe Coil Problems," *J. Appl. Phys.* 39(6), 2829-38 (May 1968).



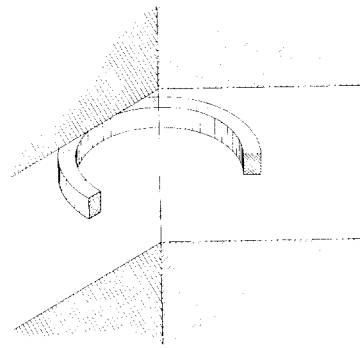
(a) CASE 1: COIL ABOVE TWO-CONDUCTOR PLANE.



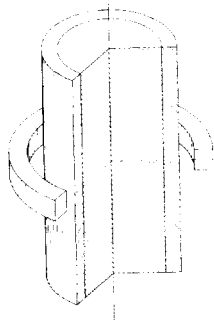
(b) CASE 2: REFLECTION-TYPE COIL (AS USED IN PHASE-SENSITIVE INSTRUMENT) ABOVE A TWO-CONDUCTOR PLANE.



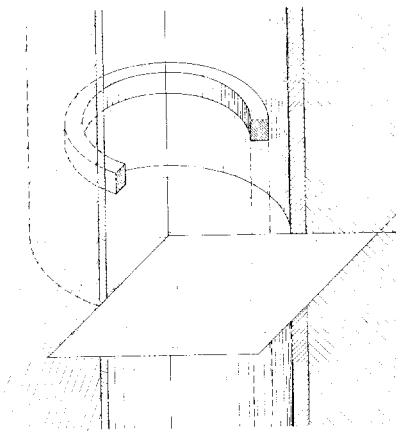
(c) CASE 3: THROUGH-TRANSMISSION COILS (AS USED IN PHASE-SENSITIVE INSTRUMENT).



(d) CASE 4: COIL BETWEEN TWO-CONDUCTING PLANES (FOR SPACING MEASUREMENTS).



(e) CASE 5: COIL ENCIRCLING TWO CONDUCTOR ROD.



(f) CASE 6: COIL INSIDE TWO CONDUCTOR TUBE.

Fig. 23.1. Eddy-Current Testing Cases for Which Solutions Have Been Obtained in the Form of Integral Equations.

office of Industrial Cooperation. A paper⁵ on this instrument has been published and an abstract is given below.

A new portable phase-sensitive eddy-current instrument has been developed at the Oak Ridge National Laboratory. It operates on either alternating current or its own rechargeable

batteries at 50 and 500 kHz. The instrument can be used for a wide range of metal or cladding thickness measurements and also for sorting and identifying metals according to their conductivities. It is insensitive to lift-off over a wide range of measurements and features ease of setup and operation along with good stability.

Coil Focus Studies. --- We are experimentally investigating the focusing effects of reflection-type eddy-current coils for use with the phase-sensitive instrument. The size of the focus or effective diameter of the eddy currents within the specimen is important because of its relation to the ability to detect small discontinuities and to resolve the response from a small discontinuity near other discontinuities. To measure the focus we scan a coil across a metal plate that has a step change in thickness on the reverse side. The length of scan required to change the instrument response from within 1% of the value on the initial thickness to within 1% of the value on the final thickness is the focal diameter of the coil. This focal diameter depends on the shielding effect of the metal housing of the probe surrounding the coil and the diameter of the coil and appears to be independent of the thickness being measured. The smallest focal diameter achieved thus far is 0.114 in. for an 0.036-in.-OD coil in an 0.063-in.-ID aluminum tube. We will attempt to reduce the focal diameter by building smaller coils and using different shielding materials.

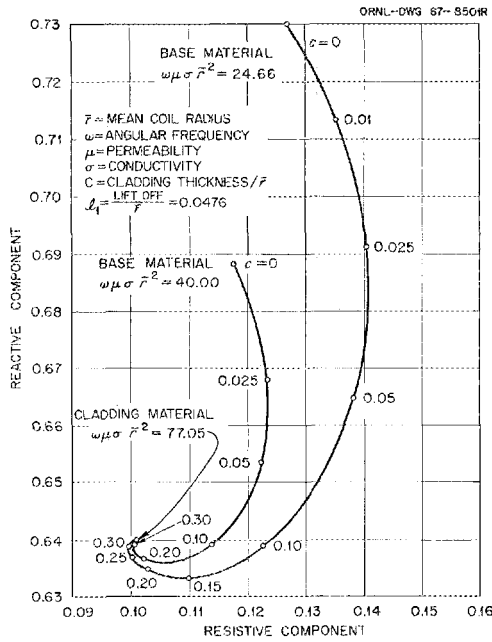


Fig. 23.2. Variation of Normalized Impedance with Cladding Thickness.

⁵C. V. Dodd, "A Portable Phase-Sensitive Eddy Current Instrument," *Mater. Evaluation* 26(3), 33-36 (March 1968).

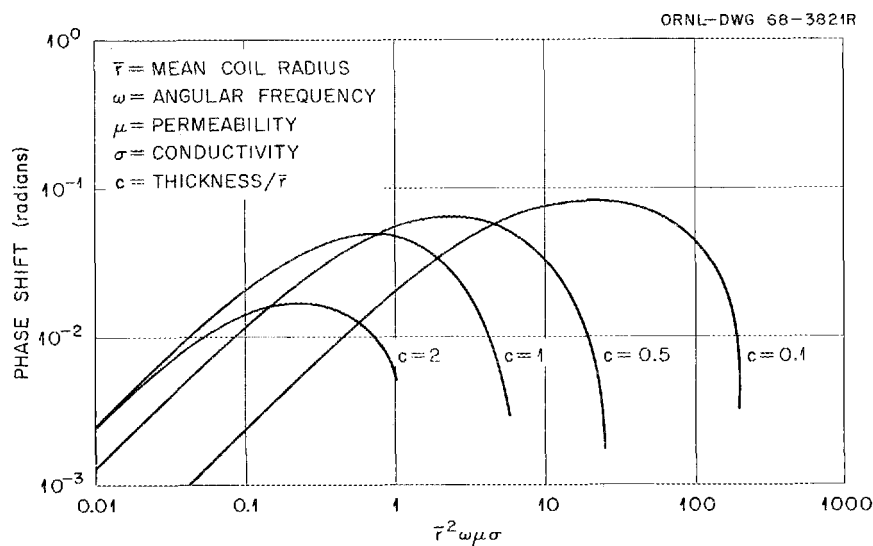


Fig. 23.3. Curves of Phase Shift for Determination of Optimum Frequency and Coil Dimensions for Various Thicknesses of Metal.

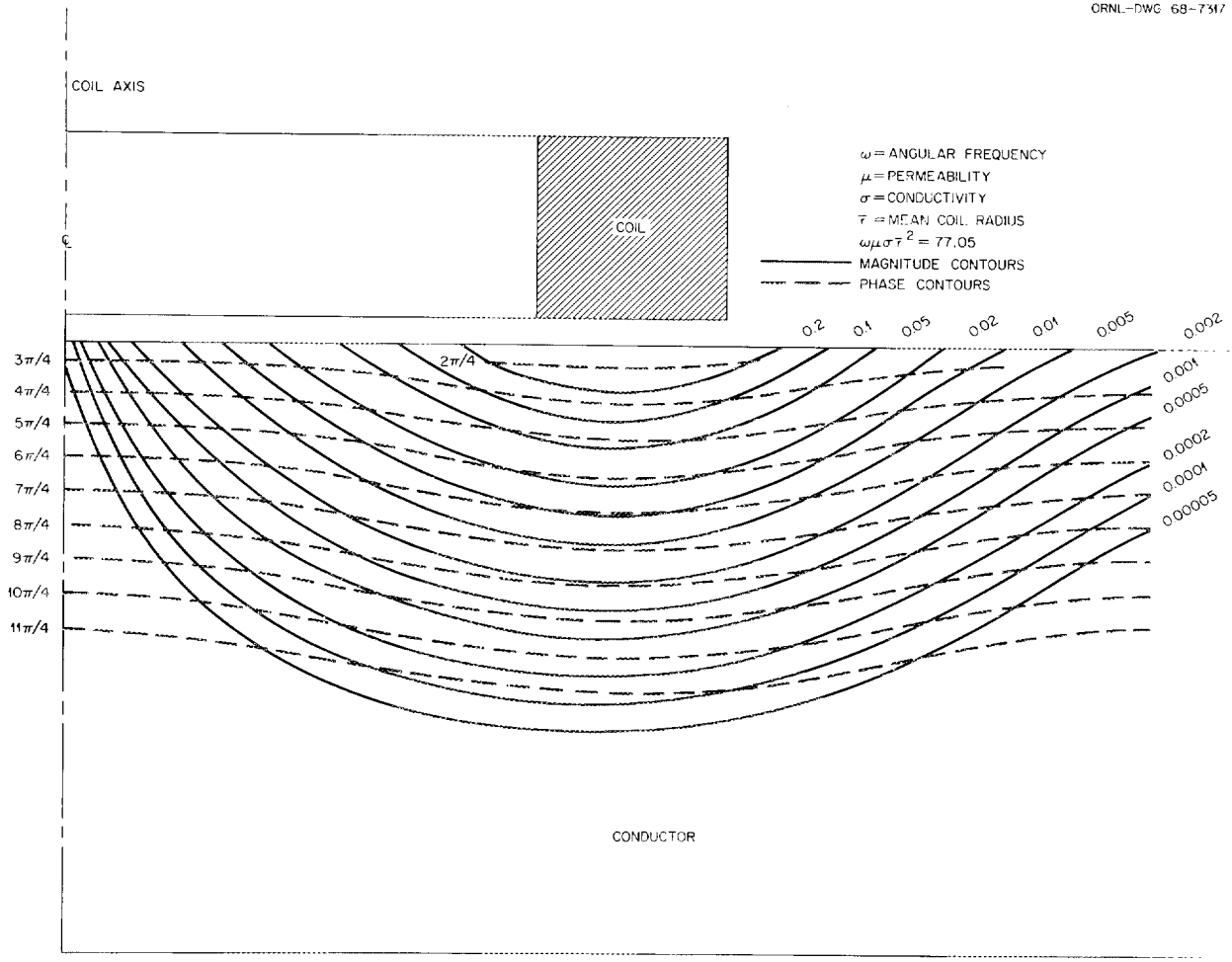


Fig. 23.4. Phase and Magnitude Contours of the Defect Sensitivity for a Coil Above a Conducting Plane.

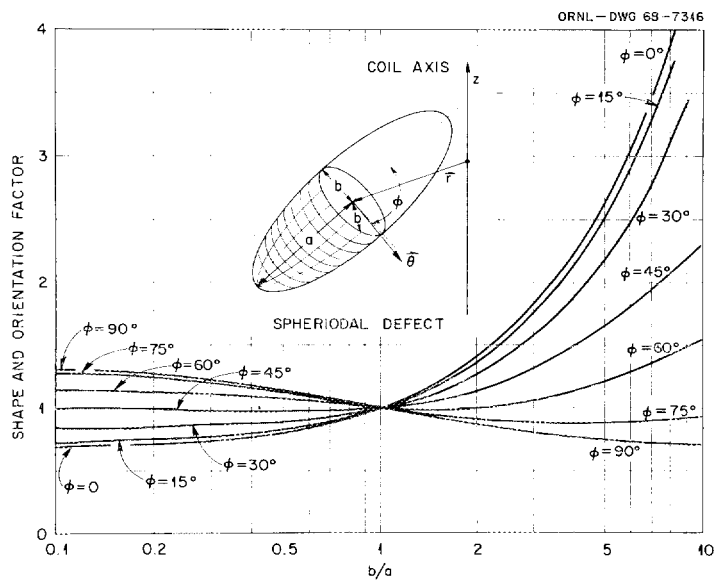


Fig. 23.5. Shape-and-Orientation Factor of a Spheroidal Defect.

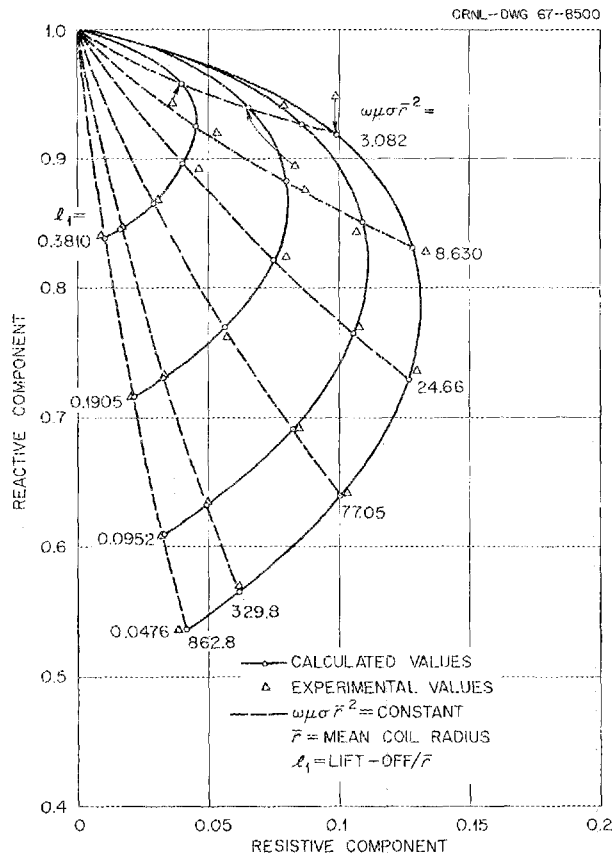


Fig. 23.6. Variation of Experimental and Calculated Values of Normalized Impedance with Frequency and Lift-Off.

Temperature-Compensated Probes

We are attempting to reduce the effect of temperature variations on eddy-current coils used with bridge-type instruments. One of the major contributions to thermal drift (change of response with temperature) of a coil is the change of direct-current resistance with temperature. We tested over a range of temperatures coils wound from copper wire, manganin wire, and a nickel-base alloy wire containing 20% Cr, 3% Al, and smaller amounts of copper or iron. Copper has a resistivity of $1.73 \mu\text{ohm-cm}$ with a temperature coefficient of about $0.39\%/^{\circ}\text{C}$, manganin has a resistivity of $48 \mu\text{ohm-cm}$ with a coefficient that varies from $+0.001$ to $-0.001\%/^{\circ}\text{C}$ between 20 and 35°C , and the nickel-base alloy has a resistivity of $113 \mu\text{ohm-cm}$ with a coefficient that varies from $+0.002$ to $-0.002\%/^{\circ}\text{C}$ between -55 and 100°C . Although there was a net gain in temperature stability by use of the higher resistivity wire, the overall test sensitivity was reduced. Coils wound from the manganin wire exhibited the smallest

temperature coefficient, but the nickel-base alloy was useful over a larger temperature range.

ULTRASONIC TEST METHODS

K. V. Cook H. L. Whaley

Fabrication of Reference Notches

We are continuing to work on the problems encountered in inspecting tubing by ultrasonic methods. A major problem is the establishment of realistic ultrasonic notch standards for calibration. Since electrical discharge machining (EDM) appears to be a reliable method for making both inner- and outer-surface notches, we are continuing our notch fabrication studies and can now machine longitudinal and transverse notches reproducibly in tubing with bores as small as 0.050 and 0.180 in., respectively. However, difficulties have been encountered in tungsten- and molybdenum-base alloys because machining these alloys apparently introduces microcracking in the bottom of the notches. If the cracking becomes excessive, the true notch depth cannot be determined. This condition was noted particularly in unalloyed tungsten, where cracks propagated in all directions from the machined notch. Further studies are in progress to determine the cause of this problem.

We are continuing to determine reference curves for both longitudinal and transverse notches as materials are available. The calibration curves for short transverse notches ($1/32$ and $1/16$ in. long) appear to be almost identical to those for longitudinal notches. This observation is based on data for austenitic stainless steel, Hastelloy C, Zircaloy, and W-26% Re.

We developed a technique for preparing silicone rubber replicas of the complete inner surfaces of tube standards by rotating the tube in a small jeweler's lathe while the rubber hardens. When properly executed, this procedure gives a hollow replica that collapses under application of a vacuum and is easily removed from the inner surface of the tube. The amount of rubber used must be carefully controlled, particularly for small-diameter tubing, to avoid formation of a solid plug, the removal of which usually results in destruction of the replica. This method of replicating is particularly useful for rapid, accurate measurement of transverse notch standards. A side benefit is the ability to examine the entire inner surface of the tube. This work on fabrication of reference notches has been partially funded by the High-Temperature Materials program.

Optical Visualization of Ultrasound

We continued our studies with the schlieren system for direct visual imaging of continuous ultrasonic beams and ultrasonic pulses.⁶ The basis of the technique is that ultrasound being propagated through a transparent liquid or solid will diffract portions of a collimated beam of light passing simultaneously through the material. This light can be gathered and displayed to yield a representation of the ultrasound. By directly observing the propagation of the ultrasound under simulated test conditions, we can learn much to aid in the design of new test setups.

In our first system we used 2-in.-diam achromatic lenses to produce the collimated light field from a variety of pulsed and continuous light sources and viewed the image on a ground glass screen. With this system ultrasound has been observed in water, Plexiglas, and polystyrene. Among the many phenomena observed were multiple reflections from inside metal plates and transmission into the bore of thin-walled tubing. This system was quite useful but too restricted because of its relatively small (2-in.-diam) viewing area and the loss of sensitivity from viewing the image on the ground glass screen. To correct these deficiencies, a system using 6-in.-diam parabolic mirrors was designed and fabricated, and the optics was changed to allow

⁶H. L. Whaley, K. V. Cook, R. W. McClung, and L. S. Snyders, "Optical Methods for Viewing Ultrasonic Propagation in Transparent Media," to be published in the proceedings of the Fifth International Conference on Nondestructive Testing, Montreal, Canada, May 21--26, 1967.

detection and display of the image in a closed-circuit television system. The system is much more sensitive with mirrors than it was with lenses. Figure 23.7 is a diagram of the revised equipment.

Frequency Analysis

In many ultrasonic test situations the effect of the multiple frequencies in the transmitted and reflected pulses is not clearly evident. However, it is generally recognized that frequency plays an important part in many tests, most of which are based on amplitude. For example, differences in the characteristic frequency spectra of transducers may help explain why one transducer will perform adequately in a given test while another supposedly similar transducer will not. A better understanding of the role of frequency in a given test situation should improve reproducibility.

An ultrasonic frequency analysis system was developed to study these frequency effects. Reflected pulses of ultrasonic energy can be selected with gating networks, amplified, and analyzed for amplitude as a function of the frequencies included in the pulse. System components were chosen to allow the use of ultrasonic instruments commonly employed in nondestructive testing. Figure 23.8 is a block diagram of the frequency analysis equipment. The system has been carefully studied both to determine factors that might bias the output and to increase the signal-to-noise ratio for low-level signals. The x-y recorder was incorporated so that information can be conveniently catalogued as well as presented on a cathode ray tube during operation.

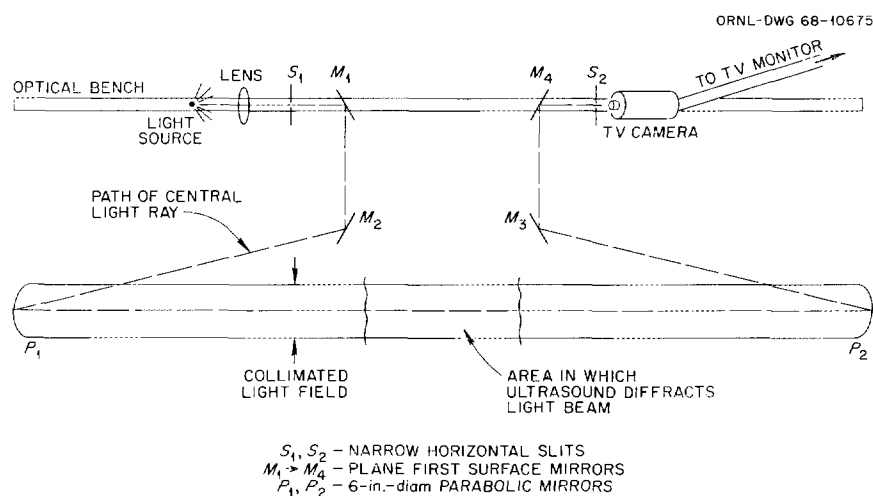


Fig. 23.7. Schematic Drawing of Schlieren System Using Parabolic Mirrors for Optical Visualization of Ultrasound.

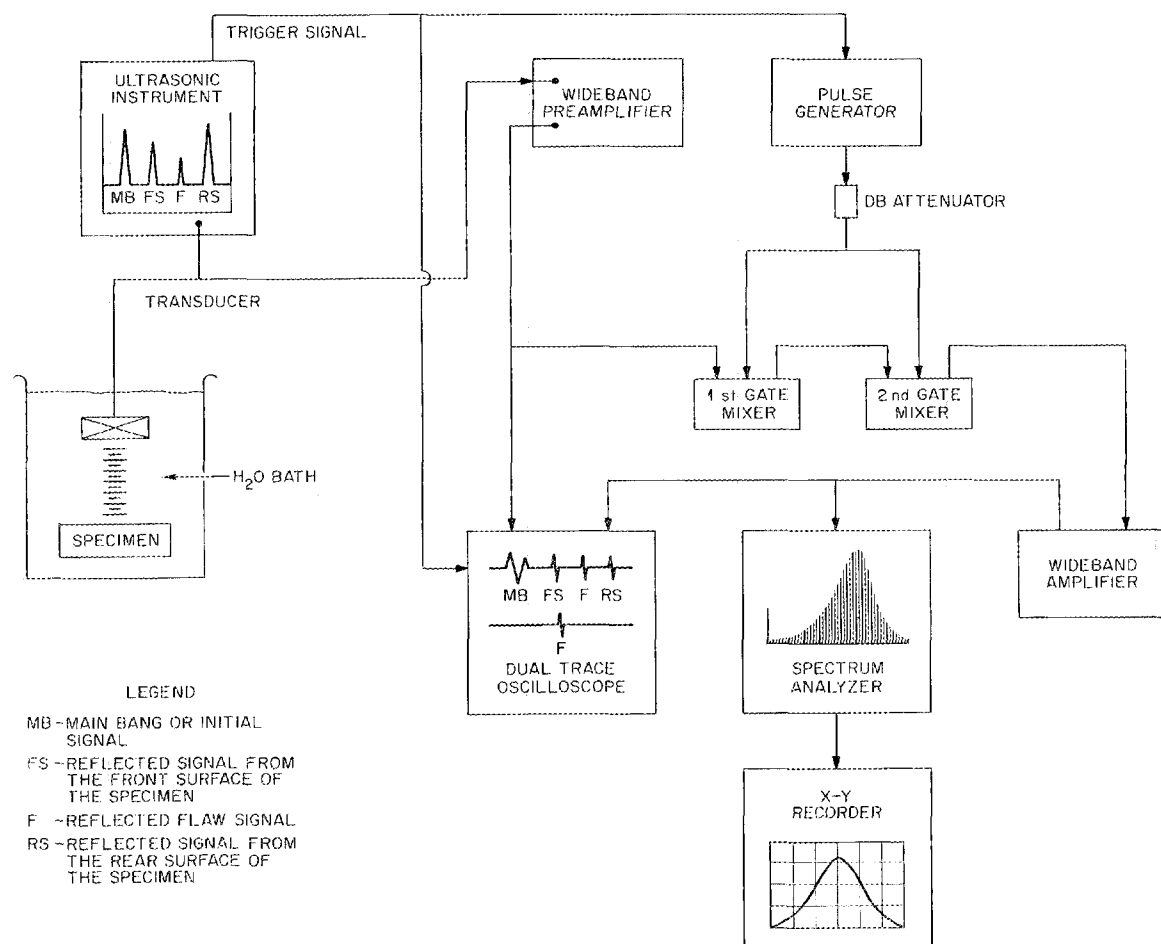


Fig. 23.8. Ultrasonic Frequency Analysis System.

As an example of early application of the system, characteristic spectra were examined from a variety of transducers of the types normally used in ultrasonic testing. We found that some transducers are remarkably broadbanded when excited by a short rise-time voltage spike and may not have peak response near the nominal (supplier listed) frequency. This information can be used in a number of ways. For example, the broad distribution of energy across the frequency spectrum may partially explain the occasional anomalous behavior of transducers as instrument receiver frequency is changed. Calibration curves have been prepared to enable quantitative determination of the amplitude of each portion of a displayed frequency spectrum. With these curves meaningful comparisons can be made between spectra obtained at different system sensitivities. Preliminary studies were made on the change in

the frequency spectrum of reflections from different interfaces.

PENETRATING RADIATION METHODS

B. E. Foster S. D. Snyder

Holography

We are studying the technique of making high-quality reflection holograms using a 2-rw helium-neon gas laser. The purpose is to familiarize ourselves with the associated problems in holography as well as the appropriate technical requirements for good holograms. Upon completion of these studies, we plan to develop techniques to use holography for examination of both surface and subsurface discontinuities in metals and

ceramics. These techniques will not necessarily involve the use of laser light.

The work surface for making holograms consists of a thick aluminum block that is shock mounted on four sections of large-diameter vacuum hose. This mounting provides an area that is relatively free of building vibrations.

Difficulty was encountered in maintaining efficient ratios of intensities between the reference and object beams of laser light. This impeded qualitative comparison between holograms made with different design angles or different subjects. Further, we could not directly observe the laser beam because of the possible eye hazard. We resolved this problem of intensity measurement by fabricating a light meter with a photosensitive field-effect transistor as a detector, an associated power supply, and a microammeter. We are also investigating both the depth-of-field limitations with the existing equipment and comparing single- and multiple-beam systems that use diverging light beams.

Quantitative Attenuation Measurement

For several years we have successfully used an x-ray attenuation technique for measuring the variations in composition and density or thickness of specimens. The method consisted of passing an x-ray beam through the specimen, monitoring the attenuated radiation beam with a thallium-activated sodium iodide crystal with associated electronics, and displaying the resultant signal on a strip-chart recorder.

Many determinations require the averaging of lengthy scans and relating this strip chart average to the property of interest with a previously determined calibration curve. With many scans per specimen, visual chart averaging can be quite laborious and slow. Therefore, we developed and installed circuitry to obtain the chart average electronically and give a digital print-out at the conclusion of each scan.

24. Sintered Aluminum Products Development

W. R. Martin

Aluminum alloys dispersion strengthened by aluminum oxide are commonly referred to as Sintered Aluminum Products (SAP) and are powder-metallogically produced. These alloys are attractive for many applications because of good strength, low density, and good compatibility with many of the environments found in nuclear systems. However, SAP lacks sufficient elevated-temperature ductility for most engineering applications and is fraught with fabrication problems that affect the uniformity of properties from billet to billet, anisotropy of properties in tubular products, and competitive economics.

Since the demise of an active HWO CR program, our close-out effort has been to conclude the investigations on primary billet fabrication and effect of secondary working. We have continued our search for dispersion-strengthened aluminum alloys (DSA) with suitable elevated temperature ductility and the causes of the low ductility in SAP type materials.

PRIMARY BILLET PROCESS DEVELOPMENT

We completed the development of a fabrication process for SAP billets.¹ Upon subsequent extrusion this material has uniform properties with strength greater than commercial SAP with equivalent oxide concentration. The general processing steps employed for the production of SAP are ball-milling of atomized powder, cleaning, vacuum hot pressing, vacuum heat treatment, and extrusion and secondary working.

During the previous year our efforts have been concentrated on selection of the billet consolidation process, study of the effects of impurities, and demonstration of the entire process on a pilot plant scale. Concurrently the feasibility studies on nondestructive test methods were completed.

¹G. L. Copeland, M. M. Martin, D. G. Harman, and W. R. Martin, *Effect of Powder and Process Variables on the Properties of Sintered Aluminum Products*, ORNL-TM-2215 (May 1968); presented at International Conference on Powder Technology jointly sponsored by ASTM and IITRI, Chicago, Illinois, May 20-23, 1968.

Selection of a Process for the Consolidation of Ball-Milled Aluminum-Aluminum Oxide Flake

G. L. Copeland M. M. Martin

Two processes designated B and D were selected for evaluation on the pilot plant scale. These processes differ only in the sequence of the vacuum heat treatment used to dehydrate the oxide. In process B we vacuum hot press as-milled powder and then vacuum anneal the billet immediately before extrusion. In process D the powder is vacuum annealed before vacuum hot pressing. Both processes produce equally strong rods, but process B extrusions exhibit better uniformity of strength and lower hydrogen contents. Process B is more easily adapted to production in that a solid billet rather than a low-density loose powder is vacuum annealed and is thus the more desirable technique for consolidation of SAP powder for subsequent extrusion.

Effect of Impurities Introduced During Billet Fabrication on the Properties of Extruded Rod

G. L. Copeland M. M. Martin

During production, SAP becomes contaminated with three elements that could influence the uniformity and thermal stability of the material. Iron in the form of small particles is included during ball-milling from mill and ball wear. Carbon contamination results from the organic materials used as surfactant and vehicle during ball-milling. Hydrogen is produced by the decomposition of any alumina hydrates or adsorbed water remaining after the billet anneal.

The iron particles included during ball-milling react with aluminum at high temperatures. Electron microprobe analysis indicated qualitatively that the reaction product was composed of iron and aluminum in the proportions of FeAl₃. We processed five rods differing in tramp iron content up to 3.5 wt % to determine if this reaction had any effect on the stability of mechanical properties. The tensile strengths at 450°C of

the as-extruded rods were compared to the strength after annealing 40 hr in vacuum at 600°C. The changes in strength upon annealing are small and random with respect to iron content. The change in uniform elongation is a consistent slight decrease, which does not depend on iron content. Thus, we conclude that iron as inclusions up to 3.5 wt % has no significant effect on the magnitude or thermal stability of tensile properties of SAP rods.

Much of the carbon in SAP is in the form of small inclusions, which we believe are Al_4C_3 , in agreement with electron microprobe analysis. Since aluminum carbide decomposes readily in contact with water to produce hydrocarbon gas, the effect of the carbide inclusions in SAP on thermal stability is of concern where moisture is present. We produced five rods with differing carbon contents up to 2 wt % by blending finely powdered Al_4C_3 with portions of a batch of SAP powder and processing to extruded rods in the normal manner. Sections of the rods were annealed at 600°C for 40 hr in vacuum and in air with an 11°C dew point. Tensile tests performed at 450°C on the extruded rod and after the stability tests show that the strength and uniform elongation changes observed after annealing are not significant with respect to normal variations and are random with respect to carbon content. We conclude that carbon contents up to 2 wt % in the form of Al_4C_3 inclusions are not detrimental to the magnitude or thermal stability of mechanical properties of SAP rods.

High concentrations of hydrogen in SAP have been shown to cause structural instabilities at high temperature.² To examine the effect of hydrogen on thermal stability, we compared the as-extruded strength of several rods containing up to 25 ppm H to the strength

after annealing for 40 hr at 600°C in vacuum and in air. The vacuum and air heat treatments tended to lower the tensile strength without evidence of blistering with one exception. Blistering was observed in the air anneal of an extrusion that contained 5.3 ppm H and was accompanied by a significant decrease in strength. The uniform elongation was not significantly affected by the heat treatment or the hydrogen level. We conclude on the basis of strength reductions that the hydrogen content in SAP should be kept less than 5 ppm to ensure thermal stability of tensile properties.

Reproducibility of Product Fabricated from Billet Process B

G. L. Copeland M. M. Martin

To determine the overall reproducibility of billet fabrication process B, we examined extrusions from nine billets (4 in. in diameter X 4 to 6 in. long) produced under the same conditions. The mechanical properties and chemical composition of these rods and SAP 895 are given in Table 24.1. The chemical composition of the ball-milled powder is given for comparison. The strength within any given billet was uniform. The maximum range observed was less than 2% of the mean.

The expected variations (3σ) among billets is $\pm 10\%$ of the mean. This spread in process reproducibility appears to be due to differences in milling, since the average strength correlates well with the oxide content. We

²N. Hansen and E. Adolph, *Effect of Heat Treatment on the Structural Stability of Sintered Aluminum Products*, RISO-25 (May 1961).

Table 24.1. Comparison of Composition and Strength of ORNL and Commercial SAP

Product	Impurity Content (wt %)			Oxide Content (wt %)	Tensile Properties at 450°C ^a	
	Fe	C	H		Ultimate Tensile Strength (psi)	Uniform Elongation (%)
			$\times 10^{-4}$		$\times 1000$	
ORNL milled SAP powder ^b	0.2-0.4	1.0-1.5		8.70 ± 0.86^c		
ORNL SAP ^d	0.2-0.4	0.15-0.30	1.7-3.7	9.32 ± 0.58^c	13.83 ± 0.47^c	0.67 ± 0.09^c
SAP 895 ^e	0.6	0.21	1-3	11.4^f	12.87^f	0.69^f

^aStrain rate 0.002 min⁻¹.

^bTen identical 27-lb batches.

^cStandard deviation.

^dNine billets produced from nine of the above ball-mill batches, three specimens per rod, two rods per billet. 156 to 1 total reduction.

^eCommercial 2-in.-diam SAP 895 extruded 30 to 1 at ORNL for a total reduction ratio of 510.

^fThere were insufficient samples from different batches for a determination of standard deviation.

believe that further improvement in our billet-to-billet strength variations depends upon better control of the as-milled oxide content. Although comparable data have not been found for SAP 895, the allowed range of 9 to 12% Al_2O_3 would indicate strength variations similar to those observed for ORNL material. The minimum strength value observed in our reproducibility study was 12,940 psi. The microstructures of our material and SAP 895 are compared by transmission electron microscopy in Fig. 24.1. In comparing the structures, one should be aware that SAP 895 has received a total reduction in area of approximately 510 to 1 compared to 156 to 1 for the ORNL material. This additional hot working should have resulted in slightly

improved oxide distribution and corresponding increase in strength. The excellent uniformity and closer spacing of the oxide in our material accounts for its higher strength at a given oxide concentration. We believe that the better oxide distribution in our material results from the elimination of intentional agglomeration of individual particles during ball-milling. Commercial SAP milling practice welded the particles together,³ whereas we add sufficient surfactant and milling vehicle to maintain individual flake particles.

³D. Gualandi and P. Jehenson, "Powder Metallurgy of Al- Al_2O_3 Composites (SAP) for Nuclear Applications," pp. 36-59 in *Modern Developments in Powder Metallurgy*, Vol. 3, Plenum Press, New York, 1966.

PHOTO 93043

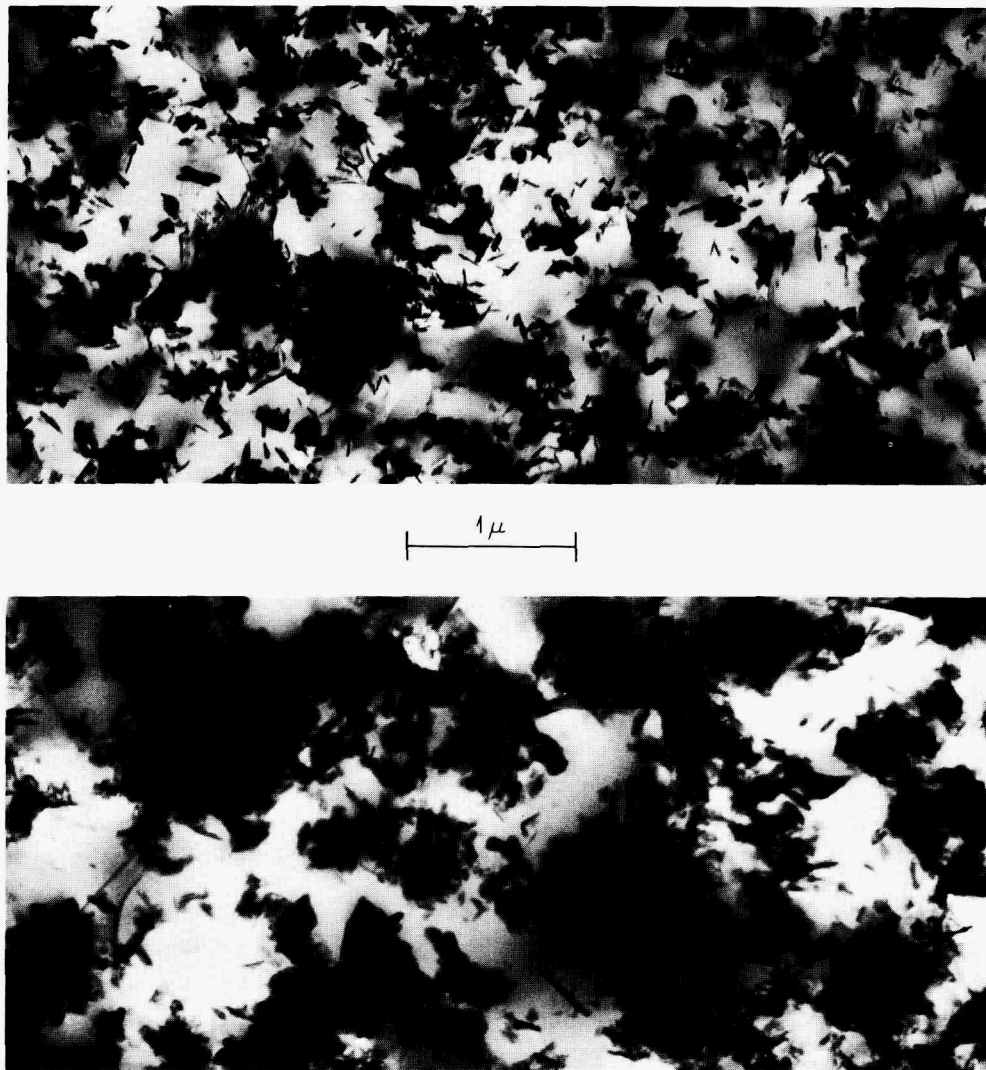


Fig. 24.1. Comparison of Transmission Electron Microstructure of ORNL 10% Al_2O_3 Material (Top) with SAP 895 (Bottom).

Nondestructive Testing of Intermediate SAP Fabrication Products

H. L. Whaley

We completed the feasibility studies on nondestructive tests for the SAP materials with which we have been working. The results of this investigation have been reported,⁴ and the abstract follows.

Several techniques were developed for the nondestructive evaluation of sintered aluminum powder materials. An entirely new air-settling technique was developed for the measurement of flake thickness of powders. Eddy-current techniques and equipment were adapted for the determination of oxide content in both powders and extrusions. X-ray attenuation techniques were applied for the measurement of homogeneity of extruded billets. Equipment and results are described in detail for each test method.

The air-settling technique by which flake thickness was measured provided the surprising result that the thickness range of the flake particles in a given batch of powder is extremely small relative to the thickness variations within a given particle. In fact, particles were commonly found whose thickness variations were as great as the range for an entire powder sample. Various types of powders had about the same mean thicknesses within experimental error. Typical results for a powder sample are a thickness range of about 0.5μ and a mean thickness near 1.0μ .

To reduce the variability of SAP wafers compacted for determination of oxide content in powders, a through-transmission eddy-current test was developed to replace the reflection technique initially used. This technique tended to integrate the effects of wafer variability and gave significantly more consistent results. This approach is capable of determining oxide content of sintered aluminum powders to an accuracy of $\pm 0.5\%$ with appropriate calibration. Similar accuracy can be obtained with a reflection technique on extruded SAP billets.

We obtained calibration curves that demonstrate that existing techniques and equipment are applicable to the determination of the homogeneity of extruded SAP billets by x-ray attenuation measurements. These curves show that a 1% change in density or thickness is detectable in billets up to at least 4.0 in. in diameter (and probably larger). Billets up to 56 in. long can be

scanned in a single pass, and billets much longer may be inspected by repositioning.

MECHANICAL PROPERTY STUDIES

Anisotropy in Mechanical Properties of Extruded Commercial SAP Materials⁵

T. M. Nilsson

The anisotropy in mechanical properties of an extruded bar of commercial SAP 895 (Al-10.3 wt % Al_2O_3) was determined by tensile testing at room temperature and 450°C of specimens cut at various angles to the extrusion direction. Properties were strongly dependent upon orientation. Strength was relatively low, not only in the transverse direction but also at orientations between the longitudinal and transverse directions. In fact, the material was weakest in an orientation about 25° from the extrusion direction. At 450°C uniform elongation appears to be lowest in the longitudinal direction. Cylindrical specimens cut at 60° to the extrusion direction seem to exhibit the best combination of high-temperature strength and ductility. The fracture, at both 450°C and room temperature, of specimens cut at 30° , 45° , and 90° to the extrusion direction is especially brittle and has a characteristic striated appearance with the striation parallel to the extrusion direction.

The factor most likely to be responsible for the anisotropy is the nonuniform oxide particle distribution produced during extrusion.

Influence of Working in Various Directions on the Microstructure and High-Temperature Mechanical Properties of an Extruded SAP Alloy⁶

T. M. Nilsson

Bars of commercial SAP 895 – sintered aluminum product containing about 10.5 wt % Al_2O_3 – were further worked in directions transverse and parallel to the initial extrusion direction. The original extrusion ratio was about 20. The extruded structure was very sensitive to transverse working, and only transverse extrusion and swaging at high temperature could be accomplished without difficulties. High-temperature

⁴H. L. Whaley, *Development of Nondestructive Tests for Sintered Aluminum Powder Materials*, ORNL topical report in preparation.

⁵Summary of paper accepted for publication by *Journal of Nuclear Materials*.

⁶Summary of a paper to be submitted for publication.

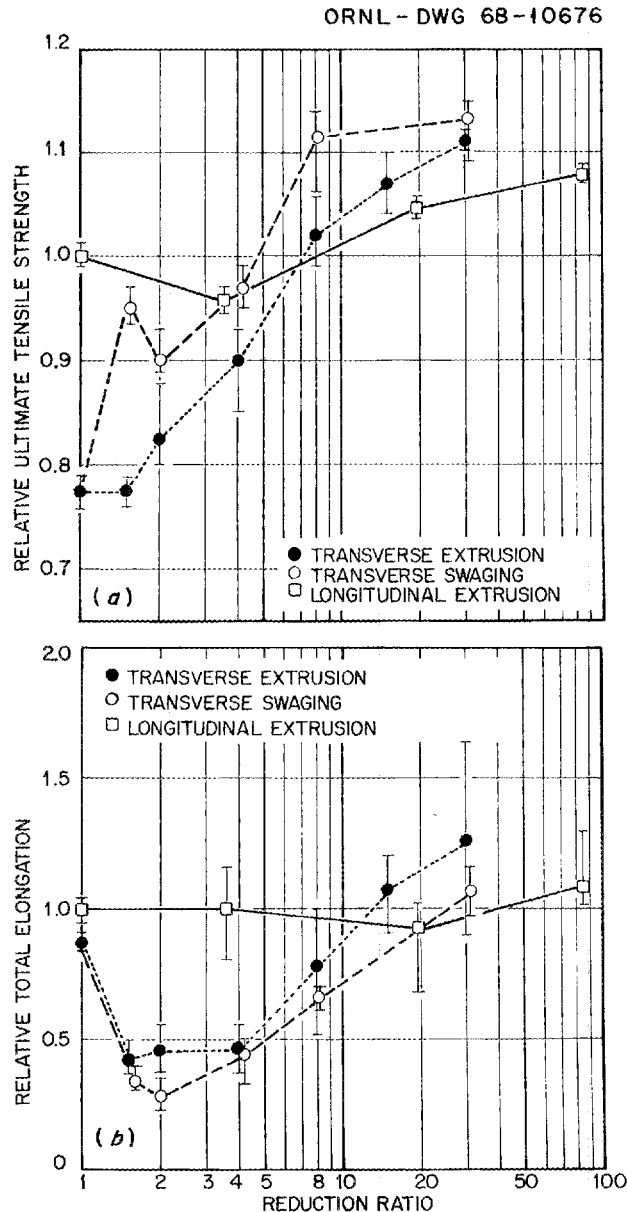


Fig. 24.2. Relative Tensile Strength (a) and Ductility (b) at 450°C of SAP 895 as a Function of Reduction and Direction During Secondary Working. Original longitudinal values correspond to 1.0.

mechanical properties were determined by tensile testing at 450°C in the new working direction. After small transverse reductions mechanical properties were low but they were restored to the level of the original extruded material after a transverse reduction of about 8:1. At a transverse reduction of 30:1, both strength and ductility exceeded the initial longitudinal values significantly; especially noteworthy was the more than

doubled uniform elongation. After further longitudinal extrusion, mechanical properties in general increased, but variations were small. The relative variations in high-temperature strength and ductility are shown in Fig. 24.2 as functions of reduction and direction during secondary working.

The dispersion of the oxide phase improved during secondary working, partly because individual particles broke and partly because particle clusters diminished in size. However, after transverse working, mechanical properties did not increase accordingly before the structure was sufficiently realigned into the new working direction. The improvement in uniform elongation after transverse swaging appeared to be connected with the complicated alignment of the resulting structure. Also, material with this structure had a lower yield point but a higher ultimate tensile strength than the transversely extruded material. The relations between alignment and mechanical properties should be examined closer in future work since this relationship may be extremely important for the improvement of the tube-burst properties of SAP and other dispersion-strengthened aluminum alloys.

Fracture Characteristics of SAP

D. G. Harman T. A. Nolan⁷

We characterized the fracture of SAP alloys over the temperature range of -196 to 450°C using the scanning electron microscope. This instrument has an extreme depth of focus and a wide range of magnifications, which allow direct viewing of the entire fracture surface as well as any local area of interest. We have studied fracture initiation and propagation for experimental ORNL SAP as well as commercial products, paying special attention to the effects of fabrication, impurity defects, and dispersoid distribution.

Figure 24.3 shows the effect of test temperature on the fracture appearance of SAP as viewed in the scanning electron microscope. The fractures differ only in the size of the features; the same ductile fracture process takes place at both high and low temperature. This is in agreement with our earlier conclusions based on conventional replication fractography.⁸

Figure 24.4 shows the effect of various defects on the fracture. Nonmetallic inclusions initiate shear "cones" during the early stages of room-temperature tests [see

⁷Physics Department, Technical Division, ORGDP.

⁸D. G. Harman and K. Farrell, *Metals and Ceramics Div. Ann. Progr. Rept. June 30, 1966*, ORNL-3970, pp. 131-35.

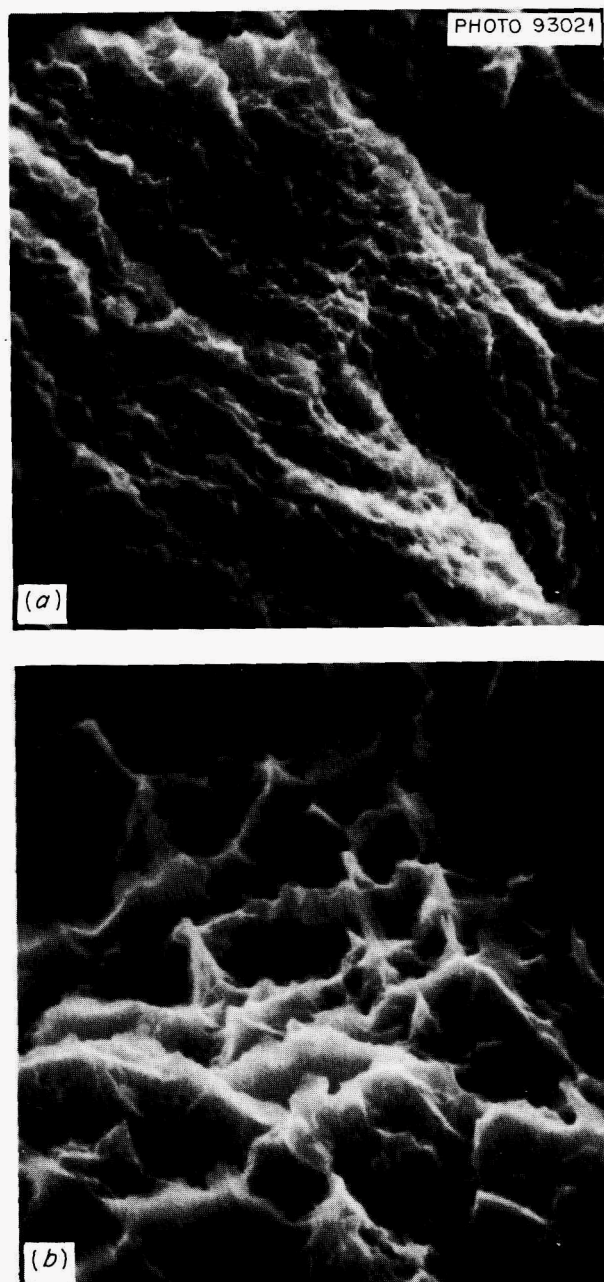


Fig. 24.3. Scanning Electron Fractographs Showing Effect of Test Temperature on the Fracture Characteristics of SAP. 10,000X. Reduced 8%. (a) XAP-001 fractured at -200°C . (b) XAP-001 fractured at 450°C .

Fig. 24.4(a) and (b)]. Because of the extensive ductility, however, these local fractures do not seriously weaken the material. Figure 24.4(c) shows that the presence of a large inclusion does not affect the high-temperature fracture. This is in agreement with the billet process development study, reported earlier in

this chapter, which indicated iron and aluminum carbide had little effect on the properties of the extruded product. Figure 24.4(d) shows the fracture surface of a material that had been improperly consolidated during the high-temperature compaction and extrusion. This explains the low strength displayed by this material.

Mechanical Properties of Commercial SAP

D. G. Harman

Design considerations for use of SAP as extruded tubing are generally based on extensive longitudinal rod data and a knowledge of the transverse-to-longitudinal ratios. Because the mechanical properties depend strongly upon test conditions, which are often omitted in the literature, we tested several commercial alloys, SAP 895, SAP 930, XAP-001, and XAP-005, to provide baseline data for our development program. Tensile properties were obtained from sections of commercially extruded 2-in.-diam \times 18-ft-long solid rods. The tensile specimens were machined parallel to the extrusion axis from positions near the outer perimeter as well as from regions nearer the center. Transverse specimens were machined at 90° to the extrusion direction and intersecting the center line of the rod. Tensile data were obtained at room temperature at a strain rate of 0.02 min^{-1} and at 450°C at strain rates of 0.02, 0.002, and 0.0002 min^{-1} .

The strength and ductility of the longitudinal specimens from the center and near-surface locations were nearly the same for all testing conditions and for all materials.

All material showed much lower values for the transverse properties than for the longitudinal. The strain-rate dependence of the strength at 450°C was about the same for both testing directions; however, the magnitude of the difference in properties depended upon the material and the testing. The transverse-to-longitudinal strength ratio decreased with decreasing strain rate because of the lower strength levels. For SAP 895, for example, this ratio decreased from 0.89 to 0.65.

The high-temperature total elongation measured in the transverse direction differed from that measured longitudinally for all materials. Equally low transverse elongations were obtained at all strain rates, whereas the longitudinal elongation decreased with decreasing strain rate. In this case, the transverse-to-longitudinal ductility ratio increased with decreasing strain rate. For example, for SAP 895 the ratio increased from 0.30 to 0.91.

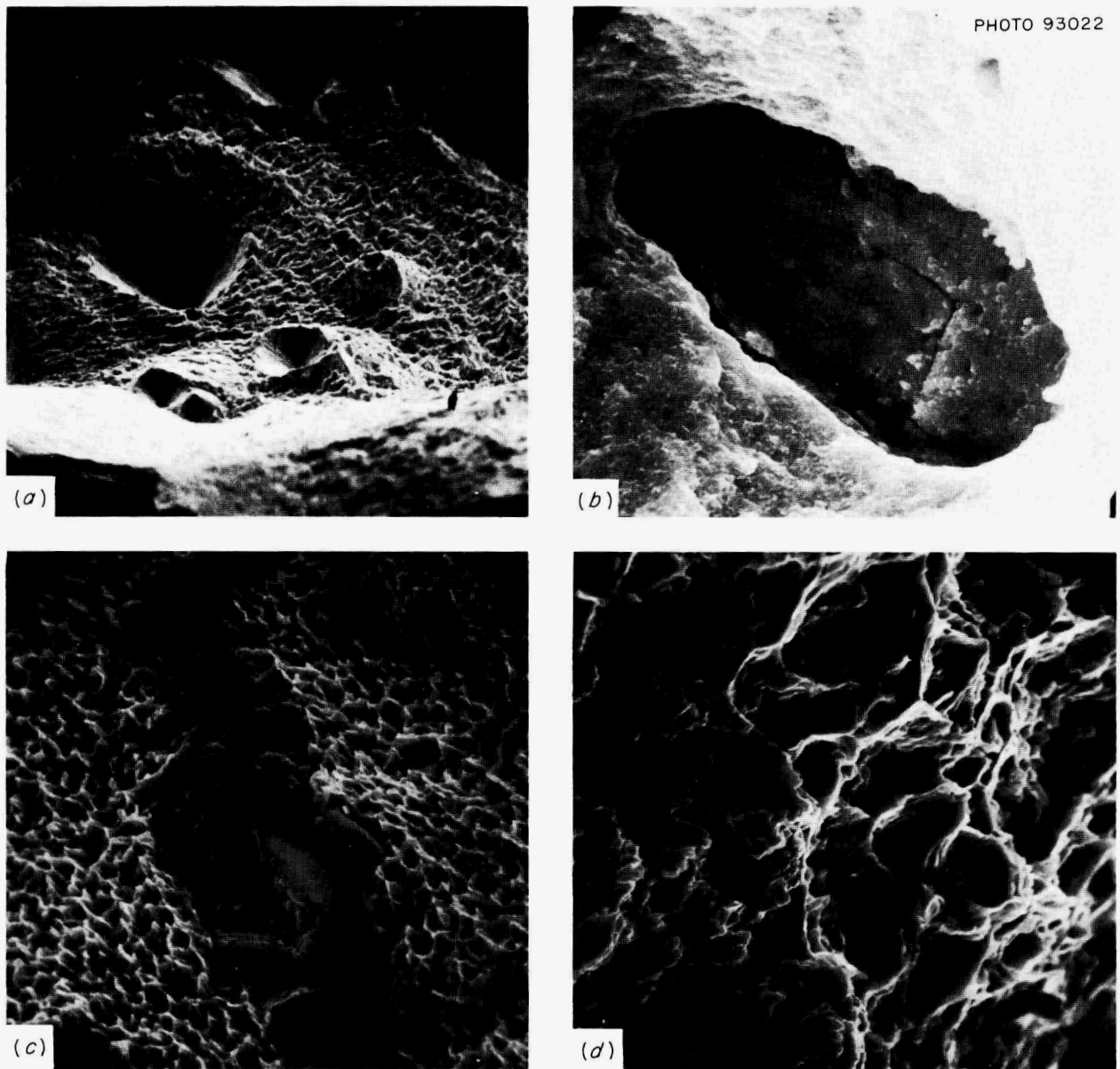


Fig. 24.4. Scanning Electron Fractographs Showing Effects of Material Defects on the Fracture Characteristics of SAP. Reduced 10%. (a) Room-temperature fracture showing "shear cone" fracture initiation sites. The cone fractures were arrested by material deformation before the final fracture. 100X. (b) Large brittle particle located at shear cone apex in (a). 3000X. (c) 450°C fracture with a large inclusion, which had no effect on the surrounding fracture features. 1000X. (d) 450°C fracture showing deleterious effect of inadequate powder consolidation during fabrication. 1000X.

Nuclear reactor applications of SAP require fairly long extruded shapes. We tested 18-ft-long extruded rods of XAP-005, SAP 895, and SAP 930 at three locations along them to determine uniformity of mechanical properties. At 450°C the mechanical properties of the three materials showed a significant

dependence on specimen location. Figure 24.5 shows the experimental results at 0.0002 min^{-1} strain rate for the longitudinal and transverse specimens. All three materials exhibited longitudinal-strength variations of at least 10% along the extrusion. Variations in transverse strength were as high as 35%.

ORNL-DWG 68-10677

○ ULTIMATE TENSILE STRENGTH
 △ 0.2% YIELD STRENGTH

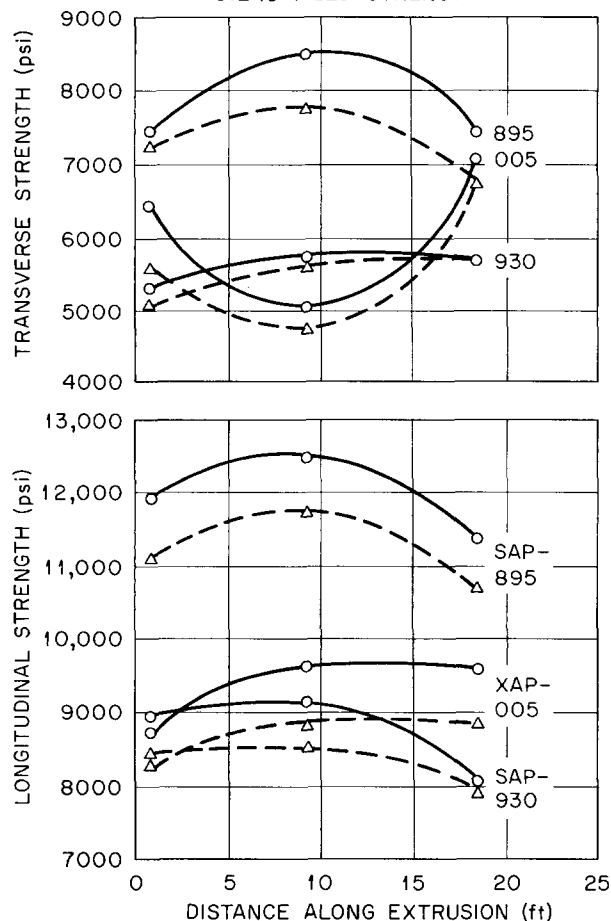


Fig. 24.5. Longitudinal and Transverse Strengths of Three 18-ft Extrusions (SAP 895, SAP 930, and XAP-005) Tested at 450°C and 0.0002 min⁻¹.

DEVELOPMENT OF NEW DISPERSION-STRENGTHENED ALUMINUM ALLOYS

G. L. Copeland

The objective of this phase of the program is to develop dispersion-strengthened aluminum alloys with suitable high-temperature ductility. Our approach is to produce alloys that should minimize the effect of three mechanisms that may be responsible for the low ductility of SAP at elevated temperature. (1) Lack of work hardening in the alloy allows deformation to occur locally with no uniform elongation once necking begins. (2) Gas collection at the incoherent oxide-matrix interface results in holes, which grow by vacancy condensation until failure occurs. (3) Strain results in the soft matrix pulling away from the hard oxide particles. The resulting voids grow by vacancy diffusion until failure occurs.

The first two mechanisms were suggested by the deformation and fracture characteristics observed during the process development of unalloyed SAP. The third mechanism has been suggested by Nilsson⁹ in his thesis on the ductility of SAP.

Thus far, we have produced alloys containing the solid-solution strengthener magnesium and alloys containing the compound-forming elements Mo, Fe, Zr, Cr, Ti, and V. Alloyed powders were made by atomizing liquid alloys so that a fine particle size was obtained with rapid quenching. The atomization of prealloyed powders for this program was investigated by the Illinois Institute of Technology Re-

⁹T. M. Nilsson, *Investigation of the Ductility of Dispersion Strengthened Aluminum-Aluminum Oxide Alloys*, Ph.D. Thesis, The Technical University of Denmark, November 1965.

Table 24.2. Dispersion-Strengthened Aluminum Alloys Being Studied

Alloy Type	Chemical Composition ^a (wt %)							Milling Times (hr)
	Mg	Mo	Fe	Zr	Cr	Ti	V	
Standard	0	0	0	0	0	0	0	0, 8, 10, 12
M-2	2	0	0	0	0	0	0	0, 8, 10, 12
M-4	4	0	0	0	0	0	0	0, 8, 10, 12
M-5	5	0	0	0	0	0	0	8, 10, 12
M-6	6	0	0	0	0	0	0	0, 8, 10, 12
M-10	10	0	0	0	0	0	0	8, 10
A-602	0	6	0	2	0.2	0.2	0.2	0, 8, 12
A-204	0	2	0	4	0.2	0.2	0.2	0, 8, 10, 12
A-222	0	2	2	2	0.2	0.2	0.2	0, 8, 10, 12
A-620	0	6	2	0	0.2	0.2	0.2	0
A-440	0	4	4	0	0.2	0.2	0.2	0, 8, 10

^aNominal composition, remainder aluminum.

search Institute under subcontract. Atomizing the aluminum-magnesium alloys and the Al-4% Mo-4% Fe composition presented no particular problems in melt sizes up to 30 lb. The melts containing zirconium tended to be sluggish, possibly because chilling in the tundish produced precipitation of the intermetallic compound or because oxides were present in the

melting crucible. Atomizing the powders into water was found to be best because of the difficulty of collection of fine powders in a dry chamber. The alloyed powders were then ball-milled, consolidated, and extruded according to our process for unalloyed SAP. The alloys listed in Table 24.2 have been produced and are being studied.

25. Sol-Gel Fast Reactor Fuels

A. L. Lotts

To obtain the full economic potential of fast breeder reactors, it is necessary to recycle periodically the fuel from the reactor. This requires that the spent fuel be chemically processed, the fissile isotopes be reconstituted along with fertile isotopes, and the recovered fuel be incorporated into refabricated fuel elements. The sol-gel process is an ideal process to employ in reconstituting fuel from the chemical processing of spent fuel elements. Accordingly, our objective is to assess sol-gel-derived (U,Pu)O₂ fuel for use primarily in Liquid-Metal-Cooled Fast Breeder Reactors and in the Fast Flux Test Facility.

The primary task areas of this program are: (1) the preparation of (U,Pu)O₂ fuel by the sol-gel process, (2) the development of fabrication procedures for incorporating the mixed oxide fuel into a suitable fuel rod component, (3) out-of-reactor testing to characterize and obtain data on the sol-gel products, and (4) the irradiation testing of the fuel under conditions that will allow an extrapolation to fast reactor conditions. We are performing all but the first of these task areas; the Chemical Technology Division is responsible for the preparation of the fuel. A summary of our activity follows. In addition, we have placed a large effort on the design, construction, and installation of additional plutonium fabrication and characterization equipment beyond that reported here.

DEVELOPMENT OF FABRICATION PROCESSES

J. D. Sease

Fast reactors operating at high specific powers will require small-diameter fuel pins with a high fissile loading. Typically, an oxide-fueled liquid-metal-cooled fast reactor fuel pin will be about 1/4-in. in diameter with a 24-in. fueled length and contain (²³⁸U-20% ²³⁹Pu)O₂. An economical fabrication process that will yield a fuel capable of high burnup will be necessary. The targeted high burnup of 100,000 Mwd/MT with oxide fuels requires a fuel density 80 to 90% of theoretical to accommodate fission products. To satisfy these requirements, we are investigating various fabri-

cation processes for sol-gel-derived (U,Pu)O₂ fuels. During the year, we concentrated on developing pelletizing and Sphere-Pac fabrication processes and fueling irradiation capsules by these processes. We plan to develop extrusion as a means of fabricating sol-gel fuel.

Sphere-Pac Process Development

R. B. Fitts A. R. Olsen
J. Komatsu¹

The development of the Sphere-Pac process for fuel rod fabrication has been discussed previously.^{2,3} In this technique a coarse bed of microspheres is formed in a container, and smaller spheres are infiltrated to fill the interstices. Low-energy vibration (<7g, 60 cps) settles the bed to maximum density. Our previous work with two sizes of microspheres (500 and <44 μ in diameter) reproducibly yielded fuel rods with a volume loading of 85 ± 1%. Spread of 10% in sphere diameters about the nominal sizes has a negligible effect on loading density. We increased volume loadings to 88% by infiltrating small spheres into a denser coarse bed obtained by blending two sizes of large microspheres before loading. The diameter ratio of these spheres is approximately 4. With the development of this "blended bed" technique and the evolution of a graphical correlation that will predict the finished Sphere-Pac bed densities for any combination of sphere sizes and blending or infiltration steps, the laboratory scale development is complete. A report covering this work is in preparation.

¹Foreign visitor on leave from the Japanese Power Reactor and Nuclear Fuel Development Corporation, Japan.

²A. R. Olsen and R. B. Fitts, *Metals and Ceramics Div. Ann. Progr. Rept. June 30, 1967*, ORNL-4170, p. 220.

³F. G. Kitts, R. B. Fitts, and A. R. Olsen, "Sol-Gel Urania-Plutonia Microsphere Preparation and Fabrication into Fuel Rods," pp. 195-210 in *Intern. Symp. Plutonium Fuel Technol., Scottsdale, Ariz. 1967, Nucl. Met.*, Vol. 13, American Institute of Mining, Metallurgical, and Petroleum Engineers, New York, 1968.

Pellet Development

W. L. Moore R. A. Bradley
R. L. Hamner

In a preliminary investigation, Hamner and Robbins⁴ demonstrated that pellets with densities from 70 to 92% of theoretical could be produced from various forms of sol-gel-derived urania, with the density depending on the powder preparation, the pressure used in forming the pellet, and the sintering conditions.

We have investigated the pelletization of urania-plutonia, using two different types of powder derived from the sol-gel process. One type was prepared by crushing microspheres that had been dried at 170°C and sieving through a 325-mesh screen. The other was produced by tray-drying mixed urania-plutonia sols at 95°C under an argon purge and grinding the dried particles to -325 mesh in a fluid energy mill. Pellets with densities from 80 to 93% of theoretical were produced from crushed microsphere powder by pressing at 15,000 to 30,000 psi and sintering in Ar-4% H₂ at 1450°C. Pellets pressed from the tray-dried powder and sintered under similar conditions had densities from 70 to 90% of theoretical.

We investigated the effect of forming pressure and sintering temperature on the density of pellets pressed from tray-dried urania-plutonia. We found a quadratic relationship between green and sintered density and that the sintering temperature in the range 1350 to 1550°C has no effect. As reported by Adwick and Reilly⁵ for coprecipitated uranium-plutonium oxide, the oxidation state of the uranium appears to play a major role in the densification kinetics of sol-gel urania-plutonia.

We are continuing our efforts to establish a process that will reproducibly yield pellets of the required density.

CHARACTERIZATION OF (U,Pu)O₂ FUELS

J. D. Sease A. R. Olsen

The preirradiation characterization of a fuel material is absolutely necessary in understanding the fabrication process and in the interpretation of irradiation results. Characterization is divided into the examination of the fuel material as produced and the determination of basic properties of the material.

⁴Ceramics Technology Group, unpublished.

⁵A. G. Adwick and W. S. C. Reilly, "The Role of Oxygen/Metal Ratios During Sintering and Oxidation of Some Uranium-Plutonium Oxides," pp. 215-35 in *Science of Ceramics*, Vol. 3, Academic Press, London, 1967.

Analytical Chemistry

W. H. Pechin

The characterization of the mixed oxide fuel requires a number of chemical and physical measurements of known precision and accuracy. The major requirements are: uranium, plutonium, and oxygen contents, density, gas release on heating, and impurity content. The analytical procedures for these determinations are being pursued concurrently with the fabrication development.

The uranium and plutonium contents of the fuel are determined by coulometric titration. Present experience on duplicate determinations indicates a 95% confidence interval for (U-20% Pu)O₂ of 0.800 ± 0.007 U and 0.200 ± 0.002 Pu. Oxygen content is being determined by the "Nitrox" method. Multiple analyses by this method indicate a precision of ±0.006 for the oxygen-to-metal ratio.

The density of sintered pellets is determined from the pellet dimensions and weight. There has not been sufficient experience with centerless ground pellets to determine the precision of this measurement, but it is expected to be better than ±1%. Microsphere densities are determined from mercury porosimeter measurements. This method requires some care to ensure that the spaces between the microspheres are filled with mercury so that the proper sample volume is used in calculating the bulk density. Fine microspheres (approx 50 μ) require a pressure of 100 psi.

The present gas-release equipment can measure only to 1200°C; equipment is now being constructed to extend this capability to above 2000°C. The various metallic impurities are determined by spectroscopic analysis.

Thermal Conductivity

P. H. Spindler D. L. McElroy

With our radial heat flow apparatus,⁶ the thermal conductivity λ of small specimens of packed beds of ThO₂ microspheres was measured in N₂, Ar, and He as a function of gas pressure, temperature, and packing density. These variables produced significant changes in λ of the various powders, and this requires further study. Therefore, we constructed a second radial heat flow apparatus to allow measurements to 4 atm and 1400°K. Performance data from this system will establish the design of a similar system for installation

⁶J. P. Moore, R. K. Williams, R. S. Graves, and D. L. McElroy, *Metals and Ceramics Div. Ann. Progr. Rept. June 30, 1967*, ORNL-4170, p. 39.

in the Interim Plutonium Laboratory for physical property measurements on plutonium-bearing materials.

The determinate and indeterminate errors of a technique for measuring λ of small quantities of powders from 300 to 1300°K were analyzed.⁷ The results on a 58%-dense MgO powder in nitrogen gas as a function of temperature and pressure are presented. Comparison of these results with data obtained by previous investigators on a similar powder indicates that the present technique may have serious error sources.

IRRADIATION TESTING

A. R. Olsen

Last year⁸ we reported on the initial phase of a program to determine the irradiation performance of sol-gel-derived (U,Pu)O₂ fuels as a function of sol-gel process variables and fabrication techniques. The program has been expanded to include comparative tests of the Sphere-Pac, extrusion, and pellet forms in both thermal and fast flux environments. Thermal flux irradiations permit the use of instrumented capsules and the achievement of high burnup in relatively short periods of time. Such tests are designed to supplement the fast-flux irradiation tests in the EBR-II, where the fission-rate distribution and temperature profiles in the fuel are more typical of anticipated LMFBR operating conditions. The program also includes tests of fuel

performance under off-normal conditions such as power transients.

Uninstrumented Irradiation Tests

A. R. Olsen R. B. Fitts J. Komatsu¹

The six capsules that have been or are being irradiated to date in this series are described in Table 25.1. These capsules were designed⁸ for irradiation tests in the Engineering Test Reactor X-basket facilities. Each capsule contains four test fuel rods. The failure of some rods in the first two experiments, 43-99 and 43-100, because of inadvertent overpower operation (>50 kw/ft peak linear heat rating) was discussed previously.⁸ A detailed report on these tests is in preparation. Experiments 43-103 and 43-112 completed their scheduled irradiation with no failures and are being examined.

Experiment 43-103 was designed to establish the basic performance characteristics of oxide fuel fabricated by the Sphere-Pac process and to compare the performance with pelletized fuel. Examination of this capsule has just begun; the only conclusion that can be

⁷Modified abstract of Paper presented at the 7th Conference on Thermal Conductivity, NBS, Gaithersburg, Maryland, Nov. 13-16, 1967.

⁸A. R. Olsen and R. B. Fitts, *Metals and Ceramics Div. Ann. Progr. Rept. June 30, 1967*, ORNL-4170, pp. 125-27.

Table 25.1. Noninstrumented Irradiation Screening Tests of Sol-Gel-Derived Urania-Base Bulk Oxide Fuels

Experiment	Fuel		Number of Rods	Peak Target Burnup (% FIMA) ^a	Peak Linear Heat Rating (w/cm)	Test Objective	Status
	Form	Composition					
43-99	Sphere-Pac	(²³⁵ U-20% Pu)O ₂	2	5 ^b	650 ^b	Thermal reactor test of fast-reactor fuel	Report in preparation
43-100	Sphere-Pac	(²³⁵ U-20% Pu)O ₂	2	10 ^b	650 ^b	Same as 43-99	Report in preparation
43-103	Sphere-Pac	UO ₂ (20% ²³⁵ U)	3	4	540	Test Sphere-Pac fabrication with low-density microspheres	Being examined
	Pellet	UO ₂ (20% ²³⁵ U)	1				
43-112	Sphere-Pac	(²³⁸ U-15% Pu)O ₂	3	0.5	550	Compare mixed oxide performance with UO ₂	Being examined
		UO ₂ (20% ²³⁵ U)	1				
43-113	Sphere-Pac	(²³⁸ U-15% Pu)O ₂	3	10	550	Same as 43-112 with high burnup	In reactor (approx 4% FIMA)
		UO ₂ (20% ²³⁵ U)	1				
43-115	Sphere-Pac	(²³⁸ U-15% Pu)O ₂	3	5	600	Same as 43-112 with intermediate burnup and higher heat rating	In reactor (approx 2% FIMA)
		UO ₂ (20% ²³⁵ U)	1				

^aFissions per initial metal atom.

^bThese are preirradiation calculated values. Rods failed in reactor from overpowering at a peak burnup of 1.5% FIMA, with peak linear heat ratings in excess of 1500 w/cm.

Table 25.2. Comparison of Burnup Analysis with Predictions by ANISN Calculation

Fuel Rod	Fuel Burnup (% FIMA)		
	Isotopic Analysis	Radiochemical Analysis ^a	ANISN Predictions
43-112-1	0.46	0.50	0.49
43-112-2 ^b	0.61	0.68	0.71
43-112-3	0.67	0.68	0.69
43-112-4	0.57	0.55	0.54

^aAverage from ¹³⁷Cs, ¹⁴⁴Ce, and ⁸⁹Sr determinations.

^bInitial fuel was UO₂ enriched to 20% ²³⁵U; all others were (²³⁸U-15% Pu)O₂.

drawn is that there is no evidence of circumferential strain on the cladding at burnup levels of approximately 4% FIMA (40,000 Mwd/MT) for either the pellet or Sphere-Pac fuel rods.

Experiment 43-112 was removed from the reactor after one cycle to confirm our revised techniques, described later in this chapter, for calculating burnup rates for plutonium-enriched fuels. Table 25.2 compares the predicted burnup levels with the results of postirradiation analysis. The agreement is remarkably good. Examination of selected sections from these fuel rods is incomplete. The postirradiation gamma scans indicate that there was no significant axial movement of the fuel during irradiation. The transverse sections in Figs. 25.1 and 25.2 clearly show a radial redistribution of the fuel. The in-reactor restructuring of the fuel in the central high-temperature region from a low-density Sphere-Pac bed into a dense annular ring of fuel with radially oriented columnar grains is typical of oxide fuels regardless of the fabrication procedure. The initial distributed porosity in the as-fabricated fuel collects to produce the central void. The primary mechanism in this restructuring phenomenon has been hypothesized to be vaporization and condensation in the thermal gradient at temperatures^{9,10} above about 1500°C. The microstructures of both the UO₂ and the (U,Pu)O₂ Sphere-Pac fuels show clear metallographic evidence of this mode of fuel densification with the growth of dendrites on the inner surface of microspheres at the periphery of the densified annular region. At lower temperatures, densification is generally accepted as resulting from sintering. This is also demonstrated in these Sphere-Pac fuels in that microporosity present in the small microspheres before irradiation has disappeared even in the spheres near the cladding at temperatures estimated to be about 900°C. Precise definition of the temperatures for various in-reactor microstructural changes will be determined in the

instrumented capsule irradiation tests. The uninstrumented tests examined to date indicate that Sphere-Pac fuels will provide in-reactor performance comparable with that of pelletized fuels of similar smear density.

Instrumented Tests

R. B. Fitts V. A. DeCarlo¹¹

Instrumented capsule tests in the ORR will be used to investigate the basic in-reactor characteristics of sol-gel-derived (U,Pu)O₂ fuels. Since a knowledge of the fuel temperatures is fundamental to the analysis and understanding of fuel behavior, the capsule has been designed to monitor fuel central and cladding-surface temperatures and fuel rod heat generation rates. In the overall instrumented program the primary characteristics to be investigated include in-reactor thermal conductivity, fuel restructuring, and fission-gas release. The influence of fuel composition, stoichiometry, density, fabrication history, and burnup on these temperature-sensitive properties will be investigated.

The first series of these tests has two primary objectives.

1. The characteristic temperatures for microstructural changes will be determined for sol-gel (U,Pu)O₂ Sphere-Pac and pellet fuels. These data are needed for the analysis of uninstrumented tests.
2. The fuel central temperature will be investigated as a function of heat generation rate and fuel rod surface temperature, and this information will be used to develop and refine a mathematical expression for the in-reactor thermal conductivity of sol-gel fuels.

Future series of instrumented tests will be used to determine the in-reactor thermal characteristics of new sol-gel fuel fabrication developments, advanced fuels, and fuel rod designs as they develop.

The design of the instrumented ORR capsule is shown in Fig. 25.3. It contains two 3-in.-long fuel rods, which operate at approximately equal heat generation rates. The rods are instrumented in three ways: a central thermocouple measures fuel central temperature, each

⁹J. Belle, *Uranium Dioxide: Properties and Nuclear Application*, p. 322, U. S. Government Printing Office, Washington, D.C., 1961.

¹⁰C. Michelson, J. L. Scott, and E. L. Long, Jr., *An Evaluation of UO₂ Irradiated at 1600 to 2400°C*, ORNL-3930 (May 1966).

¹¹Reactor Division.

fuel rod has three thermocouples in the NaK annulus to monitor cladding temperature, and four sets of calorimeter thermocouples are in the outer Zircaloy-2 wall at the midplane of each fuel rod to monitor heat generation.

The central fuel temperature may be maintained constant at a predetermined level in the 850 to 2100°C range. The cladding surface temperature will be less

than 700°C, depending on the heat generation rate, and the capsule will be suitable for operation with fuel linear heat ratings up to approximately 20 kw/ft. The initial tests will be for only one ORR cycle to minimize the effects of temperature cycles on microstructural changes. The burnup per cycle will vary, depending upon the fuel linear heat rating, up to approximately 1.5% FIMA.

R-44608

0.15 in.

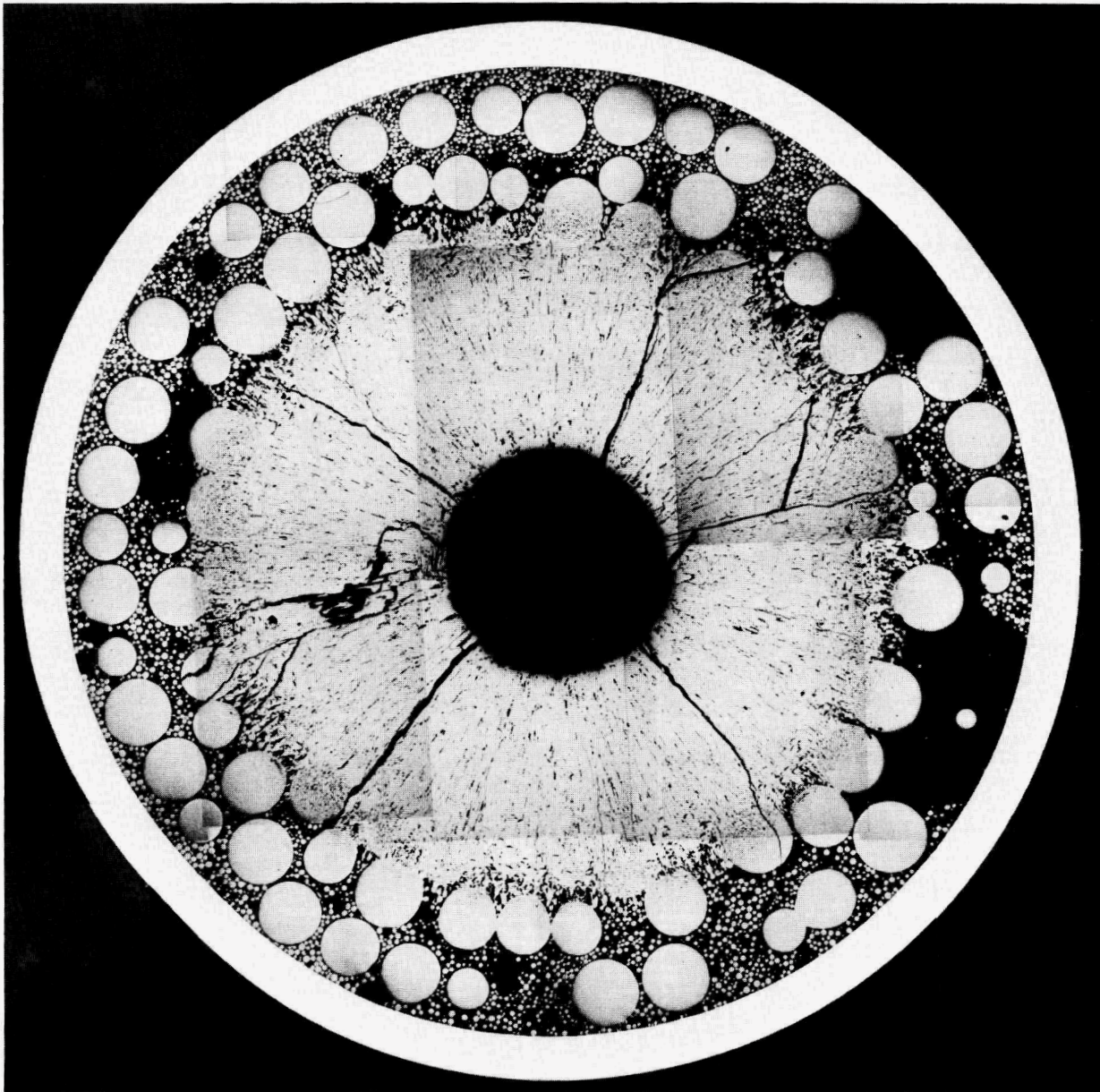


Fig. 25.1. Sphere-Pac UO_2 Fuel Irradiated in Experiment 43-112 to 0.7% FIMA at a Peak Linear Heat Rating of 450 w/cm.

The first capsule in this series operated for one cycle (51 days) in the ORR poolside facility. The fuel rods were both loaded with 8.8-g/cm^3 Sphere-Pac (U-15% Pu) O_2 identical to that used in three of the noninstrumented ETR capsules. The capsule and fuel rods operated successfully at selected fuel heat

generation rates between 2 and 15 kw/ft. The only serious difficulty was one 3-day period during which the fuel central thermocouple behaved erratically. This is as yet unexplained. Otherwise, the capsule and instrumentation performed as expected to fulfill the primary test objective – capsule design confirmation.

R-44609

0.15 in.

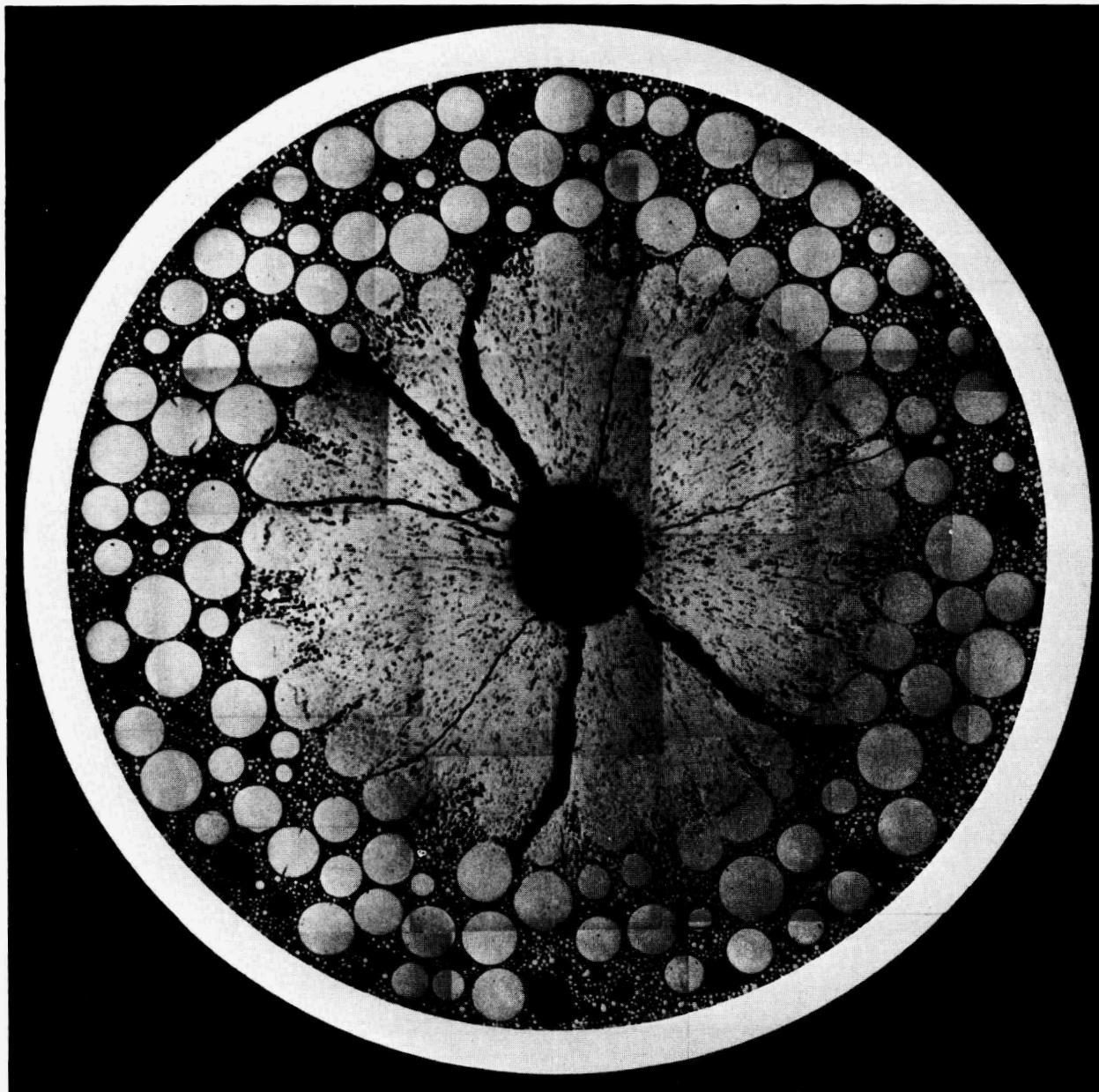


Fig. 25.2. Sphere-Pac (U-15% Pu) O_2 Fuel Irradiated in Experiment 43-112 to 0.7% FIMA at a Peak Linear Heat Rating of 485 w/cm.

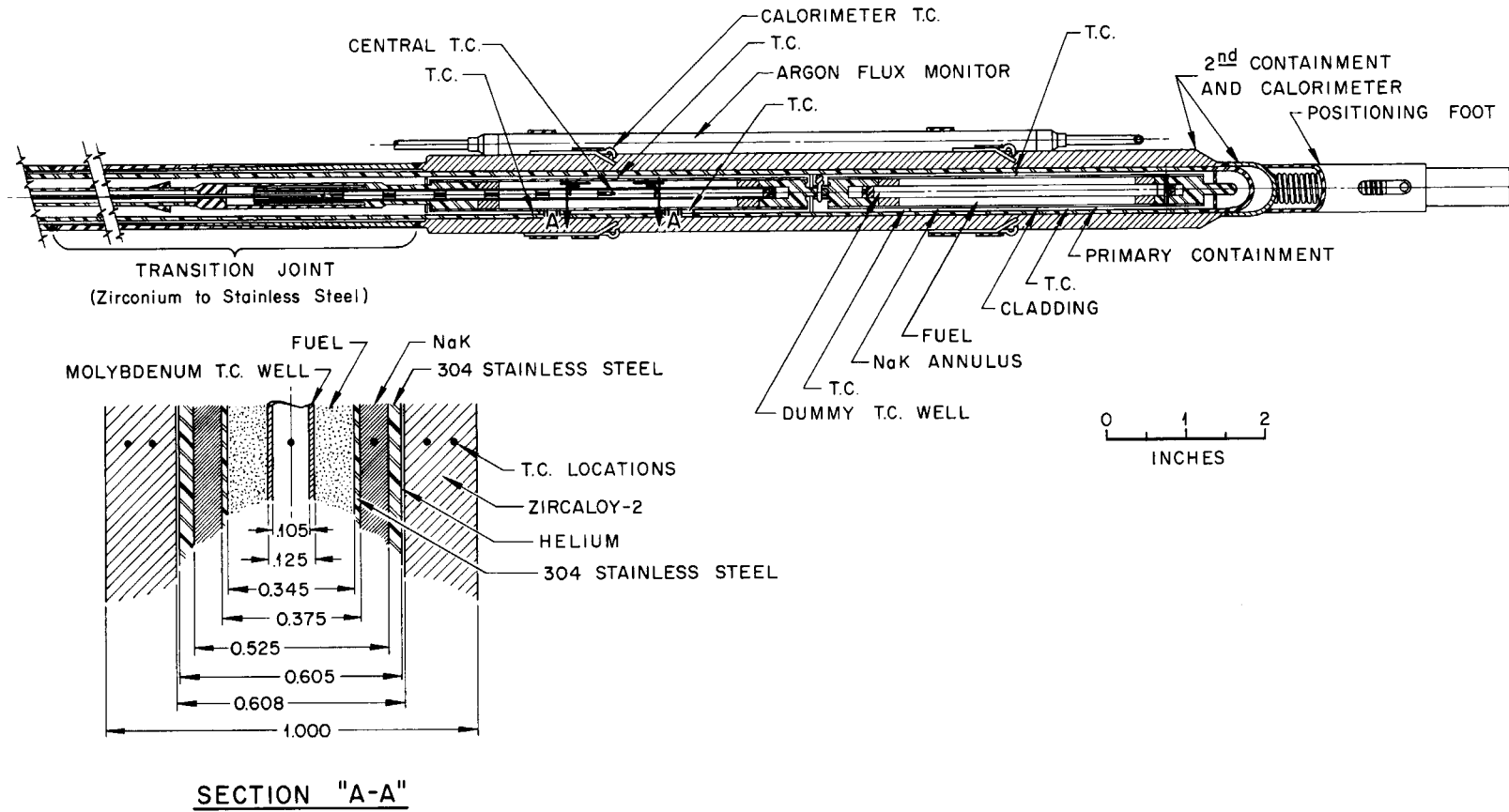


Fig. 25.3. ORR Instrumented Capsule SG-1.

A secondary test objective was to begin to study mixed oxide Sphere-Pac bed performance. Large amounts of data are obtained in this type of test and must be analyzed in detail to obtain information on fuel behavior. A computer code is being prepared to sort, store, and manipulate the data. However, it is significant to note that preliminary analysis of selected data from throughout the test run indicates that the thermal conductivity of a Sphere-Pac fuel rod is as good as or better than that reported¹² for pellet rods of equivalent smear density.

Transient Irradiation Tests

C. M. Cox J. D. Jenkins¹³ M. K. Preston¹⁴

The behavior of fuel pins under power and temperature transients will have a marked influence on both fuel element design and safety analysis. We formulated a program that is oriented toward the development of experimentally verified, computerized models to predict the behavior of fuel pins with respect to fuel densification and relocation, fission-gas release, fuel swelling, cladding deformation, failure mechanisms and thresholds, and failure propagation during transients of varying severity, up to and including fuel pin failure. The most important variables in determining the transient performance of a fuel pin are expected to be its prior operating history, fuel density, fuel fabrication form, and degree and type of axial restraint.

We reviewed the available facilities for performing these experiments, and the Transient Reactor Test Facility (TREAT) was chosen for its relatively long pulse width, availability of existing capsule designs, approval for testing plutonium-bearing fuel, and the availability of a neutron radiography facility for interim test capsule examination. We obtained approval-in-principle for performing our experiments at TREAT and expect to begin the first series of experiments in August, 1968. This series will include 13 capsules, six of which will have three separate fuel columns. We have completed the design of the fuel rods and have procured hardware for the first experiments.

In the second series of experiments, the effects of prior irradiation history will be investigated by preirra-

diation in thermal and fast neutron spectra before the transient tests. In all of these experiments, the fuel pins will be prototypic LMFBR fuel pins with (U-20% Pu)O₂ fuel.

A significant limitation of using a thermal reactor such as TREAT to simulate hypothesized fast reactor conditions is the nonuniform heat generation rate across the fuel pin, due to depression of the thermal neutron flux. For prototypic LMFBR mixed oxide fuel elements, the radial heat generation rates typically drop by a factor of about 2 from surface to center. This results in a peaking of the transient temperature profiles at roughly half to three-fourths the fuel radius, which is not consistent with the approximately parabolic temperature profiles expected in fast reactors. An obvious possible solution is the use of neutron filters, and we are currently engaged in a series of detailed reactor physics calculations to examine the effects of several possible neutron filters.

Fast Flux Irradiation Tests

A. R. Olsen

We have received approval-in-principle for the irradiation of five encapsulated test rods containing Sphere-Pac (²³⁵U-20% Pu)O₂ in the EBR-II. These rods are scheduled for incorporation into a 19-rod subassembly to be installed in a row-4 position.

Design of the fuel rods is complete, and most of the hardware has been procured. The fuel pins are designed so that two of the five rods can be remotely assembled into transient test capsules after the EBR-II irradiation. The rods will operate at linear heat ratings of about 16 kw/ft to a burnup level of 3 to 4% FIMA.

The encapsulated rods will provide the necessary lead irradiation tests for a larger number of sol-gel fuel test rods to be irradiated without double encapsulation in a 37-pin subassembly. This subassembly will include test rods fabricated by Babcock and Wilcox, with whom we are currently developing a coordinated test program. The details have not been established, but the tests will provide comparative information on four fabrication processes for sol-gel fuel (pellets, extrusions, Vi-Pac and Sphere-Pac) and two types of synthesis for pellet fuels (sol-gel and coprecipitation).

APPLIED MATHEMATICS DEVELOPMENT

R. B. Fitts W. H. Pechin
C. M. Cox A. R. Olsen

We developed various general calculation techniques to evaluate irradiation tests and fuel materials. These

¹²W. E. Bailey *et al.*, "Thermal Conductivity of Uranium-Plutonium Oxide Fuels," pp. 293-308 in *Intern. Symp. Plutonium Fuel Technol.*, Scottsdale, Ariz. 1967, *Nucl. Met.*, Vol. 13, American Institute of Mining, Metallurgical, and Petroleum Engineers, New York, 1968.

¹³Reactor Division.

¹⁴General Engineering Division.

may be used either individually or as a set, the results of one code being used as input to or to check the results from another. They range in complexity from computerization of routine calculations through development of calculations that consider material properties and structures as functions of temperature while they determine temperature profiles to the adaptation of a complex existing neutron physics code to experimental irradiation capsule calculations.

We wrote SFXØ6 in the BASIC language¹⁵ for use on the local CEIR remote computer consoles to calculate a neutron energy spectrum from dosimetry data. The code fits to the data a spectrum that consists of Maxwell-Boltzman thermal and fast neutron distributions and a $1/E$ distribution in the intermediate energies. This form has been found to be a close approximation to the flux-energy spectrum for well moderated core and reflector positions in light water test reactors.¹⁶

We have applied the SFXØ6 spectrum as a shell source with the ANISN neutron transport theory code¹⁷ to calculate heat generation rates as a function of radius in our test fuel pins. These results have agreed within $\pm 10\%$ with the heat generation calculated from postirradiation burnup analyses.

We have written two computer programs for calculating fuel-pin steady-state radial temperature profiles based on the radial heat source distribution predicted from ANISN or from other neutron physics calculations. PETPØ6 is a BASIC language code that calculates the temperature distribution based on the operating fuel geometry, the predicted heat generation distribution, and a simplified model for fuel thermal conductivity. The thermal conductivity is based upon empirical observations of the structures and densities associated with particular temperature ranges in UO_2 and ThO_2 . This code has given good correlation with observed melting in (U--20% Pu) O_2 fuels but has been

largely superseded by the PROFILE code. This is a larger FORTRAN code, which allows the user to choose between a fuel conductivity function prepared by General Electric¹² for (U,Pu) O_2 and a more general function of the form,

$$k = (A + B/T + CT^3)f(P), \quad (1)$$

where A , B , and C are constants and $f(P)$ is a porosity correction factor. The program includes an option that will predict the fuel structure changes, central void development, and revised thermal profile resulting from fuel densification, which are in turn determined by temperature. The results may be tabulated or plotted. The accuracy of our fission-rate distribution calculations is confirmed by postirradiation burnup analyses based on radiochemical and isotopic analysis.

Radiochemical analytical data for specific fission products such as ^{137}Cs , ^{144}Ce , ^{89}Sr , and ^{90}Sr are reduced to burnup data by the use of BURCØ6. This code is available in both the BASIC and FORTRAN languages.

The computer code CIBUØ6 is a FORTRAN language code for calculating fuel burnup from changes in isotopic analysis. The method differs slightly from that proposed¹⁸ by the ASTM. The plutonium-to-uranium ratios are calculated from chemical analysis of the fuel before and after irradiation. One calculates the fissions of ^{235}U from the pre- and postirradiation ratios of ^{236}U to ^{235}U , the fissions of ^{239}Pu from the increases in isotopic abundance of ^{240}Pu and ^{241}Pu , and the ^{241}Pu fissions from the increase in ^{242}Pu isotopic abundance.

The codes for both techniques of burnup analysis are operable and provide good comparative burnup values, which agree well (as reported earlier in this chapter) with the burnup levels predicted by the preirradiation calculation techniques.

¹⁵R. B. Fitts, W. H. Pechin, C. M. Cox, and A. R. Olsen, *Calculations for Irradiation Testing* (in preparation).

¹⁶W. B. Lewis and T. D. Marshall, *Distribution of Neutron Density and Neutron Flux*, IDO-16614 (July 22, 1960).

¹⁷W. W. Engle, Jr., *A Users Manual for ANISN*, K-1693 (March 20, 1967).

¹⁸ASTM Tentative Method E-244-T, "Tentative Method of Test for Atom Percent Fission in Uranium and Plutonium Fuel," *1967 Book of ASTM Standards, American Society for Testing and Materials*, Vol. 31, Philadelphia, Pa., May 1967.

26. Joining Research on Nuclear Materials

G. M. Slaughter

We studied the effects of minor alloying elements, individually and combined, on the weldability of Incoloy 800 using the VARESTRAINT Test (weld metal) and the Duffer's Gleeble (heat-affected zone). Incoloy 800 is basically an iron-nickel-chromium ternary with minor additions of titanium and aluminum. ASTM specifications¹ permit a range of 0.15 to 0.60% for titanium and aluminum. Initial work was concentrated on the effects of titanium and aluminum within these composition limits on weldability. Subsequently, we investigated the effects of sulfur and phosphorus on alloys containing nominal aluminum and titanium contents.

SPECIAL ALLOY PREPARATION

W. J. Werner R. E. McDonald D. A. Canonico

The alloys studied were all melted and prepared specifically for this program by the Materials Processing Group. Raw materials (Fe, Ni, Cr, Ti, Al, S, and P) were purchased at as high a purity as was economically feasible (all were 99.9% pure or better).

Melting and fabrication were done under rigid laboratory control to minimize contamination during processing. Alloys prepared for the VARESTRAINT and Gleeble Tests were designed for studying the individual and combined effects of titanium and aluminum.

Additional alloys for the Gleeble study were formulated to study the effects of sulfur and phosphorus on weldability. Titanium and aluminum levels for these alloys were nominally 0.38%; sulfur and phosphorus concentrations were varied from 0.010 to 0.020%. Some alloys were formulated for studying the combined effects of sulfur and phosphorus. The success of this phase of the program was evidenced by the fact that the actual compositions obtained were quite close to those desired.

¹1966 *Book of ASTM Standards, Part 7*, B 409 - 65 T, pp. 744-57, American Society for Testing and Materials, Philadelphia, 1966.

VARESTRAINT TESTING

D. A. Canonico W. J. Werner

The influence of aluminum and titanium on the hot cracking of Incoloy 800 was investigated at Rensselaer Polytechnic Institute² using its VARESTRAINT Test.³ Welding conditions for the test series are: arc voltage, 12 v; arc current, 340 amp; travel speed, 4.5 in./min; shielding gas, argon at 4 cfh; electrode, 1/8-in.-diam W-2% ThO₂.

After testing, the specimen area that received a predetermined amount of strain during welding was polished to a depth of approximately 0.010 in. All crack-length measurements were made at this depth.

The VARESTRAINT Test results obtained for the experimental Incoloy 800 alloys are presented in Fig. 26.1. The Incoloy 800 data from the original study on commercial alloys⁴ are included for comparison. The threshold for hot-crack initiation in the ternary alloy (Ni, Fe, Cr only) was above 0.5% augmented strain. This same alloy exhibited a total crack length of 0.012 in. after testing at 1% augmented strain. At this same strain, the commercial material exhibited a total crack length over 0.6 in. Obviously, the crack susceptibility was much greater for the commercial alloys than for the experimental alloys; this indicates that very small amounts of unaccounted-for trace elements may also be playing an important role. Titanium and aluminum additions to the experimental ternary alloys increased susceptibility toward hot cracking; however, there was no correlation between the level of the titanium and aluminum, either combined or individually, and total crack length for a given augmented strain. That is, the VARESTRAINT Test was unable to separate the effects of titanium or aluminum on the susceptibility of

²Work performed on subcontract under the direction of W. F. Savage and C. D. Lundin, Department of Materials Engineering, Rensselaer Polytechnic Institute, Troy, N.Y.

³W. F. Savage and C. D. Lundin, "The VARESTRAINT Test," *Welding J. (N.Y.)* 44(10), 433-s-42-s (1965).

⁴D. A. Canonico and W. J. Werner, *Metals and Ceramics Div. Ann. Progr. Rept. June 30, 1967*, ORNL-4170, p. 139.

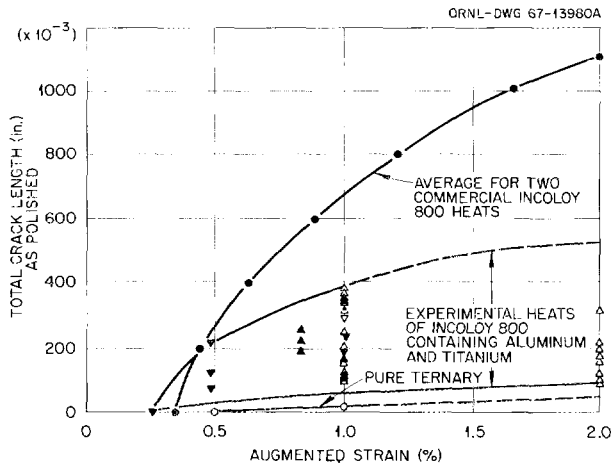


Fig. 26.1. VARESTRAINT Results for the Experimental Heats of Incoloy 800 Composition. The results of two commercial heats have been included for comparison.

Incoloy 800 toward hot cracking. The range of total crack length at 1% augmented strain for the aluminum- and titanium-bearing alloys was 0.08 to 0.35 in.

HOT-DUCTILITY TESTING

D. A. Canonico W. J. Werner

Hot-ductility tests⁵ were performed on the experimental alloys with the Duffer's Gleeble.⁶ This test measures the mechanical properties of simulated weld heat-affected zones at high temperature, and, therefore, is a useful means for evaluating weldability. Zero ductility temperatures (ZDT) and zero strength temperatures (ZST) were determined for the alloys. Zero ductility temperature is defined as that temperature at which plastic deformation before fracture is zero. Zero strength temperature is defined as that temperature at which the tensile strength of the alloy goes to zero. Recovery (of ductility) on cooling from the ZDT is obviously another measure of susceptibility toward hot cracking.

All of the alloys had ZDT's of about 2400°F; the ternary, which contained no added Ti, Al, S, or P, had the highest at 2450°F. Surprisingly, there was no ill effect on the ZDT or on recovery from Ti, Al, Ti + Al, S, P, or S + P. A finite if not spectacular effect had been expected when titanium and aluminum were added and even more when sulfur and phosphorus were added. These results are in contrast to what one would

⁵E. F. Nippes *et al.*, "An Investigation of the Hot Ductility of High-Temperature Alloys," *Welding J. (N.Y.)* 34(4), 183-s-96-s (1955).

⁶Duffer's Associates, Inc., Troy, N.Y.

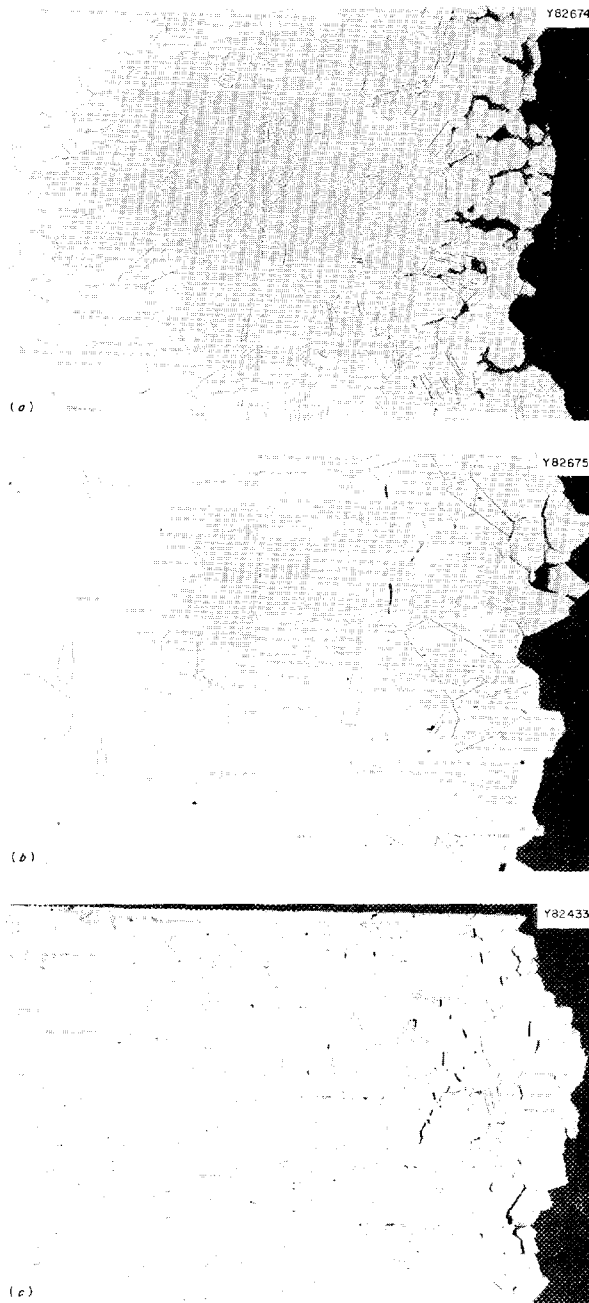


Fig. 26.2. Effect of Aluminum-Plus-Titanium Additions on the Microstructure of the Experimental Incoloy 800 Alloys. 100X. Reduced 47.5%. (a) <0.05% Al, <0.01% Ti. (b) 0.13% Al, 0.095% Ti. (c) 0.52% Al, 0.51% Ti.

expect from the phase diagram, which predicts melting point lowering, and the classical work of Pease,⁷ which predicts that sulfur and/or phosphorus will have dele-

⁷G. R. Pease, "The Practical Welding Metallurgy of Nickel and High-Nickel Alloys," *Welding J. (N.Y.)* 36, 330-s (1957).

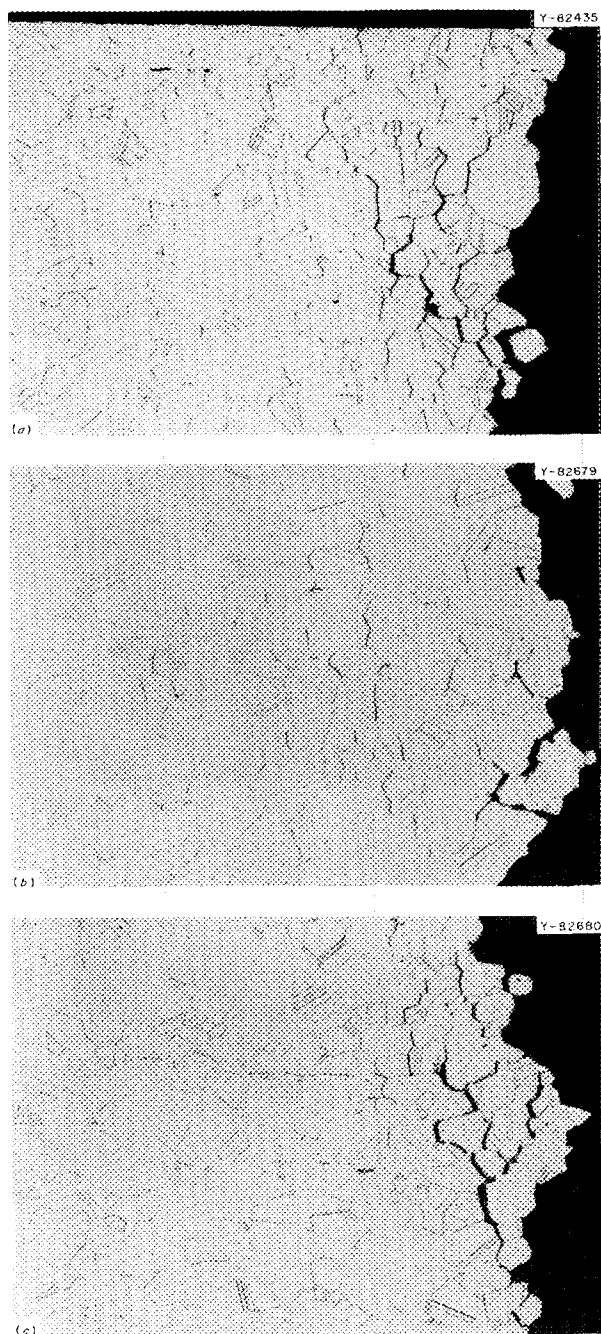


Fig. 26.3. The Effect of Sulfur and Phosphorus Additions on the Microstructure of the Experimental Incoloy 800 Alloys Containing Approximately 0.38% Al and 0.38% Ti. 100X. Reduced 48%. (a) 0.010% S, 0.001% P. (b) 0.002% S, 0.010% P. (c) 0.008% S, 0.010% P.

rious effects on the weldability of nickel-containing alloys.

Zero-strength temperatures for the aluminum- and titanium-bearing alloys decreased systematically, as

expected, with increasing (Ti + Al) content. No correlation was found between sulfur or phosphorus content and ZST.

The Gleeble specimens were examined metallographically. Figure 26.2 shows the variation in microstructure with (Ti + Al) content. Increasing (Ti + Al) results in heavy and well-defined laminations. Similar studies with an aluminum-rich alloy showed laminations and evidence of liquation within the laminae. The titanium-rich alloy showed neither laminations nor liquation; however, it did have pronounced grain-boundary embrittlement and show intergranular failure.

Figure 26.3 shows the sulfur and phosphorus effects. Figure 26.3(a) shows the effect of sulfur alone. Here we see a number of discrete inclusions aligned in the working direction. The mode of failure is intergranular, and there are some additional intergranular cracks. Figure 26.3(b) shows the phosphorus effect. Here there are continuous fine laminae. Once again failure is intergranular, and only a few cracks are adjacent to the fracture interface. Figure 26.3(c) shows the microstructure resulting from the presence of both sulfur and phosphorus. The sulfur effect is obviously dominant.

Thus, the mode of failure of the synthetic heat-affected-zone specimens does appear to be influenced elementally. High aluminum contents seem to exaggerate banding and increase the tendency toward liquation in the laminae. The presence of sulfur results in discrete precipitate particles. Reducing the sulfur or maintaining the phosphorus at levels of 0.01 wt % eliminated the discrete precipitate and caused the alloy to revert to a lamellar microstructure.

ELECTRON-BEAM MICROPROBE ANALYSIS

D. A. Canonico W. J. Werner

The unexpected similarity between sulfur- and phosphorus-bearing experimental Incoloy 800 alloys and those without these elements presented the impetus for an electron-beam microprobe study of a sulfur-bearing alloy. The alloy with 0.010% S [its microstructure is shown in Fig. 26.3(a)] was submitted for analysis. Table 26.1 contains the results, which indicate that sulfur is associated with titanium (and/or aluminum) in the inclusions seen. As was expected, the microprobe analysis also showed a high percentage of titanium in the large "pink" (titanium carbonitride) precipitate particles. A strong titanium-sulfur association was seen in the finer inclusions. The microprobe data, because of the beam size, are on the whole qualitative; however, the results seem to be quite definitive.

PHOTO 93023

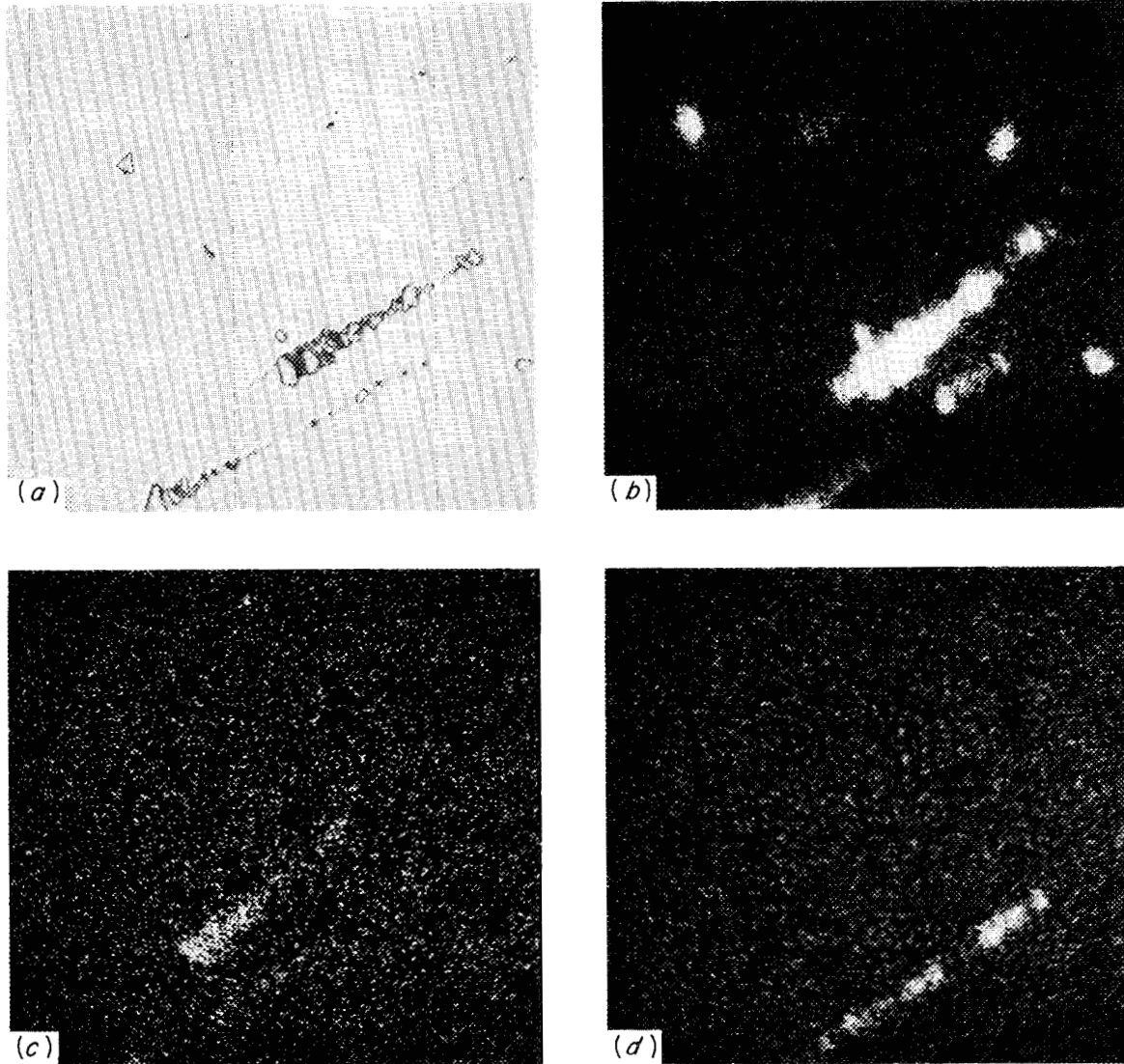


Fig. 26.4. X-Ray Scanning Images of a Sulfur-Bearing Experimental Incoloy 800 Alloy. (a) Light optics. (b) Ti K α . (c) Al K α . (d) S K α .

Table 26.1. Electron-Beam Microprobe Analysis of an Experimental Incoloy 800 Alloy that Contained Aluminum, Titanium, and Sulfur

Area	Chemical Composition (wt %)		
	Al	Ti	S ^a
Matrix	0.2	0.2	x
Large precipitates	0.7	80.8	x
Stringers ^b	≥25.0	≥36.0	>10x
Grain boundaries ^c			
with precipitate	Same	Increase	Increase
without precipitate	Same	Slight increase	Depletion

^ax represents nominal sulfur content in the matrix.

^bSemiquantitative.

^cQualitatively compared to matrix.

Figure 26.4 contains x-ray scanning images from the sample that was investigated. A definite association between sulfur and titanium is pictorially evident. A photomicrograph of the area scanned is included for comparison. The large angular particles seen in the photomicrograph are the titanium-rich "pink" carbo-nitride. The sulfur appears to be associated with the smaller precipitate particles.

The strong association between sulfur and titanium suggests an explanation for the 2400°F Gleeble ZDT plateau. Some support for this argument is found in Table 26.2, which was compiled from thermodynamic data presented in *Thermochemistry for Steel Making*.⁸ The free energies of formation at 298°K for TiS and Al₂S₃ are surpassed only by that of the known excellent sulfide former MgS. They are superior (or at least equal) to MnS. In view of these data and the

Table 26.2. The Free Energy of Formation at 298.15°K for Selected Sulfides

Compound	ΔF_f° (cal/mole)
Al ₂ S ₃	-65,670
FeS	-32,640
MgS	-92,900
MnS	-59,300
NiS	-30,700
TiS	-60,700

results of this study, it appears reasonable to hypothesize that titanium is combining with the sulfur and eliminating it as a detriment to the weldability of these nickel-rich alloys.

Other factors that seem to support this premise are: (1) the work of Pepe⁹ at Rensselaer on maraging steel, wherein he found that the grain growth in the constitutionally liquated region of the heat-affected zone was controlled by a TiS precipitate whose melting point appeared to be about 2400°F; (2) the fact that sulfur is reputedly harmful, yet its presence in the experimental alloys was innocuous. It appears reasonable to assume that somehow its influence has been overcome.

The seemingly innocuous effect of both aluminum and phosphorus has not been explained. Further work involving these elements is under way.

⁸J. F. Elliot *et al.*, *Thermochemistry for Steelmaking*, Vol. I, sponsored by the American Iron and Steel Institute, Addison-Wesley Publishing Company, Reading, Mass., 1963.

⁹J. J. Pepe, Private Communication, Rensselaer Polytechnic Institute, Troy, N.Y., April, 1967.

27. Zirconium Metallurgy

P. L. Rittenhouse

The present generation of nuclear reactors makes use of a number of zirconium alloys as fuel cladding, pressure tubes, and fuel channels. Although these alloys have relatively low neutron cross sections, there is continuing pressure to reduce the mass of all nonfissionable material associated with the reactor core. We hope, by controlling the texture of zirconium alloy tubing and, thereby, its anisotropy of properties, to permit the use of thinner tubes and cladding without loss in safety factor, to result in more economical nuclear power.

STRAIN BEHAVIOR IN UNIAXIALLY TESTED ZIRCALOY TUBING¹

P. L. Rittenhouse

Tensile specimens from seven commercially fabricated lots of annealed Zircaloy tubing were tested to examine the influence of texture on the anisotropy of strain behavior. Diametral and wall-thickness strains were measured after testing. These strains were linear functions of total strain, as indicated in Fig. 27.1. The slopes measure relative resistance to flow and, therefore, the relative distribution of basal poles in the plane perpendicular to the axis of the tubing. We found the ratio of the slopes to be inversely proportional to the ratio of the basal pole texture coefficients in the strain directions.

The method of analysis described is general and could be used to study anisotropy and texture in tubing of any material. To correlate the slopes with any particular component of the texture, as we have with the basal pole, the crystallographic deformation behavior of the material must be known.

EFFECT OF TEXTURE ON THE TORSIONAL YIELDING OF ZIRCALOY TUBING²

P. L. Rittenhouse

The physical and mechanical properties of zirconium alloys are highly anisotropic. The anisotropy is caused by crystallographic textures developed during fabrica-

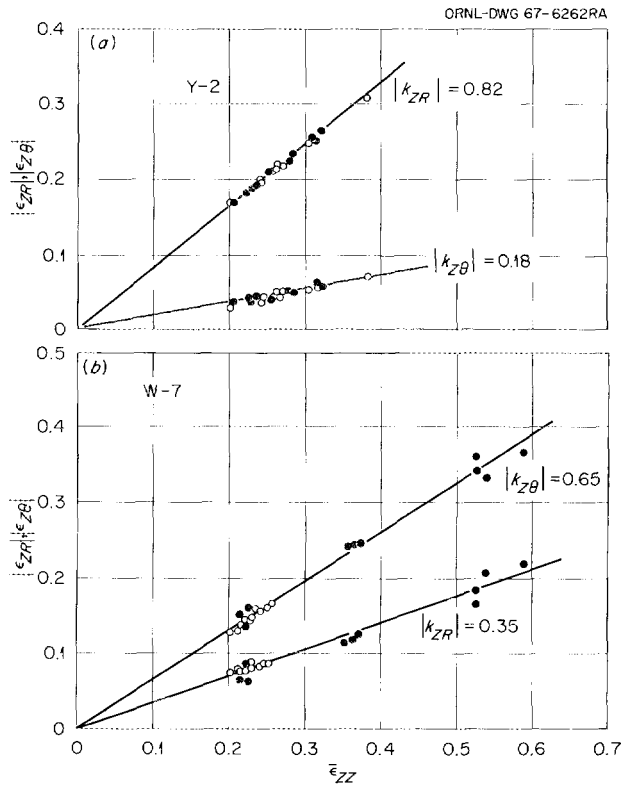


Fig. 27.1. Diametral and Wall-Thickness Strains vs Axial Strain for Zircaloy Tubing. The diameter strain is $\bar{\epsilon}_{Z\theta}$, the wall strain is $\bar{\epsilon}_{ZR}$. (a) Material Y-2; $k_{Z\theta}/k_{ZR} = 0.22$ compared to an inverse ratio of basal pole texture coefficients of 0.31. (b) Material W-7; $k_{Z\theta}/k_{ZR} = 1.8$ compared to an inverse ratio of 1.6.

tion. Our aim has been to measure the effect of texture on the uniaxial and biaxial properties of small-diameter Zircaloy tubing.

We have torsion tested more than a dozen lots of thin-walled Zircaloy tubing. This test defines the point on the plane stress yield surface at which the ratio of

¹ Abstracted from *J. Nucl. Mater.* 24, 310-15 (1967).

² Abstracted from a paper to be given at the ASTM Symposium on "Application Related Phenomena of Zirconium and Hafnium Alloys," Philadelphia, Nov. 5-7, 1968.

axial tension to tangential compression is -1.0 . The yield theories used for isotropic materials are not applicable in our case, so we modified these, permitting the ratio of axial to tangential yield strength to differ from unity, and obtained a predicted minimum torsion yield strength. The ratios of our experimental torsion yields to those predicted ranged from 1.0 to 1.5.

We can explain this range of torsion yield ratios by considering the textures that are present in the different tubing lots. The strength of the material in any direction is proportional to the concentration of basal poles in that direction. Therefore, for Zircaloy tubing in which most of the grains have basal poles parallel to the tube radius the radial direction is strongest. In the torsion test, however, the stress in this direction is zero. Neither the axial nor tangential direction is texture strengthened, so the torsion yield approaches the modified theory minimum torsion yield. If the texture is such that most grains have basal poles parallel to the tangential direction, this direction is strengthened and the torsion yield is higher than predicted.

Our results have demonstrated that texture can be quantitatively related to the anisotropy of mechanical properties of Zircaloy tubing. Also, although the isotropic yield conditions are not directly applicable to anisotropic materials, they can be modified to a form useful in the analysis of the effects of texture on anisotropy.

TEXTURES IN DEFORMED ZIRCONIUM SINGLE CRYSTALS³

D. O. Hobson

Zirconium single crystals of various specific orientations were deformed by rolling and drawing. The resulting textures were determined and are related to the deformation modes that produced them. The crystals deformed predictably by slip and by combinations of up to third-order twinning with three twinning modes. Twinning played a major role in initial texture formation. Texture changes produced by slip occurred only at the higher reductions. The twinning sequences that produced each intensity peak during the initial reductions could be identified. Schmid factor criteria were useful in predicting which deformation modes to expect for each crystal orientation and fabrication procedure. The application of these results to polycrystalline material is discussed.

³Abstracted from *Trans. Met. Soc. AIME* 242, 1105-10 (June 1968).

EXAMINATION OF ORIENTATION FACTORS FOR THE DEFORMATION SYSTEMS OF ZIRCONIUM UNDER BIAXIAL STRESS CONDITIONS⁴

D. O. Hobson

The measurement of critical resolved shear stress for the operation of deformation systems in metals and, indeed, predicting which systems will operate under a particular set of stresses in a material of multiple deformation modes is of importance in the study of texture development and plastic flow. This paper examines the geometrical aspects of the influence of a biaxial stress state (idealized rolling) on the deformation modes of zirconium. One slip and three twinning modes comprising 21 deformation systems are considered. Orientation (Schmid) factors are computed for all orientations and all deformation systems, and the values are plotted on a coordinate system that allows specimen orientation, operative deformation system, and orientation factor to be shown without ambiguity. The data presented in this paper are useful in two ways. They allow the accurate determination of the resolved shear stress in a balanced biaxial tension-compression stress state, and they permit the prediction of the deformation modes and systems that will operate for any specimen orientation in this stress state.

INHOMOGENEOUS DEFORMATION IN ZIRCALLOY TUBING⁵

D. O. Hobson P. L. Rittenhouse

Zircaloy tubing is used as fuel cladding in commercial nuclear power reactors. This is an application for which the integrity, predictability, and reliability of material behavior are of great importance. We recently found that many lots of Zircaloy tubing tested in tension deform to polygonal rather than circular cross sections. Such behavior has been heretofore unrealized and should be of immediate concern to both the design engineer and the metallurgist.

Logically, the noncircular cross sections result from a circumferential variation in plastic properties and, therefore, in texture. To test this postulate we examined the diffracted x-ray intensity from (0001), $\{10\bar{1}0\}$, $\{11\bar{2}0\}$, and $\{10\bar{1}1\}$ planes parallel to the tubing surface around the entire circumference. Tubing that

⁴Abstract of a paper to be presented at Fall Meeting of the Metallurgical Society of AIME, Detroit, Oct. 14-17, 1968.

⁵Abstracted from a paper presented at the 97th Annual Meeting of AIME, New York City, Feb. 18-22, 1968.

deformed to a circular cross section showed less than 5% variation in diffraction intensity around the circumference from any of these planes. Greater intensity variations were found for all the tubing materials that developed noncircular cross sections during deformation. In each instance the number of intensity maxima and minima was consistent with the number of sides of the polygons, Fig. 27.2.

The explanation for the existence of these circumferential texture gradients involves (1) the limited number of crystallographic deformation systems that are available to provide the macroscopic plastic strain produced during fabrication and (2) the details of the deformation processes that are peculiar to various methods of tubing fabrication.

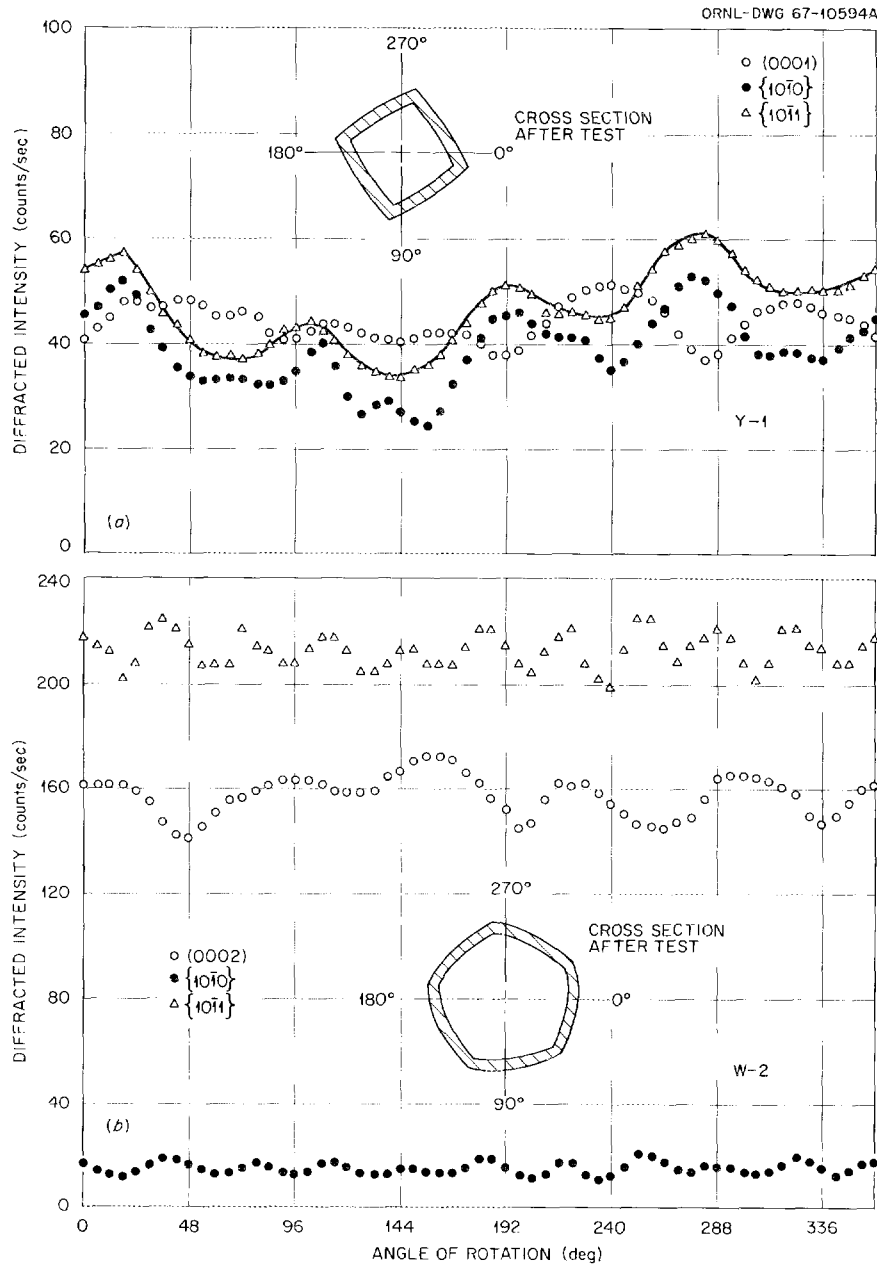


Fig. 27.2. Variation in Diffraction Intensity of (0002), $\{10\bar{1}0\}$, and $\{10\bar{1}1\}$ as a Function of Location Around the Tubing. (a) Material Y-1; square cross section and four-cycle intensity variation. (b) Material W-2; "five cycle" variation.

DEVICE FOR STUDYING TEXTURE VARIATION AROUND TUBING⁶

D. O. Hobson

A device for studying variations in radial pole densities around tubing and thus detecting texture inhomogeneities is described. Rapid interchange of specimens is possible and a range of tubing sizes can be accommodated. All specimens are automatically centered and held at the optimum position for diffraction. The slight defocussing due to the curvature of the tube surface is provided for. The beam divergence as a function of specimen radius is adjusted by collimation of the incident beam, so the tube can be treated as a flat-plate specimen. No complicated absorption factor corrections are needed.

TEXTURE GRADIENTS IN THIN-WALLED ZIRCALOY TUBING⁷

E. Tenckhoff P. L. Rittenhouse

The preferred crystallographic orientation (texture) that develops during fabrication of Zircaloy tubing has considerable influence on mechanical properties. Examinations of many deformed metals have shown that the texture of the outer layer may be different from that of the inner parts. Thus, to determine the influence of texture on mechanical behavior we must either select a specimen in which texture does not vary through the cross section or, if this is impossible, integrate the texture variation into the analysis. In either case it is necessary to determine the texture in layers below the surface of the deformed metal.

We developed techniques to allow us to measure these textures. Tube sections are machined in such a manner that a ring containing material from different layers of the tube wall is obtained. This ring is thinned to a maximum thickness of 0.002 in. by chemical dissolution and then bent elastically to the flat surface required for the reflection measurements with the texture goniometer.

We examined tubes with different processing histories, including tube reducing with either diameter or wall reduction predominant, cold drawing, and ball swaging. The intensity of basal poles and their spread into the transverse direction varied markedly, depending on the layer examined and the processing condi-

tions. From the outer to the inner surface the sharpness of the texture would rise, fall, remain constant, or show an extremum. Similarly the preferred position of basal poles varied from 0 to 45° from the radial toward the tangential direction. Although the position of the basal pole is generally believed to be unaffected by alpha annealing, in some Zircaloy tubes it changed to the radial direction from positions as great as 40° toward the tangential direction.

Our results give a more detailed insight into the formation of texture during fabrication and help in correlating texture with mechanical properties.

TUBING FABRICATION

D. O. Hobson P. L. Rittenhouse
T. M. Nilsson E. Tenckhoff

The texture of Zircaloy tubing at each intermediate stage of fabrication depends on all fabrication steps to that point. To achieve texture control we must know the contribution that each step in the procedure makes to the final texture. We have devised and are carrying out an experimental series of tubing fabrications to determine the effect on texture and quality of various processing variables and techniques. This program will (1) show in detail how fabrication events affect texture, (2) allow control of texture in the finished product, and (3) demonstrate the most economical and efficient method of tubing production.

HYDRIDE ORIENTATION IN ZIRCALOY TUBING⁸

P. L. Rittenhouse

Zircaloy tubing used as fuel cladding in water reactors absorbs a fraction of the corrosion-produced hydrogen. When the solubility limit of hydrogen in Zircaloy is exceeded, platelets of zirconium hydride are precipitated. The effect of this precipitate on the properties of the material depends upon the distribution, morphology, and orientation of the platelets. Platelets oriented perpendicular to a direction of stress are particularly harmful to ductility.

The orientation of hydride platelets in Zircaloy is thought to be influenced by crystallographic texture, fabrication history, degree of cold work, grain size, hydrogen level, and precipitation conditions, but our intent here is to show only the effect of texture and stress direction during precipitation on the orientation

⁶ Abstract of paper to be submitted to *Norelco Reporter*.

⁷ Abstracted from a paper to be given at the ASTM Symposium on "Application Related Phenomena of Zirconium and Hafnium Alloys," Philadelphia, Nov. 5-7, 1968.

⁸ Published in *Trans. Am. Nucl. Soc.* 10(2), 464 (1967).

of hydride in annealed material. We have correlated the difference in the values of the basal pole texture coefficients TC in the radial R and tangential θ directions with the hydride trace distribution on the surface perpendicular to the tubing axis. When $TC_R > TC_\theta$, a condition for which the basal planes are preferentially oriented parallel to the tangential direction, the hydride traces paralleled the tangential direction. This correlation between traces of the hydride platelets and the basal planes persisted for $TC_R < TC_\theta$. The orientation of hydride precipitated under hoop stress was identical to that in the unstressed material

when $TC_R > TC_\theta$. However, when $TC_\theta > 1.5 > TC_R$, the number of platelets perpendicular to the tangential direction was greater in stressed than in unstressed material.

In pressure tube and cladding applications, for which the tubing is subjected to hoop stresses, the most desirable texture is obviously one with basal poles parallel to the radial direction ($TC_R \gg TC_\theta$). The hydride platelets in material of this texture will be parallel to the stress, will have little effect on ductility, and will not be unfavorably reoriented during service.

Part IV. Reactor Development Support*

28. Assistance in Research Reactor Core Procurement

G. M. Adamson, Jr.

This program was begun to assist the Division of Reactor Development and Technology, Washington, D.C., in their management of research reactor fuel procurement. The program is divided into three tasks: (1) direct technical assistance to RDT when requested, (2) adapting and understanding of nondestructive testing techniques when applied to dispersion-type fuel elements, and (3) solving of technical problems encountered by the fabricators. The latter item is restricted to relatively short-range problems, principally to assure the availability of an experienced, up-to-date group of experts.

This program is closely integrated with related work on dispersion fuel elements reported in Fuel Element Fabrication Development, Part III Chapter 20, and High Flux Isotope Reactor Materials Development, Chapter 31.

FUEL ASSISTANCE AND PROCUREMENT

R. J. Beaver

This phase includes standardization of specifications, review of technical requirements for procurement packages, and participation in fuel procurement as well as quality control audits of fuel fabricators.

In the procurement phase of this program, the order for 50 stationary fuel elements and 10 control rod elements by the USAEC New York Operations Office

*The program LMFBR Cladding and Structural Materials Development is combined with the closely related Mechanical Properties Research in Part III, Chap. 22.

for the Air Force Nuclear Test Reactor (AF-NETR) at Wright-Patterson Air Force Base was completed by the National Lead Company. We were responsible for technical supervision and inspection. Based upon our inspection, we recommended approval to ship six control rod fuel elements in August 1967, and the remaining elements were delivered in January 1968.

Procurement of two PM Type 4 nuclear reactor cores for the Navy's reactor in Antarctica was initiated by the AEC New York Operations Office, who selected Nuclear Materials and Equipment Corporation (NUMEC), Apollo, Pennsylvania, as the contractor. We are providing the technical assistance and inspection to this AEC office. This job is requiring that we work with four industrial companies and two AEC offices. Our major effort to date has been reviewing, commenting on, and recommending approval of more than 200 submittals covering their intended manufacturing and inspection procedures. All of the UO₂ pellets required for this procurement were processed by NUMEC. The National Lead Company at Albany, New York, completed their qualification work associated with manufacturing the europium titanate-stainless steel control plates, and we recommended approval for them to proceed with production.

Review of specifications has centered on the fuel element for the AF-NETR utilizing experience developed during procurement. We reviewed these specifications in detail with the responsible parties at AF-NETR and RDT. The revised specifications were approved by RDT and delivered to the AEC New York Operations Office for procurement.

The Oak Ridge Research Reactor (ORR) fuel element specifications were revised and circulated for review. Revisions to the fuel element specifications for the Army's MH1A reactor were begun. We assisted the Fuels Engineering Branch of RDT in audits of the performance of NUMEC on the ZPPR and PM Type 4 core work, Battelle Northwest on their fuel element qualification for the Phoenix Program, Atomics International on their performance in producing ATR and ETR fuel elements, and the National Lead Company in reviewing their prequalification results on ATR fuel elements. Two papers^{1,2} were presented at the AEC-Industry Meeting on Water Reactor Fuel Element Technology in Washington, D.C., on January 29 and 30, 1968.

FABRICATION OF ATR FUEL PLATES

M. M. Martin J. H. Erwin
W. R. Martin

When the fuel for the Advanced Test Reactor (ATR) was changed from U_3O_8 to UAl_3 , the fuel plates began showing a nonuniform deformation near both ends of the cores. This phenomenon, commonly called dog-boning, is observed particularly in highly loaded plates where the fuel powder volume fraction is large.

Since the original ORNL development of ATR fabrication techniques³ was with U_3O_8 fuel, this phenomenon had not been encountered. However, when special instrumented fuel plates for the ATR were fabricated,⁴ we noted that dogboning was much more severe in the plates containing UAl_3 than those with U_3O_8 . However, we had previously⁵ fabricated UAl_3 plates for the ORR, containing lower UAl_3 fuel concentrations, without encountering such a problem. Since the fabrication schedules for the instrumented and standard plates do differ, we rolled two types of standard ATR plates to elucidate general difficulties and determine the amount of dogboning encountered with ORNL fabrication

procedures. Two plates (19, which is the widest and thickest, and 8, which is an average plate) were fabricated; in each case 53 wt % UAl_x was used dispersed in aluminum powder.

As expected, dogboning was a problem with both plates. It was more severe in the larger plate, with the maximum amounts measured in four metallographic samples being 65 and 100% for plates 8 and 19, respectively. When averaged over an 0.08-in. length, the values were about 55 and 70%. Comparable results from radiographic density were 52 and 58%, and those from direct measurements by x-ray attenuation techniques⁶ were 56.3 and 63.7%. The x-ray attenuation values were obtained from well established calibration data. However the radiographic values are preliminary and are shown only to indicate initial results. Additional plates are being examined to provide data on the reproducibility expected with these various techniques. The primary differences between the two plates are the cladding thickness and total rolling reduction, of which only the former appears to contribute to the degree of nonuniform deformation in the core.

EXAMINATION OF ARC-MELTING TECHNIQUES FOR THE PREPARATION OF UAl_x

J. T. Venard⁷ W. R. Martin

The principal method used commercially to prepare powdered UAl_x intermetallic fuel is arc melting and grinding. When using this procedure, commercial producers have encountered troubles with free uranium present in the cores of rolled plates and with control of the amount of fuel within a core. To help understand these problems, uranium-aluminum compounds with approximately 75 wt % U were melted in a water-cooled copper hearth and allowed to solidify into 2-in.-diam buttons. To effect proper mixing, the buttons were turned over and remelted up to six times. No free uranium in the as-cast microstructure was found in any buttons examined. However, gross microstructure variations are observed within each button, such as shown in Fig. 28.1. Preliminary microprobe analysis indicates that UAl_3 , UAl_4 , and free aluminum are present. The multiplicity of types of microstructure

¹G. M. Adamson, Jr., *Fabrication of Research Reactor Fuel Elements*, ORNL-TM-2197 (June 1968).

²G. M. Adamson, Jr., and R. W. Knight, *HFR Fuel Element Production and Operation*, ORNL-TM-2196 (June 1968).

³R. J. Beaver, P. Patriarca, and G. M. Adamson, Jr., *Procedures for Fabricating Aluminum-Base ATR Fuel Elements*, ORNL-3632 (June 1964).

⁴J. H. Erwin, W. J. Werner, and M. M. Martin, *Development and Fabrication of Instrumented-Plate Advanced Test Reactor Fuel Elements*, ORNL-4268 (in press).

⁵W. J. Werner, M. M. Martin, and J. H. Erwin, *Metals and Ceramics Div. Ann. Progr. Rept. June 30, 1966*, ORNL-3970, pp. 107-9.

⁶B. E. Foster, S. D. Snyder, and R. W. McClung, *Continuous Scanning X-Ray Attenuation Technique for Determining Fuel Inhomogeneities in Dispersion Core Fuel Plates*, ORNL-3737 (January 1965).

⁷Present address, LMFBR Program, Argonne National Laboratory, 9700 South Cass Avenue, Argonne, Ill., 60439.

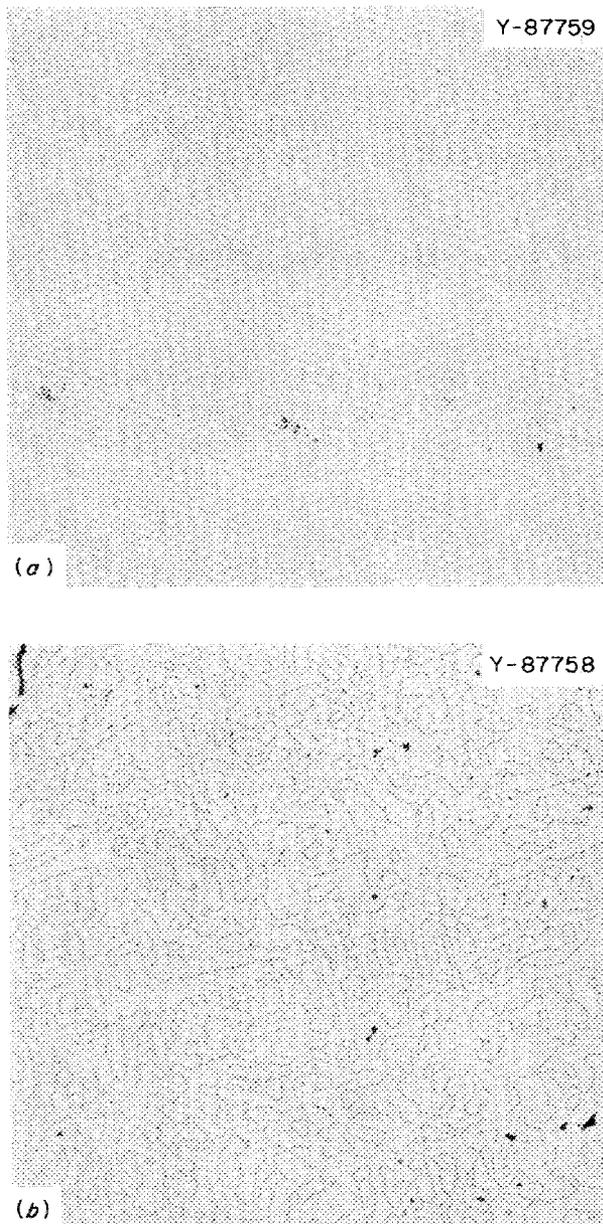


Fig. 28.1. Typical Variations in Microstructure Within a Sample of As-Cast Arc-Melted Uranium-Aluminum Intermetallic Fuel (74 wt % U). (a) Preliminary microprobe analysis indicates microstructure consists of aluminum in UAl_4 . (b) Analysis shows two compounds present, UAl_3 and UAl_4 .

within a given button may be influencing subsequent fabrication steps, such as grinding and crushing of the buttons to produce powder, and could possibly cause segregation. Alternate melting techniques that would reduce the segregation and nonuniform mixing during melting are being examined.

CLUMPING OF B_4C POWDERS IN DISPERSION FUEL ELEMENTS

A. K. Chakraborty W. R. Martin

Boron carbide powder, which is used as a burnable poison in several dispersion fuel elements, tends to agglomerate when blended with the aluminum powder matrix, causing inhomogeneity. We found that fine B_4C powders, less than 30μ in diameter, clump loosely together to give an agglomerate size from 200 to 1500μ if exposed to the atmosphere; the cause was adsorption of moisture on the particle surface. Vacuum drying made a large difference in particle size; an effective dehydration was obtained by heating the powder for 1 hr at $150^\circ C$ under vacuum. The size distribution was then 60% 5μ , 30% 10μ , 9% 15μ , and 1% 20μ . If exposed to air after such a treatment, the powder absorbs water even more rapidly than previously. If only moderate amounts of moisture are present in the B_4C , the use of vacuum-dried aluminum powder is usually sufficient to prevent clumping.

FUEL HOMOGENEITY

B. E. Foster S. D. Snyder

Twenty experimental fuel plates were fabricated to allow calibration of the x-ray attenuation scanning technique for various loadings of U_3O_8 , UAl_3 , and $UAl_3Si_{0.4}$ in aluminum matrices. Six of these plates had HFIR outer-annulus fuel contours and dimensions, six had HFIR inner-annulus fuel contours and dimensions, and the remaining eight were flat-core ATR-type plates. For each of the HFIR contours there were two plates with each fuel type. For each of the core materials, one plate contained the nominal HFIR uranium loading and the other contained a 25% increased uranium loading. The ATR-type flat-core plates were all U_3O_8 -aluminum cores, six with nominal and two with 25% increased uranium loading. These were made for a parametric study of the quantitative evaluation of fuel homogeneity with radiography.

The HFIR-type inner- and outer-annulus plates with nominal loadings were fabricated to provide a control standard to ensure consistency with the old primary calibration curve relating uranium content to attenuation. This calibration had been determined in 1962 and has been validated many times since then.

In addition to the complete scanning of all these plates for fuel content, specific 0.078×2 -in. sections in all the HFIR-type plates were scanned for calibration of both the x-ray attenuation and radiographic techniques. These sections were subsequently machined from the

plates, measured for density, and finally chemically analyzed for uranium content.

The resultant uranium content for specific attenuation values with the control plates was high by an average of 5% when compared to the original calibration. We investigated the possible causes of this bias, without successful resolution. We scanned and sectioned a Metals and Controls production-fabricated inner-annulus HFIR plate. The data obtained were randomly scattered around the original calibration curve with a maximum deviation of 5% in both high and low directions. This is far in excess of the maximum 1% deviation we have observed in the past. We became suspicious of the machining accuracy of these samples, since 8 of the 17 were between 0.092 and 0.100 in. wide rather than the desired 0.078 in. Consequently, another Metals and Controls inner-annulus plate was scanned and sampled. The sample boundaries were precisely scribed and sample identifying numbers scribed in each full sample width before machining. This plate was machined with no dimensional errors, and we are confident that the areas of the scanned samples coincide with the machined samples. We measured sample density by our usual alcohol displacement method and an alternate more rapid pycnometer method. The maximum difference between the two methods was 0.3%. The final results from chemical analysis show a reduction in the deviation from the original calibration curve to an average of +1.2% with a scatter band from -1.5% to +3.2%.

We are studying the use of radiography and densitometry to determine the qualitative and quantitative capabilities and limitations for the detection and measurement of fuel inhomogeneity in dispersion-core fuel plates. We made aluminum samples 0.078, 0.125, 0.250, and 0.500 in. in diameter and with thicknesses ranging from 0.011 to 0.137 in. These specimens when placed on a fuel plate are used to simulate a given percentage increase in fuel loading (from about 3 to 45%), and may be then related to the change in radiographic film density. Over a limited range a percentage increase in total aluminum thickness will produce a change in x-ray attenuation approximately equal to that from the same percentage increase in fuel concentration.

Preliminary data indicate that a simulated 45% increase in fuel loading 0.078 in. in diameter results in a density measurement with the 1/8-in. aperture on the densitometer equivalent to only about a 20% increase in fuel. However, the density measurement with the 0.078-in. aperture on the densitometer is equivalent to approximately a 35% increase in fuel.

The data thus far indicate that a simulated fuel increase of 3.5% with a diameter of 0.500 in. is not

visible to the eye in a dispersion core fuel plate. Actually the minimum visually detectable fuel increase is approximately 7% with a diameter of 0.125 in. For an area 0.078 in. in diameter slightly higher than an 8% fuel increase is also visible.

WELDING DEVELOPMENT

G. M. Slaughter

The electron-beam process is being investigated as a means for welding aluminum fuel plates to side plates for ATR-MTR-ORR type research reactor fuel elements (see also Fuel-Plate-to-Side-Plate Welding Development in Chapter 31). Such a procedure would result in a more positive attachment than is achieved by roll swaging. Test welds have indicated that the process is definitely feasible, and the cross section of a demonstration weld between pieces of type 6061 aluminum is shown in Fig. 28.2. Good plate tie-in was achieved and the weld exhibits excellent contour. The small amount of microfissuring observed in the weld bead can probably be minimized or eliminated if type 2219 aluminum side plates are used. Additional development work on prototype assemblies currently is under way.

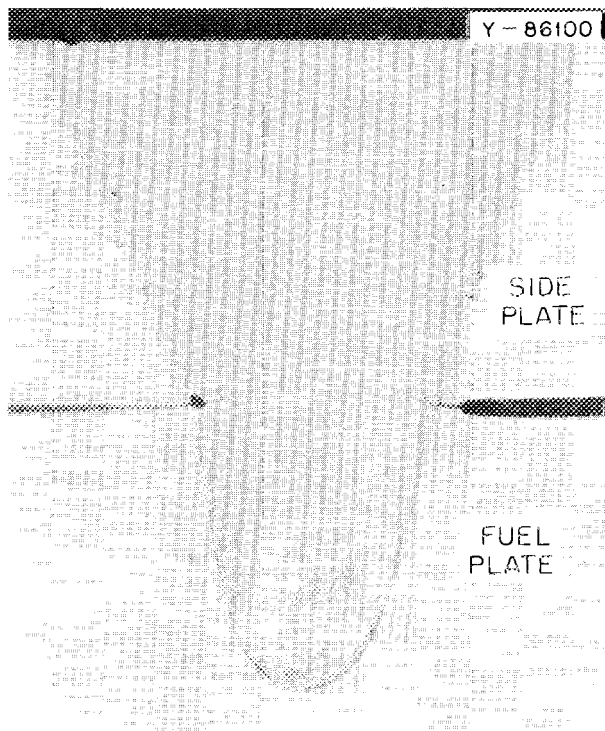


Fig. 28.2. Electron-Beam Welded Joint of 6061 Aluminum Side Plate to 6061 Aluminum Fuel Plate. Good plate tie-in was achieved, and the weld exhibits excellent contour. The small amount of microfissuring can probably be overcome by the use of 2219 aluminum side plates. Etchant: HF, H₂O. 23X.

29. Gas-Cooled Reactor Program

J. H. Coobs

Our materials effort in support of the Gas-Cooled Reactor Program is directed primarily toward development of unclad ceramic fuel elements for high-temperature gas-cooled converter reactors (HTGR's) such as the Fort St. Vrain Reactor being constructed by Gulf General Atomic for Public Services Corporation of Colorado. Proposed fuel elements consist of prismatic graphite blocks containing coated (Th,U)O₂ or (Th,U)C₂ particles and are designed to retain much of the fission-product activity within the fuel element to simplify maintenance.

Our program consists principally of developing fabrication techniques for loading bonded coated particles into fuel elements and preparing, characterizing, and irradiation testing coating materials, coated particles, and simulated bonded fuel elements. An important part of the irradiation test program now utilizes HFIR target positions. Specimens from the first such experiment, which operated for three cycles to an estimated maximum fluence of 7×10^{21} neutrons/cm² (>0.18 Mev) at 750 to 1100°C, are being examined, and another experiment to test only bonded coated particles is being prepared. Results from previous irradiation experiments in ETR and DFR are highlighted below.

A significant supporting effort for HTGR's involves the characterization of constituents for use in concretes for prestressed concrete vessels proposed for large power stations. We also began studies of corrosion resistance and other properties of weldments of nickel-base alloys proposed for advanced steam generators and have contributed to the examination and interpretation of irradiation experiments on fuel rods proposed for a gas-cooled fast breeder reactor (GCFR).

BONDING OF COATED-PARTICLE FUELS

R. L. Hamner H. Buetler¹
J. M. Robbins

Our fuel development for advanced HTGR's is concerned with demonstrating remote manufacture of

¹ Present address, Sulzer Bros., Winterthur, Switzerland.

recycle fuel, which will contain ²³³U from irradiated thorium and is an important economic feature of the reactor. We have developed equipment and techniques for bonding coated particles into rods (called sticks) for loading into holes in the hexagonal graphite fuel

PHOTO 89047



Fig. 29.1. Experimental HTGR Fuel Stick that Was Carbonized in Place, Broken, and Partially Ejected from Its Graphite Support Tube.

elements.² The fuel sticks are formed by injection of a phenolic resin binder into the blended bed of coated fuel and ThO_2 (fertile) particles in a suitable mold. Graphite powder is mixed with the resin before injection to increase the amount of residual carbon in the structure, and maleic anhydride is added to the mix to catalyze the hardening (curing) of the bonded sticks. The cured fuel sticks are removed from the mold and carbonized by heating slowly to 1000°C in a stream of inert gas. The close packing of coated particles in the fuel sticks is illustrated in Fig. 29.1, which shows a broken section of an experimental stick in a graphite support tube.

The outer pyrolytic carbon coating preferred for the coated particles is a high-density isotropic layer deposited at low temperatures (about 1250°C) and high deposition rates from propane or propylene. During early experiments we noted that some coatings were broken after bonding. Cracking always appeared to

originate in the matrix because of severe shrinkage of the resin-base bonding material during carbonization, and these cracks tended to propagate through the coatings on some particles, as shown in Fig. 29.2(a). Examination of the surface properties of the coated particles disclosed the presence of pores about $0.1\ \mu$ in diameter. Apparently this porosity contributes to a strong bond between the resin and coating, because we further observed that the resin would not bond to smooth surfaces of dense anisotropic carbon coatings that have little if any open porosity. This lack of tendency to bond was utilized to eliminate the cracking of coatings. We deposited a thin nonbonding anisotropic layer on the surface of the preferred coating and then deposited over this a thin sacrificial outer layer that would bond tightly to the resin but would crack without affecting the preferred coating. The function of the two special layers is well illustrated in Fig. 29.2(b), where the two outer layers are thicker than necessary. A practical application is illustrated in Fig. 29.3, in which the two outer layers are thin enough to have little effect on manufacturing cost or fuel packing

²J. M. Robbins, H. Beutler, and R. L. Hamner, *GCR Program Semiann. Progr. Rept. Sept. 30, 1967*, ORNL-4200, pp. 4-25.

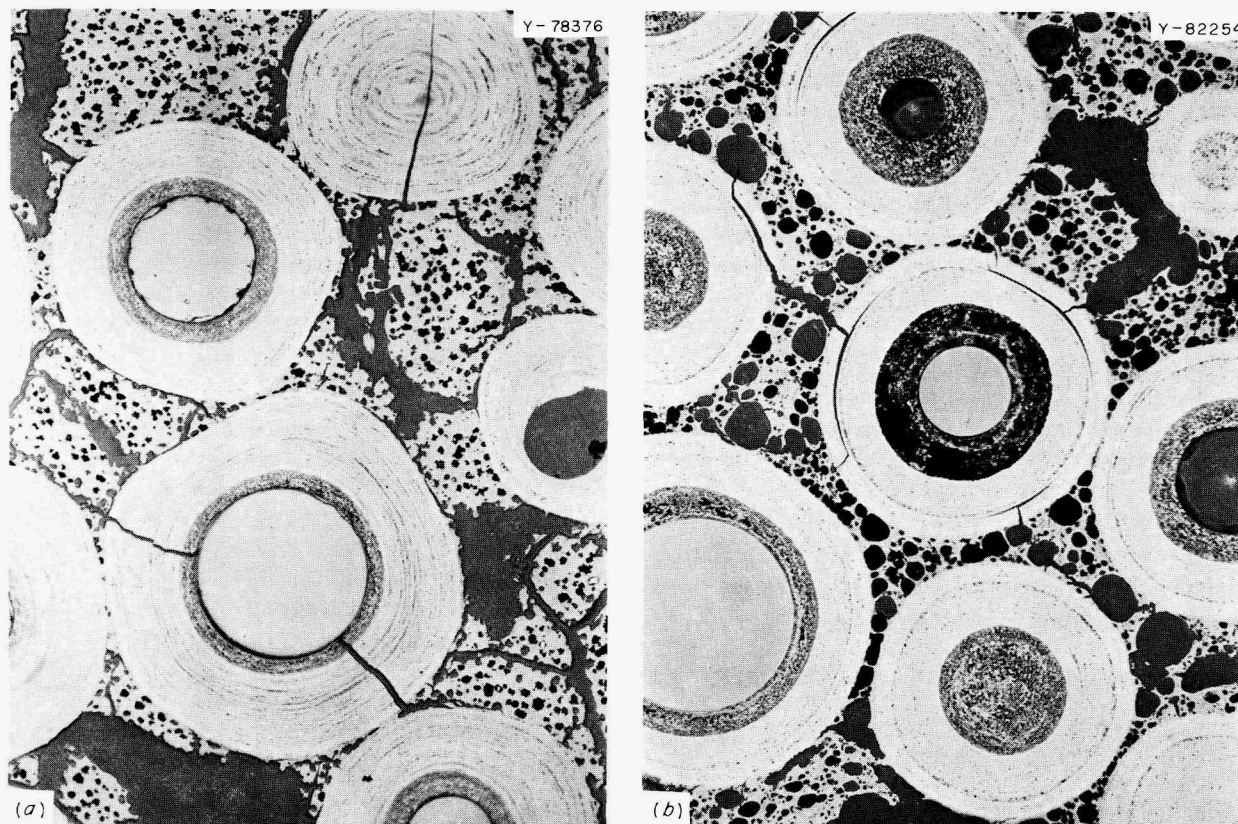


Fig. 29.2. Polished Sections of Bonded Fuel Sticks. 75X. (a) Cracks in bonding matrix propagate through some two-layer coatings. (b) Addition of nonbonding and sacrificial coating layers prevents cracking of base coatings.

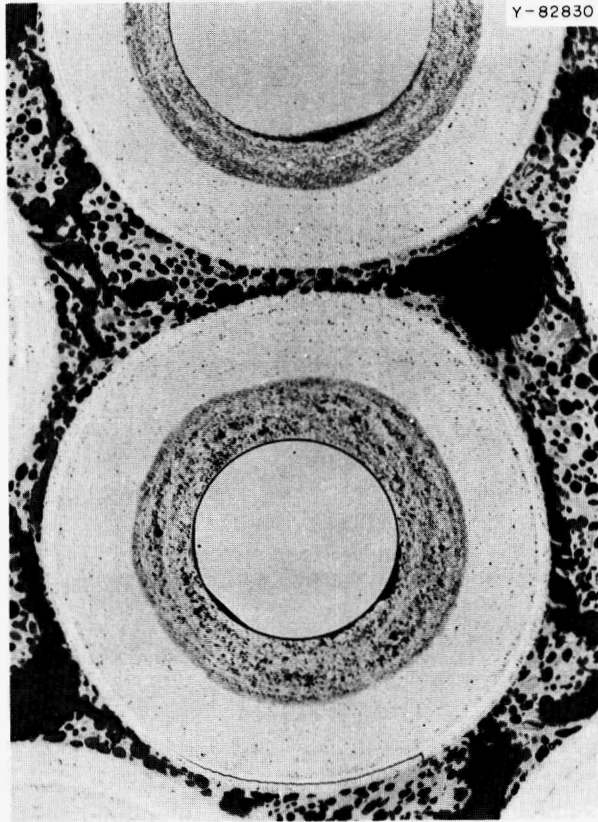


Fig. 29.3. Polished Section of Coated UO_2 Particles Having Thin Nonbonding and Sacrificial Layers and Bonded into Fuel Stick as for a Successful Irradiation Experiment. 145X.

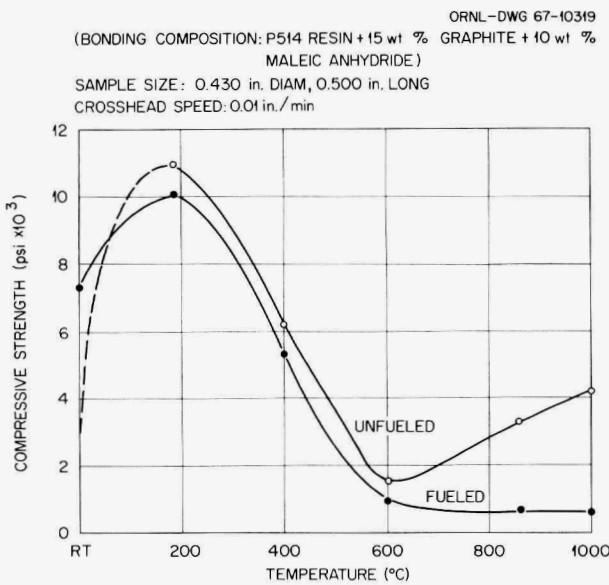


Fig. 29.4. Compressive Strength of Fueled and Unfueled Resin-Bonded Sticks After Various Heat Treatments.

density. Coated particles of the type shown in Fig. 29.3 were bonded into fuel sticks, and these have performed well in two sweep-capsule irradiation experiments at 1250°C to a fuel burnup exceeding 30%.

During the fabrication development we also studied the changes occurring in the bonded sticks during curing and carbonizing treatments and measured the effects of several modifications in manufacturing processes on their mechanical properties. The dimensions of bonded sticks change very little during heat treatment, but specimens consisting only of bonding material continued to shrink and lose weight up to 800°C . As shown in Fig. 29.4, the bonded sticks are strongest after heating at about 180°C , while completely carbonized sticks retain only 5 to 10% of their as-cured strength. Increases in curing time at 80°C and in the graphite content of the resin-base binder both appeared to increase the strength of carbonized sticks, but variations in injection procedures had little if any effect.²

SUPPRESSING INFILTRATION OF PYROLYTIC CARBON INTO POROUS BUFFER COATINGS DURING APPLICATION OF OUTER COATING LAYERS

H. Beutler¹

We have noted infiltration of pyrolytic carbon into porous buffer coatings during deposition of high-density isotropic outer layers at low temperature. In recent development work on large-scale application of coatings the carbon added to the porous coatings during the application of the outer coating filled 20 to 70% of the open porosity of the buffer layer.³ Such extensive infiltration is, of course, highly undesirable, since it drastically reduces the capacity of the porous coating for storing fission products. Neither metallography nor microradiography reveals infiltration of high-density pyrolytic carbon into buffer coatings. We always find a distinct interface between the porous buffer coating and the high-density outer layer. However, infiltration of pyrolytic carbon into porous buffer coatings is clearly evidenced by density calculations based either on carbon analyses and measurement of coated-particle dimensions or on carbon analyses and density measurements of outer coatings and entire coated particles. This infiltration was also confirmed in an experiment in which a porous alumina disk specimen was coated in propylene at 1250°C along with a batch of particles.

³W. H. Pechin, B. E. Foster, and S. D. Snyder, *Metals and Ceramics Div. Ann. Progr. Rept. June 30, 1967*, ORNL-4170, pp. 216-17.

Metallography revealed that carbon had infiltrated the entire 0.15-in.-thick specimen.

Since the infiltration of pyrolytic carbon into porous materials during the thermal decomposition of a hydrocarbon is strongly temperature dependent⁴ we investigated the possibility of reducing the infiltration by appropriate temperature control of the coating process. In two separate coating runs we applied high-density isotropic coatings on ThO₂ particles that had previously been coated with a 38- μ -thick buffer coating having a density of 0.80 g/cm³. The first coating experiment was carried out according to our standard application technique at a temperature of 1250°C. However, in the second experiment, we started the coating process at 1500°C, cooled the furnace rapidly (within 60 sec), and stabilized it at 1270°C during the remainder of the coating run.

We measured the density of the outer coating layer on coating fragments removed from disk specimens. From this, the carbon content, and the coated-particle density we calculated the density of the buffer coating after the application of the outer coating. We found that in our standard coating run the densities of the porous coatings increased from 0.80 to 1.20 g/cm³. Starting the coating experiment at a higher temperature (1500°C) successfully suppressed the infiltration of carbon into the porous coating, and the density in the buffer layer increased only insignificantly, from 0.80 to 0.85 g/cm³. The short high-temperature coating exposure did not affect the density of the outer coating. We conclude, therefore, that appropriate temperature control of the coating process can successfully prevent carbon infiltration.

IMPROVED COMPUTER PROGRAM FOR PREDICTING COATED-PARTICLE IRRADIATION BEHAVIOR

J. W. Prados⁵ T. G. Godfrey
J. L. Scott

In a series of papers⁶⁻¹⁰ we described a mathematical model and an associated computer program, STRETCH, for calculating the stress-strain history of a spherical pyrolytic carbon coating surrounding a fuel microsphere during irradiation. The stresses are produced by combined loading resulting from internal fission-gas pressure and fast-neutron damage to the pyrolytic-carbon structure. If we assume that failure will occur when some function of the stress-strain state in the

coating exceeds a critical value, the model can be used to predict the safe operating lifetime for a coated particle of given dimensions and properties irradiated in a given environment.

The early versions of these calculations⁶⁻⁸ incorporated the assumption of elastic behavior in the pyrolytic carbon coating. However, more recent experiments¹¹ demonstrated that pyrolytic carbon exhibits significant creep under fast-neutron irradiation even at low temperatures, and major modifications in our calculation procedures were required to permit a suitable representation of this inelastic behavior. The physical assumptions, working equations, and general computational strategy involved in predicting a coated particle's stress-strain-irradiation history were described in an earlier paper;¹⁰ however, the revised computer program incorporating the pyrolytic-carbon creep calculations had not been previously documented. We have now given instructions¹² for providing input data for these calculations, a listing of the computer program itself, and a sample of the output generated. The program is written in FORTRAN IV, H-Level, for the IBM System 360 computers;¹³ it should be adaptable with minor modification to other machines having FORTRAN-IV compilers.

⁴R. L. Bickerdike and W. Watts, Materials Laboratory, Royal Aircraft Establishment, Farnborough, England, unpublished research.

⁵Consultant from the University of Tennessee.

⁶J. W. Prados and J. L. Scott, *Analysis of Stress and Strain in Spherical Shells of Pyrolytic Carbon*, ORNL-3553 (June 1964).

⁷J. W. Prados and J. L. Scott, "Mathematical Model for Predicting Coated-Particle Behavior," *Nucl. Appl.* 2, 402-14 (1966).

⁸J. W. Prados, *A Computer Program for Predicting Coated-Particle Behavior*, ORNL-TM-1385 (March 1966).

⁹J. W. Prados, "Calculation of Creep in Spherical Pyrolytic-Carbon Shells Under Combined Radiation Damage and Internal Pressure," *Trans. Am. Nucl. Soc.* 9(2), 382-83 (1966).

¹⁰J. W. Prados and J. L. Scott, "The Influence of Pyrolytic-Carbon Creep on Coated-Particle Fuel Performance," *Nucl. Appl.* 3, 488-94 (1967).

¹¹R. J. Price and J. C. Bokros, "Mechanical Properties of Neutron-Irradiated Pyrolytic Carbons," *J. Nucl. Mater.* 21, 158-74 (1967).

¹²J. W. Prados and T. G. Godfrey, *STRETCH, A Computer Program for Predicting Coated-Particle Irradiation Behavior; Modification IV, December, 1967*, ORNL-TM-2127 (April 1968).

¹³*IBM System Library Manual, IBM System/360 FORTRAN IV Language, Form C28-6515-4*, IBM Corporation, White Plains, N.Y., 1966.

REVISED COMPARISON OF PREDICTED AND OBSERVED COATED-PARTICLE IRRADIATION PERFORMANCE

J. W. Prados⁵ T. G. Godfrey
A. R. Olsen

We recently developed improved techniques for calculating the influence of fast-neutron-induced dimensional changes and creep on coated-particle irradiation performance^{12,14} and applied them to revise our predictions of the burnups at failure for coated particles irradiated in ETR X-basket experiments 1 and 2. Comparisons between our earlier predictions and the observed irradiation performance of coated particles in these experiments were previously presented.^{15,16}

The properties and assumptions employed in our revised calculations were those used in the previous comparisons, with the following exceptions: (1) the coating rupture criterion was taken as an "effective creep stress"^{12,14} of 60,000 psi rather than a tangential tensile stress of 30,000 psi, (2) the release of fission gas from the kernels of particles irradiated at the low temperatures (nominally 400°C) was taken as 10% rather than 100%, (3) the irradiation creep coefficient

was decreased from 1.5×10^{-27} to 1.0×10^{-27} psi^{-1} $(\text{neutrons}/\text{cm}^2)^{-1}$ (>0.18 Mev), and (4) densification of outer coatings in accordance with the Bokros-Schwartz model¹⁷ was incorporated into the calculations. The revised predictions are compared with experimental results in Table 29.1 and Fig. 29.5. In general, the agreement between observed and predicted failures has been significantly improved, although several batches that survived the irradiation were still predicted to fail. As previously reported,¹⁵ particles with granular outer coatings most frequently exhibited this anomaly; apparently the properties we have assumed for the granular coatings are conservative.

¹⁴J. W. Prados and T. G. Godfrey, "Improved Method for Calculating Creep of Spherical, Anisotropic Pyrolytic-Carbon Coatings," *GCR Program Semiann. Progr. Rept. Mar. 31, 1968*, ORNL-4266 (in press).

¹⁵J. H. Coobs *et al.*, *GCR Program Semiann. Progr. Rept. Sept. 30, 1967*, ORNL-4200, pp. 37-46.

¹⁶J. H. Coobs *et al.*, *GCR Program Semiann. Progr. Rept. Sept. 30, 1966*, ORNL-4036, pp. 31-45.

¹⁷J. C. Bokros and A. S. Schwartz, "A Model to Describe Neutron-Induced Dimensional Changes in Pyrolytic Carbon," *Carbon* 5, 481-92, (1967).

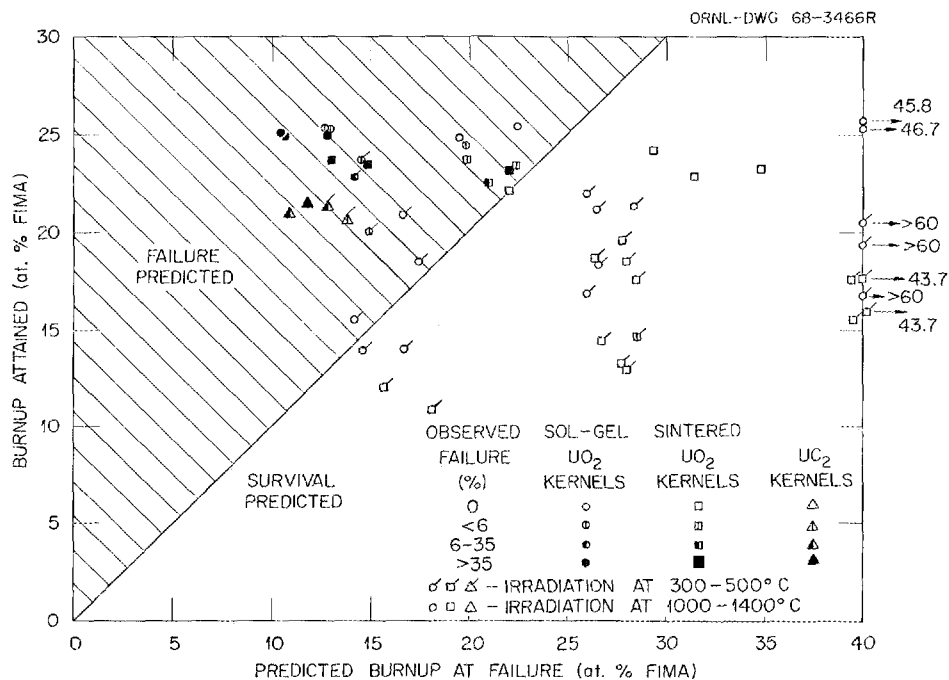


Fig. 29.5. Comparison of Observed and Predicted Performance of Pyrolytic-Carbon-Coated Particles Irradiated in ETR X-Basket Experiments 1 and 2.

Table 29.1. Performance Comparison of X-Basket 1 and 2 Coated Particles^a

X-Basket 1						X-Basket 2						
Lot	Type of Coating, ^b Inner/Outer	Nominal Temperature ^c (°C)	Burnup Attained (%)	Predicted Burnup at Failure (%)	Particle Failures (%)	Lot	Type of Coating, ^b Inner/Outer	Nominal Temperature ^c (°C)	Burnup Attained (%)	Predicted Burnup at Failure (%)	Particle Failures (%)	
Sintered Oxide						Sol-Gel Oxide						
OR-339	L/G	400	10.8	18.1	0	YZ-60	L/G	400	18.5	17.4	0	
		1000	23.3	14.8	87			1400	25.3	13.0	1	
OR-341	L/G	400	17.5	28.6	0							
		1000	23.3	22.5	5							
		400	14.6	28.6	1							
OR-342	L/I	400	18.5	28.0	0	YZ-47	L/I	400	21.3	28.3	0	
		1000	23.1	22.2	39			1400	25.4	22.5	0	
		400	12.9	28.0	0							
OR-343	I/I	400	14.4	26.7	0	YZ-56	I/I	400	16.8	26.1	0	
		1000	22.5	21.0	17			1400	24.5	19.9	4	
		400	18.5	26.7	0			400	22.0	26.1	0	
OR-344	I/G	400	13.2	27.8	0	YZ-57	I/G	400	18.3	26.6	0	
		1000	22.1	21.9	0			1400	24.8	19.6	0	
		400	19.6	27.8	0			400	21.1	26.6	0	
OR-348	P/L	400	15.5	39.5	0	YZP-29	P/L	400	20.4	>60	0	
		1000	22.9	31.4	0			1400	25.3	46.7	0	
		400	17.4	39.5	0			400	16.6	>60	0	
OR-349	L/I	400	12.0	15.7	0	YZ-66	L/I	400	20.0	15.0	<1	
		1000	23.6	13.0	100			1400	25.1	13.0	70	
OR-354	P/I	400	16.6	43.8	0	YZP-28	P/I	400	19.3	>60	0	
		1000	23.2	34.8	0			1400	25.4	45.8	0	
		400	15.9	43.8	0							
					YZ-54 ^d	L/G	400	21.8	16.7	0		
							1400	25.4	12.7	1		
							400	14.0	16.7	0		
Carbide Particles						Control Samples of Sintered Oxide						
OR-352	P/I	400	20.6	13.9 ^e	2	OR-343	I/I	1400	23.7	19.9	1	
		1000	21.5	11.9 ^e	42			OR-348	P/L	1400	24.2	29.3
OR-357	P/G	400	21.3	12.9 ^e	30							
		1000	20.9	10.9 ^e	30							
						Additional Samples of Sol-Gel Oxide						
						YZ-58	L/I	400	15.5	14.2	0	
									1400	24.9	10.7	66
									400	22.8	14.2	25
						YZ-45	L/I	400	13.9	14.6	0	
									1400	25.1	10.5	100
									400	23.5	14.6	3

^aFor easy comparison, samples in the two experiments with similar coating type and particle size are listed in the same line.

^bCoating designation: L – laminar; G – granular; I – isotropic; P – porous.

^cActual irradiation temperatures are estimated to have ranged from 300 to 500°C in the low-temperature compartments and from 1000 to 1400°C in the high-temperature compartments. Nominal values reported are estimates of average temperatures prevailing over the major portion of the irradiation.

^dCorresponds to OR-339.

^eCalculated value based on minimum measured inner-layer thickness.

HIGH-TEMPERATURE FAST-NEUTRON IRRADIATION OF PYROLYTIC-CARBON-COATED ThO₂ MICROSPHERES^{1,8}

D. M. Hewette

Fast-neutron irradiation of pyrolytic carbon may produce either densification or dilation as a result of expansion in the *c* direction and contraction in the *a* direction of the individual crystallites that make up the

structure. These effects can lead to severe stress within the coatings of fuel particles used in high-temperature gas-cooled reactors and to premature failure of the coatings.

To better understand these phenomena, we irradiated four sets of pyrolytic-carbon-coated ThO₂ microspheres in the Dounreay Fast Reactor at fluences up to 4.5×10^{21} neutrons/cm² (>0.18 Mev) at temperatures near 1150°C. The coatings were carefully characterized before irradiation. The inner coatings were porous and had a density of about 0.7 g/cm³. The outer coatings all had high densities in the range 1.74 to 2.07 g/cm³, Bacon anisotropy factors (BAF) in the range 1.0 to 1.4,

^{1,8}Summary of a report in preparation.

PHOTO 91367

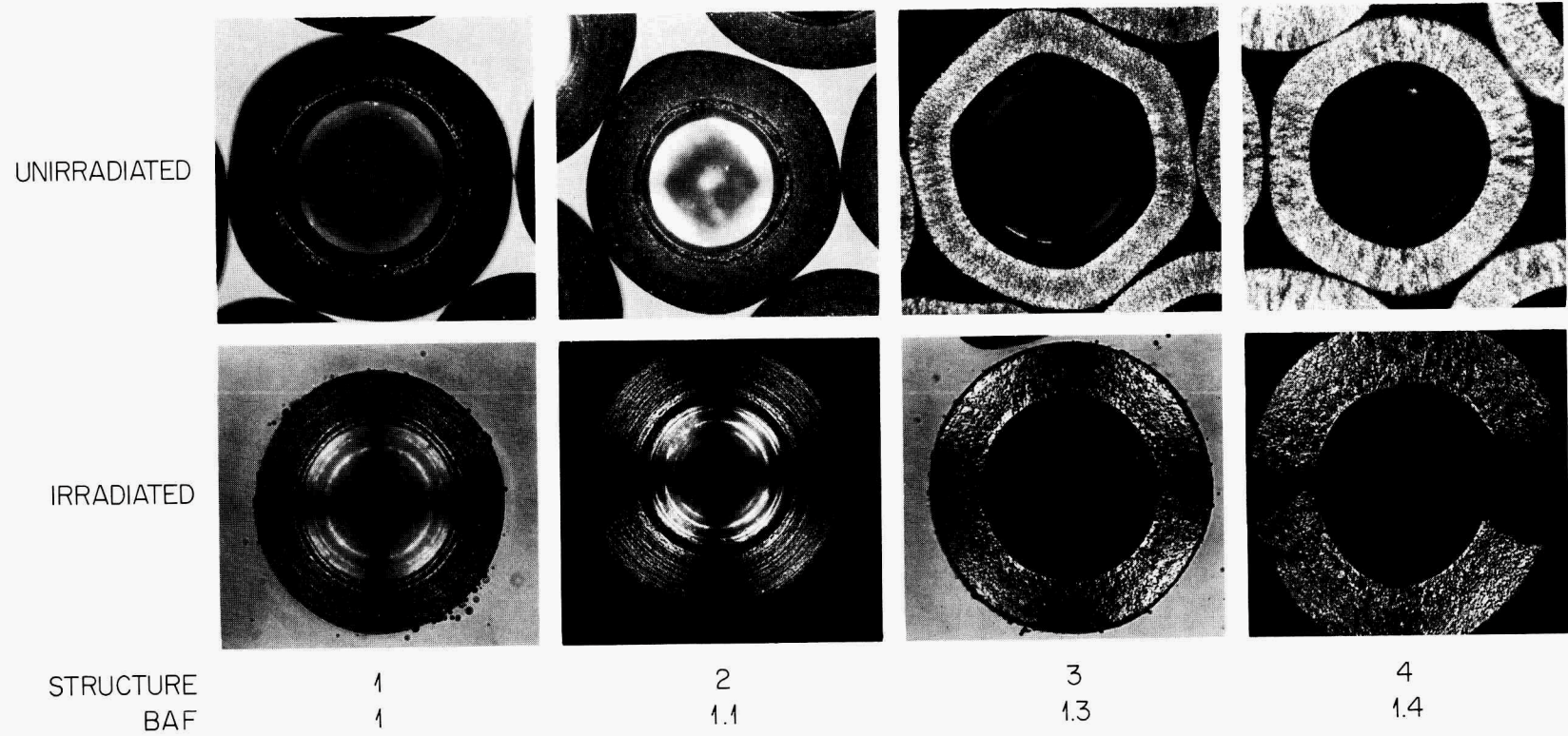


Fig. 29.6. Effect on Pyrolytic Carbon Coatings of Fast-Neutron Irradiation at 1200°C to a Fluence of 4.5×10^{21} Neutrons/cm² (>0.18 Mev.).

and apparent crystallite sizes ranging from 110 to 150 Å.

We found that the coatings with the highest anisotropy factor failed during irradiation, whereas all others were intact. Since there was virtually no burnup in the ThO_2 , we attribute failure to the effects of fast-neutron irradiation. As shown in Fig. 29.6, metallographic examination of the coatings revealed that the preferred orientation of the coatings increased if the starting densities were less than 1.9 g/cm^3 . This is evidenced by the appearance of the Maltese cross¹⁹ in the irradiated coatings of structures 1 and 2. Apparently the amount of increase in preferred orientation is dependent upon the initial preferred orientation, since structure 2, which had a higher initial BAF, shows a more intense Maltese cross. Structures 3 and 4 were anisotropic granular structures, but because of the fineness of the as-deposited granular structure the Maltese cross is obscured in the unirradiated structures. The texture of both granular specimens was coarsened during irradiation. As a result, after irradiation a Maltese cross is apparent in the outer layer of structure 3. This Maltese cross does not seem as sharp as would be expected for a

structure with an initial BAF of 1.3. The outer layer of structure 4 exhibits only a very faint Maltese cross, indicating that irradiation may have decreased its preferred orientation.

We determined the irradiation-induced density changes for the four coating types by measuring densities of fragments of the outer layers. These results are shown in Fig. 29.7 along with results obtained from disk coatings irradiated in the same experiment by Delle and Stöcker.²⁰ We see that if the initial density is 1.82 g/cm^3 or less the pyrolytic carbons densify, but if the density is greater than 1.9 they swell. Apparently as the carbons densify the preferred orientation increases.

CONCRETE FOR PRESTRESSED CONCRETE REACTOR PRESSURE VESSELS

G. Stradley L. A. Harris
J. P. Moore

The time-dependent deformation behavior and the strength of concrete as affected by the operating environment are among the most important aspects of the design and safety evaluation of a prestressed concrete reactor vessel (PCRV). The time-dependent deformation behavior or creep and shrinkage are being determined for each of three different portland cement concretes by the Waterways Experiment Station and The University of Texas. We are characterizing the three concretes and their individual constituents so that the time-dependent deformation behavior will be more meaningful. These studies are a portion of a larger program²¹ to provide information to assess the long-range performance and safety of PCRV structure.

Three different types of aggregate – limestone, graywacke, and chert – are being used with the same type II portland cement to produce the three concretes under study. We are characterizing the aggregates by properties such as size, shape, surface roughness, mineralogical class, and chemical composition, using techniques such as x-ray diffraction, chemical analysis, petrographic examination, differential thermal analysis (DTA), thermal gravimetric analysis (TGA), and screen analysis. We are also determining such properties of the

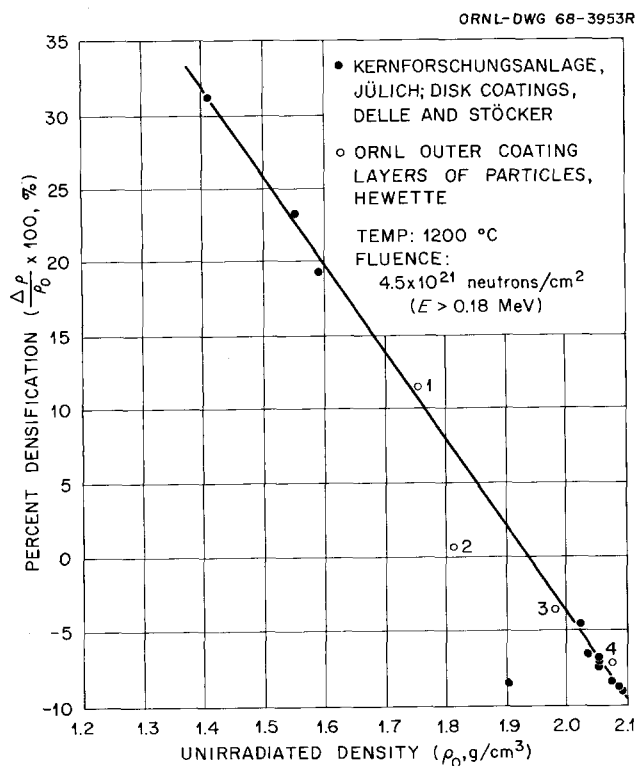


Fig. 29.7. Densification of Pyrolytic Carbon During High-Temperature Fast-Neutron Irradiation. The numbers refer to the structure types in Fig. 29.6.

¹⁹R. J. Gray and J. V. Cathcart, *J. Nucl. Mater.* 19, 81–89 (1966).

²⁰W. Delle and H. J. Stöcker, "Results of High-Temperature Irradiation of Graphite and Pyrolytic Carbon in the Dounreay Fast Reactor, Scotland," Paper from the Conference of the Working Committee on Carbon of the German Ceramic Society held on October 13, 1967 in Basel, Switzerland.

²¹G. D. Whitman, *GCR Program Semiann. Progr. Rept. Sept. 30, 1967*, ORNL-4200, p. 166.

aggregates as strength, modulus of elasticity, Poisson's ratio, and coefficient of thermal expansion. This has required the establishment of standards for the x-ray diffraction phase and the development of techniques for making thin sections for petrographic examination.

The type II portland cement is being characterized by many of the above techniques, such as chemical analysis, x-ray diffraction, DTA, and TGA. Properties such as specific surface area, strength, modulus of elasticity, Poisson's ratio, and coefficient of thermal expansion are being measured.

The three concrete mixes were designed by the Waterways Experiment Station to achieve a compressive strength of 6000 psi at the age of 28 days. We are characterizing the limestone, graywacke, and chert concretes at various ages by determining their compressive and splitting tensile strengths, Poisson's ratios, and moduli of elasticity. The coefficients of thermal expansion and the thermal conductivities of the three concretes are being measured as functions of age and moisture content. An apparatus was designed and built for measuring the coefficient of thermal expansion of concrete from room temperature to 350°F (177°C). A radial heat-flow device was constructed for measuring the thermal conductivity of concrete from room temperature to 400°F (200°C). Initial results for the characterization of the concretes and the individual constituents have been reported.²²

Being able to maintain a constant amount of moisture or moisture level in a specimen of hardened concrete and being able to establish nondestructively the amount of moisture present at that level are very important factors in a study on concrete because of the significant effect of moisture on many properties of concrete. We investigated the use of organic coatings to provide a positive seal for maintaining a constant moisture level in specimens. We concluded²¹ that organic coatings alone were not satisfactory. A specimen must be contained in a metal jacket to absolutely prevent the loss of moisture from it.

We reviewed²² the various methods and means of nondestructively measuring the amount of moisture present in hardened concrete. These methods include the measurement of changes in various electrical properties, neutron- or gamma-radiation scatter and absorption, and microwave attenuation due to changes in the moisture content of the hardened concrete. We are employing the neutron scatter and absorption technique in our study.

²²J. G. Stradley, *GCR Program Semiann. Progr. Rept. March 31, 1968*, ORNL-4266 (in press).

PROPERTIES OF NICKEL ALLOY WELDMENTS FOR ADVANCED HTGR STEAM GENERATORS

J. P. Hammond

We are evaluating welds in conventional and advanced alloys for HTGR steam generator applications, especially for the critical superheater and reheater sections. Because economy dictates the use of a variety of alloys in the same component, emphasis in our program is focused on dissimilar-metal welds. These welds must have good resistance to high-temperature steam corrosion as well as adequate strength consistent with good ductility and structural stability.

The alloy combinations presently under investigation are listed in Table 29.2 in the order of their expected elevated-temperature strength. Inert gas shielded tungsten-arc welds were made on 1/2-in.-thick plate with "V" bevels and 5/32-in.-diam filler wire. In addition to compatibility tests with steam from 1100 to 1400°F, weldability, stress-corrosion cracking susceptibility at 1100°F, and stress-rupture properties will be determined.

A subcontract was let with Southern Nuclear Engineering Company, Dunedin, Florida, to provide facilities and engineering services for the steam-corrosion work. Steam taken directly from lines of the Bartow Plant of the Florida Power Corporation flows past specimens at about 5 ft/sec and 900 psig pressure. Ten of the alloy combinations in Table 29.2 are scheduled to complete 3000-hr autoclave exposures at 1100 and 1200°F in late July 1968.

Table 29.2. Alloy Combinations for Steam Generators

Alloy Code	Base Metal	Base Metal	Filler Metal
A9	Inconel 625	Inconel 625	Inconel 625
A13	Inconel 625	Incoloy 800	Inconel 625
A12	Inconel 625	Incoloy 800	Inconel 82
A18	IN 102	IN 102	IN 102
A19	IN 102	Incoloy 800	IN 102
A20	IN 102	Incoloy 800	Inconel 82
A5	Hastelloy X	Hastelloy X	Hastelloy X
A6	Hastelloy X	Incoloy 800	Hastelloy X
A8	Hastelloy X	Incoloy 800	Hastelloy W
A7	Hastelloy X	Incoloy 800	Inconel 82
A2	Incoloy 800	Incoloy 800	Inconel 82
A14	Inconel 600	Inconel 600	Inconel 62
A3	Inconel 600	Inconel 600	Inconel 82
A16	2-1/4 Cr-1 Mo	Incoloy 800	Inconel 82
A4	Type 304 stainless steel	Type 304 stainless steel	Type 308 stainless steel

Average general corrosion rates and kinetics of scaling attack will be established in the separate regions of interest of weldments by scale-thickening measurements. Tensile and creep properties and fracture duc-

tilities will be established on weldments after steam exposure, and these will be compared with values obtained for the as-welded and welded-and-aged condition.

30. Heavy Section Steel Technology

D. A. Canonico

Nuclear power stations now being built require pressure vessels of sizes (diameters and thicknesses) that are at the forefront of or are beyond the service experience of plate manufacturers and vessel fabricators. Fracture modes of these vessels are of special interest because of the dangers peculiar to nuclear reactors, should a major failure of a pressure vessel occur. The Heavy Section Steel Technology (HSST) Program is an engineering effort begun to study the structural behavior of the thick plates and vessels needed for large reactors, with emphasis on the effects of flaws, inhomogeneities, and discontinuities under in-service operating and accident conditions. A responsibility of the program is to monitor and evaluate research efforts sponsored by industry in nondestructive and in-service inspections and to recommend and perform, if necessary, work that will assure that results obtained are practically applicable. Extensive property testing programs, including transition temperature and fracture behavior of current pressure vessel steels, will be performed on thick-section plates, weldments, and forgings. The program culminates in simulated service tests with full-thickness, full-sized pressure vessels. Results of the program will be directly applicable to the needs of the nuclear power industry and should influence significantly the codes and standards for fabrication, inspection, and operation of such vessels.

The participation of the Metals and Ceramics Division in this program is as both consultants and experimentalists. First, we have the responsibility of serving on the staff of the Program Office as metallurgical consultants. Within this framework, we are expected to contribute to decisions that require a metallurgical background and to assist in the preparation of pertinent publications. In addition, we are involved experimentally in those tasks that require the experience and facilities available within the Division.

During the past year, *Technology of Steel Pressure Vessels for Water-Cooled Nuclear Reactors* was published. We contributed to four chapters.¹⁻⁴ This document is a state-of-the-art review of the light-water nuclear pressure vessel technology and has, for all

practical purposes, become a handbook for the industry.

As an example of our experimental commitment, we have investigated the effect of flame-cutting on the steel base metal. There has been much conjecture regarding the depth of the heat-affected zone (HAZ) due to flame cutting. Heat-affected-zone depths ranging from essentially zero to 4 in. have been estimated by those working actively in the field; however, to our knowledge, no definitive data were available to support these claims. A sizable economic justification exists for establishing the depth of the HAZ since the ASME Boiler Code (Section III) requires that the mechanical properties be determined for plate materials that are used in the fabrication of nuclear pressure vessels. If the HAZ depth is in excess of 0.5 in., considerable machining would be required during sample preparation to assure that the properties of the HAZ do not oppose the actual values. Thus, a limited study was undertaken to determine the actual depth resulting from a typical commercial flame-cutting operation.

Material was obtained from ASTM A533, Grade B, Clad I-plates purchased for the HSST Program. These plates were rolled to 12-in. thickness and subsequently flame cut to 20 × 10 ft. After cutting, the plates were normalized, austenitized, quenched, tempered, and stress relieved for 40 hr at 1150°F. The material used for this study was obtained from the flame-cut edges of the plates.

The macroscopic contour of the HAZ across the 12-in. thickness and the microstructure of the HAZ at the quarter-thickness position (3 in. below the surface) are shown in Fig. 30.1. We found that the depth of the

¹D. A. Canonico, P. Patriarca, and G. C. Robinson, Jr., "Materials," Chap. 4 in *Technology of Steel Pressure Vessels for Water-Cooled Nuclear Reactors*, ORNL-NSIC-21 (December 1967).

²R. G. Berggren, D. A. Canonico, J. L. English, and P. Patriarca, "Effect of Environment on Materials," Chap. 5, *ibid.*

³D. A. Canonico, R. W. McClung, E. C. Miller, S. E. Moore, and P. Patriarca, "Quality Assurance," Chap. 9, *ibid.*

⁴R. G. Berggren, R. W. McClung, and E. C. Miller, "Testing and Service Performance Surveillance," Chap. 10, *ibid.*

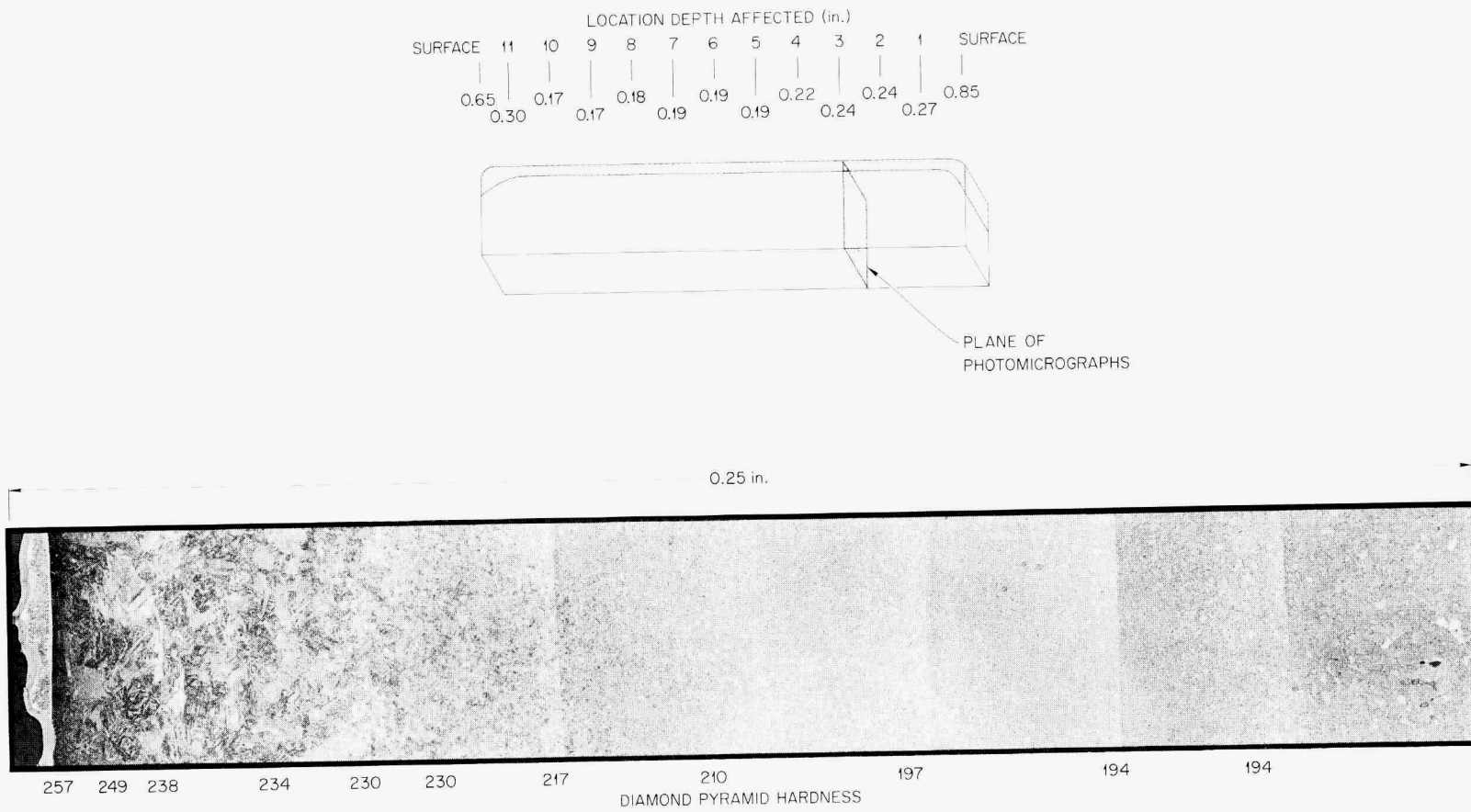


Fig. 30.1. Variation of Microstructure of a 12-in.-Thick Plate with Distance from a Flame-Cut Edge.

Y-86784

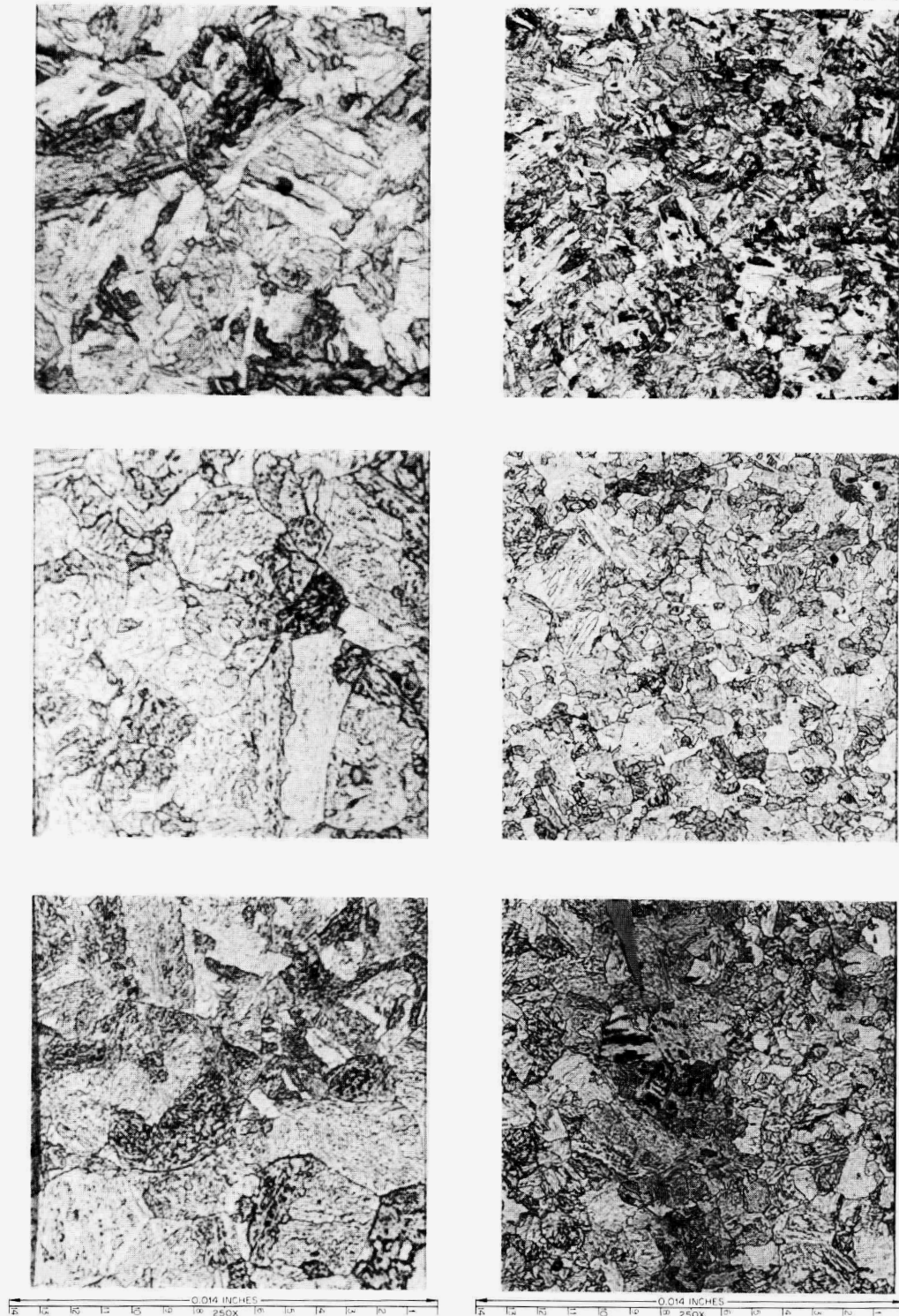


Fig. 30.2. Microstructures of HSST Plate 1 at Various Locations and Two Magnifications. Top, surface; middle, quarter thickness; bottom, midthickness.

HAZ at the plate surfaces approached 3/4 to 1 in. This depth dropped rapidly to between 3/16 and 1/4 in. The microstructure is typical of a weld heat-affected zone; that is, it contains the grain-coarsened region adjacent to the fusion line, which gradually blends into a fine-grained region, which in turn blends into the unaffected base metal.

The results of this study show that the depth of the HAZ is minimal (maximum of about 1/4 in. if the surface effects are ignored). It need not be considered in normal specimen or weld-joint preparations since the conventional machining practices will remove more than this amount.

We also investigated the microstructures that prevail at various depths in the heat-treated HSST plate 1. Fortunately, both an isothermal transformation diagram (IT) (for a composition quite similar to A533, Grade B) and the measured time-temperature cooling data for HSST plate 2 were available to aid in the interpretation. Since the continuous transformation relationships can be inferred from the IT diagram, the

microstructures appeared to be wholly bainitic. The surface of the plate, due to its faster cooling rate (approx 6°F/sec), contained a finer bainite (lower transformation product) than the quarter-thickness and midthickness locations (both of which cooled at a rate of about 0.5°F/sec). Figure 30.2 compares the microstructures that were present at the three locations cited above. The difference in microstructure was reflected in the notch toughness (-80 vs +20°F for the drop-weight nil-ductility transition temperature) and in the strength (85,000 vs 70,000 psi yield). In fact, the plate possessed nearly identical microstructures and mechanical properties across its entire 9-in. center portion.

The response of the 12-in.-thick ASTM A533, Grade B plate to the quench-and-temper heat treatment was indeed gratifying. Although the plate was heat treated to meet the ASTM Class I requirements (minimum 50,000 psi yield strength), the actual tensile properties at the quarter-thickness location will satisfy the Class II requirements (minimum yield strength of 70,000 psi).

31. High Flux Isotope Reactor Materials Development

G. M. Adamson, Jr.

The High Flux Isotope Reactor (HFIR) is being operated by ORNL for the production of research quantities of transplutonium elements. The efforts in the Metals and Ceramics Division are aimed at following the fuel element procurement, in the development of improved fuel elements and control rods, and in the development and fabrication of the isotope targets.

The reactor has now used 21 fuel assemblies, with an average core lifetime of 2296 Mwd. No operating difficulties were encountered with any of these elements. While the fuel element performance to date has been outstanding, there is considerable economic incentive to reduce cost by achieving longer operating cycles. Consequently, the present limited materials effort is directed toward achieving a higher fuel loading with as few changes as possible in the present element. Until it is shown to be unsatisfactory, the prime effort will continue with the U_3O_8 dispersion.

This development program is integrated with other work on the development of dispersion fuel plates discussed in Part III, Chapter 20 and in Chapter 28. Target fabrication is reported in Chapter 32.

HFIR FUEL ELEMENT MANUFACTURE

R. W. Knight

Assistance to Metals and Controls, Incorporated,¹ the production contractor for the HFIR fuel elements, has continued throughout the past year. Several changes have been made in the production procedure to increase reliability and reduce cost. In May 1968, the final fuel element on the second contract was shipped to ORNL on the predicted schedule. Work is continuing at M and C on a new contract.

None of the 60 fuel assemblies delivered to date has met all the specifications; in fact, only 18 inner elements and one outer element have met specifications. However, after an ORNL review of the deviations, all elements have been accepted for use at design

¹A division of Texas Instruments, Incorporated, Attleboro, Mass.

Table 31.1. Total Fuel Element Rejections by Groups

Group	Type	Numbers	Elements with Deviations	Total Deviations
1	Outer	1-12	12	88
	Inner		11	48
2	Outer	13-24	12	74
	Inner		12	35
3	Outer	25-36	12	92
	Inner		9	13
4	Outer	37-48	12	37
	Inner		7	18
5	Outer	49-60	11	35
	Inner		2	2

power. As shown by Table 31.1, in which the elements have been placed in groups of 12, each representing a six-month production period, a marked increase in the number of acceptable elements has been occurring with time; the improvement also is obvious in the decreasing number of deviations. The cause of the deviations is shown graphically in Fig. 31.1. The waivers have resulted for a wide variety of causes. All items in the specifications have been met with a reasonable frequency; only a few items have appeared on the reject list with sufficient frequency to warrant changes in the specifications, and none of these changes have been major. As in previous years, the two largest causes of rejects are the related quantities, diameter and wall thickness. After the high rejection for wall thickness in group 4, the procedures were modified by adding a third stretching ring at the midplane; the change was obviously effective. While waiver values are shown for overpenetration and channel spacing, all elements accepted have been repaired so all of these attributes are within specifications.

The fuel plate yields for plates in groups of approximately 5000 are presented in Fig. 31.2. These results, although favorable, do not show the improvement found with the elements but are quite erratic. They indicate that fuel plate recoveries are very close to the

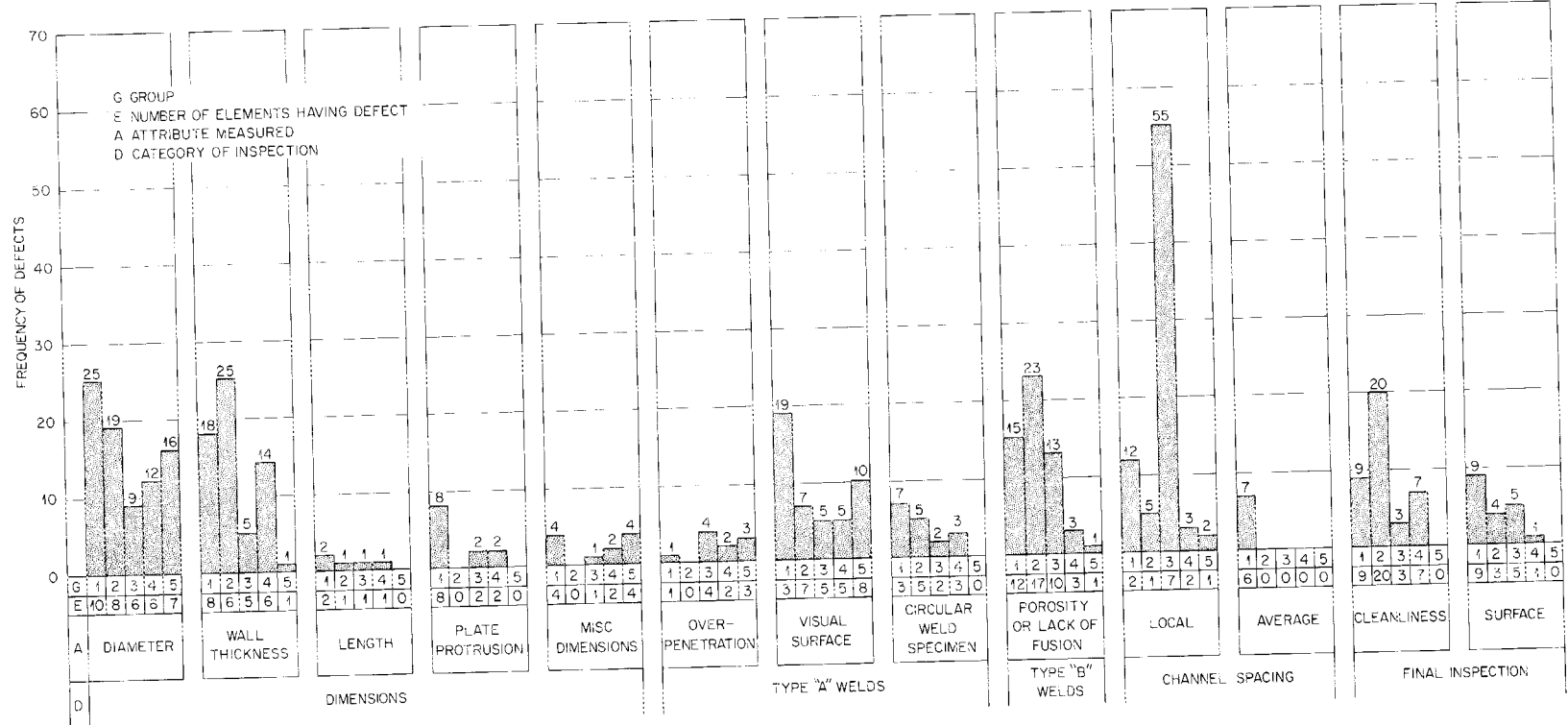


Fig. 31.1. HFIR Fuel Element Waivers.

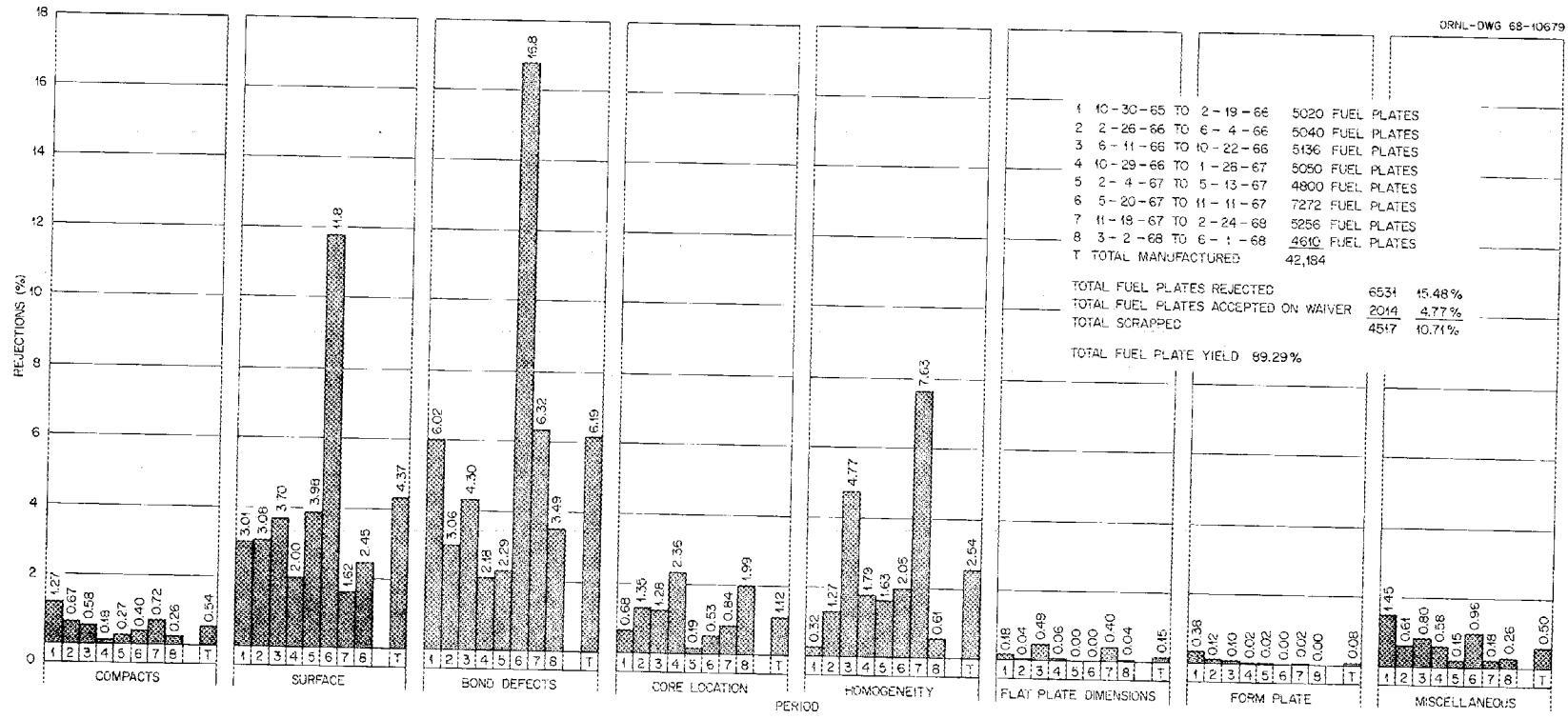


Fig. 31.2. HFIR Fuel Plate Rejections.

present technical limits of manufacturing, and a small change in processing can cause a significant fluctuation. The reject rates for the three periods during this year are 20.1, 9.99, and 4.84%, and the total reject rate for the 42,184 plates is 10.71%. Significant excursions during this period are apparent in surface condition, bond defects, and homogeneity. The excursions in surface and bond defects were associated with a single cause. These plates exhibited a slightly roughened surface, which, when examined metallographically, revealed very small surface blisters approximately 0.005 in. in diameter and 0.0025 in. deep and an indication in other areas of grain-boundary melting. Analysis of the alloy in the area of the surface blister revealed an increase in magnesium content, indicating the possibility of eutectic melting. With this in mind, the hot-bonding temperature and annealing temperature were reduced to 485°C and the blister rate went back to normal. The fuel plates exhibiting the slightly roughened surface without blisters were used in a special fuel element, which has been used in the reactor without problems. The increase in homogeneity rejections in group 7 was associated with an operator bias. The operator was retrained and the rejections were reduced.

Previously we had encountered raw material differences that affect production.² Since there has now been a complete turnover of material, the effects of these differences can be reported.

The aluminum powder used in the core varies from batch to batch in particle size and shape. This requires changes in pressing pressures between 22.5 and 30 tsi to obtain equivalent compact densities. No variation is encountered within a batch.

Batch-to-batch differences in frame and cover plate stock are reflected in the formability of the fuel plate and in the longitudinal shrinkage of side plate 4 which, with the new material, has increased 1/16 in. The production effect of these material variables is significant; however, in each case, manufacturing adjustments have been made and losses have been held to nearly zero.

Approximately 400 kg of U₃O₈ have been manufactured this year to provide material for continuing production of fuel elements. All tube stock, alclad plate, and sheet have been manufactured and received for the contract extension of 108 fuel assemblies.

POSTIRRADIATION EXAMINATION OF HFIR FUEL ELEMENTS

R. W. Knight A. E. Richt

A postoperation examination was made of fuel assembly 5 in the High Radiation Level Examination Laboratory. To maintain the fuel plate temperatures below the operating temperature, it was necessary to cool the elements in the vertical position in the HFIR pool for a period of about one year.

Both a dimensional and a metallographic examination were made. Figure 31.3 shows top and side views of the outer-annulus element. The side plates exhibited an oxide coating but no oxide spalling. The upper end view shows no fuel plate distortion. Figure 31.4 shows the lower end of the inner element. Partial blockage of some of the channels is evident; this blockage was attributed to oxide that had spalled off the fuel plates during storage in the HFIR spent-fuel pit. This material was very loosely attached and was easily removed for analysis. An analysis showed the material to be aluminum oxide.

Length and diameters were measured to determine the fuel element stability. All dimensions taken were essentially the same as the as-manufactured dimensions and within the original tolerances except the outside diameters at the horizontal midplane of the elements, which increased 0.009 and 0.008 in. for the outer and inner annuli, respectively. Some increase was expected because this is the area of the first welds during manufacture, the area of maximum shrinkage and stress, and the area where during final machining a considerable volume of material was removed. The fuel elements then operate at a temperature high enough to allow stress relief. Channel-spacing was measured for every tenth channel. Although measuring difficulties were encountered, no channels were out of specification. All channels were also viewed with back lighting and appeared to be in excellent condition.

Four complete fuel plates were removed from the outer fuel element for detailed examination. No visual evidence of blisters or distortion was observed. Gamma scanning indicated that the burnup distribution within the fuel plates was quite close to the predicted profiles. As shown in Fig. 31.5, some spalling of the corrosion-product film had occurred in the higher temperature regions of the individual fuel plates. As expected, the oxide film varied in thickness over the plate surfaces, ranging from 0.0005 in. thick over the low-temperature regions of the plates to 0.0020 in. thick immediately adjacent to the spalled region. These film thicknesses

²R. W. Knight, *Metals and Ceramics Div. Ann. Progr. Rept.* June 30, 1967, ORNL-4170, pp. 173-75.

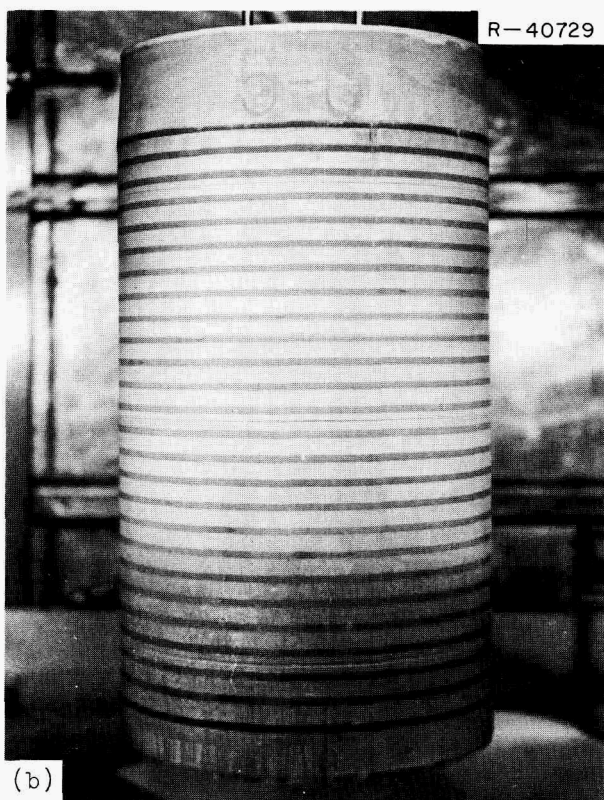
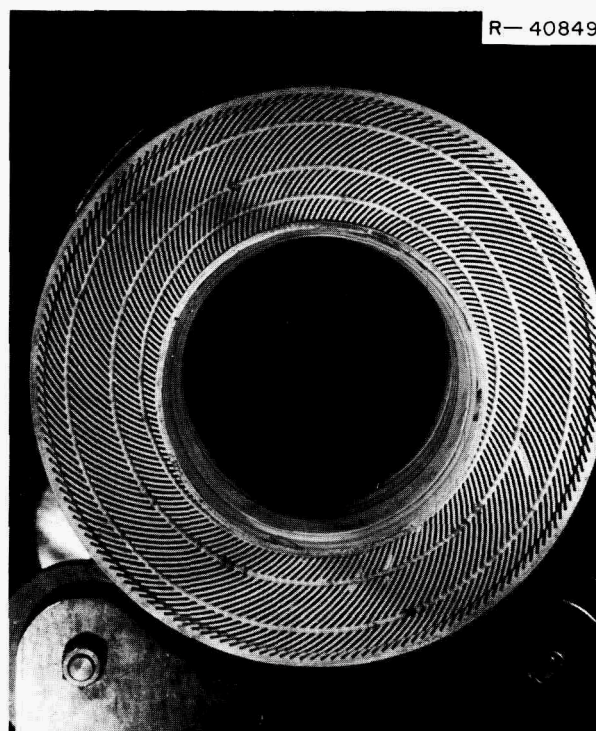
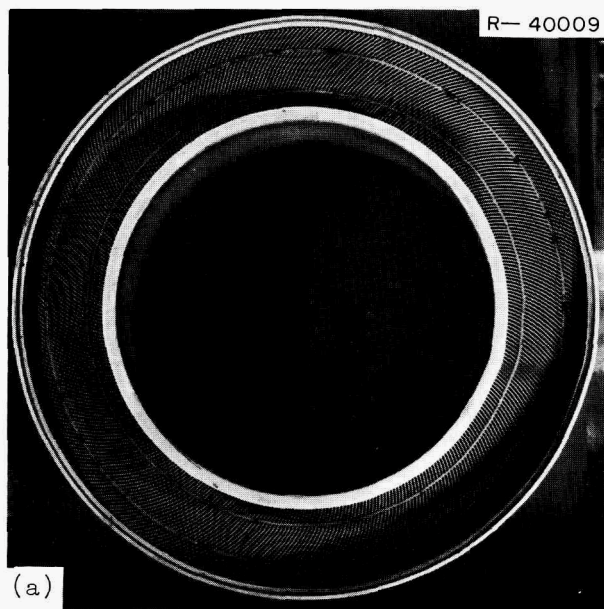


Fig. 31.3. Typical Appearance of HFIR Outer-Annulus Fuel Element. (a) Top view. (b) Side view.

Fig. 31.4. Bottom View of HFIR Inner-Annulus Fuel Element. Note partial blockage of coolant channels by white deposit.

are two to three times greater than that expected from reactor service. However, the oxide film undoubtedly increased significantly in thickness during the cooling period, since, at least initially, the temperatures approached operating temperatures.

Metallographic examination of sections of the fuel plates revealed no evidence of blistering, core-cladding separation, or fuel breakup. No incipient cracks were found at the corners of the particles where failure usually starts. Corrosion of the cladding did not appear to be excessive; we estimate that less than 0.0015 in. of the normally 0.010-in.-thick cladding was lost to corrosion. Even in areas of high burnup, the increase in core thickness was less than 0.001 in. Typical examples of the microstructure of the fuel plates are shown in Fig. 31.6. To our knowledge, these are the first photomicrographs of an aluminum-base fuel material that clearly show the fission-product-recoil damage zone surrounding the individual fuel particles. We also observed considerable variation in the extent of reaction between the U_3O_8 particles and the aluminum matrix material in different regions of the HFIR fuel

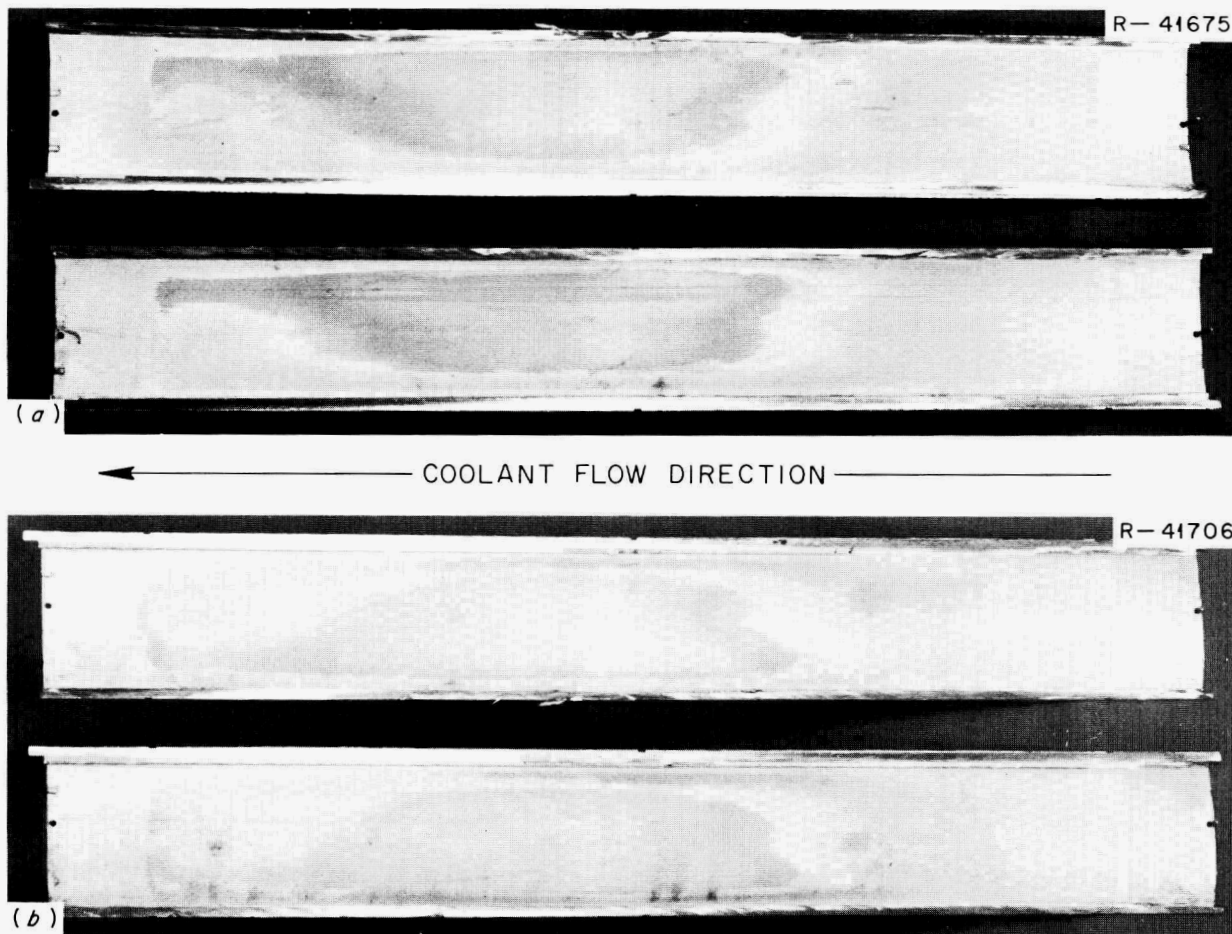


Fig. 31.5. Typical Appearance of Surfaces of HFIR Fuel Plates. Regions where the oxide film had spalled from the plate surfaces are clearly delineated by the dark, irregularly shaped areas. Approximately 1/4X. (a) Concave surfaces, with inner edges up. (b) Convex surfaces, with inner edges down.

plates. We determined the volume fraction of aluminum remaining in the fuel core of the various specimens and plotted the results as a function of the estimated fuel-core irradiation temperature. As shown in Fig. 31.7, the extent of reaction is primarily a function of the irradiation temperature and is relatively insensitive to burnup, although these temperatures are considerably lower than would be required for a comparable amount of reaction without irradiation.

Sections of the fuel plates were subjected to postirradiation heat treatments to determine the breakaway

swelling or blistering temperature. As shown in Fig. 31.8, the postirradiation blistering temperature of the HFIR fuel is significantly higher than that reported³ for other U_3O_8 -aluminum dispersion fuels.

After irradiation to its expected life, this element appears to be in excellent shape with no evidence of potential failure. It appears to be stable both dimensionally and structurally.

³M. J. Graber, G. W. Gibson, and M. Zukor, *Annual Progress Report on Reactor Fuels and Materials Development for FY 1967*, IN-1131, p. 47.

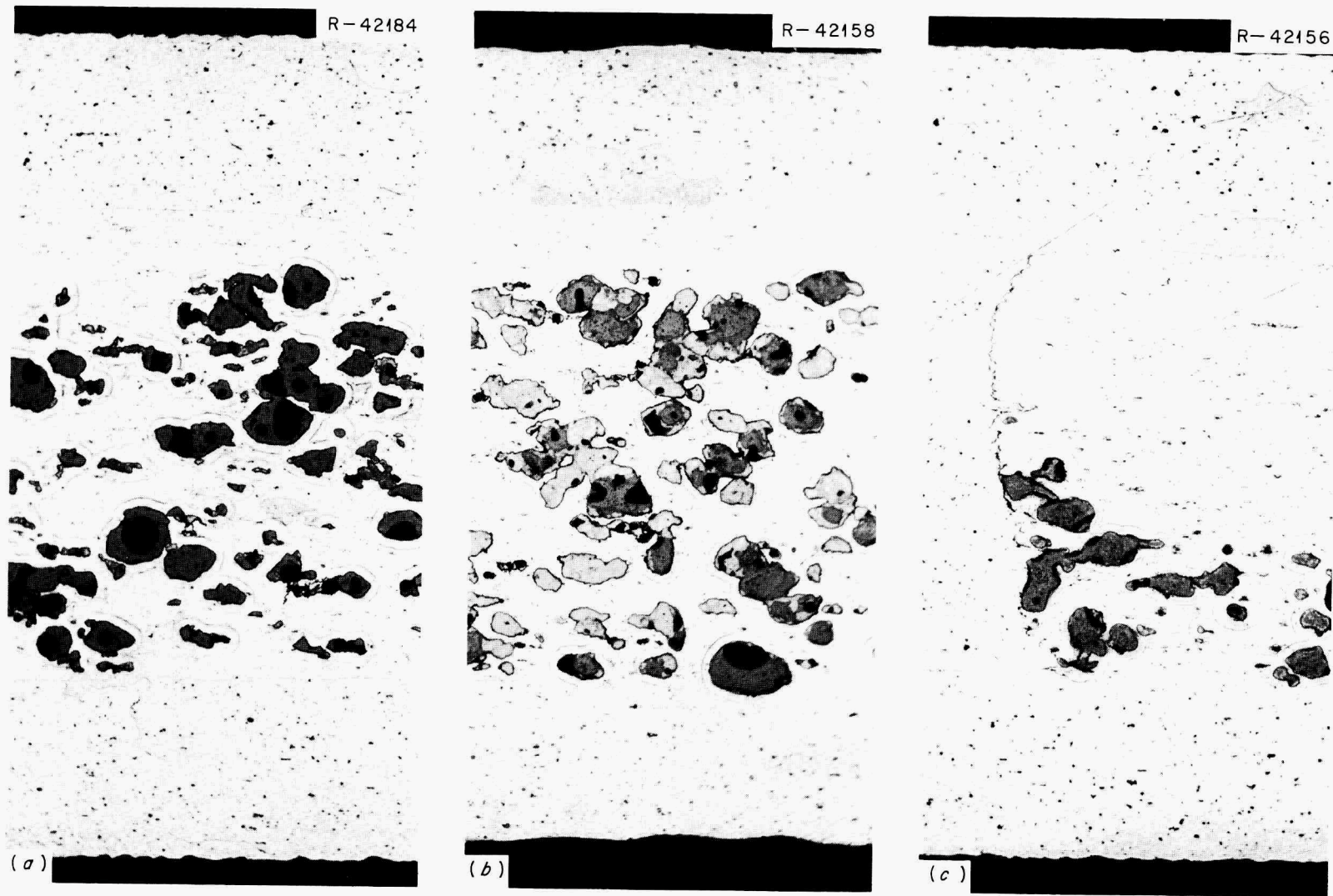


Fig. 31.6. Typical Microstructure of Sections from HFIR Fuel Plates. 100X. Etchant: 30% KOH. (a) Region of minimum burnup and lowest irradiation temperature (3.6×10^{20} fissions/cm³ at 70°C). (b) Region of intermediate burnup and maximum temperature (6.2×10^{20} fissions/cm³ at 155°C). (c) Region of maximum burnup and intermediate temperature (16.5×10^{20} fissions/cm³ at 140°C).

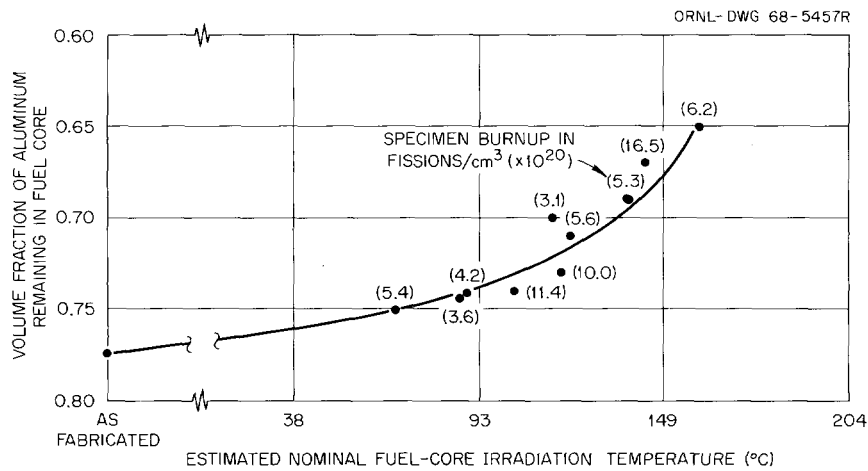


Fig. 31.7. Effect of Irradiation Temperature upon the Extent of Reaction in HFIR Fuel Plate Cores.

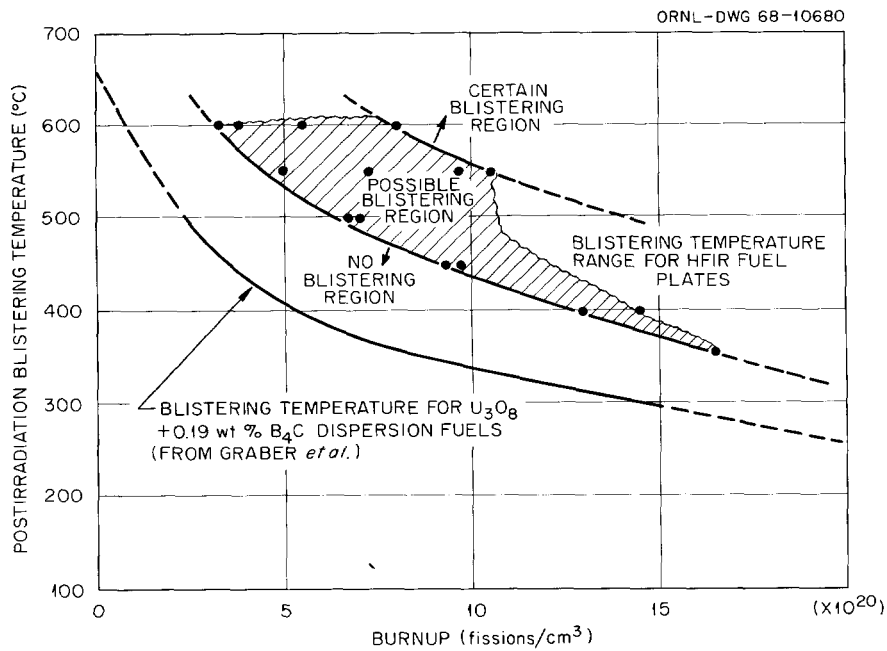


Fig. 31.8. Postirradiation Blistering Temperature of U_3O_8 -Aluminum Dispersion Fuel Plates. Lower curve is from ref. 3.

ADVANCED FUEL PLATE FABRICATION

M. M. Martin J. H. Erwin

We are investigating the fabricability of HFIR fuel plates containing a 25% increase in uranium loading. The investigation includes use of "high fired" U_3O_8 , which is equivalent to that now being used for HFIR fuel elements, and UAl_x -type intermetallics. Characteristics of the fuel compounds and matrix powder are given in Table 31.2.

Full-size HFIR-type fuel plates containing the materials in Table 31.2 and clad with aluminum alloy 6061 have been fabricated with the nominal uranium loading and a 25% increase. Identical pressing and rolling conditions were used to make all the plates. Previously, we reported⁴ the compressibility, densification, and

⁴M. M. Martin, *Metals and Ceramics Div. Ann. Progr. Rept. June 30, 1967, ORNL-4170, pp. 177-79.*

Table 31.2. Characterization of Fuel Compounds and Matrix Aluminum for Fuel Section of HFIR Fuel Plates

Characteristics	Fuel Compounds			Matrix Aluminum
	U ₃ O ₈	UAl ₃	UAl ₃ Si _{0.4}	
Uranium content, wt %	84.8	73.9	71.7	
Silicon content, wt %			3.8	0.1
Toluene density, g/cm ³	8.33	6.87	6.79	2.70
Bulk density, g/cm ³	3.8	2.9	2.7	1.2
Surface area, ^a m ² /g	0.037	0.091	0.130	0.30
Sieve analysis, ^b wt %				
+100	0.0	0.0	0.0	0.0
-100 +170	1.2	1.0	0.8	2.7
-170 +200	50.2	21.0	17.3	5.1
-200 +230	16.9	16.7	16.6	4.3
-230 +270	18.5	16.2	15.3	5.3
-270 +325	10.1	17.7	18.6	6.2
-325	3.1	27.4	31.4	76.4

^aStatic krypton BET determination.

^bConditions: Cenco shaker, 100-g sample, 30 min duration.

Table 31.3. Summary of Thickness Measurements Observed in Experimental HFIR Fuel Plates

Plate Type	Fuel	Uranium Content	Fuel Concentration	Core Thickness (in.)		Cladding Thickness (in.)	
				Average	Maximum	Average	Minimum
Inner annulus	U ₃ O ₈	16.288	31.2	0.0280	0.0306	0.0111	0.0090
	UAl ₃	16.288	36.1	0.0296	0.0322	0.0102	0.0071
	UAl ₃ -Si	16.288	36.8	0.0279	0.0307	0.0111	0.0089
	U ₃ O ₈	20.360	37.1	0.0285	0.0301	0.0108	0.0092
	UAl ₃	20.360	43.3	0.0292	0.0295	0.0106	0.0090
	UAl ₃ -Si	20.360	44.2	0.0291	0.0312	0.0105	0.0085
Outer annulus	U ₃ O ₈	19.785	42.5	0.0286	0.0292	0.0107	0.0102
	UAl ₃	19.785	49.9	0.0285	0.0302	0.0107	0.0092
	UAl ₃ -Si	19.785	50.8	0.0290	0.0292	0.0105	0.0095
	U ₃ O ₈	24.731	49.8	0.0284	0.0320	0.0108	0.0081
	UAl ₃	24.731	58.9	0.0291	0.0324	0.0104	0.0074
	UAl ₃ -Si	24.731	59.9	0.0297	0.0320	0.0102	0.0076

retained void volume for each of the loadings and fuel compound-aluminum dispersions.

Table 31.3 summarizes the maximum core and minimum cladding thicknesses usually found within 0.2 in. of the core ends along with the average thickness of the cores and cladding. We note that the values show no definite trend with fuel concentration and type of fuel. This is surprising in view of the large differences in compressive yield strength of the fuel dispersions containing U₃O₈ and UAl_x. However, metallographic examination reveals that the aluminum filler extends beyond the fuel portion of the UAl_x-type cores after

rolling, as shown in Figs. 31.9 and 31.10. Projections up to 0.450 in. in length and 0.025 in. in width were observed in the intermetallic plates. This type of projection was not observed in the U₃O₈ plates, and whether it would have any effects on operation is not known. Although the intermetallic fuel plates do not meet present HFIR specification, it appears that the aluminum filler section associated with the unique HFIR core geometry has prevented the severe thinning of cladding (dogboning) that is usually observed in high-loaded UAl_x fuel plates having the customary square-core geometry, such as in ATR plates.

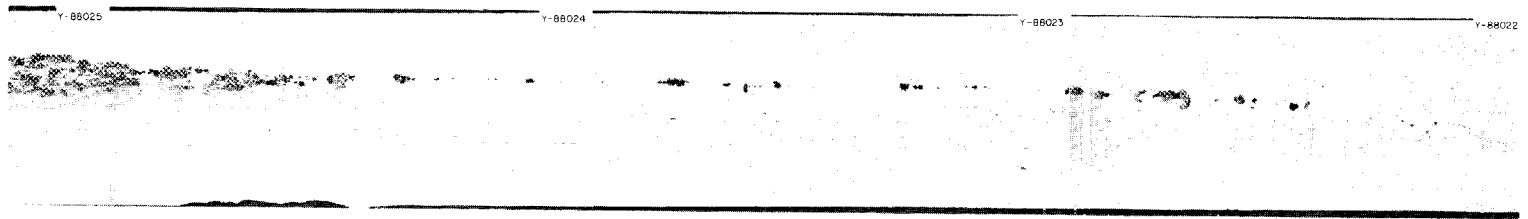


Fig. 31.9. Longitudinal Section from Core End in Experimental HFIR Fuel Plate Made with Uranium-Aluminum Intermetallic Fuel. Note filler portion extending beyond fuel section. Etched 45 sec with 1% HF. 50X. Reduced 56%.

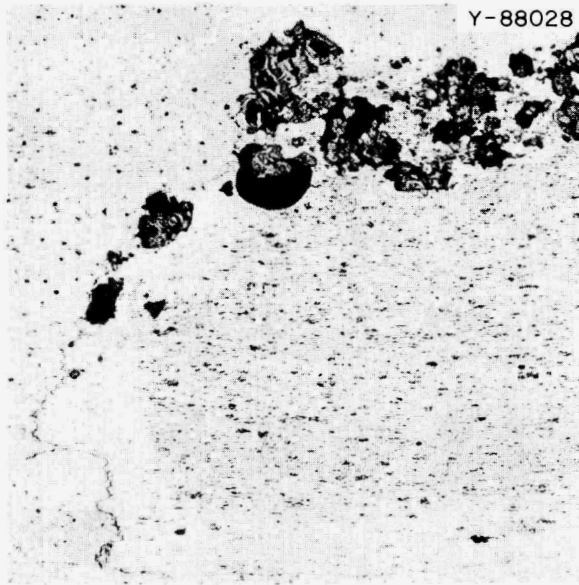


Fig. 31.10. Transverse Section from Core Edge in Experimental HFIR Fuel Plate Made with Uranium-Aluminum Inter-metallic Fuel. Note filler portion extending beyond fuel section. Etched 45 sec with 1% HF. 100X.

CHARACTERIZATION OF BURNED U_3O_8 POWDERS

J. T. Venard⁵

In our quest for a more economical fuel for HFIR, we became interested in a material referred to as "burned U_3O_8 ." This material is obtained very early in the processing scheme used by Y-12 for the production of the dead-burned U_3O_8 now used in HFIR.

The burned U_3O_8 that was characterized came from a single 2-kg lot of -100 mesh depleted material supplied by Y-12. The microstructure of the material appears in Fig. 31.11. Lines from a Debye-Scherrer powder camera sample were indexed to the hexagonal form of U_3O_8 , and no lines were found for metallic uranium. Microprobe analysis of metallic chips showed some to be primarily iron, others primarily aluminum, and still others a copper-zirconium combination, but no free uranium.

The surface area of $0.46 \text{ m}^2/\text{g}$, density of $7.94 \text{ g}/\text{cm}^3$, and screen analysis of 14.7% +170 mesh, 71.1% -170 +325 mesh, and 14.2% -325 mesh disagree greatly with current specifications for HFIR. The material also

⁵Present address, LMFBR Program, Argonne National Laboratory, 9700 South Cass Avenue, Argonne, Ill. 60439.

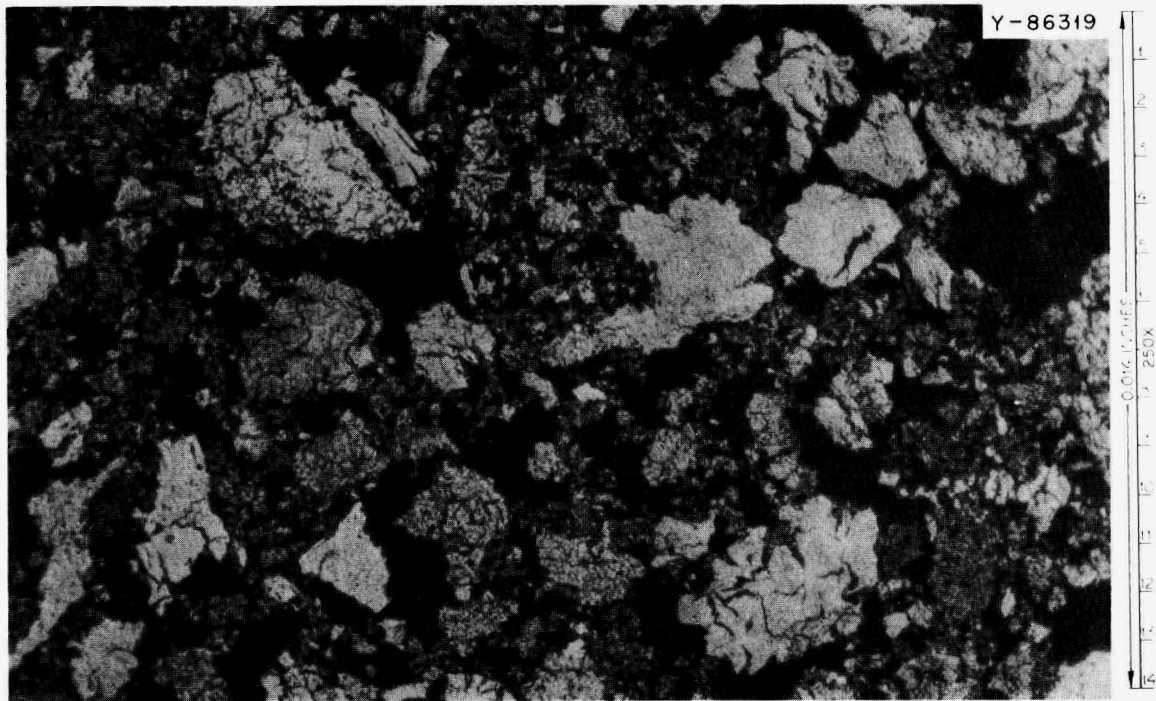


Fig. 31.11. Photomicrograph of Burned U_3O_8 Showing Particle Shape and Internal Cracking.

exceeds the specification with respect to F, Fe, Mn, and Si impurity levels. The chemical purity of the material is not, however, felt to be a serious problem since starting material that can be selected will affect these impurity levels. The high surface area and low density of this fuel powder are probably inherent characteristics of the process, and their importance must await fabrication and irradiation performance experience before a judgement is made.

All the above information gives one a reasonably clear picture of the "characteristics" of this fuel material. The decision on whether or not it will perform adequately as HFIR fuel must be based on additional blending, homogeneity, fabrication, and irradiation experiments now in progress.



Fig. 31.12. Special Electron-Beam Gun for Welding Inside a 4-3/4-in.-diam Tube.

FUEL-PLATE-TO-SIDE-PLATE WELDING DEVELOPMENT

A. G. Cepolina G. M. Slaughter

Electron-beam welding is being investigated to improve the reliability and quality of the joints between fuel plates and side plates of the HFIR fuel elements. The potential advantages for HFIR over the present arc-welding process have been discussed.⁶ Investiga-

⁶R. G. Donnelly, *Metals and Ceramics Div. Ann. Progr. Rept. June 30, 1967*, ORNL-4170, pp. 181-82.

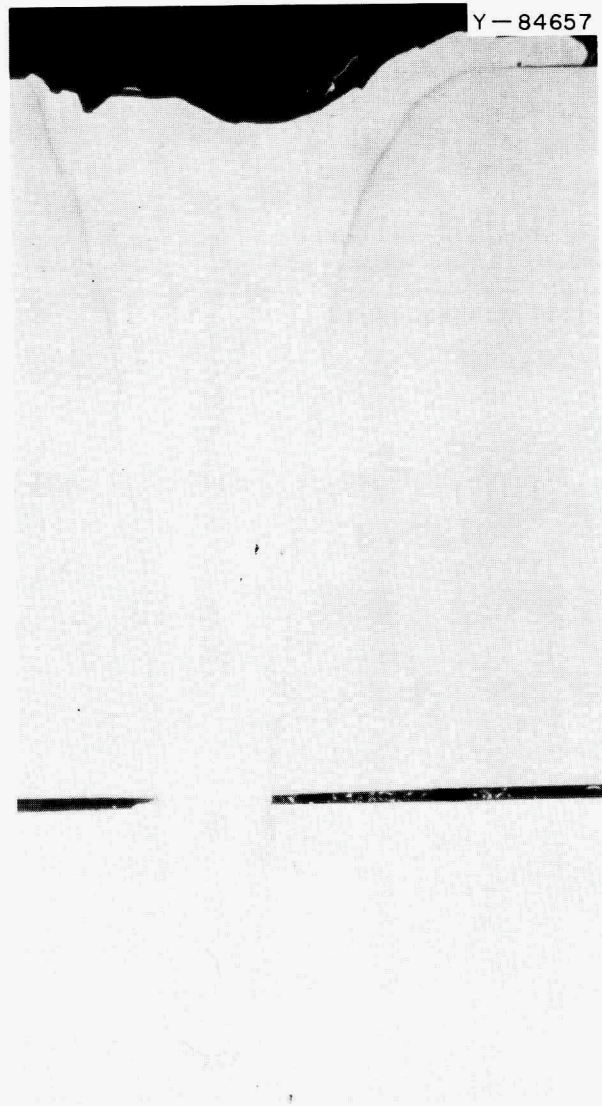


Fig. 31.13. Weld of a Fuel Plate to a 1/2-in.-Thick Type 6061 Aluminum Side Plate. Welding conditions: 200 ma, 19 kv, 25 in./min. The high depth-to-width ratio of an electron-beam weld should markedly reduce distortion. Etch: 2% HF in H₂O. 12X.

tions to date indicate that control of penetration is more easily attained with the electron-beam process.

General feasibility of the electron-beam process was demonstrated on a flat test specimen. However, a definite problem was expected in developing equipment for welding inside the inner tubes; of particular concern was the space limitation imposed by the 4-3/4-in. inside diameter of the inner fuel element. To resolve this problem, we engaged Brad Thompson Industries, Indio, California, to design and construct an electron-beam gun to fit inside a tube of this size and penetrate 1/2-in.-thick aluminum. This gun is shown in Fig. 31.12.

We witnessed the testing of this gun at the manufacturer's plant; the performance met the specified criteria. The presence of aluminum vapors from the molten weld metal kept the electron beam unstable when the applied voltage was greater than 18 kv. Below 18 kv no instability problems were evident.

Metallographic examination of test welds made at the Brad Thompson Industries plant showed good uniformity of penetration, excellent bead contour, and sound joints. No weld cracking was found with type 2219 aluminum side plates and only minor amounts with type 6061. Figure 31.13 shows a typical weld in the 1/2-in.-thick side plate.

As a result of these experiments, we feel that the electron-beam process is feasible for welding the HFIR elements. With a pumping system able to evacuate the metal vapors more rapidly, the beam stability should be improved. After installation of our own electron-beam welder, additional development will be conducted to determine the optimum welding conditions for each fuel-plate-to-side-plate configuration (inner and outer tube welds). An important factor in the determination of these conditions will be the reproducibility in penetration obtained with each combination of parameters.

COOLANT CHANNEL SPACER ATTACHMENT

A. G. Cepolina C. H. Wodtke

The construction of advanced HFIR fuel elements with longer lives and higher operating temperatures might require the use of thin longitudinal spacers to keep the fuel plates rigid during operation. Also, the presence of such spacers might permit reducing the number of fuel-plate-to-side-plate welds. Welding processes applicable to this problem must give very slight but well-controlled penetration.

The results of ultrasonic welding studies have been reported.⁷ A flow-test assembly was successfully fabricated and adequately withstood the service, and fretting-type corrosion did not seem to be a problem. However, the production rate attainable with this process was quite slow, the bond quality seemed to be inconsistent, and tip life was relatively short.

Spot welding is being actively pursued as an alternate means for attaching these spacers. Both capacitor discharge and electronically controlled machines were investigated; however, the controls available with the latter seem to make it more desirable. Preliminary welds on thin aluminum sheets made with a low-inertia electronically controlled machine at Sciaky Brothers, Incorporated, of Chicago looked especially promising. Test weld microsections showed that penetration was limited to about 0.003 in. We have engaged Sciaky to join aluminum wires to a full-length dummy HFIR fuel plate as a means of determining basic feasibility.

ALTERATION TO THE FABRICATION PROCEDURES FOR HIGH FLUX ISOTOPE REACTOR CONTROL PLATES

J. H. Erwin

To continue our effort in the reduction of control element cost, we examined the probable effects of tantalum compact simplification, as shown in Fig. 31.14. We replaced the 12 tantalum-aluminum compacts machined to four different lengths with nine similar compacts of equal length. The uniform replacement compacts eliminate the machining operation but present two uninterrupted interfaces in the thickness of the tantalum, and these joints extend the full length of this section of the core. Samples cut from a special plate containing only stacked tantalum-aluminum compacts were subjected to tensile and bend tests. Typical data from the tensile tests, summarized in Table 31.4, indicate comparable strengths between tantalum-to-tantalum and tantalum-to-aluminum-end interfaces and both of these weaker than the tantalum-to-aluminum-edge interface. However, the 2200-lb/in. strength is ample since the major concern is rupture during explosive forming when all components are held in compression.

We fabricated one inner plate to incorporate the use of chemically cleaned unclad 6061 cover plates⁸ and

⁷C. H. Wodtke, *Metals and Ceramics Div. Ann. Progr. Rept. June 30, 1967*, ORNL-4170, p. 183.

⁸J. H. Erwin, *Metals and Ceramics Div. Ann. Progr. Rept. June 30, 1967*, ORNL-4170, pp. 179-81.

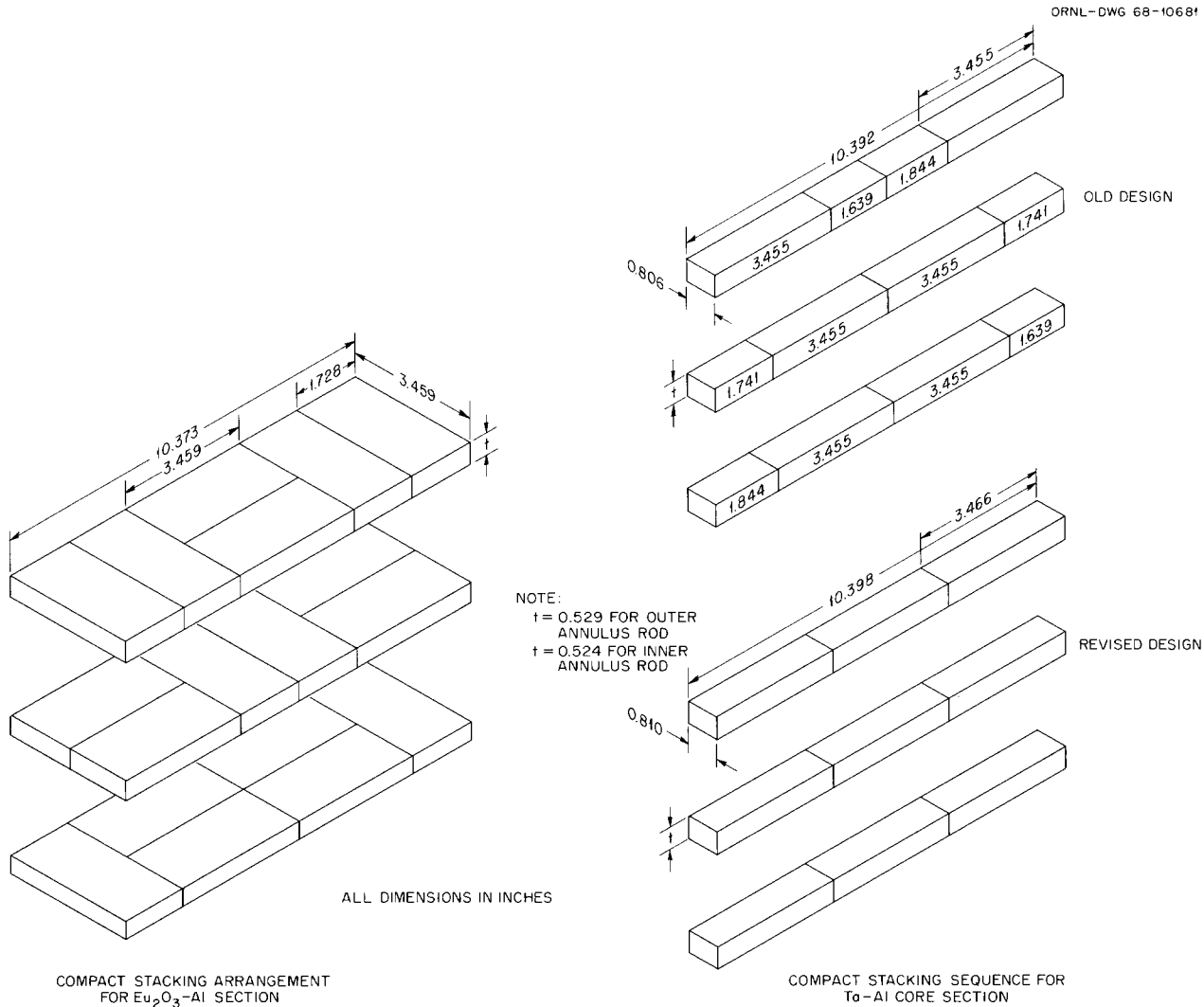


Fig. 31.14. Core Stacking Arrangement for Old and Revised HFIR Control Plate Billets.

Table 31.4. Ultimate Strength of HFIR Control Plates at the Tantalum Core Interfaces

Interface	Tensile Samples		
	Number Tested	Load to Failure (lb/in.)	
		Range	Average
Tantalum to tantalum	7	2200-3000	2580
Tantalum to aluminum edge	4	4000-4500	4325
Tantalum to aluminum end	3	2050-3500	3000

unmachined tantalum-aluminum compacts in the billet assembly. This plate has been made a part of an inner control element. Radiographic examination of the poison section of the plate indicates no separation of the compacts as a result of forming into the circular section. These improvements have now been incorporated into the control plate fabrication process.

32. High Flux Isotope Reactor Target Development

A. L. Lotts

The goal of the Transuranium Project is to produce gram quantities of the heavier transuranium elements for research by successive neutron captures in ^{239}Pu . Plutonium-239 is converted to ^{242}Pu , ^{243}Am , and ^{244}Cm in reactors at Savannah River. Target elements containing principally these three isotopes are fabricated at ORNL and are irradiated in the High Flux Isotope Reactor at a flux of approximately 3×10^{15} neutrons $\text{cm}^{-2} \text{sec}^{-1}$. In addition, special target elements consisting of higher isotopes are fabricated periodically and irradiated in the HFIR. The target elements are removed periodically from the HFIR and reprocessed in the Transuranium Processing Facility (TRU). At the TRU the product actinides are separated and the target actinides are recovered and fabricated into recycle target elements, which are returned to HFIR for further irradiation.

Our tasks in this program have included the design and validation of the original targets, the development of equipment and techniques for fabricating these elements both in glove boxes and remotely, the monitoring of the performance of the target elements in HFIR, and the design and fabrication of modified targets that may withstand HFIR service conditions. The principal activities during the past year have been the fabrication of recycle targets and special target elements, further investigation of the target failures that were reported previously, and irradiation of modified targets that may withstand the HFIR service conditions.

TRU TARGET FABRICATION OPERATIONS

J. E. Van Cleve E. J. Manthos

During irradiation in the HFIR, the target actinide oxides are encased in an assembly consisting of 30 individual elements. Each target element¹ consists of 35 individually jacketed pressed pellets, each composed of a mixture of approximately 10 vol % actinide oxides

¹M. K. Preston, Jr., J. E. Van Cleve, J. D. Sease, and A. L. Lotts, *Metals and Ceramics Div. Ann. Progr. Rept. June 30, 1966*, ORNL-3970, pp. 179-81.

dispersed in aluminum. The pellets are contained in a type X8001 aluminum tube with discontinuous fins. These fins are subsequently attached to the target rod sheath, which positions the element in the target array and through which cooling water flows during reactor operation. Manufacture of the targets consists of three parts: (1) pellet fabrication, (2) assembly and welding of the target element, and (3) inspection of the finished element.

Equipment to remotely fabricate these targets in the TRU has been developed, installed, and used to fabricate the first of the standard curium-bearing targets. The pertinent data used to evaluate the quality of the pellets for each target are presented in Table 32.1. The table also lists all of the various rods fabricated during the past year.

The K series (curium oxide) targets were fabricated completely in the remote facility and represent the first targets handled there. Extreme difficulty with the feeder mechanism caused the very large deviation in the pellet length on rod K-21, as several of the pellets were grossly heavy; however, the weight and length measurement showed that the pellets were acceptable.

The three special targets, prefix S, contained small amounts of isotopes exposed for experimental purposes. The pellets were blended in the shielded cave and pressed and loaded in the cell. The rods were remotely sectioned. After their exposure, the pellets were separated and shipped to the requester. A remotely operated saw was built to perform the sectioning. We feel that this type of irradiation and sectioning will be performed at a higher rate as the techniques become better known.

The six low-density pellet rods, prefix E, were fabricated in the Interim Alpha Laboratory. These rods contain ^{242}Pu recovered after the fabrication of the original HFIR targets. The targets were fabricated to show that the irradiation lifetime of the target would be greatly extended by adding void space in the pellets to accommodate the fission and transmutation products. These targets are presently being exposed in the HFIR Flux trap and will stay in until they fail or greatly

Table 32.1. Targets and Rabbits Fabricated in the TRU
from July 1, 1967 to June 30, 1968

Rod	Oxide Form	Major Isotope	Actinide Weight (g)	Weight of Oxide (g)	Pellet Length Standard Deviation (in.)
					$\times 10^{-3}$
K 11	Microspheres	^{244}Cm	4.57	6.55	13.0
K 12	Microspheres and shards	^{244}Cm	4.57	6.55	6.5
K 14	Microspheres and shards	^{244}Cm	4.47	6.40	10.4
K 19	Microspheres	^{244}Cm	4.42	6.66	17.3
K 21	Shards	^{244}Cm	4.50	6.45	55.6 ^a
K 20	Microspheres	^{244}Cm	4.45	6.37	6.6
S 16		^{244}Pu			
		^{252}Cf			
		^{248}Cm			
S 13		^{252}Cf			
S 12		^{244}Pu			
		^{252}Cf			
		^{248}Cm			
R 01 ^b		^{253}Es	1 μg		
E 70	Shards	^{242}Pu	8	10.36	4.7
E 71	Shards	^{242}Pu	8	10.36	7.1
E 72	Shards	^{242}Pu	8	10.36	5.8
E 73	Shards	^{242}Pu	6	7.76	4.4
E 74	Shards	^{242}Pu	6	7.76	4.5
E 75	Shards	^{242}Pu	8	10.36	4.5
TRL-1		^{252}Cf	0.700		

^aDue to malfunctioning of feeder.

^bRabbit.

exceed the exposure planned for any of the standard targets.

The einsteinium rabbit, prefix R, is the first rabbit remotely fabricated in the TRU facility. The physical shape was designed around using as much as possible of our standard fabrication equipment and the stock target rod material for construction. An entirely new remote welder was designed and fabricated to make the closure weld and also be able to make closure welds on shipping containers. The rabbit contained 1 μg of ^{253}Es and two flux monitors. After exposure the rabbit was sectioned and the pellet and flux monitors were removed.

Target TRL-1 is a californium source to be used for fast neutron activation studies. The source material, approximately 700 μg ^{252}Cf , was pressed into a standard pellet and loaded into a container designed to use the standard fabrication equipment. The source fabrication is completed, and it is presently in use in the TRL.

Several requests for ^{244}Cm oxide have been filled. The following steps are required to complete such a request. We receive the material as the precipitated

hydroxide and then calcine it to oxide to 800°C in air in our thermal cleaning furnace. The oxide is then removed from the crucibles and weighed into shipping containers. The weight of the oxide is determined with the "Batch Scale," by a modified procedure. The weight of ^{244}Cm is determined by running the shipping container on a remote calorimeter. The shipping container, with the gasketed cap screwed on tightly, is placed in a stainless steel outer container; the lid is welded on, and the package is shipped to the requester. The quality of the seal weld is determined only by a visual examination. Seven shipments containing approximately 64 g of curium oxide have been made following this procedure.

ANALYSIS OF HFIR TARGET PERFORMANCE

J. E. Van Cleve E. J. Manthos

Irradiation of 17 HFIR targets, which had been exposed in the Savannah River Reactors (SRL) for approximately 12 months before they were irradiated in HFIR, was terminated after 7-2/3 23-day cycles of

exposure in the HFIR. Actually, curium activity had been detected in the HFIR primary coolant water after five cycles; at this time five failed targets were isolated.² Five of the remaining targets failed after one additional cycle of exposure, six targets failed after 2 cycles, and one target showed no visible evidence of failure. The first target that failed had been irradiated to 39% FIMA and a fluence of 6.36×10^{22} neutrons/cm² (thermal) and 1.04×10^{22} neutrons/cm² (fast) (>0.82 Mev). The maximum fluence that any of the failed targets received was 7.49×10^{22} neutrons/cm² (thermal) and 1.42×10^{22} neutrons/cm² (fast).

At the time of failure, two groups of targets were being irradiated in the HFIR. In addition to the failed targets, which had previously been exposed in SRL, a second group of targets had been irradiated in the HFIR only. Both groups were similar in design except that the SRL targets each contained 10 g ²⁴²Pu, while the virgin HFIR targets contained 8 g. Each of the targets contained 35 individually jacketed aluminum matrix pellets pressed to 90% of theoretical density and containing ²⁴²Pu dispersed as PuO₂. The cladding and cover sheath were fabricated from X8001 aluminum.

Irradiation of the virgin HFIR targets continued until June 16, 1968, when they were removed from the reactor and transferred to the TRU for recovery of the contained transuranium elements. At the time of removal, the virgin targets had accumulated fluences ranging from 8.19 to 9.09×10^{22} neutrons/cm² (thermal) and 2.51 to 2.82×10^{22} neutrons/cm² (fast) (>0.82 Mev).

All of the SRL targets were visually examined at the TRU before they were chemically processed. We also examined three special targets that had been irradiated for 3 and 5 cycles and saw no evidence of failure. We also plan to visually examine the virgin HFIR targets for evidences of failure before they are processed.

Three metallographic sections at the region of failure were obtained from two of the SRL targets and submitted to the HRLEL for analysis. In addition, sections of the cover sheath were obtained and submitted for mechanical properties testing, heat treating studies and metallography, density determinations, and electron microscopy. Sections of sheaths that had been irradiated in SRL and HFIR, and in HFIR only for 3 and 5 cycles were also submitted.

Data from the failed targets and from the ETR irradiations of ²³⁹Pu prototypes^{3,4} were analyzed, and a model to explain the failure was developed. According to the failure model, target life will be improved if the plutonium loading is reduced and if more porosity is made available within the pellet. Six "low-density"

²⁴²Pu targets were fabricated and are being irradiated in the HFIR. As of June 16, 1968, these targets have been irradiated for 9 cycles and accumulated a fluence of 4.10×10^{22} neutrons/cm² (thermal) and 1.37×10^{22} neutrons/cm² (fast) (>0.82 Mev). According to the failure model, these targets should achieve greater than 26 cycles exposure before failure occurs.

An interim progress report⁵ detailing the history of the SRL targets and describing the preliminary results of investigation has been written. A more detailed investigation of the failure and an irradiation program for the investigation of the effects of high neutron exposure on aluminum and aluminum alloys are being carried out. Two special targets containing tensile specimens have been irradiated for 3 and 5 cycles in the HFIR. The package containing the specimens is presently being disassembled in the HRLEL.

TRU Inspection Results

E. J. Manthos

Each of the 17 SRL target elements was examined at the TRU before it was chemically processed. The first five failed targets we examined^{2,5} more intensively than the later failures, which were irradiated in the HFIR for an additional cycle or two. At the end of each cycle, the targets were individually tested at the HFIR in a nitrogen sweep gas apparatus for the presence of ¹³¹I and ¹³³Xe. Any target that showed the presence of these isotopes was assumed to be failed and was transferred to the TRU. At the end of the second cycle, all the remaining SRL targets were removed from the HFIR.

At the TRU, inspection of these targets consisted of removal of the cover sheath and examination of the target for cracking. The failed regions on each target were also photographed. The maximum number of cracks observed on the first five failed targets was three; and all of the cracks had formed at the approximate center of the pellet column, which also corresponded to

²A. L. Lotts et al., *Metals and Ceramics Div. Ann. Progr. Rept. June 30, 1967*, ORNL-4170, pp. 187-91.

³A. R. Olsen, J. D. Sease, A. E. Richt, J. W. Ullman, and S. D. Clinton, *Trans. Am. Nucl. Soc.* 9(1), 66 (1966).

⁴A. R. Olsen, J. D. Sease, A. E. Richt, and J. W. Ullman, *Metals and Ceramics Div. Ann. Progr. Rept. June 30, 1966*, ORNL-3970, pp. 182-84.

⁵A. L. Lotts, R. E. Adams, J. E. Bigelow, R. T. King, E. L. Long, Jr., E. J. Manthos, and J. E. Van Cleve, *Analysis of Failure of HFIR Target Elements Irradiated in SRL and in HFIR - An Interim Status Report*, ORNL-TM-2236 (in preparation).

the maximum flux region. We observed an increase in the number of cracks on targets that had been irradiated further. Cracks had also formed above and below the center of the pellet column. One target that had been irradiated for one additional cycle contained 13 cracks; five of them are shown in Fig. 32.1. We saw no cracks on one target that had been irradiated for one additional cycle; however, it was so scarred during removal of the cover sheath that a crack might have been masked. The SRL target exposures are summarized in Table 32.2.

In addition to the SRL targets, two special targets that had been irradiated in HFIR for 3 cycles and one that had been irradiated for 5 cycles were also examined before they were sectioned and disassembled. These targets appeared normal, with no evidences of cracking. A section of the cover sheath from a 3-cycle target and from the 5-cycle target were transferred to the HRLEL for further examination and preparation into specimens suitable for transmission electron microscopy.

Table 32.2. Results of the Visual Examination of the SRL Targets After Failure

Target	Exposure ^a in HFIR (number of 23-day cycles)	Fluence ^b (neutrons/cm ²)		Number of Cracks
		Thermal ×10 ²²	Fast (> 0.82 Mev) ×10 ²²	
56A	5-1/3	6.36	1.04	1
6A	5-2/3	6.48	1.08	2
34A	5-2/3	6.48	1.08	3
10A	5-2/3	6.60	1.00	2
35A ^c	5-2/3	6.48	1.08	0
32A	6-2/3	6.94	1.22	3
55A	6-2/3	7.04	1.15	10
11A	6-2/3	6.91	1.24	13
18A	6-2/3	7.04	1.15	1
42A	6-2/3	6.99	1.24	0
47A	6-2/3	6.97	1.26	5
38A	7-2/3	7.49	1.42	3
46A	7-2/3	7.55	1.31	6
41A	7-2/3	7.44	1.39	7
40A	7-2/3	7.44	1.39	4
48A	7-2/3	7.45	1.38	2
13A	7-2/3	7.55	1.31	4

^aAll targets had also been irradiated at SRL for approximately one year.

^bThe fluence listed is maximum that each target received and was calculated for conditions at Reactor midplane.

^cTarget 35A did not contain any cracks; however, the nitrogen sweep gas test showed the presence of volatile fission products.

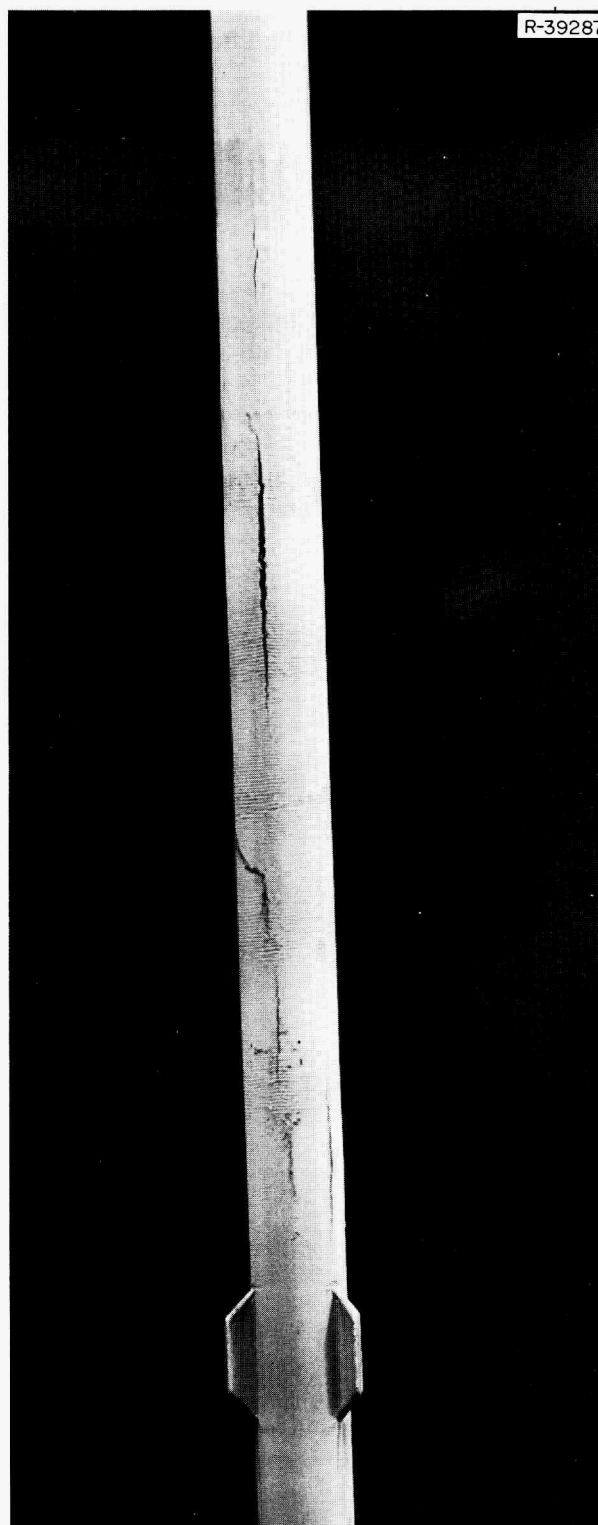


Fig. 32.1. Target 11A, Showing 5 of the 13 Cracks.

Irradiation of the 14 original virgin HFIR targets was continued without incident for a total of 17 cycles. They were removed from the HFIR on June 16, 1968, and transferred to the TRU for processing and recovery of the contained transuranium elements. Each of these targets will be stripped of its cover sheath and visually examined for evidence of failure before it is processed. Sections of the cover sheaths will also be obtained and transferred to the HRLEL for further examination.

Mechanical Properties

R. T. King E. L. Long, Jr.

The embrittlement of aluminum due to irradiation damage has been studied. Descriptions of the studies can be found in Part III, Chapter 21 of this report. Several important points may be summarized regarding the observations of neutron damage behavior in X8001 aluminum irradiated to 1×10^{22} neutrons/cm².

High neutron fluences substantially reduce the elevated-temperature ductility of the as-irradiated X8001 aluminum alloy, even though the room-temperature ductility of the alloy does not change. High neutron fluences are responsible for a large increase in the ultimate strength of as-irradiated X8001 aluminum, which persists up to a test temperature of approxi-

mately 316°C. The ductility of the irradiated alloy is completely recovered by annealing for 1 hr at 538°C before testing at 149°C. Lower temperature 1-hr annealing treatments do not increase ductility.

The irradiation produces approximately 10^{15} voids/cm³ whose diameters range from 100 to 600 Å. Preirradiation of the alloy in a high predominantly thermal neutron flux increases the void density but decreases the average void size. The voids present after irradiation anneal out in 1 hr at 260°C. Subboundaries and other structural imperfections evidently serve as sinks for these vacancy aggregates. Annealing the irradiated alloy for 24 hr at 600°C causes the formation of gas bubbles ranging from 1 to 16 μ in diameter. These bubbles are predominantly stabilized by hydrogen and cause 7 to 10% volume swelling.

The supersaturated silicon produced by $^{27}\text{Al}(n,\gamma)$ reactions forms no observable precipitate during irradiation. However, fine precipitate particles do form in the matrix during a postirradiation anneal of 1 hr at 120°C; the size and density of the particles increase with increasing annealing temperature up to at least 260°C. The cold-worked structure of the irradiated alloy is retained to higher temperatures than the normal recovery range of the unirradiated alloy. The silicon precipitate undoubtedly plays an important role in this stabilization process.

33. Cladding Materials for SNAP-8

J. R. Weir, Jr. H. E. McCoy, Jr. D. G. Harman

The SNAP-8 is an electrical generating system being developed for use in future space vehicles. The reactor is NaK cooled, fueled and moderated with zirconium hydride containing ^{235}U , and reflected with beryllium. The fuel element is clad with Hastelloy N. We have found that this alloy is subject to a type of thermal neutron damage that results in reduced strength and ductility at high temperatures. We were asked to determine (1) the magnitude of the property changes in Hastelloy N due to irradiation, (2) whether the properties could be improved significantly by thermal-mechanical treatments or by changes in alloy composition, and (3) the property changes in several other candidate cladding materials.

During the first year of this study,¹ we found that irradiation in the range of 650 to 760°C to thermal fluences of 2 to 3×10^{20} neutrons/cm² reduced the postirradiation fracture ductility of standard Hastelloy N. Under certain conditions of test temperature and strain rate, the fracture strain was only a few tenths of a percent in wrought materials² and in tubes.³ We also found that small changes in alloy composition were very effective in improving the properties and that various thermal-mechanical treatments did not affect the postirradiation properties significantly.¹

During the past year, we compared the postirradiation properties of several candidate cladding materials. These materials included Hastelloy X, Incoloy 800 with various titanium levels, type 304 stainless steel, a modified type 304L stainless steel containing 0.2% Ti, and several heats of modified Hastelloy N containing additions of titanium, zirconium, and niobium. The

work on the modified Hastelloy N is also of interest to the Molten Salt Reactor Program and is discussed further in Chapter 34 of this report.

The designers felt that failure would result from the inability of the material to deform plastically rather than from overstressing. Hence, the strain at fracture is the most important parameter in this study and our results are presented on this basis in Figs. 33.1 and 33.2. The nickel-base alloys (Fig. 33.1) are characterized by a very distinct ductility minimum as a function of strain rate. The titanium-modified Hastelloy N exhibits some improvement over standard Hastelloy N, but Hastelloy X is significantly better than both standard and modified Hastelloy N. The iron-base alloys (Fig. 33.2) were generally more ductile than the nickel-base alloys. The fracture strain of type 304 stainless steel decreased with decreasing strain rate (or decreasing stress), whereas the fracture strain of the titanium-modified type 304L stainless steel and Incoloy 800 increased with decreasing strain rate. The one heat of Incoloy 800 containing 0.10% Ti and 0.12% C had markedly higher ductility at low strain rates than any of the other alloys. Since Incoloy 800 is a candidate LMFBR alloy, its postirradiation properties are also discussed in Part III, Chapter 22 of this report.

Several laboratory melts of modified Hastelloy N containing various concentrations of titanium were irradiated and then creep tested in an effort to determine the titanium concentration required to give optimum resistance to irradiation damage. The results of tests at 650 and 760°C are summarized in Fig. 33.3. The general trend at both temperatures is that the properties continue to improve with increasing titanium level. The minimum level required for significant improvement seems to be slightly higher at 760 than at 650°C (0.5 compared with 0.3%). At both temperatures there seems to be little additional improvement over the range of 0.5 to 0.8% Ti.

Other modified alloys of the Hastelloy N type had very good postirradiation properties. For an alloy with 1% Zr, at 760°C the rupture life was 100 times that of standard Hastelloy N and the fracture strain was 12%

¹H. E. McCoy, Jr., and J. R. Weir, Jr., *Metals and Ceramics Div. Ann. Progr. Rept. June 30, 1967*, ORNL-4170, pp. 160-61.

²H. E. McCoy, *Effects of Irradiation on the Mechanical Properties of Two Vacuum-Melted Heats of Hastelloy N*, ORNL-TM-2043 (January 1968).

³H. E. McCoy, Jr., and J. R. Weir, "Stress-Rupture Properties of Irradiated and Unirradiated Hastelloy N Tubes," *Nucl. Appl.* 4, 96-104 (1968).

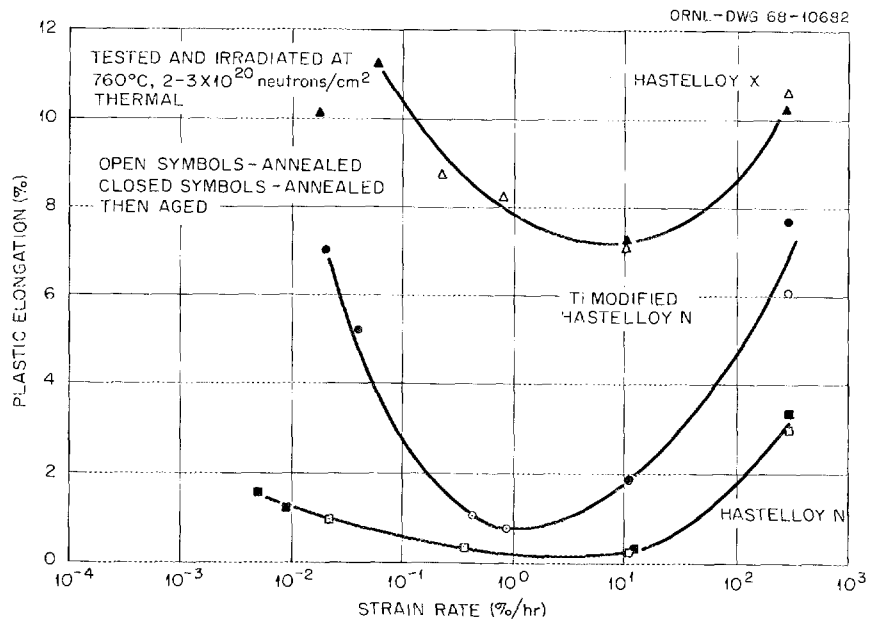


Fig. 33.1. The Effect of Strain Rate on the Postirradiation Ductility of Three Nickel-Base Alloys. The titanium-modified Hastelloy N had the nominal percentage composition of Ni-12 Mo-7 Cr-0.2 Mn-0.5 Ti-0.05 C.

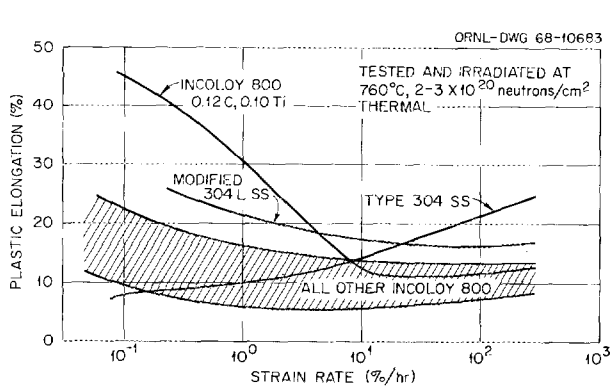


Fig. 33.2. The Effect of Strain Rate on the Postirradiation Ductility of Incoloy 800 and Stainless Steel. The modified type 304L stainless steel had the percentage composition of Fe-19.5 Cr-11 Ni-1 Mn-0.05 Si-0.2 Ti-0.012 C.

compared with 1% for standard Hastelloy N under comparable conditions. An alloy containing 2% Nb and 0.5% Ti showed an 80-fold improvement in rupture life and a fracture strain of 20%.

Although our program disclosed that several improved alloys could probably be developed, a project decision was made that the properties of standard Hastelloy N were adequate for satisfactory operation of the reactor. The latter part of this fiscal year was spent in testing specimens that were already irradiated, and our program will terminate July 1, 1968.

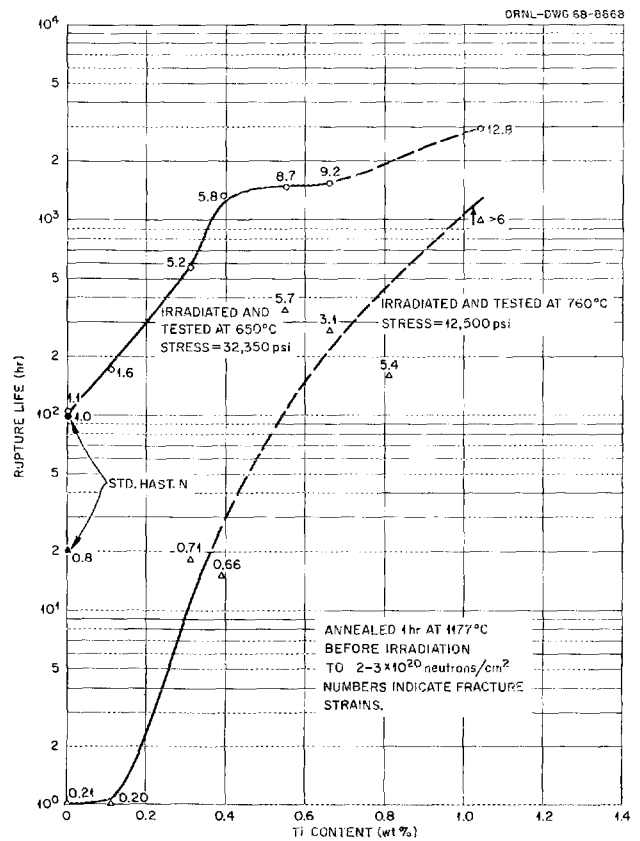


Fig. 33.3. Variation of Postirradiation Creep Properties of Modified Hastelloy N with Titanium Content.

34. Molten-Salt Reactor Program

J. R. Weir, Jr. H. E. McCoy, Jr.

The Molten-Salt Reactor Program is an ORNL program for the development of a thermal breeder. A significant milestone is the successful design, construction, and operation of the MSRE, which uses the liquid fuel salt ${}^7\text{LiF}$ -29.1 mole % BeF_2 -5 mole % ZrF_4 -0.9 mole % UF_4 , a graphite moderator, and Hastelloy N as the metallic structural material. The reactor operates at a peak temperature of 650°C , and the thermal power (8 Mw) is transferred to an air radiator by a coolant of LiF -34 mole % BeF_2 . The MSRE went critical on June 1, 1965 and had operated 72,441 Mwhr by April 1, 1968. The reactor is presently shut down in preparation for operation with ${}^{233}\text{U}$ fuel, another step toward the operation of a thermal breeder based on the ${}^{232}\text{Th}$ - ${}^{233}\text{U}$ cycle.

Our main involvement with the operation of the MSRE has been a surveillance program in which we follow the property changes of the Hastelloy N and the graphite. The primary function of this program is to ensure the continued safe operation of the MSRE. Also, the samples that we remove are used by the Reactor Chemistry Division to study the behavior of fission products.

The successful operation of the MSRE and an accumulation of general information that supports the basic molten-salt thermal breeder concept have inspired the proposal of a demonstration experiment involving a small reactor designated the Molten Salt Breeder Experiment (MSBE). It is proposed that the MSBE be the minimum size required to demonstrate breeding, perhaps 100 to 200 Mw (electrical), be complete with power generating capabilities, and be operational by 1976. The Project is presently optimistic about the continued development of a chemical processing scheme for removing fission products and protactinium from a molten salt containing thorium and ${}^{233}\text{U}$. Thus the single-fluid concept is presently favored, in which the fertile and fissile salts are combined into a single fluoride salt containing LiF , BeF_2 , ${}^{233}\text{UF}_4$, and ThF_4 . The reactor consists of a Hastelloy N vessel, graphite

prisms arranged to obtain specific flow channels and the proper moderation, and an undermoderated outer blanket with low fission density and a high probability of neutron capture.

Thus the materials for the MSBE are the same as for the MSRE, namely graphite and Hastelloy N, but the requirements on both are more severe. The graphite must resist the penetration of salt (requiring a pore diameter of $1\ \mu$), resist the penetration of fission products (requiring a surface diffusivity of helium of below $10^{-8}\ \text{cm}^2/\text{sec}$), and maintain these properties to very high neutron fluences. The dimensional changes that occur in presently available graphites under irradiation indicate that the expected lifetime of the graphite is about 3×10^{22} neutrons/ cm^2 ($>50\ \text{kev}$). Although the graphite can be replaced, the reactor would suffer an economical penalty and a loss in the ease of operation normally associated with fluid fuel reactors. We can design a very attractive reactor that utilizes presently available graphites, but we are seeking a better graphite. We designed and operated an irradiation facility in HFIR for obtaining a fluence of 1×10^{22} neutrons/ cm^2 ($>50\ \text{kev}$) in about four months. Also, we enlisted the assistance of commercial vendors in obtaining suitable graphites and investigated techniques for sealing graphite with either molybdenum or pyrolytic carbon to reduce the surface diffusivity.

The Hastelloy N vessel and associated piping must last for the entire plant life of 30 years. The high-temperature strength and ductility of Hastelloy N are reduced by irradiation, but we have modified Hastelloy N with a small titanium addition to improve its resistance to irradiation damage. This development involves procurement, irradiation damage studies, joining, and corrosion.

Molten Salt Reactor work reported elsewhere in this report includes the diffusion of titanium in Hastelloy N in Part I, Chapter 4; the nature of molybdenum fission product in fuel solutions in Part I, Chapter 10; and the production of ${}^{233}\text{U}$ -bearing fuel in Chapter 37.

MSRE SUPPORT

MSRE Materials Surveillance Program

W. H. Cook

The effects of the MSRE environment on its graphite moderator, grade CGB, and its primary structural alloy, Hastelloy N, are periodically monitored through the MSRE surveillance program. The facilities also permit us to expose some Hastelloy N specimens to higher fluxes and fluences than those encountered by the structural Hastelloy N in the MSRE. These specimens provide data useful for predicting future limits for the Hastelloy N in the MSRE or in some future reactor. We are also using the MSRE surveillance facilities to study the effects of irradiation and the fluoride salts on alloys, advanced and new grades of graphite, and graphite-to-metal joints. The details of the surveillance facilities and specimens have been presented previously.^{1,2}

Three groups of surveillance samples have been removed from the MSRE to date. The details concerning the specimens are given in Table 34.1. We have reported²⁻⁴ on the examination of groups 1 and 2 and are presently examining those from group 3. The important observations to date follow.

¹W. H. Cook and A. Taboada, *Metals and Ceramics Div. Ann. Progr. Rept. June 30, 1966*, ORNL-3970, pp. 193-95.

²W. H. Cook, *Metals and Ceramics Div. Ann. Progr. Rept. June 30, 1967*, ORNL-4170, pp. 192-95.

³W. H. Cook, *MSR Program Semiann. Progr. Rept. Aug. 31, 1967*, ORNL-4191, pp. 196-200.

⁴W. H. Cook, *MSR Program Semiann. Progr. Rept. Feb. 29, 1968*, ORNL-4254, p. 183.

1. The Hastelloy N specimens from the core are discolored only slightly.
2. Metallographic sections of the Hastelloy N show no evidence of corrosion. An 0.002-in. reaction layer forms where the Hastelloy N is in direct contact with the graphite.
3. The graphite is in excellent physical condition. The specimens in group 3 had a thin surface film visible only under special lighting.
4. The Hastelloy N specimens from outside the core were oxidized to a depth of about 0.002 in. but showed no evidence of nitriding.

Several special grades of graphite have been included in this program in an effort to further determine the behavior of the fission products. Some of the materials have already been removed and are undergoing detailed examination by the Reactor Chemistry and Metals and Ceramics Divisions. Several compositions of modified Hastelloy N have been included in the surveillance program, and the most significant result to date is that the corrosion resistance of these materials is not significantly different from that of standard Hastelloy N.

Properties of Hastelloy N Surveillance Specimens

H. E. McCoy, Jr.

We have run postirradiation creep and tensile tests to determine the effects of exposure to the MSRE environment on the mechanical properties. We have completed our tests on groups 1 and 2 (see Table 34.1).

Table 34.1. MSRE Surveillance Program

	Insertion		Removal		Time at 645 ± 10°C (hr)	Fluence (neutrons/cm ²)	
	Date	Mwhr	Date	Mwhr		Thermal	> 1.22 Mev
Group 1							
Core ^a	9/8/65	0.0066	7/28/66	8,682	4,800	1.3 × 10 ²⁰	3.1 × 10 ¹⁹
Group 2							
Core ^a	9/13/66	8,682	5/9/67	36,247	5,500	4.1 × 10 ²⁰	1.0 × 10 ¹⁹
Vessel ^b	8/24/65	0	6/5/67	36,247	11,000	1.3 × 10 ¹⁹	5.5 × 10 ¹⁸
Group 3							
Core ^a	9/13/66	8,682	4/3/68	72,441	15,289	9.4 × 10 ²⁰	2.3 × 10 ²⁰
Core ^b	6/5/67	36,247	4/3/68	72,441	9,789	5.3 × 10 ²⁰	1.3 × 10 ²⁰
Vessel ^b	8/24/65	0	5/7/68	72,441	20,789	2.6 × 10 ¹⁹	1.1 × 10 ¹⁹

^aStandard Hastelloy N.

^bModified Hastelloy N.

The detailed results have been reported previously,⁵⁻⁷ and the important observations are summarized below.

1. The tensile ductility of standard Hastelloy N was reduced significantly by irradiation. There was an unexpected reduction in the room-temperature ductility; intergranular fractures and strains in the range of 35 to 40% were observed. The fracture strain increased to about 50% at 200°C and decreased precipitously above 500°C. Above 500°C the fracture strain generally decreased as the test temperature increased or the strain rate decreased.

2. The creep-rupture strength and fracture strain of standard Hastelloy N at 650°C were reduced by irradiation. The reduction in rupture life was greatest at high stresses and diminished as the stress level was decreased. The fracture strain was a minimum value of 0.5% in creep tests of a few hours duration and increased slowly to 2 to 3% for 1000-hr creep tests.

3. The property changes in standard Hastelloy N at elevated temperatures are comparable with those noted for materials irradiated to comparable fluences in the ORR in helium.

4. We can compare the effects of thermal fluences of 1.3×10^{20} and 1.3×10^{19} neutrons/cm². The tensile properties are still changing markedly, but the creep-rupture properties are about the same.

5. The titanium- and zirconium-modified Hastelloy N specimens removed in group 2 had not been heat treated before irradiation to obtain the optimum properties. Their postirradiation mechanical properties were only slightly better than those observed for the standard alloy, they did not age, and their corrosion resistance was acceptable.

MSBR DEVELOPMENT

Procurement and Evaluation of Special Grades of Graphite

W. H. Cook O. B. Cavin

The graphite for future molten salt breeder reactors must have (1) maximum accessible pore entrance diameters less than 1 μ to prevent salt absorption, (2) a surface diffusivity less than 10^{-8} cm²/sec for fission gases such as ¹³⁵Xe, and (3) reasonable dimensional

stability to at least 3×10^{22} neutrons/cm² (>50 kev) at 700°C. These requirements are not independent, and we are finding that some work will be required for commercial vendors to produce the desired graphite in suitable shapes. Extruded shapes about 10 ft long will be needed for the MSBE, and future reactors will involve lengths up to 20 ft.

Because of the importance of graphite in molten salt reactors, we have kept several commercial vendors informed of our program. Several have responded by providing candidate materials, and our evaluations have been made available. We hope that this process will lead to the development of improved graphites with several vendors having the fabrication capability.

We need to know several properties of these graphites, including density, pore spectra, mechanical properties, permeability, crystallite size, preferred orientation, and lattice constants. We already can measure many of these, and we have expanded our capabilities to include gas permeability and x-ray diffraction studies. Equipment has been developed to measure the gas permeability of graphite from 10^{-1} to 10^{-10} cm²/sec. We have attempted to measure the crystallite size by x-ray line broadening, but several other factors contribute. Hence, we will have to analyze our results by more sophisticated methods that allow us to separate the various factors. Lattice parameter measurements on several types of graphite show that the length of the *a*-axis is quite constant but the *c*-axis varies markedly with grade and thermal history.

Gas Impregnation of Graphite with Carbon

R. L. Beatty D. V. Kiplinger

One of the requirements for graphite to be used in a molten-salt breeder reactor is a surface permeability low enough to prevent xenon absorption. Calculations suggest that a helium permeability of less than 10^{-8} cm²/sec at the graphite surface will permit the xenon to be purged from the salt by helium bubbles before significant amounts can penetrate the graphite. Since commercially available graphites usually have helium permeabilities some six or seven orders of magnitude higher than this required level, it is necessary to consider coating or sealing the graphite surface by some means.

Carbon is the preferred surface sealing material because it does not impose the parasitic neutron absorption penalties associated with refractory metals. However, the sealing carbon, which is deposited by pyrolysis of a hydrocarbon gas, has a crystalline character markedly different from that of the base

⁵H. E. McCoy, *An Evaluation of the Molten Salt Reactor Experiment Hastelloy N Surveillance Specimens - First Group*, ORNL-TM-1997 (November 1967).

⁶H. E. McCoy, Jr., *Metals and Ceramics Div. Ann. Progr. Rept. June 30, 1968*, ORNL-4170, pp. 195-96.

⁷H. E. McCoy *et al.*, *MSR Program Semiann. Progr. Rept. Aug. 31, 1967*, ORNL-4191, p. 200.

graphite. Experience with graphite irradiation predicts that neutron-induced dimensional changes of the substrate and sealing carbons will probably differ also. Therefore, if the pyrolytic carbon is applied simply as a coating, it may spall during irradiation. To counteract this we are developing a process for depositing the pyrolytic carbon in the near-surface pores.

Our gas-impregnation method employs a chamber in which the atmosphere is cycled between vacuum and hydrocarbon while the graphite substrate is heated inductively to 800 to 1000°C. The important variables are substrate temperature, cycle frequency, concentration and pressure of hydrocarbon gas, and original substrate porosity. Using this vacuum-pressure pulsing technique, we sealed specimens of POCO grade AXF graphite to helium permeabilities less than 10^{-9} cm²/sec with no measurable thickness of surface coating. Twelve sealed specimens representing useful ranges of experimental variables will be irradiated in a HFIR target capsule to determine fast-neutron irradiation stability.

Surface Sealing Graphite with Molybdenum

W. C. Robinson, Jr.

Chemical vapor deposition is one of the methods being investigated to decrease the gas permeability of structural graphite for the MSBR. The initial objective is to obtain a helium permeability below 10^{-8} cm²/sec with a minimum thickness of molybdenum deposit.

First we developed a small assembly, which attaches to a Veeco leak detector, for estimating the helium permeability of coated samples of our geometry. Although this apparatus can measure helium flow rates between about 7×10^{-6} and 1.5×10^{-10} cm³/sec, most of the samples coated had permeabilities above $7 \times$

10^{-6} cm³/sec. Therefore, the effectiveness of a coating technique was tested by measuring the pressure to which the sample could be pumped by the Veeco leak detector before and after impregnation. The ability of a particular thickness of molybdenum to seal the graphite samples was dictated by the permeability of the original graphite. The as-received AXF graphite, which was initially studied in this investigation, varied considerably in permeability, with pumping pressure ranging from 0.001 to 0.15 torr from sample to sample.

The surface condition of the as-received graphite proved to be of extreme importance; fingerprints on the surface of the graphite reduced the effectiveness of the coatings. Removing the fingerprints by annealing the graphite in air at 600°C for 0.5 hr before coating produced a very rough surface and opened large pores, which are much more difficult to seal than the pores in the as-received samples. Thus we used argon and vacuum for the precoating heat treatment. These treatments did not completely remove all surface contamination but are the most effective treatment available to us to date.

Two chemical vapor deposition techniques for metal coatings have been investigated. In one, molybdenum is deposited from MoF₆ and hydrogen at a constant pressure. Molybdenum deposits on the surface as the MoF₆ is reduced there. In the other, a vacuum inside the graphite sample during deposition pulls the reacting gases into the graphite pores before the chemical reaction. We refer to these as the constant pressure and pressure differential techniques.

For the constant pressure technique, the ability of a particular deposit thickness of molybdenum to reduce the pumping pressure is shown in Fig. 34.1, which depicts the difference in pumping pressure of the uncoated and coated sample as a function of coating

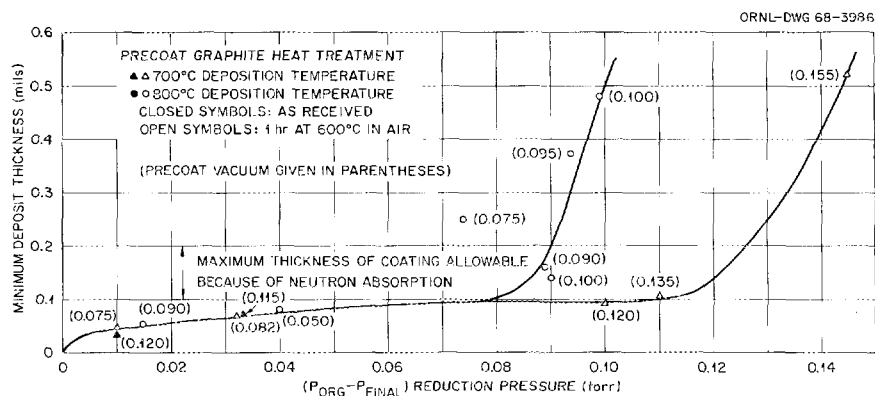


Fig. 34.1. Change in Pressure Drop Across a Graphite Specimen with Coating Thickness.

thickness. The coatings at 700°C are more efficient than those at 800°C, particularly on samples that originally pumped to pressures between 0.08 and 0.11 torr. The initial experiments using the pressure differential techniques indicate that the penetration of the metal is deeper with this technique. For example, a pressure drop of 0.16 torr was obtained with a deposit ranging from 1.4×10^{-4} to 2.0×10^{-4} in. This pressure drop is approximately 30% higher than can be obtained with an equivalent coating thickness applied by the constant pressure method.

Thus our findings have been qualitative, each suggesting some change in coating procedure or technique. We have not worked out a technique whereby we can routinely reduce the permeability of graphite to the desired level with no more than 2×10^{-4} in. of molybdenum.

Graphite Irradiation

C. R. Kennedy

Because of the very high fluences anticipated for graphite in MSBR's (approx 10^{22} neutrons/cm² >50 kev), only a few reactors in the world are suitable for an irradiation test program. Fortunately one of these reactors, the High Flux Isotope Reactor (HFIR), is located in Oak Ridge, and two target pin positions were made available for this work. The experimental facility shown in Fig. 34.2 was designed for irradiating graphite cylinders 1 in. high X 0.4 in. OD X 0.1 in. ID at 700 to 720°C. The experiments are not instrumented, and a

uniform axial temperature distribution is obtained by the addition of small tungsten susceptors. The actual temperatures are determined⁸ by measuring the expansion and annealing characteristics of SiC.

Two experiments were run early in the year to confirm the design. They ran quite well and only a few modifications were necessary. The flux in the facility was measured to be 1.2×10^{15} neutrons cm⁻² sec⁻¹ (>50 kev).

The necessary design changes were made, and two long-term irradiation experiments were built and installed. These experiments have just completed five reactor cycles, have been removed for evaluation, and appeared to have performed very well. The materials in these experiments fall into three categories: (1) materials for direct comparison with experiments by PNL, UK, and GA, including grades AGOT, UK isotropic, and H 315-A; (2) materials of potential interest for MSBR applications; and (3) experimental grades with controlled raw materials and processing for isolating the important variables in irradiation damage.

Graphites that demonstrate poor dimensional stability in these experiments will be replaced with other materials before reinsertion into HFIR. As our surface sealing work progresses, sealed specimens will be irradiated to determine the integrity of the coating.

⁸R. P. Thorne, V. C. Howard, and B. Hope, *Radiation-Induced Changes in Porous Cubic Silicon Carbide*, TRG-Report-1024 (November 1965); *Proc. Brit. Ceram. Soc.* 7, 449-59 (February 1967).

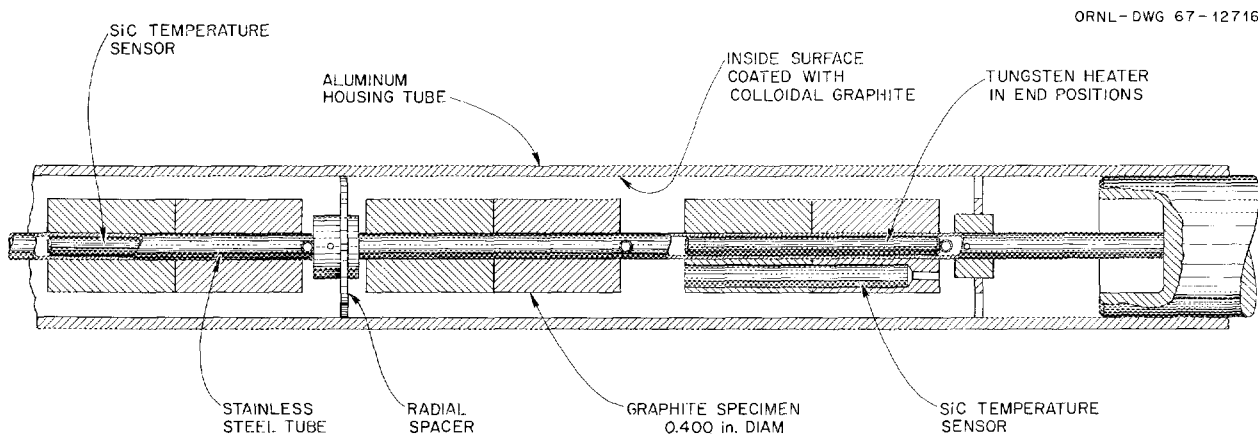


Fig. 34.2. A Section of the Facility for Irradiating Graphite in the HFIR. The outer tube is 0.5 in. OD X 32 in. long and occupies a position in the target pin cluster.

Development of a Modified Hastelloy N with Improved Resistance to Irradiation Damage

H. E. McCoy, Jr. C. E. Sessions R. E. Gehlbach

We found previously⁹ that small additions of titanium, zirconium, and hafnium improve the resistance of Hastelloy N to damage by radiation. For further development we chose a titanium-modified alloy having the nominal composition Ni-12% Mo-7% Cr-0.5% Ti-0.1 to 4% Fe-0.2 to 0.6% Mn-0.1% maximum Si-0.08% maximum C-0.001% maximum B. We have obtained twenty-five 100-lb melts and one 5000-lb melt of this general composition for further study. Our irradiation tests show that for a material annealed 1 hr at 1177°C and irradiated to a thermal fluence of 5×10^{20} neutrons/cm² (1) the creep-rupture life is unaffected at test temperatures of 650 and 760°C and (2) the fracture strain is reduced, showing a minimum of about 3% at a strain rate of about 0.1%/hr. We also observed that the material has the optimum resistance to radiation damage after the anneal at 1177°C, which produces a fairly coarse grain size.

A recent observation is that the postirradiation properties at 650°C deteriorate very rapidly as the irradiation temperature is increased. Electron microscope studies show that the microstructure is drastically different for the stressed portions of specimens irradiated at 650 and 760°C and tested at 650°C. The specimen irradiated at 650°C contained massive grain-boundary precipitate particles and a large amount of matrix precipitation. The specimen irradiated at 760°C was free of precipitate, and helium bubbles were observed along the grain boundaries. Thus, the morphology of the precipitate formed at 650°C results in superior mechanical properties to that obtained at 760°C. We shall attempt to find heat treatments that will produce the desired precipitate distribution before irradiation at 760°C.

As reported in Part III, Chapter 22 of this report, the properties of unirradiated titanium-modified alloy are very sensitive to the carbon and titanium concentrations. Electron microscopy showed that the titanium-modified Hastelloy N alloy is basically a solid solution with fine precipitates present. These precipitates have been identified as Mo₂C and Ti(C,N,B). They likely play a critical role in determining the mechanical properties.

Weldability of Hastelloy N

D. A. Canonico

We reported previously that the small plates of the titanium-modified Hastelloy N showed excellent weld-

ability under unrestrained conditions.¹⁰ We have now obtained a large heat (5000 lb) of this alloy and can make large welds in fully restrained plates. The restrained welds are more comparable with conditions encountered in fabricating large components. Our first welds in the large heat of the modified alloy (designated heat 7320) showed profuse weld metal cracking. Further tests showed that the cracks form in the underlying pass when the next pass is made. We have investigated the use of dissimilar filler metals for joining heat 7320 and find that satisfactory welds can be obtained with several filler metals including (1) heat 5090, an air-melted heat of standard Hastelloy N; (2) heat 67-526, a small vacuum melt of standard Hastelloy N containing 0.5% Ti and 16% Mo; and (3) heat 67-550, a small vacuum melt containing 0.7% Ti.

Further welds have been made in some of the 100-lb heats under fully restrained conditions. These welds appear to be free of cracks. Hence, we conclude that the welding problems are associated with impurities present in the large heat. Further work will be done to determine the impurity and how it can be eliminated from future melts.

Residual Stress Measurements in Hastelloy N Welds

A. G. Cepolina D. A. Canonico

We began to determine the distribution and magnitude of residual stresses that prevail in Hastelloy N weldments. In addition to determining fundamental information for metallurgists and designers, it permits us to evaluate the effects of postweld heat treatments on the stresses and to optimize the stress-relief conditions.

A technique was developed to continuously determine the stress as a function of distance from the weld center line. We adapted the "boring Sachs" method, which was originally set up for the determination of the distribution of residual stresses in pipes. Since plane strain and plane stress can both be expressed with the same equations, the relationships for the pipe will be valid for a disk. The terms in the equations concerning longitudinal stresses are eliminated in a planar specimen.

⁹H. E. McCoy, Jr., and J. R. Weir, Jr., *Metals and Ceramics Div. Ann. Progr. Rept. June 30, 1967*, ORNL-4170, pp. 197-98.

¹⁰D. A. Canonico and H. E. McCoy, Jr., *Metals and Ceramics Div. Ann. Progr. Rept. June 30, 1967*, ORNL-4170, pp. 198-200.

For this study, a 12-in.-diam \times 1/2-in.-thick piece of Hastelloy N was used. Two 6-in.-diam circular bead-on-plate tungsten-arc welds were made simultaneously on each side of the plate. The weld parameters used for this study provided heat inputs of 7500 j/in. for each weld or a total of 15,000 j/in. The strain was measured while a series of concentric sections were machined on a lathe, beginning at the center of the disk.

The equations applicable for translating the tangential strain to both radial and tangential stress are given below:

$$\sigma_r = \frac{E\epsilon_t}{2} \left(\frac{R_0^2}{R^2} - 1 \right), \quad (1)$$

$$\sigma_t = E \left[(A_0 - A) \frac{d\epsilon}{dA} - \left(\frac{A_0 - A}{2A} \right) \epsilon_t \right], \quad (2)$$

where:

σ_r = radial stress, psi

σ_t = tangential stress, psi

E = Young's modulus for the disk material

ϵ_t = total tangential strain measured on the external rim

R_0 = disk radius, in.

R = internal hole (cut) radius, in.

A_0 = initial disk area, in.²

A = internal hole (removed metal) area, in.²

The tangential residual stress (with respect to the weld axis) is a function of $d\epsilon_t/dR$, the change of the tangential strain with radius. To evaluate $d\epsilon_t/dR$, the experimental reading of strain and radius must be fitted with a continuous function. The curve fitting and slope determination at various values of R were computerized. The tangential and radial stresses are then determined as a function of location across the weldment.

In our initial experiments, we investigated the residual stresses that prevail due to welding and the effect on these stresses of postweld heat treatments of 1 hr at 1177°C and 6 hr at 871°C. The results of these studies are shown in Fig. 34.3. The as-welded Hastelloy N specimen contained residual stress levels in the tangential direction over 55,000 psi and in the radial direction over 15,000 psi. Postweld heat treatments reduced both residual stresses to less than 5000 psi. The 1177°C treatment for 1 hr seemed to provide the best stress relief. The tangential and radial residual stresses were nearly identical (between 2500 and 4000 psi) in the

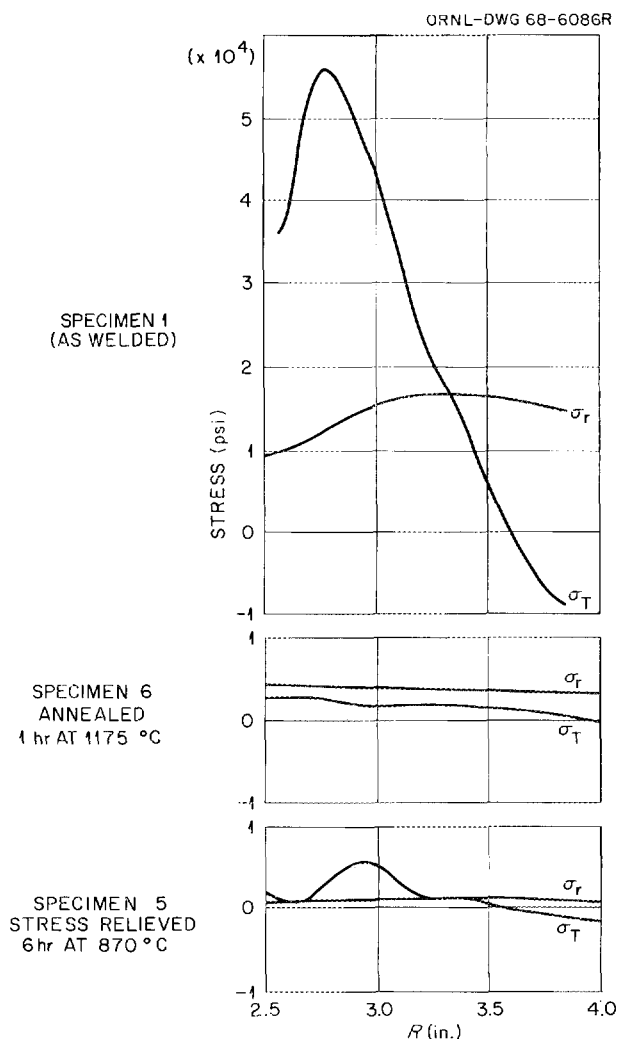


Fig. 34.3. Residual Stresses in Various Hastelloy N Weldments.

region of the weld. The 6-hr treatment at 871°C also decreased the residual stress level; however, a peak value of about 5000 psi did occur quite near the weld center line. A short distance away the residual stresses approached zero.

Interestingly, the highest residual stress in the as-welded specimen occurred about 1/4 in. from the weld center line toward the center of the specimen. This may be a real effect or it may be due to the specimen configuration. This point will be investigated further. The results of this study show that a heat treatment of 871°C provides quite adequate stress relief. The effect of even lower postweld heat treatments will be studied.

Oxidation of Hastelloy N

B. McNabb, Jr.

In a reactor system Hastelloy N is exposed to both fluoride salts and the reactor cell environment of nitrogen contaminated with oxygen. Thus, the oxidation resistance of the alloy is of considerable importance. Most of the early oxidation work on this alloy involved air-melted materials that contained fairly large concentrations of residual elements, particularly silicon. We are presently considering vacuum-melted material with some modifications in the alloying additions, and we must determine whether these changes reduce the oxidation resistance appreciably.

We tested both commercial and laboratory melts at 760 and 982°C. Most of our results are for scaling tests in which the test piece was cooled to ambient temperature every 25 hr. However, continuous tests indicate the same trends. Several significant observations have been made.

1. Silicon is very beneficial. The results for several commercial heats, in which the concentrations of other elements may vary appreciably, show a very strong correlation between scaling and the silicon concentration.

2. Vacuum-melted materials are generally less resistant to scaling than air-melted alloys, principally because of their lower silicon contents.

3. In a series of small melts of the base composition Ni-12% Mo-7% Cr-0.2% Mn-0.5% C, additions of Al, Ti, Zr, and Hf up to 1% were all equally beneficial.

4. In alloys having base compositions of Ni-16% Mo-7% Cr-4% Fe-0.5% Mn-0.05% C-0.5% Si, aluminum and zinc were beneficial and titanium was detrimental.

5. Iron was generally beneficial in all alloys.

These studies show that the scaling resistance of Hastelloy N is reduced appreciably by vacuum melting and that the addition of small amounts of titanium will have relatively minor effects. The oxidation resistance at 760°C appears adequate for continuous service.

Corrosion

A. P. Litman J. Koger

We are studying the compatibility of Hastelloy N with several fluoride salts, which can be classified as fuel, blanket, and coolant. The fuel salt is LiF and BeF₂ in a molar ratio of 2 with a few tenths of a percent of UF₄. The blanket salt composition is LiF-2% BeF₂-25% ThF₄. Both would be used in a two-fluid breeder, but

the single-fluid reactor will use a salt containing both ThF₄ and UF₄ having the approximate composition LiF-20% BeF₂-12% ThF₄-0.3% UF₄. The coolant salt that we are investigating is NaBF₄-8% NaF. The most attractive characteristics of this salt are its relatively low liquidus temperature (383°C) and its low cost (<\$0.50/lb).

We are presently investigating the compatibility of each salt with Hastelloy N using thermal convection loops operating in the nominal temperature range of 500 to 700°C. Two additional materials that are involved in our program are type 304L stainless steel and titanium-modified Hastelloy N. The former material is included to determine whether this cheaper alloy could be utilized in cooler parts of the system and the latter to ensure that the composition modifications that we have made in Hastelloy N are not deleterious. We are using a new type of thermal convection loop that enables us to remove metal tabs for periodic examination and to take salt samples without disturbing the loop operation.

The following significant observations have been made.

1. We have operated a Hastelloy N fuel salt loop for 55,000 hr at a peak temperature of 700°C without incident, indicating the excellent compatibility of these materials.
2. A type 304L stainless steel fuel salt loop has operated for 44,000 hr at a peak temperature of 675°C with only minor changes in flow characteristics. The removable specimens in this loop exhibit weight changes equivalent to about 0.002 in./year.
3. Hastelloy N loops containing fuel and blanket salts with removable specimens indicate corrosion rates equivalent to 1×10^{-4} in./year (based on 3000 hr operation).
4. The coolant salt appears a bit more aggressive, with corrosion rates of almost 5×10^{-4} in./year (based on 4000 hr operation).
5. In all cases where the titanium-modified Hastelloy N and standard Hastelloy N specimens were tested under comparable conditions, the titanium-modified alloy corroded more slowly. We attribute this reduction primarily to the lower iron content of the modified alloy. This observation also supports diffusion studies reported in Part I, Chapter 4 of this report, in which the diffusion rate of titanium was not high enough for this very reactive element to contribute appreciably to the corrosion rate.

Graphite Brazing Development

W. J. Werner

We are developing¹¹ procedures for brazing large graphite pipes to Hastelloy N. Although we are continuing to study direct brazing, a major part of our studies has been the use of thin (0.0002 to 0.0005 in.) chemically deposited metallic coatings on graphite for enhancing brazeability. Thus, the conventional ductile corrosion-resistant brazing materials such as pure copper and Pd-40% Ni would be applicable. Both molybdenum and tungsten have been deposited on high-density, low-permeability graphite, and we found that several brazing filler metals readily wet and flow on the coated graphite. X-ray diffraction studies showed that molybdenum had reacted with the graphite to form a thin layer of molybdenum carbide.

We devised a 1-in.-diam test joint of mating cones to determine the strength of joints of graphite to Hastelloy N and to molybdenum. The graphite was high-density, low-permeability, isotropic material.¹² The graphite-to-Hastelloy N joints were brazed with copper. These specimens fractured normal to the longitudinal axis of the graphite within the tapered portion of the specimen. The exact position of fracture varied from specimen to specimen. This was taken as an indication of the extent of cracking at the mating surfaces due to differential thermal expansion. Thus, the effects of stresses due to differential thermal expansion were more severe than anticipated.

The coated graphite-to-molybdenum test specimens were brazed with both copper and Pd-35% Ni-5% Cr as the brazing filler metal. A few uncoated graphite-to-molybdenum joints were also brazed with the carbide-forming Pd-Ni-Cr alloy. We encountered difficulties with the copper-brazed specimens. The joints failed at the mating surfaces at low strengths, and there was little evidence of brazing or pyrolytic coating present after failure. All the joints brazed with Pd-Ni-Cr failed in the graphite below the junction at a stress of about 3000 psi.

Experimental results on full-size joints (3.5-in. OD X 0.5-in. wall) are preliminary. The specimens consisted of (1) chemically vapor coated graphite directly brazed to Hastelloy N with copper and (2) a similar joint but brazed with Pd-Ni-Cr and incorporating an intermediate transition material to accommodate expansion differ-

ences.¹³ Both induction and furnace heating were employed. Induction brazing is especially attractive in view of the large number of joints needed and the length and configuration of the reactor components.

Our experiments have indicated that the low-expansion transition metal method is considerably more attractive than the direct approach. We fabricated a copper-brazed coated graphite-to-molybdenum-to-Hastelloy N joint that showed no visual or radiographic evidence of cracking. Good flow of the brazing filler metal was noted radiographically throughout the joint area. To date, this particular joint has been thermally cycled ten times between 200 and 700°C with cooldown to room temperature after cycles 1, 3, 5, and 10 for radiography. The radiographs indicate that the joint is still sound. Direct joints of graphite to Hastelloy N, on the other hand, have exhibited severe cracking.

We have also examined the effect of various surface conditioning or cleaning treatments on the wetting and flow of brazing alloys (Pd-Ni-Cr and Au-Ni-Mo) on graphite. Samples of POCO graphite were polished through the 600-grit paper and submitted to the several treatments. No differences between wettability or flowability were noted within either set of brazed specimens, and it appears that a good clean machined surface is sufficient for adequate wettability and flowability of these alloys.

Graphite-to-Hastelloy N Transition Joints

J. P. Hammond

To eliminate damaging thermal strain in graphite-to-Hastelloy N joints for cyclic temperature service, composites using the graded transition joint concept¹⁴ are being developed. These use a series of segments whose coefficient of thermal expansion changes gradually across the joint. We have accomplished this by inserting a series of (Ni-30% Fe)-matrix tungsten dispersions fabricated by liquid-phase sintering. The concentration of tungsten, which approximates graphite in coefficient of expansion, decreases gradually along the joint and thereby increases the expansion coefficient to near that of Hastelloy N.

¹¹W. J. Werner, *Metals and Ceramics Div. Ann. Progr. Rept. June 30, 1967*, ORNL-4170, p. 205.

¹²Manufactured by POCO Graphite, Inc., Garland, Tex.

¹³W. J. Werner and G. M. Slaughter, "Brazing Graphite to Hastelloy N for Nuclear Reactors," *Welding Eng.* 53(3), 65 (March 1968).

¹⁴F. Zimmer, "New Ways to Bond Dissimilar Materials," *Metal Progr.* 83, 101-8 (January 1963).

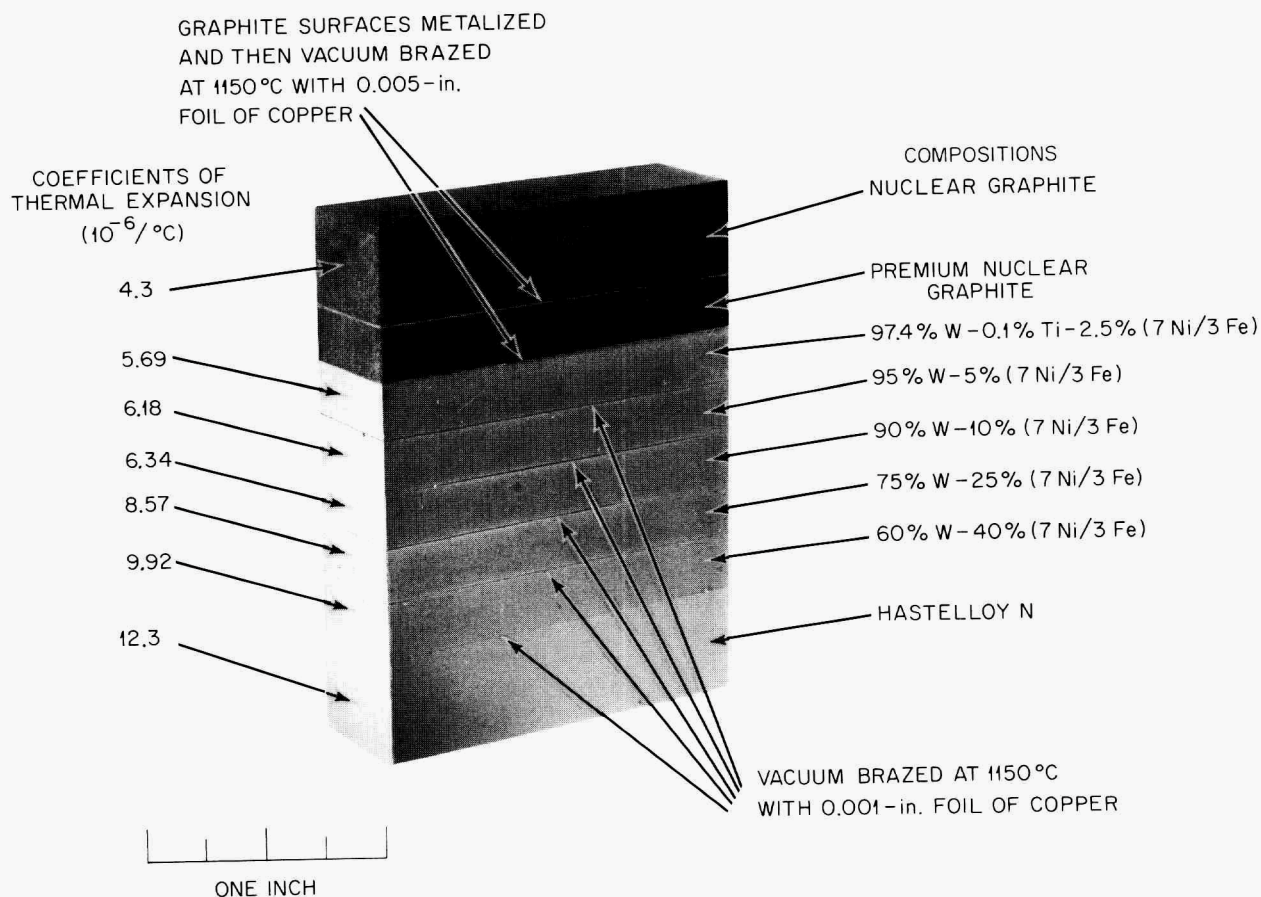


Fig. 34.4. Transition Joint, Graphite-to-Hastelloy N.

Several preliminary composites of the description illustrated in Fig. 34.4 have been fabricated for testing. This joint incorporates a more radiation-resistant grade of graphite¹⁵ between the nuclear graphite being joined and the series of heavy-metal alloys to mitigate strain that arises due to irradiation-induced dimensional instability in the graphite. The composite is made by fabricating the segments individually (the premium-quality graphite is formed by hot isostatic pressing); these segments are then joined together in the two-step brazing operation indicated in Fig. 34.4. The adjoining materials, including the brazing alloys, show metallurgical compatibility. The heavy-metal alloys are very tough and, since they display a marked capacity for deformation without cracking, we contemplate that

sheet-rolling could be an economical part-manufacturing process.

The composite shown in Fig. 34.4 has been subjected to 12 service-simulating thermal cycles between 700 and 400°C without any adverse effects. Corrosion tests in molten fluoride salts are still in process; however, the basic materials involved showed good resistance to corrosion. Heavy-metal alloys based on molybdenum are being investigated to supplement those containing tungsten. The molybdenum alloys have an advantage over tungsten in that fast neutron displacement damage would anneal out of the molybdenum alloys at lower temperatures. Composites of transitional metal carbides in graphite fabricated by hot isostatic pressing will be examined as an improvement for the irradiation-resistant graphite member. From this variety of materials, compositions providing a linear gradient in thermal expansion between graphite and Hastelloy N may be selected.

¹⁵D. C. Carmichael, W. C. Chard, and M. C. Brockway, *Dense Isotropic Graphite Fabricated by Hot Isostatic Compaction*, BMI-1796 (March 1967).

Radiation Stability of Brazing Alloys of Interest for Graphite

W. J. Werner H. E. McCoy, Jr.

We irradiated a series of commercial and experimental brazing filler metals that are promising for joining Hastelloy N and refractory-metal low-expansion transition sections to high-density graphite. Since we were primarily interested in the damage to the brazing filler metal itself and since graphite joints are difficult to test and the data are subject to scatter, we used Hastelloy N test specimens. Miller-Peaslee specimens¹⁶ were irradiated 1128 hr at 760°C in a single test capsule in the poolside position in the ORR. The thermal and fast (>2.9 Mev) fluences were 2.43×10^{20} and 2.03×10^{19} neutrons/cm², respectively. The brazing filler metals used in the study are shown in Table 34.2.

Shear strains for the as-brazed and unirradiated samples were calculated from the actual specimen brazing clearance determined metallographically. For the reactor specimens, the average brazing gap of the unirradiated specimens was used. All of the brazing filler metals seem to have adequate strength and shear strain for nuclear system joints.

Table 34.2. Brazing Filler Metals
Used in Irradiation Test

Alloy	Brazing Application
Copper	Pyrolytic-molybdenum-coated graphite to molybdenum or Hastelloy N and molybdenum to Hastelloy N
Pd-Ni-Cr	Graphite to molybdenum or Hastelloy N
Cu-Ni-Cr-Be	Graphite to molybdenum or Hastelloy N
Cu-Ni-Ta-Be	Graphite to molybdenum or Hastelloy N

Nondestructive Testing of Graphite-to-Metal Joints

K. V. Cook H. L. Whaley

We are developing nondestructive testing techniques to detect nonbond in various designs of graphite-to-metal joints. Our preliminary studies indicate that an

acceptable pulse-echo ultrasonic method can be developed for certain joint configurations. Mechanical scanning is difficult for the tapered joint design. We assembled a turntable device and associated equipment to allow precision three-dimensional scanning in our large ultrasonic immersion tank.

We demonstrated that the ultrasonic method (using the turntable scanning device) could distinguish bond and nonbond on one joint design. Both Hastelloy N-to-graphite and molybdenum-to-graphite joints have been examined. In one Hastelloy N-to-graphite joint only one area was bonded. The destructive test of this joint resulted in the separation of the graphite material in the bonded area, as shown in Fig. 34.5. As is evident, only one portion of the joint, the dark area, was bonded, coinciding with the prediction based on the ultrasonic examination. These results demonstrate the feasibility of the ultrasonic pulse-echo method for this particular joint configuration. We are determining the optimum sensitivity of this technique to nonbonding.

A second joint design is a tensile specimen with the graphite-to-metal joint in the gage length. The maximum diameter of the specimen is 1.00 in. and the joint is a 30° cone, so the joint diameter varies from 1 in. to a point. The graphite is the male part of the joint and the Hastelloy N the female part. Calibration is difficult since both the curvature of the joint and the area that reflects the ultrasonic energy vary with the diameter and the reflected signal varies as the diameter changes even for complete nonbond. A further complication is the metal thickness varying from the outer surface of the specimen to the joint interface. Attempts to test this joint with the pulse-echo ultrasonic method have been unsuccessful thus far; however, we feel that it is possible to tolerate some variation in our test and plan to pursue this technique when modifications on our mechanical system are completed.

Other joint designs to be fabricated will also require investigation by nondestructive techniques. These needs are being coordinated closely with the Welding and Brazing Group.

¹⁶F. M. Miller and R. L. Peaslee, *Welding J.* 34, 144-s-150-s (1958).

PHOTO 89768



Fig. 34.5. Results of a Destructive Test on a Graphite-to-Metal Brazed Joint. The dark area, where the graphite material separated due to the presence of good bond, coincides with the area that the ultrasonic test had predicted to be bonded.

35. Reactor Evaluation

A. L. Lotts

The total cost of producing heat or power by nuclear energy is composed of a number of components such as reactor capital costs, reactor operating costs, and fuel cycle cost. For several years ORNL has been evaluating various new reactor concepts, pointing out which reactor concepts are most economical, and indicating areas of technology in which research and development might be profitable. Such evaluations require the consideration of a number of interacting variables that must be evaluated by several different disciplines. Our role has been to evaluate fabrication costs for fuel elements and fuel element performance. Thus we work in cooperation with chemical engineers of the Chemical Technology Division on fuel cycle studies and with physicists and reactor design engineers in the Reactor Division on both fuel cycle studies and fuel performance evaluation.

The emphasis this year has been on updating *Civilian Nuclear Power, A Report to the President - 1962* and assisting in the evaluation of desalination reactors. Although these have been the end results of our work, we have tried to improve our efficiency, precision, and capability through the development of additional models and computer codes for economic studies. We also started the development of a model and computer code for performance of pin-type fuel elements. This work is an attempt to coordinate more effectively our present performance evaluations with irradiation experiments being conducted at ORNL and elsewhere. Since the work was started only in the latter part of the year, it has not yet progressed sufficiently to enable a report on the details.

COMPUTER PROGRAM DEVELOPMENT

A. L. Lotts

We had previously written computer codes for estimating fuel element fabrication costs for a variety of fuel element concepts.^{1,2} These we have continued to update and improve as required to perform current evaluations. The revisions are reported below.

We also met some new tasks in our economic evaluation work, which required the development of new models and codes. For example, during the year we were asked (1) to estimate the economically optimum schedule for building fuel fabrication plants in a growing nuclear economy and (2) to estimate the optimum time to start recycle of ^{233}U in a high-temperature gas-cooled reactor economy. The recycle of ^{233}U , which results from using the ^{233}U -thorium cycle, requires special facilities and, therefore, substantial investment. Computer codes that have more general application were developed for each of these problems.

Fuel Fabrication Costs

F. J. Homan

An existing computer program was modified to gain increased flexibility and to reflect the latest thinking related to fuel element fabrication for fast reactors. It is now possible to calculate costs for fabrication of fast reactor axial and radial blankets in separate, independent facilities or in the same facility. In addition, the case where axial and radial blankets are not of the same material can now be handled. New subroutines were added to systematize the output and increase the amount of information available. Equipment costs and manpower requirements for individual fabrication steps can now be output, as well as a complete breakdown of the capital cost of the entire fabrication facility. A curve-fitting subroutine determines equation parameters for curves of capital cost of the plant, annual operating costs, and hardware costs as functions of plant throughput. A detailed report³ has been prepared to describe this fuel element fabrication cost computer program,

¹A. L. Lotts, *Metals and Ceramics Div. Ann. Progr. Rept. June 30, 1964*, ORNL-3670, pp. 254-55.

²T. N. Washburn and F. R. Winslow, *Metals and Ceramics Div. Ann. Progr. Rept. June 30, 1966*, ORNL-3970, p. 207.

³A. L. Lotts, T. N. Washburn, and F. J. Homan, *FABCØST 9, A Computer Code for Estimating Fabrication Costs for Rod-Bundle Fuel Elements*, ORNL-4287 (in press).

which is for pin-type fuel elements. The general methods are described in another publication.⁴

Plant Optimization

F. J. Homan

Fuel element fabrication can account for up to 20% of the total power cost from a nuclear electric power station. This gives a strong incentive to minimize fabrication costs. The cost of fabrication is heavily influenced by the size of the fabrication plant with respect to the total market. Fuels can be more cheaply fabricated in a single large facility than in several smaller ones with the same total capacity, assuming all plants are fully utilized. This is due to the inherent economies of scale. On the other hand, it is inefficient and expensive to operate a partially utilized large facility.

The growing nuclear economy presents a problem to industrial planners. A plant of sufficient size to meet present fabrication demands will be too small to meet near future demands, making another plant necessary almost immediately. Therefore, an oversized plant must be built and operated below full capacity for a period of time. But the question is, how much oversize should the first plant be? Furthermore, how much oversize should subsequent plants be? We developed a method to achieve a balance between the cost benefits of scale and the disadvantage of partial utilization. Basically, the method involves internal generation of numerous possible schemes, calculation of the levelized cost of fuel element fabrication by each scheme, and selection of the scheme with the lowest levelized cost figure. The method is based on current data and technology and is intended as a tool in seeking a solution to minimal fuel fabrication costs and not as the solution itself. A basis for the assignment of initial fabrication prices was evolved as part of this study, and a method of application is suggested. The optimum plant size sequence method is in the process of being issued as an ORNL report.

Recycle Delay Code

F. J. Furman

Considerable economy, both in cost and preservation of natural resources, may be achieved by advanced converter and breeder reactors, as compared with

⁴A. L. Lotts and T. N. Washburn, "Use of Computer Codes in Estimating Fuel Element Fabrication Costs," *Nucl. Appl.* 4, 307-19 (May 1968).

present-day reactors, by recycling the converted or bred fuel. However, fuel must be recycled in large, highly automated reprocessing and refabrication plants to obtain these economies. Thus, when a power reactor system is in the early stages of growth, recycle operations may not be economical. The "DELAY" computer code, written in FORTRAN IV, calculates the optimum time to initiate large-scale recycle operations.⁵

The code input data include reactor mass balances for both recycle and nonrecycle operation and an assumed reactor industry growth rate. Fuel and storage requirements are then calculated for a selected time of recycle startup. These requirements are then fed to a plant-size optimization routine to determine optimum plant sizes, times of plant startups, and costs. The cost information is used to calculate total yearly costs, which are converted to present worth and summed to yield a total cost. Other times for recycle operation startup are calculated by the same method, and the total cost differences are compared to select the optimum time for recycle startup and the costs incurred by delays.

COST ANALYSIS

A. Goldman

The cost of producing power by nuclear energy is the sum of capital, operating, and fuel cycle costs. To achieve reductions in cost, the problem must be regarded in its entirety, since each category interacts with the others. As part of the overall approach to the problem of reducing power costs, our role is to evaluate fuel element fabrication costs and performance as they relate to the fuel cycle component of total cost.

The method used to estimate fuel fabrication costs uses computer programs to perform the many calculations required. Fabrication procedures and flowsheets are selected and analyzed for capital and operating increments at each point in the processes, and the results for a wide range in production rates are stored in the computer program. Estimated hardware costs for similar production rates are also stored. The input parameters for each concept to be estimated are based upon the specific design, the fabrication process desired, and financial data as stated in the ground rules for the particular study.

⁵F. J. Furman, R. B. Pratt, F. J. Homan, and A. L. Lotts, *DELAY - Computer Program for Predicting the Economically Optimum Time to Initiate Recycle in a Growing Reactor Industry*, report in preparation.

Over the past year our efforts have been concentrated on the preparation of new computer programs that will handle fast breeder concepts with their separate core and blanket zones and the application of these programs to the reactor systems of interest to the Fuel Recycle Task Force, as well as to parametric studies of other reactor concepts.⁶⁻¹¹

Fuel Recycle Task Force

A. Goldman

We have continued to participate in the AEC Fuel Recycle Task Force (FRTF) activities as part of their contribution toward updating *Civilian Nuclear Power, A Report to the President -- 1962*. We have developed fuel fabrication cost estimates for the approximately 40 reactor concepts considered in the FRTF study. These included pressurized-water and boiling-water reactors (including plutonium recycle for each); heavy-water-moderated organic-cooled reactors with alternate fuels of low-enriched uranium monocarbide, natural uranium monocarbide, natural uranium metallic fuel, thorium-uranium oxide, and thorium-uranium alloy; heavy-water-moderated boiling-light-water reactors with natural UO₂ fuel; high-temperature gas-cooled reactor; steam-cooled breeder reactor; gas-cooled fast reactor; and liquid-metal-cooled fast breeder reactors.

The estimates have been incorporated into a draft of the FRTF report on *Reactor Fuel Cycle Costs for Nuclear Power Evaluation*, which has been transmitted to the AEC for review. The cost estimates have also been utilized by the Systems Analysis Task Force of the AEC in a mathematical simulation study of the projected future growth patterns of the U.S. central station electric power generation system.

Desalination

A. Goldman

The desalination program at ORNL is concerned with reactors as heat sources and with distillation plants. Our

⁶*An Evaluation of Advanced Converter Reactors*, WASH-1087 (draft) (March 1968). Official Use Only.

⁷*An Evaluation of Alternate Coolant Fast Breeders*, WASH-1090 (draft) (April 1968). Official Use Only.

⁸W. R. Gall *et al.*, *An Evaluation of Steam-Cooled Fast Reactors*, ORNL-4245 (draft) (March 1968). Official Use Only.

⁹L. L. Bennett *et al.*, *An Evaluation of Gas-Cooled Fast Reactors*, ORNL-4206 (draft) (March 1968). Official Use Only.

¹⁰ORNL Staff, *An Evaluation of Heavy-Water-Moderated Organic-Cooled Reactors*, WASH-1083 (draft) (March 1968). Official Use Only.

¹¹*An Evaluation of Heavy-Water-Moderated Boiling-Light-Water-Cooled Reactors*, WASH-1086 (draft) (March 1968). Official Use Only.

efforts have been concerned with the former and in particular with methods of reducing fuel fabrication costs to decrease total water costs. The emphasis in the past year has been divided into three main reactor concepts. In the first bare metal fuel is cooled with sodium in a fast-breeder design; in the second uranium metal or oxide, clad in Zircaloy, is cooled with pressurized light water; and in the third concept, clad oxide fuel in a fast breeder design is cooled with sodium. We have prepared parametric fuel fabrication costs for the PWR concept to illustrate the sensitivity of fabrication costs to fuel rod diameter. The results have been incorporated into fuel cycle studies within the Reactor Division, which indicate that such pressurized water reactors when operated at low temperatures may offer desalination plants a source of inexpensive heat. The overall survey of such low-temperature PWR systems is now being prepared as an ORNL report, and further fuel fabrication cost estimates are being prepared, based on refined input specifications.

Similar fuel fabrication cost estimates on the fast breeder concepts have been provided the Reactor Division for both core and blanket studies.

HTGR Low Enrichment Study

R. B. Pratt

Fuel element fabrication costs have been estimated for a proposed low-enrichment Dragon Project HTGR concept. The fuel element consists of five annular graphite cylinders filled with bonded coated particles. The cylinders are joined at the element base by integral graphite webs, which are slotted to permit coolant passage. Fabrication steps investigated include purchase and machining of graphite, fuel kernel preparation, particle coating, element loading and bonding, and inspection.

On the assumption that the production requirements for 1-, 10-, and 30-reactor industry sizes would be 80, 800, and 2400 kg U/day, we estimated that the fabrication costs would be \$166.28, \$108.38, and \$98.23/kg of heavy metal, respectively. Graphite costs were based on a fine-grained, machinable grade. Fuel was assumed to be 3%-enriched UO₂ sol-gel microspheres, coated with layers of pyrolytic carbon and silicon carbide and bonded into narrow annuli in the graphite cylinders. The low enrichment eliminates the need for highly enriched uranium and thorium-²³³U recycle facilities. The estimated costs include operating, capital, and hardware costs for fabrication of such an element but do not include nuclear fuel costs, use charges, nor nuclear fuel losses. The accuracy of the estimation is considered to be $\pm 20\%$.

HTGR Recycle Delay Analysis

F. J. Homan R. B. Pratt

We calculated the economically optimum time for large-scale HTGR recycle operation startup as an aid to the planning of the HTGR Recycle Development Program. The results show that the most favorable time to start recycle operations is seven to eight years after the first 1000 Mw (electrical) HTGR goes on-line.

The data entered into the calculations were:

1. mass balances for recycle and non-recycle,¹²
2. predicted growth curves for the HTGR industry,¹³
3. estimated cost curves for HTGR reprocessing¹⁴ and refabrication,¹⁵⁻¹⁷
4. estimated cost curves for fuel element storage,¹⁸ and
5. estimated cost curves for waste storage.¹⁴

Varying the input data over wide ranges had little effect on the calculated time for recycle startup. Replacement of the most optimistic HTGR growth curve with a very pessimistic curve changed the optimum recycle startup less than two years. Present worth factors of 0 to 15% had no effect on the recycle startup date, while increasing the scaling factor for reprocessing and refabrication plants from 0.51 to 0.75 changed the optimum date by less than two years. We concluded that the optimum date for recycle startup was insensitive to large changes in input parameters. A report on this analysis is being prepared.¹⁹

¹²D. R. Vondy and T. B. Fowler, *Computer Code TONG for Zero-Dimensional Reactor Depletion Calculations*, ORNL-TM-1633 (June 1967).

¹³S. Donelson, personal communication, Gulf General Atomic, Inc.

¹⁴J. T. Roberts, Chemical Technology Division, personal communication.

¹⁵F. N. Washburn, A. L. Lotts, and F. E. Harrington, *Comparative Evaluation of Sol-Gel Fuel Fabrication Costs*, ORNL-TM-1979 (September 1967).

¹⁶A. L. Lotts, D. A. Douglas, Jr., and R. L. Pilloton, *Refabrication Technology and Costs for High-Temperature Gas-Cooled Reactor Fuels*, ORNL-TM-1115 (May 1965).

¹⁷F. E. Harrington, Chemical Technology Division, personal communication.

¹⁸W. H. Seden, *HTGR Long-Term Spent Fuel Storage Costs*, GAMD-7994 (Sept. 1, 1967).

¹⁹F. J. Furman, R. B. Pratt, and A. L. Lotts, *Prediction of Economically Optimum Time to Initiate Recycle for the High-Temperature Gas-Cooled Reactor Industry Using Computer Program DELAY*, report in preparation.

FUEL PERFORMANCE ANALYSIS

R. E. Adams A. Goldman

The ability of a fuel element to perform satisfactorily to its design burnup is a major factor in defining the economics of nuclear power systems. We have evaluated the materials and fuel element performance of several reactor concepts from the aspect of design and the operating environment to identify potential problem areas that may limit the ability of the systems to perform as proposed. The reactor systems investigated as part of the ORNL contribution to the updating of the *Civilian Nuclear Power, A Report to the President ... 1962* are discussed below.

Heavy-Water-Moderated Organic-Cooled Reactors

Several varieties of heavy-water-moderated organic-cooled reactors (HWOCR), which differed principally in the type of fuel elements used, were examined. Three had rod bundles clad with sintered aluminum powder (SAP). Fuel for these was natural or slightly enriched uranium carbide (NUC and EUC) or thorium-uranium oxide (TUO). Two had nested annular tubes of natural uranium metal (NUM) or thorium-uranium metal (TUM) with coextruded zirconium alloy claddings. Details of the evaluation have been published.¹⁰

We found SAP cladding to be feasible for these reactor systems. It is compatible with organic coolants and with hyperstoichiometric UC at the proposed times and temperatures. We conclude that consistent properties can be attained in fuel cladding tubes and that strength will be adequate at proposed operating temperatures and times. A major limitation is that its ductility at low strain rates will be limited to about 0.5%. Data are lacking on effects of compressive and biaxial stresses and on long-time creep effects.

Of principal concern from the aspect of fuel element performance are the effects of fuel swelling and fission-gas release on the ability of the fuel cladding to maintain its integrity. We conclude that all fuel elements will operate satisfactorily at the heat ratings and temperatures proposed. With the EUC fuel element, fuel swelling coupled with low cladding ductility will necessitate rigid control of gap thickness between fuel and cladding to achieve design burnup. The problem is less critical at the lower burnup level proposed for the NUC fuel element. The TUO fuel element, as designed, appears to have insufficient void space to accommodate released fission gases. We conclude that it may be necessary to increase the end plenum length to 3.9 in.

(from 1.3 in.) to achieve design burnup. Fuel swelling and fuel tube stability are the critical parameters for the metal fueled systems, and additional data are necessary to establish performance characteristics. With the NUM fuel tubes, excessive fuel swelling could lead to collapse of the inner cladding or failure of the outer cladding as a result of plastic strain instability, and the estimated 1% swelling per 1000 Mwd/ton will limit maximum exposures to about 7000 Mwd/ton. With the TUM fuel tubes, the much lower swelling rates of about 2% per 10,000 Mwd/ton and the fuel tube geometry will cause only a 0.006-in. increase in thickness and less than 0.5% cladding strain at maximum average burnup of 20,000 Mwd/ton. Principal uncertainty will be potential fuel tube distortion and maintenance of uniform coolant channel spacing during the long fuel element exposure.

Heavy-Water-Moderated Light-Water-Cooled Reactor

The fuel element for the proposed heavy-water-moderated light-water-cooled reactor (HWBLW) has Zircaloy-4-clad natural UO_2 fuel rods in 5-ft-long bundles stacked in vertical pressure tubes. The proposed maximum burnup level is about 11,000 Mwd/ton. The proposed operating limits slightly exceed those achieved in current power reactors but are within limits for planned large boiling water reactors. An analysis of fuel rod performance, based on fuel swelling, thermal expansion, and fission-gas release, suggests it may be desirable to provide a small void plenum (approx 0.6 in. long) at one end of the fuel rod. We concluded that with some additional development the fuel element could operate satisfactorily at proposed conditions.

Steam-Cooled Fast Breeder Reactors

Fuel element performance was analyzed for three different steam-cooled fast breeder reactor designs. All used UO_2 - PuO_2 fuel. The high pressure (3700 psi coolant) design had type 19-9 DL stainless steel cladding, while the intermediate-pressure design (2680 psi) and the low-pressure design (1250 psi) used Inconel 625.

Steam-cooled fast reactors impose severe requirements on fuel cladding materials because of the combined effects of high coolant pressures and temperatures, the high fast neutron exposures, and the high burnups required. No prototype fuel elements have been tested for any of the reactors. Steam-cooled superheater elements have been tested at comparable temperatures, pressures, and times in thermal reactors at burnups to a few thousand megawatt days per ton.

Sodium-cooled rods have been tested in fast reactors at lower temperature and coolant pressures to burnups in excess of 50,000 Mwd/ton. Thus, projected burnups of approximately 100,000 Mwd/ton represent considerable extrapolations of existing technology, and considerable testing and development would be required to define materials limitations and optimize fuel element designs. Major problem areas are summarized below.

Coolant-cladding compatibility appears satisfactory for Inconel 625. Austenitic stainless steels have shown marginal performance in high-temperature steam environments because of stress corrosion cracking, and we believe that the 19-9 DL cladding would not be satisfactory for this application. Moreover, a compatibility problem may develop between the mixed oxide fuel and the cladding since some surface reactions have been observed under irradiation.

All three concepts propose internal preuse pressurization of the fuel rods to prevent cladding collapse from the high coolant pressures during initial operation. Our analysis indicates that preuse pressurization should be increased for both the low- and high-pressure designs. The high-pressure design will also require an increase in void plenum volume to accommodate internal pressures at the end of life.

Radiation effects will reduce cladding ductility and rupture strength. On this basis, the limiting fuel element life was judged to occur when the cladding stress resulting from fission-gas pressure would develop 1% cladding strain. Maximum burnup levels based on this criterion are about 100,000, 53,000, and 62,000 Mwd/ton for the low-, intermediate-, and high-pressure designs, respectively.

Fuel swelling will also contribute to cladding stress. The magnitude of stress from this effect will depend on the ability of swelling fuel to flow into the internal porosity provided. Available high-exposure data on similar fuels indicate an increasing resistance toward such accommodation as burnups exceed about 50,000 Mwd/ton. Since fuel temperatures for the steam-cooled reactors are somewhat higher, fuel may flow more readily. We concluded that maximum burnup levels for the steam-cooled reactors cannot now be defined.

From the aspect of fuel performance, the intermediate pressure design appears most conservative, and we consider that fuel elements will probably perform satisfactorily to burnups of 50,000 Mwd/ton.

We believe that the low-pressure-design maximum heat ratings should be reduced about 10% to avoid operation with molten fuel. A 30% increase in preuse pressurization should avoid fuel rod collapse without creating excessive internal pressures. The maximum

burnup limit will probably be controlled by fuel swelling and cannot be defined at this time. We believe that the 19-9 DL cladding proposed for the high-pressure design will not be satisfactory because of potential stress corrosion cracking. A significant increase in fuel rod preuse pressurization and an increased void plenum would be required to reach design burnup.

Gas-Cooled Fast Reactors

The proposed fuel element has mixed oxide pellets clad in type 316 stainless steel. Two designs were evaluated: a reference design (GCFR-4) with maximum heat rating and cladding temperature of 17.8 kw/ft and 1435°F, and a derated design operating at 16.3 kw/ft and 1315°F.

The fuel element design includes a proposed manifold system to equalize pressures across the fuel cladding. Thus, fission-gas pressure and fuel cladding collapse are not potential problems.

Fuel swelling would be the major source of cladding stress. The ultimate burnup limitation would depend on the extent to which fuel swelling can be accommodated within the fuel rod without exceeding the assumed 1% cladding strain limit imposed by radiation damage. Thus, fuel element life will be governed principally by the magnitude of cladding restraint.

These designs offer less restraint toward fuel swelling than has prevailed during most experimental tests on similar fast reactor fuels. However, fuel temperatures are also slightly higher, so the greater fuel plasticity and low internal pressure may decrease the required restraint.

As with steam-cooled reactors, a potential problem of incompatibility may exist between the fuel and the cladding; cladding-coolant compatibility will depend on coolant impurities. Corrosion from either source will reduce cladding strength.

We believe that the heat ratings and temperatures proposed for the reference design would result in molten fuel and probably lead to premature failure through fuel slumping and expansion effects, but the proposed conditions for the derated design are feasible.

We concluded that burnup limitations as a function of cladding strength and maximum allowable operating temperatures must be defined by experimental testing before such limits can be usefully applied to these designs.

Carbide-Fueled LMFBR

A conceptual design of an advanced fuel element for a carbide-fueled LMFBR was also evaluated. The design

proposed a sodium-bonded, vented fuel rod, operating at maximum heat rating of 67 kw/ft and 1350°F maximum cladding temperature. The design assumed that heat transfer problems could be solved and a cladding material compatible with sodium and with properties similar to type 316 stainless steel would be developed. Low fuel swelling rates of approximately 1.8% per 10,000 Mwd/ton were anticipated on the basis that the high fuel temperatures would release most fission gases, and average burnup levels of 111,000 Mwd/ton were assumed.

The proposed element was felt to be a major extrapolation of present technology. Initial operation at the heat ratings proposed is considered feasible (test data exist up to about 40 kw/ft), although the effects of thermal stresses and possible deterioration of the sodium bond conductance could cause early failure. Fuel-cladding compatibility has not been established, and at the high inner-cladding temperature (approx 1550°F max) carburization of the cladding is likely. The possibility of doping the fuel to stabilize the carbon exists.

An analysis of carbide fuel irradiation data indicates that fuel swelling is temperature dependent, and low swelling is obtained only at low fuel temperatures or in cases where cladding restraint is considerable. Carbides are notable for their ability to retain fission gases, and no cases of fission-gas release in excess of 30% have been reported for fuels operating up to 3000°F. Even at peak power regions of a rod in this design, more than 50% of the fuel would operate at temperatures below 3000°F. An optimistic minimum swelling rate of 5.4% per 10,000 Mwd/ton was assumed for peak power regions. On this basis, the fuel would contact the cladding at 42,000 Mwd/ton. Cladding restraint would be small for the proposed 0.015-in.-thick cladding at operating temperatures, so a burnup limit of about 55,000 Mwd/ton was estimated to be optimistic for the fuel rod.

We concluded that the proposed design offers little chance of achieving the design burnup and represents an ultimate goal to be achieved if successful solutions can be developed for all recognized problems.

HTGR Evaluation

Two high-temperature gas-cooled reactor designs prepared and submitted by Gulf General Atomics (GGA) were examined. The designs were termed the "Reference Design" and "Backup Design." The latter reflects the current state of HTGR technology as exemplified by the Fort St. Vrain power station now under

construction, but in accordance with the AEC Advanced Converter Task Force ground rules, it is a 1000 Mw (electrical) single-reactor concept. The Reference Design is intended to represent the more favorable performance that should be possible in an HTGR after successful completion of development programs.

We found that the coated-particle graphite-matrix fuels common to both designs have been demonstrated in reactor systems in the United States and abroad in numerous irradiation tests under widely varying conditions. We calculated the maximum fuel temperatures in both designs to be less than the 1500°C values specified by GGA, even with conservative values for thermal conductivity. Our calculations indicated that maximum tangential strains of about 1.6% will occur in the particle coatings as the result of fuel kernel swelling, fission-gas pressure, and fast neutron damage in the pyrolytic carbon coatings, whereas failures are predicted to occur at 5% and greater. Thus, we concluded

that there is a design margin in the fuel performance, which might allow higher power density operation or greater fuel densities per core volume.

Evaluation of the proposed graphite core block designs and comparison with the results of irradiation tests at high temperatures to fast-neutron doses of about 5×10^{21} led to the conclusion that cracking of the graphite blocks and/or jamming of the blocks in the core might occur. No penalty was assigned to this concept since the irradiation data are so fragmentary that it is not clear that the problem exists. If necessary, the situation could be eased by specifying a graphite with relatively better irradiation stability, reducing graphite maximum temperatures, designing the blocks to permit some movement, or ordering fuel exposures.

The results of our analyses have been drafted.²⁰

²⁰Staff of ORNL, *Core Evaluation of High-Temperature Gas-Cooled Reactors*, ORNL-4194 (draft).

36. Terrestrial Low-Power Reactor

G. M. Slaughter

The Terrestrial Low-Power Reactor (TLPR) Program Office was established at ORNL in September 1966. This office acts as an extension of the Division of Reactor Development and Technology of the AEC and assists in the detailed planning, coordination, and evaluation of the activities of the TLPR program to be carried out by the AEC's laboratories and industrial contractors.

The program presently has two basic objectives. The first is the development of technology for reactor electric power systems, initially covering the range of 30 to 200 kw (electrical), that may have various applications, such as oceanographic power plants and remote terrestrial power plants. The systems are to serve as stationary power plants and may be either attended or unattended. The second objective is to prepare the conceptual design of a terrestrial power systems test facility. The facility is to have provisions for testing both reactor and isotopic power plant systems under environmental conditions of the various potential applications.

We have been involved in the selection of structural materials and fuels for these systems.

MATERIALS SELECTION

G. M. Slaughter

In the course of the TLPR program, it has become evident that some major advantages should be associated with the use of titanium as the structural material for water reactor systems. An examination of the flowsheets for water reactor plants, particularly those for the Army Package Power Reactor (APPR), discloses that the water-treatment systems are responsible for a large fraction of the instrumentation, controls, plumbing, and other equipment. A study of the basic water chemistry problems indicates that most or all of this equipment could be eliminated by use of a hermetically sealed system built of a single corrosion-resistant structural material.¹ While the data available on conventional water reactor systems are not sufficient to determine whether this will indeed prove possible,

titanium appears likely to be much better than stainless steel or Inconel, the next-best contenders.² If all or most of the water-treatment equipment could be eliminated through the use of titanium, the reduction in costs, complexity, maintenance, transportation, and field assembly problems would be very great indeed and would far more than justify any increase in cost that might stem from the use of titanium.

Consequently, over the past year we have determined the state of the art of fabricating and welding titanium and its alloys and have kept abreast of the corrosion work being performed. A number of trips were made to installations directly involved in the development and usage of titanium. A large number of reports covering many aspects of the technology of titanium were also reviewed. An analysis of all the information obtained indicates that the technology of titanium has advanced to a high degree in the past few years. Its corrosion resistance, fabricability, and weldability are such that it appears feasible to consider it as a structural material for TLPR applications.

FUELS EVALUATION

W. S. Ernst

The TLPR program at ORNL has been designing a 11.75 Mw (thermal) pressurized water reactor for remote applications. The primary objective has been to minimize fuel cycle costs within the basic ground rule that the supporting technology be state of the art. This precludes new concepts that would require extensive testing. One of the principal goals affecting both fuel performance and economics is a 50-Mwyr core life. This is a stringent goal considering the present operating experience.

¹A. P. Fraas, *Conceptual Designs for TLPR Plants with Boiling Water Reactors*, ORNL-TM-2012 (to be published).

²G. H. Jenks and J. C. Griess, *Water Chemistry in Pressurized and Boiling Water Power Reactors*, ORNL-4173 (November 1967).

During the past year we assisted the TLPR program by evaluating several fuel types considered for use in this reactor. The performance of fuel as it pertains to TLPR requirements was assessed by evaluating the literature and personal communications. Pellets of UO_2 contained in a metal tube still represent the fuel configuration in which technology is most advanced.

Calculations concerning fuel performance indicate that the average linear heat rating of the fuel will be about 2.3 kw/ft and the peak about 5.9 kw/ft. For a 50-Mwyr core life, the average expected fuel burnup will be about 21,250 Mwd/ton and the peak about 42,500 Mwd/ton. The heat ratings are conservative and certainly state of the art, but the expected burnups are high with respect to current commercial practice. However, these burnups are in line with those forecast for a number of large pressurized water reactors now under construction.

Evidence that the desired fuel performance in a TLPR can be obtained comes from the success of the SA-1 experiment in the Dresden Reactor and the blanket elements in the Shippingport PWR-1 core. Fuel and cladding in these cases have seen irradiation conditions that bracket those expected in a TLPR. Burnups exceeding 50,000 Mwd/ton at average linear heat ratings of about 6 kw/ft are expected for the SA-1 at the end of the experiment. Currently this experiment is

in excellent condition. The SA-1 experiment, in essence, approaches reasonably closely a prototype test for full-size TLPR fuel elements. On this basis we believe the fuel element designed for the TLPR will perform as expected.

Core fabrication costs³ as well as the complete fuel cycle costs⁴ have been estimated for the TLPR. Fabrication costs were based on a plant throughput chosen as representative of the size plant in which specialized fuels such as the TLPR core might be fabricated. Since military application of the TLPR probably will be its primary function, the economic rules as applied to military users were applied. Military nuclear fuel cycle analyses differ from conventional commercial analyses in two important aspects: (1) no use charge is applied while the fuel is in the field and (2) no commercial interest is applied. Under these conditions, a core for the TLPR was estimated to cost about \$233,000 or approximately \$266/kg U. The fuel cycle costs were estimated to be below 12 mills/kwhr for a range of loadings and lattice pitches near the TLPR fuel configuration. These fuel cycle costs assume that the 50-Mwyr core lifetime will be obtained.

³Personal communication, A. E. Goldman to W. S. Ernst, Jr., May 14, 1968.

⁴Personal communication, Carl Copenhaver, Reactor Division.

37. Thorium Utilization

A. L. Lotts

The development of the thorium- ^{233}U fuel cycle has for several years been an objective of the Chemical Technology and Metals and Ceramics Divisions. This work primarily involves the development of processes, the engineering of processes and equipment, and the demonstration of equipment and facilities for reprocessing bred fuels on a pilot scale. Recently, the primary emphasis in the program has been the development of a refabrication process for prismatic graphite fuel elements containing coated particles, an advanced design of the fuel elements employed by Gulf General atomic in the Fort St. Vrain Reactor. The project is to culminate in a demonstration of the refabrication of this advanced fuel element containing thorium and ^{233}U .

Accordingly, we are developing pilot-scale processes and equipment for the recycle of these advanced HTGR fuels. The work includes process development, engineering development, equipment design, pilot-scale demonstration of processing, product evaluation, and irradiation testing. The program is tied quite closely to the Gas-Cooled Reactor Project, particularly that aspect of the program dealing with the testing of coated-particle fuels, which is reported in Chapter 29 of this report. Since our pace was slowed, we concentrated on solving critical problems in refabrication processing technology.

Another part of the program deals with the preparation of facilities suitable for reprocessing and refabrication development for the thorium- ^{233}U cycle. A description of the present status of the TURF, as well as a service activity in TURF aimed at the preparation of a ^{233}U -bearing salt, is contained in the subsequent sections.

THORIUM-URANIUM RECYCLE FACILITY

J. M. Chandler¹

Because ^{232}U decay in recycle fuel produces increasing radioactivity with time and necessitates biological protection, we have constructed the Thorium-Uranium Recycle Facility (Fig. 37.1). This facility permits

the development and evaluation of a variety of integrated fuel processing and refabrication schemes at the necessary pilot-scale levels. Concurrently with placing this facility into operation, some design of the fabrication line for fueled-graphite equipment was accomplished; in addition, equipment was installed and operated for the preparation of ^{233}U -bearing salt for the Molten-Salt Reactor.

TURF Building Construction and Procurement

J. W. Anderson ²	S. E. Bolt ³
J. M. Chandler ¹	J. P. Jarvis ²
S. Mann ¹	D. M. Shepherd ²

A portion of the Thorium-Uranium Recycle Facility was completed by Blount Brothers Construction Company of Montgomery, Alabama, on September 15, 1967, and accepted by the Laboratory for occupancy. This permitted acceptance of the facility before total completion to expedite the installation of processing equipment in cell G for the MSRE ^{233}U fuel preparation experiment. The remainder of the facility was completed and accepted for occupancy on October 2, 1967.

During the last several months of construction an intensive effort was made to test performance of the major utility service systems and the operational equipment in the facility. To realize the maximum effectiveness from this testing program, we prepared detailed test procedures to be used by the contractor in testing the following plant systems: water, steam and condensate, compressed air, electrical power distribution, waste, gas, fire protection, heating, ventilating and air conditioning, and electromechanical systems.

Immediately upon our occupancy, Rust Engineering Company began installing the out-of-cell processing

¹On loan from Chemical Technology Division.

²On loan from General Engineering Division.

³On loan from Reactor Division.

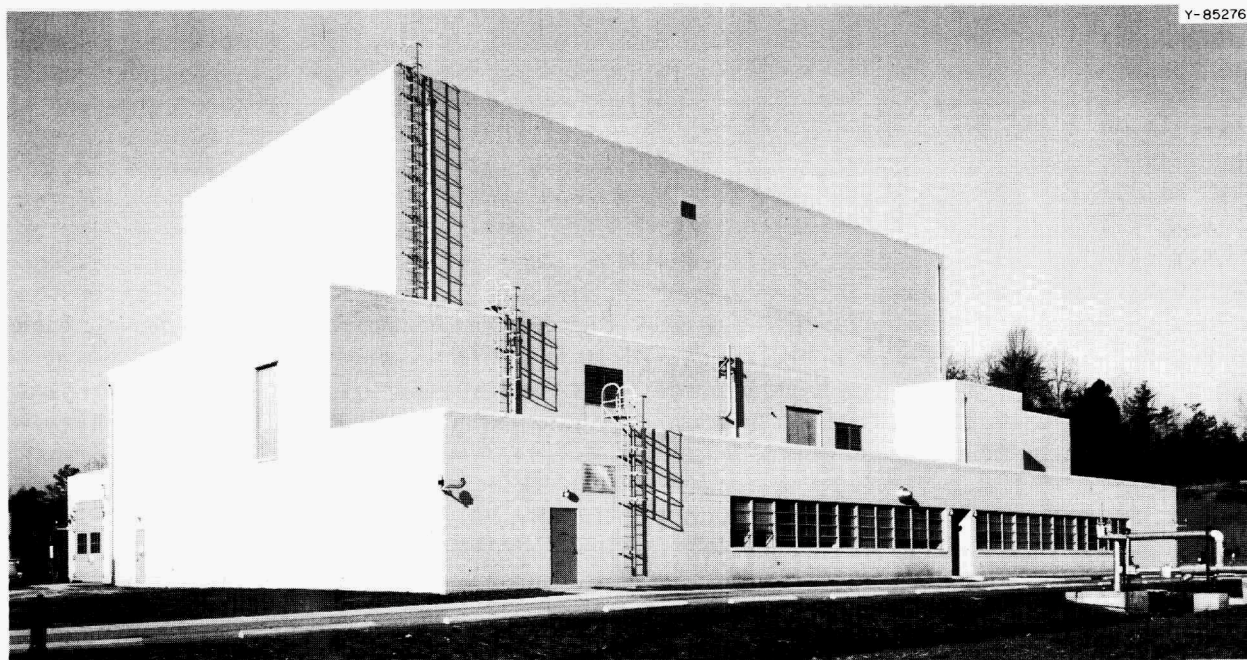


Fig. 37.1. The Thorium-Uranium Recycle Facility.

equipment for cell G, in-cell crane and manipulator systems, various service plugs in service sleeves throughout the cell bank, viewing windows at cell operating modules, and the equipment mounting pad on the floor in cells C and D (shown in Fig. 37.2). This portion of the construction program, authorized as cost-plus-fixed-fee participation, was completed on January 15, 1968, at approximately 15% less than the estimated cost. Painting was completed on March 9, 1968.

The installation of special equipment in the facility by the Laboratory began November 1, 1967, and was completed on March 15, 1968. This work consisted primarily of installation of master-slave manipulators, special sampling equipment for the liquid waste tanks, a pneumatic-tube solid sample conveyor system for cells C, D, and E, and the facility radiation and contamination monitoring and control equipment. Also, we cleaned and filled the zinc bromide window tanks in cells G and F. The filling of the remainder of the window tanks has been deferred until facility operations require shielded viewing windows in other cells. The Laboratory's participation in the construction project has included the procurement and installation of special-purpose equipment costing \$1,753,000. This participation was concluded on March 15, 1968, within the estimated time and cost. Sol-gel sphere-forming equipment and the remaining zinc bromide shielding media have been deferred until the end of 1969. The fuel fabrication equipment has not yet been authorized.

Concurrent with the construction operations by Rust Engineering Company and the Laboratory, the TURF operating staff prepared and executed procedures whereby the facility was checked out and placed into normal operating condition. Some of the items were operator training and rechecking of the utility service systems, operation of the in-cell crane and manipulator systems, installation of Raschig rings in a liquid waste tank, calibration of all three hot waste tanks with checkout of the waste tank sampling station and all the instrumentation and controls for operating and maintaining the waste tanks, replacement of the absolute filters in both the cell exhaust and hot off-gas filter pits, and testing of the filter pit and checkout of the complete facility ventilating and air conditioning system with dioctyl phthalate. Plans were also developed and placed into effect for preventive maintenance on all operating equipment and for coordinating various programs for testing and inspection of equipment essential to safe operation.

A number of improvements to the facility were made. These include landscaping of the site by the Plant and Equipment Division, identification of equipment and service lines within the facility, installation of an argon supply system for maintaining a purge and blanket on shielded viewing windows, installation of neutron threshold detector instruments on both the first and third floor levels of the facility, and the installation of an additional constant alpha air monitor.

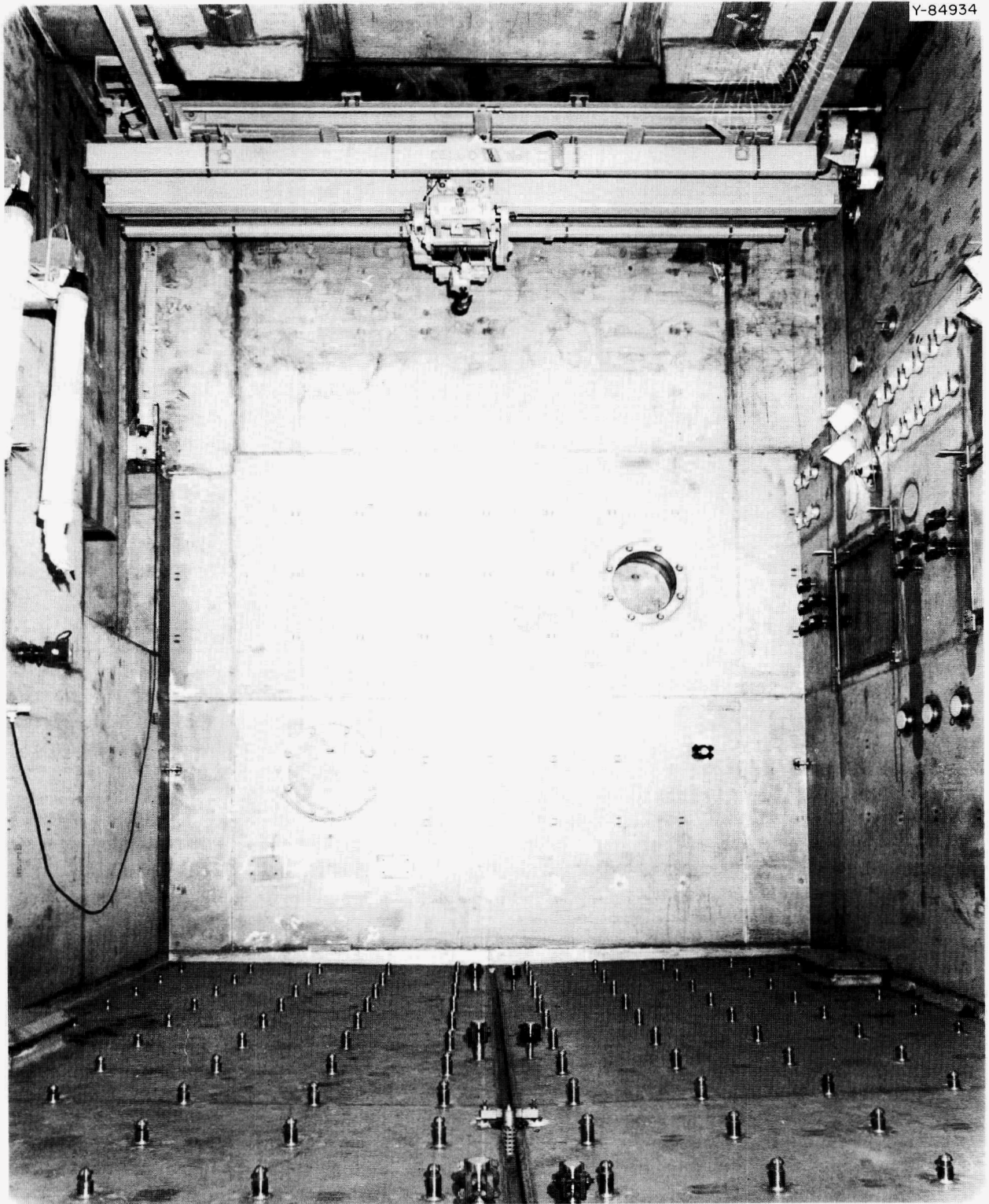


Fig. 37.2. Cell D, Showing Equipment-Mounting Pad Installed.

An emergency manual for the facility was prepared, and assembly of data for the facility operating manual began with manuals for a number of the facility utility service systems.

The safety analysis for the facility was drafted during the latter part of 1967, and the facility received preoperational review by the AEC on January 21, 1968. These efforts resulted in approval of the facility to carry out the MSRE ^{233}U fuel preparation experiment and tentative approval of operation of the facility in the broad spectrum of research activities for which it was designed and constructed.

Preparation of ^{233}U Fuel for the MSRE

S. E. Bolt³

Operation of the Molten-Salt Reactor with ^{233}U fuel will provide valuable nuclear and chemical data for future molten-salt reactors. Plans have been completed for refueling and operating the MSRE with this type fuel. Approximately 39.5 kg of 91.4%-enriched ^{233}U as ^7LiF -27 mole % UF_4 eutectic salt will be required by the MSRE. This material is being prepared in remotely operated equipment in cell G of TURF because of the 222 ppm ^{232}U in ^{233}U . Details of the progress on this work may be reviewed elsewhere.⁴

DESIGN OF FUELED-GRAPHITE LINE

J. D. Sease

To demonstrate the technical and economic feasibility of refabricating recycle fuel for HTGR's, we plan to design, install, and operate a pilot-scale demonstration line in TURF. The fuel elements fabricated in the line will consist of graphite blocks with holes for fuel and for passage of coolant gas. The fuel holes will be filled with a carbonaceous matrix containing microspheres of ^{235}U , ^{233}U , and thorium as either the oxide or carbide coated with pyrolytic carbon, silicon carbide, or both. Only oxide particles will be coated in the line. The reference fuel element for the line is based on the proposed Public Service of Colorado, Fort St. Vrain Reactor (PSC) element and consists of a hexagonal graphite block 14.5 in. across the flats and 31 in. long, containing some 200 fuel channels about 0.5 in. in diameter. The line will be capable of processing approximately 20 kg of fuel per 24-hr day; this is equivalent to two PSC elements.

⁴Chem. Technol. Div. Ann. Progr. Rept. May 31, 1968, ORNL-4272 (in preparation).

Originally, the design for the fueled-graphite line was to be completed in 1969, with operation to begin in 1972; however, now completion of the design is not required until 1972, with operation in 1974. At the time of the program change, we had completed approximately 80% of the conceptual design of this line and about 5% of the detailed design. Resumption of the design of the line is scheduled to begin in 1970. A detailed description of the status of the fueled-graphite line is contained in the Thorium Utilization annual reports.⁵

FUELED-GRAPHITE DEVELOPMENT

F. J. Furman J. D. Sease

Our objective is to provide economical processes for remote refabrication of thorium- ^{233}U -bearing HTGR fuels. Presently, our main concern is with processes dealing with the fuel particles. This work is divided into four parts: particle handling, particle coating, particle inspection, and bonding of fuel particles.

Particle Handling

J. T. Meador F. J. Furman

In the TURF, over 10 kg/day of particles will have to be remotely transferred between the forming, sizing, coating, inspection, and blending operations involved in the fuel refabrication process. To accomplish these transfers, we developed a pneumatic particle transfer system.

During the past year, we emphasized development of connecting devices in the pneumatic transfer lines to allow the transfer path to be changed remotely. We developed a diverter valve that will switch the transfer path from one line to another and joints that will connect two or more lines into one. This equipment was tested together with previously developed cut-off valves, hoppers, and feed devices and found to be highly reliable. Over long-term usage, only negligible abrasion occurs on pyrolytic-carbon-coated particles.

Particle Coating

R. B. Pratt C. F. Sanders
W. H. Pechin

Deposition of pyrolytic carbon coatings on nuclear fuels is probably one of the more difficult and

⁵R. G. Wymer and A. L. Lotts (compilers), *Status and Progress Report for Thorium Fuel Cycle Development Dec. 31, 1966 and Dec. 31, 1967*, in preparation.

expensive steps associated with the fabrication of HTGR fuel elements. Analysis has shown that increasing the production scale of coated fuels can reduce the cost of this step.⁶ Therefore, we have directed our efforts toward development of a pilot-scale process⁷ for depositing pyrolytic carbon coatings on sol-gel microspheres in quantities to 10 kg/day. Not only do we have the normal problems associated with increasing the scale of a process; we are also concerned with ensuring that the process is suitable for remote fabrication of ²³³U-bearing recycle fuels in the TURF. We are establishing cold processing equipment, delineating coating parameters, seeking control of coating properties, and designing and fabricating an in-cell prototype remotely operated fluidized-bed coating system. Significant progress was made in each of these areas.

The 5-in.-ID coating furnace system has become existing technology and is operating routinely. A sufficient number of coating parameters have been defined that coatings can be reproducibly controlled over a wide range of specifications.⁸ Efforts in this area include a continuing investigation of deposition of low-density buffer coatings from acetylene as well as a main effort toward characterization of high-density coatings produced from propane and propylene.

During the past year, our knowledge of coating nuclear fuel particles has increased sufficiently to enable final design and construction of a prototype remotely operated coating system.⁹ The system is 95% complete and awaiting checkout and startup.

The design of the prototype coater, including its furnace and service disconnects, is shown in Fig. 37.3. The assembly consists of the following functional modules: the base, the subbase (including disconnect blocks), the water-cooled shell, and the furnace internals, including the coating chamber, gas-injector manifold, and heating element.

⁶A. L. Lotts, D. A. Douglas, Jr., and R. L. Pilloton, "Refabrication Technology and Costs For High-Temperature Gas-Cooled Reactor Fuels," pp. 167-97 in *Proceedings of the Conference on Fuel Cycles of High-Temperature Gas-Cooled Reactors, Brussels, June 10-11, 1965*, ed. by D. Tytgat, European Atomic Energy Community (EURATOM), Brussels, May 1966, EUR-2780.e.

⁷R. B. Pratt, J. D. Sease, and A. L. Lotts, *Pilot-Scale Equipment Development for Pyrolytic-Carbon Coating*, ORNL-4302 (in press).

⁸R. B. Pratt, J. D. Sease, and A. L. Lotts, "Pyrolytic Carbon Coating in an Engineering Scale System," paper presented at the Winter Meeting of the American Nuclear Society, Chicago, Illinois, 1967.

⁹J. D. Sease and S. E. Bolt, "Fueled-Graphite Fabrication Equipment," *Status and Progress Report for Thorium Fuel Cycle Development Dec. 31, 1966* (in preparation).

Experience has proven coating of particles to be a high-maintenance process step. Accordingly, the remote coater design reflects a maintenance philosophy that provides for modular replacement of components and repair or renovation of defective modules in a gloved maintenance area.

The remote coater also serves as a vehicle for demonstrating proposed instrumentation philosophies. Preprogrammed and manual operation are provided. Critical system parameters are automatically monitored and safety interlocked. In addition, this information is designed for compatibility with a data logging and computer control system proposed for the ultimate fueled graphite fabrication process.

Particle Inspection

F. J. Furman

In a typical HTGR, the fuel loading tolerances are $\pm 1\%$ for the complete core or $\pm 5\%$ for an individual fuel element. To obtain the tolerances required, the size and density of the fuel particles before and after coating must be accurately known. In a large-scale production facility, these determinations must be made swiftly to control the process. Conventional determinations of particle size by microradiography and density by sink-float or combustion are too slow. We favor a particle-size analyzer that will determine rapidly and precisely the diameter of a large number of particles and at the same time count the number of particles in a given weight of material.

Considerable progress has been made in the past year in achieving these aims. We obtained a particle size analyzer, which, after development, should fulfill these needs. The principle of operation is as follows. The sample, which may be in air or a clear fluid, passes in front of a light beam. The magnitude of the light-beam interruption is proportional to the size of the particle. The decrease in light produces a proportional dip in photodetection output current, which is electronically shaped so that it can be accepted by a pulse-height analyzer. The pulse-height analyzer presently used consists of ten channels, each calibrated to count particles with a 10- μ range of diameters, so any one calibration covers a total range of 100 μ . The counter can be calibrated for particles from 150 to 850 μ in diameter. Analysis of the particle counts in each of the channels gives the mean diameter, particle size distribution, and -- combined with a weight measurement -- particle density.

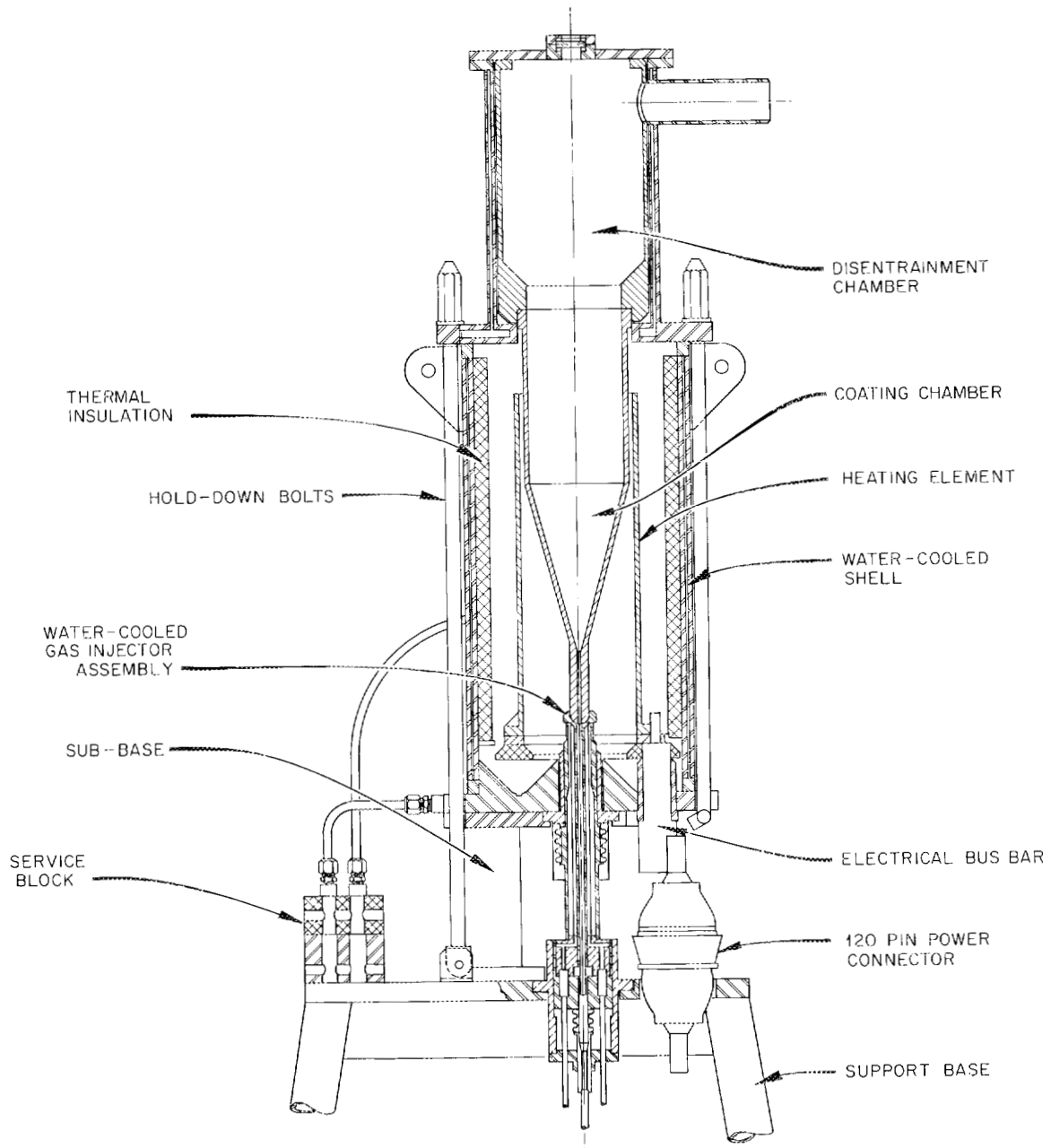


Fig. 37.3. Prototype Remote Fluidized Bed Coater.

Bonding of Fuel Particles

C. F. Sanders F. J. Furman

The bonding of fuel particles is necessary to prevent spilling of the particles if a fuel element breaks. The fuel particles will be bonded into 1/2-in.-diam 30-in.-long sticks, which can be inspected before insertion into the hexagonal carbon elements. The bonding agent now used is a mixture of phenolic resin, maleic anhydride as accelerator, and carbon dust as filler.

Fuel sticks 12 in. long are now being produced. They contain particles of two different sizes and will be used to test techniques for recovering ^{233}U separate from ^{235}U , as will be done in the actual recycle of HTGR fuels.

For the fabrication of the experimental fuel sticks, we developed a molding system that can be easily automated. It uses single swaged molds with removable end plugs. The molds are filled with particles by two or three adjustable-orifice feeders, which can be closely controlled to give selected ratios of particle types. After the mold is loaded with particles, the bonding mixture is injected, and the assembly is baked to polymerize the resin. After being baked, the sticks are hydraulically ejected and the molds are returned to be cleaned and reused. The fuel sticks are inspected and inserted into the hexagonal block.

COATING OF HIGH-ACTIVITY PARTICLES

E. S. Bomar

Personnel at BNWL requested three lots of coated microspheres for use in physics experiments. Each lot contained about 250 g of microspheres of ZrO_2 with 8% of $^{233}\text{UO}_2$, $^{235}\text{UO}_2$, or $^{239}\text{PuO}_2$. The Chemical Technology Division prepared the microspheres by the sol-gel method, and we applied a nominal coating of $100\ \mu$ of pyrolytic carbon in a fluidized bed.

These fuels differed in two ways from materials with which we had prior experience; namely, they were much less dense and decreased 7 to 10% in volume due to the transformation from monoclinic to tetragonal structure on heating to approximately 1000°C , which is below the coating temperature.

The $^{239}\text{PuO}_2$ - ZrO_2 microspheres were coated without complication, giving a product having a surface alpha count of a few hundred counts per minute per gram of particles. The $^{235}\text{UO}_2$ - ZrO_2 showed an order of magnitude less radioactivity, as would be expected. However, we had difficulty with the $^{233}\text{UO}_2$ - ZrO_2

material due to its smaller average particle size, which required operation of the coating furnace under conditions that led to a highly stressed coating. The coating on quite a few particles cracked from the increase in volume of the oxide core on transforming to the less dense monoclinic phase during cooling. Surface alpha activity ranged up to 10^5 counts $\text{min}^{-1}\ \text{g}^{-1}$.

IRRADIATION OF THORIA-BASE BULK OXIDE FUELS

A. R. Olsen

The irradiation testing and evaluation of metal-clad thoria-base bulk oxide fuels are continuing. The current program, listed in Table 37.1 along with the status of each test, is restricted to the completion of irradiation tests that were started before July 1967. The results of earlier tests in this series have been reported.¹⁰⁻¹²

Examination of the three pellet rods, given an extended irradiation to attain scheduled burnup levels of approximately 150,000 Mwd/MT, is essentially complete. The burnup analyses for these tests indicate that the actual burnup level was only about 100,000 Mwd/MT. Examination of the microstructures shows that the fuel operated at linear heat ratings of less than the proposed 12 kw/ft, which would account for the lower burnup during the long exposure period of approximately 1190 effective full power days. A report on the low-heat-rating thoria-base fuel tests is in preparation.

The microstructure of the $(\text{Th}-5\%\text{Pu})\text{O}_2$ Sphere-Pac fuel shown in Fig. 37.4 can be compared with the UO_2 and $(\text{U,Pu})\text{O}_2$ Sphere-Pac fuels discussed in Part III, Chapter 25, of this report. All three fuels were exposed under similar conditions, and the mode of in-reactor

¹⁰A. R. Olsen, *Metals and Ceramics Div. Ann. Progr. Rept. June 30, 1967*, ORNL-4170, pp. 220-23.

¹¹A. R. Olsen, J. D. Sease, R. B. Fitts, and A. L. Lotts, *Fabrication and Irradiation Testing of Sol-Gel Fuels at Oak Ridge National Laboratory*, ORNL-TM-1971 (September 1967); paper presented at the symposium on Sol-Gel Processes for the Production of Ceramic Nuclear Fuels, Turin, Italy, Oct. 2-3, 1967.

¹²A. R. Olsen, J. H. Coobs, and J. W. Ullmann, "Current Status of Irradiation Testing of Thorium Fuels at Oak Ridge National Laboratory," pp. 475-94 in *Thorium Fuel Cycle* (Proceedings of Second International Thorium Fuel Cycle Symposium, Gatlinburg, Tenn., May 3-6, 1966), R. G. Wymer, Coordinator, U.S. Atomic Energy Commission/Division of Technical Information, Oak Ridge, Tenn., February 1968.

fuel restructuring is similar. However, the higher melting point of the thoria-base fuel is apparent in the extent of restructuring. Many of the microspheres in the cooler outer radial position were lost in the metallographic preparation of the (Th-5% Pu)O₂ sec-

tion, indicating essentially no inter-sphere sintering in this region. Additional Sphere-Pac test rods with higher heat ratings and higher burnup will be available from the ETR-IV group during the coming year.

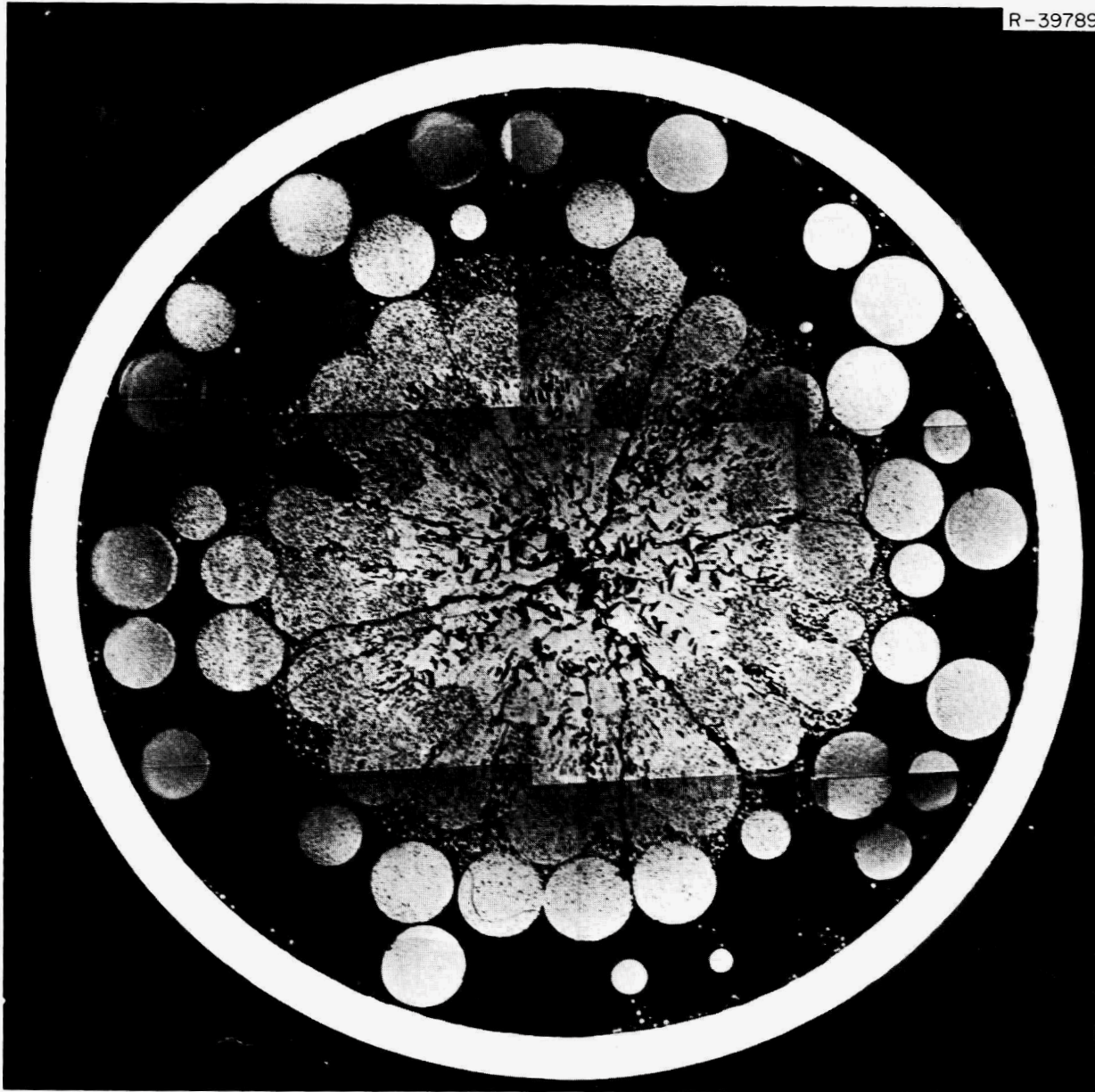


Fig. 37.4. (Th-5% Pu)O₂ Fuel Rod, Fabricated by Sphere-Pac and Irradiated to 0.5% FIMA at 450 w/cm with a Cladding Temperature of 450°C.

Table 37.1. Thoria-Base Fuel Rods Currently Being Irradiated or Examined⁴

Designation	Number of Rods	Type of Oxide	Density (% of Theoretical)	Fuel Rod Dimensions (cm)			Linear Heat Rating (w/cm)	Peak Burnup (Mwd/MT metal)	Objective	Status
				Length	OD	Wall				
MTR-II	2	Sol-Gel S ThO ₂ -4.5% UO ₂ Vi-Pac	88 to 89	57	0.8	0.06	600	100,000	Obtain higher heat rating by increasing enrichment	Being examined
MTR-III	6	Sol-Gel 35 ThO ₂ -4.5% UO ₂ Vi-Pac	86 to 89	30	1.1	0.06	820	100,000	Compare oxide calcining atmospheres and higher heat ratings obtained by increasing diameter	4 awaiting examination, 2 being examined
ETR-II	6	BNL Sol-Gel ThO ₂ -4% ²³³ UO ₂ Vi-Pac	90	48	1.3	0.09	630	30,000 to 100,000	Study effects of remote fabrication and oxide recalcining	1 examined, 1 being examined, 4 in reactor
ETR-III	5	Sol-Gel ThO ₂ -5% PuO ₂ Sphere Pac	88	48	1.3	0.09	770	10,000 to 70,000	Study ThO ₂ blanket material with gradually increasing heat rating and provide high-protactinium low-fission-product material for chemical processing	2 being examined, 2 awaiting examination
ETR-IV	6	Sol-Gel ThO ₂ -5% PuO ₂ Sphere Pac	84	24	1.3	0.09	650 to 1000	20,000 to 100,000	Study sol-gel ThO ₂ -PuO ₂ microsphere performance as vibratorily compacted beds at various heat ratings and burnup levels	In reactor
Sphere-Pac	4	Sol-Gel ThO ₂ -5% PuO ₂	84	19	0.64	0.025	450	5,000	Test sol-gel ThO ₂ -PuO ₂ microspheres with high cladding temperatures	Examined; report in preparation
Pellet Rods	3	ThO ₂ -4.5% UO ₂	91	11.4	0.79	0.06	400	150,000	Investigate swelling and gas release of ThO ₂ -base fuels at very high burnup	Report in preparation

⁴ETR-II, ETR-III, and ETR-IV rods are clad with Zircaloy-2; all other fuel rods are clad with type 304 stainless steel.

Part V. Other Program Activities

38. Metallography

R. J. Gray

As a service group to the Metals and Ceramics Division and to other divisions at this Laboratory, we are responsible for specimen preparation and examination for both radioactive and nonradioactive materials. We must assist in the interpretation of microstructures or carry out the complete study if the requester desires. Techniques for all phases of metallography must always be improved or replaced as required to maintain a high standard of quality. We also engage in equipment development and modification and investigate alternate methods of performing metallographic services, which might be applied to the general program requests.

ALPHA METALLOGRAPHY FACILITY¹

R. J. Gray B. C. Leslie

A new alpha metallography glove box line has been fabricated and installed (Fig. 38.1). The installation is designed primarily for the handling of plutonium and its alloys, and the operating discipline is complete containment for all processes. A negative air pressure of -0.5 to 1.0 in. water gage is maintained for normal operations; if required, argon can be substituted as the internal atmosphere. The various operations in the eight glove boxes are (1) cutting, grinding, and mounting; (2) mechanical polishing; (3) vacuum deposition etching; (4) microscopic inspection; (5) vacuum cathodic etching; (6) chemical and electrolytic etching; (7) replica-

tion and minor repairs of equipment; and (8) microscopy and photomicrography.

We grind specimens by a lapping method and mechanically polish on a conventional 8-in. motor-driven wheel as well as on vibratory polishing units. The inspection microscope is a modified Leitz Metallux. The metallograph is a highly modified Bausch and Lomb Research I instrument, which has been divided so that the inverted microscope is within the glove box. Illumination, visual examination, and photomicrography are coupled with the microscope through three optical relays.

In addition to the eight glove boxes in a line, two glove boxes are isolated. One is used for microhardness testing and mensuration and the other is equipped for photomacrography and mensuration.

ELECTRON MICROGRAPHIC EXAMINATION OF RADIOACTIVE MATERIALS

J. L. Miller, Jr.

We recently added electron microscopy to the list of services available in the remote metallographic facility in the High Radiation Level Examination Laboratory (HRLEL). The use of two-stage plastic-carbon replicas allows routine examination of highly radioactive (>30,000 r/hr) materials as well as alpha-emitting materials.² This replication technique has been applied

¹Presented at the 22nd AEC Metallography Group Meeting in San Diego, Calif., June 19-21, 1968.

²J. L. Miller, Jr., "Replication of Irradiated Materials for Electron Microscopy," presented at the 22nd AEC Metallography Group Meeting in San Diego, Calif., June 19-21, 1968.

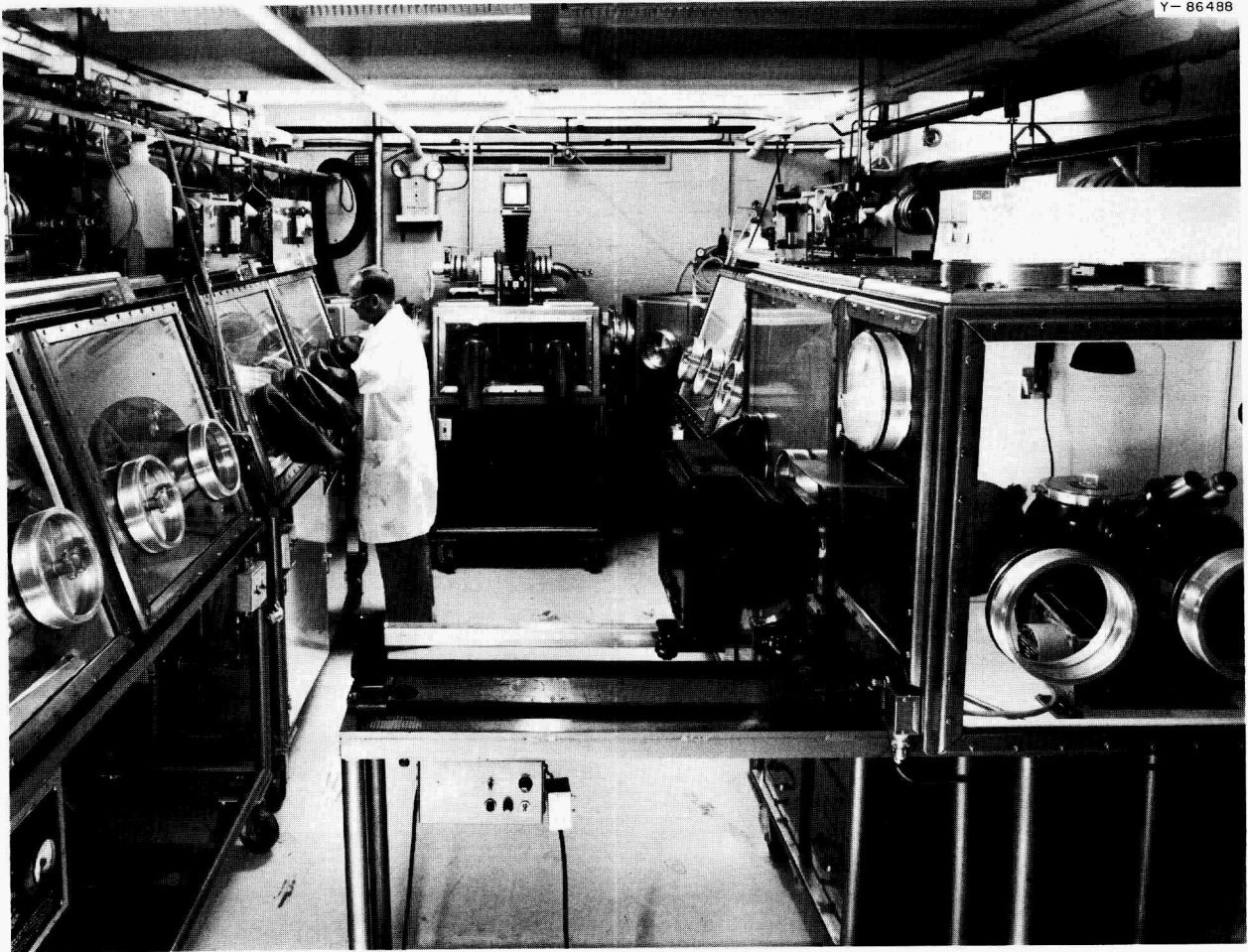


Fig. 38.1. Metallography Glove Box Line in Interim Alpha Facility in Building 3019.

to metallographic as well as fractographic surfaces with resultant resolutions consistently better than 100 Å.

Because of drift and subsequent pile-up of carbon, plastic-carbon replicas often were unsatisfactory when extremely fine details were to be measured. Substitution of chromium for carbon as a replicating medium eliminated the pile-up problem and yielded very distinct details. However, the chromium replicas are more suitable for polished or etched specimens than for relatively rough fractured surfaces because the metallic replica is more susceptible to damage from stresses generated during removal of the primary plastic replica. Examples of results obtained by these replication techniques on irradiated materials are shown in Fig. 38.2.

CORRELATION OF COMPOSITION AND HEAT TREATMENT WITH THE MICROSTRUCTURES OF URANIUM CARBIDES

M. B. Sears³ R. J. Gray
L. M. Ferris³ B. C. Leslie

Optical photomicrographs, at magnifications of 250 and 1000X, of 78 different arc-cast and heat-treated uranium carbide specimens were reported.⁴ Specimens with total carbon-to-uranium atom ratios from 0.4 to

³Chemical Technology Division.

⁴M. J. Bradley, R. J. Gray, L. M. Ferris, and B. C. Leslie, *Coordination of Composition and Heat Treatments with the Microstructures of Uranium Carbide*, ORNL-3515 (July 1968).

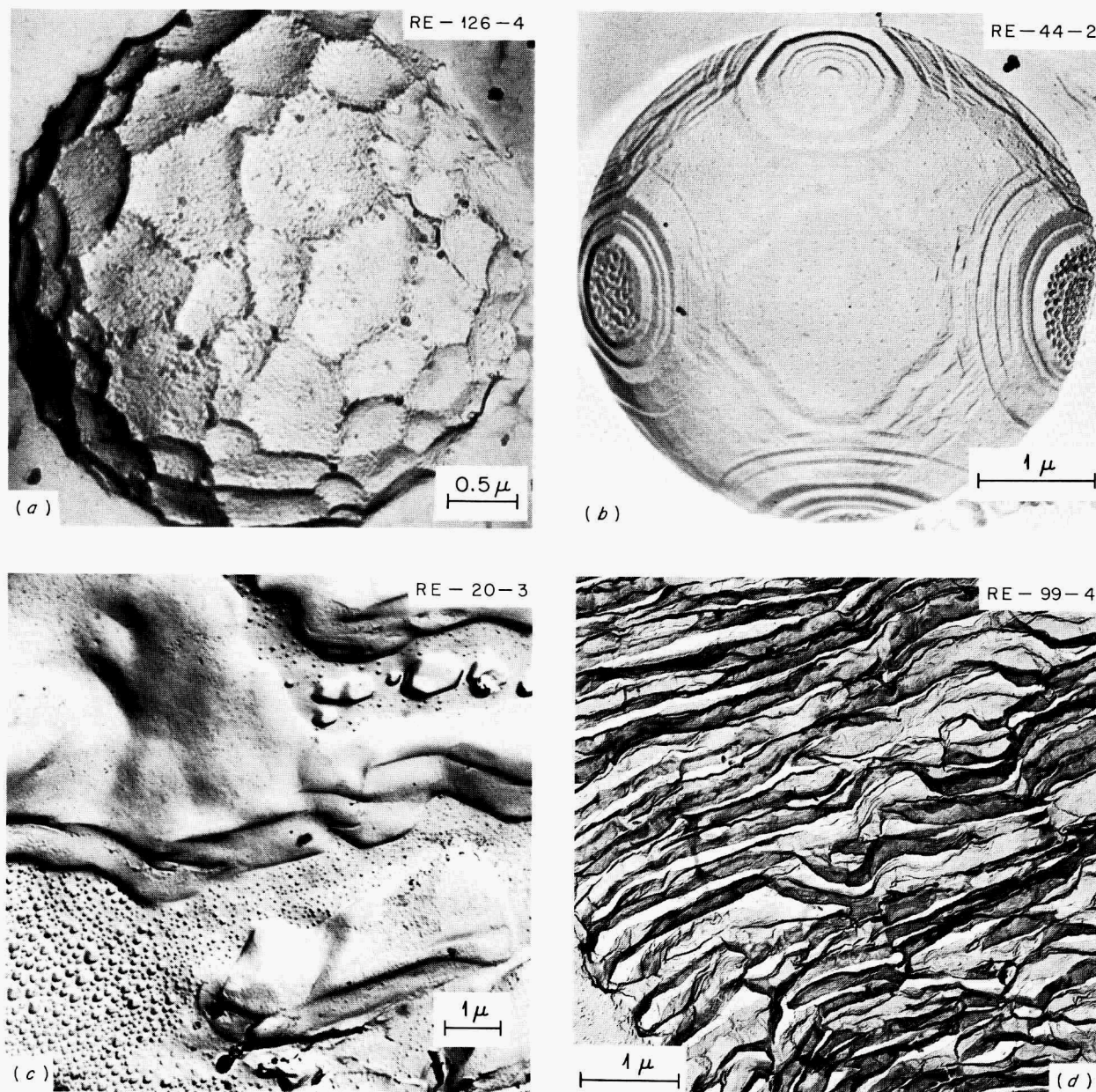


Fig. 38.2. Electron Micrographs of Various Irradiated Materials. (a) Carbon secondary replica of a crystallographic hole in zirconium carbide. (b) Fractograph of uranium nitride fuel showing coalescence of fission gas on grain surfaces – carbon secondary replica. (c) Carbon secondary replica of a fabrication void in a microsphere (unirradiated). (d) Chromium secondary replica of a pearlitic steel.

2.4 (2 to 11 wt % C) were included, but the major emphasis was on the UC-UC₂, UC-U₂C₃, and U₂C₃-UC₂ regions of the phase diagram. The phases present were identified by x-ray diffraction analysis of the specimens at room temperature and in many cases were

further confirmed by determining the hydrolysis products. The specimens were also analyzed for uranium, total carbon, free carbon, oxygen, nitrogen, and tungsten to provide as complete a characterization as possible.

ELECTRON MICROPROBE ANALYSIS

H. V. Mateer R. S. Crouse

Small areas (approx $3\ \mu$ in diameter) on the surface of metallographic specimens can be chemically analyzed through the use of the electron microprobe. Characteristic x-rays generated on the surface of the sample are separated by both diffracting crystals and energy discrimination; the intensity of characteristic x-rays generated is directly related to the concentration of the element in the sample.

A combination of high continuous background radiation from the electron bombardment and inherent instrument instability over long counting periods makes working with low element concentrations on the electron microprobe difficult. Segregation of tantalum (nominal composition 800 ppm) in a zone-refined single crystal of niobium was confirmed by comparing the variation in tantalum concentration across a frozen zone with the radiation across the interface of a melted and refrozen zone. Background measurements were made on a single crystal of niobium containing no tantalum. Solid-state electronics improved instrument stability so that 25-min counts (detectability limit 180 ppm) could be made with some confidence.

In another problem involving low concentrations, a series of Nb-1% Zr samples that had been exposed to lithium at elevated temperatures showed zirconium depletion at the surfaces. The electron microprobe was used to determine the depth of the depleted zone and, by extrapolation, the surface concentration of zirconium. Data obtained was to be subjected to a least-squares fit on the IBM 360 computer to determine diffusion coefficients. Automatic step-scanning of the sample and the use of a CEIR computer program to convert intensity data to concentrations made the gathering and processing of large amounts of data possible. A large area a precise distance from the surface of the specimen was analyzed with a stigmated beam ($40 \times 3\ \mu$) with its major axis parallel to the surface of the sample.

The use of a partially evacuated flow proportional thin-window detector extended the range of elements detectable with the electron probe to include carbon and oxygen.

EVALUATION OF THE BAUSCH AND LOMB RESEARCH II METALLOGRAPH¹

R. S. Crouse R. J. Gray

A newly developed commercial Bausch and Lomb Research II metallograph was evaluated this year. The

operation of this instrument and its performance pertaining to resolution, field flatness, lighting, photography, and special modes of operation were compared with the older Research I metallograph; the new instrument was superior on most counts. Ease of operation is outstanding.

The instrument as received showed signs of not having been properly inspected at the factory; however, in-the-field corrections by a Bausch and Lomb service representative on some uneven lighting problems, dust in the projection system, and de-centered objective lenses were very successful. A half-wave plate was modified for full rotation to extend the usefulness of the instrument in examining weakly birefringent materials.

QUANTITATIVE TELEVISION MICROSCOPY¹

T. M. Kegley, Jr.

The evaluation of the Quantimet television microscope was continued.⁵ We made grain size analyses of ASTM standard grain size charts and area analyses of known area-fraction charts. Point count and Quantimet area analyses were made from the same nickel-bakelite compact and the results were compared with density measurements.

The ASTM grain size number as determined by Quantimet analysis of the ASTM charts was within 0.2 of the nominal ASTM grain size numbers 0 through 8. The grain size as determined by the Quantimet depended on the magnification employed. For the same grain size, the apparent ASTM grain size number decreased (or grain size increased) as the magnification decreased. For example, when the ASTM grain size 8 chart was analyzed, grain size numbers of 7.47, 7.77, and 7.85 were obtained with the 4.2, 8.5, and 17.6X objectives, respectively, with the epidiastroscope attachment. This apparent decrease in the ASTM grain size number was related to a resolution effect, which caused a loss of projection near each grain boundary junction.

In the analysis of the test charts representing area fractions of 10, 20, 30, 40, and 50%, the mean values obtained (Table 38.1) were within 0.15% of the area-fraction values determined by the Gaertner measuring microscope. Volume fraction measurements of a 20 vol % nickel-bakelite compact derived from density measurement, point count analysis, and Quantimet area analysis were in remarkably close agreement — within 0.15% (see Table 38.2). The performance of the

⁵T. M. Kegley, Jr., *Metals and Ceramics Div. Ann. Progr. Rept. June 30, 1967*, ORNL-4170, pp. 233-34.

Quantimet in the grain size and area measurements of known standards was quite acceptable.

Table 38.1. Quantimet Analysis of Area-Fraction Test Charts

Test Card	Area Analysis with Gaertner Measuring Microscope (%)		Quantimet Area Analysis (%)		
	Area Fraction	Duplicate Analysis Deviation	Area Fraction	Range	Standard Deviation
A-7	10.03	0.000	10.01	9.9–10.1	±0.06
A-6	19.77	0.021	19.75	19.7–19.8	±0.05
A-1	29.67	0.008	29.81	29.3–30.3	±0.4
A-2	30.23	±0.01 ^a	30.15	30.0–30.3	±0.12
A-5	41.08	0.019	41.04	40.8–41.4	±0.19
A-4	48.49	0.015	48.41	48.0–48.7	±0.26

^aStandard deviation.

In actual practice with standard metallographic specimens, our major criticism is the need for moderately high contrast in the microstructure for the instrument to define and measure areas of interest. Specimens that meet these contrast requirements can be measured expeditiously and within an acceptable error.

Table 38.2. Volume Fraction Measurements of Nickel-Bakelite Compact

Volume Percentage	Method of Determination
20.02	Immersion density measurements
20.05 ± 0.74 ^a	Analysis with Swift automatic point counter
20.15 ± 0.61 ^a	Quantimet

^aStandard error.

39. Rover Rocket Materials

R. E. Clausing

We continued to provide materials support to the AEC-NASA Space Nuclear Propulsion Office on the Rover Nuclear Rocket Program.¹ We are providing technical liaison between NASA and some contractors and performing experimental work in certain areas. We concluded the thermal fatigue testing of nozzle tube configurations and the elevated-temperature testing of tubing materials reported in progress last year. More recent effort has been directed mostly toward materials problems that may arise as the result of exposure to the space environment.

THE THERMAL FATIGUE PROPERTIES OF NOZZLE COOLANT TUBES

D. G. Harman A. E. Carden²

The nozzles for nuclear rockets are typical of most regeneratively cooled rocket nozzles in that the inner surface that contacts the hot exhaust gas is formed by brazing together large numbers of suitably shaped thin-walled tubes. The cryogenic propellant (liquid hydrogen) is forced into these tubes and is vaporized to keep the nozzle from melting. The propellant is then fed into the reactor. The thin-walled tubes are supported externally by relatively heavy sections and are firmly joined to them. These heavy sections remain at low temperatures while the interior nozzle surfaces become quite hot. Thermal expansions of up to 2% may be produced in the tubes, and thermal cycling may produce low-cycle thermal fatigue failures. Apparatus was developed to permit simulation of the thermal and mechanical constraints operating in an actual nozzle,³

and the results of tests have been reported⁴ and are abstracted below.

Multiple-tube specimens of type 347 stainless steel and Hastelloy X were cycled from -200 to 1600, 1800, and 1900°F. Fatigue failures in the form of intergranular cracks were observed through the tube crowns after 23 to 87 thermal cycles. The number of thermal cycles to failure was decreased by increasing the test temperature, holding at this temperature for longer times, or denting the tube crowns before test. Fatigue life increased with decreasing tube diameters, and this was applied to the analysis of a typical nozzle configuration. No appreciable difference was noted between the type 347 stainless steel and the Hastelloy X test specimens.

Simplified single-tube specimens were tested in a specialized low-cycle fatigue apparatus developed under the direction of A. E. Carden at the University of Alabama. Thermal and mechanical effects can be programmed and controlled independently. This apparatus was used specifically to determine the effect of the minimum in the tensile ductility of Hastelloy X near 1300°F on the low-cycle fatigue of the alloy and to provide other data for correlation with the simulated service tests. The fatigue data have been reported elsewhere⁵ and only the abstract is included here.

The low cycle fatigue of Hastelloy X at elevated temperature is presented. Isothermal data at 800, 1300, 1500, and 1800°F are presented with cyclic thermal fatigue data for 600 to 1800°F, 800 to 1300°F, and 1300 to 1800°F. These tests were performed in an Instron machine with separate temperature control. The purpose was to determine the effect of a minimum tensile ductility at or near 1300°F, the effect of the stress-temperature arrangement, and the effect of temperature and frequency. Based on a correlation of strain range with life, the results show no significant deterioration to the fatigue properties at 1300°F; increasing the temperature lowers the strain fatigue curve; and the stress-temperature arrangement shows no adverse effect on this alloy. In general, the thermal fatigue data agree with the isothermal data at the maximum temperature. Only a few tests were performed to investigate the frequency effect, but no significant change could be seen for the 360 and 420 cycles per hour as compared to the base-line data at 36

¹E. A. Franco-Ferreira, *Metals and Ceramics Div. Ann. Progr. Rept. June 30, 1967*, ORNL-4170, pp. 238-44.

²Consultant from the University of Alabama.

³A. E. Carden, D. G. Harman, and E. A. Franco-Ferreira, "Thermal Fatigue Analysis of a Cryogenically Cooled Rocket Nozzle," pp. 102-1--102-12 in *Southeastern Symposium on Missiles & Aerospace Vehicles Sciences*, Vol. II, American Astronautical Society, Southeast Section, Huntsville, Ala., 1966.

⁴D. G. Harman, *Thermal Fatigue of Rocket Nozzle Cooling Tubes*, ORNL-TM-2089 (in preparation).

⁵A. E. Carden and T. B. Slade, "Low-Cycle Fatigue of Hastelloy X," presented at the ASTM Annual Meeting, June 1968, San Francisco.

cycles per hour. Although the tests included appreciable creep strains, the results agreed with those of the other 36-cycles per hour sawtooth extension cycle data.

Correlation of the results^{4,5} is in progress and will be the subject of a topical report.

EFFECTS OF SPACE ENVIRONMENT ON NERVA MATERIALS

R. E. Clausing

Exposure of the NERVA engine to the environment of space may produce some materials problems not encountered in ground tests. A committee composed of representatives from the NASA Space Nuclear Propulsion Office at Cleveland, Aerojet General Corporation, Westinghouse Astronuclear Laboratory, Oak Ridge National Laboratory, and Thompson-Ramo-Wooldridge attempts to define such problem areas and to ensure that the NERVA design and fabrication are consistent with reliable operation in the space environment.

The tendency of atomically clean surfaces to adhere strongly is one of the most important space-related phenomena to be considered. Adhesion and friction of clean surfaces are not well understood, but it has been demonstrated that the presence or absence of adsorbed gases on otherwise atomically clean surfaces can completely alter adhesional and frictional properties of both pure materials and engineering alloys. To better assess the importance of these effects on the materials in the NERVA system it is necessary to know (1) the specific environment at the location of particular components in the engine and (2) how this environment will influence adhesion and friction. We provide information on both of these subjects by implementing the two experimental studies described briefly below.

Outgassing of NERVA Fuel Elements

The gaseous atmosphere at any point in the NERVA engine will depend upon the temperature and history of the entire engine system; however, in the present design it will be determined primarily by the outgassing of the graphite reactor. This outgassing cannot be accurately estimated because of the special nature of the core material, its configuration, and its coating. Experimental data must be sought for the actual core elements at temperatures and pressures similar to those expected in space operation. We have designed and are assembling an experiment to obtain such measurements.

The data obtained will include both the quantity and species of gases released from fuel elements as a function of configuration, temperature, and pretreat-

ment. Measurements will be made on both single elements and a cluster of seven. Temperatures from room temperature to 2000°R will be used for outgassing, and pretreatments will be provided to produce conditions similar to those encountered (1) after launching but before the first firing in space and (2) after the engine has been fired once and subjected to the postfiring cool-down procedure but not restarted. The tests are to be conducted using quarter-length fuel element sections; however, several full-length single-element tests will be made to confirm the extrapolation of the data from partial elements to full-length elements. The gases evolved will be measured quantitatively in a specially designed ultrahigh-vacuum system.

Adhesion of NERVA Materials

This program is being conducted through an ORNL subcontract with the Syracuse University Research Corporation. Dr. R. G. Aldrich is the principal investigator, and R. E. Clausing of the ORNL Metals and Ceramics Division is the project monitor. The program is providing information on the adhesion of graphites and metals to themselves and to other materials in various controlled environments. Special emphasis is placed on the effect of surface contamination from the gaseous environment on adhesion.

The technique used in these experiments is based upon that developed by D. V. Keller of Syracuse University.⁶ The experimental plan is to (1) produce an initial surface that is atomically clean, (2) measure its adhesion properties, (3) provide a known gaseous contamination, and (4) measure the change in adhesion produced by the contamination with hydrogen and oxygen. The results of the tests are given in Table 39.1. They indicate that for some materials it is not possible to produce surfaces that will adhere by any of the usual cleaning procedures, including thermal cleaning or electron or ion bombardment. Others have shown that engineering alloys can be made to adhere if mechanical shearing occurs or if mechanical rubbing motions are permitted. Our apparatus has now been modified to permit a controlled rubbing action. This has produced adhesion without the need for other surface cleaning in the case of the only alloy tested thus far. Table 39.1 also shows that oxygen is more effective than hydrogen in inhibiting adhesion for materials that could be compared.

⁶K. I. Johnson and D. V. Keller, *J. Appl. Phys.* 38, 1896-1904 (1967).

Table 39.1. Summary of Adhesion Tests

Couple	Adhesion Obtained	Result for Various Conditions ^a								Pressure (torr) to Inhibit Adhesion		
		1	2	3	4	5	6	7	8	H ₂	O ₂	
Type 440 stainless steel ^b	No	—	—	—	—	—	—	—	—	<i>c</i>	<i>c</i>	<i>c</i>
PO-3 graphite ^b	No	—	—	—	—	—	—	—	—	<i>c</i>	<i>c</i>	<i>c</i>
Pyrolytic graphite ^b	No	—	—	—	—	—	—	—	—	<i>c</i>	<i>c</i>	<i>c</i>
Pyrolytic graphite } ZTA graphite }	Yes	+	<i>c</i>	+	+	+	+	+	+	<i>c</i>	70	10 ⁻⁵
Pure titanium ^b	Yes	—	—	—	—	+	<i>c</i>	<i>c</i>	<i>c</i>	<i>c</i>	70	10 ⁻⁶
Ti-5% Al-2.5% Sn ^{b,d}	Yes	—	—	—	<i>c</i>	<i>e</i>	<i>e</i>	<i>e</i>	+	<i>e</i>	<i>e</i>	<i>e</i>

^aSpecimen conditions: (1) As received, laboratory air; (2) as received, 10⁻⁶ torr; (3) as received, 10⁻⁹ torr; (4) vacuum baked to 250°C; (5) degassed at higher temperatures; (6) argon ion bombarded; (7) cleaned by electron bombardment; (8) mechanically rubbed. Results: +, adhesion observed; —, adhesion not observed.

^bBoth specimens of same material.

^cNot tested.

^dAlloy in the EL1 condition.

^eBeing tested.

40. Dispersion Strengthening of Aluminum-Base Alloys

Joseph P. Hammond

Experimental methods that gave remarkably good properties were developed for dispersion hardening aluminum alloys. The objective was to develop materials with enhanced elevated-temperature strength and, especially, improved low-strain-rate fracture ductility for fuel cladding in organic-cooled heavy-water-moderated reactors. Effort to improve the properties of SAP (Al_2O_3 dispersed in aluminum) for near-term application in these reactors is treated in Part III, Chapter 24, of this report.

A principal shortcoming of the conventional SAP procedure of hardening aluminum is that the "open" milling method used to introduce the dispersant, allowing the aluminum to react with air as it is ground, gives insufficiently fine and uniform dispersions. The practice is to achieve low interparticle spacing, an important strength-related variable, by ball-milling for long periods. Unfortunately, however, the amount of oxide formed increases with milling time, and materials with desired strength generally have too high an oxide loading for optimum toughness and ductility. We have eliminated this objection of the conventional SAP process by devising a means for achieving extraordinarily fine dispersions in aluminum independent of the type or amount of oxide introduced.

The method involves embedment of the dispersant by grinding in a high-energy ball mill. The dispersant may be introduced in its final form or as an unstable oxide for reacting with a constituent of the matrix to form the dispersant *in situ*. Grinding is performed for one or two days in a hermetically sealed drum under the protection of argon, with petroleum ether containing 0.5% stearic acid used as a grinding liquid.² The petroleum ether is then evaporated off, and the mixture

is vacuum annealed and then consolidated by cold pressing and bare extrusion at 500°C.

A variety of dispersion-hardened aluminum alloys were processed by this method. Some show exceptionally high strengths at elevated temperatures, while others have good high-temperature strengths with substantially improved low-strain-rate fracture ductility. The mechanical properties of two such experimental alloys are compared in Table 40.1 with properties of commercial SAP.

Alloy 3 of Table 40.1, hardened by 4% ultrafine SiO_2 reacting in finely ground Al-11% (2.3 at. %) Ce eutectic splat, was much stronger at 450°C than SAP with 11% oxide (alloy 2), yet it contained only 4% oxide. Electron transmission micrographs of the SiO_2 additive and the Al-11% Ce powder with the SiO_2 ground in it are shown in Fig. 40.1 and illustrate the exceedingly fine and uniform dispersion of the reactant in this material before consolidation.

The oxide dispersant in alloy 4 of Table 40.1 was formed by reacting 4% ultrafine fibrillar boehmite (AlOOH) in finely milled Al-5.5% Mg powder. This material has as good elevated-temperature strength as alloy 1, a SAP with higher oxide content (6%), and an improved low-strain-rate ductility. The excellent dispersion obtained in this alloy is shown in the electron transmission micrograph of Fig. 40.2.

¹This material was from the discontinued program "Dispersions in Solids" and not reported previously because of patent restrictions.

²X-ray diffraction analyses of powders processed by this method give aluminum crystallite sizes around 230 Å, compared to 1300 to 1600 Å for commercial SAP powders.

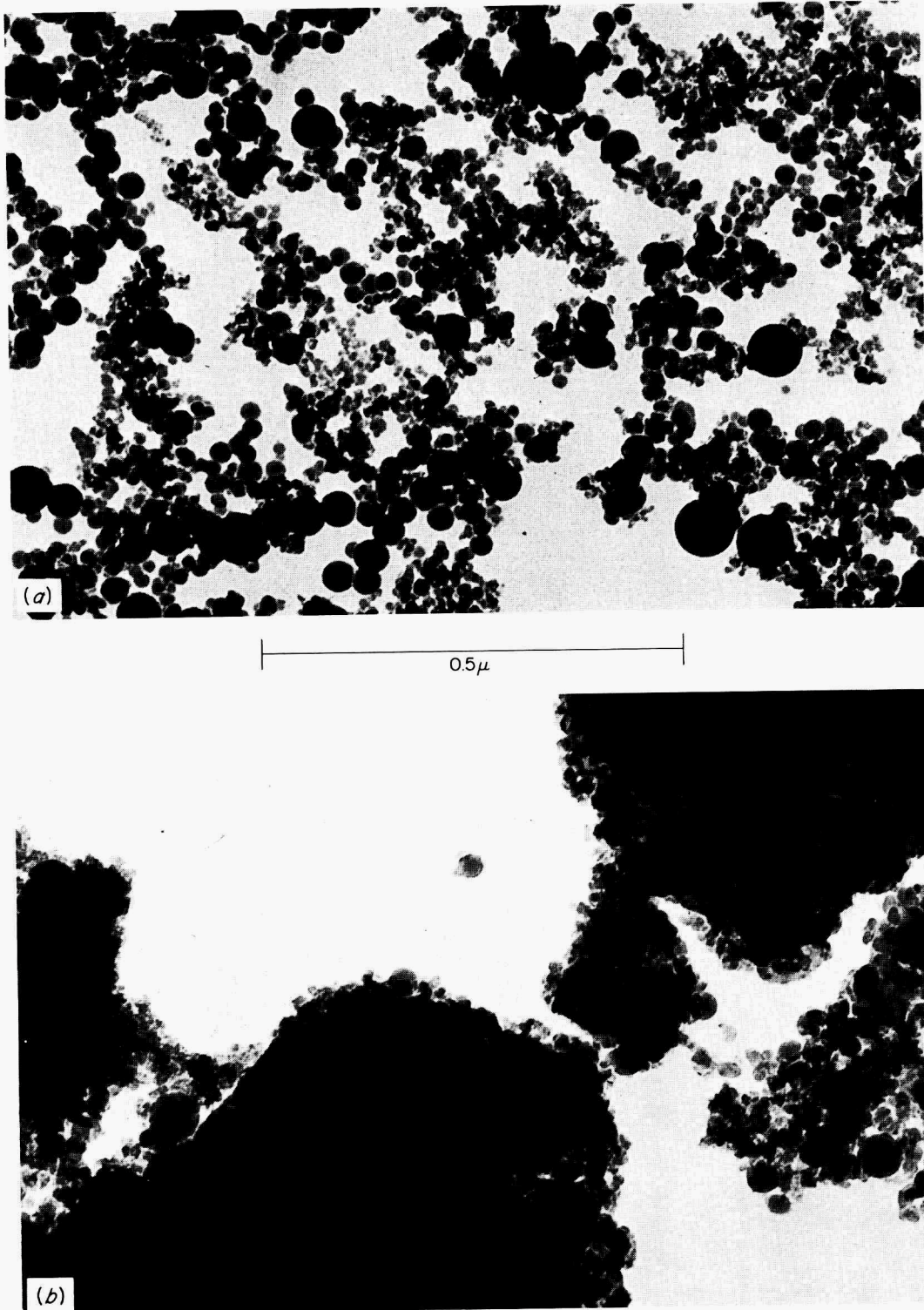


Fig. 40.1. Transmission Electron Micrographs of (a) Amorphous SiO_2 Oxygen Carrier and (b) Al-11% Ce Powder After Being Milled with SiO_2 in it.

Table 40.1. Comparison of Tensile Properties of Two Experimental Aluminum Alloys with Conventional SAP-Type Materials

Alloy	Description	Strain Rate (min ⁻¹)	Test Temperature (°C)	Yield Strength, 0.2% Offset (psi)	Ultimate Tensile Strength (psi)	Total Elongation (%)
1	XAP-001 ^a (with 6% Al ₂ O ₃)	0.02	25-29	32,000	38,270	11.5
		0.02	450	10,280	11,280	2.7
		0.002	450	9,690	10,400	1.8
		0.0002	450	8,650	9,170	1.3
2	SAP 895 ^a (with 11% Al ₂ O ₃)	0.2	25-29	33,310	40,220	9.9
		0.02	450	13,490	14,650	2.0
		0.002	450	12,410	12,900	1.4
		0.0002	450	10,720	11,390	1.1
3	Experimental Al-11% Ce splat with 4% SiO ₂ ^b	0.02	25-29	60,820	76,300	6.6
		0.02	450	18,838	19,411	0.59
		0.002	450	16,162	16,818	0.37
		0.0002	450	14,720	15,120	0.93
4	Experimental Al-5.5% Mg filings with 4% AlOOH ^c	0.02	25-29	53,640	61,830	6.12
		0.02	450	11,440	11,770	5.45
		0.002	450	9,810	10,300	3.60
		0.0002	450	8,800	9,290	2.26

^aCommercial alloy in which the oxide was formed in aluminum powder by reaction with air during open ball-milling with a proprietary grinding liquid. Powder consolidated and extruded at 25:1 reduction.

^bOxide dispersant formed by chemical reaction from 140-A SiO₂ additive milled for one day into the Al-11% Ce powder. Mixture was annealed at 450°C, cold pressed, and extruded at 500°C at 20:1 reduction.

^cOxide dispersant formed by chemical reaction from fibrillar AlOOH (50 Å diam × 1000 Å long) milled for one day into the Al-5.5% Mg powder. Mixture was annealed at 500°C, cold pressed, and extruded at 500°C at 20:1 reduction.

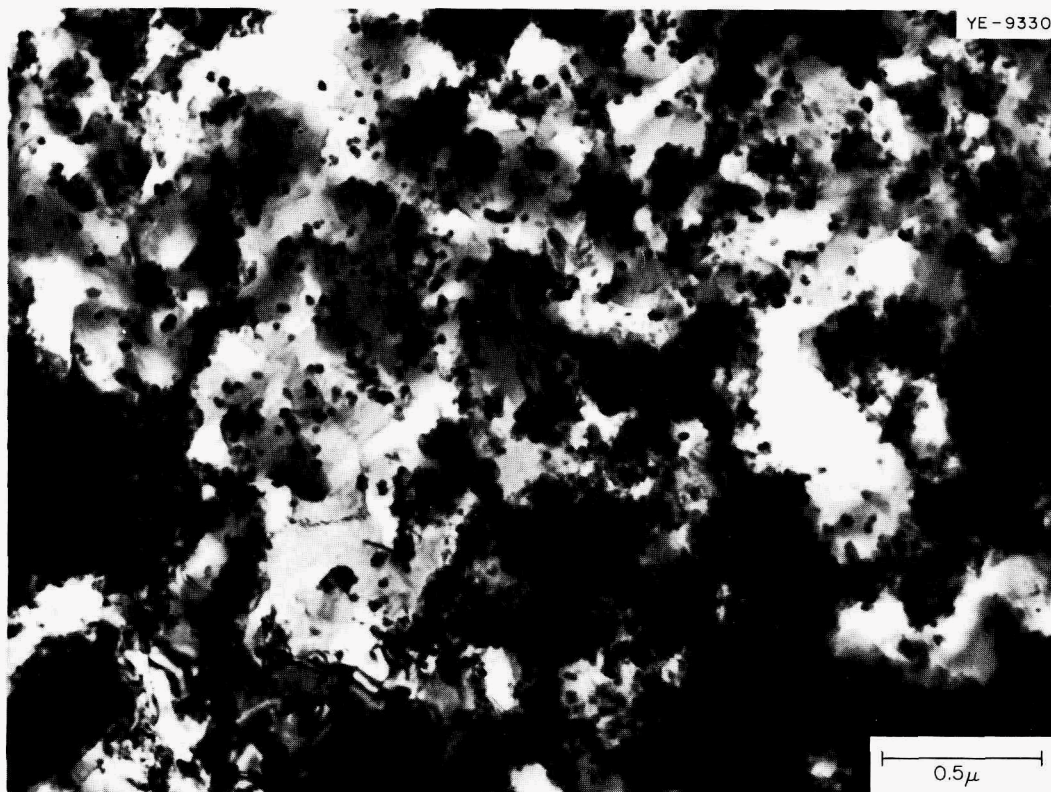


Fig. 40.2. Transmission Electron Micrograph of Alloy Formed from Al-5.5% Mg Powder Reacted with 4% Fibrillar Boehmite (AlOOH). Longitudinal section.

41. Army Pulsed Radiation Facility Reactor Assistance

A. P. Litman

We have provided metallurgical assistance during the fabrication and testing of a U-10% Mo alloy core for the Army Pulsed Radiation Facility Reactor (APRFR). In addition to overseeing quality control during fabrication and coating of the components, we provided service during the criticality and pulse testing program and evaluated the core after test. At the present time we are coordinating a core-alloy development program.

This work is sponsored by the U.S. Army Ballistic Research Laboratories through interagency agreement with the U.S. Atomic Energy Commission.

EVALUATION OF THE APRFR CORE¹

A. P. Litman W. J. Leonard
M. I. Lundin²

The Army Pulsed Radiation Facility Reactor (APRFR), an essentially unmoderated, unreflected prompt-burst machine with a U-10% Mo alloy core, is a modified version of the ORNL Health Physics Research Reactor. An APRFR core was recently fabricated at the Y-12 Plant, tested to damage in the ORNL Critical Experiments Facility,³ and analyzed for metallurgical integrity.

The U-10% Mo core components are induction-melted vacuum castings, heat treated for retention of the body-centered-cubic gamma phase. The core (Fig. 41.1) contains approximately 113 kg of 93.2%-enriched uranium as a U-10% Mo alloy in the form of an 8.9-in.-diam cylindrical assembly about 8 in. long. This assembly is composed of a stationary outer shell of stacked nesting rings of several thicknesses held together by nine 0.78-in.-diam fuel alloy bolts, three movable fuel rods (the mass adjustment, regulating, and pulse rods), and a movable inner shell that serves as a

safety block. All finished parts were either aluminum-plated or nickel electroplated for fission-product retention and protection against oxidation and stress-corrosion cracking by exposure to air.⁴ The plated aluminum was partially converted to uranium-aluminum intermetallics, either during plating or by post-plating heat treatment.⁵

The performance test program totaling 48 pulses was carried out in two stages in which successively increasing pulse energies were generated. The first stage started with a reactivity addition that generated 10^{15} fissions. On the 31st pulse 3.7×10^{17} fissions occurred, the reactor period was 12.5 μ sec, and the integrated leakage flux was 8.8×10^{11} neutrons/cm² at a distance 206 cm (6.75 ft) from the core surface. The second stage starting with pulse 32 proceeded in a similar sequential fashion except that the last reactivity addition generated 2.7×10^{17} fissions.

Progressive damage to the core occurred as a result of inertial and thermal stresses induced during fission (peak temperature, 900°C) and included cracking and buckling of a few fuel rings, bending of the mass-adjustment, regulating, and pulse rods, and 1% permanent set to the bolts. Maximum damage occurred during pulse 31. Delayed crack propagation occurred on some bolts that failed in torsion during maintenance but was not observed on the fuel rings that cracked during testing. The U-10% Mo gamma phase was retained during the test and the partially converted aluminum plating showed superior protection compared to the nickel plating.

Comparison of the tensile properties of the U-10% Mo alloy at room temperature and at 205°C before and after the test revealed a slight strengthening, a small ductility decrease, and a modest increase in Young's modulus.

¹Summary of papers presented at the American Nuclear Society, Chicago, November 5-9, 1967, and Toronto, Ontario, Canada, June 10-13, 1968.

²Reactor Division.

³J. T. Mihalcz et al., "Superprompt Critical Behavior of a Uranium-Molybdenum Assembly," *Trans. Am. Nucl. Soc.* 10, 611 (1967).

⁴J. W. Pridgeon, *Stress-Corrosion Cracking in Uranium-Molybdenum Alloys*, Y-1417 (Aug. 12, 1963).

⁵R. T. Bell, *Aluminum Ion Plating of Uranium-Molybdenum Alloy Fast-Burst Reactor Elements*, Y-1617 (June 6, 1968).

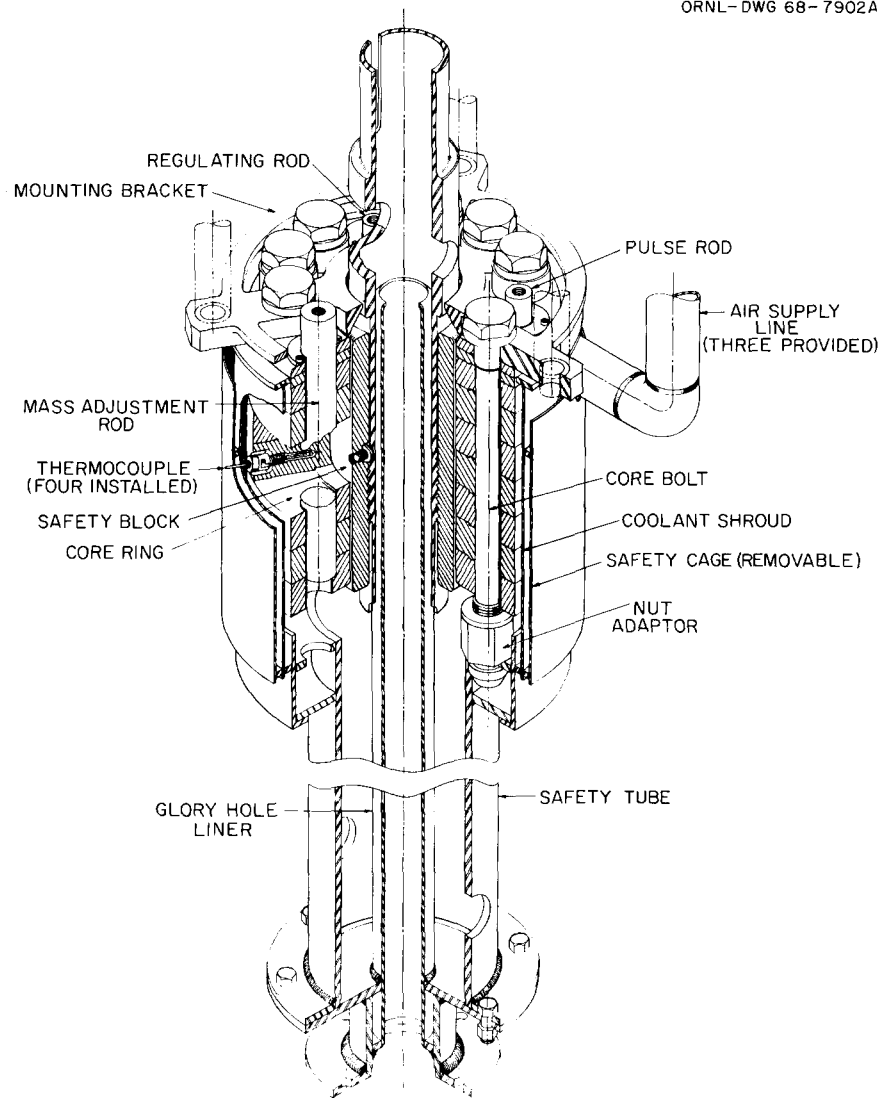


Fig. 41.1. Army Pulsed Radiation Facility Reactor Core Assembly.

CORE ALLOY DEVELOPMENT

A. P. Litman W. J. Leonard

We began to develop a core alloy with properties superior to those of U-10% Mo for superprompt critical systems of the type under consideration. From a physical metallurgical standpoint, the core alloy should (1) exhibit dimensional and microstructural stability during thermal cycling and (2) resist stress-corrosion cracking in air. With respect to reactor performance criteria, it should also have properties that promote maximum neutron yield Y and minimum pulse width at half peak power, $\omega_{1/2}$. According to Kazi⁶ and Mitsis,⁷

$$Y \propto \sigma_u^{3/4} / E^{5/8} \text{ and } \omega_{1/2} \propto (\sigma_u^{1/4} E^{1/8})^{-1},$$

where σ_u is the ultimate tensile strength and E is the modulus of elasticity. A search of the available data on uranium alloys disclosed that uranium containing 8 to 12% Nb has properties that would give 70% improvement in Y over U-10% Mo at 580°C with no sacrifice in $\omega_{1/2}$. Accordingly, we feel that uranium-niobium alloys are strong candidates for this application.

⁶A. H. Kazi, *Notes on the Effect of Alloy Properties on Fast Pulse Reactor Performance*, AMXBR-TG/10-67 (Jan. 3, 1967).

⁷G. J. Mitsis, *Effects of Alloy Properties on Burst Performance*, Memo for Record, Ballistic Research Laboratories, Aberdeen Proving Ground, Maryland (July 6, 1965).

Papers and Publications

Papers and Oral Presentations

Compiled by Frances A. Scarboro

13th Refractory Composites Working Group, Seattle, Wash., July 18–20, 1967

J. I. Federer* and J. E. Spruiell, "Formation and Characterization of an A15-Type Structure in Chemical Vapor-Deposited Tungsten-Rhenium Alloys"

Gordon Conference on Corrosion, New London, N.H., July 24–28, 1967

J. V. Cathcart,* G. F. Petersen, and C. J. Sparks, "The Structure of Thin Oxide Films on Nickel"

American Crystallographic Association Summer Meeting, University of Minnesota, Minneapolis, Aug. 20–25, 1967

L. A. Harris* and H. L. Yakel, "Structural Studies of Binary Oxide Compounds of Beryllium Oxide"

C. J. Sparks, Jr.,* "Increased X-Ray Intensities Using Graphite as a Monochromator"

14th Annual International Symposia on Microscopy, Cambridge, England, Aug. 21–25, 1967

R. J. Gray,* "Techniques for Revealing the Microstructure in Metallography"

International Conference on Hyperfine Interactions Detected by Nuclear Radiation, Pacific Grove, Calif., Aug. 25–30, 1967

J. C. Love,* G. Czjzek, J. J. Spijkerman, and D. K. Snediker, "Mossbauer Experiments with Nickel-61"

International Conference on the Strength of Metals and Alloys, Shiba Park, Tokyo, Japan, Sept. 4–8, 1967

B.T.M. Loh, "Dynamics of Slip Band Formation"

Symposium on Thermodynamics of Nuclear Materials with Emphasis on Solution Systems, Vienna, Austria, Sept. 4–8, 1967

J. M. Leitnaker,* "The Ideality of the UC-UN Solid Solution"

Conference on Chemical Vapor Deposition of Refractory Metals, Alloys, and Compounds, Gatlinburg, Tenn., Sept. 12–13, 1967

K. Farrell,* J. T. Houston, and A. C. Schaffhauser, "The Growth of Grain Boundary Gas Bubbles in Chemically Vapor Deposited Tungsten"

J. I. Federer* and J. E. Spruiell, "Formation and Characterization of an A15-Type Structure in Chemical Vapor-Deposited Tungsten-Rhenium Alloys"

*Speaker.

- W. R. Martin,* R. L. Heestand, R. E. McDonald, and G. A. Reimann, "Application of Chemical Vapor Deposition to the Production of Tungsten Tubing"
- H. E. McCoy* and J. O. Stiegler, "Mechanical Behavior of CVD Tungsten at Elevated Temperatures"
- W. C. Robinson,* F. H. Patterson, J. D. Fleming, and C. D. Gorton, "Chemical Vapor Deposition Statistical Parametric Study"
- 1967 Fall Meeting of the American Ceramic Society, Nuclear Division, Urbana, Ill., Sept. 19--22, 1967
- A. T. Chapman,* G. W. Clark, D. E. Hendrix, C. S. Yust, and O. B. Cavin, "Substructure and Precipitates in UO₂ Single Crystals"
- R. A. Potter,* J. M. Leitnaker, and T. G. Godfrey, "Synthesis and Fabrication of Uranium Carbonitride"
- US/Japan Information Exchange Meeting on Ceramic Nuclear Fuels, Pacific Northwest Laboratory, Battelle Memorial Institute, Richland, Wash., Sept. 25--29, 1967
- A. L. Lotts* and T. G. Godfrey, "Nuclear Fuels Development at the Oak Ridge National Laboratory"
- Libby-Cockcroft Exchange on Nuclear Fuels, Pleasanton, Calif., Sept. 25--29, 1967
- J. L. Scott* and T. G. Godfrey, "Nuclear Fuels Development at the Oak Ridge National Laboratory"
- CNEN Symposium on Sol-Gel Processes for the Production of Ceramic Nuclear Fuels, Turin, Italy, Oct. 2--3, 1967
- A. R. Olsen,* J. D. Sease, R. B. Fitts, and A. L. Lotts, "Fabrication and Irradiation Testing of Sol-Gel Fuels at Oak Ridge National Laboratory"
- T. N. Washburn, A. L. Lotts, and F. E. Harrington, "Comparative Evaluation of Sol-Gel Fuel Fabrication Costs," (Presented by A. R. Olsen)
- American Welding Society 1967 National Fall Meeting, Houston, Tex., Oct. 2--5, 1967
- R. G. Donnelly* and R. J. Beaver, "Welding Development for Isotopic Power Capsules"
- 1967 Nuclear Metallurgy Symposium on Plutonium Fuels Technology, Phoenix, Ariz., Oct. 4--6, 1967
- F. G. Kitts,* R. B. Fitts, and A. R. Olsen, "Sol-Gel Urania-Plutonia Microsphere Preparation and Fabrication into Fuel Rods"
- Symposium on Underwater Welding, Cutting, and Hand Tools, Battelle Memorial Institute, Columbus, Ohio, Oct. 10--11, 1967
- C. H. Wodtke,* "Underwater Plasma Arc Cutting"
- 11th Conference on Analytical Chemistry in Nuclear Technology, Gatlinburg, Tenn., Oct. 10--12, 1967
- R. W. McClung,* "Nondestructive Testing Techniques -- Instrumentation and Methods"
- American Society for Metals, Seminar on Ductility, Cleveland, Ohio, Oct. 14--15, 1967
- J. O. Stiegler and J. R. Weir, Jr.,* "Effects of Irradiation on Ductility"
- Electrochemical Society Meeting, Corrosion Division, Symposium on Mechanical Properties of Surface Reaction Products, Chicago, Ill., Oct. 15--20, 1967
- R. E. Pawel,* "Stress Measurements During Gaseous Reactions of Refractory Metals"
- 27th National Fall Conference of the Society for Nondestructive Testing, Cleveland, Ohio, Oct. 16--19, 1967
- W. H. Bridges* and R. W. McClung, "Computerized Information Retrieval -- a Nondestructive Memory for Nondestructive Testers"
- C. V. Dodd,* "A Portable Phase-Sensitive Eddy-Current Instrument"
- B. E. Foster* and S. D. Snyder, "Evaluation of Variables in the Measurement of Fuel Concentration Variations in Fuel Rods"

*Speaker.

H. L. Whaley,* K. V. Cook, R. W. McClung, and L. S. Snyders, "Optical Methods for Studying Ultrasonic Propagation in Transparent Media"

1967 Fall Meeting of the Metallurgical Society, Cleveland, Ohio, Oct. 16–19, 1967

L. K. Barrett and C. S. Yust,* "Progressive Shape Changes of the Void During Sintering"

R. W. Carpenter* and J. C. Ogle, "Rolling and Recrystallization Substructure in Very Thin Foils of Copper and Iron"

R. E. Clausing,* "The Desorption of Hydrogen, Deuterium, Carbon Monoxide, and Oxygen from Polycrystalline Tungsten as the Result of Electron Bombardment"

D. G. Harman* and T. A. Nolan, "Mechanical Properties and Fracture of Al-Al₂O₃ Alloys"

D. O. Hobson,* "Analysis of Textures in Deformed Zirconium Single Crystals"

R. T. King* and J. R. Weir, "The Effect of Cyclotron-Injected Helium on the Mechanical Properties of Stainless Steel"

C. C. Koch* and G. R. Love, "The Vanadium-Techneium Alloy System"

C. C. Koch* and C. J. McHargue, "The Influence of Plastic Deformation on the fcc ⇌ dhcp Phase Transformation in Cerium"

T. S. Lundy* and A. J. Mortlock, "The Near-Surface Effect for Diffusion in Silver and Gold"

T. A. Nolan and D. G. Harman,* "Analysis of the Fracture of Aluminum Oxide (SAP) by Electron Microscopy"

P. L. Rittenhouse,* "A Quantitative Assessment of the Effect of Crystallographic Texture on the Yield and Flow of Zircaloy-2"

R. A. Vandermeer and J. C. Ogle,* "Texture Inhomogeneities in Cold-Rolled Columbium"

Conference on Incipient Failure Diagnosis for Assuring Safety and Availability of Nuclear Power Plants, Gatlinburg, Tenn., Oct. 30–Nov. 1, 1967

R. W. McClung,* "State of the Art of Nondestructive Testing for Service and Post-Operation Examination of Reactor Pressure Vessels"

1967 Thermionic Conversion Specialist Conference, Palo Alto, Calif., Oct. 30–Nov. 2, 1967

J. I. Federer,* W. C. Robinson, Jr., and R. M. Steele, "Effect of Deposition Conditions on the Orientation of Chemical Vapor-Deposited Tungsten and Molybdenum"

C. E. Sessions* and J. H. DeVan, "Thermal Convection Loop Tests of Refractory Alloys in Lithium"

American Chemical Society, Atlanta, Ga., Nov. 1–3, 1967

G. P. Smith,* W. E. Smith, and J. Brynestad, "Entanglement of Nickel(II) Ions in the Lattice of Zinc Chloride-Rich Melts"

20th Annual Pacific Coast Regional Meeting of the American Ceramic Society, San Francisco, Calif., Nov. 1–4, 1967

J. M. Robbins and R. L. Hamner,* "Bonding of Pyrolytic-Carbon-Coated Fuel Particles for HTGR Applications"

American Physical Society Meeting, Clemson, S.C., Nov. 2–4, 1967

J. C. Love,* G. Czjzek, and F. E. Obenshain, "Hyperfine Interaction of Nickel-61"

F. E. Obenshain, G. Czjzek, J.L.C. Ford, J. C. Love, and H.H.F. Wegener, "Coulomb Recoil Implantation Mössbauer Experiments with Germanium-73"

American Nuclear Society Winter Meeting, Chicago, Ill., Nov. 5–9, 1967

G. L. Copeland* and W. R. Martin, "The Ball-Milling of Aluminum Powder for Production of Aluminum-Al₂O₃ Oxide Dispersions"

*Speaker.

C. W. Cunningham, B. Fleischer, L. C. Fuller, W. R. Huntley,* and D. H. Jansen, "Design and Operation of Turbine Nozzle and Blade Screening Tests in Potassium Vapor"

M. I. Lundin,* A. P. Litman, and W. J. Leonard, "Design and Metallurgical Aspects of the Army Pulsed Radiation Facility Reactor"

E. J. Manthos,* R. E. Adams, R. T. King, E. L. Long, Jr., J. E. Van Cleve, Jr., and A. L. Lotts, "Postirradiation Examination of Failed HFIR Target Elements"

M. M. Martin* and W. R. Martin, "A Study of Processes for SAP Powder Consolidation"

R. B. Pratt, J. D. Sease,* and A. L. Lotts, "Pyrolytic-Carbon Coatings in an Engineering-Scale System"

P. L. Rittenhouse,* "Hydride Orientation in Zircaloy Tubing"

American Society of Mechanical Engineers, Pittsburgh, Pa., Nov. 12-17, 1967

W. O. Harms* and A. P. Litman, "Compatibility of Materials for Advanced Space Nuclear Power Systems"

International Congress on Vacuum Metallurgy, Strasbourg, France, Nov. 13-17, 1967

D. T. Bourgette,* "Effect of Vacuum Environment on the Behavior of Metals and Alloys"

7th Thermal Conductivity Conference, Gaithersburg, Md., Nov. 13-16, 1967

M. Barisoni, R. K. Williams,* and D. L. McElroy, "Physical Properties of Indium From 77 to 350°K"

J. P. Moore, D. L. McElroy,* and R. S. Graves, "Thermal Conductivity of a 58% Dense MgO Powder in Nitrogen"

J. P. Moore,* R. K. Williams, and D. L. McElroy, "Physical Properties of Chromium from 77 to 400°K"

American Society for Nondestructive Testing and Society of American Materials Process Engineers Joint Meeting, Huntsville, Ala., Nov. 13, 1967

R. W. McClung,* "Recent Advances in Nondestructive Testing in the Nuclear Field"

25th High-Temperature Fuels Committee Meeting, General Atomic Division, General Dynamics Corporation, San Diego, Calif., Dec. 5-7, 1967

J. L. Scott,* "High-Temperature Fuel Work at the Oak Ridge National Laboratory"

13th AEC Coated-Particle Fuels Working Group Meeting, Gulf General Atomic, San Diego, Calif., Dec. 12-13, 1967

J. H. Coobs* and O. Sisman, "Coated-Particle Fuels Development at Oak Ridge National Laboratory for Period Jan. 15-Oct. 15, 1967"

5th International Conference on Solid State Physics, Manchester, England, Jan. 3-6, 1968

G. Czjzek,* J. C. Love, and F. E. Obenshain, "Hyperfine Interactions of Nickel-61 Measured by the Mössbauer Effect"

97th Annual Meeting of the American Institute of Mining, Metallurgical, and Petroleum Engineers, New York, Feb. 25-29, 1968

E. E. Bloom and J. O. Stiegler, "Helium Bubbles in Irradiated Austenitic Stainless Steel" (Presented by R. T. King)

K. Farrell* and J. T. Houston, "Thermal Rejection of Gas Bubbles from Electrodeposited Nickel"

R. E. Gehlbach* and H. E. McCoy, "Effect of Thermo-Mechanical Treatments on Precipitation in Hastelloy N"

R. W. Hendricks,* R. W. Carpenter, and R. W. Gould, "A Small-Angle X-Ray Scattering Investigation of Inhomogeneities in Aluminum-Zinc Alloys"

R. T. King,* "Some Observations on the Effects of Cyclotron-Injected Gases in Face-Centered Cubic Metals"

C. C. Koch and G. R. Love,* "Reaction Morphologies and Superconducting Properties in Technetium-Vanadium Alloys"

*Speaker.

B.T.M. Loh,* "A Graphical Method for Determining the Schmid Factor"

P. L. Rittenhouse and D. O. Hobson,* "Inhomogeneous Deformation in Zircaloy Tubing"

W. C. Robinson, Jr.,* and J. I. Federer, "Thermodynamic Considerations of the Chemical Vapor Deposition Process"

A. C. Schaffhauser,* J. T. Houston, and K. Farrell, "Effect of Gas Bubbles on Recrystallization and Grain Growth in Tungsten"

J. O. Stiegler and K. Farrell,* "The Observation of Gas Bubbles in Solids"

S. C. Weaver* and J. E. Spruiell, "Helium Bubble Migration in Uranium Nitride"

A. Wolfenden* and K. Farrell, "Comparison of Theories of the Growth of Gas Bubbles in Solids with Experimental Data"

M. H. Yoo,* "Interaction of Slip Dislocations with Twins in Hexagonal Close-Packed Metals"

1968 Westec Conference, Los Angeles, Calif., Mar. 11--14, 1968

W. R. Martin,* C. W. Dean, R. E. McDonald, and G. A. Reimann, "Fabrication of Tungsten and Tungsten-Alloy Tubing"

National Association of Corrosion Engineers, Cleveland, Ohio, Mar. 18--21, 1968

J. H. DeVan,* "Kinetic Processes in Liquid Metal Corrosion"

R. L. Klueh,* "Interactions in Alkali Metal Solutions Containing Oxygen"

American Physical Society Meeting, Berkeley, Calif., Mar. 18--21, 1968

H. L. Davis* and J. S. Faulkner, "Effect of Uniaxial Tension on the Fermi Surface of Metallic Copper"

J. S. Faulkner* and H. L. Davis, "Constant Energy Surface for Aluminum by the Korringa-Kohn-Rostoker Method"

American Institute of Chemical Engineers, Materials Engineering and Science Conference and Exposition, Philadelphia, Pa., Mar. 31--Apr. 5, 1968

R. J. Beaver* and M. M. Martin, "The Status of Europium Compounds for Reactivity Control in Nuclear Reactors"

J. L. Scott* and S. C. Weaver, "Fuels for Water Reactors"

American Chemical Society Meeting, San Francisco, Calif., Mar. 31--Apr. 5, 1968

G. P. Smith,* W. E. Smith, and J. Brynstad, "Coordination Behavior of Nickel(II) in ZnCl₂-Rich Melts of ZnCl₂-CsCl"

49th Annual Meeting of the American Welding Society, Chicago, Ill., Apr. 1--5, 1968

D. A. Canonico,* N. C. Cole, and G. M. Slaughter, "The Development of High-Temperature Brazing Alloys"

D. A. Canonico* and H. E. McCoy, "Welding Studies on Modified Hastelloy N"

N. C. Cole,* R. G. Gilliland, and G. M. Slaughter, "Welding of Tungsten and Tungsten Alloys"

American Nuclear Society National Topical Meeting, Cincinnati, Ohio, Apr. 2--4, 1968

J. R. Weir, Jr.,* J. O. Stiegler, and E. E. Bloom, "Irradiation Behavior of Cladding and Structural Materials"

70th Annual Meeting of the American Ceramic Society, Chicago, Ill., Apr. 20--25, 1968

J. P. Moore,* W. Fulkerson, and D. L. McElroy, "The Thermal Conductivity, Electrical Resistivity, and Seebeck Coefficient of Uranium Mononitride from 77 to 400°K"

L. E. Poteat and C. S. Morgan,* "Diffusion of Thorium in Thorium Dioxide"

*Speaker.

American Physical Society Meeting, Washington, D.C., Apr. 22–25, 1968

J. O. Betterton, Jr.,* J. O. Scarbrough, H. L. Davis, and W. Fulkerson, "The Low Temperature Specific Heat of Uranium Nitride"

H. L. Davis,* "Effect of Uniaxial Tension on the Fermi Surface of Metallic Copper"

RDT/SNS Meeting on Materials Development for Space Reactor Power Systems, Washington, D.C., Apr. 23–24, 1968

N. C. Cole and G. M. Slaughter, "Tungsten Metallurgy Review" (presented by A. C. Schaffhauser)

J. H. DeVan, B. Fleischer,* and A. P. Litman, "Status of Program on Lithium Corrosion of Refractory Alloys at the Oak Ridge National Laboratory"

J. I. Federer,* W. C. Robinson, G. A. Reimann, and R. E. McDonald, "Vapor Fabrication of Tungsten-Rhenium Alloys"

W. Fulkerson,* "The Status of Uranium Nitride Development Program at the Oak Ridge National Laboratory"

A. C. Schaffhauser,* K. Farrell, and J. O. Stiegler, "Evaluation of As-Deposited and Wrought CVD Tungsten"

A. C. Schaffhauser* and W. R. Martin, "Status of Tungsten Metallurgy Program at the Oak Ridge National Laboratory"

R. L. Stephenson, "Creep-Rupture Properties of Tungsten and Tungsten Alloys" (presented by A. C. Schaffhauser)

S. C. Weaver* and J. L. Scott, "Status of Uranium Nitride Development at the Oak Ridge National Laboratory" (Confidential)

Southern Metals Conference, Knoxville, Tenn., Apr. 24–26, 1968

R. J. Gray,* "Metallographic Characterization"

R. W. McClung,* "A Survey of Nondestructive Testing"

American Institute of Mining, Metallurgical, and Petroleum Engineers Refractory Metals Symposium, Washington, D.C., Apr. 25–26, 1968

H. Inouye,* "Interactions of Refractory Metals with Active Gases in Vacua and Inert Gas Environments"

26th High-Temperature Fuels Committee Meeting, Combustion Engineering, Inc., Windsor, Conn., Apr. 30–May 2, 1968

R. B. Fitts and A. L. Lotts,* "High-Temperature Fuel Work at the Oak Ridge National Laboratory"

Atomic Energy Commission Corrosion Symposium, Battelle Memorial Institute, Columbus, Ohio, May 6–8, 1968

R. L. Klueh,* "The Effect of Oxygen in Sodium on the Compatibility of Sodium with Tantalum and Niobium"

A. P. Litman and J. W. Koger,* "Corrosion of Hastelloy N Alloys in Sodium Fluoroborate Coolants for Molten Salt Reactors"

A. P. Litman,* W. J. Leonard, and D. B. Lloyd, "Dissimilar Metal Mass Transfer in a Bimetallic NaK Heat Rejection System"

C. E. Sessions and J. H. DeVan,* "Mass Transfer Phenomena in Refractory Metal–Lithium Systems"

C. E. Sessions* and T. S. Lundy, "Diffusion of Titanium in Modified Hastelloy N"

3rd International Conference on Electron and Ion Beam Science and Technology, Boston, Mass., May 6–9, 1968

C. W. Dean,* R. E. McDonald, R. E. Reed, and J. F. Emery, "Sources of Contamination During Electron-Beam Melting"

D. S. Easton* and J. O. Betterton, "Purification of Zirconium and Other Refractory Metals in an Ultrahigh Vacuum Zone Refiner with Analysis of Partial Pressures"

*Speaker.

14th Refractory Composites and Metal Matrix Composite Working Group Meeting, Wright-Patterson Air Force Base, Ohio, May 13–15, 1968

J. E. Spruiell,* “Chemical Vapor Deposition of Silicon Carbide from Silicon Tetrachloride-Methane-Hydrogen Mixtures”

International Conference on Powder Technology, Jointly sponsored by the American Society for Testing and Materials and the Illinois Institute of Technology Research Institute, Chicago, Ill., May 20–23, 1968

G. L. Copeland,* M. M. Martin, D. G. Harman, and W. R. Martin, “Effect of Powder and Process Variables on the Properties of Sintered Aluminum Products”

Interamerican Conference on Materials Technology, San Antonio, Tex., May 20–24, 1968

R. W. McClung,* “Nondestructive Test Development for Nuclear Reactor Programs at the Oak Ridge National Laboratory”

14th Annual Meeting of the American Nuclear Society, Toronto, Canada, June 9–13, 1968

C. M. Cox* and H.G.F. Wilsdorf, “The Crystallization of Amorphous Germanium by Reactor Neutrons”

J. I. Federer,* W. C. Robinson, Jr., and R. B. Pratt, “Flame Reactor Preparation of Fissionable Oxide Powders”

R. T. King* and J. R. Weir, Jr., “The Effect of Irradiation on the Mechanical Properties of Aluminum Alloys”

A. P. Litman and J. W. Koger,* “Compatibility of Fluoroborate Coolant Salts with Hastelloy N for Molten Salt Reactors”

A. P. Litman,* W. J. Leonard, and D. B. Lloyd, “Compatibility of a Type 316 Stainless Steel-NaK 78 Nb–1% Zr Alloy Heat Rejection System”

A. P. Litman,* W. J. Leonard, and M. I. Lundin, “Evaluation of a U–10% Mo Alloy and Consideration of an Alternate Alloy for Pulse Reactor Cores”

A. P. Litman,* H. E. McCoy, and J. H. DeVan, “Fluoride Salts for Heat Transfer Applications”

M. M. Martin,* J. H. Erwin, and W. R. Martin, “Effect of Type and Concentration of Fuel on the Void Volume in Aluminum Dispersion-Type Fuel Plates”

J. O. Stiegler, E. E. Bloom,* and J. R. Weir, “Electron Microscopy of Irradiated EBR-II Fuel Cladding”

American Vacuum Society Meeting, Beverly Hills, Calif., June 10–13, 1968

R. L. Stephenson,* “Evaluation of the High Temperature Creep Properties of Refractory Metal Alloys in Vacuum”

American Society for Engineering Education, Diamond Jubilee Meeting, University of California, Los Angeles, June 17–20, 1968

J. L. Scott,* “Mechanisms of Swelling and Gas Release in Nuclear Materials”

Libby-Cockcroft Meeting on Irradiation Effects on Structural Materials, Battelle Memorial Institute, Richland, Wash., June 19–21, 1968

J. R. Weir,* E. E. Bloom, D. G. Harman, C. E. Sessions, and H. E. McCoy, “Effects of Small Titanium Additions on High-Temperature Radiation Damage in Type 304 Stainless Steel, Type 316 Stainless Steel, Incoloy 800, and Hastelloy N”

J. R. Weir,* E. E. Bloom, and J. O. Stiegler, “Observations on Intergranular Fracture in the Presence of Helium Bubbles”

J. R. Weir,* R. T. King, E. E. Bloom, and J. O. Stiegler, “Formation and Annealing of Voids in Stainless Steels and Aluminum Alloys”

*Speaker.

22nd AEC Metallography Group Meeting, San Diego, Calif., June 19--21, 1968

R. S. Crouse* and R. J. Gray, "Evaluation of the Bausch and Lomb Research II Metallograph"

C.K.H. DuBose* and C. Jones, "Techniques for the Preparation of Transmission Electron Microscopy Specimens from Tubing"

R. E. Gehlbach,* "Electron Microscope-Microprobe Analysis of Precipitation"

R. J. Gray* and B. C. Leslie, "An Alpha Metallography Facility"

T. M. Kegley, Jr., "The Quantimet Television Microscope -- Its Operation and Evaluation" (presented by R. S. Crouse)

J. L. Miller, Jr.,* "Replication of Irradiated Materials for Electron Microscopy"

American Society for Testing and Materials Symposium on the Effects of Radiation on Structural Metals, San Francisco, Calif., June 23--28, 1968

E. E. Bloom* and J. R. Weir, Jr., "Development of Austenitic Stainless Steels with Improved Resistance to Elevated-Temperature Irradiation Embrittlement"

R. T. King, "The Effect of Cyclotron-Injected Helium on the Mechanical Properties of Stainless Steel" (presented by E. E. Bloom)

R. T. King and J. R. Weir, Jr.,* "The Effect of Irradiation on the Mechanical Properties of Aluminum Alloys"

R. W. Swindeman,* "Low-Cycle Fatigue Study of Niobium Alloy D-43"

H. E. McCoy and J. R. Weir,* "Development of a Titanium-Modified Hastelloy with Improved Resistance to Radiation Damage"

*Speaker.

Publications

Compiled by Meredith R. Hill

- Abraham, M. M., C. B. Finch, and G. W. Clark, "Electron Spin Resonance of Tripositive Curium in ThO_2 and CeO_2 ," *Phys. Rev.* **168**(3), 933–35 (April 1968).
- Adamson, G. M., Jr., *Fabrication of Research Reactor Fuel Elements*, ORNL-TM-2197 (June 1968).
- Askill, John, *A Bibliography on Tracer Diffusion in Metals: Part V. Self and Impurity Diffusion in Simple Metal Oxides*, ORNL-3795, Part V (January 1968).
- Aungst, R. C., T. B. Correy, F. V. Daly, F. W. Davis, J. M. Fox, Jr., E. H. Franks, N. C. Jessen, R. E. Lorentz, C. R. Mayne, E. C. Miller, G. M. Slaughter, W. R. Smith, Sr., C. C. Stone, and C. R. Sutton, "Nuclear Power," pp. 87.1–87.34 in *Welding Handbook*, 5th ed., sect. 5 (ed. by A. L. Phillips), American Welding Society, New York, 1967.
- Bannister, M. J., "Crystallite Size Measurements on Thoria Gel," *J. Am. Ceram. Soc.* **50**(11), 619–23 (November 1967).
- Barrett, Lida K., and C. S. Yust, "Progressive Shape Changes of the Void During Sintering," *Abstr. Bull. Inst. Metals Div.* **2**(2), 57 (1967); and *Trans. Met. Soc. AIME* **239**(8), 1172–80 (August 1967).
- Beaver, R. J., A. E. Richt, and M. M. Martin, *Irradiation Behavior of Aluminum-Base Dispersions Containing Europium Oxides*, ORNL-4199 (January 1968).
- Beaver, R. J., J. W. Tackett, J. H. Erwin, G. M. Slaughter, and W. J. Kucera, *Initial Development of HFIR Fuel Assemblies*, ORNL-4108 (October 1967).
- Berggren, R. G., D. A. Canonico, J. L. English, and P. Patriarca, "Effect of Environment on Materials," Chap. 5, pp. 150–281 in *Technology of Steel Pressure Vessels for Water-Cooled Nuclear Reactors, A Review of Current Practice in Design, Analysis, Materials, Fabrication, Inspection, and Test*, ed. by G. D. Whitman, G. C. Robinson, Jr., and A. W. Savolainen, ORNL-NSIC-21 (December 1967).
- Berggren, R. G., R. W. McClung, and E. C. Miller, "Testing and Service Performance Surveillance," Chap. 10, pp. 629–68 in *Technology of Steel Pressure Vessels for Water-Cooled Nuclear Reactors, A Review of Current Practice in Design, Analysis, Materials, Fabrication, Inspection, and Test*, ed. by G. D. Whitman, G. C. Robinson, Jr., and A. W. Savolainen, ORNL-NSIC-21 (December 1967).
- Betterton, J. O., Jr., and J. O. Scarbrough, "Low-Temperature Specific Heats of Zr-Ti, Zr-Hf, and Zr-Sc Alloys," *Phys. Rev.* **168**(3), 715–25 (April 1968).
- Bjerrum, N. J., H. L. Davis, and G. P. Smith, "The Optical Spectrum of Bismuth(I) in the Molten Aluminum Bromide–Sodium Bromide Eutectic," *Inorg. Chem.* **6**(8), 1603 (August 1967).
- Bjerrum, N. J., and G. P. Smith, "Lower Oxidation States of Bismuth. Bi_8^{2+} Formed in AlCl_3 – NaCl Melts," *Inorg. Chem.* **6**(11), 1968–72 (November 1967).
- Bloom, E. E., *In-Reactor and Postirradiation Creep-Rupture Properties of Type 304 Stainless Steel at 650°C*, ORNL-TM-2130 (March 1968).
- Bloom, E. E., and J. O. Stiegler, "Helium Bubbles in Irradiated Austenitic Stainless Steel," (Abstract) *J. Metals* **20**(1), 40A (January 1968).
- Bogue, D. C., *The Yield Stress and Plastic Strain Theory for Anisotropic Materials*, ORNL-TM-1869 (July 1967).
- Borie, Bernard, "The Darwin Dynamical Theory of X-ray Diffraction," *Acta Cryst.* **23**(2), 210–16 (August 1967).

- Boston, C. R., "Densities of Molten BiCl_3 and AlCl_3 Mixtures," *J. Chem. Eng. Data* **13**(1), 117--18 (January 1968).
- Boston, C. R., D. W. James, and G. P. Smith, "The Ultraviolet Spectrum of the Nitrate Ion in Molten Mixtures of Alkali Metal Nitrates," *J. Phys. Chem.* **72**(1), 293--95 (January 1968).
- Boston, C. R., Jorulf Brynstad, and G. P. Smith, "Effect of Melting on the Electronic Spectra of Cs_3NiCl_5 and CsNiCl_3 ," *J. Chem. Phys.* **47**(9), 3193--97 (November 1967).
- Bourgette, D. T., "Vaporization Behavior of Haynes Alloy No. 25 in High Vacuum at Elevated Temperature," pp. 289--303 in *Intern. Trans. Vacuum Met. Conf., 1967*, ed. by E. L. Foster, American Vacuum Society, New York, 1968.
- Bourgette, D. T., "Materials in vacuum environment," *J. Metals* **19**(12), 50--58 (December 1967).
- Brandon, C. A., D. R. Cuneo, G. B. Engle, and E. L. Long, Jr., "BeO-Graphite In-Reactor Compatibility at 1500°C and Resulting ^6Li Distribution," *Nucl. Appl.* **4**(1), 23--30 (January 1968).
- Brandon, C. A., D. R. Cuneo, G. B. Engle, and E. L. Long, Jr., *An Irradiation Experiment to Study the Compatibility of BeO with Graphite at 1500°C Part II. Operation and Postirradiation Evaluation*, ORNL-TM-1799 (October 1967).
- Brooks, C. R., J. E. Spruiell, and C.K.H. DuBose, "Electron Microscopic Observations of Dislocations in Nickel and Ni-Mo Alloys," *Mater. Res. Bull.* **3**, 381--88 (May 1968).
- Brooksbank, R. E., J. P. Nichols, and A. L. Lotts, "The Impact of Kilorod Facility Operational Experience on the Design of Fabrication Plants for ^{233}U -Th Fuels," pp. 321--40 in *Thorium Fuel Cycle* (Proceedings of Second International Thorium Fuel Cycle Symposium May 3--6, 1966), R. G. Wymer, Coordinator, U.S. Atomic Energy Commission/Division of Technical Information, Oak Ridge, Tenn., February 1968.
- Brynstad, Jorulf, and G. P. Smith, "Isosbestic Points and Internally Linear Spectra Generated by Changes in Solvent Composition or Temperature," *J. Phys. Chem.* **72**(1), 296--300 (January 1968).
- Brynstad, Jorulf, C. R. Boston, and G. P. Smith, "Electronic Spectra and Coordination of Nickel Centers in Liquid Lithium Chloride--Potassium Chloride Mixtures," *J. Chem. Phys.* **47**(9), 3179--89 (November 1967).
- Brynstad, Jorulf, and G. P. Smith, "Electronic Spectra and Coordination Geometry of Nickel Centers in Liquid Mixtures of Magnesium Chloride and Potassium Chloride," *J. Chem. Phys.* **47**(9), 3190--93 (November 1967).
- Buchanan, Mary G., and R. W. Hendricks, *Program Weight: A FORTRAN IV Program for Evaluation of Weighting Functions Used in Small-Angle X-Ray Scattering*, ORNL-TM-1950 (September 1967).
- Bunshah, R. F., M. A. Orehoski, A. Simkovich, R. K. Pitler, J. Morley, D. Bourgette, and S. Nelson, "Vacuum Metallurgy 1967 -- Part 1, a review of the International Conference held in New York, June 13--16," *J. Metals* **19**(10), 35--39 (October 1967).
- Bunshah, R. F., M. A. Orehoski, A. Simkovich, R. K. Pitler, J. Morley, D. Bourgette, and S. Nelson, "Vacuum Metallurgy 1967 -- Part 2, a review of the International Conference held in New York, June 13--16," *J. Metals* **19**(11), 69--75 (November 1967).
- Canonico, D. A., P. Patriarca, and G. C. Robinson, Jr., "Materials," Chap. 4, pp. 85--149 in *Technology of Steel Pressure Vessels for Water-Cooled Nuclear Reactors, A Review of Current Practice in Design, Analysis, Materials, Fabrication, Inspection, and Test*, ed. by G. D. Whitman, G. C. Robinson, Jr., and A. W. Savolainen, ORNL-NSIC-21 (December 1967).
- Canonico, D., R. W. McClung, E. C. Miller, S. E. Moore, and P. Patriarca, "Quality Assurance," Chap. 9, pp. 577--628 in *Technology of Steel Pressure Vessels for Water-Cooled Nuclear Reactors, A Review of Current Practice in Design, Analysis, Materials, Fabrication, Inspection, and Test*, ed. by G. D. Whitman, G. C. Robinson, Jr., and A. W. Savolainen, ORNL-NSIC-21 (December 1967).
- Carpenter, R. W., and J. C. Ogle, "Rolling and Recrystallization Substructure in Very Thin Foils of Copper and Iron," *Abstr. Bull. Inst. Metals Div.* **2**(2), 101 (1967).
- Cathcart, J. V., G. F. Petersen, and C. J. Sparks, "Oxidation Rate and Oxide Structural Defects," Chap. 14, pp. 333--46 in *Surfaces and Interfaces, I -- Chemical and Physical Characteristics*, ed. by J. J. Burke, N. L. Reed, and Volker Weiss, Syracuse University Press, Syracuse, New York, 1967.

- Cathcart, J. V., and G. F. Petersen, "Structural Characteristics of the Oxide on the (111) of Copper," *J. Electrochem. Soc.* **115**(6), 595–97 (June 1968).
- Chang, Ji Young, "Miniature High Temperature Graphite Furnace," *Rev. Sci. Instr.* **39**(5), 756–60 (May 1968).
- Clausing, R. E., "The Desorption of Hydrogen, Deuterium, Carbon Monoxide, and Oxygen from Polycrystalline Tungsten as the Result of Electron Bombardment," *Abstr. Bull. Inst. Metals Div.* **2**(2), 81 (1967).
- Collins, W. C., D. G. Scott, J. W. Tackett, and P. W. Turner, "Welding of the Control Plates for the High Flux Isotope Reactor," *Welding J. (N. Y.)* **46**(10), 833–41 (October 1967).
- Coobs, J. H., and O. Sisman, *Coated-Particle Fuels Development at Oak Ridge National Laboratory for Period January 15, 1967, to October 15, 1967*, ORNL-TM-2061 (December 1967).
- Copeland, G. L., and W. R. Martin, "The Ball Milling of Aluminum Powder for Production of Aluminum- Al_2O_3 Dispersions," (Summary) *Trans. Am. Nucl. Soc.* **10**(2), 478 (November 1967).
- Copeland, G. L., M. M. Martin, D. G. Harman, and W. R. Martin, *Effect of Powder and Process Variables on the Properties of Sintered Aluminum Products*, ORNL-TM-2215 (May 1968).
- Cunningham, C. W., B. Fleischer, L. C. Fuller, W. R. Huntley, and D. H. Jansen, "Design and Operation of Turbine Nozzle and Blade Screening Tests in Potassium Vapor," (Summary) *Trans. Am. Nucl. Soc.* **10**(2), 428–29 (November 1967).
- Cunningham, J. E., *Severe Radiation Damage to Aluminum Alloys*, ORNL-TM-2138 (March 1968).
- Davis, H. L., J. S. Faulkner, and H. W. Joy, "Calculation of the Band Structure for Copper as a Function of Lattice Spacing," *Phys. Rev.* **167**(3), 601–7 (March 1968).
- Dean, C. W., and R. E. McDonald, *High-Purity Shape Casting with an Electron-Beam Furnace*, ORNL-TM-1935 (October 1967).
- Dean, C. W., R. E. McDonald, and C. F. Leitten, Jr., "High-Purity Shape Casting with an Electron-Beam Furnace," pp. 262–67 in *Record of the IEEE 9th Annual Symposium on Electron, Ion, and Laser Beam Technology, Berkeley, 9–11 May 1967*, R.F.W. Pease, ed., San Francisco Press, San Francisco, 1967.
- DeVan, J. H., "Corrosion of Iron- and Nickel-Base Alloys in High-Temperature Sodium and NaK," pp. 643–59; DeVan, J. H., A. P. Litman, J. R. DiStefano, and C. E. Sessions, "Lithium and Potassium Corrosion Studies with Refractory Metals," pp. 675–95 in *Alkali Metal Coolants* (Proceedings of a Symposium, Vienna, 28 November–2 December, 1966), International Atomic Energy Agency, Vienna, 1967.
- Dodd, C. V., and W. E. Deeds, "Electromagnetic Forces in Conductors," *J. Appl. Phys.* **38**(13), 5045–51 (December 1967).
- Dodd, C. V., "A Portable Phase-Sensitive Eddy Current Instrument," *Mater. Evaluation* **26**(3), 33–36 (March 1968).
- Dodd, C. V., and W. E. Deeds, "Analytical Solutions to Eddy-Current Probe Coil Problems," *J. Appl. Phys.* **39**(6), 2829–38 (May 1968); also ORNL-TM-1987 (November 1967).
- Easton, D. S., and J. O. Betterton, "Purification of Zirconium and Other Refractory Metals in an Ultrahigh Vacuum Zone Refiner with Analysis of Partial Pressures," (Abstract) *J. Electrochem. Soc.* **115**(3), 75C (March 1968).
- Farrell, K., J. T. Houston, and A. C. Schaffhauser, "The Growth of Grain Boundary Gas Bubbles in Chemically Vapor Deposited Tungsten," pp. 363–90 in *Proceedings of the Conference on Chemical Vapor Deposition of Refractory Metals, Alloys, and Compounds, Gatlinburg, Tennessee, September 12–14, 1967*, ed. by A. C. Schaffhauser, American Nuclear Society, Hinsdale, Illinois.
- Farrell, K., A. C. Schaffhauser, and J. O. Stiegler, "Recrystallization, Grain Growth and the Ductile-Brittle Transition in Tungsten Sheet," *J. Less-Common Metals* **13**(2), 141–55 (August 1967).
- Farrell, K., B.T.M. Loh, and J. O. Stiegler, "Morphologies of Bubbles and Voids in Tungsten," *Am. Soc. Metals, Trans. Quart.* **60**(3), 485–93 (September 1967).
- Farrell, K., A. C. Schaffhauser, and J. O. Stiegler, "Bend Yield Stresses in Tungsten Sheet," *J. Less-Common Metals* **13**(5), 548–58 (November 1967).

- Farrell, K., and J. T. Houston, "Thermal Rejection of Gas Bubbles from Electrodeposited Nickel," (Abstract) *J. Metals* **20**(1), 42A (January 1968).
- Faulkner, J. S., H. L. Davis, and H. W. Joy, "Calculation of Constant-Energy Surfaces for Copper by the Korringa-Kohn-Rostoker Method," *Phys. Rev.* **161**(3), 656-64 (September 1967).
- Federer, J. I., W. C. Robinson, and R. M. Steele, "Effect of Deposition Conditions on the Orientation of Chemical Vapor-Deposited Tungsten and Molybdenum," pp. 287-95 in *1967 IEEE Conference Record of the Thermionic Conversion Specialist Conference, October 30-November 1, 1967, Palo Alto, California*, The Institute of Electrical and Electronics Engineers, New York.
- Federer, J. I., W. C. Robinson, Jr., and R. B. Pratt, "Flame Reactor Preparation of Fissionable Oxide Powders," (Summary) *Trans. Am. Nucl. Soc.* **11**(1), 130 (June 1968).
- Federer, J. I., and J. E. Spruiell, "Formation and Characterization of an A15-Type Structure in Chemically Vapor Deposited Tungsten-Rhenium Alloys," pp. 443-58 in *Proceedings of the Conference on Chemical Vapor Deposition of Refractory Metals, Alloys, and Compounds, Gatlinburg, Tennessee, September 12-14, 1967*, ed. by A. C. Schaffhauser, American Nuclear Society, Hinsdale, Illinois.
- Federer, John Irvin, *Formation and Characterization of the A15-Type Structure in Chemical Vapor Deposited Tungsten-Rhenium Alloys*, ORNL-TM-1888 (August 1967), M. S. Thesis, the University of Tennessee.
- Fitts, R. B., J. D. Sease, and A. L. Lotts, "Preparation of Ceramic Nuclear Fuels by Sol-Gel Extrusion," pp. 28-33, vol. 63 in "Preparation of Nuclear Fuels, Nuclear Engineering-Part XVIII," A. D. Tevebaugh and D. L. Keller, eds., *Chem. Eng. Progr. Symp. Ser.* **80**, American Institute of Chemical Engineers, New York, 1967.
- Flamm, H. J., *An Entrained-Fluidized-Bed System for Pyrolytic Carbon Coating of Microspheres*, ORNL-TM-2113 (April 1968).
- Foster, B. E., and S. D. Snyder, "Evaluation of Variables in the Measurement of Fuel Concentration Variations in Nuclear Fuel Rods," *Mater. Evaluation* **26**(2), 27-32 (February 1968).
- Franco-Ferreira, E. A., and L. C. Williams, *Fabrication of Instrumented Fuel Elements and In-Pile Capsules*, ORNL-4190 (December 1967).
- Fulkerson, W., D. L. McElroy, and J. P. Moore, "Comments on a Paper by E. Patrassi, Die Wärmeleitfähigkeit von Urandioxid bei sehr hohen Temperaturgradienten (The Thermal Conductivity of UO₂ at Very High Temperature Gradients)," *J. Nucl. Mater.* **26**(2), 223-26 (May 1968).
- Fulkerson, W., J. P. Moore, R. K. Williams, R. S. Graves, and D. L. McElroy, "Thermal Conductivity, Electrical Resistivity, and Seebeck Coefficient of Silicon from 100 to 1300°K," *Phys. Rev.* **167**(3), 765-82 (March 1968).
- Gehlbach, R. E., and H. E. McCoy, "Effect of Thermo-Mechanical Treatments on Precipitation in Hastelloy N," (Abstract) *J. Metals* **20**(1), 91A (January 1968).
- Gould, R. W., and R. W. Hendricks, "A High-Temperature Vacuum Sample Holder for the Kratky Camera," *J. Sci. Instr. Ser. 2*, **1**(6), 681 (June 1968).
- Gray, R. J., "Technology Forecast '68," *Metal Progr.* **93**(1), 58-70 (January 1968).
- Gray, R. J., "Present Status of Metallography," pp. 17-62 in "Fifty Years of Progress in Metallographic Techniques," *Am. Soc. Testing Mater. Spec. Tech. Publ.* **430**, American Society for Testing and Materials, Philadelphia, Pa., (April 1968); also ORNL-TM-1733 (July 1967).
- Haas, P. A., F. G. Kitts, and H. Beutler, "Preparation of Reactor Fuels by Sol-Gel Processes," pp. 16-27, vol. 63 in "Preparation of Nuclear Fuels, Nuclear Engineering-Part XVIII," A. D. Tevebaugh and D. L. Keller, eds., *Chem. Eng. Progr. Symp. Ser.* **80** American Institute of Chemical Engineers, New York, 1967.
- Hammond, J. P., *Physical, Mechanical, and Irradiation Properties of Thorium and Thorium Alloys*, ORNL-4218 (April 1968).
- Handler, G. S., and H. W. Joy, "S Limit in Helium. Movement of a System on an Energy Surface in Parameter Space," *J. Chem. Phys.* **47**(12), 5074-77 (December 1967).

- Harman, D. G., and T. A. Nolan, "Mechanical Properties and Fracture of Al-Al₂O₃ Alloys," *Abstr. Bull. Inst. Metals Div.* 2(2), 30 (1967).
- Harman, D. G., and T. A. Nolan, *Fracture of Al-Al₂O₃ Alloys: Fracture Analysis of the Commercial SAP-Type Alloy XAP-001*, ORNL-TM-1826 (July 1967).
- Harms, W. O., and A. P. Litman, *Compatibility of Materials for Advanced Space Nuclear Power Systems*, ORNL-TM-1964 (October 1967).
- Harris, L. A., and H. L. Yakel, "The Crystal Structure of La₂Be₂O₅," *Acta Cryst.* B24(5), 672--82 (May 1968).
- Heestand, R. L., D. W. Short, and W. C. Robinson, "Chemical Vapor Deposition of Ceramic Compounds," pp. 175--91 in *Proceedings of the Conference on Chemical Vapor Deposition of Refractory Metals, Alloys, and Compounds, Gatlinburg, Tennessee, September 12--14, 1967*, ed. by A. C. Schaffhauser, American Nuclear Society, Hinsdale, Illinois.
- Hendricks, R. W., R. W. Carpenter, and R. W. Gould, "A Small-Angle X-Ray Scattering Investigation of Inhomogeneities in Aluminum-Zinc Alloys," (Abstract) *J. Metals* 20(1), 68A (January 1968).
- Hendricks, R. W., and B. S. Borie, "On the Determination of the Metastable Miscibility Gap from Integrated Small-Angle X-Ray Scattering Data," pp. 319--34 in *Small-Angle X-Ray Scattering* (Proceedings of the Conference held at Syracuse University, June 1965), ed. by H. Brumberger, Gordon & Breach, New York, 1967.
- Hendricks, R. W., and P. W. Schmidt, "Calculation of Weighting Functions for Collimation Corrections in Small-Angle X-Ray Scattering," *Acta Phys. Austriaca* 26(2-3), 97--122 (1967).
- Hewette, D. M., II, R. L. Beatty, H. Beutler, J. H. Coobs, A. R. Olsen, and J. W. Prados, *Preirradiation Data for the Pyrolytic-Carbon-Coated Sol-Gel UO₂ Particles for the ETR X-Basket-2 Irradiation Experiment*, ORNL-TM-2097 (May 1968).
- Hobson, D. O., "Analysis of Textures in Deformed Zirconium Single Crystals," *Abstr. Bull. Inst. Metals Div.* 2(2), 100 (1967).
- Hobson, D. O., "Textures in Deformed Zirconium Single Crystals," *Trans. Met. Soc. AIME* 242(6), 1105--10 (June 1968).
- Hobson, D. O., *Preliminary Study of Pyrolytic Tungsten Deposition*, ORNL-TM-2074 (January 1968).
- Inouye, H., and J. M. Leitnaker, "Equilibrium Nitrogen Pressures and Thermodynamic Properties of UN," *J. Am. Ceram. Soc.* 51(1), 6--9 (January 1968).
- Joy, H. W., and H. J. Silverstone, "Valence States of Carbon in π -Electron Systems. II. Excited States and Ions," *Mol. Phys.* 13(2), 149--56 (October 1967).
- King, R. T., and J. R. Weir, "The Effect of Cyclotron-Injected Helium on the Mechanical Properties of Stainless Steel," *Abstr. Bull. Inst. Metals Div.* 2(2), 30 (1967).
- King, R. T., "Some Observations on the Effects of Cyclotron-Injected Gases in Face-Centered Cubic Metals," (Abstract) *J. Metals* 20(1), 41A (January 1968).
- King, Roy Thomas, *Numerical Methods for Sintering by Volume Diffusion*, ORNL-TM-2014 (January 1968); Ph.D. Thesis, Carnegie-Mellon University.
- King, R. T., and J. R. Weir, Jr., "The Effect of Irradiation on the Mechanical Properties of Aluminum Alloys," (Summary) *Trans. Am. Nucl. Soc.* 11(1), 146--47 (June 1968).
- Kitts, F. G., R. B. Fitts, and A. R. Olsen, "Sol-Gel Urania-Plutonia Microsphere Preparation and Fabrication in Fuel Rods," pp. 195--210 in *Intern. Symp. Plutonium Fuels Technol., Scottsdale, Ariz., 1967*, *Nucl. Met.* 13, American Institute of Mining, Metallurgical and Petroleum Engineers, New York, 1968.
- Knight, R. W., J. Binns, and G. M. Adamson, Jr., *Fabrication Procedures for Manufacturing High Flux Isotope Reactor Fuel Elements*, ORNL-4242 (June 1968).
- Koch, C. C., and G. R. Love, "Vanadium-Techetium Alloy System," *Abstr. Bull. Inst. Metals Div.* 2(2), 104 (1967).

- Koch, C. C., and C. J. McHargue, "The Influence of Plastic Deformation on the fcc \rightleftharpoons dhcp Phase Transformation in Cerium," *Abstr. Bull. Inst. Metals Div.* **2**(2), 117 (1967).
- Koch, C. C., R. H. Kernohan, and S. T. Sekula, "Superconductivity in the Technetium-Vanadium Alloy System," *J. Appl. Phys.* **38**(11), 4359–64 (October 1967).
- Koch, C. C., and G. R. Love, "Reaction Morphologies and Superconducting Properties in Technetium-Vanadium Alloys," (Abstract) *J. Metals* **20**(1), 56A (January 1968).
- Koch, C. C., and G. R. Love, "An Investigation of the Vanadium–Technetium Alloy System," *J. Less-Common Metals* **15**(1), 43–58 (May 1968).
- Kollie, T. G., "Specific Heat Determinations by Pulse Calorimetry Utilizing a Digital Voltmeter for Data Acquisition," *Rev. Sci. Instr.* **38**(10), 1452–63 (October 1967).
- Kopp, O. C., and L. A. Harris, "Synthesis of Grunerite and Other Phases in the System $\text{SiO}_2\text{-NaOH-Fe-H}_2\text{O}$," *Am. Mineralogist* **52**(11,12), 1681–88 (November–December 1967).
- Larsen-Badse, Jorgen, *Indentation Creep of Soft Metals*, ORNL-TM-1862 (July 1967).
- Larsen-Badse, Jorgen, *The Temperature and Time Dependence of the Hardness of Iron and Nickel*, ORNL-TM-1861 (July 1967).
- Leitnaker, J. M., "The Ideality of the UC-UN Solid Solution," pp. 317–30 in *Thermodynamics of Nuclear Materials, 1967*, International Atomic Energy Agency, Vienna, 1968.
- Leitten, C. F., Jr., and R. J. Beaver, "Use of Lanthanide Oxide Neutron Absorbers in Pressurized Water Reactors," *Nucl. Appl.* **4**(6), 399–417 (June 1968).
- Litman, A. P., W. J. Leonard, and M. I. Lundin, "Evaluation of U-10% Mo Alloy and Consideration of an Alternate Alloy for Pulse Reactor Cores," (Summary) *Trans. Am. Nucl. Soc.* **11**(1), 154–55 (June 1968).
- Litman, A. P., H. E. McCoy, and J. H. DeVan, "Fluoride Salts for Heat-Transfer Applications," (Summary) *Trans. Am. Nucl. Soc.* **11**(1), 128–29 (June 1968).
- Litman, A. P., W. J. Leonard, and D. B. Lloyd, "Compatibility of NaK with Type-316 Stainless Steel and Nb–1% Zr Alloy in a Heat Rejection System," (Summary) *Trans. Am. Nucl. Soc.* **11**(1), 117 (June 1968).
- Litman, A. P., and J. W. Koger, "Compatibility of Fluoroborate Coolant Salts with Hastelloy N for Molten Salt Reactors," (Summary) *Trans. Am. Nucl. Soc.* **11**(1), 143 (June 1968).
- Loh, B.T.M., "A Graphical Method for Determining the Schmid Factor," (Abstract) *J. Metals* **20**(1), 17A (January 1968).
- Lotts, A. L., and T. N. Washburn, "Fuel Element Fabrication," pp. 87–91 in Kirk-Othmer, *Encyclopedia of Chemical Technology*, 2nd ed., vol. 14, John Wiley & Sons, New York, 1967.
- Lotts, A. L., and T. N. Washburn, "Use of Computer Codes in Estimating Fuel Element Fabrication Costs," *Nucl. Appl.* **4**(5), 307–19 (May 1968).
- Love, G. R., "Computer-Directed Plotting of X-Ray Pole Figures," *Trans. Met. Soc. AIME* **242**(4), 746–47 (April 1968).
- Love, G. R., *Calcomp Plotting of X-Ray Pole Figures*, ORNL-TM-2018 (January 1968).
- Love, J. C., G. Czjzek, J. J. Spijkerman, and D. K. Snediker, "Mössbauer Experiments with Nickel-61," pp. 124–29 in *Hyperfine Structures and Nuclear Radiations*, ed. by E. Matthias and D. A. Shirley, North-Holland Publishing Company, Amsterdam, 1968.
- Love, J. C., and F. E. Obenshain, "Mössbauer Investigations of Nickel Alloys," (Abstract) *Bull. Am. Phys. Soc.* **13**, 667 (April 1968).
- Lundin, M. I., A. P. Litman, and W. J. Leonard, "Design and Metallurgical Aspects of the Army Pulsed Radiation Facility Reactor," (Summary) *Trans. Am. Nucl. Soc.* **10**(2), 609–11 (November 1967).
- Lundy, T. S., and A. J. Mortlock, "Near-Surface Effect for Diffusion in Silver and Gold," *Abstr. Bull. Inst. Metals Div.* **2**(2), 20 (1967).

- Lundy, T. S., "Discussion of 'Diffusion of Palladium, Silver, Cadmium, Indium, and Tin in Aluminum'," *Trans. Met. Soc. AIME* **242**(5), 956 (May 1968).
- MacPherson, R. E., and R. J. Gray, *Development of a 500-kw NaK-to-Air Radiator*, ORNL-4159 (January 1968).
- Mantnos, E. J., R. E. Adams, R. T. King, E. L. Long, Jr., J. E. Van Cleve, Jr., and A. L. Lotts, "Postirradiation Examination of Failed HFIR Target Elements," (Summary) *Trans. Am. Nucl. Soc.* **10**(2), 480–81 (November 1967).
- Martin, M. M., J. H. Erwin, and W. R. Martin, "Effect of Type and Concentration of Fuel on the Void Volume in Aluminum Dispersion-Type Fuel Plates," (Summary) *Trans. Am. Nucl. Soc.* **11**(1), 107–8 (June 1968).
- Martin, M. M., and W. R. Martin, "A Study of Processes for SAP Powder Consolidation," (Summary) *Trans. Am. Nucl. Soc.* **10**(2), 478–79 (November 1967).
- Martin, W. R., and J. R. Weir, "Solutions to the Problems of High-Temperature Irradiation Embrittlement," pp. 440–57 in *Effects of Radiation on Structural Metals*, *Am. Soc. Testing Mater. Spec. Tech. Publ.* 426, American Society for Testing and Materials, Philadelphia, Pa., 1967.
- Martin, W. R., R. L. Heestand, R. E. McDonald, and G. A. Reimann, *Application of Chemical Vapor Deposition to the Production of Tungsten Tubing*, ORNL-TM-1889 (July 1967).
- Martin, W. R., R. L. Heestand, R. E. McDonald, and G. A. Reimann, "Application of Chemical Vapor Deposition to the Production of Tungsten Tubing," pp. 303–14 in *Proceedings of the Conference on Chemical Vapor Deposition of Refractory Metals, Alloys, and Compounds, Gatlinburg, Tennessee, September 12–14, 1967*, ed. by A. C. Schaffhauser, American Nuclear Society, Hinsdale, Illinois.
- McClung, R. W., "Nondestructive Test Development for Nuclear Reactor Programs at the Oak Ridge National Laboratory," pp. 246–53 in *Materials Technology – An Interamerican Approach* (Interamerican Conference on Materials Technology, May 20–24, 1968, San Antonio, Texas), The American Society of Mechanical Engineers, New York, 1968.
- McClung, R. W., "State of the Art of Nondestructive Testing for Service and Postoperation Examination of Reactor Pressure Vessels," pp. 165–67 in *Incipient Failure Diagnosis for Assuring Safety and Availability of Nuclear Power Plants* (Conference Proceedings, Gatlinburg, Tennessee, October 30–November 1, 1967), CONF-671011 (January 1968).
- McClung, R. W., "Inspection of Small Specialty Welds and Brazed Joints for Nuclear Service," pp. 182–204 in *Proceedings of the 1967 Symposium on Nondestructive Testing of Welds*, ed. by T. F. Drouillard, The American Society for Nondestructive Testing, Evanston, Illinois, 1968.
- McCoy, H. E., Jr., *Effects of Irradiation on the Mechanical Properties of Two Vacuum-Melted Heats of Hastelloy N*, ORNL-TM-2043 (January 1968).
- McCoy, H. E., Jr., and J. R. Weir, Jr., "Stress-Rupture Properties of Irradiated and Unirradiated Hastelloy N Tubes," *Nucl. Appl.* **4**(2), 96–104 (February 1968).
- McCoy, H. E., Jr., *An Evaluation of the Molten Salt Reactor Experiment Hastelloy N Surveillance Specimens – First Group*, ORNL-TM-1997 (November 1967).
- McCoy, H. E., Jr., and J. R. Weir, Jr., *In- and Ex-Reactor Stress-Rupture Properties of Hastelloy N Tubing*, ORNL-TM-1906 (September 1967).
- McCoy, H. E., Jr., and J. O. Stiegler, *Mechanical Behavior of Chemically Vapor Deposited Tungsten at Elevated Temperatures*, ORNL-4162 (September 1967).
- McCoy, H. E., and J. O. Stiegler, "Mechanical Behavior of CVD Tungsten at Elevated Temperatures," pp. 391–425 in *Proceedings of the Conference on Chemical Vapor Deposition of Refractory Metals, Alloys, and Compounds, Gatlinburg, Tennessee, September 12–14, 1967*, ed. by A. C. Schaffhauser, American Nuclear Society, Hinsdale, Illinois.
- McDonald, R. E., and G. A. Reimann, *Floating-Mandrel Extrusion of Tungsten and Tungsten-Alloy Tubing*, ORNL-4210 (February 1968).

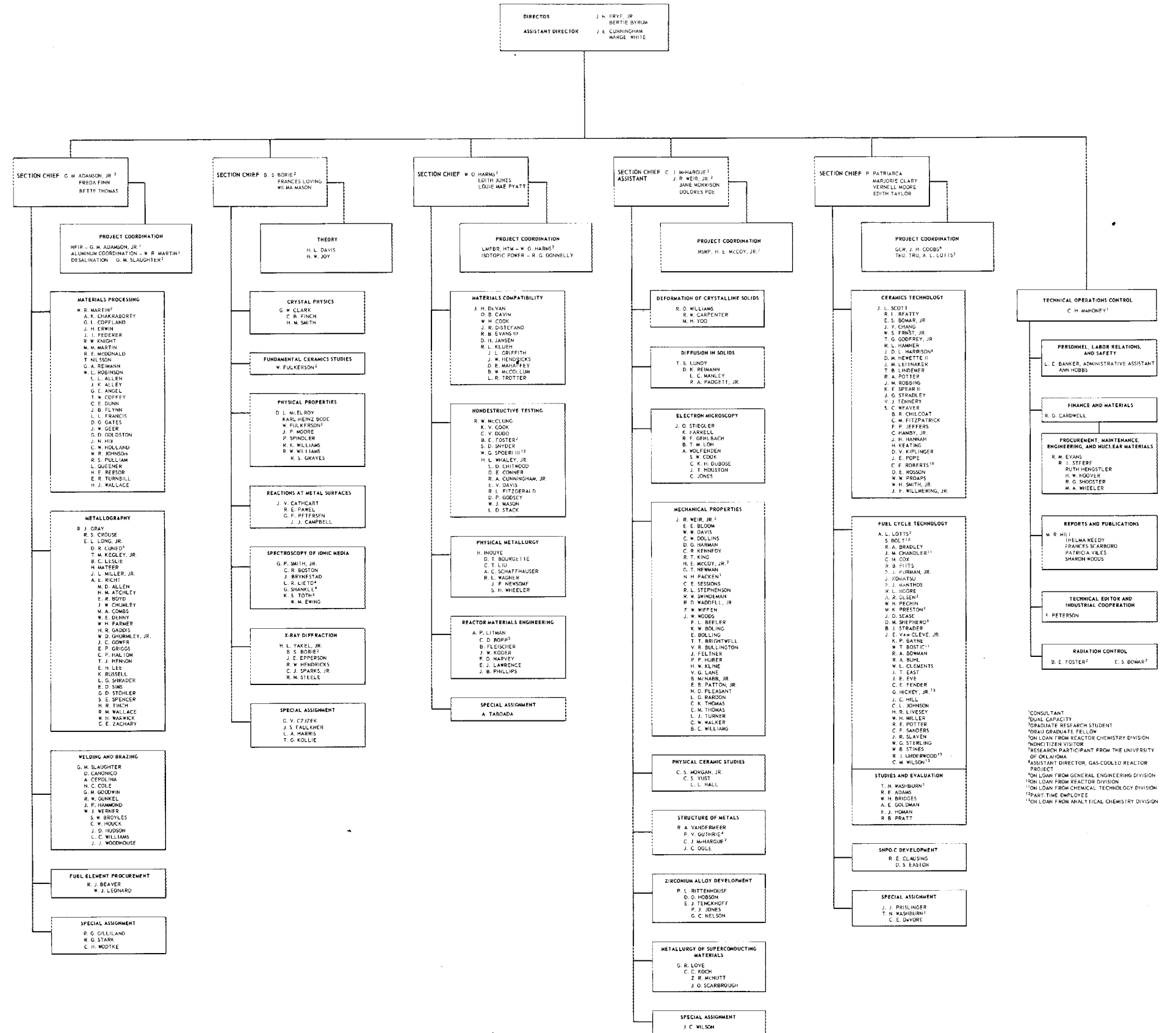
- McElroy, D. L., and W. Fulkerson, "Temperature Measurement and Control," pp. 105–267 in *Techniques of Metal Research*, vol. 1, Part 1, Techniques of Materials Preparation and Handling, ed. by R. F. Bunshah, Wiley, New York, 1968.
- Melton, C. E., and H. W. Joy, "Theoretical Evidence for NH_4 and H_3O ," *J. Chem. Phys.* **48**(11), 5286–87 (June 1968).
- Moncrief, E. C., and A. P. Litman, *Corrosion of the Volatility Pilot Plant INOR-8 Dissolver After Seven Cold Dissolution Runs*, ORNL-TM-1907 (July 1967).
- Moore, J. P., D. L. McElroy, and R. S. Graves, "Thermal Conductivity and Electrical Resistivity of High-Purity Copper from 78 to 400°K," *Can. J. Phys.* **45**(12), 3849–65 (December 1967).
- Morgan, C. S., and D. H. Bowen, "Inert Gas Bubbles in Neutron-irradiated Magnesium Oxide," *Phil. Mag.* **16**(139), 165 (July 1967).
- Morgan, C. S., and L. L. Hall, "Effect of Isostatic Pressure on Sintering," *J. Am. Ceram. Soc.* **50**(7), 382–83 (July 1967).
- Mortlock, A. J., *The Near-Surface Diffusion Anomaly in Gold*, ORNL-4141 (July 1967).
- Murdock, J. F., and C. J. McHargue, "Self-Diffusion in Body-Centered Cubic Titanium-Vanadium Alloys," *Acta Met.* **16**(4), 493–500 (April 1968).
- Nolan, T. A., and D. G. Harman, "Analysis of the Fracture of Aluminum Oxide (SAP) by Electron Microscopy," *Abstr. Bull. Inst. Metals Div.* **2**(2), 58 (1967).
- Obenshain, Felix, Gordon Czjzek, J.L.C. Love, and H.H.F. Wegener, "Coulomb-Recoil-Implantation-Mössbauer Experiments with ^{73}Ge ," (Abstract) *Bull. Am. Phys. Soc.* **13**(2), 235 (February 1968).
- Olsen, A. R., J. H. Coobs, and J. W. Ullmann, "Current Status of Irradiation Testing of Thorium Fuels at Oak Ridge National Laboratory," pp. 475–94 in *Thorium Fuel Cycle* (Proceedings of Second International Thorium Fuel Cycle Symposium May 3–6, 1966) R. G. Wymer, Coordinator, U.S. Atomic Energy Commission/Division of Technical Information, Oak Ridge, Tennessee, February 1968.
- Olsen, A. R., J. D. Sease, R. B. Fitts, and A. L. Lotts, *Fabrication and Irradiation Testing of Sol-Gel Fuels at Oak Ridge National Laboratory*, ORNL-TM-1971 (September 1967).
- Patterson, F. H., W. C. Robinson, Jr., and T. L. Hebble, *The Statistical Design and Analysis of Chemical Vapor Deposition Experiments*, ORNL-TM-2066 (December 1967).
- Pawel, R. E., and T. S. Lundy, "The Use of Electrochemical Sectioning in the Study of Diffusion in Tungsten," *J. Electrochem. Soc.* **115**(3), 233–37 (March 1968).
- Pawel, R. E., "The Effect of Anodic Films on the Gaseous Oxidation of Tantalum. II. Films Formed in Phosphoric Acid Solutions," *J. Electrochem. Soc.* **114**(12), 1222–27 (December 1967).
- Peterson, Sigfred, "Ignition and Combustion of Reactor Materials," *Nucl. Safety* **9**(1), 10–14 (Jan.–Feb. 1968).
- Picklesimer, M. L., "Anodizing for Controlled Microstructural Contrast by Color," *Microscope* **15**(4th quart.), 472–79 (October 1967).
- Prados, J. W., and T. G. Godfrey, *STRETCH, A Computer Program for Predicting Coated-Particle Irradiation Behavior; Modification IV, December 1967*, ORNL-TM-2127 (April 1968).
- Prados, J. W., R. L. Beatty, H. Beutler, J. H. Coobs, A. R. Olsen, and J. L. Scott, "Development of Coated-Particle Fuels for Advanced Gas-Cooled Reactors," pp. 273–92 in *Thorium Fuel Cycle* (Proceedings of Second International Thorium Fuel Cycle Symposium May 3–6, 1966) R. G. Wymer, Coordinator, U.S. Atomic Energy Commission/Division of Technical Information, Oak Ridge, Tennessee, February 1968.
- Prados, J. W., and J. L. Scott, "The Influence of Pyrolytic-Carbon Creep on Coated-Particle Fuel Performance," *Nucl. Appl.* **3**(8), 488–94 (August 1967).
- Pratt, R. B., J. D. Sease, and A. L. Lotts, "Pyrolytic-Carbon Coating in an Engineering-Scale System," (Summary) *Trans. Am. Nucl. Soc.* **10**(2), 510–11 (November 1967).

- Prislinger, J. J., and S. H. Jury, *Fabrication of an Improved Frost-Point Hygrometer Sensing Element*, ORNL-TM-2123 (April 1968).
- Reed, R. E., and C. J. McHargue, "Effect of Fabrication Method on the Texture of Aluminum Rods," *Trans. Met. Soc. AIME* 242(2), 180–82 (February 1968).
- Reed, R. E., and C. J. McHargue, "Deformation Bands and the Formation of $\langle 111 \rangle$ - $\langle 001 \rangle$ Fiber Textures in Aluminum," *Trans. Met. Soc. AIME* 239(10), 1604–12 (October 1967).
- Rittenhouse, P. L., and D. O. Hobson, "Inhomogeneous Deformation in Zircaloy Tubing," (Abstract) *J. Metals* 20(1), 106A (January 1968).
- Rittenhouse, P. L., "Strain Behavior in Uniaxially Tested Zircaloy Tubing," *J. Nucl. Mater.* 24(3), 310–15 (December 1967).
- Rittenhouse, P. L., "Hydride Orientation in Zircaloy Tubing," (Summary) *Trans. Am. Nucl. Soc.* 10(2), 464 (November 1967).
- Rittenhouse, P. L., "Determination of the Anisotropy of Yielding and Flow in Zircaloy-2 from a Single Test," *J. Nucl. Mater.* 23(2), 183–91 (August 1967).
- Rittenhouse, P. L., "A Quantitative Assessment of the Effect of Crystallographic Texture on the Yield and Flow of Zircaloy-2," *Abstr. Bull. Inst. Metals Div.* 2(2), 100 (1967).
- Robinson, W. C., F. H. Patterson, J. D. Fleming, and C. W. Gorton, "Chemical Vapor Deposition Statistical Parametric Study," pp. 109–25 in *Proceedings of the Conference on Chemical Vapor Deposition of Refractory Metals, Alloys, and Compounds, Gatlinburg, Tennessee, September 12–14, 1967*, ed. by A. C. Schaffhauser, American Nuclear Society, Hinsdale, Illinois.
- Robinson, W. C., Jr., and J. I. Federer, "Thermodynamic Considerations of the Chemical Vapor Deposition Process," (Abstract) *J. Metals* 20(1), 88A and 154A (January 1968).
- Robinson, W. C., F. H. Patterson, J. D. Fleming, and C. W. Gorton, *Chemical Vapor Deposition Statistical Parametric Study*, ORNL-TM-1890 (July 1967).
- Schaffhauser, A. C., J. T. Houston, and K. Farrell, "Effect of Gas Bubbles on Recrystallization and Grain Growth in Tungsten," (Abstract) *J. Metals* 20(1), 43A (January 1968).
- Scott, J. L., "Fuel Element Performance," *Nucl. Safety* 8(4), 331–39 (Summer 1967).
- Sease, J. D., R. B. Pratt, and A. L. Lotts, "Remote Fabrication of Thorium Fuels," pp. 341–57 in *Thorium Fuel Cycle* (Proceedings of Second International Thorium Fuel Cycle Symposium May 3–6, 1966) R. G. Wymer, Coordinator, U.S. Atomic Energy Commission/Division of Technical Information, Oak Ridge, Tennessee, February 1968.
- Sessions, C. E., and J. H. DeVan, "Thermal Convection Loop Tests of Refractory Alloys in Lithium," pp. 326–31 in *1967 IEEE Conference Record of the Thermionic Conversion Specialist Conference, October 30–November 1, 1967, Palo Alto, California*, Institute of Electric and Electronic Engineers, New York.
- Silverstone, H. J., and H. W. Joy, "Valence States of Carbon in π -Electron Systems. I. Alternant-Hydrocarbon Ground States," *J. Chem. Phys.* 47(4), 1384–92 (August 1967).
- Slaughter, G. M., E. A. Franco-Ferreira, and P. Patriarca, "Welding and Brazing of High Temperature Radiators and Heat Exchangers," *Welding J. (N.Y.)* 47(1), 15–22 (January 1968).
- Smith, W. E., Jorulf Brynestad, and G. P. Smith, "Two Different Tetrahedral–Octahedral Coordination Equilibria for Nickel(II) in Molten Zinc Chloride–Cesium Chloride Mixtures," *J. Am. Chem. Soc.* 89, 5983–84 (November 1967).
- Smith, W. E., and G. P. Smith, "Densities of Molten Zinc Chloride and Its Mixtures with Cesium Chloride," *J. Chem. Eng. Data* 13(1), 123–24 (January 1968).
- Spear, K. E., and J. M. Leitnaker, *Review and Analysis of Phase Behavior and Thermodynamic Properties of the Plutonium-Nitrogen System*, ORNL-TM-2106 (March 1968).
- Spruiell, J. E., B. F. Shuler, and F. H. Patterson, "Deformation Studies of Thermochemically Deposited Tungsten Sheet," *Trans. Met. Soc. AIME* 239(11), 1763–67 (November 1967).

- Stephenson, R. L., *Creep-Rupture Properties of Unalloyed Tantalum, Ta-10% W and T-111 Alloys*, ORNL-TM-1994 (December 1967).
- Stiegler, J. O., and J. R. Weir, Jr., *Effects of Irradiation on Ductility*, ORNL-TM-2019 (January 1968).
- Stiegler, J. O., and K. Farrell, "The Observation of Gas Bubbles in Solids," (Abstract) *J. Metals* **20**(1), 13A (January 1968).
- Stiegler, J. O., E. E. Bloom, and J. R. Weir, "Electron Microscopy of Irradiated EBR-II Fuel Cladding," (Summary) *Trans. Am. Nucl. Soc.* **11**(1), 146 (June 1968).
- Stiegler, J. O., K. Farrell, and H. E. McCoy, "Stress-Induced Growth of Gas Bubbles in Solids," *J. Nucl. Mater.* **25**(3), 340-43 (March 1968).
- Stiegler, J. O., K. Farrell, B.T.M. Loh, and H. E. McCoy, "Nature of Creep Cavities in Tungsten," *Am. Soc. Metals, Trans. Quart.* **60**(3), 494-503 (September 1967).
- Thurber, W. C., J. R. DiStefano, T. G. Kollie, H. Inouye, H. E. McCoy, and R. L. Stephenson, "Recent Studies on the Columbium-1% Zirconium Alloy," pp. 59-77 in *High Temperature Refractory Metals* (Metallurgical Society Conferences) vol. 34, ed. by R. W. Fountain, J. Malt, and L. S. Richardson, Gordon & Breach, New York, 1966.
- Tolson, G. M., and A. Taboada, *MSRE Control Elements: Manufacture, Inspection, Drawings, and Specifications*, ORNL-4123 (July 1967).
- Tunstall, J. N., and C. V. Dodd III, *A Computer Program to Solve Eddy-Current Problems*, K-1740 (April 1968).
- Vandermeer, R. A., and J. C. Ogle, "Texture Inhomogeneities in Cold-Rolled Columbium," *Abstr. Bull. Inst. Metals Div.* **2**(2), 101 (1967).
- Venard, J. T., *Compatibility of Dispersion Strengthened Aluminum with Uranium Monocarbide*, ORNL-TM-2010 (January 1968).
- Venard, John Thomas, *Investigation of Certain Ternary Systems Containing Thorium and Uranium*, ORNL-TM-2015 (January 1968), M. S. Thesis, the University of Tennessee.
- Venard, J. T., J. E. Spruiell, and O. B. Cavin, "Lattice Parameters Across the UN-ThN Pseudobinary," *J. Nucl. Mater.* **24**(2), 245-46 (November 1967).
- Washburn, T. N., A. L. Lotts, and F. E. Harrington, *Comparative Evaluation of Sol-Gel Fuel Fabrication Costs*, ORNL-TM-1979 (September 1967).
- Weaver, Samuel Cavin, *Helium Gas Bubble Migration in Uranium Mononitride in a Temperature Gradient*, ORNL-TM-2016 (December 1967), M.S. Thesis, the University of Tennessee.
- Weaver, S. C., and J. E. Spruiell, "Helium Bubble Migration in Uranium Nitride," (Abstract) *J. Metals* **20**(1), 30A (January 1968).
- Werner, W. J., and G. M. Slaughter, "Brazing Graphite to Hastelloy N for Nuclear Reactors," *Welding Eng.* **53**(3), 65 (March 1968).
- Williams, R. O., "Analytical Solutions for Representing Fiber Textures as Axial Pole Figures," *J. Appl. Phys.* **38**(10), 4029-33 (September 1967).
- Williams, R. O., "The Representation of the Textures of Rolled Copper, Brass, and Aluminum by Biaxial Pole Figures," *Trans. Met. Soc. AIME* **242**(1), 105-15 (January 1968).
- Wolfenden, A., and K. Farrell, "Comparison of Theories of the Growth of Gas Bubbles in Solids with Experimental Data," (Abstract) *J. Metals* **20**(1), 31A (January 1968).
- Yoo, M. H., "Interaction of Slip Dislocations with Twins in Hexagonal Close-Packed Metals," (Abstract) *J. Metals* **20**(1), 71A (January 1968).
- The following quarterly progress reports have been issued during this reporting period:
- Patriarca, P., *Fuels and Materials Development Program Quart. Progr. Rept. June 30, 1967*, ORNL-TM-1941; *Sept. 30, 1967*, ORNL-TM-2020; *Dec. 31, 1967*, ORNL-TM-2090; *Mar. 31, 1968*, ORNL-TM-2217 (Official Use Only).

METALS AND CERAMICS DIVISION

SEPTEMBER 1, 1968



INTERNAL DISTRIBUTION

- | | |
|--|-------------------------|
| 1-3. Central Research Library | 77. H. Inouye |
| 4-5. ORNL -- Y-12 Technical Library,
Document Reference Section | 78. R. G. Jordan (K-25) |
| 6-30. Laboratory Records Department | 79. M. A. Kastenbaum |
| 31. Laboratory Records, ORNL R.C. | 80. M. T. Kelley |
| 32. ORNL Patent Office | 81. E. M. King |
| 33. Laboratory Shift Supervisor | 82. R. B. Korsmeyer |
| 34. G. M. Adamson, Jr. | 83. J. A. Lane |
| 35. L. G. Alexander | 84. C. E. Larson |
| 36. R. J. Beaver | 85. A. P. Litman |
| 37. D. S. Billington | 86. A. L. Lotts |
| 38. A. L. Boch | 87. T. S. Lundy |
| 39. E. G. Bohlmann | 88. H. G. MacPherson |
| 40. E. S. Bomar | 89. W. R. Martin |
| 41. B. S. Borie | 90. R. W. McClung |
| 42. G. E. Boyd | 91. H. C. McCurdy |
| 43. R. B. Briggs | 92. D. L. McElroy |
| 44. J. V. Cathcart | 93. C. J. McHargue |
| 45. J. M. Chandler | 94. A. J. Miller |
| 46. G. W. Clark | 95. E. C. Miller |
| 47. W. C. Colwell | 96. MIT Practice School |
| 48. J. H. Coobs | 97. C. S. Morgan |
| 49. J. A. Cox | 98. M. L. Nelson |
| 50. F. L. Culler | 99. S. M. Ohr |
| 51. J. E. Cunningham | 100. A. R. Olsen |
| 52. G. V. Czjzek | 101-102. R. B. Parker |
| 53. J. H. DeVan | 103. P. Patriarca |
| 54. J. H. Erwin | 104. S. Peterson |
| 55. J. S. Faulkner | 105. J. W. Prados |
| 56. D. E. Ferguson | 106. H. P. Raaen |
| 57. G. W. Flack | 107. P. L. Rittenhouse |
| 58. A. P. Fraas | 108. A. W. Savolainen |
| 59. J. H. Frye, Jr. | 109. O. Sisman |
| 60. W. Fulkerson | 110. J. L. Scott |
| 61. J. H. Gillette | 111. H. E. Seagren |
| 62. R. J. Gray | 112. J. D. Sease |
| 63. J. L. Gregg | 113. G. M. Slaughter |
| 64. W. R. Grimes | 114. G. P. Smith, Jr. |
| 65. J. P. Hammond | 115. J. T. Stanley |
| 66. W. O. Harms | 116. P. E. Stein (K-25) |
| 67. C. S. Harrill | 117. J. O. Stiegler |
| 68-73. M. R. Hill | 118. D. A. Sundberg |
| 74. N. E. Hinkle | 119. D. B. Trauger |
| 75. A. S. Householder | 120. J. E. Van Cleve |
| 76. A. P. Huber (K-25) | 121. T. N. Washburn |
| | 122. M. S. Wechsler |

- | | |
|----------------------|-----------------------------------|
| 123. A. M. Weinberg | 128. H. L. Yakel |
| 124. J. R. Weir, Jr. | 129. C. M. Adam, Jr. (consultant) |
| 125. G. D. Whitman | 130. Leo Brewer (consultant) |
| 126. R. O. Williams | 131. L. S. Darken (consultant) |
| 127. J. C. Wilson | 132. J. A. Krumhansl (consultant) |

EXTERNAL DISTRIBUTION

133. D. F. Cope, RDT, AEC, Oak Ridge National Laboratory
134. N. Engel, Georgia Institute of Technology
135. V. D. Frechette, Alfred University
136. Angelo Giambusso, AEC, Washington
137. W. W. Grigorieff, Assistant to the Executive Director,
Oak Ridge Associated Universities
138. R. F. Hehemann, Case Institute of Technology
139. E. E. Hoffman, GE, Cincinnati
140. O. C. Kopp, University of Tennessee
141. J. Korringa, Ohio State University
142. W. J. Larkin, AEC, Oak Ridge Operations
143. C. F. Leitten, Jr., Linde Division, Union Carbide Corporation
144. J. J. Lombardo, NASA, Lewis Research Center
145. W. D. Manly, Union Carbide Corporation, New York
146. C. L. Matthews, RDT, AEC, Oak Ridge National Laboratory
147. P. W. McDaniel, AEC, Washington
148. T. W. McIntosh, AEC, Washington
149. R. R. Nash, NASA, Washington
150. E. F. Nippes, Rensselaer Polytechnic Institute
151. R. E. Pahler, AEC, Washington
152. R. M. Parke, MAB, National Academy of Science, Washington
153. H. B. Rahner, Savannah River Operations
154. F. N. Rhines, University of Florida
155. F. C. Schwenk, AEC, Washington
156. J. Simmons, AEC, Washington
157. E. E. Sinclair, AEC, Washington
158. L. M. Slifkin, University of North Carolina
159. E. E. Stansbury, University of Tennessee
160. D. K. Stevens, AEC, Washington
161. Dorothy Smith, AEC, Washington
162. J. A. Swartout, Union Carbide Corporation, New York
163. A. Van Echo, AEC, Washington
164. Watt Webb, Union Carbide Metals
165. J. Weertman, Northwestern University
166. G. W. Wench, AEC, Washington
167. M. J. Whitman, AEC, Washington
168. C.H.T. Wilkins, University of Alabama
169. Laboratory and University Division, AEC, Oak Ridge Operations
- 170-391. Given distribution as shown in TID-4500 under Metals, Ceramics, and Materials category (25 copies – CFSTI)